SCHOLARLY PUBLICATIONS

A CURRENT AWARENESS BULLETIN
OF RESEARCH OUTPUT

@DTU

(81st Edition)

SEPTEMBER 2019

BY: CENTRAL LIBRARY

DELHI TECHNOLOGICAL UNIVERSITY
(FORMERLY *DELHI COLLEGE OF ENGINEERING)*
GOVT. OF N.C.T. OF DELHI
SHAHBAD DAULATPUR, MAIN BAWANA ROAD
DELHI 110042

PREFACE

This is the **Eighty first** Issue of Current Awareness Bulletin started by Delhi Technological University, Central Library. The aim of the bulletin is to compile, preserve and disseminate information published by the faculty, students and alumni for mutual benefits. The bulletin also aims to propagate the intellectual contribution of Delhi Technological University (DTU) as a whole to the academia.

The bulletin contains information resources available in the internet in the form of articles, reports, presentations published in international journals, websites, etc. by the faculty and students of DTU. The publications of faculty and student which are not covered in this bulletin may be because of the reason that the full text either was not accessible or could not be searched by the search engine used by the library for this purpose.

The learned faculty and students are requested to provide their uncovered publications to the library either through email or in CD, etc. to make the bulletin more comprehensive.

This issue contains the information published during **September, 2019**. The arrangement of the contents is alphabetical. The full text of the article which is either subscribed by the university or available in the web is provided in this bulletin.

Central Library

CONTENTS

1. A deterministic time-delayed SIR epidemic model: mathematical modeling and analysis, ***6.Abhishek Kumar, 6.Kanica Goel and 3.Nilam***, Applied Mathematics, DTU

2. Adaptive Sitting Plan Algorithm Based On Henon Chaotic Map ***6.Ashish Kumar***[1], ***3.N S Raghava***[2], [1]IT and [2]Electronics, DTU

3. AN EFFECT OF ANKLE FOOT ORTHOSIS ON THE MUSCLE ACTIVITY OF DROP FOOT PATIENT: A CASE STUDY, FALAH HASANABDULSADAH, FAISAL HASAN, ***3.QASIM MURTAZA*** and SIDDHARTH BHARDWAJ, Mechanical, DTU

4. An examination of colorectal cancer burden by socioeconomic status: evidence from GLOBOCAN 2018, ***3.Rajesh Sharma***, Management, DTU

5. Aβ, Tau, and α-Synuclein aggregation and integrated role of PARK2 in the regulation and clearance of toxic peptides, ***6.Dhiraj Kumar***, ***3.Pravir Kumar***, Biotechnology, DTU

6. DESIGN AND STUDY OF A SOLAR THERMAL SYPHON PUMP, Md. Zishan Akhter, Md. Sarwar Khan, Md Sameer Farooque, ***6.Kaushalendra K. Dubey***, Gopal P. Sinha, Mechanical, Production, Industrial and Automobile, DTU

7. Design of Power Efficient 4:2 Compressors Using PFAL and Modified PFAL Adiabatic Logic Families, ***6.A. Mann***, ***6.N. Malhotra***, K. Gupta and ***3.N. Pandey***, Electronics and Communication, DTU

8. Development and characterization of non-coding RNA based simple sequence repeat markers in Capsicum species, Vandana Jaiswal, Abdul Rawoof, ***6.Meenakshi Dubeya***, Sushil Satish Chhapekar, Vineet Sharma and ***3.Nirala Ramchiarya***, Biotechnology, DTU

9. Elucidations on the Effect of Lanthanum Doping in ZnO Towards Enhanced Performance Nanogenerators, Pandey Rajagopalan, ***7.1.Pramila Jakhar***, I.A. Palani, Vipul Singh and Sang Jae Kim, Electrical, DTU

10. Forecasting Landslide in Chukha from Index Properties of Soil-Research to Policy Making, Nimesh Chettri, ***3.Raju Sarkar***, Kirtan Adhikari and Indra Bdr Chettri, Civil, DTU

11. High Gain Quasi Mutually Coupled Active Impedance Source Converter Utilizing Reduced Components Count, Avneet Kumar, Sajid Kamal, M Raghuram, ***8.1.Deepankar***, Santosh K. Singh and Xiaogang Xiong, Electrical and Electronics, DTU

12. Human Action Recognition Using Modified Bag of Visual Word based on Spectral Perception, ***6.Om Mishra***[1], ***3.Rajiv Kapoor***[1] and ***3.M.M. Tripathi***[2], [1]Electronics and Communication and [2]Electrical, DTU

13. Impact of cryogenic cooling during machining: A Literature Review, ***6.Anurag Sharma***, ***3.R.C. Singh*** and ***3.Ranganath M.Singari***, Mechanical, DTU

14. Inverse Band Reject and All Pass Filter Structure Employing CMOS CDBAs, ***3.Ram Bhagat***[1], ***3.D. R. Bhaskar***[2] and ***3.Pragati Kumar***[1], [1]Electrical and [2]Electronics, DTU

15. Linking knowledge management practices to organizational performance using the balanced scorecard approach, ***6.Meenu Chopra*** and ***3.Vikas Gupta***, DSM, DTU

16. Low power analog comb filter for biomedical applications, ***6.Sajal K. Paul***, Chandan Kumar Choubey and Gaurav Tiwari, DTU

17. Measuring the flexibility index for a supply chain using graph theory matrix approach, Rajesh Kumar Singh and ***3.Pravin Kumar***, Mechanical, DTU

18. Military Dog Based Optimizer and its Application to Fake Review Detection, Ashish Kumar Tripathi, ***3.Kapil Sharma*** and Manju Bala, IT, DTU

19. Nanomaterial-Modified Conducting Paper: Fabrication, Properties, and Emerging Biomedical Applications, ***6.Saurabh Kumar***, ***3.Chandra Mouli Pandey***, Amir Hatamie, Abdolreza Simchi, Magnus Willander, and ***3.Bansi D. Malhotra***, Biotechnology and Chemistry, DTU

20. Non-linearity of the Single Layer Graphene Field Effect Transistors, ***6.MUNINDRA*** and ***3.Deva Nand***, Electronics, DTU

21. Objective functions of distribution network expansion planning - a comprehensive and exhaustive review, Mandhir Kumar Verma, ***3.Vinod Kumar Yadav*** and V. Mukherjee, Electrical, DTU

22. Optimized Resonant Converter by Implementing Shunt Branch Element as Magnetizing Inductance of Transformer in Electric Vehicle Chargers, Vijaya Vardhan Reddy. P, H.M. Suryawanshi, ***7.1.Girish G. Talapur***, and Makarand Sudhakar Ballal, Electrical, DTU

23. Renewable Energy Fed DC Microgrid: An Overview, ***7.Apoorva Mishra*** and ***3.J.N Rai***, Electrical, DTU

24. Sentiment Analysis on Twitter Data: A Survey, ***6.Abhilash Mittal*** and ***3.Sanjay Patidar***, Computer Science, DTU

25. Sentiment Cognition from Words Shortlisted by Fuzzy Entropy, ***6.Srishti Vashishtha***, and ***3.Seba Susan***, IT, DTU

26. Study and first law analysis of Gas Turbine-HRSG-ORC co-generation system with change in atmospheric temperature, ***6.Priyanshu Thakur*** and ***3.PV Ram Kumar***, Mechanical, DTU

27. Synthesis and assessment of carboxymethyl tamarind kernel gum based novel superabsorbent hydrogels for agricultural applications, ***6.Khushbu***, ***3.Sudhir G. Warkar*** and ***3.Anil Kumar***, Applied Chemistry, DTU

28. TRAFFIC NOISE ANALYSIS USING RLS-90 MODEL IN URBAN CITY, ***3.Rajeev Kumar Mishra***, ***6.Ankita R. Mishra*** and ***6.Amit Singh***, Environmental, DTU

29. Tribological behavior of carbon coating for piston ring applications using Taguchi approach, ***6.Ankit Tyagi***, ***6.SM Pandey***, ***3.Qasim Murtaza***, ***3.R.S. Walia***, Mohit Tyagi, Mechanical, DTU

30. Visual Object Tracking by Fusion of Audio Imaging in Template Matching Framework, Satbir Singh, Arun Khosla and ***3.Rajiv Kapoor***, Electronics, DTU

31. Word sense disambiguation using implicit information, ***3.Goonjan Jain*** and D.K. Lobiyal, Applied Mathematics, DTU

1. *Chancellor*

2. *Pro Vice Chancellor*

2.1. *Ex Pro Vice Chancellor*

3. *Faculty*

3.1. *Ex Faculty*

4. *Teaching-cum-Research Fellow*

4.1.*Asst. Librarian*

5. *Alumni*

6. *Research Scholar*

6.1. *Ex Research Scholar*

7. *PG Scholar*

7.1. *Ex PG Scholar*

8. *Undergraduate Student*

8.1. *Ex Undergraduate Student*

Theory in Biosciences
https://doi.org/10.1007/s12064-019-00300-7

ORIGINAL ARTICLE

A deterministic time-delayed SIR epidemic model: mathematical modeling and analysis

Abhishek Kumar[1] · **Kanica Goel**[1] · **Nilam**[1]

Received: 27 January 2019 / Accepted: 29 August 2019
© Springer-Verlag GmbH Germany, part of Springer Nature 2019

Abstract
In this paper, a deterministic model for transmission of an epidemic has been proposed by dividing the total population into three subclasses, namely susceptible, infectious and recovered. The incidence rate of infection is taken as a nonlinear functional along with time delay, and treatment rate of infected is considered as Holling type III functional. We have structured a deterministic transmission model of the epidemic taking into account the factors that affect the epidemic transmission such as social and natural factors, inhibitory effects and numerous control measures. The delayed model has been analyzed mathematically for two equilibria, namely disease-free equilibrium (DFE) and endemic equilibrium. It is found that DFE is locally and globally asymptotically stable when the basic reproduction number (R_0) is less than unity. It has also been shown that the delayed system for DFE at $R_0 = 1$ is linearly neutrally stable. The existence of an endemic equilibrium has been shown and found that under some conditions, endemic equilibrium is locally asymptotically stable, and is globally asymptotically stable when $R_0 > 1$. Further, the endemic equilibrium exhibits Hopf bifurcation under some conditions. Finally, an undelayed system has been analyzed, and it is shown that at $R_0 = 1$, DFE exhibits a forward bifurcation.

Keywords Epidemic · Delay SIR model · Holling type III treatment rate · Nonlinear incidence rate · Stability · Bifurcation

Introduction

The structure of deterministic mathematical models for observing and controlling the spread of various human diseases is of public health interest in the light of the fact that the mathematics helps to formulate effective mechanisms for controlling their spread. Since the first compartmental model is given by Kermack and McKendrick (1927), various mathematical models involving some complex assumptions (Gumel et al. 2006; Korobeinikov and Maini 2005; Kumar and Nilam 2018, 2019a; b, 2019; Dubey et al. 2013, 2015; Cui et al. 2017; Xiao and Ruan 2007; Li and Zhang 2017; Huang et al. 2010; Goel and Nilam 2019; Hattaf and Yousfi 2009; Hattaf et al. 2013; Zhou and Fan 2012; Dubey et al. 2016; Naresh et al. 2009; Xu and Ma 2009; Wang and Ruan 2004; Wang 2002; Li Michael et al. 1999; Zhang and Suo 2010) have been proposed and considered, for instance, SIR, SIS, SEIR and SEIRS models. In recent times, considerable attention has been paid to study the dynamics of epidemic models with epidemiologically meaningful time delays. In the context of disease transmission, delays can be caused by a variety of factors. The most well-known reasons for a delay are (1) the latency of the infection in a vector and (2) the latency of the infection in an infected host (Huang et al. 2010; Li and Liu 2014). In these cases, some time should elapse before the level of infection in the infected host or the vector reaches a sufficiently high level to transmit the infection further.

It is well known that disease transmission progress plays a vital role in epidemic dynamics; that is, applying different incidence rates can potentially change the behaviors of the system. In many epidemic models, numerous incidence functions with or without delay are widely used in different epidemiological backgrounds (Li and Liu 2014). The incidence rate can also be modeled by many other kinds of more general functions. It is interesting whether the functional form of the incidence rate can change the epidemic dynamics

✉ Nilam
rathi.nilam@gmail.com

Abhishek Kumar
abhishek.dtu14@gmail.com

Kanica Goel
kanica.dtu2016@gmail.com

[1] Department of Applied Mathematics, Delhi Technological University, Delhi 110042, India

Published online: 06 September 2019

or not. Liu et al. (1986) suggested a nonlinear saturated incidence function $\beta SI^l/\left(1+\alpha I^h\right)$ to model the impact of behavioral changes to certain communicable diseases, where βSI^l describes the infection force of the disease and $1/\left(1+\alpha I^h\right)$ measures the inhibition effect from the behavioral change of the susceptible people when the number of infectious people increases; l, h and β are all positive constants, and α is a nonnegative constant. The case $l = h = 1$, i.e., the function $\beta SI/(1+\alpha I)$, was used by Capasso and Serio (1978) to represent a "protection measure" in modeling the cholera epidemics in Bari in 1973.

The resources of the health system available to the public determine how well the diseases are controlled. Particularly, the capacity of the hospital setting and the effectiveness and efficiency of treatment may influence the recovery rate (Cui et al. 2017). In this manner, consideration of the treatment rate is very important. For this, numerous authors (Kumar and Nilam 2018, 2019a, b; Kumar et al. 2019; Dubey et al. 2013, 2015) have suggested various treatment rates such as Monod–Haldane functional type and Holling type I and II. To contribute to the study of saturated treatment, we incorporate the Holling type III (Dubey et al. 2013, 2016) treatment rate, which characterizes the case in which removal rate initially is rapid with increment in infectives, and afterward, it develops gradually, finally settling to a saturated value. Any subsequent expansion in infectives will not influence the recovery/removal rate. This case relates to a known disease which has re-emerged and has available treatment methods.

In this article, we propose and analyze a mathematical susceptible—infected—recovered model to gain a better understanding of transmission and subsequent control of the spread of infectious/communicable disease via a combination of nonlinear saturated incidence and Holling type III treatment rates. We incorporate time delay in incidence rate as the incubation period of the disease. We discuss the positivity and boundedness of the model solution. Further, we find the equilibrium points of the model and discuss the local and global stability of the equilibria. The stability of equilibria is discussed in terms of the basic reproduction number (van den Driessche and Watmough 2002), Routh–Hurwitz criterion and Lyapunov functional. Moreover, bifurcation analysis and an undelayed system are also discussed. Our goal is to study the effect of nonlinear incidence along with time delay and Holling type III treatment, on the transmission dynamics of the infectious disease in the human population.

The remaining part of the manuscript is organized as follows: In "The mathematical model and its basic properties" section, the mathematical model is presented together with its basic properties as positivity and boundedness of the solutions. In "Equilibria and their stability analysis" section, a rigorous analysis of the model is provided including the existence and local stability analysis of model equilibria. The "Global stability" section analyzes the global stability of the equilibrium points. The stability of the undelayed system is presented in "Undelayed system" section. Finally, a discussion is presented in "Discussion" section.

The mathematical model and its basic properties

In this section, we present a deterministic epidemic model to prevent an outbreak of an epidemic. We assume that the human population under consideration is $N(t)$. We divide $N(t)$ into three isolated compartments or classes $X(t), Y(t)$ and $Z(t)$. Here, $X(t)$ represents the susceptible population, $Y(t)$ represents the compartment of infectious individuals, and recovered individuals are represented by $Z(t)$. The useful postulates for the model formulation are as follows.

Postulates

(A1) The nonlinear incidence rate is given by the function $F(Y)$.
(A2) It is supposed that all the newborns are susceptible.
(A3) The force of infection at any time t is given by $\alpha X(t)F(Y(t-\tau))$ (Kumar and Nilam 2018; Naresh et al. 2009), because those infected at the time $(t-\tau)$ become infectious τ time later.
(A4) The total population is supposed to be large enough to be adequately described by a deterministic model and is divided into compartments (or classes) based on the disease status.

The susceptible population is generated via recruitment by birth at a constant rate A. The natural death rate is supposed to be the same for all the individuals and is represented by μ. The contact capable of leading the infection in the human population is assumed as a rate α (transmission rate of infection). The protection measures (psychological or inhibitory effect) are considered at a rate β. The infected people also die due to disease-related death at a rate σ (disease–induced mortality). The rate of cure of infection is ω, and limitation rate in the treatment of infected is φ. The rate of recovery from infection is θ. These assumptions lead to the following nonlinear system of the delay differential equations to describe the changes in $X(t), Y(t)$ and $Z(t)$ with respect to time t:

$$\begin{aligned}
\frac{\mathrm{d}X(t)}{\mathrm{d}t} &= A-\mu X(t)-\frac{\alpha X(t)Y(t-\tau)}{1+\beta Y(t-\tau)},\\
\frac{\mathrm{d}Y(t)}{\mathrm{d}t} &= \frac{\alpha X(t)Y(t-\tau)}{1+\beta Y(t-\tau)}-(\mu+\sigma+\theta)Y(t)-\frac{\omega Y^2(t)}{1+\varphi Y^2(t)},\\
\frac{\mathrm{d}Z(t)}{\mathrm{d}t} &= \frac{\omega Y^2(t)}{1+\varphi Y^2(t)}+\theta Y(t)-\mu Z(t).
\end{aligned} \tag{1}$$

Here, time lag $\tau > 0$ represents the incubation period of the disease, defined as a fixed time during which the infectious agents develop in the vector, and it is only after that time that the infected vector can infect a susceptible individual.

For biological reasons, the initial conditions are nonnegative continuous functions as

$$X(\rho) = x(\rho); \quad Y(\rho) = y(\rho); \quad Z(\rho) = z(\rho), \tag{2}$$

where $H(\rho) = (x, y, z)^{\mathrm{T}} \in C$, are functions such that $x, y, z \geq 0, (-\tau \leq \rho \leq 0)$. C denotes the Banach space $C\left([-\tau, 0], \mathbb{R}^3_+\right)$ of continuous functions mapping the interval $[-\tau, 0]$ into $\mathbb{R}^3_+$ with the supremum norm

$$H = \sup_{\rho \in [-\tau, 0]} |H(\rho)|,$$

where $|\cdot|$ is any norm in $\mathbb{R}^3_+$.

The fundamental theory of functional differential equations (Hale and Verduyn Lunel 1993) implies for any initial conditions (2), system (1) has a unique solution $(X(t), Y(t), Z(t))$. The non-negativity and boundedness of the solution with a positive initial value (2) is guaranteed by the following theorem:

Theorem 1 *All solutions of model* (1) *starting in* $\mathbb{R}^3_+$ *are bounded and enter the set* $\Gamma = \left\{(X, Y, Z) \in \mathbb{R}^3_+ : X(t) + Y(t) + Z(t) = N(t) \leq \frac{A}{\mu}\right\}$.

Proof We assume that the model-dependent variables and parameters are nonnegative. Continuity of the right-hand side of system (1) and its derivative imply that the model is well posed for $N(t) > 0$. The invariant region for the existence of the solutions can be obtained as given below:

$$\frac{\mathrm{d}[X(t) + Y(t) + Z(t)]}{\mathrm{d}t} = \frac{\mathrm{d}N(t)}{\mathrm{d}t} \leq A - \mu N(t) \tag{3}$$

$$\Rightarrow \quad 0 < \liminf\ N(t) \leq \limsup\ N(t) \leq \frac{A}{\mu} (\text{as } t \to \infty). \tag{4}$$

Since $N(t) > 0$ on $[-\tau, 0]$ by assumption $N(t) > 0$ for all $t \geq 0$. Therefore, from (3) above, $N(t)$ cannot blow up to infinity in finite time. The model system is dissipative (solutions are bounded), and therefore, the solution exists globally for all $t > 0$ in the invariant and compact set $\Gamma = \left\{(X, Y, Z) \in \mathbb{R}^3_+ : X(t) + Y(t) + Z(t) = N(t) \leq \frac{A}{\mu}\right\}$. As $N \to 0, X(t), Y(t)$ and $Z(t)$ also tend to zero, each of these terms tends to zero as $N(t)$ does. It is therefore natural to interpret these terms as zero when $N(t) = 0$.

Remark In the region Γ, the elementary results, for example local existence, uniqueness and continuity of solutions, are valid for model (1). Therefore, there exists a unique solution $(X(t), Y(t), Z(t))$ of model (1) starting in the interior of Γ that exists on a maximal interval $[0, \infty)$ if solutions remain bounded (Naresh et al. 2009).

Since the first two equations of model (1) are independent of $R(t)$, it is convenient to study the first two equations of system (1) for theoretical analysis. The reduced model is as follows:

$$\begin{aligned} \frac{\mathrm{d}X(t)}{\mathrm{d}t} &= A - \mu X(t) - \frac{\alpha X(t) Y(t - \tau)}{1 + \beta Y(t - \tau)}, \\ \frac{\mathrm{d}Y(t)}{\mathrm{d}t} &= \frac{\alpha X(t) Y(t - \tau)}{1 + \beta Y(t - \tau)} - (\mu + \sigma + \theta) Y(t) - \frac{\omega Y^2(t)}{1 + \varphi Y^2(t)}. \end{aligned} \tag{5}$$

The initial conditions are

$$X(\rho) = x(\rho); \quad Y(\rho) = y(\rho) \tag{6}$$

Theorem 2 *All state variables* $(X(t), Y(t))$ *of the reduced model* (5) *with the initial condition* (6) *are nonnegative.*

Proof First we show that $X(t)$ is nonnegative for all $t \geq 0$. On the contrary, it is assumed that there exist $t_1 > 0$ be the first time such that $X(t_1) = 0$, and then by the first equation of system (5), we have $X'(t_1) = A > 0$, and hence, $X(t) < 0$ for $t \in (t_1 - \varepsilon, t_1)$, where $\varepsilon > 0$ is sufficiently small. This contradicts $X(t) > 0$ for $t \in [0, t_1)$. It follows that $X(t) > 0$ for $t > 0$. Now, we prove that positivity of solution $Y(t)$. Integrating the second equation of system (5) from 0 to t for $0 < t \leq \tau$, by applying the variation of constant formula and the step-by-step integration method, we obtain:

$$Y(t) = Y(0) \mathrm{e}^{-(\mu + \sigma + \theta)t} \cdot \mathrm{e}^{\int_0^t F(X(\delta), Y(\delta - \tau), Y(\delta)) \mathrm{d}\delta}$$

where $F(X(\delta), Y(\delta - \tau), Y(\delta)) = \left(\frac{\alpha X(\delta) Y(\delta - \tau)}{(1 + \beta Y(\delta - \tau)) Y(\delta)} - \frac{\omega Y(\delta)}{\varphi Y^2(\delta) + 1}\right)$.

It is easy to see that $Y(t) > 0$ for all $0 \leq t \leq \tau$. Integrating the second equation of system (5) from τ to t for $\tau < t \leq 2\tau$ gives

$$Y(t) = Y(\tau) \mathrm{e}^{-(\mu + \sigma + \theta)t} \cdot \mathrm{e}^{\int_\tau^t F(X(\delta), Y(\delta - \tau), Y(\delta)) \mathrm{d}\delta}$$

Note that $Y(t) > 0$ for all $\tau \leq t \leq 2\tau$, and this procedure can easily carry on. It follows that for all $t > 0$, we have $Y(t) > 0$. This completes the proof.

Equilibria and their stability analysis

In this section, we analyze the equilibrium points of system (5). The equilibrium solutions of a time-delayed system are equivalent to the corresponding system with zero delays

(Kumar and Nilam 2018). There are only two types of equilibria for our model, namely

1. $Q = \left(\frac{A}{\mu}, 0\right)$, disease- or infection-free equilibrium.
2. $Q^* = (X^*, Y^*)$, endemic or positive equilibrium.

Infection-free steady state

In this subsection, we analyze system (5) by finding its equilibria and their stability analysis. The steady state of system (5) satisfies the following system of equations:

$$A - \mu X(t) - \frac{\alpha X(t) Y(t)}{1 + \beta Y(t)} = 0 \tag{7}$$

$$\frac{\alpha X(t) Y(t)}{1 + \beta Y(t)} - (\mu + \sigma + \theta) Y(t) - \frac{\omega Y^2(t)}{1 + \varphi Y^2(t)} = 0. \tag{8}$$

Systems (7)–(8) has the infection-free equilibrium $Q = \left(\frac{A}{\mu}, 0\right)$, that is, there is no infection present in the community and all people are susceptible. The characteristic equation (the corresponding matrix (J_1) is given in "Appendix") of system (5) at Q is given by the following equation:

$$(\mu + \lambda)\left(\lambda - \frac{\alpha A}{\mu} e^{-\lambda\tau} + (\mu + \sigma + \theta)\right) = 0 \tag{9}$$

The term $\frac{\alpha A}{\mu(\mu+\sigma+\theta)} e^{-\lambda\tau}$ at $\tau = 0$ is known as basic reproduction number denoted as R_0. The threshold parameter R_0 is helpful in describing the spread of an infectious disease. Thus, R_0 for the model system (5) is obtained as

$$R_0 = \frac{\alpha A}{\mu(\mu + \sigma + \theta)}.$$

Analysis for $R_0 \neq 1$

One of the roots of (9) is given by $\lambda_1 = -\mu$, and the other roots can be obtained from

$$\frac{\alpha A}{\mu} e^{-\lambda\tau} - (\mu + \sigma + \theta) - \lambda = 0 \tag{10}$$

Suppose that

$$G(\lambda) = \lambda - \frac{\alpha A}{\mu} e^{-\lambda\tau} + (\mu + \sigma + \theta). \tag{11}$$

If $R_0 > 1$, it is readily seen that for λ real,

$$G(0) = (\mu + \sigma + \theta) - \frac{\alpha A}{\mu} = (\mu + \sigma + \theta)\left(1 - R_0\right),$$
$$\lim_{\lambda \to +\infty} G(\lambda) = +\infty.$$

Hence, $G(\lambda) = 0$ has a positive real root if $R_0 > 1$.

If $R_0 < 1$, we assume that Re $\lambda \geq 0$.
We see that

$$\text{Re } \lambda = \frac{\alpha A}{\mu} e^{-\text{Re } \lambda\tau} \cos \text{Im} \lambda\tau - (\mu + \sigma + \theta) < (\mu + \sigma + \theta)\left(R_0 - 1\right) < 0,$$

a contradiction to our assumption. Hence, if $R_0 < 1$ then the characteristic root λ of (10) has a negative real part.

Thus, the following theorem is proposed:

Theorem 3 *The infection-free steady state Q is locally asymptotically stable (LAS) when $R_0 < 1$ and unstable when $R_0 > 1$ for $\tau > 0$.*

Analysis at $R_0 = 1$

If $R_0 = 1$, then $\lambda = 0$ is a simple characteristic root of (9). Let $\lambda = a + ib$ be any of the other solutions, then (10) changes into:

$$a + ib + \mu + \sigma + \theta - \frac{\alpha A}{\mu} e^{-(a+ib)\tau} = 0 \tag{12}$$

By using Euler's formula and by separating real and imaginary parts, we can write

$$a + \mu + \sigma + \theta = \frac{\alpha A}{\mu} \cos b\tau e^{-a\tau}, \quad b = -\frac{\alpha A}{\mu} \sin b\tau e^{-a\tau} \tag{13}$$

Observing that $R_0 = 1$ implies $\frac{\alpha A}{\mu} = (\mu + \sigma + \theta)$. Moreover, if there exists a root satisfying both (13), then it also satisfies the equation obtained by squaring and adding them member to member,

$$(a + \mu + \sigma + \theta)^2 + b^2 = (\mu + \sigma + \theta)^2 e^{-2a\tau}. \tag{14}$$

For (14) to be verified, we must have $a \leq 0$. Thus, we propose the following theorem:

Theorem 4 *The infection-free steady state Q of system (5) is linearly neutrally stable if $R_0 = 1$ for $\tau > 0$.*

Endemic steady state

To establish the existence of an endemic equilibrium $Q^*(X^*, Y^*)$, the right-hand side of system (5) is equated to zero. Thus, the solution of following a set of algebraic equations gives the endemic equilibrium point $Q^*(X^*, Y^*)$ for the proposed model system:

$$\begin{aligned} A - \mu X^* - \frac{\alpha X^* Y^*}{1 + \beta Y^*} &= 0, \\ \frac{\alpha X^* Y^*}{1 + \beta Y^*} - (\mu + \sigma + \theta) Y^* - \frac{\omega Y^{*2}}{1 + \varphi Y^{*2}} &= 0. \end{aligned} \tag{15}$$

The solution of (15) gives the following:

1. $X^* = \frac{A(1+\beta Y^*)}{\mu+(\mu\beta+\alpha)Y^*}$,
2. Y^*.

Here, Y^* is given by the following cubic equation:

$$P(Y^*) = K_0 + K_1 Y^* + K_2 Y^{*2} + K_3 Y^{*3} = 0 \tag{16}$$

where

$$\begin{aligned}
K_0 &= A\alpha - \theta\mu - \mu^2 - \mu\sigma = \mu(\mu+\sigma+\theta)\big(R_0 - 1\big),\\
K_1 &= -(\alpha+\beta\mu)(\theta+\mu+\sigma) - \mu\omega,\\
K_2 &= \mu(\theta+\mu+\sigma)\varphi\big(R_0 - 1\big) - (\alpha+\beta\mu)\omega,\\
K_3 &= -(\alpha+\beta\mu)(\theta+\mu+\sigma)\varphi.
\end{aligned}$$

Next, we propose the following result for the existence of endemic equilibrium:

Theorem 5 *If $R_0 > 1$, then there are either one or three positive endemic equilibria, and if all equilibria are simple roots and if $R_0 \le 1$ then no positive endemic equilibria exist.*

Proof It is evident from the expressions of K_1, K_2, K_3 and K_4 that K_3 is always negative. Suppose $R_0 > 1 (K_0 > 0)$. The leading coefficient K_3 is negative. Hence, $\lim_{Y^*\to\infty} P(Y^*) = -\infty$. Also, note that $P(0) > 0$ when $R_0 > 1$. $P(Y^*)$ is a continuous function of Y^*, and by applying fundamental theorem of algebra, it is evident that (16) can have at most three real roots. By a geometric argument, it is readily seen that there is either one or three positive endemic equilibria, if all equilibria are simple roots. However, when $R_0 < 1$, the coefficients K_0, K_1, K_2 and K_3 all are negative, and then by a fundamental theorem of algebra, we know that (16) cannot have any positive real root, and when $R_0 = 1$, the coefficients K_0 is zero and other coefficients K_1, K_2 and K_3 all are negative, and then by a fundamental theorem of algebra, we know that this polynomial cannot have any positive real root.

Stability analysis of endemic or positive equilibria

To investigate the local stability of system (5) at endemic equilibrium (Q^*), we linearize system (5) at Q^* and obtained the characteristic equation (the corresponding matrix (J_2) is given in "Appendix") which is as given below:

$$\begin{aligned}
&\lambda^2 + M_1\lambda + N_1 + \big(M_2\lambda + N_2\big)e^{-\lambda\tau} = 0\\
&M_1 = \frac{(1+Y^*\beta)\big(\theta+2\mu+\sigma+Y^{*3}(\alpha+\beta(\theta+2\mu+\sigma))\varphi^2 + Y^*(\alpha+\beta(\theta+2\mu+\sigma)+2(\theta\varphi+2\mu\varphi+\sigma\varphi+\omega))\big)}{(1+Y^*\beta)^2(1+Y^*\varphi)^2}\\
&\quad + \frac{(1+Y^*\beta)Y^{*2}\big(2\alpha\varphi+(\theta+2\mu+\sigma)\varphi^2+2\beta(\theta\varphi+2\mu\varphi+\sigma\varphi+\omega)\big)}{(1+Y^*\beta)^2(1+Y^*\varphi)^2},\\
&M_2 = \frac{-X^*\alpha}{(1+Y^*\beta)^2},\\
&N_1 = \frac{(1+Y^*\beta)(\mu+Y^*(\alpha+\beta\mu))(\theta+\mu+\sigma)}{(1+Y^*\beta)^2},\\
&N_2 = \frac{-X^*\alpha\mu}{(1+Y^*\beta)^2}.
\end{aligned} \tag{17}$$

Theorem 5 *For $\tau > 0$, system (5) at Q^* is locally asymptotically stable if $M_1^2 - 2N_1 - M_2^2 > 0$ and $N_1^2 - N_2^2 > 0$ are satisfied simultaneously.*

Proof At endemic equilibrium Q^*, the characteristic equation of the system for $\tau > 0$ is given by (17):

$$\lambda^2 + M_1\lambda + N_1 + \big(M_2\lambda + N_2\big)e^{-\lambda\tau} = 0.$$

For $\tau > 0$, by corollary 2.4 in Ruan and Wei (2003), it follows that a characteristic root of (17) must cross the imaginary axis for the occurrence of instability for a specific value of the delay τ. Accordingly, we assume that $\lambda = i\omega, \omega > 0$ is the root of the characteristic (17). Putting $\lambda = i\omega$ in (17) gives the following:

$$\begin{aligned}
&-\omega^2 + N_1 + M_2\omega\sin\omega\tau + N_2\cos\omega\tau\\
&\quad + i\big(M_2\omega\cos\omega\tau - N_2\sin\omega\tau + M_1\omega\big) = 0
\end{aligned} \tag{18}$$

Using Euler's formula and separating the real and imaginary part of (18), we get

$$M_2\omega\sin\omega\tau + N_2\cos\omega\tau = \omega^2 - N_1 \tag{19}$$

$$M_2\omega\cos\omega\tau - N_2\sin\omega\tau = -M_1\omega \tag{20}$$

Squaring and adding both sides of Eqs. (19) and (20) yields

$$\omega^4 + \big(M_1^2 - 2N_1 - M_2^2\big)\omega^2 + \big(N_1^2 - N_2^2\big) = 0 \tag{21}$$

Setting $\omega^2 = Z_1$, (21) becomes

$$Z_1^2 + MZ_1 + T = 0. \tag{22}$$

Here, $M = \left(M_1^2 - 2N_1 - M_2^2\right)$ and $T = \left(N_1^2 - N_2^2\right)$.

Clearly, if $M = \left(M_1^2 - 2N_1 - M_2^2\right) > 0$ and $T = \left(N_1^2 - N_2^2\right) > 0$ are satisfied simultaneously, and then by Routh–Hurwitz Criterion (22) will always have roots with the negative real part. It contradicts our assumption for instability that $\lambda = i\omega$ is a root of (17). Hence, Q^* is locally asymptotically stable for $\tau > 0$.

Hopf bifurcation analysis

In this section, we discuss the Hopf bifurcation of system (5).

If $T = \left(N_1^2 - N_2^2\right)$ in (22) is negative, then there is unique positive ω_0 satisfying (22), i.e., there is a single pair of purely imaginary roots $\pm i\omega_0$ to (22).

From Eqs. (19) and (20), τ_n corresponding to ω_0 can be obtained as

$$\tau_n = \frac{1}{\omega_0}\arccos\left(\frac{\left(N_2 - M_1M_2\right)\omega_0^2 - N_1N_2}{M_2^2\omega_0^2 + N_2^2}\right) + \frac{2n\pi}{\omega_0}, \quad n = 0, 1, 2, \ldots. \tag{23}$$

Endemic equilibrium Q^* is stable for $\tau < \tau_0$ if transversality condition holds true, i.e., if $\frac{\mathrm{d}}{\mathrm{d}\tau}(\mathrm{Re}(\lambda))\Big|_{\lambda=i\omega_0} > 0$.

Differentiating (17) with respect to τ, we get

$$\left(2\lambda + M_1 + M_2\mathrm{e}^{-\lambda\tau} - \left(M_2\lambda + N_2\right)\tau\mathrm{e}^{-\lambda\tau}\right)\frac{\mathrm{d}\lambda}{\mathrm{d}\tau} = \lambda\left(M_2\lambda + N_2\right)\mathrm{e}^{-\lambda\tau}$$

$$\left(\frac{\mathrm{d}\lambda}{\mathrm{d}\tau}\right)^{-1} = \frac{\left(2\lambda + M_1 + M_2e^{-\lambda\tau} - \left(M_2\lambda + N_2\right)\tau\mathrm{e}^{-\lambda\tau}\right)}{\lambda\left(M_2\lambda + N_2\right)\mathrm{e}^{-\lambda\tau}} = \frac{\left(2\lambda + M_1\right)}{\lambda\left(M_2\lambda + N_2\right)\mathrm{e}^{-\lambda\tau}} + \frac{M_2}{\lambda\left(M_2\lambda + N_2\right)} - \frac{\tau}{\lambda}$$

$$\left(\frac{\mathrm{d}\lambda}{\mathrm{d}\tau}\right)^{-1} = \frac{\left(2\lambda + M_1\right)}{-\lambda\left(\lambda^2 + M_1\lambda + N_1\right)} + \frac{M_2}{\lambda\left(M_2\lambda + N_2\right)} - \frac{\tau}{\lambda}$$

$$\begin{aligned}
&\frac{\mathrm{d}}{\mathrm{d}\tau}(\mathrm{Re}(\lambda))^{-1}\Big|_{\lambda=i\omega_0} = \mathrm{Re}\left(\frac{\mathrm{d}\lambda}{\mathrm{d}\tau}\right)^{-1}\Big|_{\lambda=i\omega_0} \\
&= \mathrm{Re}\left(\frac{\left(2i\omega_0 + M_1\right)}{-i\omega_0\left(-\omega_0^2 + iM_1\omega_0 + N_1\right)} + \frac{M_2}{i\omega_0\left(iM_2\omega_0 + N_2\right)} - \frac{\tau}{i\omega_0}\right) \\
&= \mathrm{Re}\left(\frac{1}{\omega_0}\left(\frac{\left(2i\omega_0 + M_1\right)}{\left(\omega_0^2 - N_1\right)i + M_1\omega_0)} + \frac{M_2}{\left(-M_2\omega_0 + iN_2\right)} + i\tau\right)\right) \\
&= \frac{1}{\omega_0}\left(\frac{2\omega_0\left(\omega_0^2 - N_1\right) + M_1^2\omega_0}{\left(\omega_0^2 - N_1\right)^2 + \left(M_1\omega_0\right)^2} - \frac{M_2^2\omega_0}{\left(M_2\omega_0\right)^2 + N_2^2}\right)
\end{aligned} \tag{24}$$

$= \frac{2\omega_0^2 + \left(M_1^2 - 2N_1 - M_2^2\right)}{\left(M_2\omega_0\right)^2 + N_2^2}$ [since, from Eqs. (19), (20), $\left(\omega_0^2 - N_1\right)^2 + \left(M_1\omega_0\right)^2 = \left(M_2\omega_0\right)^2 + N_2^2$].

Under the condition $M_1^2 - 2N_1 - M_2^2 > 0$, we have $\frac{\mathrm{d}}{\mathrm{d}\tau}(\mathrm{Re}(\lambda))\Big|_{\lambda=i\omega_0} > 0$.

Thus, the transversality condition holds and Hopf bifurcation occurs at $\omega = \omega_0, \tau = \tau_0$.

By summarizing the above analysis, we arrive at the following theorem.

Theorem 6 *The endemic equilibrium (EE) of system (5) is locally asymptotically stable for $\tau \in [0, \tau_0)$, and it exhibits Hopf bifurcation at $\tau = \tau_0$.*

Global stability

We suppose that

$$H(X(t)) = \alpha X(t), \quad F(Y(t)) = \frac{Y(t)}{1 + \beta Y(t)}.$$

To prove our results, we need the following assumptions:

(H1) $H(0) = F(0) = 0; H'(X) > 0$, for all $X, Y > 0$.

(H2) $F'(Y) > 0; \frac{\partial^2 F(Y)}{\partial Y^2} \leq 0$, for all $X, Y > 0$.

(H3) $\frac{F(Y)}{F(Y^*)} \leq 1; \frac{(\mu+\sigma+\theta)Y + \frac{\omega Y^2}{1+\varphi Y^2}}{H(X^*)F(Y)} \geq 1$ or $\frac{F(Y)}{F(Y^*)} \geq 1; \frac{(\mu+\sigma+\theta)Y + \frac{\omega Y^2}{1+\varphi Y^2}}{H(X^*)F(Y)} \leq 1$ for all $X, Y > 0$.

Theorem 7 *Suppose that assumptions (H1–H3) are satisfied.*

1. *If $R_0 > 1$, the endemic equilibrium $Q^*(X^*, Y^*)$ is globally asymptotically stable (GAS) for any $\tau \geq 0$.*
2. *If $R_0 \leq 1$, the infection-free equilibrium $Q(X_0, 0) = Q\left(\frac{A}{\mu}, 0\right)$ is globally asymptotically stable (GAS) for any $\tau \geq 0$.*

Proof (1) Let us consider any solution $(X(t), Y(t))$ of system (5) with the initial conditions. For any $\tau \geq 0$, we define the function $U_1(t)$ as follows:

$$U_1(t) = X(t) - \int_{X^*}^{X(t)} \frac{H(X^*)}{H(\eta)} \mathrm{d}\eta + Y(t) - \int_{Y^*}^{Y(t)} \frac{F(Y^*)}{F(\eta)} \mathrm{d}\eta.$$

Korobeinikov and Maini (2005) showed that Q^* is the only internal stationary point and the minimum point of $U_1(t) \to \infty$ at the boundary of the positive quadrant. Therefore, Q^* is the global minimum point, and the function is bounded from below.

Let

$$U_2 = \int_0^{\tau} \left[\frac{F(Y(t-\xi))}{F(Y^*)} - 1 - \ln \frac{F(Y(t-\xi))}{F(Y^*)} \right] \mathrm{d}\xi.$$

It easy to see that $U_2 \geq 0$ and $U_2 = 0$ if and only if $Y(t-\xi) = Y^*$ for all $\xi \in [0, \tau]$. For any positive $Y(t-\xi)$ for ξ in $[0, \tau]$, U_2 will be finite and can be differentiated. Then, the derivative of U_2 satisfies

$$\begin{aligned}
\frac{\mathrm{d}U_2}{\mathrm{d}t} &= \frac{\mathrm{d}}{\mathrm{d}t} \int_0^{\tau} \left[\frac{F(Y(t-\xi))}{F(Y^*)} - 1 - \ln \frac{F(Y(t-\xi))}{F(Y^*)} \right] \mathrm{d}\xi \\
&= \int_0^{\tau} \frac{\mathrm{d}}{\mathrm{d}t} \left[\frac{F(Y(t-\xi))}{F(Y^*)} - 1 - \ln \frac{F(Y(t-\xi))}{F(Y^*)} \right] \mathrm{d}\xi \\
&= -\int_0^{\tau} \frac{\mathrm{d}}{\mathrm{d}\xi} \left[\frac{F(Y(t-\xi))}{F(Y^*)} - 1 - \ln \frac{F(Y(t-\xi))}{F(Y^*)} \right] \mathrm{d}\xi \\
&= -\left[\frac{F(Y(t-\xi))}{F(Y^*)} - 1 - \ln \frac{F(Y(t-\xi))}{F(Y^*)} \right]_{\xi=0}^{\tau} \\
&= -\frac{F(Y(t-\tau))}{F(Y^*)} + \frac{F(Y(t))}{F(Y^*)} + \ln \frac{F(Y(t-\tau))}{F(Y)}.
\end{aligned}$$

Now, we study the behavior of Lyapunov functional

$$V_1 = U_1(t) + \left(\mu + \sigma + \theta + \frac{\omega Y^*}{1 + \varphi Y^{*2}} \right) Y^* U_2$$

The derivative of V_1 along the solution of (5) is given by:

$$\begin{aligned}
\frac{\mathrm{d}V_1}{\mathrm{d}t} &= \left(1 - \frac{H(X^*)}{H(X)}\right)\dot{X}(t) + \left(1 - \frac{F(Y^*)}{F(Y)}\right)\dot{Y}(t) \\
&\quad + \left(\mu + \sigma + \theta + \frac{\omega Y^*}{1 + \varphi Y^{*2}} \right) Y^* \frac{\mathrm{d}U_2}{\mathrm{d}t} \\
&= \left(1 - \frac{H(X^*)}{H(X)}\right)(\mu X^* + H(X^*)F(Y^*) \\
&\quad - \mu X - H(X)F(Y(t-\tau))) + \left(1 - \frac{F(Y^*)}{F(Y)}\right) \\
&\quad \times \left(H(X)F(Y(t-\tau)) - (\mu + \sigma + \theta)Y - \frac{\omega Y^2}{1 + \varphi Y^2} \right) \\
&\quad - \left(\mu + \sigma + \theta + \frac{\omega Y^*}{1 + \varphi Y^{*2}} \right) Y^* \\
&\quad \times \left(\frac{F(Y(t-\tau))}{F(Y^*)} - \frac{F(Y)}{F(Y^*)} - \ln \frac{F(Y(t-\tau))}{F(Y)} \right).
\end{aligned}$$

By noting that

$$\ln \frac{F(Y(t-\tau))}{F(Y)} = \ln \frac{H(X^*)}{H(X)} + \ln \frac{H(X)F(Y(t-\tau))}{H(X^*)F(Y)},$$

and

$$\left(\mu + \sigma + \theta + \frac{\omega Y^*}{1 + \varphi Y^{*2}} \right) Y^* = H(X^*)F(Y^*),$$

it is easy to see that

$$\begin{aligned}
\frac{\mathrm{d}V_1}{\mathrm{d}t} &= \frac{\mu}{H(X)}(H(X) - H(X^*))(X^* - X) + H(X^*)F(Y^*) \\
&\quad \times \left(1 - \frac{H(X^*)}{H(X)} + \ln \frac{H(X^*)}{H(X)} \right) + H(X^*)F(Y^*) \\
&\quad \times \left(1 + \ln \frac{H(X)F(Y(t-\tau))}{H(X^*)F(Y)} - \frac{H(X)F(Y(t-\tau))}{H(X^*)F(Y)} \right) \\
&\quad + H(X^*)F(Y^*) \left(\left(\frac{F(Y)}{F(Y^*)} - 1 \right) \right. \\
&\quad \left. \times \left(1 - \frac{(\mu + \sigma + \theta)Y + \frac{\omega Y^2}{1 + \varphi Y^2}}{H(X^*)F(Y)} \right) \right).
\end{aligned}$$

Here,

$$\begin{aligned}
&1 - \frac{H(X^*)}{H(X)} + \ln \frac{H(X^*)}{H(X)} \leq 0; \text{ for all } X > 0, \text{ and} \\
&1 + \ln \frac{H(X)F(Y(t-\tau))}{H(X^*)F(Y)} \\
&\quad - \frac{H(X)F(Y(t-\tau))}{H(X^*)F(Y)} \leq 0; \text{ for all } Y(t-\tau) > 0, \quad X > 0.
\end{aligned} \tag{25}$$

For monotonically increasing function $H(X)$, $H(X) \geq H(X^*)$ holds when $X \geq X^*$, and hence, the following inequalities hold:

$$(X^* - X)(H(X) - H(X^*)) \leq 0. \tag{26}$$

Hence, by condition (H3) and inequalities (25)–(26), all the conditions of corollary 5.2 of Kuang (1993) hold true. Hence, Q^* is globally asymptotically stable for any $\tau \geq 0$ when $R_0 > 1$.

(2) We consider the Lyapunov functional

$$V_2 = X(t) - \int_{X_0}^{X(t)} \frac{H(X_0)}{H(\eta)} \mathrm{d}\eta + Y(t) + H(X_0) \int_0^{\tau} F(Y(t-\xi))\mathrm{d}\xi. \tag{27}$$

Let

$$U_3 = \int_0^{\tau} F(Y(t-\xi))\mathrm{d}\xi.$$

The derivative of U_3 is

$$\begin{aligned}\frac{\mathrm{d}U_3}{\mathrm{d}t} &= \int_0^{\tau} \frac{\mathrm{d}}{\mathrm{d}t} F(Y(t-\xi))\mathrm{d}\xi = -\int_0^{\tau} \frac{\mathrm{d}}{\mathrm{d}\xi} F(Y(t-\xi))\mathrm{d}\xi \\ &= -F(Y(t-\tau)) + F(Y(t)).\end{aligned}$$

Hence, we obtain

$$\begin{aligned}\frac{\mathrm{d}V_2}{\mathrm{d}t} &= \left(1 - \frac{H(X_0)}{H(X)}\right)\dot{X}(t) + \dot{Y}(t) + H(X_0)\frac{\mathrm{d}U_3}{\mathrm{d}t} \\ &= \left(1 - \frac{H(X_0)}{H(X)}\right)(\mu X^* - \mu X - H(X)F(Y(t-\tau))) \\ &\quad + \left(H(X)F(Y(t-\tau)) - (\mu+\sigma+\theta)Y - \frac{\omega Y^2}{1+\varphi Y^2}\right) \\ &\quad - H(X_0)F(Y(t-\tau)) + H(X_0)F(Y(t)) \\ &= -\frac{\mu}{H(X)}(X - X_0)\big(H(X) - H(X_0)\big) - \frac{\omega Y^2}{1+\varphi Y^2} \\ &\quad + (\mu+\sigma+\theta)\left(\frac{H(X_0)F(Y(t))}{(\mu+\sigma+\theta)} - Y\right).\end{aligned}$$

It holds that $\lim_{t\to\infty} \frac{\mathrm{d}V_2}{\mathrm{d}t} = 0$, which yields $\lim_{t\to\infty} X(t) = X_0$ and $\lim_{t\to\infty} Y(t) = 0$.

Now,

$$\big(X - X_0\big)\big(H(X) - H(X_0)\big) \geq 0, \tag{28}$$

and the condition (H2) ensures that $F(Y) \leq \frac{\partial F(0)}{\partial Y} Y$ for all $Y > 0$. Hence,

$$\frac{H(X_0)F(Y(t))}{(\mu+\sigma+\theta)} - Y \leq \left(\frac{H(X_0)\frac{\partial F(0)}{\partial Y}}{(\mu+\sigma+\theta)} - 1\right)Y = \big(R_0 - 1\big)Y. \tag{29}$$

Therefore, $R_0 < 1$ ensures that $\frac{\mathrm{d}V_2}{\mathrm{d}t} \leq 0$ for all $X(t), Y(t) \geq 0$. Hence, again from corollary 5.2 of Kuang (1993), we have that Q is stable.

Furthermore, also for $R_0 = 1$, $\frac{\mathrm{d}V_2}{\mathrm{d}t} = 0$ implies that $X(t) = X_0$. Hence, it can be shown that $Q(X_0, 0)$ is the largest invariant set in $\{(X(t), Y(t)) | \dot{V}_2 = 0\}$. With the help of the classical Lyapunov–LaSalle invariance principle (Hale and Verduyn Lunel 1993; Sastry 1999), Q is globally stable.

This completes the proof of Theorem 7.

Undelayed system

In this section, we consider the case of instantaneous transmission of primary infection. We perform a qualitative analysis of system (5) without delay, i.e., we set $\tau = 0$. This analysis has interest in itself and will also allow getting some information on the stability of coexistence equilibrium in the case with delay.

It is useful to investigate the stability properties of system (5), without delay, near the criticality (that is, at Q and $R_0 = 1$). To this aim, we use the bifurcation theory approach developed in Buonomo and Cerasuolo (2015), which is based on the center manifold theory (Sastry 1999). In particular, we are interested to assess if there is a stable coexistence equilibrium bifurcation form Q, and Q changes from being stable to unstable. This behavior is called forward bifurcation (Buonomo and Cerasuolo 2015).

Now, for the undelayed system, we propose the following result:

Theorem 8 *When $\tau = 0$, system (5) exhibits a forward bifurcation at Q and $R_0 = 1$.*

Proof Clearly, from the expression of R_0 it can be seen that R_0 is directly related to α. Subsequently, we choose α as the bifurcation parameter. Moreover, $R_0 = 0$ implies that $\alpha = \alpha^* = \frac{\mu(\mu+\sigma+\theta)}{A}$. Since the linearization technique is not applicable to check the stability behavior at $R_0 = 1$, so we use center manifold theory (Sastry 1999). For this, we redefined $X = x_1$ and $Y = x_2$, and then system (5) takes the form

$$\begin{aligned}\frac{\mathrm{d}x_1}{\mathrm{d}t} &= A - \mu x_1 - \frac{\alpha x_1 x_2(t)}{1+\beta x_2(t)} \equiv f_1, \\ \frac{\mathrm{d}x_2}{\mathrm{d}t} &= \frac{\alpha x_1 x_2(t)}{1+\beta x_2(t)} - (\mu+\sigma+\theta)x_2 - \frac{\omega x_2^2}{1+\varphi x_2^2} \equiv f_2.\end{aligned} \tag{30}$$

The Jacobian matrix J' of the model system (30) evaluated at $R_0 = 1$ and $\alpha = \alpha^*$ around the disease-free equilibrium is

$$J' = \begin{bmatrix} -\mu & -\frac{\alpha^* A}{\mu} \\ 0 & 0 \end{bmatrix}.$$

J' has a simple zero eigenvalue while the other eigenvalue is negative. The right eigenvector $w = \left[w_1, w_2\right]^{\mathrm{T}}$ of J' corresponding to zero eigenvalue can be obtained as given below:

$$w_1 = -\frac{\alpha^* A}{\mu^2}, \quad w_2 = 1$$

Similarly, the left eigenvector $u = \left[u_1, u_2\right]$ of J' corresponding to zero eigenvalue is obtained as $[0, 1]$. The nonzero partial derivatives associated with the functions f_1 and f_2 evaluated at $R_0 = 1$ and $\alpha = \alpha^*$ are

$$\left(\frac{\partial^2 f_2}{\partial x_1 \partial x_2}\right)_Q = \left(\frac{\partial^2 f_2}{\partial x_2 \partial x_1}\right)_Q = \alpha^*,$$
$$\left(\frac{\partial^2 f_2}{\partial x_2^2}\right)_Q = -\frac{2\beta\alpha^* A}{\mu} - 2\omega \text{ and } \left(\frac{\partial^2 f_2}{\partial x_2 \partial \alpha^*}\right)_Q = \frac{A}{\mu}.$$

Using Theorem 4.1 given in Castillo-Chavez and Song (2004), the coefficients a_1 and b_1 can be computed as

$$\begin{aligned} a_1 &= \sum_{k,i,j=1}^{2} u_k w_i w_j \left(\frac{\partial^2 f_k}{\partial x_i \partial x_j}\right)_Q \\ &= u_2\left(2w_1 w_2 \alpha^* - w_2^2\left(\frac{2\beta\alpha^* A}{\mu} + 2\omega\right)\right) \\ &= -\left(2\frac{\alpha^* A}{\mu^2}\alpha^* + \frac{2\beta\alpha^* A}{\mu} + 2\omega\right) < 0 \end{aligned}$$

and

$$\begin{aligned} b_1 &= \sum_{k,i=1}^{2} u_k w_i \left(\frac{\partial^2 f_k}{\partial x_i \partial \beta^*}\right)_Q \\ &= u_2\left(w_2 \frac{A}{\mu}\right) \\ &= \frac{A}{\mu} > 0. \end{aligned}$$

From the expressions of a_1 and b_1, it is evident that $a_1 < 0$ and $b_1 > 0$. Therefore, from Theorem 4.1 of Castillo-Chavez and Song (2004) bifurcation is forward. This completes the proof.

Theorem 9 *For $\tau = 0$, system (5) at Q^* is locally asymptotically stable if $M_1 + M_2 > 0$ and $N_1 + N_2 > 0$ are satisfied simultaneously.*

Proof At endemic equilibrium Q^*, the characteristic equation of system (5) is obtaining by putting $\tau = 0$ in (17) as given below:

$$\lambda^2 + M_1\lambda + N_1 + \left(M_2\lambda + N_2\right) = 0 \tag{31}$$

Clearly, if $M_1 + M_2 > 0$ and $N_1 + N_2 > 0$ are satisfied simultaneously, and then by Routh–Hurwitz Criterion (31) will always have roots with the negative real part, and hence, system (5) at Q^* for $\tau = 0$ is locally asymptotically stable.

Discussion

In this study, we have proposed and analyzed a novel SIR epidemic model along with nonlinear incidence rate, time delay (describing the incubation period) and Holling type III treatment rate. The analysis of the model has been discussed in terms of a threshold parameter R_0. The mathematical analysis has shown that DFE is locally asymptotically stable when $R_0 < 1$ and unstable when $R_0 > 1$ for time delay $\tau > 0$ which describes that disease can be eliminated from the community when $R_0 < 1$ and it will persist when $R_0 > 1$. Further, we have shown that the DFE at $R_0 = 1$ is linearly neutrally stable for time delay $\tau > 0$ which reveals that disease may persist at a very low level in society and exhibits a forward bifurcation for the time delay $\tau = 0$, i.e., there is a stable coexistence equilibrium Q^* bifurcating from Q, and Q changes from being stable to unstable. We have shown that EE is locally asymptotically stable under the conditions stated in Theorems 5 and 9 for $\tau > 0$ and $\tau = 0$, respectively. Furthermore, conditions for Hopf bifurcation have also been discussed. Moreover, it has also shown that both DFE and EE are globally asymptotically stable when $R_0 \leq 1$ and $R_0 > 1$ respectively.

Acknowledgements The authors acknowledged Delhi Technological University for providing the monetary help for this research. The authors thank the handling editor and anonymous reviewers for their careful reading of our manuscript and their insightful comments and suggestions.

Compliance with ethical standards

Conflict of interest The authors declare that they have no conflict of interest.

Appendix

1. The linearized matrix corresponding to the infection-free equilibrium $Q(\frac{A}{\mu}, 0)$ is

$$J_1 = \begin{pmatrix} -\mu & -\frac{\alpha A}{\mu}e^{-\lambda\tau} \\ 0 & \frac{\alpha A}{\mu}e^{-\lambda\tau} - (\mu+\sigma+\theta) \end{pmatrix}$$

2. The linearized matrix corresponding to the endemic equilibrium is

$$J_2 = \begin{pmatrix} -\mu - \frac{\alpha Y^*}{1+\beta Y^*} & -\frac{\alpha X^*}{(1+\beta Y^*)^2}e^{-\lambda\tau} \\ \frac{\alpha Y^*}{1+\beta Y^*} & \frac{\alpha X^*}{(1+\beta Y^*)^2}e^{-\lambda\tau} - (\mu+\sigma+\theta) - \frac{2\omega Y^*}{\left(1+\varphi Y^{*2}\right)^2} \end{pmatrix}$$

References

Buonomo B, Cerasuolo M (2015) The effect of time delay in plant-pathogen interactions with host demography. Math Biosci Eng 12(3):473–490

Capasso V, Serio G (1978) A generalization of the Kermack–McKendrick deterministic epidemic model. Math Biosci 42:43–61

Castillo-Chavez C, Song B (2004) Dynamical models of tuberculosis and their applications. Math Biosci Eng 1:361–404

Cui Q, Qiu Z, Liu W, Hu Z (2017) Complex dynamics of an SIR epidemic model with nonlinear saturated incidence rate and recovery rate. Entropy. https://doi.org/10.3390/e19070305

Dubey B, Patara A, Srivastava PK, Dubey US (2013) Modelling and analysis of a SEIR model with different types of nonlinear treatment rates. J Biol Syst 21(3):1350023

Dubey B, Dubey P, Dubey Uma S (2015) Dynamics of a SIR model with nonlinear incidence rate and treatment rate. Appl Appl Math 2(2):718–737

Dubey P, Dubey B, Dubey US (2016) An SIR model with nonlinear incidence rate and Holling type III treatment rate. Appl Anal Biol Phys Sci Springer Proc Math Stat 186:63–81

Goel K, Nilam (2019) A mathematical and numerical study of a SIR epidemic model with time delay. Nonlinear Incid Treat Rates Theory Biosci. https://doi.org/10.1007/s12064-019-00275-5

Gumel AB, Connell Mccluskey C, Watmough J (2006) An SVEIR model for assessing the potential impact of an imperfect anti-SARS vaccine. Math. Biosci. Eng. 3:485–494

Hale J, Verduyn Lunel SM (1993) Introduction to Functional Differential Equations. Springer, New York

Hattaf K, Yousfi N (2009) Mathematical model of influenza A (H1N1) infection. Adv Stud Biol 1(8):383–390

Hattaf K, Lashari AA, Louartassi Y, Yousfi N (2013) A delayed SIR epidemic model with general incidence rate. Electr J Qual Theory Differ Equ 3:1–9

Huang G, Takeuchi Y, Ma W, Wei D (2010) Global Stability for delay SIR and SEIR epidemic models with nonlinear incidence rate. Bull Math Biol 72:1192–1207

Kermack WO, McKendrick AG (1927) A contribution to the mathematical theory of Epidemics. Proc R Soc Lond A 115(772):700–721

Korobeinikov A, Maini PK (2005) Nonlinear incidence and stability of infectious disease models. Math. Med. Biol. 22:113–128

Kuang Y (1993) Delay differential equations with applications in population dynamics. Academic Press, San Diego

Kumar A, Nilam (2018) Stability of a time delayed SIR epidemic model along with nonlinear incidence rate and Holling type II treatment rate. Int J Comput Methods 15(6):1850055

Kumar A, Nilam (2019a) Dynamical model of epidemic along with time delay; Holling type II incidence rate and Monod–Haldane treatment rate. Differ Equ Dyn Syst 27(1–3):299–312

Kumar A, Nilam (2019b) Mathematical analysis of a delayed epidemic model with nonlinear incidence and treatment rates. J Eng Math 115(1):1–20

Kumar A, Nilam, Kishor R (2019) A short study of an SIR model with inclusion of an alert class, two explicit nonlinear incidence rates and saturated treatment rate. SeMA J 10:10. https://doi.org/10.1007/s40324-019-00189-8

Li M, Liu X (2014) An SIR epidemic model with time delay and general nonlinear incidence rate. Abstr Appl Anal 2014, Article ID 131257

Li Michael Y, Graef JR, Wang L, Karsai J (1999) Global dynamics of a SEIR model with varying total population size. Math Biosci 160:191–213

Li GH, Zhang YH (2017) Dynamic behaviors of a modified SIR model in epidemic diseases using nonlinear incidence rate and recovery rates. PLoS ONE 12(4):e0175789

Liu WM, Levin SA, Iwasa Y (1986) Influence of nonlinear incidence rates upon the behavior of SIRS epidemiological models. J Math Biol 23(2):187–204

Naresh R, Tripathi A, Tchuenche JM, Sharma D (2009) Stability analysis of a time delayed SIR epidemic model with nonlinear incidence rate. Comput Math Appl 58:348–359

Ruan S, Wei J (2003) On the zeros of transcendental functions with applications to stability of delay differential equations with two. Dyn Contin Discrete Impuls Syst Ser A Math Anal 10:863–874

Sastry S (1999) Analysis, stability and control. Springer, New York

van den Driessche P, Watmough J (2002) Reproduction numbers and sub-threshold endemic equilibria for compartment models of disease transmission. Math Biosci 180:29–48

Wang WD (2002) Global behavior of an SEIRS epidemic model with time delays. Appl Math Lett 15:423–428

Wang W, Ruan S (2004) Bifurcation in an epidemic model with constant removal rates of the infectives. J Math Anal Appl 21:775–793

Xiao D, Ruan S (2007) Global analysis of an epidemic model with nonmonotone incidence rate. Math Biosci 208(2):419–429

Xu R, Ma Z (2009) Stability of a delayed SIRS epidemic model with a nonlinear incidence rate. Chaos Solut Fractals 41:2319–2325

Zhang Z, Suo S (2010) Qualitative analysis of an SIR epidemic model with saturated treatment rate. J Appl Math Comput 34:177–194

Zhou L, Fan M (2012) Dynamics of a SIR epidemic model with limited medical resources revisited. Nonlinear Anal RWA 13:312–324

Publisher's Note Springer Nature remains neutral with regard to jurisdictional claims in published maps and institutional affiliations.

Adaptive Sitting Plan Algorithm Based On Henon Chaotic Map

Ashish Kumar, N S Raghava

Abstract: Examinations are an essential part of colleges, universities and academic institutes, where students go through many stages of evaluation scheme for better assessment. An organized structure of an exam hall with a proper sitting arrangement of students leads the implementation process of examination. A fraudulent behaviour such as cheating in examinations can hamper the efforts of many students; it is the Machiavellian behaviour of students which is being increased with technology and the rapid growth of the internet. In this paper, we have designed two algorithms, the first algorithm generates automatic sitting arrangement plan for examination halls to prevent mismanagement, prohibited material, and cheating during examinations and the second algorithm deals with Henon chaotic map to rescheduled the sitting plan. It is based on the sitting allocation methodology to generate random allocation in classrooms for every exam to prevent cheating from their surrounding locations. To preserve academic integrity, it is required to decrease the possibility of cheating in the examination hall. Maximum utilization of classrooms and less human resources are the main objectives of the proposed algorithms. Proposed work has been applied to university, and it gives a better environment during examination with the less human resource in a less executable time rather than a manual sitting plan allocation methods.

Index Terms: Allocation, cheating, classrooms, examination, Henon chaotic map, management, sitting arrangement.

1 Introduction

Exams are the critical phase in every academic institute, and it also takes place in a competitive exam where many students enrolled themselves to get a job or admission [1] [2], and it is conducted at immense scale. In order to write exams in the given time frame, it is necessary to adjust the students in the classroom along with efficient management. To conduct an examination, the exam controller takes in charge of all the responsibilities which are related to exams [3]. Arrangements of desks in a classroom most often are fixed, and it cannot be transferred from the place, which leads to an administrator or exam controller for the students have to take concrete steps to the seating arrangement of seats in each classroom. Before the examination, the sitting plan of every classroom is generated and is also shared with students. When the student finds the right place for his sitting according to the sitting plan, then for each exam, the student has to sit in the same place that was already designated during the examination. Invigilators are sent by the authority in classrooms to monitor students and also for conducting exams successfully. In a classroom, during the examination, its corresponding attendance sheet is also essential to calculate a total number of present students and absentees to maintain records of student whether student has appeared or not in the examination. Exam sheets are collected in the end, and it also verified with the attendance sheet as shown in Fig. 1. Exam seating allocation algorithm is required to accommodate students in such a way that all the students of different discipline can write their exam efficiently without any interruptions [4] [5]. Many institutes do not use algorithms or techniques to generate seating allocation plan, it is based on some basic rules, number of students, size of classrooms, number of disciplines in the institute, time slots and types of examinations. A cooperative seating arrangement can trouble the invigilators, and there are more chances for students to copy content from their neighbor's exam sheet. Generally, in many institutes, Seats are allocated to students in a traditional approach with some facile rules, which increases the cost and time to get a feasible solution. There are possibilities of error in manual approach which are like, few seats are left empty, overlapping of seats between students, no seat is allocated to student, and there is also the fear that two adjacent students are writing the same paper. Having said that, question papers are distributed to students and increases the sore difficulties of invigilators and makes a complex system. Positive academic behaviour is developed with a proper sitting plan during the examination and even in classrooms during theory lectures to maintain discipline [6]. In this paper, we have designed two algorithms to preserve academic integrity; the first algorithm generates automatic sitting arrangement plan for examination halls to prevent prohibited material and cheating during examinations. The second algorithm deals with Henon chaotic map; It is associated with the sitting plan to generate random allocation in classrooms for every exam to prevent cheating from their surrounding locations. To conduct the examination in the institute, sitting plan along with its corresponding attendance for better monitoring is required. Cheating is common phenomena in human nature, which is also replicated in academic because of a few students. Cheating can be done in various ways which are mentioned below:

- To answer the questions given in the exam, copying content from the adjacent student's answer sheet from the same discipline in the examination hall.
- Cheating is also done through state-of-the-art technology.
- Once a student knows his sitting position in the examination hall, then there is a possibility that for the next upcoming exam, a student may write answers or text on the desk, and may hide exams related content.

- ***Ashish Kumar*** *is currently pursuing Ph.D. degree program in Department of Information Technology, Delhi Technological university, Delhi, India 110042 E-mail: ashishkumar@dtu.ac.in*
- ***N.S. Raghava*** *is working as a Professor in Electronics and Communication Engineering Department at Delhi Technological University. His area of specialization is Antenna and Propagation, Cloud Computing, Information Security, Microwave Engineering. E-mail: nsraghava@dce.ac.in*

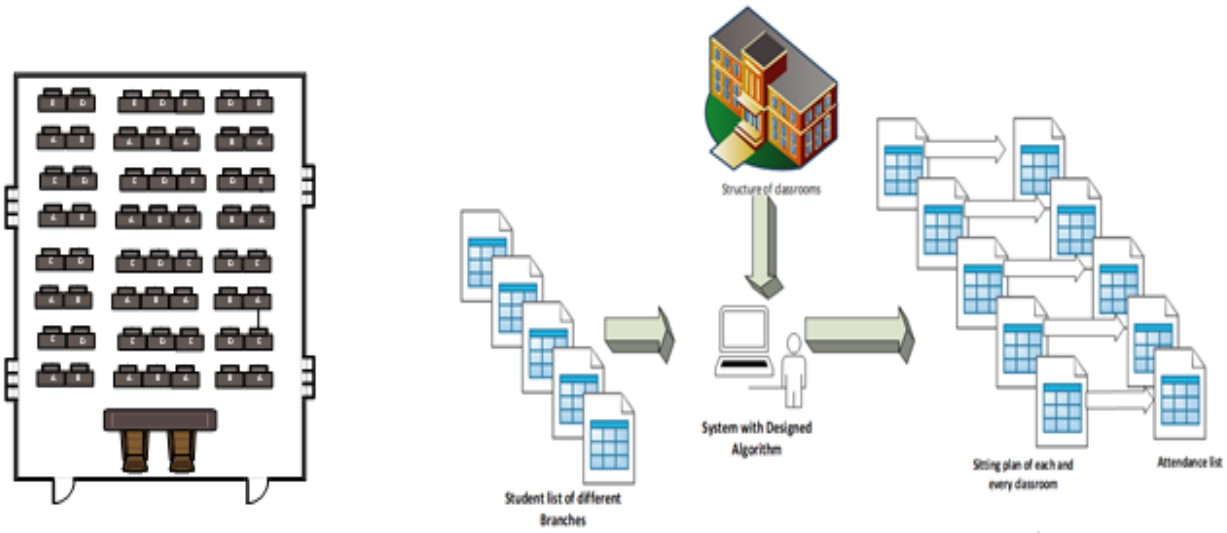

(a) Classroom plan of distribution *(b) comprehensive procedure*

Figure. 1. *Architecture of sitting plan algorithm*

2 PROPOSED ALGORITHM

In many institutes, sitting allocation plan is designed by members of exam cell or by the exam controller, and it is required to have a large number of human resources to create an environment to generate a proper sitting plan. Many meetings of faculties with board members are placed before the examination to facilitate students for a proper atmosphere to write their exams. In order to reduce the enormous load, this paper introduces two algorithms. Student database is considered as input for the proposed algorithms. The first algorithm deals with the allocation of seats in classrooms with detailed attendance sheet of students of every classroom whereas the second algorithm is designed to generate a random sitting plan to prevent unethical things during the examination. Figure. 1.(a) Demonstrates the proposed algorithm, where different discipline participates in the examination process.

2.1 Adaptive Sitting Allocation Algorithm

The education system also has an essential contribution to the economic growth of any country and education system is assessed by the educational environment and knowledge of the student. To do this, an examination is required for better assessment, through this, the foundation of the students' future is laid. Various disciplines of institute participate in examination process simultaneously. At the initial stage, a number of registered students who are going to appear in exam are identified and count number of students in each discipline. The second input for this algorithm is based on classrooms, where two parameters are taken: size of classroom and number of classrooms. The size of the examination hall defines how many students can be accommodated for the examination. Generally, examination halls consist of tables which are arranged in a row-column fashion. Maximum Utilization of examination halls is one of the primary objectives of the proposed algorithm.

Step (1): Initially, student list is prepared by system and roll numbers are extracted and are stored in an array. It is also dependent on the number of disciplines n. It is also found by the system administrator that in which column roll numbers of students are written in the file. The number of students in every discipline may be the same or may not be the same, so column size is taken maximum in the account for the driven approach.

TABLE I. PSEUDO CODE OF STEP (1)

```
1. for i ← 1 to n do
2. filename ← file(i).xlsx
3. [num, text(i)] ← xlsread (filename, size)
4. extracted only roll numbers from the list by specified that
   column
5. m(i) ← size(text(i));
6. end for
```

Step (2): Roll numbers of each branch are stored in a separate list, and the number of students of different discipline is counted. For maximum utilization of classrooms or examination halls, student data lists are equally divided into four parts. An administrator finalizes four different lists with the manual and automatic approaches. Therefore, the creation of these four list entirely depends upon the examination controller. In two ways allotment can proceed further. A total number of students are counted by using the following equation.

$$M = \sum_{i=1}^{n} m_{(i)} \qquad (1)$$

Where M represents a total number of students in the institute.

a) Automatically System Generated List

In this approach, the system works itself to divide the total number of students list into four equal parts, and processed lists are further used as input for step 3.

TABLE II: PSEUDO CODE OF STEP 2.(A)

```
total = 0
text = emptylist
for  i = 1: n do
text←text+text(i)
total←total+m(i)
end for
d←total/4;
rem←total%4
list1 = text(1 : d)
list2 = text(d + 1 : 2d)
list3 = text(2d + 1 : 3d)
list4 = text(3d + 1 : 4d + rem)
```

b) Manual Approach to Generate a List

In this approach, lists are prepared by a member of the examination cell. Manually, we have taken four lists to allocate student in examination halls. Various disciplines enrolled and wrote their exams. So, it is considered that students of the same discipline can be found at a nearby location. For example, A, B, C, D, E, F, G are different discipline, and the lists are created in such a way that there is not much difference in size of the list or ideally the number of students in the list should be equal.

$$list1 = A + G$$
$$list2 = B + H$$
$$list3 = C + E$$
$$list4 = D$$

Step (3): Classroom's structure is constructed in a row, column fashion. In which, the position of desks is fixed, and it is assumed that table or desk will not be moved from one classroom to another classroom. The classroom is taken as a matrix, and it is also found that how many classes have the same number of columns, those classes are put together in which the number of columns are same and treated as a single classroom. Let us consider, the class1 dimension is M1 × N and class2 dimension is M2 × N, then these two classrooms can be merge and can be treated as a single classroom having the strength to accommodate student will be (M1 × M2) × N. same is followed with other classrooms.

Step (4): In this section, step3 is repeated until all the classrooms of the institute are covered. Sitting plan which is generated by step 3., divided into a separate and individual sitting plan for every classroom. Attendance lists of classrooms are also generated itself by the proposed algorithm on the basis of sitting plan.

TABLE III. PSEUDO CODE FOR STEP (3)

```
Initialize: ptr1=1, ptr2=1, ptr3=1, ptr4=1
for i←1: total number of rows
   for j ←1: N
      if (i and j both variables are not divisible by 2)
            if (ptr1<= size of list1)
            c (i, j) ← list1(ptr1,1)
            ptr1=ptr1+1;
            else
               c (i, j) ← seat is empty
            end

      else if (i is not divisible by 2 and j is divisible by 2)
             if (ptr2<= size of list2)
            c (i, j) ← list2(ptr2,1)
            ptr2=ptr2+1;
            else
               c (i, j) ← seat is empty
            end

       else if (i is divisible by 2 and j is not divisible 2)
                   if (ptr3<= size of list1)
            c (i, j) ← list3(ptr3,1)
            ptr1=ptr3+1;
            else
               c (i, j) ← seat is empty
            end
       else (i and j are divisible by 2)
            if (ptr4<= size of list4)
            c (i, j) ← list4(ptr4,1)
            ptr4=ptr4+1;
            else
               c (i, j) ← seat is empty
            end
      end
   end
end
```

(a)Content on Wall

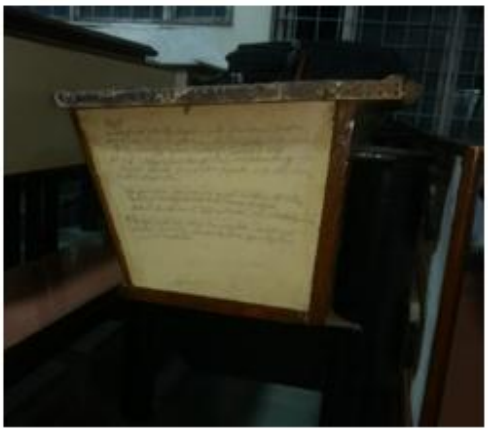

(b) Content on Desk

Figure 3. Prohibited text content on desk and wall

2.2 Random sitting allocation using Henon chaotic map

Henon chaotic map is introduced in sitting allocation methodology to provide a random sitting allocation for every examination hall. Sometimes students write the relevant content of the next exam on a desk or table and enclosure walls as shown in Fig. 3., it helps them to copy content from the table or desk to their answer sheets. One more way that once a student knows his location as per sitting plan, a student may hide notes or book near to their surrounding location. Subsequently, for a legitimate reason, student come out from examination hall. Meanwhile, student receives answers from the hidden material. Chaotic maps are widely used in various field of science; therefore, different chaotic maps are also associated with chaos theory. Chaotic maps are mainly used to generate pseudo-random numbers and can be used as per the requirement of research [7].

Step (1): Henon chaotic map [8][9] was discovered in 1978, and mostly, it is used as a pseudo-random number generator in security systems. Two dimensional discrete-time nonlinear dynamical Henon chaotic map generates a pseudo-random binary sequence which has been described as below in (2).

$$Xn+1 = 1+Yn - aXn$$
$$Yn+1 = bXn \qquad n=0, 1, 2\ldots \qquad (2)$$

Here, the parameters, a and b are of prime importance as the dynamic behaviour of the system depends on these values.

The system cannot be chaotic unless the value of a and b are 1.4 and 0.3 respectively.

Step (2): In adaptive sitting allocation algorithm, four lists were generated in two ways. Here, the size of each list is taken for further approach. This sequence is converted into [1, size(list)] using modular arithmetic as shown in Fig. 4.

TABLE IV. PSEUDO CODE FOR STEP(2).

while until all the list are covered do

$X \in \{-I, I\}$ Where I is an integer

$New_X \leftarrow floorsizeoflist(i) \times X$

$New_X \leftarrow mod(New_X, size\ of\ list(i))$

- Remove all duplicate numbers from and replaced by those numbers which are having zero frequency.
- Remove duplicate numbers from the sequence $New_X[\ ]$and replace by those numbers which are having 0 frequency count in sequence list as shown in fig. 4.

end while

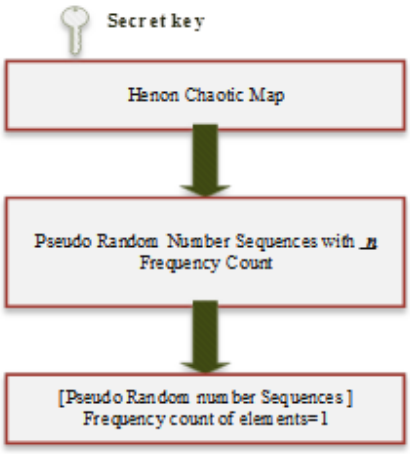

Figure 4. Pseudo-random numbers generation using Henon chaotic map

TABLE V. ATTENDANCE SHEET FOR THE CLASSROOM A

ATTENDANCE SHEET ROOM NO: HALL-01											
CO	**BOOKLET NO.**	**SIGNATURE**	**ME**	**BOOK. NO.**	**SIGNATURE**	**EE**	**BOOK. NO.**	**SIGNATURE**	**EC**	**BOOKLET NO.**	**SIGNATURE**
CO/01			ME/01			EE/01			EC/01		
CO/02			ME/02			EE/02			EC/02		
CO/03			ME/03			EE/03			EC/03		
C0/04			ME/04			EE/04			EC/04		
CO/05			ME/05			EE/05			EC/05		
CO/06			ME/06			EE/06			EC/06		
CO/07			ME/07			EE/07			EC/07		
CO/08			ME/08			EE/08			EC/08		
CO/09			ME/09			EE/09			EC/09		
CO/10			ME/10								
CO/11			ME/11								
CO/12			ME/12								

TABLE VI. SITTING PLAN FOR CLASSROOM A

ROOM NO. HALL -01							
CO/01	EE/01	CO/02	EE/02	CO/03	EE/03		CO/04
ME/01	EC/01	ME/02	EC/02	ME/03	EC/03		ME/04
CO/05	EE/04	CO/06	EE/05	CO/07	EE/06		CO/08
ME/05	EC/04	ME/06	EC/05	ME/07	EC/06		ME/08
CO/09	EE/07	CO/10	EE/08	CO/11	EE/09		CO/12
ME/09	EC/07	ME/11	EC/08	ME/11	EC/09		ME/12
CO/01- CO/12 =12				**ME/01-ME/12=12**			
EE/01 -EE/09= 09				**EC/01- EC/09=09**			
TOTAL= 42							

Step (3): Now, the Random sequence is used to shuffle the roll numbers of a student's list; pseudo-random sequence is used to rearrange the list by its indexing position with new index position using the Newx [ ] matrix. Later this shuffled list is utilized to regenerate the new sitting plan.

3 Experimental Results and Discussion

Sitting plan is prepared by locating the number of students in the examination hall. Generally, when the individuals of the institutes do this work, it takes a lot of time and resources. In order to reduce the complexity of the system and prevent unethical practices, this paper helps in many ways. Proposed algorithm gives impressive results, and when the algorithm is implemented and tested, the drawbacks that were found in the traditional approaches seem to be moved away through this proposed algorithm. In this section, experimental results of the proposed algorithm are given to appreciate the efficiency of the proposed security system. MATLAB 7.9 software with 8 GB ram is used for implementation of proposed algorithm along with the use of Microsoft excel worksheet for reading and writing operations. The proposed algorithm generates table V and Table VI and it shows that the proposed algorithm works appropriately without any overlapping or underlapping problem and also reduce the cost of the prior implemented system. Henon chaotic map plays an important role to generate a new sitting plan for every exam, which helps institute to prevent cheating and misconduct of students.

4 Conclusion and Future Work

Cheating is a common practice among students, and their human behaviour brings it. Academic Institute cannot stop the trend of imitating the students completely, but by creating an improved environment, the ideal education system can be prepared. Sitting plan gives proper management for conducting the examination process. A system with MATLAB and Microsoft excel worksheet is enough to generate a sitting plan; it takes a few seconds instead of taking several weeks. The education system is the backbone of any country, and many academic institutions are working to make it strong towards this direction. If a healthy examination process is governed by an institute, then by the results obtained, many steps can be taken to improve the education system, and this is only possible by the cooperation of teachers and students. Institute for upcoming exams can train those students who could not get a good result in an examination. The Henon chaotic map has been used to generate a random sittings plan to prevent cheating during the examination; it helps invigilators and also students for better assessment. It is possible in upcoming that how this input could be taken automatically by the system itself for the maximum utilization of examination halls.

References

[1] Clark, B.R.: The Higher Education System: Academic Organization in Cross-national Perspective. Univ of California Press, (1986).

[2] Mizruchi, M.S.: Who controls whom? an examination of the relation between management and boards of directors in large american corporations. Academy of Management review 8(3), 426–435 (1983).

[3] Klemm, W.: Use and mis-use of technology for online, asynchronous, collaborative learning. Computer-supported collaborative learning in higher education, 172–200 (2005).

[4] Burke, E.K., Elliman, D., Weare, R.: A genetic algorithm based university timetabling system. In: Proceedings of the 2nd East-west International Conference on Computer Technologies in Education, vol. 1, pp. 35–40 (1994)

[5] Hill, K.T., Wigfield, A.: Test anxiety: A major educational problem and what can be done about it. The Elementary School Journal 85(1), 105–126 (1984).

[6] Biggs, J.B.: Teaching for Quality Learning at University: What the Student Does. McGraw-Hill Education (UK), (2011).

[7] Petrisor, E.: Entry and exit sets in the dynamics of area preserving Henon map. Chaos, Solitons & Fractals 17(4), 651–658 (2003).

[8] Guo-hui, L., Shi-ping, Z., De-ming, X., Jian-wen, L.: An intermittent linear feedback method for controlling he´ non-like attractor. Journal of Applied Sciences, 288–290 (2001).

[9] Raghava, N. S., and Ashish Kumar. "Aishwarya Deep and Abhilasha Chahal,"." Improved LSB method for Image Steganography using Henon Chaotic Map", open journal of information security and applications 1.1 (2014).

ResearchGate

See discussions, stats, and author profiles for this publication at: https://www.researchgate.net/publication/335758414

AN EFFECT OF ANKLE FOOT ORTHOSIS ON THE MUSCLE ACTIVITY OF DROP FOOT PATIENT: A CASE STUDY

Article · September 2019

CITATIONS
0

READS
36

4 authors:

Faisal Hasan
Aligarh Muslim University
61 PUBLICATIONS **208** CITATIONS
SEE PROFILE

Qasim Murtaza
Delhi Technological University
57 PUBLICATIONS **418** CITATIONS
SEE PROFILE

Siddharth Bhardwaj
Aligarh Muslim University
15 PUBLICATIONS **14** CITATIONS
SEE PROFILE

Falah Hasan Abdulsadah
Aligarh Muslim University
2 PUBLICATIONS **0** CITATIONS
SEE PROFILE

Some of the authors of this publication are also working on these related projects:

Project conjugate heat transfer within cavity View project

Project EMG based rehabilitation/prosthetic control View project

All content following this page was uploaded by Falah Hasan Abdulsadah on 12 September 2019.

The user has requested enhancement of the downloaded file.

International Journal of Mechanical and Production Engineering Research and Development (IJMPERD)
ISSN (P): 2249-6890; ISSN (E): 2249-8001
Vol. 9, Issue 3, Jun 2019, 1535-1540
© TJPRC Pvt. Ltd.

TRANS STELLAR
• Journal Publications • Research Consultancy

AN EFFECT OF ANKLE FOOT ORTHOSIS ON THE MUSCLE ACTIVITY OF DROP FOOT PATIENT: A CASE STUDY

FALAH HASANABDULSADAH[1], FAISAL HASAN[1], QASIM MURTAZA[2] & SIDDHARTH BHARDWAJ[1]

[1]*Department of Mechanical Engineering, Aligarh Muslim University, Aligarh, India*

[2]*Department of Mechanical Engineering, Delhi Technological University, Delhi, India*

ABSTRACT

This paper presents a case study for a drop foot patient, analyzing the muscle activation via electromyography (EMG)while using different types of ankle foot orthosis (AFO) and compare it with muscle activity of bare foot movement during stair climbing and gait. EMG activity in stair climbing and gait was recorded without and with wearing three types of AFO materials (Polypropylene (PP), carbon fiber composite material (CF), Polylactic Acid(PLA)) under different backpack load (0 Kg, 5 kg, 10 kg, 25 kg). EMG signals recorded from the two lower limb muscles (gastrocnemius and tibialis anterior) showed that amplitude of EMG increased with increasing load during stair climbing and gait. The Normalized EMG-RMS (NER) of both the muscle group was greater instair climbing compared to gait. NER of gastrocnemius was greater than tibialis anterior for both the task under the same load condition. While using PLA-AFO on drop foot lower limb, the NER of both the muscle was comparable to the NER value of normal limb in both the task. The study of muscle activation under different backpack load during stair climbing can be used to design orthoses device and interface with intelligent control based on EMG for human activities lower muscle.

KEYWORDS*: *Normalizing, Muscle Activation, Backpack Load, Electromyography (EMG) & Ankle Foot Orthoses (AFO)

Received: Apr 21, 2019; **Accepted**: May 11, 2019; **Published**: Jun 11, 2019; **Paper Id.**: IJMPERDJUN2019161

A CASE STUDY

INTRODUCTION

Walking and stair climbing are common tasks encountered in day to day living. Manifesting these tasks are highly dependent on the strength and functioning of lower limb [1], [2], [3], [4], [5]. Researchers have studied the effectsof step height [6], gait velocity [7], age [8] and staircase aberration on lower limb biomechanics [9]. Both endo and exo-orthosis have proven their efficacy in improving patient gait suffering from lower limb pathology. Studies have shown the positive changes in gait ability of patients with knee and hip implants [11], [12], amputees with artificial limbs [13] and athletes with anterior cruciate ligament deficiencies [14]. Study have also been conducted to show the effect of orthosis material on gait kinematics[10].

Drop foot is the abnormality in gait caused due to improper flexion of the ankle and is commonly occurred after stroke, spinal cord injury, or other nervous disorders. In drop foot, the patient is unable to lift the affected feet which results in dragging of ankle during the swing phase of the gait cycle. Various powered and non-powered ankle foot orthosis (AFO) are available which are used to treat the pathology and support the foot during swing phase. However the AFO are sometimes found uncomfortable to the patient and does not promote

muscle atrophy [15]. Hence it is important to study the muscle activation while using these AFOs.

Surface Electromyography (EMG) provides a non-invasive way to investigate the muscular effort in the form of summed action potentials. EMG have been used to provide both the insight into neuralcontrol strategies for different tasks in gait cycle [1], [16], [17] as well as, to indicate the knee joint loadings at the knee due to increased knee height [18].

In the present paper a case study has been presented for the muscle activity of gastrocnemius and tibialis anterior of the drop foot patient while using three different types of AFO with four different backpack loading conditions and compared it with the muscle activity of normal foot.

METHODOLOGY

A drop foot patient (age = 24 years, height = 160 cm and weight = 56 kg) was recruited for the case study through local advertisement. The patient suffered drop foot in right leg and have never used any orthotic aid to support the drop foot. The study was approved by the university ethics board and a written consent was taken from the subject after explaining the experimental task.

Ankle Foot Orthosis (AFO)

Three different types of AFO viz. Polypropylene (PP), carbon fiber composite (CF) and Polylactic Acid (PLA) were tested and compared with the bare foot condition during gait and stair climbing task. Figure 1shows the different AFO used for the study.

Figure 1: Ankle Foot Orthosis- (a) PP, (b) CF and (c) PLA

Design of Experiment

The experiment consisted of measuring the EMG activity of Gastrocnemius (GA) and Tibialis anterior (TA) of the right leg (affected with drop foot) during gait and stair climbing task with and without (bare foot) the AFOs. The two tasks were carried out at five different backpack load conditions viz. 0 kg (without backpack), 5 kg, 10 kg and 25 kg. Between each loading condition a time gap of 5 minutes was given to subside fatigue. The stair climb (rise = 180 mm, tread = 280 mm, width = 450 mm) consisted of climbing 6 stairs in a row without any hand support while, the gait task consisted of subject performing the gait at his normal pace for 2.5 meters (the distance was marked on the ground). In a separate trial the two tasks were conducted to record the muscle activity of GA and TA of patient's left leg (unaffected leg) in bare foot condition to allow comparison with the drop foot muscle activity while using different AFO and loading conditions.

EMG Instrumentation and Data Acquisition

EMG was measured with the aid of bipolar active EMG electrodes (SX230, Biometrics Ltd, UK). The electrodes were pre amplified with biometrics subject unit and base unit (Biometrics DLK 900). The EMG data was recorded at sampling frequency of 1000 Hz into the PC using Data LINK acquisition software. Reference electrode was attached to the lunate bone of the right wrist.

Procedure

First the participant was given introduction to the AFO and briefed about the experimental purpose. Skin preparation was done before placing the EMG sensors over the tested muscle groups as per the SENIAM standards. With each loading condition the subject was asked to carry the backpack on his shoulder and carry out the gait and stair climb task while the EMG data is continuously recorded in the PC. Figure 2shows the patient performing the two tasks. After recording the muscle activity of affected foot (drop foot) for the two task in different loading and AFO, trials were conducted to record the EMG activity of GA and TA of unaffected leg for different backpack loads in bare foot condition.

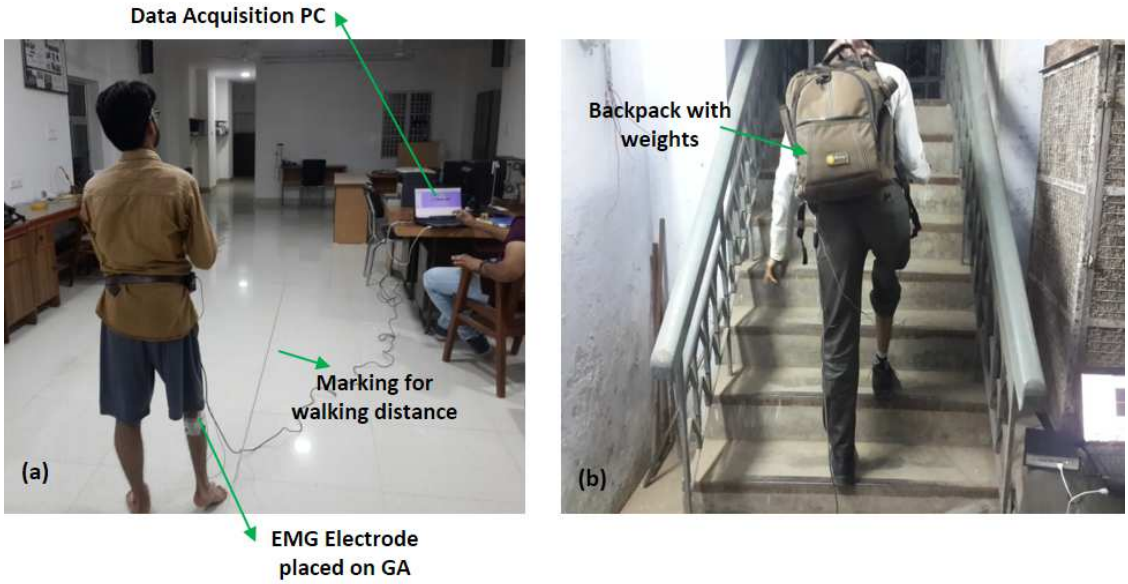

Figure 2: Patient Performing (a) Gait and (b) Stair Climb Task

Approach for the Analysis

After completion of the experimental trial, post processing of the EMG data was done with Data LINK PC software. Root mean square (RMS) of the EMG data were evaluated for successive time strap of 125 ms and then normalized using peak dynamic normalization method.

$$\text{nRMS} = \frac{(\text{RMS}_{\text{EMG}})_{\text{mean}} - (\text{RMS}_{\text{EMG}})_{\text{min}}}{(\text{RMS}_{\text{EMG}})_{\text{max}} - (\text{RMS}_{\text{EMG}})_{\text{min}}}, \quad (1)$$

Where, nRMS= Normalized RMS

$(\text{RMS}_{\text{EMG}})_{\text{mean}}$ = Mean EMG-RMS during the task.

$(\text{RMS}_{\text{EMG}})_{\text{min}}$ = Minimum EMG-RMS during task.

$(\text{RMS}_{\text{EMG}})_{\text{max}}$ = Maximum EMG-RMS during the task.

RESULTS

A sample result for the recorded EMG data and evaluated EMG-RMS for patient wearing CF AFO with 10 Kg load for gait and stair climbing task is shown in Figure 3. The results showed that muscle activation EMG amplitudes of both the muscles in the tasks increases with increasing backpack loads. The maximum EMG-RMS of GA was greater than TA for both the gait and stair climbing task for all the AFO tested as well as for bare foot. Figure 4 summarizes the normalized EMG-RMS (NER) for different experimental conditions.

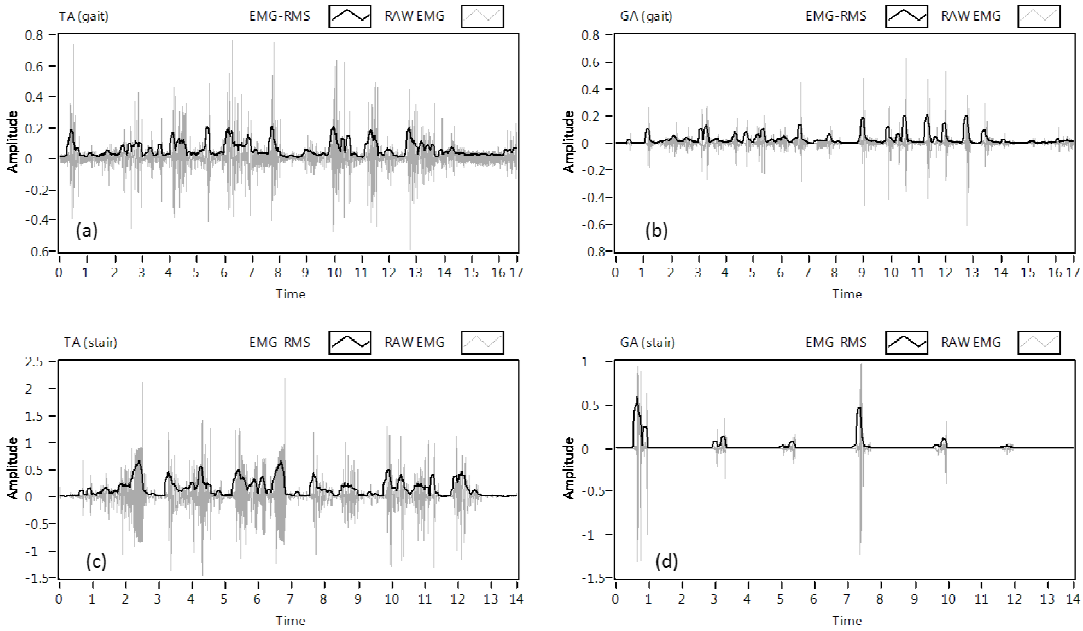

Figure 3: EMG-RMS Data for TA and GA During Gait(a, b) and Stair Climb (c,d) Respectively for Patient Wearing CF AFO and Backpack Load of 10 kg

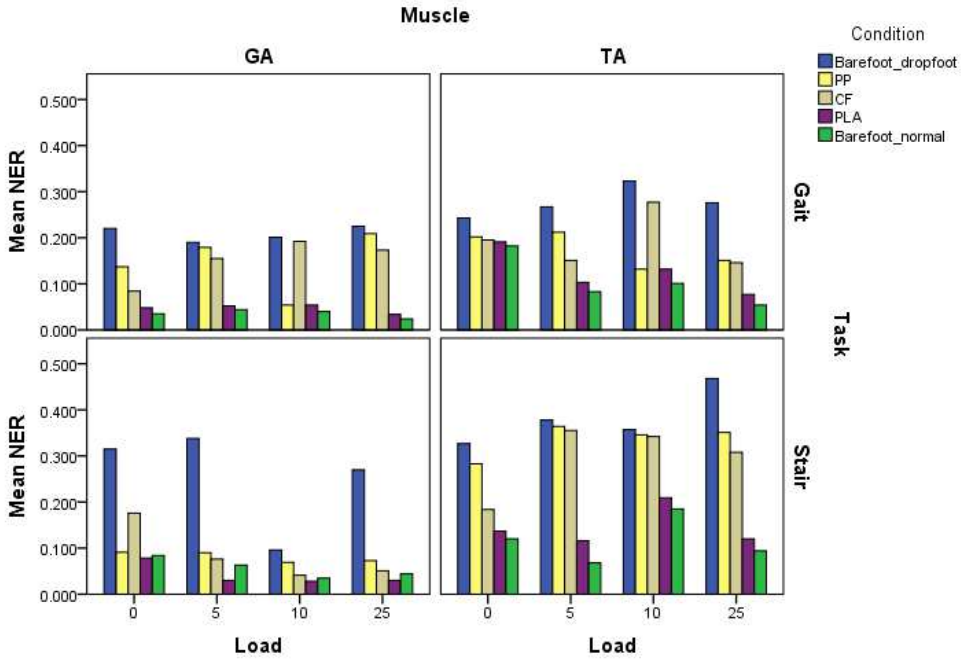

Figure 4: Normalized EMG RMS (NER) for the Tested Loads and AFOs

CONCLUSIONS

The Normalized EMG-RMS (NER) of both the muscle group was greater in stair climbing compared to gait. NER of gastrocnemius was greater than tibialis anterior for both the task under the same load condition. While using PLA-AFO on drop foot lower limb, the NER of both the muscle was comparable to the NER value of normal limb in both the task.

REFERENCES

1. *G., Graichen F., Rohlmann A.(1995) : Is staircase walking a risk for the fixation of hip implants. J, Biomech, [1] Andriacchi, T.P., Andersson, G.B.J., Fermier R.W., Stern, D., &Galante J.O.(1980) : A study of lower-limb mechanics during stairclimbing.J, Bone Joint Surg, 62, 749–757*
2. *Andriacchi T.P., Galante J.O., &Fermier R.W.(1982): The influence of total knee-replacement design on walking and stair climbing.J, Bone Joint Surg, 64, 1328–1335*
3. *Bergmann G., Graichen F., Rohlmann A.(1995) : Is staircase walking a risk for the fixation of hip implants. J, Biomech, 5, 535–553*
4. *Haightd.J., Lerner Z.F., Board W.J.(2014) : A comparison of slow, uphill and fast, level walking on lower extremity biomechanics and tibiofemoral joint loading in obeseand nonobese adults. J. Orthop. Res, 32(2), 324–330.*
5. *Townsend M.A., Lainhart S.P., Shiavi R. (1978) :Variability and biomechanics of synergy patterns of some lower-limb muscles during ascending and descending stairs and level walking. Med. Biol. Eng. Comput, 16, 681– 688*
6. *Spanjaard M., Reeves N.D., Van dieen J.H., Baltzopoulos V., Maganaries C.N.(2008) : Lower-limb biomechanics during stair descent. J. Exp. Biol, 211, 1368–1375*
7. *Spanjaard M., Reeves N.D., Van dieen J.H., Baltzopoulos V., Maganaries C.N. (2009) :Influence of gait velocity on gastronomies muscle fascicle behavior during stair negotiation, J. Electromyogr. Kinesiol, 19, 304–313*
8. *Nadeau S., Mcfadyen B.J., Malouin F.(2003) : Frontal and sagittal plane analyses of the stair climbing task in healthy adults aged over 40 years, Clin. Biomech, 18, 950–959*
9. *Riener R., Rabuffetti M., Frigo C.(2002) : Stair ascent and descent at different inclinations, Gait and Posture, 15, 32–44*
10. *AbdulsadahF.H, Murataza Q, Hasan F,Hussain K. M. (2018): Improvement in Gait Cycle with Ankle Foot Orthosis, HWWE 2018, Kerela, India.*
11. *Blazkiewicz M.(2013): Muscle force distribution during forward and backward locomotion, ActaBioeng. Biomech,15, 3–9*
12. *Costigan P.A., D Eluzio K.J., Wyss U.P.(2006): Knee and hip kinetics during normal stair climbing, Gait and Posture, 16, 31–37*
13. *Powers C.M., Boyd L.A., Torburn L. Perry J. (1997): Stair ambulation in persons with transtibial amputation, J. Rehabil. Res. Dev, 34, 9–18*
14. *Kowalk D.L., Duncan J.A. Mccue F.C., Vaughan C.L.(1997) : Anterior cruciate ligament reconstruction and joint dynamics during stair climbing, Med. Sci. Sports Exerc, 29, 1406–1413*
15. *Hoque, L., Kamal, S. M., & Ahmed, Z. (2013). Isolation, identification and antimicrobial sensitivity pattern of bacterial isolates from tracheal aspirate of ICU patients of central Dhaka, Bandladesh. Int j res appl nat soc sci, 1(7), 11-6.*

16. *Hesse S., Werner C., Matthias K., Stephen K., Berteanu M. (1999): Non-velocity-related effects of a rigid double-stopped ankle–foot orthosis on gait and lower limb muscle activity of hemiparetic subjects with an equinovarus deformity, Stroke, 30, 1855–1861.*

17. *Silder A., Besier T., Delp S.L.(2012) : Predicting the metabolic cost of incline walking from muscle activity and walking mechanics, J. Biomech, 45, 1842–1849*

18. *Sutherland D.H.(2001) : The evolution of clinical gait analysis, Kinesiological EMG, Gait and Posture, 14, 61–70*

19. *Barkema D.D., Derrick T.R., Martin P.E.(2012) : Heel height affects lower extremity frontal plane joint moments during walking, Gait Posture, 35, 483–488*

View publication stats

EPMA Journal
https://doi.org/10.1007/s13167-019-00185-y

RESEARCH

An examination of colorectal cancer burden by socioeconomic status: evidence from GLOBOCAN 2018

Rajesh Sharma [1]

Received: 4 May 2019 / Accepted: 14 August 2019
© European Association for Predictive, Preventive and Personalised Medicine (EPMA) 2019

Abstract

Aim and background Colon and rectum (colorectal) cancer cause substantial mortality and morbidity worldwide. The management and control of a complex disease such as cancer cannot rely on the old strategy of "one disease one medicine" and must make a transition into new-age practices involving predictive, preventive, and personalized medicine (PPPM) at its core. Adoption of PPPM approach to cancer management at the policy level requires quantification of cancer burden at the country level. For this purpose, we examine the burden of colorectal cancer in 185 countries in 2018. Based on results, we discuss the opportunities presented by PPPM and challenges to be encountered while adopting PPPM for the treatment and prevention of colorectal cancer.

Data and methods Age- and sex-wise estimates of colorectal cancer were procured from the GLOBOCAN 2018. The country- and region-wise burden of colorectal cancer in 185 countries was examined using all-age and age-standardized incidence and mortality estimates. Human development index (HDI) was employed as the indicator of socioeconomic status of a country. Mortality-to-incidence ratio (MIR) was employed as the proxy of 5-year survival rate.

Results Globally, colorectal cancer claimed an estimated 880,792 lives (males 484,224; females 396,568) with 1.85 million new cases (males 1.03 million; females 823,303) were estimated to be diagnosed in 2018. Globally, the age-standardized incidence rate (ASIR) was 19.7/100,000, whereas age-standardized mortality rate (ASMR) recorded to be 16.3/100,000 in 2018. Age-standardized rates were the highest in developed countries led by Hungary with ASIR of 51.2/100,000 followed by South Korea with ASIR of 44.5/100,000. ASMR followed the patterns of ASIR with the highest ASMR recorded by Hungary (21.5 per 100,000) and Slovakia (20.4 per 100,000). Globally, MIR stood at 0.48, and among the countries recording more than 1000 cases, Nepal registered the highest MIR of 0.83 and the lowest was recorded by South Korea (0.27). The age-standardized rates exhibited nonlinear association with HDI, whereas MIR was negatively associated with HDI.

Conclusion Colorectal cancer causes a substantial burden worldwide and exhibit a positive association with the socioeconomic status. With the aid of improving screening modalities, preventable nature of the disease (due to dietary and lifestyle risk factors) and improving treatment procedures, the burden of CRC can largely be curtailed. The high burden of CRC in developing countries, therefore, calls for effective prevention strategies, cost-effective screening, and early-stage detection, cost-effective predictive, and personalized treatment regime.

Keywords Colorectal Cancer · Incidence · Mortality · Predictive preventive personalized medicine · Precision medicine · GLOBOCAN

Introduction

Globally, the burden of communicable diseases has been falling, and mortality and morbidity due to noncommunicable diseases have been rising since the last three decades [1]. The burden of communicable diseases has been proved to be amenable to interventions such as vaccination, public hygiene, and improvement in basic healthcare infrastructure. This, however, is not true for noncommunicable diseases such as cancer which lack an easy solution as a vaccine to treat every kind of neoplasia. Colorectal cancer (CRC) is one of the amenable causes of death and also has been one of the leading cancer groups causing substantial mortality and morbidity worldwide [1, 2]. CRC was previously considered to be a

✉ Rajesh Sharma
rajesh.sharma@dtu.ac.in

[1] University School of Management and Entrepreneurship, Delhi Technological University, Vivek Vihar- Phase II, Delhi 110095, India

Published online: 11 September 2019

disease of affluence, but as the countries are climbing up the development hierarchy, its burden has risen sharply in developing countries exemplified by surges in countries such as Japan, Singapore and China [3]. Although the CRC burden has been the greatest in developed countries and rising in developing ones, survival rates, which depend crucially upon the stage of diagnosis, are significantly different in countries with different socioeconomic level [4]. The heterogeneous patterns of incidence, mortality, and survival implicate a gap in cancer detection and treatment in countries as per their socioeconomic status.

The majority of colorectal neoplasia are adenocarcinomas originating from epithelial cells of the colorectal mucosa; other rare types include neuroendocrine, squamous cell, adenosquamous, spindle cell, and undifferentiated carcinomas [5]. Around 80–90% of newly diagnosed cases are sporadic with slow growth from adenomatous polyps to adenoma to adenocarcinoma while the rest (10–20%) is related to familial histories such as familial adenomatous polyposis (FAP) and hereditary nonpolyposis (HNPCC) [6]. The slow march of cancer from polyps to frank carcinoma can be arrested by employing screening methods such as stool-based procedures (e.g., fecal occult blood test and fecal immunochemical test) and structural examinations (e.g., colonoscopy, flexible sigmoidoscopy), thereby resulting in improved survival and low mortality rates [7].

Tackling the burden of a disease as complex as cancer requires new-age strategies such as predictive, preventive, and personalized medicine (PPPM) which is aiming to shift the focus of cancer therapeutics from reactive to a preventive and predictive one to provide individualized treatment paradigms to cancer patients [8–10]. In cancer management, this approach seeks to separate a healthy person from a patient, low-risk individual from the at-risk population, and a low-grade tumor from a high-grade tumor to offer precise and personalized medicine [8]. To devise proper cancer policy and implement PPPM strategies at the patient or provider level, it is pertinent to examine the recent estimates of the burden of cancer-in-question (CRC here) at the macro-level.

In this study, we examined the CRC burden using estimates from GLOBOCAN 2018 which produced country-, age-, and sex-wise estimates of the incidence, mortality, and prevalence of colorectal carcinoma in 185 countries for the year 2018 [11]. The socioeconomic status of a nation was gauged using country-level human development index (HDI)—a summary indicator of income, education, and longevity [12]. Five-year survival rate due to CRC was proxied using mortality-to-incidence ratio (MIR) which has been employed as the proxy of survival rates before [13–16]. An examination of CRC burden is expected to aid policy making and devise appropriate policy interventions to tackle a public health threat that is growing but is also amenable to prevention and early detection.

Data and methods

We procured the estimates of CRC burden from GLOBOCAN 2018, which provided age-, sex-, and country-wise incidence, mortality, and prevalence estimates of 36 neoplasia for 185 countries for the year 2018 [11, 17]. GLOBOCAN 2018 provided incidence and mortality estimates for each cancer group for 21 regions defined by United Nations Population Division (UNPD) in 18 nonoverlapping age groups (0–4, 5–9, 10–14, 15–19, 20–24, 25–29, 30–34, 35–39, 40–44, 45–49, 50–54, 55–59, 60–64, 65–69, 70–74, 75–79, 80–84, and > 85 years). The complete GLOBOCAN 2018 estimation framework and calculation of various population health metrics are detailed elsewhere [11, 17]. The full set of GLOBOCAN 2018 results is available in the Global Cancer Observatory (http://gco.iarc.fr [18]). We procured data of CRC encoded as C18-C21 (colon, rectum, and anus) as per International Classification of Diseases tenth revision (ICD-10). In this study, we examine the CRC burden in terms of all-age incidence and mortality along with age-standardized rates expressed in terms of 100,000 person-years. The age-standardized incidence rate (ASIR) of a country was calculated using following formula.

$$ASIR_i = \sum_j \frac{C_{ij} * P_{ij} * w_j}{TP_i} \quad (1)$$

In the above equation, i indexes the country and j indexes the age group. C_{ij} denotes number of cases in jth age group in ith country, P_{ij} denotes population in ith country in jth age group, TP_i denotes total population of ith country and w_j is the weight of jth age group ascribed by world population reference standard. The age-standardized mortality rate (ASMR) for different countries was calculated similarly by replacing number of cases (C_{ij}) by number of deaths (D_{ij}) in equation 1.

The 5-year survival rate of CRC was proxied using mortality-to-incidence ratio (MIR), which was calculated as the ratio of all-age death counts to all-age incident cases. MIR has been previously employed as a proxy for 5-year survival rate in the case of different neoplasia [13–16]. While we report estimates for all 185 countries, we focus primarily on the heavily burdened countries and regions. In addition to examining the country-wise burden of colorectal carcinoma, we also examined its relationship with a country's socioeconomic status measured using its human development index (HDI) [12, 19]. HDI, an indicator of human development constructed by United N ations Development Program (UNDP), is a summary index of three indicators: health (life expectancy at birth), education (mean years of schooling and expected number of years of schooling)[1],

[1] UNDP defines mean number of years of schooling as the number of years of schooling received by people ages 25 and older, and expected years of schooling s defined as number of years of schooling that a child of school entrance age can expect to receive if prevailing patterns of age-specific enrolment rates persist throughout life [12].

and income (gross national income (GNI) per capita)[12]. Country-specific value for each of the indicators was rescaled by UNDP on 0 to 1 scale with 0 corresponding to the lowest value and 1 to the highest reported value of the variable and the final HDI of a country is calculated as the geometric mean of the three indicators [12] using the following equation:

$$HDI = \sqrt[3]{II * EI * HI} \quad (2)$$

In the above equation, II is the income index, EI denotes the education index, and HI denotes the health index. As GLOBOCAN estimates were available for the year 2018, and HDI data was available for 2017, we extrapolated the values of HDI for the year 2018 using the country-specific HDI values in the years 2016 and 2017. It was done to make the HDI values consistent with the values of CRC burden in the year 2018. Data analysis was conducted using Python 3.6, MS Excel 2016, and Stata 13.0 statistical software.

Results

Globally, there were an estimated 1.85 million newly diagnosed CRC cases with ASIR estimated to be 19.7 per 100,000 person-years in 2018. Sex-wise, there were 1.03 million incident cases in males and 823,303 cases in females (Table 1). CRC claimed an estimated 880,792 lives in 2018, out of which there were 484,224 males and 396,568 females. The ASMR was estimated to be8.9 per 100,000 person-years in 2018. Region-wise, colorectal cancer burden was the highest in East Asia with 736,573 incident cases (males 426,342 and females 310,231) and 325,128 deaths (males 183,346 and females 141,782). In terms of all-age incidence, North America ranked second with 179,771 cases (93,898 males; 85,873 females) followed by central and eastern Europe with 164,998 (males 84,951 and females 80,047) cases. In terms of deaths, however, central and eastern Europe ranked second after East Asia with 94,545 deaths (males 48,025 and females 46,520). Country-wise, China ranked first with 521,490 cases and 247,563 deaths followed by the USA with 155,098 cases and 54,611 deaths in 2018 (Table 1).

Age-standardized rates were the highest in developed regions led by Australia/New Zealand region with ASIR of 36.7/100,000 followed by northern Europe with ASIR of 32.1/100,000. ASIR was the lowest in south-central Asia at 4.9 per 100,000 person-years in 2018. ASMR was again the highest in central and eastern Europe (15.2/100,000) followed by southern Europe (11.5/100,000) with south-central Asia registering the lowest ASMR of 3.6/100,000 in 2018. Top-3 countries with highest ASIR were Hungary (51.2/100,000), South Korea (44.5 per 100,000) and Slovakia (43.8 per 100,000) in 2018 (Table 1; Fig. 1a). The estimated ASMR was again the highest in developed countries led by Hungary (21.5/100,000) and Slovakia (20.4 per 100,000) (Table 1; Fig. 1b). Among the countries with more than 1000 incident cases in 2018, ASIR varied 13-fold from Bangladesh with ASIR of 3.8/100,000 to 51.2/100,000 recorded by Hungary. ASMR varied 7-fold in these countries (> 1000 cases) ranging from Bangladesh with ASMR of 3.0/100,000 to Hungary which recorded ASMR of 21.5/100,000 in 2018.

Sex-wise, we noted that CRC had more proclivity towards males than females with males recording ASIR of 23.8/100,000 as against female ASIR of 21.8/100,000. The male-female difference in ASIR was the greatest in European regions, e.g., Southern Europe, male ASIR 40.4/100,000 and female ASIR 24.1/100,000. Globally, the ASMR was again higher in males (10.8/100,000) than females (7.2/100,000). The male-female difference in ASMR was the highest in European regions, e.g., central and eastern Europe, male ASMR 20.5/100,000 and female ASMR 11.9/100,000. The pattern of male dominance in terms of CRC burden was preserved across other world regions with few of the heavily burdened countries recording male age-standardized rates approximately twice as that of female age-standardized rates; for instance, Poland has an estimated male ASMR of 22.6/100,000 and female ASMR of 11.4/100,000 (Table 1). The *t* test of mean difference between male and females across countries was again found to be significant across all the metrics (bottom row of Table 1).

Across the age groups, the CRC incidence exhibited bell-shaped distribution; deaths due to CRC, however, increased monotonically with age (Fig. 2). The male dominance in terms of CRC burden was again preserved across different age groups with each of them except the oldest (85 plus) registering higher incidence as well as the death counts in males than in females (Fig. 2).

To examine the statistical relationship between CRC and HDI, we regressed ASIR and ASMR on HDI in linear form as well as by including the quadratic term (Table 2). The model including only the linear term of HDI could explain 58.7% variation in ASIR, whereas it explained 38.6% variation in ASMR. The inclusion of quadratic term resulted in a better fit of the model with regression involving both linear and quadratic term explaining 66.8% and 40.9% variation in ASIR and ASMR, respectively. CRC was generally higher in developed countries with a sharp upsurge in the positive relationship at HDI around 0.5 and 0.37 with the nonlinearity not as sharp in case of ASMR as it was in the case of ASIR (Table 2, Fig. 3).

MIR, a proxy indicator of 5-year survival rate, exhibited negative gradient with HDI (Fig. 3c). The global MIR of CRC stood at 0.48 with 140 countries recording MIR above the global MIR. Among the regions, the highest MIR (or the lowest survival rates) was recorded by African regions

Table 1 Colon and rectum cancer burden in 185 countries, 2018

	Incidence			ASIR			Deaths			ASMR			MIR		
Population	T	M	F	T	M	F	T	M	F	T	M	F	T	M	F
Australia/New Zealand	21,217	11,444	9773	36.7	41.7	32.1	7424	3893	3531	11.1	12.9	9.5	0.35	0.34	0.36
Australia	17,782	9643	8139	36.9	41.9	32.4	6131	3237	2894	10.9	12.8	9.2	0.34	0.34	0.36
New Zealand	3435	1801	1634	35.3	40.2	30.8	1293	656	637	12.1	13.4	10.9	0.38	0.36	0.39
Caribbean	10,886	5016	5870	17.9	17.9	17.8	6259	2898	3361	9.6	9.9	9.3	0.57	0.58	0.57
Bahamas	115	60	55	22.2	26.4	19.4	50	28	22	9.3	12.3	7.4	0.43	0.47	0.4
Barbados	219	118	101	38.9	50.3	28.8	101	53	48	16.6	21.4	12.4	0.46	0.45	0.48
Cuba	4238	1811	2427	17.6	16.1	18.9	2811	1228	1583	10.7	10.2	11.1	0.66	0.68	0.65
Dominican Republic	1489	730	759	13.4	13.9	12.9	858	428	430	7.4	7.9	6.9	0.58	0.59	0.57
France, Guadeloupe	183	89	94	19.8	21.2	18.5	104	61	43	9.4	13.1	6.4	0.57	0.69	0.46
France, Martinique	214	111	103	23.9	29	19.8	110	56	54	10.9	13.3	9	0.51	0.5	0.52
Haiti	949	406	543	10.8	9.9	11.7	656	267	389	7.5	6.7	8.3	0.69	0.66	0.72
Jamaica	953	380	573	24.9	21.3	28.2	467	186	281	11.2	9.8	12.4	0.49	0.49	0.49
Puerto Rico	1823	979	844	27.3	34.1	22.1	736	414	322	9.8	13.4	7.1	0.4	0.42	0.38
Saint Lucia	36	16	20	14.5	13.3	16	20	10	10	8	8.2	7.9	0.56	0.63	0.5
Trinidad and Tobago	381	191	190	19.4	21.5	17.5	188	96	92	9.3	10.8	8	0.49	0.5	0.48
Central America	19,520	9959	9561	11	12.1	10	9614	4910	4704	5.3	5.9	4.7	0.49	0.49	0.49
Belize	24	11	13	9.7	9.2	10	15	7	8	6.3	6.2	6.3	0.63	0.64	0.62
Costa Rica	1128	560	568	16.7	17.6	15.9	617	316	301	8.6	9.5	7.7	0.55	0.56	0.53
El Salvador	681	267	414	9	8.9	9.1	367	143	224	4.6	4.5	4.7	0.54	0.54	0.54
Guatemala	802	368	434	6.3	6.3	6.3	450	206	244	3.5	3.5	3.4	0.56	0.56	0.56
Honduras	573	286	287	8.2	9	7.6	340	175	165	4.5	4.9	4.1	0.59	0.61	0.57
Mexico	14,900	7795	7105	11.2	12.5	10	7084	3719	3365	5.2	5.9	4.6	0.48	0.48	0.47
Nicaragua	631	250	381	11.3	10.2	12.2	367	145	222	6.5	5.9	6.9	0.58	0.58	0.58
Panama	781	422	359	16.2	18.5	14.1	374	199	175	7.4	8.4	6.5	0.48	0.47	0.49
Central and Eastern Europe	164,998	84,951	80,047	28.8	37.5	23.2	94,545	48,025	46,520	15.2	20.5	11.9	0.57	0.57	0.58
Belarus	5680	2802	2878	31.8	41.6	26	2919	1315	1604	15.1	19.2	12.8	0.51	0.47	0.56
Bulgaria	4604	2724	1880	28.5	38.3	20.7	2714	1642	1072	14.9	21.3	10	0.59	0.6	0.57
Czechia	7838	4538	3300	32.7	42.5	24.9	3421	1974	1447	12.7	17.4	9.1	0.44	0.43	0.44
Hungary	10,809	6115	4694	51.2	70.6	36.8	5076	2867	2209	21.5	31.2	14.8	0.47	0.47	0.47
Moldova	2171	1241	930	34.2	47.3	25.2	1202	699	503	18.7	26.9	13.2	0.55	0.56	0.54
Poland	24,507	14,027	10,480	30.3	41.1	22.1	14,362	8104	6258	16.1	22.6	11.4	0.59	0.58	0.6
Romania	11,076	6500	4576	26.7	36.3	19.3	6319	3702	2617	13.7	19.2	9.5	0.57	0.57	0.57
Russian Federation	71,406	33,095	38,311	26.7	32.9	23.2	42,349	19,430	22,919	14.7	18.9	12.3	0.59	0.59	0.6
Slovakia	4624	2724	1900	43.8	60.7	31.2	2396	1376	1020	20.4	29.5	14.4	0.52	0.51	0.54

Table 1 (continued)

Population	Incidence			ASIR			Deaths			ASMR			MIR		
	T	M	F	T	M	F	T	M	F	T	M	F	T	M	F
Ukraine	22,283	11,185	11,098	25.8	33.6	21.1	13,787	6916	6871	15.1	20.3	11.9	0.62	0.62	0.62
Eastern Africa	17,125	7933	9192	7.7	7.8	7.7	12,201	5802	6399	5.7	6	5.5	0.71	0.73	0.7
Burundi	418	193	225	8.3	7.7	8.8	357	166	191	7.4	7	7.6	0.85	0.86	0.85
Comoros	18	8	10	4.3	4.1	4.5	18	8	10	4.3	4.1	4.5	1	1	1
Djibouti	41	20	21	5.6	5.8	5.5	34	18	16	4.9	5.4	4.4	0.83	0.9	0.76
Eritrea	189	95	94	6.3	7	5.8	149	77	72	5.2	5.9	4.7	0.79	0.81	0.77
Ethiopia	4716	2206	2510	7.5	7.8	7.4	3555	1745	1810	5.8	6.3	5.5	0.75	0.79	0.72
France, La Réunion	349	186	163	25.2	29.2	21.6	143	72	71	9.3	10.9	7.9	0.41	0.39	0.44
Kenya	2316	1134	1182	9.3	10	8.7	1466	738	728	6	6.8	5.4	0.63	0.65	0.62
Madagascar	827	366	461	6.1	5.5	6.5	579	258	321	4.4	4.2	4.7	0.7	0.7	0.7
Malawi	354	171	183	3.5	3.9	3.3	239	119	120	2.5	2.9	2.2	0.68	0.7	0.66
Mauritius	288	156	132	14.7	17.4	12.6	173	92	81	8.6	10.3	7.1	0.6	0.59	0.61
Mozambique	561	278	283	3.3	3.7	3	451	224	227	2.8	3.2	2.5	0.8	0.81	0.8
Rwanda	838	355	483	13.4	12.6	14.1	592	258	334	9.8	9.7	10	0.71	0.73	0.69
Somalia	599	298	301	8	8.4	7.6	539	273	266	7.4	7.9	6.9	0.9	0.92	0.88
South Sudan	509	256	253	7.1	7.5	6.7	420	216	204	6	6.6	5.5	0.83	0.84	0.81
Tanzania	2594	1004	1590	9	7.4	10.4	1767	704	1063	6.3	5.5	7	0.68	0.7	0.67
Uganda	1345	655	690	8.1	8.3	7.9	961	458	503	6.2	6.4	5.9	0.71	0.7	0.73
Zambia	355	163	192	4.6	4.9	4.4	202	103	99	2.8	3.2	2.4	0.57	0.63	0.52
Zimbabwe	793	382	411	10.1	11.6	9.1	549	269	280	7.2	8.4	6.3	0.69	0.7	0.68
Eastern Asia	736,573	426,342	310,231	26.5	32	21.3	325,128	183,346	141,782	10.9	13.3	8.7	0.44	0.43	0.46
China	521,490	303,853	217,637	23.7	28.1	19.4	247,563	142,476	105,087	10.9	13.1	8.8	0.47	0.47	0.48
Japan	148,151	82,641	65,510	38.9	49.1	29.6	57,910	30,228	27,682	12	15.2	9.2	0.39	0.37	0.42
North Korea	6566	3266	3300	18.8	22.7	15.8	3112	1415	1697	8.5	10.4	7.3	0.47	0.43	0.51
South Korea	42,363	26,143	16,220	44.5	59.5	31.3	9762	5445	4317	8.7	11.8	6.3	0.23	0.21	0.27
Mongolia	146	67	79	6.2	6.5	6	88	42	46	3.8	4	3.6	0.6	0.63	0.58
Melanesia	906	557	349	12.8	17.8	9	561	372	189	8.1	12.3	4.9	0.62	0.67	0.54
Fiji	86	43	43	10.1	11.3	9.3	50	27	23	6.2	7.9	5.2	0.58	0.63	0.53
France, New Caledonia	101	59	42	25.8	31.7	20.5	34	23	11	9	13	5.6	0.34	0.39	0.26
Papua New Guinea	684	439	245	13	19.3	8.4	447	307	140	8.7	14	4.8	0.65	0.7	0.57
Solomon Islands	25	12	13	7	7.3	6.6	21	11	10	5.9	6.7	5.1	0.84	0.92	0.77
Vanuatu	10	4	6	5.1	4.3	5.9	9	4	5	4.6	4.3	5	0.9	1	0.83
Micronesia	96	55	41	17.4	20.9	13.9	51	31	20	9.5	12.5	6.8	0.53	0.56	0.49
Guam	38	21	17	17.2	20.1	14.6	20	12	8	9.1	11.6	7.1	0.53	0.57	0.47

Table 1 (continued)

Population	Incidence			ASIR			Deaths			ASMR			MIR		
	T	M	F	T	M	F	T	M	F	T	M	F	T	M	F
Middle Africa	6010	2895	3115	7.5	7.8	7.3	4562	2232	2330	5.9	6.3	5.6	0.76	0.77	0.75
Angola	733	374	359	5.3	6	4.8	480	254	226	3.6	4.3	3.1	0.65	0.68	0.63
Cameroon	871	450	421	6.9	7.7	6.3	609	322	287	5	5.8	4.4	0.7	0.72	0.68
Central African Republic	151	78	73	5.8	6.5	5.2	139	73	66	5.4	6.3	4.8	0.92	0.94	0.9
Chad	413	214	199	5.9	6.6	5.3	325	169	156	5	5.6	4.5	0.79	0.79	0.78
Congo	152	81	71	5	5.7	4.5	102	56	46	3.5	4.1	3	0.67	0.69	0.65
Democratic Republic of Congo	3568	1627	1941	9.1	9	9.2	2831	1314	1517	7.4	7.5	7.3	0.79	0.81	0.78
Equatorial Guinea	40	24	16	5.8	6.4	5.2	30	18	12	5	5.8	4.2	0.75	0.75	0.75
Gabon	82	47	35	5.5	6.3	4.9	46	26	20	3.3	3.8	3	0.56	0.55	0.57
Sao Tome and Principe	5	3	2	6.6	9.5	4.4	3	2	1	4.1	6.6	2.2	0.6	0.67	0.5
North America	179,771	93,898	85,873	26.2	29.5	23.2	64,121	33,752	30,369	8.4	9.9	7.1	0.36	0.36	0.35
Canada	24,617	13,039	11,578	31.5	35.2	28	9494	5086	4408	10.1	12.2	8.2	0.39	0.39	0.38
USA	155,098	80,829	74,269	25.6	28.8	22.6	54,611	28,658	25,953	8.2	9.6	6.9	0.35	0.35	0.35
Northern Africa	18,810	9696	9114	9.2	10	8.6	10,902	5801	5101	5.4	6.1	4.7	0.58	0.6	0.56
Algeria	5537	2910	2627	13.9	14.8	13	3027	1684	1343	7.5	8.5	6.6	0.55	0.58	0.51
Egypt	5393	2661	2732	6.5	6.6	6.3	3041	1487	1554	3.7	3.8	3.5	0.56	0.56	0.57
Libya	675	309	366	12.6	13	12.5	404	192	212	8	8.5	7.6	0.6	0.62	0.58
Morocco	4118	2205	1913	10.9	12.2	9.8	2462	1381	1081	6.5	7.7	5.4	0.6	0.63	0.57
Sudan	1398	746	652	5.4	6.2	4.7	1004	555	449	3.9	4.7	3.3	0.72	0.74	0.69
Tunisia	1657	848	809	11.9	13	11	950	493	457	6.6	7.5	5.9	0.57	0.58	0.56
Northern Europe	75,900	41,255	34,645	32.1	37.5	27.3	32,659	17,367	15,292	11.2	13.5	9.3	0.43	0.42	0.44
Denmark	5585	2966	2619	41	45.9	36.6	1934	1003	931	12	13.7	10.5	0.35	0.34	0.36
Estonia	942	416	526	29.2	34.8	25.9	482	234	248	12.5	17.8	9.5	0.51	0.56	0.47
Finland	3440	1826	1614	24.6	28.7	21.2	1393	755	638	8.6	10.8	6.8	0.4	0.41	0.4
Iceland	168	92	76	26.2	30.5	22	82	46	36	10.9	13.4	8.6	0.49	0.5	0.47
Ireland	2968	1752	1216	34	42.4	26.4	1207	686	521	12.2	15.2	9.7	0.41	0.39	0.43
Latvia	1550	735	815	33	42.6	27.7	706	321	385	12.8	17.3	10.4	0.46	0.44	0.47
Lithuania	1831	898	933	27.2	35.6	22.1	996	535	461	12.8	19.6	8.9	0.54	0.6	0.49
Norway	4887	2530	2357	42.9	46.9	39.3	1750	915	835	13.2	15.3	11.3	0.36	0.36	0.35
Sweden	6421	3370	3051	26.9	29.7	24.3	3062	1637	1425	10.6	12.4	9	0.48	0.49	0.47
UK	47,892	26,551	21,341	32.1	37.8	27	20,957	11,186	9771	11.1	13.3	9.3	0.44	0.42	0.46
Polynesia	113	67	46	16.2	20	12.4	30	23	7	4.4	7.4	2.1	0.27	0.34	0.15
French Polynesia	47	27	20	13.9	15.9	11.6	11	9	2	3.4	5.6	1.2	0.23	0.33	0.1
Samoa	37	24	13	22.6	30.6	14.8	13	8	5	7.8	10.9	6.3	0.35	0.33	0.38

Table 1 (continued)

Population	Incidence			ASIR			Deaths			ASMR			MIR		
	T	M	F	T	M	F	T	M	F	T	M	F	T	M	F
South America	97,600	48,061	49,539	18.6	20.6	17.1	48,793	24,563	24,230	8.9	10.3	7.8	0.5	0.51	0.49
Argentina	15,692	8527	7165	25	31.5	20.2	8721	4751	3970	12.6	16.6	9.8	0.56	0.56	0.55
Bolivia	605	311	294	6.1	6.7	5.6	371	194	177	3.7	4.1	3.2	0.61	0.62	0.6
Brazil	51,783	24,737	27,046	19.6	21.1	18.6	24,482	12,031	12,451	9	10.1	8.1	0.47	0.49	0.46
Chile	5914	3002	2912	20.7	23.9	18.2	3144	1556	1588	10.2	11.9	8.9	0.53	0.52	0.55
Colombia	9140	4396	4744	15.8	16.9	15	4489	2203	2286	7.6	8.4	6.9	0.49	0.5	0.48
Ecuador	2025	902	1123	11.3	10.8	11.7	1100	507	593	5.8	5.9	5.8	0.54	0.56	0.53
French Guyana	54	32	22	21.7	26.8	17	14	8	6	5.8	7.3	4.3	0.26	0.25	0.27
Guyana	36	15	21	5	4.4	5.4	27	12	15	3.8	3.5	3.9	0.75	0.8	0.71
Paraguay	895	466	429	13.9	15	12.7	552	284	268	8.3	9	7.5	0.62	0.61	0.62
Peru	4610	2255	2355	13.3	14.2	12.4	2367	1220	1147	6.5	7.5	5.7	0.51	0.54	0.49
Suriname	94	51	43	15.4	18.8	12.7	70	38	32	11.3	14.1	8.9	0.74	0.75	0.74
Uruguay	2273	1152	1121	35	43.8	28.3	1093	555	538	15	19.3	12.1	0.48	0.48	0.48
Venezuela	4479	2215	2264	13.6	14.8	12.6	2363	1204	1159	7.1	8.1	6.2	0.53	0.54	0.51
South-Eastern Asia	95,223	53,542	41,681	14.3	17.6	11.6	52,475	29,384	23,091	7.9	9.9	6.3	0.55	0.55	0.55
Brunei	140	84	56	35	43.4	27.4	50	32	18	13.9	18.5	9.8	0.36	0.38	0.32
Cambodia	1314	637	677	11.1	13	9.9	859	414	445	7.5	8.8	6.7	0.65	0.65	0.66
Indonesia	30,017	19,113	10,904	12.1	16.2	8.4	16,386	10,279	6107	6.9	9.3	4.8	0.55	0.54	0.56
Lao PDR	652	326	326	13.9	14.9	13.1	394	197	197	8.6	9.4	8	0.6	0.6	0.6
Malaysia	6137	3342	2795	19.9	22	17.9	3414	1863	1551	11.2	12.5	9.9	0.56	0.56	0.55
Myanmar	4751	2600	2151	9.1	11.1	7.6	2960	1606	1354	5.8	7.1	4.8	0.62	0.62	0.63
Philippines	15,680	8791	6889	18.9	23.5	15.2	8821	4841	3980	11	13.9	8.9	0.56	0.55	0.58
Singapore	4202	1994	2208	36.8	38.9	34	1980	1050	930	17.3	20.2	14.6	0.47	0.53	0.42
Thailand	17,534	9015	8519	15.5	17.6	13.9	9462	4963	4499	8.4	9.7	7.4	0.54	0.55	0.53
Timor-Leste	63	33	30	8.9	9.7	8.1	45	23	22	6.5	7.1	5.9	0.71	0.7	0.73
Viet Nam	14,733	7607	7126	13.4	16	11.6	8104	4116	3988	7	8.7	5.9	0.55	0.54	0.56
Southern Africa	7167	3637	3530	13.4	16.8	11.2	3801	1979	1822	7.1	9.5	5.7	0.53	0.54	0.52
Botswana	53	35	18	2.9	4.9	1.6	28	20	8	1.7	3.2	0.8	0.53	0.57	0.44
Eswatini	30	16	14	3.6	4.6	2.9	18	11	7	2.4	3.5	1.7	0.6	0.69	0.5
Lesotho	47	27	20	3.1	4.4	2.4	35	21	14	2.5	3.6	1.8	0.74	0.78	0.7
Namibia	100	51	49	6.3	7.3	5.5	56	29	27	3.6	4.3	3.1	0.56	0.57	0.55
South Africa	6937	3508	3429	14.4	18.1	12	3664	1898	1766	7.6	10.2	6.1	0.53	0.54	0.52
South-Central Asia	88,033	53,534	34,499	4.9	6.1	3.8	63,401	39,852	23,549	3.6	4.6	2.6	0.72	0.74	0.68
Afghanistan	805	487	318	4	4.7	3.4	709	436	273	3.7	4.2	3	0.88	0.9	0.86

Table 1 (continued)

Population	Incidence			ASIR			Deaths			ASMR			MIR		
	T	M	F	T	M	F	T	M	F	T	M	F	T	M	F
Bangladesh	5549	3164	2385	3.8	4.3	3.3	4469	2605	1864	3	3.5	2.6	0.81	0.82	0.78
Bhutan	30	23	7	4.2	6	2.1	24	19	5	3.7	5.5	1.6	0.8	0.83	0.71
India	56,751	36,687	20,064	4.4	5.8	3.1	43,090	28,591	14,499	3.4	4.6	2.2	0.76	0.78	0.72
Iran	9864	5630	4234	12.9	14.6	11.1	4153	2395	1758	5.6	6.3	4.8	0.42	0.43	0.42
Kazakhstan	3049	1392	1657	15.4	17.7	14.1	2108	1023	1085	10.5	13.3	8.9	0.69	0.73	0.65
Kyrgyzstan	352	174	178	7.3	8.1	6.5	274	136	138	5.7	6.4	5	0.78	0.78	0.78
Maldives	41	30	11	11.9	15.9	7.2	20	17	3	6.3	10.5	1.8	0.49	0.57	0.27
Nepal	1432	514	918	5.8	4.4	7	1191	449	742	4.8	3.9	5.7	0.83	0.87	0.81
Pakistan	6475	3587	2888	4.2	4.5	3.8	5003	2822	2181	3.3	3.7	3	0.77	0.79	0.76
Sri Lanka	1441	734	707	5.2	5.8	4.7	968	518	450	3.4	4	2.9	0.67	0.71	0.64
Tajikistan	263	165	98	4	4.9	3.1	207	131	76	3.1	4	2.4	0.79	0.79	0.78
Turkmenistan	278	134	144	6	6.7	5.6	168	87	81	3.7	4.2	3.2	0.6	0.65	0.56
Uzbekistan	1703	813	890	6.3	6.5	6	1017	623	394	3.8	5.1	2.7	0.6	0.77	0.44
Southern Europe	119,949	69,446	50,503	31.6	40.4	24.1	53,975	30,991	22,984	11.5	15.4	8.4	0.45	0.45	0.46
Albania	402	225	177	8.4	9.6	7.2	198	115	83	3.7	4.5	3	0.49	0.51	0.47
Bosnia and Herzegovina	1818	1046	772	26.1	33	20.4	1081	628	453	13.3	18.2	9.4	0.59	0.6	0.59
Croatia	3387	1951	1436	34.1	45.9	24.9	2187	1288	899	18.9	27.4	12.7	0.65	0.66	0.63
Greece	7319	4158	3161	26.2	32.3	21.1	3430	1985	1445	9.7	12.7	7.3	0.47	0.48	0.46
Italy	49,327	26,930	22,397	29.9	36	24.8	21,172	11,491	9681	10.2	12.8	8	0.43	0.43	0.43
Macedonia FYR	996	517	479	28.4	30.9	26.3	472	248	224	12.5	14.2	11.1	0.47	0.48	0.47
Malta	302	180	122	29.1	36	23.2	121	70	51	10.6	13.2	8.6	0.4	0.39	0.42
Montenegro	210	115	95	18.6	22.7	14.9	115	62	53	9.2	11.2	7.5	0.55	0.54	0.56
Portugal	10,270	6104	4166	40	54	28.7	4261	2497	1764	13.5	18.7	9.6	0.41	0.41	0.42
Serbia	6149	3775	2374	36.7	49	26.4	3232	1966	1266	16.8	23.3	11.6	0.53	0.52	0.53
Slovenia	1987	1301	686	41.1	58.9	25.5	740	423	317	12.5	17.1	8.9	0.37	0.33	0.46
Spain	37,172	22,744	14,428	33.4	45.2	23.3	16,683	10,038	6645	12	16.8	8	0.45	0.44	0.46
Western Africa	12,734	6489	6245	6.4	6.8	6.1	8568	4440	4128	4.5	4.9	4.2	0.67	0.68	0.66
Benin	433	274	159	6.8	9.5	4.6	299	190	109	4.8	6.8	3.2	0.69	0.69	0.69
Burkina Faso	583	243	340	6.3	5.5	6.7	463	194	269	5.3	4.8	5.6	0.79	0.8	0.79
Cabo Verde	30	9	21	6.4	7.3	6.3	21	6	15	4.2	4.2	4.3	0.7	0.67	0.71
Côte d'Ivoire	737	333	404	5.8	4.9	6.9	552	259	293	4.5	3.9	5.2	0.75	0.78	0.73
Gambia	11	9	2	1.1	1.7	0.48	9	7	2	0.98	1.5	0.48	0.82	0.78	1
Ghana	1228	658	570	7.8	9.6	6.6	824	467	357	5.5	7.1	4.2	0.67	0.71	0.63
Guinea	145	77	68	2	2.1	1.8	118	65	53	1.7	1.9	1.5	0.81	0.84	0.78

Table 1 (continued)

Population	Incidence			ASIR			Deaths			ASMR			MIR		
	T	M	F	T	M	F	T	M	F	T	M	F	T	M	F
Guinea-Bissau	61	30	31	6.1	7.1	5.5	53	28	25	5.6	6.9	4.7	0.87	0.93	0.81
Liberia	102	43	59	3.9	3.4	4.3	84	37	47	3.4	3	3.6	0.82	0.86	0.8
Mali	917	385	532	10.5	9	11.7	686	290	396	8.3	7.3	9.1	0.75	0.75	0.74
Mauritania	159	70	89	6.1	5.2	6.7	111	48	63	4.5	3.8	4.9	0.7	0.69	0.71
Niger	583	305	278	5.3	5.5	5	522	284	238	4.9	5.3	4.5	0.9	0.93	0.86
Nigeria	6692	3568	3124	6.2	6.8	5.6	4059	2202	1857	4	4.5	3.5	0.61	0.62	0.59
Senegal	529	226	303	6.5	6.3	6.6	372	165	207	4.8	4.9	4.7	0.7	0.73	0.68
Sierra Leone	216	103	113	5.5	5	5.9	173	83	90	4.7	4.3	5	0.8	0.81	0.8
Togo	303	153	150	7.2	7.2	7.1	219	113	106	5.5	5.6	5.3	0.72	0.74	0.71
Western Asia	38,067	21,490	16,577	16.3	19.4	13.6	20,418	11,240	9178	8.7	10.4	7.3	0.54	0.52	0.55
Armenia	990	367	623	19.9	18.4	20.8	640	252	388	12.4	12.6	12.1	0.65	0.69	0.62
Azerbaijan	1114	668	446	10.2	13.8	7.4	774	482	292	7.1	10.2	4.8	0.69	0.72	0.65
Bahrain	120	72	48	12.6	14.2	11.2	70	40	30	8.1	8.9	7.6	0.58	0.56	0.63
Cyprus	511	338	173	24.2	34.4	15.3	242	154	88	10.2	14.6	6.5	0.47	0.46	0.51
West Bank and Gaza Strip	501	262	239	19.1	21.1	17.3	303	159	144	11.9	13.3	10.7	0.6	0.61	0.6
Georgia	645	331	314	8.7	11.1	7.1	427	226	201	5.7	7.5	4.4	0.66	0.68	0.64
Iraq	1391	763	628	6.1	7.2	5.2	813	446	367	3.7	4.4	3.1	0.58	0.58	0.58
Israel	2519	1336	1183	20.1	22.8	18	1390	717	673	9.3	11	7.9	0.55	0.54	0.57
Jordan	1105	460	645	17	14.8	19.2	589	257	332	9.3	8.5	10	0.53	0.56	0.51
Kuwait	352	195	157	13.2	12.9	14	178	97	81	7.5	7.4	7.9	0.51	0.5	0.52
Lebanon	1463	775	688	20	20.8	19.2	851	451	400	10.9	11.7	10.3	0.58	0.58	0.58
Oman	368	262	106	11	11.7	9.6	195	137	58	6.4	6.8	5.6	0.53	0.52	0.55
Qatar	142	100	42	13	13.5	13.8	79	54	25	8.7	9	9.5	0.56	0.54	0.6
Saudi Arabia	3564	2405	1159	13.1	14.9	10.6	1603	1077	526	6.3	7.3	5	0.45	0.45	0.45
Syrian Arab Republic	1890	870	1020	14.4	14.3	14.5	1248	583	665	9.5	9.7	9.4	0.66	0.67	0.65
Turkey	20,031	11,548	8483	21	27.4	16	10,033	5571	4462	10.2	13.1	7.9	0.5	0.48	0.53
United Arab Emirates	662	437	225	14.1	14.8	13.5	314	207	107	7.4	7.7	7.3	0.47	0.47	0.48
Yemen	1210	639	571	8.6	9.5	7.8	911	484	427	6.7	7.5	6	0.75	0.76	0.75
Western Europe	138,820	75,948	62,872	28.8	34.5	23.7	61,304	33,323	27,981	10.3	13.1	8	0.44	0.44	0.45
Austria	4421	2531	1890	20.7	26.3	16.1	2276	1318	958	8.9	12	6.2	0.51	0.52	0.51
Belgium	9346	5266	4080	35.3	43.8	28	3224	1669	1555	9.7	11.9	7.8	0.34	0.32	0.38
France	47,025	25,813	21,212	30.4	36.9	24.8	19,962	10,821	9141	10.2	13.1	7.9	0.42	0.42	0.43
Germany	58,047	31,026	27,021	26.2	31	22.1	27,334	14,931	12,403	10.1	13	7.7	0.47	0.48	0.46
Luxembourg	323	170	153	28.1	31.4	25.3	134	72	62	10.1	12.3	8.1	0.41	0.42	0.41

Table 1 (continued)

Population	Incidence			ASIR			Deaths			ASMR			MIR		
	T	M	F	T	M	F	T	M	F	T	M	F	T	M	F
Netherlands	14,921	8513	6408	37.8	45.3	31.1	6442	3443	2999	13.8	16.5	11.5	0.43	0.4	0.47
Switzerland	4681	2598	2083	24	28.4	20.2	1909	1054	855	8.1	10.1	6.4	0.41	0.41	0.41
World	1,849,518	1,026,215	823,303	19.7	23.6	16.3	880,792	484,224	396,568	8.9	10.8	7.2	0.48	0.47	0.48
t Test (male vs female)		2.20** (0.014)			10.27*** (0.000)			2.14** (0.016)			12.29*** (0.000)			5.00*** (0.000)	

T: Total, both sexes, all age-groups; F: Females, all age-groups; M: Males, all age-groups; ASIR: age-standardized incidence rate per 100,000 person-years; ASMR: age-standardized mortality rate per 100,000 person-years; MIR: Mortality-to-incidence ratio. Data Source: GLOBOCAN 2018 (IARC). T-test in the last column tests for the hypothesis of M (male mean) – F (female mean) = 0 against the one-sided alternate hypothesis M-F < 0; **/*** denotes statistical significance at 5%/1% respectively

(middle Africa 0.76 and eastern Africa 0.71). The MIR was also high in south-central Asia at 0.71. Although ASIR was one of the highest in Australia/New Zealand region, its MIR was one of the lowest at 0.35. Among the countries with incidence greater than 1000 in 2018, MIR exhibited a 3.6-fold variation ranging from 0.23 in South Korea to 0.83 in Nepal. Unlike ASIR and ASMR, the pattern of association of MIR with HDI was found to be strictly linear and downward sloping rather than quadratic (Fig. 3c; Table 2). HDI could explain 72.6% of the variation in MIR (Table 2) with the inclusion of quadratic term does not significantly improve the fit of the model, which is again apparent from Fig. 3c.

Globally, 1 in 24 persons (1 in 19 men and 1 in 29 women) had the risk of developing CRC during their lifetime (before the age 85) whereas the risk of dying from CRC were 1 in 37 in males and 1 in 57 in females (Table 3; Table 4 of Appendix). There was wide geographical variations between the risk of developing and dying from CRC during lifetime i.e. before the age 85 (Table 3; Table 4 of Appendix). While the odds of CRC incidence were the greatest in Australia/New Zealand region with 1 in 13 persons (males 1 in 11; females: 1 in 15) were expected to develop CRC during their lifetime, the odds of CRC death, however, were the greatest in central and eastern Europe (both sexes 1 in 28; males 1 in 20; females 1 in 36). Country-wise, odds of developing CRC were the greatest in developed countries led by Hungary with odds of CRC incidence 1 in 10 (males 1 in 7; females 1 in 13). In females, the highest odds of CRC incidence and death were estimated in Singapore (incidence 1 in 11; death 1 in 27). Fifty-three countries had more than 5% risk of CRC incidence during a person's lifetime, whereas 7 countries recorded greater than 10% risk of developing CRC. As per the development status, the CRC risk was the highest in developed countries and lowest in lesser developed and populous countries in Asia and Africa. India, for instance, had one of the lowest risks (incidence 1 in 120; death 1 in 149) of CRC incidence and mortality.

Discussion

We examined the CRC burden using estimates of incidence and mortality from GLOBOCAN 2018 [11, 17] and examined its association with socioeconomic status measured using HDI. We found that CRC incidence increases with age and has more proclivity towards males than females. While all-age incidence and mortality were the highest in high HDI countries led by China (incidence 521,490 and deaths 247,563), the age-standardized rates were the highest in very high HDI countries led by Hungary (ASIR 51.2/100,000) and South Korea (44.5/100,000); ASMR too was the highest in Hungary (21.5/100,000) followed by Slovakia (20.4/

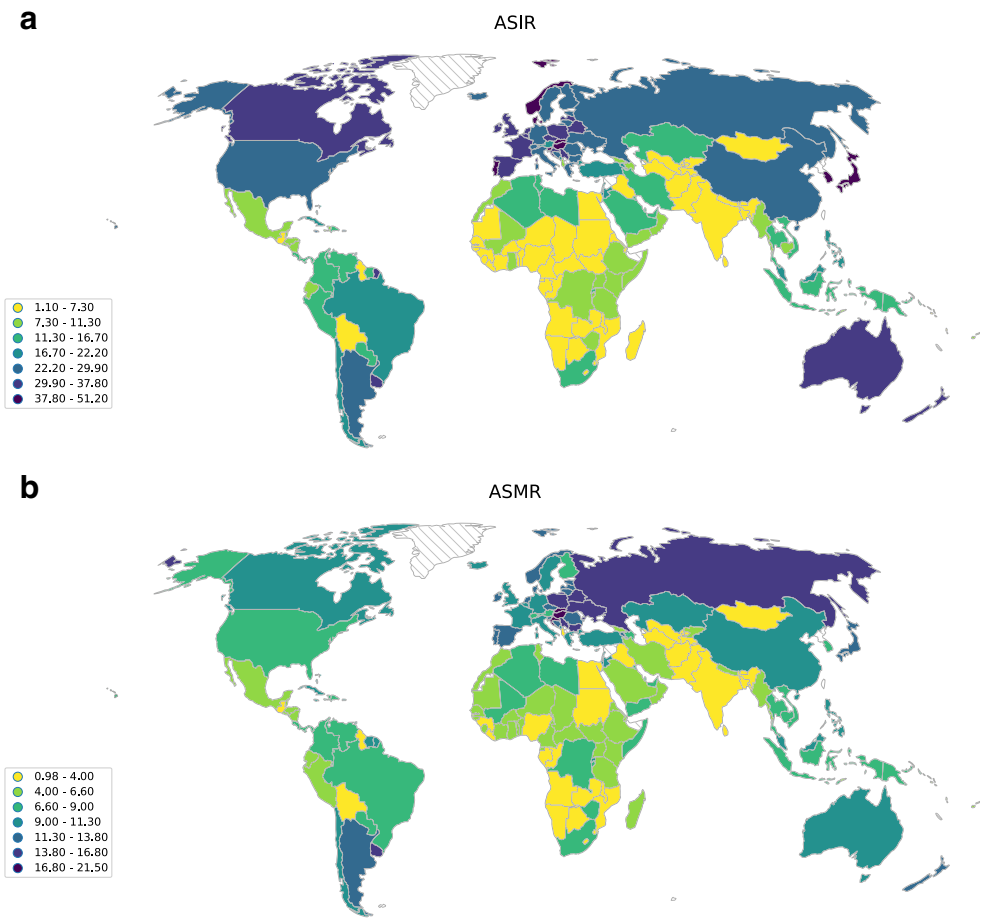

Fig. 1 Geographical distribution of colorectal cancer burden in both sexes in 2017. **a** ASIR. **b** ASMR. ASIR age-standardized incidence rate per 100,000 person-years, ASMR age-standardized mortality rate per 100,000 person-years. Data source: GLOBOCAN 2018 (IARC)

100,000). Due to large population size, East Asia led the world regions in terms of all-age incidence and death counts, whereas ASIR and ASMR were the highest in developed regions, e.g., Northern Europe recorded ASIR of 32.1/100,000 and central and eastern Europe recorded ASMR of 15.2/100,000. Both ASIR and ASMR were lowest in south-central Asia at estimated at 4.9/100,000 and 3.6/100,000, respectively, in 2018. Higher incidence in developed societies has already been documented before [20] and is attributable to a greater percentage of the older population, dietary patterns, and availability of screening procedures [21]. Higher risk of males towards CRC has been documented before and can be possibly attributed to factors such as greater prevalence of risk factors such as alcohol and smoking in males [22–24]. The differences in mortality rates, however, also reflect the role of factors other than alcohol and smoking, though it requires more research to provide conclusive evidence.

Ninety percent of CRC incidence and 92% of CRC deaths occurred in 50-plus age group (Fig. 2). As age increases, adenomatous polyps grows slowly from adenoma to frank carcinoma; therefore, CRC deaths can be prevented by the detection and removal of adenomatous polyps through early screening. Although operational screening modalities differ in terms of convenience and cost, mainly two types of screening procedures are currently employed. First is stool based, e.g., fecal occult blood test (FOBT), Guaiac-based FOBT, and fecal immunochemical test (FIT); second involves structural examinations such as flexible sigmoidoscopy and colonoscopy. Colonoscopy is considered to be the gold standard of CRC screening and diagnosis; it has higher specificity and sensitivity than the stool-based methods, the colonoscopy, however, is quite resource-intensive in comparison with stool-based methods [7]. Although different methods vary in terms of efficiency and their implementation varies geographically, randomized control trials have demonstrated that screening methods have been quite effective in early detection of adenomas and colorectal carcinoma, thereby boosting the survival rates [25–29]. There are currently two approaches to screening: population-wide and opportunistic. The population-wide screening is quite prevalent in Western countries, the opportunistic screening, however, had limited success in boosting the take-up rates [30]. As per WHO country survey on cancer control policies, FOBT-based screening procedure was available at public primary level in 82/160 of the responding countries, whereas colonoscopy was present in 70/160 countries (Table 5 of Appendix). Even in those

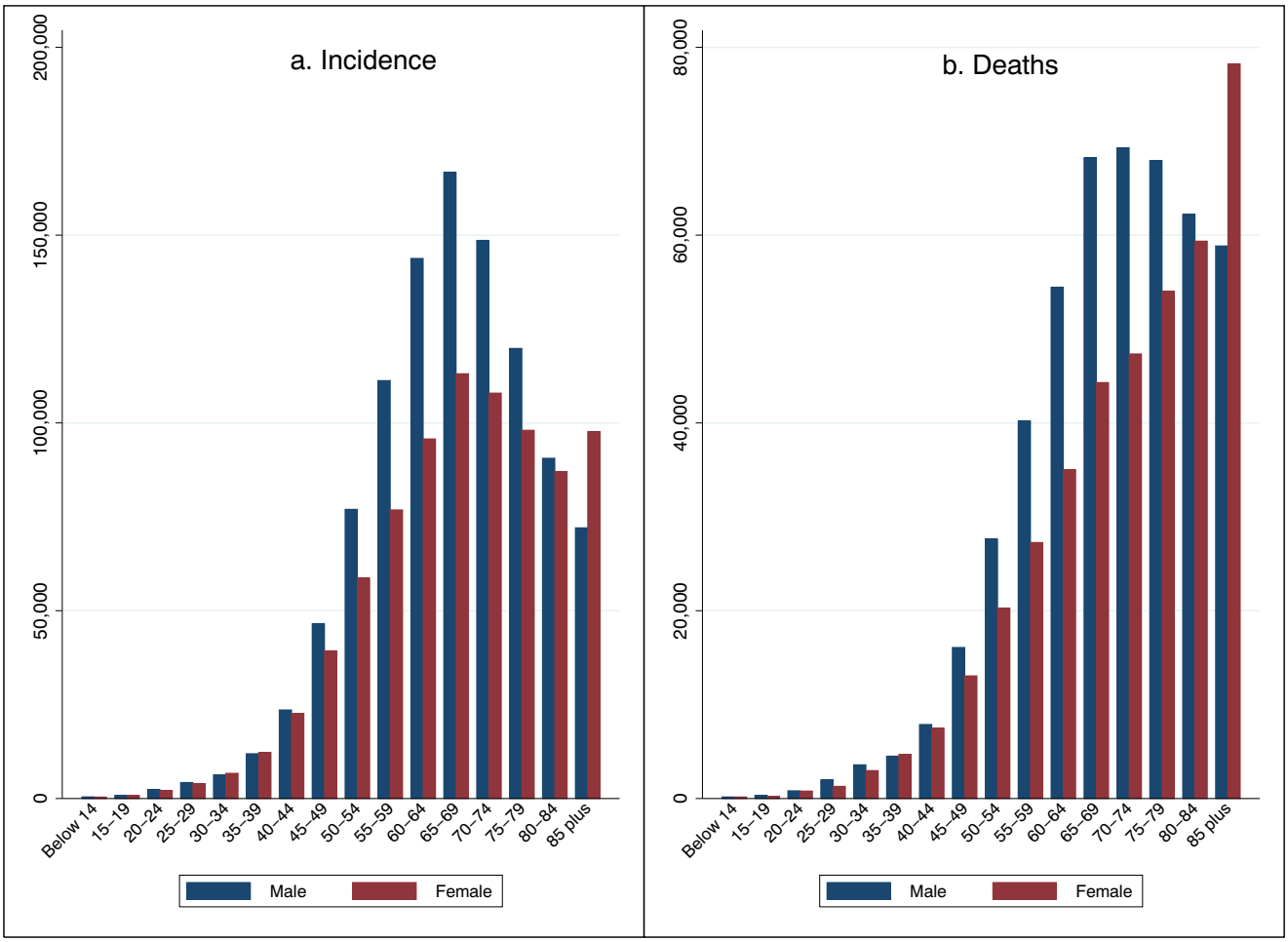

Fig. 2 Age-group and gender-wise burden of colon and rectum cancer in 2018. **a** Incidence. **b** Deaths. Data source: GLOBOCAN 2018 (IARC)

countries where these screening modalities were available, most of the countries belonged to high/very high HDI category. The US Preventive Services Task Force (USPSTF) recommends screening for CRC in the 50–75 age group; those with familial history and other high-risk population are recomended for screening at a comparatively younger age and higher frequency [7]. S A significant percentage of US citizens still had no access to screening in 2010 [31]. Moreover, heterogenous participation rates were observed in developed societies owing to differential socioeconomic status and level of education, thereby resulting in inequalities in the disease outcomes [32].

The modifiable risk factors that are associated with elevated risk of CRC include alcohol [33], smoking [34], red meat [35], obesity [36, 37], and type 2 diabetes [38], whereas fruit and vegetable consumption [39, 40] and physical activity reduce the risk of CRC [41]. The nonmodifiable risk factors of CRC include aging, familial history, preoccurrence of polyps, and inflammatory bowel diseases such as Crohn's disease and ulcerative colitis [21]. Inflammation has recently been found to be associated with increased incidence of CRC; accordingly, anti-inflammatory drugs like low-dose aspirin has been found to be effective in reducing the CRC incidence [42–44].[2]

We observed high CRC burden in Asian countries exemplified by high absolute incidence and mortality in China, Japan, India, and South Korea with these four countries accounting for 41.6% (768,755 of 1.85 million) of incident cases and 40.7% (358,325 of 880,792) of global deaths in 2018. Previous studies also reported an increased risk of colorectal carcinoma in Asian populations [3]. The increasing incidence of CRC in these countries is reflective of changing lifestyle and behavior as factors including lack of physical activity and dietary patterns have been shown to be positively associated with high incidence of colorectal neoplasia in developed countries [21, 46]. The first pillar of the PPPM approach advocates for the prevention of CRC via controlling risk factors, the vast majority of which are related to lifestyle [33–41]. Preventable nature of CRC makes it a likely target of PPPM

[2] US Preventive Services Task Force (US PSTF) recommends the use of low-dose aspirin for the prevention of colorectal cancer in high-risk patients [45].

Table 2 Association between human development and indicators of CRC burden

	ASIR as dependent Variable		ASMR as dependent Variable		MIR as dependent Variable	
HDI	56.9*** (3.4)	− 134.8*** (22.9)	16.1*** (1.3)	− 20.8* (11.0)	− 0.7839*** (0.0324)	− 0.6718** (0.2833)
HDI SQ		140.5*** (17.5)		27.0*** (8.1)		− 0.0821 (0.2108)
Intercept	− 24.0*** (2.3)	38.0*** (7.1)	− 3.4*** (0.9)	8.6*** (3.5)	1.1504*** (0.0239)	1.1142*** (0.0900)
R^2	0.5869	0.6691	0.3850	0.4101	0.7240	0.7242
Turning Point		0.4797		0.3852		

Data source: MIR was calculated directly as the ratio of all-age death numbers and no. of all-age incident cases which were procured from GLOBOCAN 2018 (IARC) and HDI estimates from UNDP. Robust standard errors are presented inside parenthesis

ASMR age-standardized mortality rate per 100,000 person-years, both sexes, *ASIR* age-standardized incidence rate per 100,000 person-years, both sexes, *MIR* mortality-to-incidence ratio, *HDI* country-wise human development index

*, **, *** represent statistical significance at 10, 5, and 1% level of significance. Turning point is calculated as $\frac{-\beta_1}{2\beta_2}$

approach to medicine. For targeted therapy and precision medicine envisaged by PPPM, diagnostic, prognostic, and therapeutic markers need to be developed and continually adopted in CRC medicine. Carcinoembryonic antigen (CEA), for instance, has been shown to be a promising prognostic biomarker for CRC [47] and preliminary research has

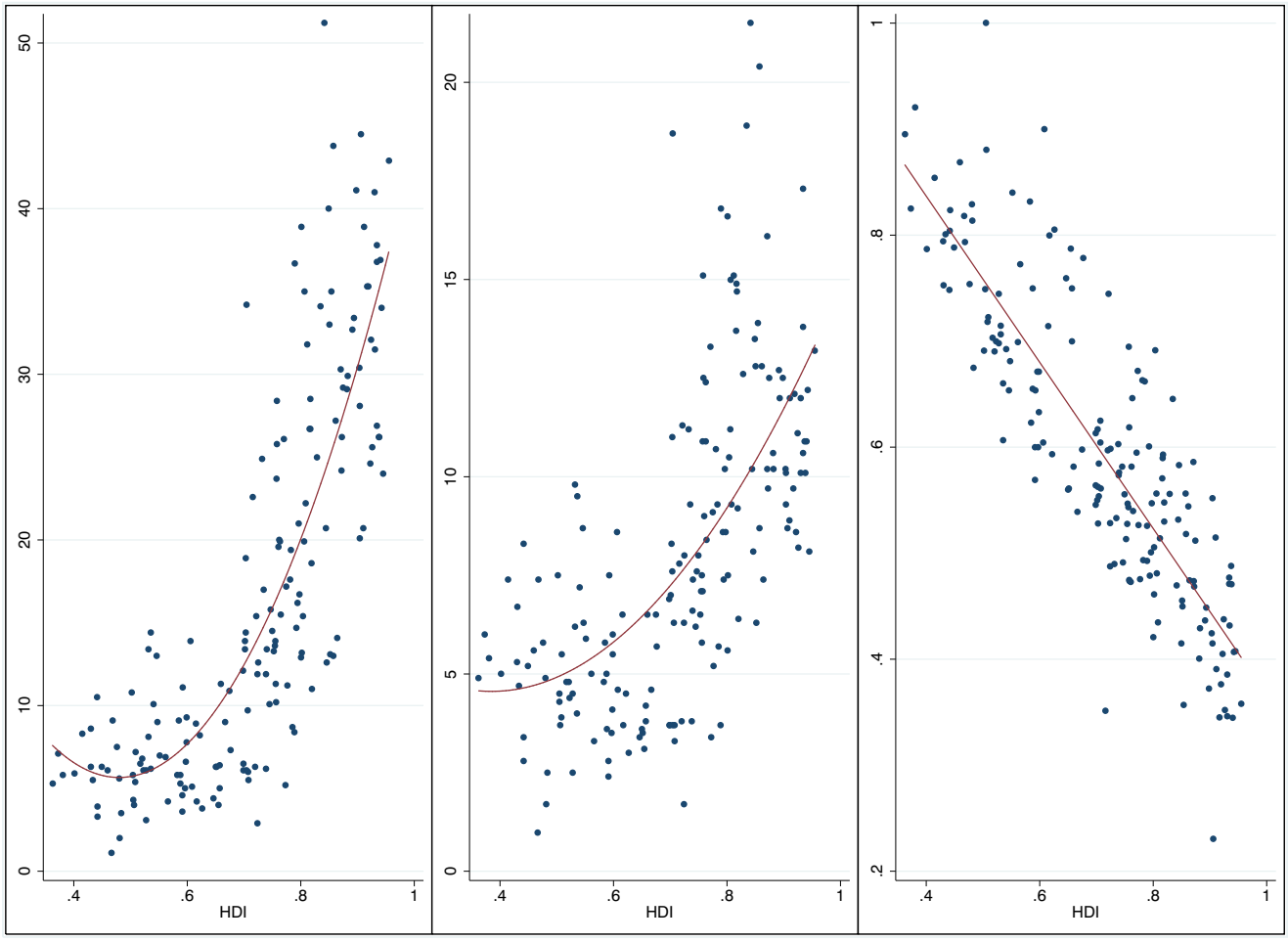

Fig. 3 Nonlinear relationship between human development and age-standardized rates. **a** ASIR vs HDI. **b** ASMR vs HDI. **c** MIR vs HDI. ASMR age-standardized mortality rate per 100,000 person-years, both sexes, ASIR age-standardized incidence rate per 100,000 person-years, both sexes, MIR mortality-to-incidence ratio, HDI human development index. Data source: MIR was calculated directly as the ratio of all-age death numbers and no. of all-age incident cases, both of which were procured from GLOBOCAN 2018 (IARC) and HDI estimates were obtained from UNDP

Table 3 Region-wise probability of incidence and death due to colorectal cancer

Population	Incidence			Deaths		
	Both	Male	Female	Both	Male	Female
Australia and New Zealand	7.83 (1 in 13)	8.98 (1 in 11)	6.75 (1 in 15)	2.77 (1 in 36)	3.16 (1 in 32)	2.4 (1 in 42)
Caribbean	3.97 (1 in 25)	4.01 (1 in 25)	3.94 (1 in 25)	2.37 (1 in 42)	2.45 (1 in 41)	2.29 (1 in 44)
Central America	2.17 (1 in 46)	2.38 (1 in 42)	1.98 (1 in 51)	1.17 (1 in 85)	1.3 (1 in 77)	1.06 (1 in 94)
Central and Eastern Europe	5.9 (1 in 17)	7.92 (1 in 13)	4.7 (1 in 21)	3.56 (1 in 28)	4.93 (1 in 20)	2.78 (1 in 36)
Eastern Africa	1.49 (1 in 67)	1.54 (1 in 65)	1.45 (1 in 69)	1.19 (1 in 84)	1.28 (1 in 78)	1.12 (1 in 89)
Eastern Asia	5.67 (1 in 18)	6.86 (1 in 15)	4.58 (1 in 22)	2.83 (1 in 35)	3.44 (1 in 29)	2.28 (1 in 44)
Melanesia	2.82 (1 in 35)	4.23 (1 in 24)	1.75 (1 in 57)	1.85 (1 in 54)	3.02 (1 in 33)	0.97 (1 in 103)
Micronesia	3.63 (1 in 28)	4.1 (1 in 24)	3.13 (1 in 32)	1.81 (1 in 55)	2.69 (1 in 37)	1.09 (1 in 92)
Middle Africa	1.72 (1 in 58)	1.84 (1 in 54)	1.63 (1 in 61)	1.47 (1 in 68)	1.61 (1 in 62)	1.37 (1 in 73)
North America	5.18 (1 in 19)	5.88 (1 in 17)	4.57 (1 in 22)	1.88 (1 in 53)	2.21 (1 in 45)	1.59 (1 in 63)
Northern Africa	1.68 (1 in 60)	1.9 (1 in 53)	1.51 (1 in 66)	1.14 (1 in 88)	1.35 (1 in 74)	0.97 (1 in 103)
Northern Europe	6.89 (1 in 15)	8.23 (1 in 12)	5.74 (1 in 17)	2.9 (1 in 34)	3.55 (1 in 28)	2.37 (1 in 42)
Polynesia	3.48 (1 in 29)	4.53 (1 in 22)	2.55 (1 in 39)	0.77 (1 in 130)	1.35 (1 in 74)	0.26 (1 in 385)
South America	3.91 (1 in 26)	4.42 (1 in 23)	3.51 (1 in 28)	2.14 (1 in 47)	2.53 (1 in 40)	1.84 (1 in 54)
South-Central Asia	0.93 (1 in 108)	1.2 (1 in 83)	0.68 (1 in 147)	0.72 (1 in 139)	0.95 (1 in 105)	0.5 (1 in 200)
South-Eastern Asia	2.92 (1 in 34)	3.65 (1 in 27)	2.35 (1 in 43)	1.84 (1 in 54)	2.36 (1 in 42)	1.46 (1 in 68)
Southern Africa	2.89 (1 in 35)	3.78 (1 in 26)	2.37 (1 in 42)	1.72 (1 in 58)	2.37 (1 in 42)	1.35 (1 in 74)
Southern Europe	6.64 (1 in 15)	8.66 (1 in 12)	4.95 (1 in 20)	2.89 (1 in 35)	3.92 (1 in 26)	2.06 (1 in 49)
Western Africa	1.15 (1 in 87)	1.24 (1 in 81)	1.07 (1 in 93)	0.9 (1 in 111)	0.99 (1 in 101)	0.82 (1 in 122)
Western Asia	3.38 (1 in 30)	4.15 (1 in 24)	2.75 (1 in 36)	2.05 (1 in 49)	2.5 (1 in 40)	1.69 (1 in 59)
Western Europe	6.12 (1 in 16)	7.48 (1 in 13)	4.94 (1 in 20)	2.6 (1 in 38)	3.32 (1 in 30)	1.99 (1 in 50)

Data source: cumulative risk of developing and dying from cancer (before age 85) were procured from GLOBOCAN 2018 and the odds were calculated using the CRC risk. Odds of developing and dying from CRC are presented inside parenthesis

identified few hormones to have prognostic and therapeutic marker properties for CRC, though more research is still needed to explore their full potential [48].

The mortality due to CRC reflects the strength of the healthcare system and infrastructure to prevent, diagnose, and treat the disease. The CRC mortality rates were in concordance with incidence rates with ASMR being the highest in Europe (e.g. Hungary (21.5 per 100,000) and Slovakia (20.4 per 100,000)). The lesser developed (low/medium HDI) countries have comparatively lower ASMR because of large population and relatively lower life expectancy, the survival rates (proxied by MIR), however, were lot higher in developed countries (high/very high HDI) as compared to the lesser developed ones. Statistically too, we found that better socioeconomic status of a country measured using HDI has had strong statistically significant negative effect on MIR (a proxy for 5-year survival rate). Low survival rates in lesser developed countries reflect screening prevalence as well as treatment modalities for CRC, which depend critically upon the stage at which malignancy gets detected. While adenomatous polyps or a low-grade tumor detected during screening can be removed by polypectomy, the late-stage tumor, however, can be treated using colectomy (partial or complete removal of colon) in conjunction with adjuvant (neo)chemotherapy and/or radiotherapy. Few of these treatment modalities such as surgery (even if cancer or polyps are detected early) are insufficiently present in less developed countries [49].

Limitations

The accuracy and validity of the estimates of CRC examined in this paper is crucially dependent upon data availability from cancer registries which is far from complete in many of the less developed countries led by Africa. Therefore, the estimates produced for few countries lacking cancer registry mostly reflect estimates from the neighboring countries [11, 17]. Moreover, for the countries lacking coverage and completeness, the GLOBOCAN estimates reported in this paper are expected to be downward biased. Second, the estimates presented in this paper were available only for 1 year (i.e., 2018) which could not be utilized to gauge the temporal patterns of the CRC burden. Third, we employed MIR as a proxy indicator of 5-year survival rate which is not an exact measure of survival rate. This indicator, however, can serve as a useful

proxy for the survival rate of colorectal neoplasia in the absence of country-wise exact measure of survival rate.

Conclusion and expert recommendations

High burden of CRC was estimated in developed countries and was correlated positively with HDI and but is also substantially high in Asian countries. It shows that as countries are moving up in the development hierarchy, they are emulating Westernized lifestyle and dietary habits which have manifested in high CRC incidence in these countries. As the vast majority of risk factors are associated with lifestyle and diet, and screening programs are available, the CRC burden can be curtailed to attain the sustainable development goal (SDG 3) of ensuring a healthy and quality life.

Against the rising burden, it is also noteworhty that CRC deaths can be prevented via primary approaches (i.e., control of risk factors) and secondary prevention using cancer screening; both of these approaches are fundamental to the preventive, predictive, and personalized approach to medicine [8–10]. PPPM approach epitomizes the changing philosophy of healthcare from illness to health, from treatment to prevention and from one-size-fits-all to personalized medicine [50]. PPPM approach to medicine requires effective cancer control policies, aware citizens (at-risk population and patient), healthcare infrastructure, and availability and affordability of various technologies (omics technologies etc) to offer personalized medicine [51, 52]. The adoption of the PPPM approach to cancer management, however, is not easy in the context of developing and less-developed countries. This is because the PPPM approach is an integrated approach that combines advantages of individual bio/medical fields through a multi-professional collaboration [9]; such multi-professional collaboration along with multi-omics approach is quite a challenging and costly task for low-resource economies. Additionally, a large percentage of people in low-resource economies are still poor and lacks access to basic healthcare facilities let alone personalized medicine. Therefore, at the policy level, the following strategies must be adopted for cancer management and control in concordance with PPPM approach to disease managment and control. First, prevention must be adopted as the first-line attack on colorectal carcinoma. The major thrust of any policy intervention must be on providing cost-effective screening services and ensure their availability at the broadest possible level. Second, universal health coverage (UHC) can ensure access to basic health services (screening and treatment), which can later be upgraded to provide precision and personalized medicine. Third, through health literacy campaigns, various preventive approaches, behavioral risk factors, and screening programs must be popularized and made available to high-risk populations. Finally, new-age screening devices, omics technologies, and diagnostic and prognostic biomarker panels suiting the low-cost requirements need to be continuously developed and adopted.

Acknowledgments The authors thank the International Agency for Research on Cancer (IARC) for making available GLOBOCAN 2018 estimates in the public domain.

Compliance with ethical standards

Conflict of interest The authors declare that they have no conflict of interest.

Ethical approval The research is conducted using data available in the public domain and does not include any human participants and/or animals.

Appendix

Table 4 Country-wise probability of incidence and death due to colorectal cancer

	Incidence			Deaths		
Country	Both	Male	Female	Both	Male	Female
Afghanistan	0.68 (1 in 147)	0.77 (1 in 130)	0.59 (1 in 169)	0.62 (1 in 161)	0.69 (1 in 145)	0.55 (1 in 182)
Albania	1.49 (1 in 67)	1.73 (1 in 58)	1.27 (1 in 79)	0.84 (1 in 119)	1.02 (1 in 98)	0.66 (1 in 152)
Algeria	2.6 (1 in 38)	2.93 (1 in 34)	2.29 (1 in 44)	1.64 (1 in 61)	1.97 (1 in 51)	1.35 (1 in 74)
Angola	1.04 (1 in 96)	1.22 (1 in 82)	0.9 (1 in 111)	0.79 (1 in 127)	0.96 (1 in 104)	0.66 (1 in 152)
Argentina	5.11 (1 in 20)	6.69 (1 in 15)	3.98 (1 in 25)	3 (1 in 33)	4.09 (1 in 24)	2.25 (1 in 44)
Armenia	4.81 (1 in 21)	4.42 (1 in 23)	5.06 (1 in 20)	3.19 (1 in 31)	3.21 (1 in 31)	3.16 (1 in 32)
Australia	7.77 (1 in 13)	8.95 (1 in 11)	6.67 (1 in 15)	2.7 (1 in 37)	3.09 (1 in 32)	2.33 (1 in 43)

Table 4 (continued)

Country	Incidence			Deaths		
	Both	Male	Female	Both	Male	Female
Austria	4.56 (1 in 22)	5.91 (1 in 17)	3.44 (1 in 29)	2.29 (1 in 44)	3.16 (1 in 32)	1.6 (1 in 63)
Azerbaijan	2.01 (1 in 50)	2.85 (1 in 35)	1.41 (1 in 71)	1.54 (1 in 65)	2.31 (1 in 43)	1 (1 in 100)
Bahamas	4.59 (1 in 22)	5.6 (1 in 18)	3.75 (1 in 27)	2.2 (1 in 45)	2.91 (1 in 34)	1.68 (1 in 60)
Bahrain	2.41 (1 in 41)	3.12 (1 in 32)	1.73 (1 in 58)	1.72 (1 in 58)	2.28 (1 in 44)	1.26 (1 in 79)
Bangladesh	0.68 (1 in 147)	0.76 (1 in 132)	0.61 (1 in 164)	0.58 (1 in 172)	0.66 (1 in 152)	0.49 (1 in 204)
Barbados	8.25 (1 in 12)	9.65 (1 in 10)	7 (1 in 14)	3.99 (1 in 25)	4.87 (1 in 21)	3.28 (1 in 30)
Belarus	6.4 (1 in 16)	8.77 (1 in 11)	5.17 (1 in 19)	3.48 (1 in 29)	4.57 (1 in 22)	2.95 (1 in 34)
Belgium	7.53 (1 in 13)	9.47 (1 in 11)	5.9 (1 in 17)	2.51 (1 in 40)	3.15 (1 in 32)	1.99 (1 in 50)
Belize	1.52 (1 in 66)	1.48 (1 in 68)	1.54 (1 in 65)	1.16 (1 in 86)	1.08 (1 in 93)	1.22 (1 in 82)
Benin	0.91 (1 in 110)	1.42 (1 in 70)	0.52 (1 in 192)	0.68 (1 in 147)	1.07 (1 in 93)	0.37 (1 in 270)
Bhutan	0.68 (1 in 147)	0.78 (1 in 128)	0.57 (1 in 175)	0.65 (1 in 154)	0.74 (1 in 135)	0.53 (1 in 189)
Bolivia	1.16 (1 in 86)	1.29 (1 in 78)	1.03 (1 in 97)	0.75 (1 in 133)	0.87 (1 in 115)	0.65 (1 in 154)
Bosnia and Herzegovina	5.19 (1 in 19)	6.61 (1 in 15)	4.07 (1 in 25)	3.19 (1 in 31)	4.34 (1 in 23)	2.33 (1 in 43)
Botswana	0.53 (1 in 189)	0.93 (1 in 108)	0.27 (1 in 370)	0.4 (1 in 250)	0.73 (1 in 137)	0.2 (1 in 500)
Brazil	4 (1 in 25)	4.42 (1 in 23)	3.68 (1 in 27)	2.09 (1 in 48)	2.43 (1 in 41)	1.85 (1 in 54)
Brunei	6.97 (1 in 14)	8.72 (1 in 11)	5.44 (1 in 18)	3.03 (1 in 33)	4.15 (1 in 24)	2.07 (1 in 48)
Bulgaria	5.67 (1 in 18)	7.82 (1 in 13)	4.1 (1 in 24)	3.47 (1 in 29)	5.05 (1 in 20)	2.36 (1 in 42)
Burkina Faso	1.21 (1 in 83)	1.05 (1 in 95)	1.32 (1 in 76)	1.11 (1 in 90)	0.98 (1 in 102)	1.18 (1 in 85)
Burundi	1.93 (1 in 52)	1.67 (1 in 60)	2.14 (1 in 47)	1.81 (1 in 55)	1.61 (1 in 62)	1.97 (1 in 51)
Cabo Verde	1.97 (1 in 51)	2.65 (1 in 38)	1.64 (1 in 61)	1.26 (1 in 79)	1.76 (1 in 57)	0.99 (1 in 101)
Cambodia	2.39 (1 in 42)	2.8 (1 in 36)	2.12 (1 in 47)	1.85 (1 in 54)	2.16 (1 in 46)	1.65 (1 in 61)
Cameroon	1.53 (1 in 65)	1.75 (1 in 57)	1.35 (1 in 74)	1.24 (1 in 81)	1.46 (1 in 68)	1.06 (1 in 94)
Canada	6.49 (1 in 15)	7.4 (1 in 14)	5.68 (1 in 18)	2.55 (1 in 39)	3.1 (1 in 32)	2.06 (1 in 49)
Central African Republic	1.19 (1 in 84)	1.43 (1 in 70)	1.01 (1 in 99)	1.16 (1 in 86)	1.41 (1 in 71)	0.98 (1 in 102)
Chad	1.07 (1 in 93)	1.23 (1 in 81)	0.93 (1 in 108)	0.97 (1 in 103)	1.11 (1 in 90)	0.85 (1 in 118)
Chile	4.65 (1 in 22)	5.45 (1 in 18)	4.03 (1 in 25)	2.62 (1 in 38)	3.11 (1 in 32)	2.25 (1 in 44)
China	5.05 (1 in 20)	5.99 (1 in 17)	4.16 (1 in 24)	2.86 (1 in 35)	3.42 (1 in 29)	2.34 (1 in 43)
Colombia	3.45 (1 in 29)	3.68 (1 in 27)	3.27 (1 in 31)	1.89 (1 in 53)	2.09 (1 in 48)	1.74 (1 in 57)
Comoros	1.01 (1 in 99)	0.83 (1 in 120)	1.14 (1 in 88)	1.01 (1 in 99)	0.83 (1 in 120)	1.14 (1 in 88)
Congo, Democratic Republic of	2.21 (1 in 45)	2.26 (1 in 44)	2.19 (1 in 46)	1.95 (1 in 51)	2.05 (1 in 49)	1.88 (1 in 53)
Congo, Republic of	1.14 (1 in 88)	1.35 (1 in 74)	0.97 (1 in 103)	0.9 (1 in 111)	1.08 (1 in 93)	0.75 (1 in 133)
Costa Rica	3.61 (1 in 28)	3.83 (1 in 26)	3.42 (1 in 29)	2.09 (1 in 48)	2.32 (1 in 43)	1.88 (1 in 53)
Côte d'Ivoire	1.11 (1 in 90)	0.91 (1 in 110)	1.35 (1 in 74)	0.95 (1 in 105)	0.79 (1 in 127)	1.13 (1 in 88)
Croatia	7.19 (1 in 14)	9.91 (1 in 10)	5.22 (1 in 19)	4.71 (1 in 21)	7 (1 in 14)	3.14 (1 in 32)
Cuba	4.12 (1 in 24)	3.74 (1 in 27)	4.45 (1 in 22)	2.76 (1 in 36)	2.66 (1 in 38)	2.85 (1 in 35)
Cyprus	5.39 (1 in 19)	7.81 (1 in 13)	3.28 (1 in 30)	2.62 (1 in 38)	3.81 (1 in 26)	1.62 (1 in 62)
Czechia	6.96 (1 in 14)	9.31 (1 in 11)	5.19 (1 in 19)	3.17 (1 in 32)	4.4 (1 in 23)	2.26 (1 in 44)
Denmark	8.99 (1 in 11)	10.29 (1 in 10)	7.85 (1 in 13)	3.18 (1 in 31)	3.71 (1 in 27)	2.74 (1 in 36)
Djibouti	0.81 (1 in 123)	1 (1 in 100)	0.65 (1 in 154)	0.75 (1 in 133)	0.97 (1 in 103)	0.56 (1 in 179)
Dominican Republic	2.66 (1 in 38)	2.62 (1 in 38)	2.68 (1 in 37)	1.64 (1 in 61)	1.66 (1 in 60)	1.62 (1 in 62)
Ecuador	2.53 (1 in 40)	2.37 (1 in 42)	2.66 (1 in 38)	1.45 (1 in 69)	1.44 (1 in 69)	1.46 (1 in 68)
Egypt	1.16 (1 in 86)	1.15 (1 in 87)	1.16 (1 in 86)	0.78 (1 in 128)	0.78 (1 in 128)	0.77 (1 in 130)
El Salvador	1.91 (1 in 52)	1.71 (1 in 58)	2.07 (1 in 48)	1.08 (1 in 93)	0.96 (1 in 104)	1.16 (1 in 86)
Equatorial Guinea	0.98 (1 in 102)	1.19 (1 in 84)	0.79 (1 in 127)	0.92 (1 in 109)	1.15 (1 in 87)	0.71 (1 in 141)
Eritrea	1.03 (1 in 97)	1.25 (1 in 80)	0.85 (1 in 118)	0.91 (1 in 110)	1.13 (1 in 88)	0.73 (1 in 137)
Estonia	6.64 (1 in 15)	8.18 (1 in 12)	5.8 (1 in 17)	3.36 (1 in 30)	4.87 (1 in 21)	2.55 (1 in 39)
Eswatini	0.59 (1 in 169)	0.77 (1 in 130)	0.49 (1 in 204)	0.46 (1 in 217)	0.67 (1 in 149)	0.34 (1 in 294)

Table 4 (continued)

Country	Incidence			Deaths		
	Both	Male	Female	Both	Male	Female
Ethiopia	1.16 (1 in 86)	1.35 (1 in 74)	1.01 (1 in 99)	0.97 (1 in 103)	1.19 (1 in 84)	0.79 (1 in 127)
Fiji	1.87 (1 in 53)	2.02 (1 in 50)	1.77 (1 in 56)	1.2 (1 in 83)	1.5 (1 in 67)	0.99 (1 in 101)
Finland	5.38 (1 in 19)	6.45 (1 in 16)	4.5 (1 in 22)	2.18 (1 in 46)	2.79 (1 in 36)	1.69 (1 in 59)
France	6.39 (1 in 16)	7.92 (1 in 13)	5.08 (1 in 20)	2.55 (1 in 39)	3.31 (1 in 30)	1.91 (1 in 52)
France, Guadeloupe	3.92 (1 in 26)	4.59 (1 in 22)	3.4 (1 in 29)	2.32 (1 in 43)	3.53 (1 in 28)	1.39 (1 in 72)
France, La Réunion	5.3 (1 in 19)	6.31 (1 in 16)	4.45 (1 in 22)	2.4 (1 in 42)	2.95 (1 in 34)	1.94 (1 in 52)
France, Martinique	4.93 (1 in 20)	5.82 (1 in 17)	4.2 (1 in 24)	2.29 (1 in 44)	2.92 (1 in 34)	1.8 (1 in 56)
France, New Caledonia	5.36 (1 in 19)	6.51 (1 in 15)	4.28 (1 in 23)	1.64 (1 in 61)	2.06 (1 in 49)	1.24 (1 in 81)
French Guyana	3.8 (1 in 26)	4 (1 in 25)	3.45 (1 in 29)	0.84 (1 in 119)	1.37 (1 in 73)	0.39 (1 in 256)
French Polynesia	3.24 (1 in 31)	4.04 (1 in 25)	2.47 (1 in 40)	0.72 (1 in 139)	1.29 (1 in 78)	0.17 (1 in 588)
Gabon	0.75 (1 in 133)	0.94 (1 in 106)	0.6 (1 in 167)	0.5 (1 in 200)	0.64 (1 in 156)	0.41 (1 in 244)
Gaza Strip and West Bank	4.01 (1 in 25)	4.65 (1 in 22)	3.47 (1 in 29)	2.81 (1 in 36)	3.27 (1 in 31)	2.43 (1 in 41)
Georgia	1.85 (1 in 54)	2.42 (1 in 41)	1.49 (1 in 67)	1.26 (1 in 79)	1.71 (1 in 58)	0.98 (1 in 102)
Germany	5.62 (1 in 18)	6.74 (1 in 15)	4.65 (1 in 22)	2.56 (1 in 39)	3.27 (1 in 31)	1.96 (1 in 51)
Ghana	2.03 (1 in 49)	2.69 (1 in 37)	1.54 (1 in 65)	1.56 (1 in 64)	2.17 (1 in 46)	1.1 (1 in 91)
Greece	5.57 (1 in 18)	7.11 (1 in 14)	4.31 (1 in 23)	2.48 (1 in 40)	3.33 (1 in 30)	1.8 (1 in 56)
Guam	3.59 (1 in 28)	3.96 (1 in 25)	3.21 (1 in 31)	1.76 (1 in 57)	2.51 (1 in 40)	1.16 (1 in 86)
Guatemala	1.28 (1 in 78)	1.27 (1 in 79)	1.29 (1 in 78)	0.8 (1 in 125)	0.8 (1 in 125)	0.79 (1 in 127)
Guinea	0.31 (1 in 323)	0.33 (1 in 303)	0.29 (1 in 345)	0.28 (1 in 357)	0.3 (1 in 333)	0.26 (1 in 385)
Guinea-Bissau	1.29 (1 in 78)	1.53 (1 in 65)	1.11 (1 in 90)	1.23 (1 in 81)	1.52 (1 in 66)	1.01 (1 in 99)
Guyana	1.85 (1 in 54)	1.54 (1 in 65)	2.08 (1 in 48)	1.53 (1 in 65)	1.42 (1 in 70)	1.61 (1 in 62)
Haiti	2.93 (1 in 34)	3.29 (1 in 30)	2.7 (1 in 37)	2.07 (1 in 48)	2.06 (1 in 49)	2.1 (1 in 48)
Honduras	1.73 (1 in 58)	2.09 (1 in 48)	1.45 (1 in 69)	0.86 (1 in 116)	0.93 (1 in 108)	0.81 (1 in 123)
Hungary	10.09 (1 in 10)	14.02 (1 in 7)	7.43 (1 in 13)	5.01 (1 in 20)	7.37 (1 in 14)	3.53 (1 in 28)
Iceland	5.98 (1 in 17)	6.84 (1 in 15)	5.15 (1 in 19)	2.78 (1 in 36)	3.44 (1 in 29)	2.17 (1 in 46)
India	0.83 (1 in 120)	1.16 (1 in 86)	0.53 (1 in 189)	0.67 (1 in 149)	0.96 (1 in 104)	0.41 (1 in 244)
Indonesia	2.33 (1 in 43)	3.19 (1 in 31)	1.62 (1 in 62)	1.58 (1 in 63)	2.16 (1 in 46)	1.11 (1 in 90)
Iran, Islamic Republic of	2.6 (1 in 38)	2.99 (1 in 33)	2.18 (1 in 46)	1.37 (1 in 73)	1.52 (1 in 66)	1.19 (1 in 84)
Iraq	1.11 (1 in 90)	1.31 (1 in 76)	0.95 (1 in 105)	0.74 (1 in 135)	0.88 (1 in 114)	0.63 (1 in 159)
Ireland	7.55 (1 in 13)	9.5 (1 in 11)	5.77 (1 in 17)	3.21 (1 in 31)	3.95 (1 in 25)	2.56 (1 in 39)
Israel	4.32 (1 in 23)	5.3 (1 in 19)	3.54 (1 in 28)	2.4 (1 in 42)	2.89 (1 in 35)	2.01 (1 in 50)
Italy	6.45 (1 in 16)	7.95 (1 in 13)	5.18 (1 in 19)	2.61 (1 in 38)	3.36 (1 in 30)	2 (1 in 50)
Jamaica	5.14 (1 in 19)	4.4 (1 in 23)	5.78 (1 in 17)	2.63 (1 in 38)	2.28 (1 in 44)	2.93 (1 in 34)
Japan	8.09 (1 in 12)	10.27 (1 in 10)	6.17 (1 in 16)	2.92 (1 in 34)	3.72 (1 in 27)	2.24 (1 in 45)
Jordan	3.34 (1 in 30)	3.14 (1 in 32)	3.54 (1 in 28)	2.04 (1 in 49)	2.01 (1 in 50)	2.08 (1 in 48)
Kazakhstan	3.14 (1 in 32)	3.81 (1 in 26)	2.79 (1 in 36)	2.4 (1 in 42)	3.17 (1 in 32)	1.99 (1 in 50)
Kenya	1.68 (1 in 60)	1.95 (1 in 51)	1.47 (1 in 68)	1.21 (1 in 83)	1.48 (1 in 68)	0.99 (1 in 101)
Korea, Democratic Republic of	3.88 (1 in 26)	4.7 (1 in 21)	3.37 (1 in 30)	2.17 (1 in 46)	2.62 (1 in 38)	1.91 (1 in 52)
Korea, Republic of	8.38 (1 in 12)	11.25 (1 in 9)	5.97 (1 in 17)	2.23 (1 in 45)	3.06 (1 in 33)	1.61 (1 in 62)
Kuwait	2.98 (1 in 34)	3.05 (1 in 33)	2.94 (1 in 34)	1.91 (1 in 52)	1.98 (1 in 51)	1.86 (1 in 54)
Kyrgyzstan	1.58 (1 in 63)	1.61 (1 in 62)	1.52 (1 in 66)	1.31 (1 in 76)	1.41 (1 in 71)	1.22 (1 in 82)
Lao People's Democratic Republic	2.72 (1 in 37)	2.99 (1 in 33)	2.51 (1 in 40)	1.97 (1 in 51)	2.23 (1 in 45)	1.78 (1 in 56)
Latvia	7.21 (1 in 14)	9.81 (1 in 10)	5.87 (1 in 17)	3.31 (1 in 30)	4.64 (1 in 22)	2.65 (1 in 38)
Lebanon	4.13 (1 in 24)	4.41 (1 in 23)	3.9 (1 in 26)	2.58 (1 in 39)	2.83 (1 in 35)	2.37 (1 in 42)
Lesotho	0.54 (1 in 185)	0.81 (1 in 123)	0.39 (1 in 256)	0.46 (1 in 217)	0.72 (1 in 139)	0.32 (1 in 313)
Liberia	0.73 (1 in 137)	0.63 (1 in 159)	0.82 (1 in 122)	0.68 (1 in 147)	0.6 (1 in 167)	0.74 (1 in 135)
Libya	2.21 (1 in 45)	2.49 (1 in 40)	1.99 (1 in 50)	1.58 (1 in 63)	1.85 (1 in 54)	1.37 (1 in 73)

Table 4 (continued)

Country	Incidence			Deaths		
	Both	Male	Female	Both	Male	Female
Lithuania	5.77 (1 in 17)	7.93 (1 in 13)	4.57 (1 in 22)	3.2 (1 in 31)	5.04 (1 in 20)	2.2 (1 in 45)
Luxembourg	6.21 (1 in 16)	7.43 (1 in 13)	5.21 (1 in 19)	2.67 (1 in 37)	3.42 (1 in 29)	2.05 (1 in 49)
Madagascar	1.35 (1 in 74)	1.19 (1 in 84)	1.47 (1 in 68)	1.07 (1 in 93)	0.98 (1 in 102)	1.15 (1 in 87)
Malawi	0.53 (1 in 189)	0.64 (1 in 156)	0.47 (1 in 213)	0.43 (1 in 233)	0.54 (1 in 185)	0.35 (1 in 286)
Malaysia	4.3 (1 in 23)	4.78 (1 in 21)	3.86 (1 in 26)	2.87 (1 in 35)	3.25 (1 in 31)	2.51 (1 in 40)
Maldives	2.28 (1 in 44)	2.94 (1 in 34)	1.55 (1 in 65)	1.57 (1 in 64)	2.4 (1 in 42)	0.67 (1 in 149)
Mali	2.07 (1 in 48)	1.75 (1 in 57)	2.33 (1 in 43)	1.78 (1 in 56)	1.56 (1 in 64)	1.96 (1 in 51)
Malta	6.63 (1 in 15)	8.56 (1 in 12)	4.99 (1 in 20)	2.81 (1 in 36)	3.62 (1 in 28)	2.16 (1 in 46)
Mauritania	1.27 (1 in 79)	1.03 (1 in 97)	1.44 (1 in 69)	1.03 (1 in 97)	0.86 (1 in 116)	1.15 (1 in 87)
Mauritius	3.08 (1 in 32)	3.8 (1 in 26)	2.55 (1 in 39)	2.04 (1 in 49)	2.47 (1 in 40)	1.71 (1 in 58)
Mexico	2.16 (1 in 46)	2.41 (1 in 41)	1.93 (1 in 52)	1.14 (1 in 88)	1.3 (1 in 77)	1 (1 in 100)
Mongolia	1.29 (1 in 78)	1.36 (1 in 74)	1.25 (1 in 80)	0.72 (1 in 139)	0.83 (1 in 120)	0.65 (1 in 154)
Montenegro	3.55 (1 in 28)	4.13 (1 in 24)	3.05 (1 in 33)	2.17 (1 in 46)	2.63 (1 in 38)	1.83 (1 in 55)
Morocco	1.92 (1 in 52)	2.26 (1 in 44)	1.63 (1 in 61)	1.33 (1 in 75)	1.67 (1 in 60)	1.05 (1 in 95)
Mozambique	0.61 (1 in 164)	0.66 (1 in 152)	0.58 (1 in 172)	0.54 (1 in 185)	0.59 (1 in 169)	0.5 (1 in 200)
Myanmar	1.73 (1 in 58)	2.13 (1 in 47)	1.43 (1 in 70)	1.28 (1 in 78)	1.58 (1 in 63)	1.06 (1 in 94)
Namibia	1.25 (1 in 80)	1.48 (1 in 68)	1.09 (1 in 92)	0.8 (1 in 125)	1.04 (1 in 96)	0.64 (1 in 156)
Nepal	1.32 (1 in 76)	1.09 (1 in 92)	1.53 (1 in 65)	1.15 (1 in 87)	0.99 (1 in 101)	1.3 (1 in 77)
New Zealand	8.14 (1 in 12)	9.13 (1 in 11)	7.23 (1 in 14)	3.12 (1 in 32)	3.51 (1 in 28)	2.77 (1 in 36)
Nicaragua	2.28 (1 in 44)	1.99 (1 in 50)	2.51 (1 in 40)	1.47 (1 in 68)	1.29 (1 in 78)	1.6 (1 in 63)
Niger	0.88 (1 in 114)	0.91 (1 in 110)	0.84 (1 in 119)	0.86 (1 in 116)	0.9 (1 in 111)	0.81 (1 in 123)
Nigeria	0.95 (1 in 105)	1.08 (1 in 93)	0.84 (1 in 119)	0.67 (1 in 149)	0.78 (1 in 128)	0.57 (1 in 175)
Norway	9.45 (1 in 11)	10.5 (1 in 10)	8.52 (1 in 12)	3.46 (1 in 29)	4.06 (1 in 25)	2.93 (1 in 34)
Oman	1.87 (1 in 53)	1.91 (1 in 52)	1.78 (1 in 56)	1.25 (1 in 80)	1.26 (1 in 79)	1.22 (1 in 82)
Pakistan	0.68 (1 in 147)	0.73 (1 in 137)	0.63 (1 in 159)	0.57 (1 in 175)	0.62 (1 in 161)	0.52 (1 in 192)
Panama	3.45 (1 in 29)	4.09 (1 in 24)	2.89 (1 in 35)	1.78 (1 in 56)	2.08 (1 in 48)	1.51 (1 in 66)
Papua New Guinea	2.96 (1 in 34)	4.8 (1 in 21)	1.61 (1 in 62)	2.1 (1 in 48)	3.69 (1 in 27)	0.96 (1 in 104)
Paraguay	2.95 (1 in 34)	3.05 (1 in 33)	2.84 (1 in 35)	2 (1 in 50)	2.09 (1 in 48)	1.91 (1 in 52)
Peru	3.03 (1 in 33)	3.3 (1 in 30)	2.8 (1 in 36)	1.66 (1 in 60)	1.92 (1 in 52)	1.45 (1 in 69)
Philippines	4.06 (1 in 25)	5.14 (1 in 19)	3.25 (1 in 31)	2.83 (1 in 35)	3.59 (1 in 28)	2.28 (1 in 44)
Poland	6.4 (1 in 16)	8.85 (1 in 11)	4.68 (1 in 21)	3.93 (1 in 25)	5.64 (1 in 18)	2.79 (1 in 36)
Portugal	8.1 (1 in 12)	11.06 (1 in 9)	5.74 (1 in 17)	3.31 (1 in 30)	4.68 (1 in 21)	2.28 (1 in 44)
Puerto Rico	5.49 (1 in 18)	6.9 (1 in 14)	4.41 (1 in 23)	2.26 (1 in 44)	3.07 (1 in 33)	1.66 (1 in 60)
Qatar	3.41 (1 in 29)	3.7 (1 in 27)	2.96 (1 in 34)	2.55 (1 in 39)	2.69 (1 in 37)	2.38 (1 in 42)
Republic of Moldova	6.56 (1 in 15)	9.27 (1 in 11)	4.83 (1 in 21)	4.05 (1 in 25)	6.02 (1 in 17)	2.84 (1 in 35)
Romania	5.46 (1 in 18)	7.57 (1 in 13)	3.95 (1 in 25)	3.25 (1 in 31)	4.65 (1 in 22)	2.3 (1 in 43)
Russian Federation	5.51 (1 in 18)	7 (1 in 14)	4.72 (1 in 21)	3.48 (1 in 29)	4.63 (1 in 22)	2.9 (1 in 34)
Rwanda	3.29 (1 in 30)	3.15 (1 in 32)	3.41 (1 in 29)	2.68 (1 in 37)	2.7 (1 in 37)	2.68 (1 in 37)
Saint Lucia	3.53 (1 in 28)	4.19 (1 in 24)	3.04 (1 in 33)	2.25 (1 in 44)	2.93 (1 in 34)	1.72 (1 in 58)
Samoa	4.32 (1 in 23)	5.98 (1 in 17)	2.89 (1 in 35)	1.07 (1 in 93)	1.5 (1 in 67)	0.76 (1 in 132)
Sao Tome and Principe	0.88 (1 in 114)	1.33 (1 in 75)	0.55 (1 in 182)	0.57 (1 in 175)	0.96 (1 in 104)	0.28 (1 in 357)
Saudi Arabia	2.37 (1 in 42)	2.8 (1 in 36)	1.85 (1 in 54)	1.3 (1 in 77)	1.58 (1 in 63)	0.99 (1 in 101)
Senegal	1.38 (1 in 72)	1.42 (1 in 70)	1.35 (1 in 74)	1.12 (1 in 89)	1.22 (1 in 82)	1.05 (1 in 95)
Serbia	6.64 (1 in 15)	9.04 (1 in 11)	4.71 (1 in 21)	3.84 (1 in 26)	5.45 (1 in 18)	2.64 (1 in 38)
Sierra Leone	1.1 (1 in 91)	0.94 (1 in 106)	1.24 (1 in 81)	1.01 (1 in 99)	0.86 (1 in 116)	1.15 (1 in 87)
Singapore	8.88 (1 in 11)	8.9 (1 in 11)	8.72 (1 in 11)	4.4 (1 in 23)	5.11 (1 in 20)	3.77 (1 in 27)
Slovakia	9.01 (1 in 11)	12.73 (1 in 8)	6.44 (1 in 16)	5.11 (1 in 20)	7.6 (1 in 13)	3.57 (1 in 28)

Table 4 (continued)

Country	Incidence			Deaths		
	Both	Male	Female	Both	Male	Female
Slovenia	8.49 (1 in 12)	12.32 (1 in 8)	5.28 (1 in 19)	3.23 (1 in 31)	4.47 (1 in 22)	2.28 (1 in 44)
Solomon Islands	1.23 (1 in 81)	1.43 (1 in 70)	1.03 (1 in 97)	1.06 (1 in 94)	1.28 (1 in 78)	0.84 (1 in 119)
Somalia	1.31 (1 in 76)	1.52 (1 in 66)	1.12 (1 in 89)	1.25 (1 in 80)	1.47 (1 in 68)	1.05 (1 in 95)
South Africa	3.12 (1 in 32)	4.09 (1 in 24)	2.55 (1 in 39)	1.84 (1 in 54)	2.55 (1 in 39)	1.44 (1 in 69)
South Sudan	1.35 (1 in 74)	1.49 (1 in 67)	1.24 (1 in 81)	1.23 (1 in 81)	1.37 (1 in 73)	1.1 (1 in 91)
Spain	7.06 (1 in 14)	9.74 (1 in 10)	4.82 (1 in 21)	3.01 (1 in 33)	4.33 (1 in 23)	1.96 (1 in 51)
Sri Lanka	0.93 (1 in 108)	1.08 (1 in 93)	0.82 (1 in 122)	0.68 (1 in 147)	0.82 (1 in 122)	0.57 (1 in 175)
Sudan	0.92 (1 in 109)	1.16 (1 in 86)	0.72 (1 in 139)	0.77 (1 in 130)	1.02 (1 in 98)	0.57 (1 in 175)
Suriname	3.89 (1 in 26)	4.88 (1 in 20)	3.18 (1 in 31)	2.87 (1 in 35)	3.39 (1 in 29)	2.46 (1 in 41)
Sweden	6.03 (1 in 17)	6.74 (1 in 15)	5.4 (1 in 19)	2.77 (1 in 36)	3.28 (1 in 30)	2.32 (1 in 43)
Switzerland	5.15 (1 in 19)	6.3 (1 in 16)	4.16 (1 in 24)	2.08 (1 in 48)	2.64 (1 in 38)	1.61 (1 in 62)
Syrian Arab Republic	2.87 (1 in 35)	2.97 (1 in 34)	2.8 (1 in 36)	2.11 (1 in 47)	2.24 (1 in 45)	2.02 (1 in 50)
Tajikistan	0.69 (1 in 145)	0.81 (1 in 123)	0.58 (1 in 172)	0.58 (1 in 172)	0.72 (1 in 139)	0.46 (1 in 217)
Tanzania	2.09 (1 in 48)	1.7 (1 in 59)	2.41 (1 in 41)	1.62 (1 in 62)	1.38 (1 in 72)	1.82 (1 in 55)
Thailand	3.2 (1 in 31)	3.71 (1 in 27)	2.8 (1 in 36)	1.74 (1 in 57)	2.07 (1 in 48)	1.48 (1 in 68)
The former Yugoslav Republic of Macedonia	5.33 (1 in 19)	5.98 (1 in 17)	4.81 (1 in 21)	2.93 (1 in 34)	3.37 (1 in 30)	2.59 (1 in 39)
The Netherlands	8.13 (1 in 12)	9.93 (1 in 10)	6.51 (1 in 15)	3.55 (1 in 28)	4.28 (1 in 23)	2.92 (1 in 34)
The Republic of the Gambia	0.15 (1 in 667)	0.21 (1 in 476)	0.1 (1 in 1000)	0.15 (1 in 667)	0.2 (1 in 500)	0.1 (1 in 1000)
Timor-Leste	1.88 (1 in 53)	1.86 (1 in 54)	1.88 (1 in 53)	1.53 (1 in 65)	1.52 (1 in 66)	1.52 (1 in 66)
Togo	1.43 (1 in 70)	1.38 (1 in 72)	1.46 (1 in 68)	1.19 (1 in 84)	1.19 (1 in 84)	1.19 (1 in 84)
Trinidad and Tobago	4.12 (1 in 24)	4.63 (1 in 22)	3.71 (1 in 27)	2.22 (1 in 45)	2.64 (1 in 38)	1.9 (1 in 53)
Tunisia	2.3 (1 in 43)	2.55 (1 in 39)	2.09 (1 in 48)	1.49 (1 in 67)	1.68 (1 in 60)	1.33 (1 in 75)
Turkey	4.27 (1 in 23)	5.64 (1 in 18)	3.21 (1 in 31)	2.43 (1 in 41)	3.16 (1 in 32)	1.88 (1 in 53)
Turkmenistan	1.29 (1 in 78)	1.45 (1 in 69)	1.18 (1 in 85)	0.69 (1 in 145)	0.84 (1 in 119)	0.58 (1 in 172)
Uganda	1.86 (1 in 54)	1.75 (1 in 57)	1.94 (1 in 52)	1.56 (1 in 64)	1.48 (1 in 68)	1.61 (1 in 62)
Ukraine	5.12 (1 in 20)	6.92 (1 in 14)	4.12 (1 in 24)	3.29 (1 in 30)	4.53 (1 in 22)	2.61 (1 in 38)
United Arab Emirates	2.93 (1 in 34)	3.3 (1 in 30)	2.25 (1 in 44)	1.72 (1 in 58)	1.85 (1 in 54)	1.51 (1 in 66)
UK	6.8 (1 in 15)	8.17 (1 in 12)	5.57 (1 in 18)	2.87 (1 in 35)	3.48 (1 in 29)	2.35 (1 in 43)
USA	5.01 (1 in 20)	5.68 (1 in 18)	4.44 (1 in 23)	1.79 (1 in 56)	2.1 (1 in 48)	1.53 (1 in 65)
Uruguay	7.54 (1 in 13)	9.54 (1 in 10)	6.1 (1 in 16)	3.73 (1 in 27)	4.91 (1 in 20)	2.94 (1 in 34)
Uzbekistan	1.22 (1 in 82)	1.21 (1 in 83)	1.22 (1 in 82)	0.75 (1 in 133)	1 (1 in 100)	0.55 (1 in 182)
Vanuatu	0.72 (1 in 139)	0.64 (1 in 156)	0.81 (1 in 123)	0.69 (1 in 145)	0.64 (1 in 156)	0.73 (1 in 137)
Venezuela, Bolivarian Republic of	2.85 (1 in 35)	3.02 (1 in 33)	2.69 (1 in 37)	1.66 (1 in 60)	1.84 (1 in 54)	1.5 (1 in 67)
Viet Nam	2.51 (1 in 40)	3.11 (1 in 32)	2.12 (1 in 47)	1.55 (1 in 65)	2 (1 in 50)	1.28 (1 in 78)
World	4.25 (1 in 24)	5.15 (1 in 19)	3.48 (1 in 29)	2.18 (1 in 46)	2.69 (1 in 37)	1.76 (1 in 57)
Yemen	1.86 (1 in 54)	2.01 (1 in 50)	1.74 (1 in 57)	1.55 (1 in 65)	1.67 (1 in 60)	1.44 (1 in 69)
Zambia	0.75 (1 in 133)	0.89 (1 in 112)	0.66 (1 in 152)	0.49 (1 in 204)	0.65 (1 in 154)	0.38 (1 in 263)
Zimbabwe	2.01 (1 in 50)	2.35 (1 in 43)	1.77 (1 in 56)	1.55 (1 in 65)	1.85 (1 in 54)	1.34 (1 in 75)

Data source: cumulative risk of developing and dying from cancer (before age 85) were procured from GLOBOCAN 2018 and the odds were calculated using the CRC risk. Odds of developing and dying from CRC are presented inside parenthesis.

Table 5 Country-wise availability of screening modalities

Population	FOBT	Colonoscopy
Afghanistan	0	0
Albania	0	0
Algeria	0	0
Angola	ND	ND
Argentina	1	1
Armenia	1	0
Australia	1	1
Austria	1	1
Azerbaijan	1	0
Bahamas	1	0
Bahrain	1	1
Bangladesh	0	0
Barbados	1	1
Belarus	ND	ND
Belgium	1	1
Belize	1	1
Benin	0	0
Bhutan	0	1
Bolivia	1	0
Bosnia and Herzegovina	ND	ND
Botswana	0	0
Brazil	1	1
Brunei	1	1
Bulgaria	1	1
Burkina Faso	0	1
Burundi	0	0
Cabo Verde	ND	ND
Cambodia	0	DK
Cameroon	1	0
Canada	1	1
Central African Republic	0	0
Chad	ND	ND
Chile	1	1
China	1	1
Colombia	1	1
Comoros	1	0
Congo	0	1
Costa Rica	1	1
Côte d'Ivoire	0	0
Croatia	1	1
Cuba	1	1
Cyprus	1	1
Czechia	1	1
Democratic Republic of Congo	ND	ND
Denmark	1	1
Djibouti	0	0
Dominican Republic	1	0
Ecuador	1	0
Egypt	1	0
El Salvador	0	0
Equatorial Guinea	0	0
Eritrea	0	0
Estonia	1	0
Eswatini	0	0
Ethiopia	ND	ND
Fiji	1	1
Finland	1	1
France	1	1
France, Guadeloupe		
France, La Réunion		
France, Martinique		
France, New Caledonia		
French Guyana		
French Polynesia		
Gabon	1	1
Gambia	0	0
Gaza Strip and West Bank		
Georgia	0	0
Germany	1	1
Ghana	0	0
Greece	1	1
Guam		
Guatemala	0	0
Guinea	0	0
Guinea-Bissau	0	0
Guyana	ND	ND
Haiti	ND	ND
Honduras	0	0
Hungary	0	0
Iceland	1	0
India	0	0
Indonesia	0	0
Iran	1	1
Iraq	0	0
Ireland	1	1
Israel	1	1
Italy	1	1
Jamaica	1	1
Japan	1	1
Jordan	1	0
Kazakhstan	1	1
Kenya	0	0
Kuwait	0	0
Kyrgyzstan	0	0
Lao PDR	DK	1
Latvia	1	1
Lebanon	0	0
Lesotho	0	0

Table 5 (continued)

Population	FOBT	Colonoscopy
Liberia	0	0
Libya	0	0
Lithuania	1	1
Luxembourg	1	1
Macedonia FYR	1	1
Madagascar	0	0
Malawi	0	0
Malaysia	0	1
Maldives	0	0
Mali	0	0
Malta	1	1
Mauritania	0	0
Mauritius	ND	ND
Mexico	DK	DK
Moldova	1	1
Mongolia	0	0
Montenegro	0	0
Morocco	0	1
Mozambique	0	0
Myanmar	0	0
Namibia	1	DK
Nepal	0	0
Netherlands	0	0
New Zealand	1	0
Nicaragua	1	1
Niger	0	0
Nigeria	0	0
North Korea	0	0
Norway	1	1
Oman	1	1
Pakistan	0	0
Panama	1	0
Papua New Guinea	1	0
Paraguay	0	0
Peru	0	0
Philippines	0	0
Poland	1	1
Portugal	1	1
Puerto Rico		
Qatar	1	0
Romania	0	0
Russian Federation	1	1
Rwanda	0	0
Saint Lucia	1	1
Samoa	1	0
Sao Tome and Principe	0	0
Saudi Arabia	0	0
Senegal	0	1
Serbia	1	1

Table 5 (continued)

Population	FOBT	Colonoscopy
Sierra Leone	ND	ND
Singapore	1	1
Slovakia	1	1
Slovenia	1	1
Solomon Islands	0	0
Somalia	0	0
South Africa	ND	ND
South Korea	1	1
South Sudan	ND	ND
Spain	1	1
Sri Lanka	0	0
Sudan	0	0
Suriname	1	1
Sweden	1	1
Switzerland	1	1
Syrian Arab Republic	1	1
Tajikistan	NR	NR
Tanzania	ND	ND
Thailand	0	0
Timor-Leste	ND	ND
Togo	0	0
Trinidad and Tobago	1	1
Tunisia	0	0
Turkey	1	1
Turkmenistan	1	1
Uganda	0	0
Ukraine	0	0
United Arab Emirates	1	0
UK	1	0
USA	1	1
Uruguay	1	1
Uzbekistan	0	0
Vanuatu	0	0
Venezuela	1	1
Viet Nam	0	0
Yemen	0	0
Zambia	0	0
Zimbabwe	0	1

All the data is procured from WHO Cancer Country Profiles. The answer to the question on screening availability was coded as follows: generally available at the public primary healthcare level (1) and not generally available at the public primary health care level (0). Data was not available for the countries for which no entry is there in the table

DK do not know, *ND* county did not respond to WHO questionnaire, *NR* country responded to WHO survey but did not responded to particular question

References

1. Roth GA, Abate D, Abate KH, Abay SM, Abbafati C, Abbasi N, et al. Global, regional, and national age-sex-specific mortality for 282 causes of death in 195 countries and territories, 1980–2017: a systematic analysis for the Global Burden of Disease Study 2017. Lancet. 2018;392:1736–88.
2. Fitzmaurice C, Akinyemiju TF, Al Lami FH, Alam T, Alizadeh-Navaei R, Allen C, et al. Global, regional, and national cancer incidence, mortality, years of life lost, years lived with disability, and disability-adjusted life-years for 29 cancer groups, 1990 to 2016: a systematic analysis for the global burden of disease study. JAMA Oncol. 2018;4:1553–68.
3. Sung JJ, Lau JY, Goh KL, Leung WK. Increasing incidence of colorectal cancer in Asia: implications for screening. Lancet Oncol. 2005;6:871–6.
4. Allemani C, Matsuda T, Di Carlo V, Harewood R, Matz M, Nikšić M. Global surveillance of trends in cancer survival 2000–14 (CONCORD-3): analysis of individual records for 37 513 025 patients diagnosed with one of 18 cancers from 322 population-based registries in 71 countries. Lancet. 2018;391:1023–75.
5. Hamilton SR, Bosman FT, Boffetta P, et al. Carcinoma of the colon and rectum. In: In Bosman FT, Carneiro F, Hruban RH, Theise ND, editors. WHO classification of tumours of the digestive system. Lyon: IARC Press; 2010. p. 134–46.
6. Taylor DP, Burt RW, Williams MS, Haug PJ, Cannon–Albright LA. Population-based family history–specific risks for colorectal cancer: a constellation approach. Gastroenterology. 2010;138:877–885.
7. Bibbins-Domingo K, Grossman DC, Curry SJ, Davidson KW, Epling JW, García FA, et al. Screening for colorectal cancer: US Preventive Services Task Force recommendation statement. JAMA. 2016;315:2564–75.
8. Grech G, Zhan X, Yoo BC, Bubnov R, Hagan S, Danesi R, et al. EPMA position paper in cancer: current overview and future perspectives. EPMA J. 2015;6:9.
9. Golubnitschaja O, Baban B, Boniolo G, Wang W, Bubnov R, Kapalla M, et al. Medicine in the early twenty-first century: paradigm and anticipation - EPMA position paper 2016. EPMA J. 2016;7:23.
10. Janssens JP, Schuster K, Voss A. Preventive, predictive, and personalized medicine for effective and affordable cancer care. EPMA J. 2018;9:113–23.
11. Bray F, Ferlay J, Soerjomataram I, Siegel RL, Torre LA, Jemal A. Global cancer statistics 2018: GLOBOCAN estimates of incidence and mortality worldwide for 36 cancers in 185 countries. CA Cancer J Clin. 2018;68:394–424.
12. UNDP (2018). Human Development Indices and Indicators 2018 Statistical Update. Available at http://hdr.undp.org/sites/default/files/2018_human_development_statistical_update.pdf (Accessed: 3.5.2019).
13. Vostakolaei F, Karim-Kos HE, Janssen-Heijnen ML, Visser O, Verbeek AL, Kiemeney LA. The validity of the mortality to incidence ratio as a proxy for site-specific cancer survival. Eur J Pub Health. 2010;21:573–7.
14. Sunkara V, Hebert JR. The colorectal cancer mortality-to-incidence ratio as an indicator of global cancer screening and care. Cancer. 2015;121:1563–9.
15. Sharma R. Breast cancer incidence, mortality and mortality-to-incidence ratio (MIR) are associated with human development, 1990–2016: evidence from Global Burden of Disease Study 2016. Breast Cancer. 2019a;26:428–45.
16. Sharma R. The burden of prostate cancer is associated with human development index: evidence from 87 countries, 1990–2016. EPMA J. 2019b;10:137–52.
17. Ferlay J, Colombet M, Soerjomataram I, Mathers C, Parkin DM, Piñeros M, et al. Estimating the global cancer incidence and mortality in 2018: GLOBOCAN sources and methods. Int J Cancer. 2019;144:1941–53.
18. Ferlay J, Ervik M, Lam F, Colombet M, Mery L, Piñeros M et al (2018). Global Cancer Observatory. Lyon, France: International Agency for Research on Cancer. Available from: https://gco.iarc.fr/, accessed [01.05.2019].
19. Human Development Database: http://hdr.undp.org/en/data# (Accessed: 3.5.2019).
20. Arnold M, Sierra MS, Laversanne M, Soerjomataram I, Jemal A, Bray F. Global patterns and trends in colorectal cancer incidence and mortality. Gut. 2017;66:683–91.
21. Haggar FA, Boushey RP. Colorectal cancer epidemiology: incidence, mortality, survival, and risk factors. Clin Colon Rectal Surg. 2009;22:191–7.
22. Devesa SS, Chow WH. Variation in colorectal cancer incidence in the United States by subsite of origin. Cancer. 1993;71:3819–26.
23. Cheng X, Chen VW, Steele B, Ruiz B, Fulton J, Liu L, et al. Subsite-specific incidence rate and stage of disease in colorectal cancer by race, gender, and age group in the United States, 1992–1997. Cancer. 2001;92:2547–54.
24. Murphy G, Devesa SS, Cross AJ, Inskip PD, McGlynn KA, Cook MB. Sex disparities in colorectal cancer incidence by anatomic subsite, race and age. Int J Cancer. 2011;128:1668–75.
25. Atkin WS, Edwards R, Kralj-Hans I, Wooldrage K, Hart AR, Northover JM, et al. Once-only flexible sigmoidoscopy screening in prevention of colorectal cancer: a multicentre randomised controlled trial. Lancet. 2010;375:1624–33.
26. Segnan N, Armaroli P, Bonelli L, Risio M, Sciallero S, Zappa M, et al. Once-only sigmoidoscopy in colorectal cancer screening: follow-up findings of the Italian Randomized Controlled Trial—SCORE. J Natl Cancer Inst. 2011;103:1310–22.
27. Schoen RE, Pinsky PF, Weissfeld JL, Yokochi LA, Church T, Laiyemo AO, et al. Colorectal-cancer incidence and mortality with screening flexible sigmoidoscopy. N Engl J Med. 2012;366:2345–57.
28. Holme Ø, Bretthauer M, Fretheim A, Odgaard-Jensen J, Hoff G. Flexible sigmoidoscopy versus faecal occult blood testing for colorectal cancer screening in asymptomatic individuals. Cochrane Database Syst Rev. 2013;9:CD0009259
29. Holme Ø, Løberg M, Kalager M, Bretthauer M, Hernán MA, Aas E, et al. Effect of flexible sigmoidoscopy screening on colorectal cancer incidence and mortality: a randomized clinical trial. JAMA. 2014;312:606–15.
30. Schreuders EH, Ruco A, Rabeneck L, Schoen RE, Sung JJ, Young GP, et al. Colorectal cancer screening: a global overview of existing programmes. Gut. 2015;64:1637–49.
31. Shapiro JA, Klabunde CN, Thompson TD, Nadel MR, Seeff LC, White A. Patterns of colorectal cancer test use, including CT colonography, in the 2010 National Health Interview Survey. Cancer Epidemiol Biomark Prev. 2012;21:895–904.
32. Decker KM, Singh H. Reducing inequalities in colorectal cancer screening in North America. J Carcinog. 2014;13:12.
33. Fedirko V, Tramacere I, Bagnardi V, Rota M, Scotti L, Islami F. Alcohol drinking and colorectal cancer risk: an overall and dose–response meta-analysis of published studies. Ann Oncol. 2011;22:1958–72.
34. Botteri E, Iodice S, Bagnardi V, Raimondi S, Lowenfels AB, Maisonneuve P. Smoking and colorectal cancer: a meta-analysis. JAMA. 2008;300:2765–78.
35. Demeyer D, Mertens B, De Smet S, Ulens M. Mechanisms linking colorectal cancer to the consumption of (processed) red meat: a review. Crit Rev Food Sci Nutr. 2016;56:2747–66.
36. Bardou M, Barkun AN, Martel M. Obesity and colorectal cancer. Gut. 2013;62:933–47.

37. Moghaddam AA, Woodward M, Huxley R. Obesity and risk of colorectal cancer: a meta-analysis of 31 studies with 70,000 events. Cancer Epidemiol Biomark Prev. 2007;16:2533–47.
38. Peeters PJ, Bazelier MT, Leufkens HG, de Vries F, De Bruin ML. The risk of colorectal cancer in patients with type 2 diabetes: associations with treatment stage and obesity. Diabetes Care. 2015;38:495–502.
39. Terry P, Giovannucci E, Michels KB, Bergkvist L, Hansen H, Holmberg L, et al. Fruit, vegetables, dietary fiber, and risk of colorectal cancer. J Natl Cancer Inst. 2001;93:525–33.
40. Van Duijnhoven FJ, Bueno-De-Mesquita HB, Ferrari P, Jenab M, Boshuizen HC, Ros MM, et al. Fruit, vegetables, and colorectal cancer risk: the European Prospective Investigation into Cancer and Nutrition. Am J Clin Nutr. 2009;89:1441–52.
41. Huxley RR, Ansary-Moghaddam A, Clifton P, Czernichow S, Parr CL, Woodward M. The impact of dietary and lifestyle risk factors on risk of colorectal cancer: a quantitative overview of the epidemiological evidence. Int J Cancer. 2009;125:171–80.
42. Rothwell PM, Wilson M, Elwin CE, Norrving B, Algra A, Warlow CP, et al. Long-term effect of aspirin on colorectal cancer incidence and mortality: 20-year follow-up of five randomised trials. Lancet. 2010;376:1741–50.
43. Rothwell PM, Fowkes FG, Belch JF, Ogawa H, Warlow CP, Meade TW. Effect of daily aspirin on long-term risk of death due to cancer: analysis of individual patient data from randomised trials. Lancet. 2011;377:31–41.
44. Burn J, Gerdes AM, Macrae F, Mecklin JP, Moeslein G, Olschwang S, et al. Long-term effect of aspirin on cancer risk in carriers of hereditary colorectal cancer: an analysis from the CAPP2 randomised controlled trial. Lancet. 2011;378:2081–7.
45. Chubak J, Kamineni A, Buist DSM, Anderson ML & Whitlock EP (2015) Aspirin use for the prevention of colorectal cancer: an updated systematic evidence review for the U.S. Preventive Services Task Force (Agency for Healthcare Research and Quality (US), 2015).
46. Gonzalez CA, Riboli E. Diet and cancer prevention: contributions from the European Prospective Investigation into Cancer and Nutrition (EPIC) study. Eur J Cancer. 2010;46:2555–62.
47. Thirunavukarasu P, Sukumar S, Sathaiah M, Mahan M, Pragatheeshwar KD, Pingpank JF, et al. C-stage in colon cancer: implications of carcinoembryonic antigen biomarker in staging, prognosis, and management. J Natl Cancer Inst. 2011;103:689–97.
48. Nikolaou S, Qiu S, Fiorentino F, Rasheed S, Tekkis P, Kontovounisios C. The prognostic and therapeutic role of hormones in colorectal cancer: a review. Mol Biol Rep. 2019:461477–86.
49. Sullivan R, Alatise OI, Anderson BO, Audisio R, Autier P, Aggarwal A, et al. Global cancer surgery: delivering safe, affordable, and timely cancer surgery. Lancet Oncol. 2015;16:1193–224.
50. Lu M, Zhan X. The crucial role of multiomic approach in cancer research and clinically relevant outcomes. EPMA J. 2018;9:77–102.
51. Horgan RP, Kenny LC. 'Omic' technologies: genomics, transcriptomics, proteomics and metabolomics. Obstet Gynaecol. 2011;13:189–95.
52. Golubnitschaja O, Kinkorova J, Costigliola V. Predictive, preventive and personalized medicine as the hardcore of 'Horizon 2020': EPMA position paper. EPMA J. 2014;5:6.

Publisher's note Springer Nature remains neutral with regard to jurisdictional claims in published maps and institutional affiliations.

Neuropeptides xxx (xxxx) xxxx

Contents lists available at ScienceDirect

Neuropeptides

journal homepage: www.elsevier.com/locate/npep

Aβ, Tau, and α-Synuclein aggregation and integrated role of PARK2 in the regulation and clearance of toxic peptides

Dhiraj Kumar, Pravir Kumar*

Molecular Neuroscience and Functional Genomics Laboratory, Delhi Technological University, Shahbad Daulatpur, Bawana Road, Delhi 110042, India

ARTICLE INFO

Keywords:
Amyloid-beta (Aβ)
Tau
Alpha-Synuclein
Alzheimer's disease (AD)
Parkinson's disease (PD)
Crosstalk
Ubiquitination

ABSTRACT

Alzheimer's and Parkinson's diseases are one of the world's leading causes of death. > 50 million people throughout the world are suffering with these diseases. They are two distinct progressive neurodegenerative disorders affecting different regions of the brain with diverse symptoms, including memory and motor loss respectively, but with the advancement of diseases, both affect the whole brain and exhibit some common biological symptoms. For instance, > 50% PD patients develop dementia in their later stages, though it is a hallmark of Alzheimer's disease. In fact, latest research has suggested the involvement of some common pathophysiological and genetic links between these diseases, including the deposition of pathological Aβ, Tau, and α-synuclein in both the cases. Therefore, it is pertinent to diagnose the shared biomarkers, their aggregation mechanism, their intricate relationships in the pathophysiology of disease and therapeutic markers to target them. This would enable us to identify novel markers for the early detection of disease and targets for the future therapies. Herein, we investigated molecular aspects of Aβ, Tau, and α-Synuclein aggregation, and characterized their functional partners involved in the pathology of AD and PD. Moreover, we identified the molecular-crosstalk between AD and PD associated with their pathogenic proteins- Aβ, Tau, and α-Synuclein. Furthermore, we characterized their ubiquitinational enzymes and associated interaction network regulating the proteasomal clearance of these pathological proteins.

1. Introduction

The aggregation of certain misfolded proteins is the chief pathogenic event that evokes neurotoxicity in many neurodegenerative disorders like Alzheimer's and Parkinson's disease (Jellinger, 2010). The major structural changes that take place are the rise in β-sheet conformation in misfolded protein that promotes oligomerization and amyloid like fibril formation (Relini et al., 2013). Moreover, the aggregation mechanism involves a crucial step of seed-nucleus formation, where the monomers form a smallest aggregate, termed as 'nucleus' that grows faster by the addition of monomers in comparison to its dissociation back into smaller aggregates and free monomers. The primary nucleation event that triggers the oligomer formation is followed by the secondary nucleation events, where a nucleus formation on the surface of previously existing aggregate, direct a fast increase in the number of oligomers. Then, they attain a fibrillar form known as "fibrillar oligomers" and result into a fibril formation, i.e. seed, which leads to a rapid generation of new fibrils with same morphology and chirality (Linse, 2019). These oligomeric forms are more toxic and can be targeted by certain oligomer eliminating compounds (Dunkelmann et al., 2018). Thus, the seed-nucleation phenomenon governs a series of misfolding, and protein-protein interaction events that exaggerate the protein aggregation process (Breydo and Uversky, 2014). Consequently, aggregated proteins become resistant to proteolysis and cellular clearance that cause chronic endoplasmic reticulum stress, mitochondrial dysfunction, reactive oxygen species formation, intense tissue inflammation and activation of apoptotic pathways leading to the neuronal loss (Rutkowski and Kaufman, 2004; Morimoto, 2008).

Although AD and PD exhibit heterogeneity at the genetic and clinical level which is affecting different regions of the brain, including acetyl-cholinergic neurons in hippocampus and dopaminergic neurons in *substantia nigra pars compacta*. Recent studies revealed significant similarity in their overlapping role of pathological proteins, including amyloid-beta, tau protein, and α-synuclein and suggestive familial link in their pathogenesis (Jellinger, 2012). For instance, above 50% of patients, suffering from AD revealed amyloid like alpha-synuclein peptide aggregates (Marsh and Blurton-Jones, 2012) while PD patients displayed frequent tau deposits (Lei et al., 2010). In addition, it has

* Corresponding author at: Molecular Neuroscience and Functional Genomics Laboratory, Department of Biotechnology, Delhi Technological University (Formerly Delhi College of Engineering), Room # FW4TF3, Mechanical Engineering Building, Shahbad Daulatpur, Bawana Road, Delhi 110042, India.
E-mail address: pravirkumar@dtu.ac.in (P. Kumar).

https://doi.org/10.1016/j.npep.2019.101971
Received 3 July 2019; Received in revised form 9 September 2019; Accepted 11 September 2019
0143-4179/ © 2019 Elsevier Ltd. All rights reserved.

Please cite this article as: Dhiraj Kumar and Pravir Kumar, Neuropeptides, https://doi.org/10.1016/j.npep.2019.101971

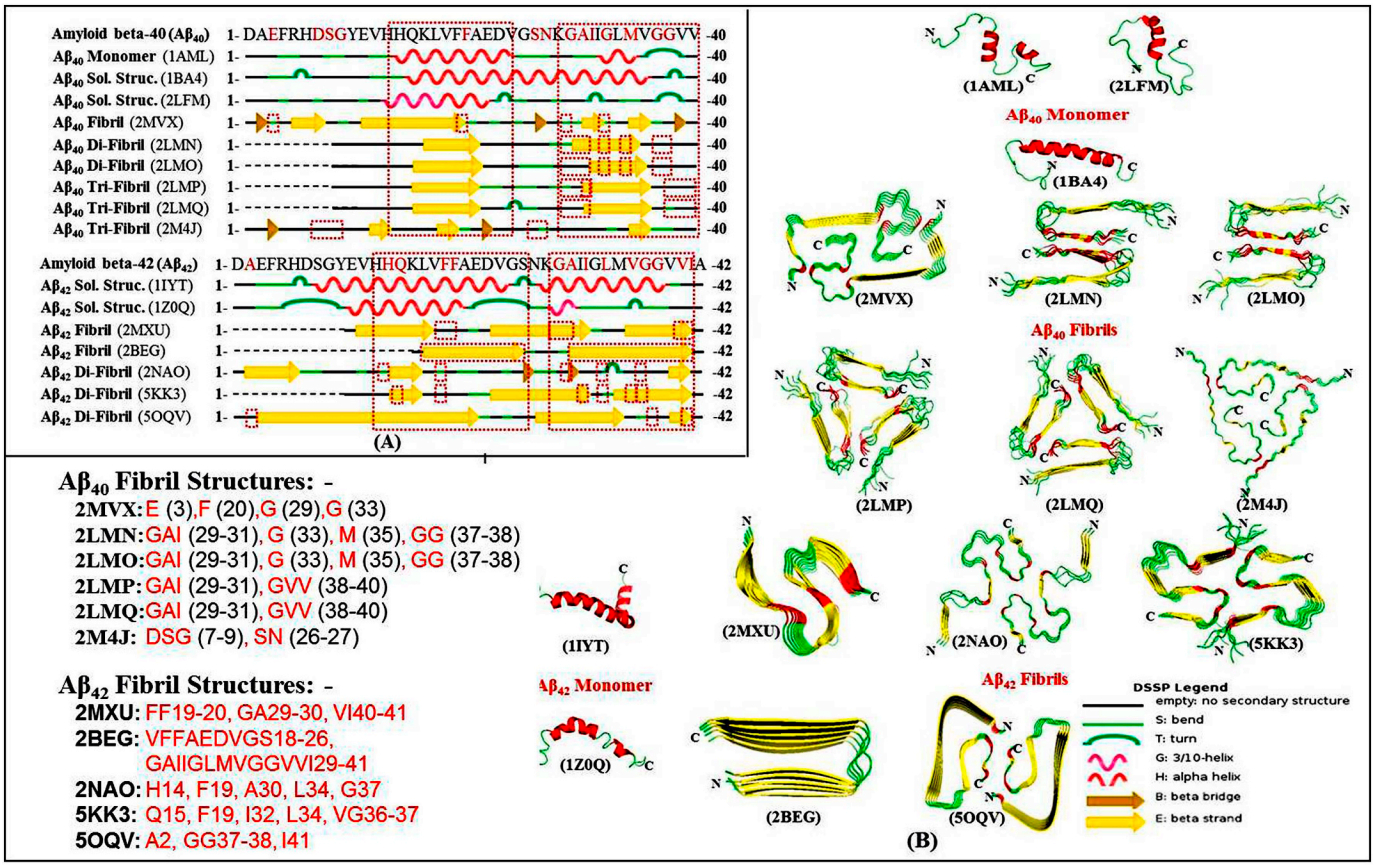

Fig. 1. Molecular basis of Amyloid beta peptide aggregation- (A) Structural changes in $A\beta_{40}/A\beta_{42}$ pathology: Helical conformation of amyloid-beta peptide gets distorted into the fibril structure rich in beta-strands and few beta-bridges. Polypeptide regions, including HQKLVFFAEDV (14-24) and GAIIGLMVGGVV (29-40) are responsible for the intra- and intermolecular fibril formation and consequent aggregation of $A\beta_{40}$ peptides. Similarly, HQKLVFFAEDVGS (14-26) and GAIIGLMVGGVVI (29-41) regions are responsible for intra- and intermolecular fibril formation and consequent aggregation of $A\beta_{42}$ peptides. Moreover, fibril-forming peptides are highlighted in red color, fibril-specific aggregation regions with red rectangles that presented the sequence motif responsible for aggregation of amyloid beta peptide. (B) 3D Structure of $A\beta_{40}/A\beta_{42}$ peptides: Aβ40 monomers (1AML, 2LFM, 1BA4) and Aβ42 monomers (1IYT, 1Z0Q) are shown in its cartoon view with aggregation prone region highlighted in red. The reported $A\beta_{40}/A\beta_{42}$ fibrils are shown in cartoon view with their aggregation prone regions in red color respectively. (2MVX: E3, F20, G29, G33; 2LMN: GAI29-31, G33, M35, GG37-38; 2LMO: GAI29-31, G33, M35, GG37-38; 2LMP: GAI29-31, GVV38-40; 2LMQ: GAI29-31, GVV38-40; 2M4J: DSG7-9, SN26-27/ 2MXU: FF19-20, GA29-30, VI40-41; 2BEG: VFFAEDVGS18-26, GAIIGLMVGGVVI29-41; 2NAO: H14, F19, A30, L34, G37; 5KK3: Q15, F19, I32, L34, VG36-37, 5OQV: A2, GG37-38, I41). (For interpretation of the references to color in this figure legend, the reader is referred to the web version of this article.)

demonstrated that the accumulation of tau proteins could take place with the help of specific strains of alpha-synuclein (Guo et al., 2013). Another study identified that Aβ Seeding escalates the formation of big sized α-synuclein oligomers that efficiently hampered neuronal SNARE-mediated vesicle fusion at synaptic junctions (Choi et al., 2015). Apart from proteinopathic similarities, some recent breakthroughs suggested a possible genetic link between these diseases in their advanced stages (Bailey et al., 2013; Singleton and Hardy, 2016; Ibanez et al., 2018; Zeng et al., 2018). For instance, LRRK2 mutant G2019S mediated phosphorylation of AβPP at T668, promoted APP intracellular domain's (AICD) nuclear translocation and consequent neurotoxicity in PD (Zeng et al., 2018). Likewise, LRRK2 is reported to directly phosphorylate tau at T149 and T153 signifying their interaction in a disease relevant manner (Bailey et al., 2013). Another study identified pathogenic mutations in AD causing genes- PSEN1 and PSEN2 in sporadic PD patients (Ibanez et al., 2018). Therefore, future research is required to establish well-defined pathological links between them.

However, these pathogenic proteins differ in their structural and functional biology, but they may share their protein-misfolding events and interact together to aggravate the disease symptoms (Barage and Sonawane, 2015; Cuanalo-Contreras et al., 2013). Moreover, they also interact with other ubiquitinational markers to relieve the proteotoxic burden inside neurons, via refolding or targeting proteins to ubiquitin proteasome system for degradation (Ciechanover and Kwon, 2015). Such a crucial ubiquitinational marker is PARK2, which is found to govern the proteasomal clearance of a wide range of substrates belonging to the nuclear proteins, cytoskeleton proteins, cell cycle regulators, heat shock proteins, neurotransmitters, and the cell signaling proteins. Some of these substrates include ataxin, Bcl-2, cyclin E, dopamine transporter, Hsp70, α-synuclein, synphilin-1, and α/β tubulin that regulates a variety of functions in different neurodegenerative disorders (Zhang et al., 2016). For instance, PARK2 regulates mitochondrial trafficking, endosomal sorting, synaptic transmission, programmed necrosis, ER stress, inflammation and cellular homeostasis. (Choong and Mochizuki, 2017; Sassone et al., 2017; Singh et al., 2018; Williams et al., 2018; Sun et al., 2019). Altogether, these findings highlight the need for a clear understanding of precise molecular mechanism behind pathogenic protein aggregation and clearance, and their interaction with other proteins to devise better diagnostic and treatment options for such neurodegenerative disorders.

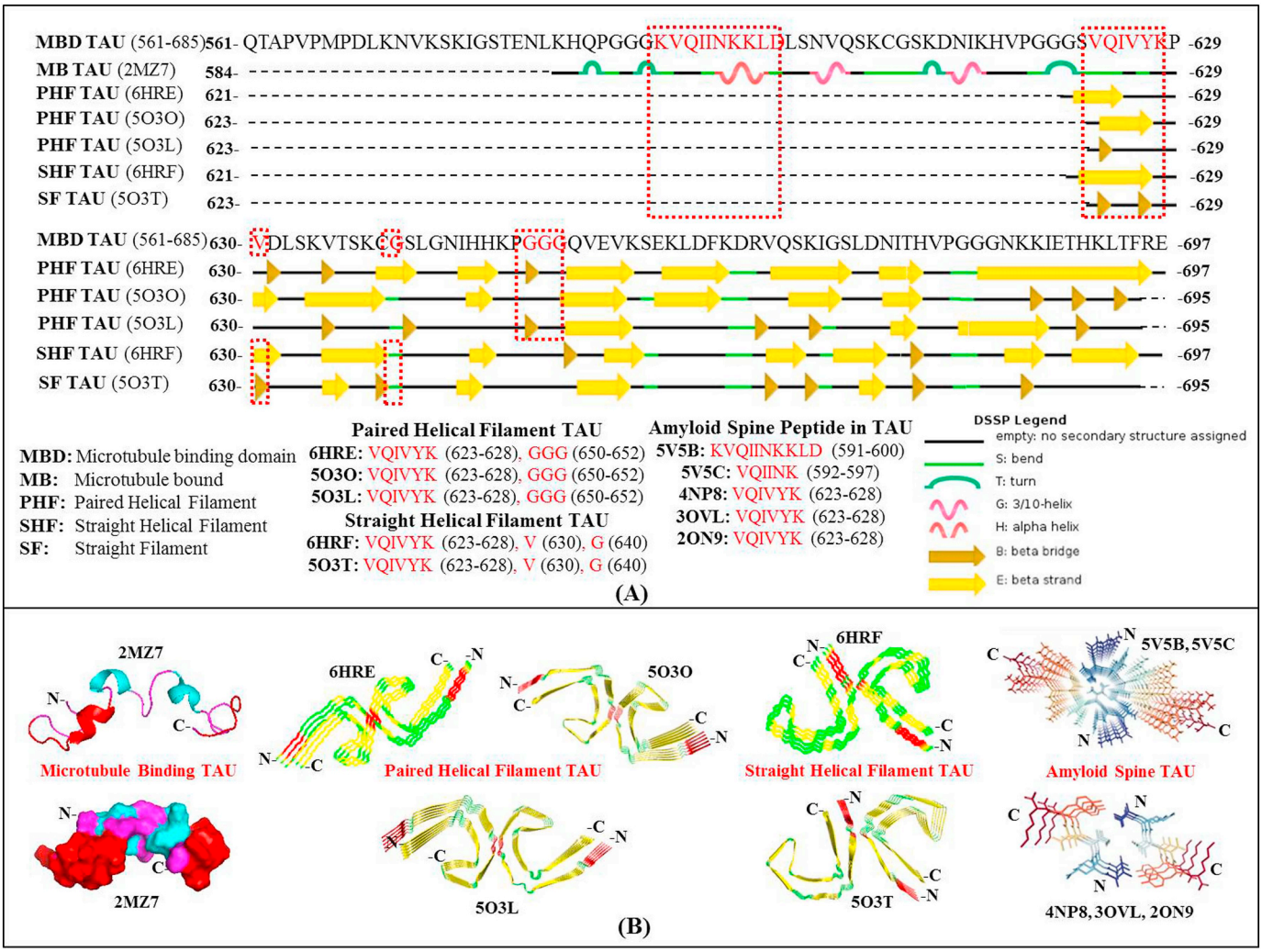

Fig. 2. Molecular basis of TAU protein aggregation- (A) Structural changes in TAU pathology: Helical conformation of microtubule binding domain is distorted into the filament structure (paired helical/ straight helical/ straight) rich in beta-strands and beta-bridges. Tripeptide glycine (650–652; Red) is responsible for paired-helical filament while valine (630; Red) and glycine (640; Red) are accountable for straight helical filament formation and consequent aggregation. Moreover, amyloid spines forming peptides are highlighted in red color that showed the sequence motif VQI(IN)/(VY)K responsible for aggregation of TAU protein in Alzheimer's disease. (B) 3D Structure of TAU protein: Microtubule binding domain of TAU (2MZ7) is shown in its cartoon and surface view with the aggregation-prone region highlighted in red. Paired-helical filaments of TAU (6HRE, 5O3O, 5O3L) reported in AD are shown in ribbon/cartoon view with their aggregation-prone regions in red color. Likewise, Straight-helical filaments of TAU (6HRF, 5O3T) reported in AD are shown in ribbon/cartoon view with their aggregation prone regions in red color. Furthermore, amyloid-spine forming TAU peptide models KVQIINKKLD and VQIVYK are shown in Licorice view that formed amyloid aggregate with help of interactions between valine and Isoleucine. (For interpretation of the references to color in this figure legend, the reader is referred to the web version of this article.)

2. Material and methods

2.1. Investigation of the molecular basis of Aβ$_{40/42}$, Tau, and α-Synuclein aggregation

The present sequences for the neurotoxic proteins were analysed for their secondary structures, and their available monomer and fibrillar structures were annotated for their hydrophobic residues responsible for aggregation.

2.1.1. Structural determination of Aβ$_{40/42}$, Tau, and α-Synuclein

The peptide sequence of Aβ$_{40/42}$, Tau and α-Synuclein were obtained from protein data bank (RCSB PDB: www.rcsb.org; Berman et al., 2000) and processed for the determination of its secondary structure by Dictionary of protein secondary structure (DSSP) database (Touw et al., 2015).

2.1.2. Macromolecular structure design and hydrophobicity annotation

The macromolecular monomeric and fibrillar structures of Aβ$_{40/42}$, Tau, and α-Synuclein proteins have been analysed for the hydrophobic or aggregation prone residues. These sites were annotated to the available 3D-structures with help of NGL viewer (http://proteinformatics.charite.de/ngl) (Rose and Hildebrand, 2015) and Pymol software (DeLano, 2002).

2.2. Characterization of the functional partners of Aβ$_{40/42}$, Tau, and α-Synuclein involved in the pathology of Alzheimer's and Parkinson's disease

The top interacting partners of the neurotoxic proteins have predicted and analysed for their role in disease pathogenesis.

2.2.1. Prediction of interacting partners of AβPP, Tau, and α-Synuclein

The interacting partners of AβPP, Tau, and α-Synuclein was determined by functional protein association networks tool called STRING, online available at https://string-db.org/. The top interactors

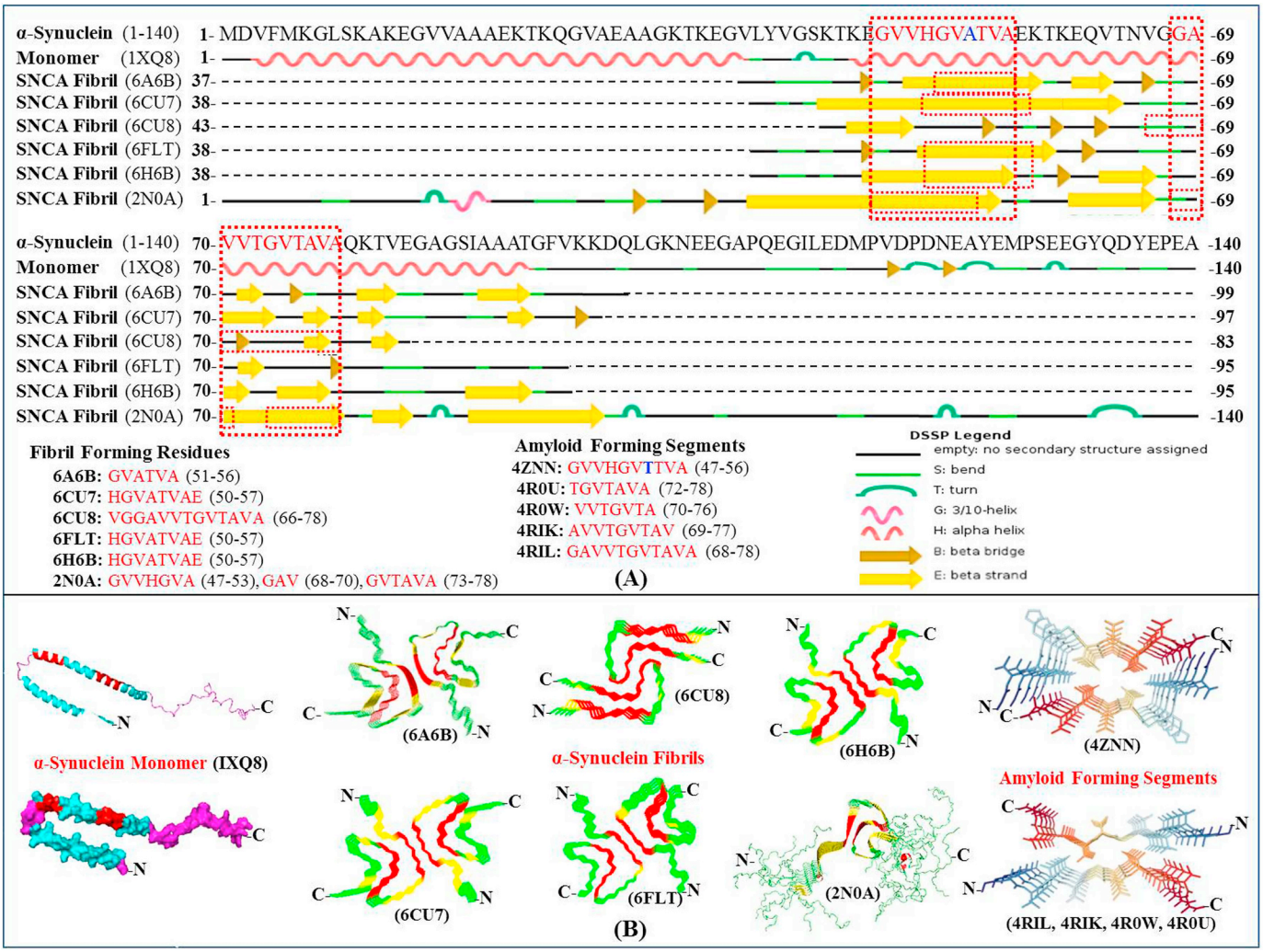

Fig. 3. Molecular basis of α-Synuclein protein aggregation- (A) Structural changes in α-Synuclein pathology: Helical conformations of synuclein monomer are distorted into the fibril structure rich in beta-strands and beta-bridges. Polypeptide regions, including GVVHGVATVAE (47-57) and GAVVTGVTAVA (68-78) are responsible for the intra- and intermolecular fibril formation and consequent aggregation of SNCA protein. Moreover, amyloid forming peptides are highlighted in red color that showed the sequence motif accountable for aggregation of SNCA protein in Alzheimer's disease. Moreover, the fibril-specific aggregation regions are shown with green rectangles. (B) 3D Structure of α-Synuclein protein: SNCA monomer (IXQ8) is shown in its cartoon and surface view with aggregation prone region highlighted in red. Reported alpha synuclein fibrils (6A6B, 6CU7, 6CU8, 6FLT, 6H6B, 2N0A) are shown in ribbon/cartoon view with their aggregation-prone regions in red color. Likewise, Straight helical filaments of TAU (6HRF, 5O3T) reported in AD are shown in ribbon/cartoon view with their aggregation prone regions in red color. Furthermore, amyloid-forming peptide models 4ZNN and 4RIL is shown in Licorice view that formed amyloid aggregate with help of interactions between their intermittent residues, glycine and valine. (For interpretation of the references to color in this figure legend, the reader is referred to the web version of this article.)

were identified with high confidence at the threshold of interaction score ≥ 0.700, and the network were generated without clustering and evidence based upon text mining, experiments, databases, co-expression, neighborhood, gene fusion and co-occurrence (Jensen et al., 2009).

2.2.2. *Protein interaction network analysis for Alzheimer's and Parkinson's disease*

Top hundred interacting partners of the AβPP, Tau, and α-Synuclein proteins were mapped on the pathways for Alzheimer's and Parkinson's disease from KEGG Pathways database and analysed for their functional association with the disease pathogenesis (Kanehisa et al., 2017).

2.3. *Investigation of the molecular crosstalk between AD and PD*

The combined AD and PD-related top-interactions of AβPP, Tau, and α-Synuclein was iterated for their interactions with another top hundred interacting partner. Those proteins that qualified their AD and PD incidence were selected and identified for their interactions with AβPP, Tau, and α-Synuclein at a high confidence threshold ≥0.7 with STRING tool, i.e. a Search Tool for the Retrieval of Interacting Genes/Proteins based on the evidence from text mining, experiments, databases, co-expression, neighborhood, gene fusion and co-occurrence (Szklarczyk et al., 2015). The interacting partner's prediction was followed by the Venn diagram analysis. Thus, the obtained proteins common to both Alzheimer's and Parkinson's disease, and were interacting with AβPP, Tau, and α-Synuclein, were screened as the key marker for AD-PD crosstalk.

2.4. *Identification of ubiquitination enzymes regulating the clearance of $A\beta_{40/42}$, Tau, and α-Synuclein*

The potential ubiquitination enzymes regulating the biology of Aβ, AβPP, Tau, and α-Synuclein proteasomal clearances were identified by determining the interaction among all the ubiquitin E1-activating enzymes, E2-conjugating enzymes, E3-ligating enzymes and deubiquitinating enzymes with AD-PD crosstalk proteins- AβPP, CAPN1, GSK3B, LRRK2, MAPT, PARK2, PLCB2, SNCA, and UBB at different confidences.

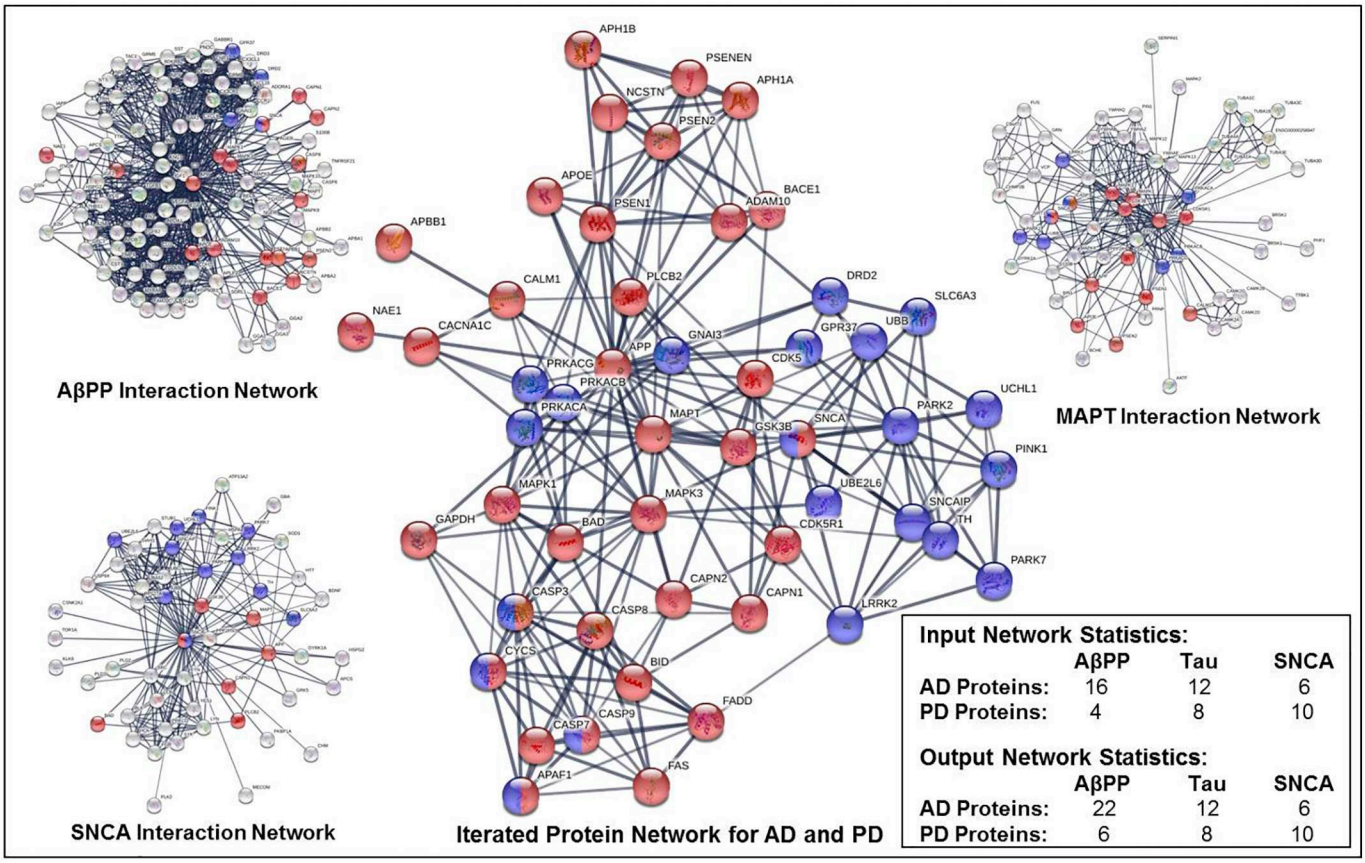

Fig. 4. Functional association network of AβPP, Tau and α-Synuclein interacting-proteins in AD and PD- The prime 100 amyloid-beta precursor interactor input proteins involved 16 AD-related proteins- ADAM10, APBB1, APOE, BACE1, CAPN1, CAPN2, CASP8, GAPDH, MAPK1, MAPK3, MAPT, NAE1, NCSTN, PSEN1, PSEN2, SNCA and 4 PD-related proteins- DRD2, GNAI3, GPR37, SNCA. Similarly, top 100 tau interactor input proteins involved 12 AD-related proteins- APOE, APP, CALM1, CASP3, CDK5, CDK5R1, GSK3B, MAPK1, MAPK3, PSEN1, PSEN2, SNCA and 8 PD-related proteins- CASP3, LRRK2, PRKACA, PRKACB, PRKACG, SNCA, PARK2, UBB. Likewise, leading 100 α-Synuclein interactor input proteins involved 6 AD-related proteins- APP, BAD, CAPN1, GSK3B, MAPT, PLCB2 and 10 PD-related proteins- LRRK2, PARK2, PARK7, PINK1, SLC6A3, SNCAIP, TH, UBB, UBE2L6, UCHL1. Moreover, the top 100 iterated interaction network of AβPP, Tau, and α-Synuclein involved the following proteins. (ADAM10-Disintegrin and metalloproteinase domain-containing protein 10; APBB1-Amyloid-beta A4 precursor protein-binding family B member 1; APH1A-Gamma-secretase subunit APH-1A; APOE-Apolipoprotein E; BACE1-Beta-secretase 1; BAD-Bcl2-associated agonist of cell death; CALM1-Calmodulin-1; CAPN1-Calpain-1 catalytic subunit; CAPN2-Calpain-2 catalytic subunit; CASP3-Caspase-3; CDK5-Cyclin-dependent-like kinase 5; CDK5R1-Cyclin-dependent kinase 5 activator 1; DRD2-D(2) dopamine receptor; GAPDH-Glyceraldehyde-3-phosphate dehydrogenase; GNAI3-Guanine nucleotide-binding protein G(k) subunit alpha; GPR37-Prosaposin receptor GPR37; GSK3B-Glycogen synthase kinase-3 beta; LRRK2-Leucine-rich repeat serine/threonine-protein kinase 2; MAPK1-Mitogen-activated protein kinase 1; MAPK3-Mitogen-activated protein kinase 3; MAPT-Microtubule-associated protein tau; NAE1-NEDD8-activating enzyme E1 regulatory subunit; NCSTN-Nicastrin; PARK2-E3 ubiquitin-protein ligase parkin; PARK7-Protein/nucleic acid deglycase DJ-1; PINK1-Serine/threonine-protein kinase PINK1; PLCB2-1-phosphatidylinositol 4;5-bisphosphate phosphodiesterase beta-2; PRKACA-cAMP-dependent protein kinase catalytic subunit alpha; PRKACB-cAMP-dependent protein kinase catalytic subunit beta; PRKACG-cAMP-dependent protein kinase catalytic subunit gamma; PSEN1-Presenilin-1; PSEN2-Presenilin-2; PSENEN-Gamma-secretase subunit PEN-2; SLC6A3-Sodium-dependent dopamine transporter; SNCAIP-Synphilin-1; TH-Tyrosine 3-monooxygenase; UBB-Polyubiquitin-B; UBE2L6-Ubiquitin/ISG15-conjugating enzyme E2 L6; UCHL1-Ubiquitin carboxyl-terminal hydrolase isozyme L1.)

Furthermore, the protein-protein interactional network among the identified proteins was designed by functional protein-association network prediction STRING tool (Szklarczyk et al., 2015).

2.5. Functional annotation of the AD-PD cross-talk and ubiquitination markers

The analysis of the biological processes, reactome pathways, molecular functions, and the protein domains of the predicted AD-PD cross talk markers and the UPS enzymes- E1s, E2s, E3s, and DUBs were performed with the help of a functional enrichment analysis tool "FunRich" version 3.1.3 (Pathan et al., 2015). It is a tool for the enrichment and interaction network analysis of genes and proteins based on data mining from the available databases, including FunRich, Uniprot, Reactome and Custom. The Unirot and reactome databases have been explored to obtain the best scoring results at very high significant *P* value, i.e. $P < .001$.

3. Results

3.1. Hydrophobic interactions are the basis of neurotoxic protein aggregation

The pathological peptides and proteins, including $A\beta_{40}$, $A\beta_{42}$, Tau, and α-synuclein in AD and PD were studied for their aggregation sites to analyze the protein folding dynamics in its diseased state. The analysis of their secondary structures revealed the transformation of their helical conformations into beta strands from their monomer to fibrillar state respectively. However, their tertiary structures have revealed the presence of crucial hydrophobic sites responsible for their intra- and inter-molecular interactions governing protein aggregation.

3.1.1. Amyloid beta peptide

The amyloid peptide existed in the two common isoforms in the brain, including $A\beta_{40}$ and $A\beta_{42}$ responsible for the senile plaques in

Table 1
Interacting partners of AβPP, Tau and α-Synuclein proteins and their corresponding functions.

Interacting proteins		Molecular functions
ADAM10	Disintegrin and metalloproteinase domain-containing protein 10	Responsible for the proteolytic release of TNF-alpha and several other cell-surface proteins, including heparin-binding epidermal growth-like factor, ephrin-A2, CD44, CDH2 and for constitutive and regulated alpha-secretase cleavage of amyloid precursor protein (APP)
APBB1	Amyloid-beta A4 precursor protein-binding family B member 1	Transcription coregulator with both coactivator and corepressor functions that forms a transcriptionally active complex with the gamma-secretase-derived amyloid precursor protein (APP) intracellular domain play a role in DNA damage response
APH1A	Gamma-secretase subunit APH-1A	Endoprotease complex that catalyzes the intramembrane cleavage of integral membrane proteins such as Notch receptors and APP
APOE	Apolipoprotein E	Mediates the binding, internalization, and catabolism of lipoprotein particles
BACE1	Beta-secretase 1	Responsible for the proteolytic processing of the amyloid precursor protein (APP)
BAD	Bcl2-associated agonist of cell death	Promotes cell death and appears to act as a link between growth factor receptor signaling and the apoptotic pathways
CALM1	Calmodulin-1	Mediates the control of a large number of enzymes, ion channels, aquaporins and other proteins through calcium-binding
CAPN1	Calpain-1 catalytic subunit	Catalyzes limited proteolysis of substrates involved in cytoskeletal remodeling and signal transduction
CAPN2	Calpain-2 catalytic subunit	Catalyzes limited proteolysis of substrates involved in cytoskeletal remodeling and signal transduction
CASP3	Caspase-3	Involved in the activation cascade of caspases responsible for apoptosis execution
CDK5	Cyclin-dependent-like kinase 5	Essential for neuronal cell cycle arrest and differentiation and may be involved in apoptotic cell death in neuronal diseases by triggering abortive cell cycle re-entry
CDK5R1	Cyclin-dependent kinase 5 activator 1	Neuron specific activator of CDK5 involved in dendritic spine morphogenesis and required for neurite outgrowth and cortical lamination
DRD2	D(2) dopamine receptor	Dopamine receptor whose activity is mediated by G proteins which inhibit adenylyl cyclase and promote cell proliferation
GAPDH	Glyceraldehyde-3-phosphate dehydrogenase	Play a role in glycolysis and nuclear functions via participating in transcription, RNA transport, DNA replication and apoptosis
GNAI3	Guanine nucleotide-binding protein G(k) subunit alpha	Function as transducers downstream of G protein-coupled receptors (GPCRs) in numerous signaling cascades
GPR37	Prosaposin receptor GPR37	Receptor for the neuroprotective and glioprotective factor prosaposin where ligand binding induces endocytosis, followed by an ERK phosphorylation cascade
GSK3B	Glycogen synthase kinase-3 beta	Acts as a negative regulator in the hormonal control of glucose homeostasis, Wnt signaling and regulation of transcription factors and microtubules
LRRK2	Leucine-rich repeat serine/threonine-protein kinase 2	Positively regulates autophagy through a calcium- dependent activation of the CaMKK/AMPK signaling pathway
MAPK1	Mitogen-activated protein kinase 1	Acts as an essential component of the MAP kinase signal transduction pathway and mediates diverse biological functions such as cell growth, adhesion, survival and differentiation through the regulation of transcription, translation, cytoskeletal rearrangements
MAPK3	Mitogen-activated protein kinase 3	Acts as an essential component of the MAP kinase signal transduction pathway and mediates diverse biological functions such as cell growth, adhesion, survival and differentiation through the regulation of transcription, translation, cytoskeletal rearrangements
NAE1	NEDD8-activating enzyme E1 regulatory subunit	Regulatory subunit of the dimeric UBA3-NAE1 E1 enzyme
NCSTN	Nicastrin	Catalyzes the intramembrane cleavage of integral membrane proteins such as Notch receptors and APP (amyloid-beta precursor protein)
PARK2	E3 ubiquitin-protein ligase parkin	Functions within a multiprotein E3 ubiquitin ligase complex, catalyzing the covalent attachment of ubiquitin moieties onto substrate proteins
PARK7	Protein/nucleic acid deglycase DJ-1	Catalyzes the deglycation of the Maillard adducts formed between amino groups of proteins or nucleotides and reactive carbonyl groups of glyoxals and functions as a protein deglycase that repairs methylglyoxal- and glyoxal-glycated proteins, and releases repaired proteins and lactate or glycolate, respectively
PINK1	Serine/threonine-protein kinase PINK1	Protects against mitochondrial dysfunction during cellular stress by phosphorylating mitochondrial proteins and triggering selective autophagy (mitophagy) by mediating activation and translocation of Parkin
PLCB2	1-phosphatidylinositol 4;5-bisphosphate phosphodiesterase beta-2	Involved in the production of the second messenger molecules diacylglycerol (DAG) and inositol 1,4,5-trisphosphate (IP3)
PRKACA	cAMP-dependent protein kinase catalytic subunit alpha	Phosphorylates a large number of substrates in the cytoplasm and the nucleus and regulates the abundance of compartmentalized pools of its regulatory subunits
PRKACB	cAMP-dependent protein kinase catalytic subunit beta	Mediates cAMP-dependent signaling triggered by receptor binding to GPCRs that regulates diverse cellular processes such as cell proliferation, the cell cycle, differentiation and regulation of microtubule dynamics, chromatin condensation and decondensation, nuclear envelope disassembly and reassembly
PRKACG	cAMP-dependent protein kinase catalytic subunit gamma	Phosphorylates a large number of substrates in the cytoplasm and the nucleus
PSEN1	Presenilin-1	Presenilin-2; Probable catalytic subunit of the gamma-secretase complex, an endoprotease complex that catalyzes the intramembrane cleavage of integral membrane proteins such as Notch receptors and APP (amyloid-beta precursor protein) and may play a role in intracellular signaling and gene expression or in linking chromatin to the nuclear membrane
PSEN2	Presenilin-2	Presenilin-2; Probable catalytic subunit of the gamma-secretase complex, an endoprotease complex that catalyzes the intramembrane cleavage of integral membrane proteins such as Notch receptors and APP (amyloid-beta precursor protein) and may play a role in intracellular signaling and gene expression or in linking chromatin to the nuclear membrane
PSENEN	Gamma-secretase subunit PEN-2	Catalyzes the intramembrane cleavage of integral membrane proteins such as Notch receptors and APP (amyloid-beta precursor protein) and modulates both endoproteolysis of presenilin and gamma-secretase activity
SLC6A3	Sodium-dependent dopamine transporter	Terminates the action of dopamine by its high affinity sodium-dependent reuptake into presynaptic terminals
SNCAIP	Synphilin-1	Isoform 2 inhibits the ubiquitin ligase activity of SIAH1 and inhibits proteasomal degradation of target proteins
TH	Tyrosine 3-monooxygenase	Plays an important role in the physiology of adrenergic neurons

(*continued on next page*)

Table 1 (*continued*)

Interacting proteins		Molecular functions
UBB	Polyubiquitin-B	Form polyubiquitin chains on target proteins and regulate different functions depending on the Lys residue of the ubiquitin that is linked
UBE2L6	Ubiquitin/ISG15-conjugating enzyme E2 L6	Catalyzes the covalent attachment of ubiquitin or ISG15 to other proteins
UCHL1	Ubiquitin carboxyl-terminal hydrolase isozyme L1	Ubiquitin-protein hydrolase involved both in the processing of ubiquitin precursors and of ubiquitinated proteins

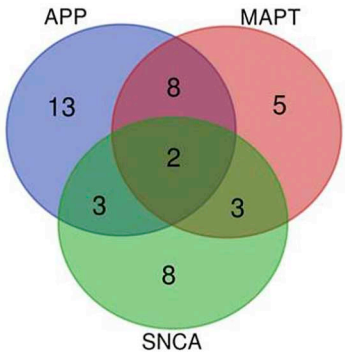

Names	total	elements
APP MAPT SNCA	2	GSK3B PARK2
APP MAPT	8	PSEN2 MAPK1 CDK5 SNCA CASP3 MAPK3 APOE PSEN1
APP SNCA	3	PLCB2 CAPN1 MAPT
MAPT SNCA	3	UBB APP LRRK2
APP	13	PSENEN BACE1 ADAM10 APH1A GNAI3 APBB1 NCSTN DRD2 CAPN2 GPR37 CASP8 GAPDH NAE1
MAPT	5	CDK5R1 PRKACA PRKACB PRKACG CALM1
SNCA	8	PINK1 SLC6A3 BAD PARK7 UBE2L6 SNCAIP TH UCHL1

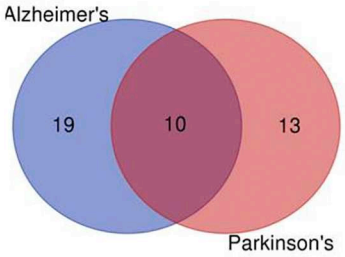

Names	total	elements
Alzheimer's Parkinson's	10	PLCB2 UBB APP GSK3B SNCA CAPN1 CASP3 PARK2 LRRK2 MAPT
Alzheimer's	19	PSENEN BACE1 ADAM10 CASSP8 APH1A APBB1 PSEN2 MAPK1 NCSTN BAD CDK5 CDK5R1 CAPN2 MAPK3 APOE CALM1 GAPDH PSEN1 NAE1
Parkinson's	13	PINK1 GNAI3 SLC6A3 DRD2 PARK7 PRKACA PRKACB UBE2L6 PRKACG GPR37 SNCAIP TH UCHL1

Key markers for AD and PD crosstalk:

APP- Amyloid beta precursor protein
GSK3B- Glycogen synthase kinase 3 beta
MAPT- Microtubule associated protein Tau
PLCB2- Phospholipase C Beta 2
CAPN1- Calpain-1 catalytic subunit
LRRK2- Leucine-rich repeat kinase 2
PARK2- Parkin
SNCA- Synuclein Alpha

Fig. 5. Crosstalk markers involved in the pathology of Alzheimer's and Parkinson's disease- The first Venn diagram analysis highlighted the common interacting partners of Aβ, Tau and α-Synuclein while the second Venn diagram analysis showed the disease incidences of their interacting proteins into Alzheimer's and Parkinson's disease.

Alzheimer's disease. We reported high content of alpha helical structure in $A\beta_{42}$ isoforms than $A\beta_{40}$. However, $A\beta_{42}$ found to exist in mono-fibril to di-fibril state while $A\beta_{40}$ reported up to tri fibrillar state in terms of their complexity. Moreover, they shared their aggregation regions, rich in hydrophobic residues with some additional amino acids. For instance, the aggregation sites responsible for intra- and intermolecular fibril formation in $A\beta_{40}$ and $A\beta_{42}$ were HQKLVFFAEDV (14-24)/GAIIGLMVGGVV (29-40) and HQKLVFFAEDVGS (14-26)/GAIIGLMVGGVVI (29-41) respectively, which were almost similar with only few residue differences. However, the sequence specific aggregation sites for individual fibrillar peptides have shown in Fig. 1 that was populated with glycine, alanine, valine, leucine, isoleucine and phenylalanine.

3.1.2. Microtubule associated Tau protein

The MAPT is a 758 amino acid residue long protein whose microtubule-binding domain spans from 561 to 697 amino acids. It is hydrophilic, unstructured and dynamic in its aggregation. Therefore, it binds to microtubule in a random coil like fashion. The amyloid spine forming TAU (5V5B, 5V5C, 4NP8, 3OVL, 2ON9) revealed the KVQIINKKLD (591-600), VQIINK (592-597) and VQIVYK (623-628) sequence motif crucial for its aggregation. In addition, Tau's fibrillar form (6HRE, 5O3O, 5O3L) identified two types of helical filaments, including paired-helical and straight-helical form. The paired-helical filaments reported intra- and inter-molecular interactions with help of VQIVYK (623-628) and GGG (650-652) residues while straight-helical filaments with help of VQIVYK (623-628) and Valine (630), and Glycine (640) residues. Moreover, the protein-specific aggregation sites and the structural changes in their secondary-structures have shown in Fig. 2.

3.1.3. Alpha-Synuclein

The α-Synuclein is a small protein of 140 amino acids chief among other isoforms, i.e. β- and γ-synuclein. The conformational changes in its native structure take place to form pre-fibrillar oligomers and consequent fibril formation. It is also reported to attain amyloid like conformations (4R0U, 4R0W, 4RIK, 4RIL) that are identified to be formed by GVVHGVTTVA (47-56), TGVTAVA (72-78), VVTGVTA (70-76), AVVTGVTAV (69-77), and GAVVTGVTAVA (68-78) segments. Furthermore, the polypeptide regions- GVVHGVATVAE (47-57) and

ARTICLE IN PRESS

Table 2
The key ubiquitin E3 ligases regulating the clearance of AD-PD crosstalk markers.

Direct regulators for AβPP, Tau, and α-Synuclein clearance

Names	Total	Elements
APP, LRRK2, MAPT, PARK2, SNCA	1	STUB1
APP, LRRK2, MAPT, SNCA	1	PARK2
GSK3B, PARK2, SNCA	2	FBXW7, SIAH1
LRRK2, PARK2, SNCA	1	FBXO7
APP, CAPN1	1	WDTC1
APP, MAPT	1	SYVN1
GSK3B, SNCA	1	TRAF6
PARK2, SNCA	4	RNF19A, SIAH2, TRIM32, NEDD4
APP	1	FBXL2
MAPT	1	MARCH7
SNCA	1	FBXO45

Indirect regulators for AβPP, Tau, and α-Synuclein clearance

Names	Total	Elements
GSK3B, LRRK2, PARK2	1	TRAF2
CAPN1, GSK3B	1	CDH1
CAPN1, PARK2	1	TRIM63
GSK3B, PARK2	5	CUL3, SKP1, RBX1, CUL1, UBE3A
LRRK2, PARK2	4	WSB1, RANBP2, HERC2, HACE1
PARK2, PLCB2	1	RNF41
GSK3B	9	UBR5, TRIM29, BIRC2, MAP3K1, PIAS1, XIAP, NHLRC1, MDM2, APC2
LRRK2	4	ERCC8, TRIM23, RHOBTB1, RHOBTB3
PARK2	149	TRAF7, MUL1, RNF114, SPSB2, RNF217, HEWE1, DET1, ASB7, HERC1, BTBD1, VPRBP, TRIM69, HECW2, FBXL18, RNF115, ASB14, HERC3, ASB11, LRRC41, FBXW4, RNF182, KLHL2, UBR1, SKP2, ASB17, RNF25, TCEB1, FBXL16, UBE3C, ASB4, RNF34, FBXL5, FBXO4, FBXL12, FBXO21, FBXO6, CDC20, MYLIP, TRIM9, TRIM11, FBXL22, KBTBD6, UBOX5, KBTBD8, ASB16, NEDD4L, ASB6, KLHL22, CDC23, RNF14, HERC4, RBCK1, ASB1, KLHL21, TCEB2, HECTD3, ASB9, FBXL3, SOCS3, ASB12, FBXW8, TRIP12, FBXL15, CUL2, ZBTB16, MGRN1, FBXL4, RNF7, CUL7, RNF19B, SPSB1, FBXO41, RNF123, RNF31, KLHL25, ITCH, HECTD1, RNF138, ARIH1, FBXO2, RFWD2, AMFR, TRIM36, UBR4, FBXL13, LRR1, MARCH5, TRIM39, KLHL20, CCNF, CUL5, FBXL19, TRIM71, SOCS1, WWP1, FBXL8, LNX1, ASB13, FBXO27, RNF111, RCHY1, TRIM21, PJA2, FBXO22, PJA1, TRIM4, FBXO17, LRSAM1, FBXO10, UBE3B, ASB8, FBXO30, SH3RF1, FBXO44, FBXW10, ASB18, RNF130, VHL, FBXO15, DZIP3, FBXW2, TRIM37, ASB5, ZNF645, FBXO9, FBXW9, ZNRF1, UBE4A, UBE3D, CDC26, ASB10, UBR2, ASB2, FBXW5, FBXL7, ASB15, FBXL14, TRIM50, ARIH2, HECTD2, FBXO11, FBXO31, FBXO40, KLHL9, KLHL11, RBBP6, TRIM41, RLIM, TRAIP

Table 3
Ubiquitinational markers for AD-PD crosstalk proteins.

Pathological Targets	Key Ubiquitin E3 ligases	Ubiquitinating E2 Conjugating Enzymes	Ubiquitin E1 Activating Enzymes	Deubiquitinating Enzymes
AβPP, Tau, α-Synuclein, LRRK2, PARK2	**STUB1**	UBE2A, UBE2B, UBE2C, UBE2F, UBE2G1, UBE2G2, UBE2H, UBE2J1, UBE2J2, UBE2K, UBE2L6, UBE2M, UBE2N, UBE2O, UBE2Q1, UBE2S, UBE2U, UBE2W, UBE2Z, UBE2L3, BIRC6, UBE2I, UBE2T	ATG7, NAE1, SAE1, UBA1, UBA3, UBA5, UBA6, UBA7	ATXN3, USP8, USP7, USP19, PSMD14, SENP3
AβPP, Tau, α-Synuclein, LRRK2	**PARK2**	UBE2A, UBE2B, UBE2C, UBE2F, UBE2G1, UBE2G2, UBE2H, UBE2J1, UBE2J2, UBE2K, UBE2L6, UBE2M, UBE2N, UBE2O, UBE2Q1, UBE2S, UBE2U, UBE2W, UBE2Z, UBE2L3	ATG7, NAE1, SAE1, UBA1, UBA3, UBA5, UBA6, UBA7	ATXN3, USP8, USP30, UCHL1, BAP1, PSMD14, USP15
AβPP, α-Synuclein, LRRK2, PARK2	**FBXO7 (FBXL2, FBXO45)**	UBE2A, UBE2B, UBE2C, UBE2F, UBE2G1, UBE2G2, UBE2H, UBE2J1, UBE2J2, UBE2K, UBE2L6, UBE2M, UBE2N, UBE2O, UBE2Q1, UBE2S, UBE2U, UBE2W, UBE2Z	ATG7, NAE1, SAE1, UBA1, UBA3, UBA5, UBA6, UBA7	USP47,UCHL1
α-Synuclein, GSK3B, PARK2	**FBXW7**	UBE2A, UBE2B, UBE2C, UBE2F, UBE2G1, UBE2G2, UBE2H, UBE2J1, UBE2J2, UBE2K, UBE2L6, UBE2M, UBE2N, UBE2O, UBE2Q1, UBE2S, UBE2U, UBE2W, UBE2Z	ATG7, NAE1, SAE1, UBA1, UBA3, UBA5, UBA6, UBA7	USP47, USP28, USP7, USP36
α-Synuclein, GSK3B, PARK2	**SIAH1**	UBE2A, UBE2B, UBE2C, UBE2F, UBE2G1, UBE2G2, UBE2H,UBE2J1, UBE2J2, UBE2K, UBE2L6, UBE2M, UBE2N, UBE2O, UBE2Q1, UBE2S, UBE2U, UBE2W, UBE2Z, UBE2I	ATG7, NAE1, SAE1, UBA1, UBA3, UBA5, UBA6, UBA7	USP19, USP4, USP6, USP15, USP20
AβPP, Tau	**SYVN1**	UBE2G2, UBE2J1, ATG3, UBE2J2, UBE2K, UBE2G1, UBE2S	ATG7, NAE1, SAE1, UBA1, UBA3, UBA5, UBA6, UBA7	ATXN3, PSMD14, USP19, VCPIP1
α-Synuclein, PARK2	**NEDD4**	UBE2A, UBE2B, UBE2C, UBE2F, UBE2G1, UBE2G2, UBE2H, UBE2I, UBE2J1, UBE2J2, UBE2K, UBE2L3,	ATG7, NAE1, SAE1, UBA1, UBA3, UBA5,	USP2, USP7, USP8, USP14, USP18, USP20, USP25,
		UBE2L6, UBE2M, UBE2N, UBE2O, UBE2Q1, UBE2S, UBE2T, UBE2U, UBE2W, UBE2Z	UBA6, UBA7	USP28, STAMBP
-Synuclein, PARK2	**RNF19A**	UBE2A, UBE2B, UBE2C, UBE2F, UBE2G1, UBE2G2, UBE2H, UBE2J1, UBE2J2, UBE2K, UBE2L6, UBE2M, UBE2N, UBE2O, UBE2Q1, UBE2S, UBE2U, UBE2W, UBE2Z, UBE2L3	ATG7, NAE1, SAE1, UBA1, UBA3, UBA5, UBA6, UBA7	–
α-Synuclein, PARK2	**SIAH2**	UBE2A, UBE2B, UBE2C, UBE2F, UBE2G1, UBE2G2, UBE2H, UBE2J1, UBE2J2, UBE2K, UBE2L6, UBE2M, UBE2N, UBE2O, UBE2Q1, UBE2S, UBE2U, UBE2W, UBE2Z, UBE2I	ATG7, NAE1, SAE1, UBA1, UBA3, UBA5, UBA6, UBA7	USP19, USP4, USP6, USP15, USP20
α-Synuclein, PARK2	**TRIM32**	UBE2A, UBE2B, UBE2C, UBE2F, UBE2G1, UBE2G2, UBE2H, UBE2J1, UBE2J2, UBE2K, UBE2L6, UBE2M, UBE2N, UBE2O, UBE2Q1, UBE2S, UBE2U, UBE2W, UBE2Z	ATG7, NAE1, SAE1, UBA1, UBA3, UBA5, UBA6, UBA7	–
AβPP, CAPN1	**WDTC1**	UBE2M	ATG7, NAE1, SAE1, UBA1, UBA3, UBA5, UBA6, UBA7	SENP8
α-Synuclein, GSK3β	**TRAF6**	UBE2N, UBE2I, UBE2K, UBE2L3, UBE2O, UBE2S	ATG7, UBA1, UBA3, UBA5, UBA6, UBA7	USP4, USP7, OTUB1, OTUB2, TNFAIP3, ZRANB1, OTUD5, OTUD7A, STAMBP, UCHL1, USP2, USP15, USP20, USP21, USP25
Tau	**MARCH7**	UBE2G2, UBE2K, UBE2N	ATG7, UBA1, UBA3, UBA5, UBA6, UBA7	USP7

Red- Highest Confidence; Blue- High Confidence; Green- Medium Confidence

GAVVTGVTAVA (68-78) found to interact and form intra- and inter-molecular fibril that have shown in Fig. 3. These α-synuclein fibrils are rich in beta-strands and beta-bridges with varied structural conformations that initiate the lewy body formation in Parkinson's disease.

3.2. Functional partners of Aβ, Tau, and α-Synuclein involved in Alzheimer's and Parkinson's disease pathology

The top-hundred interacting partners among Aβ, Tau, and α-Synuclein

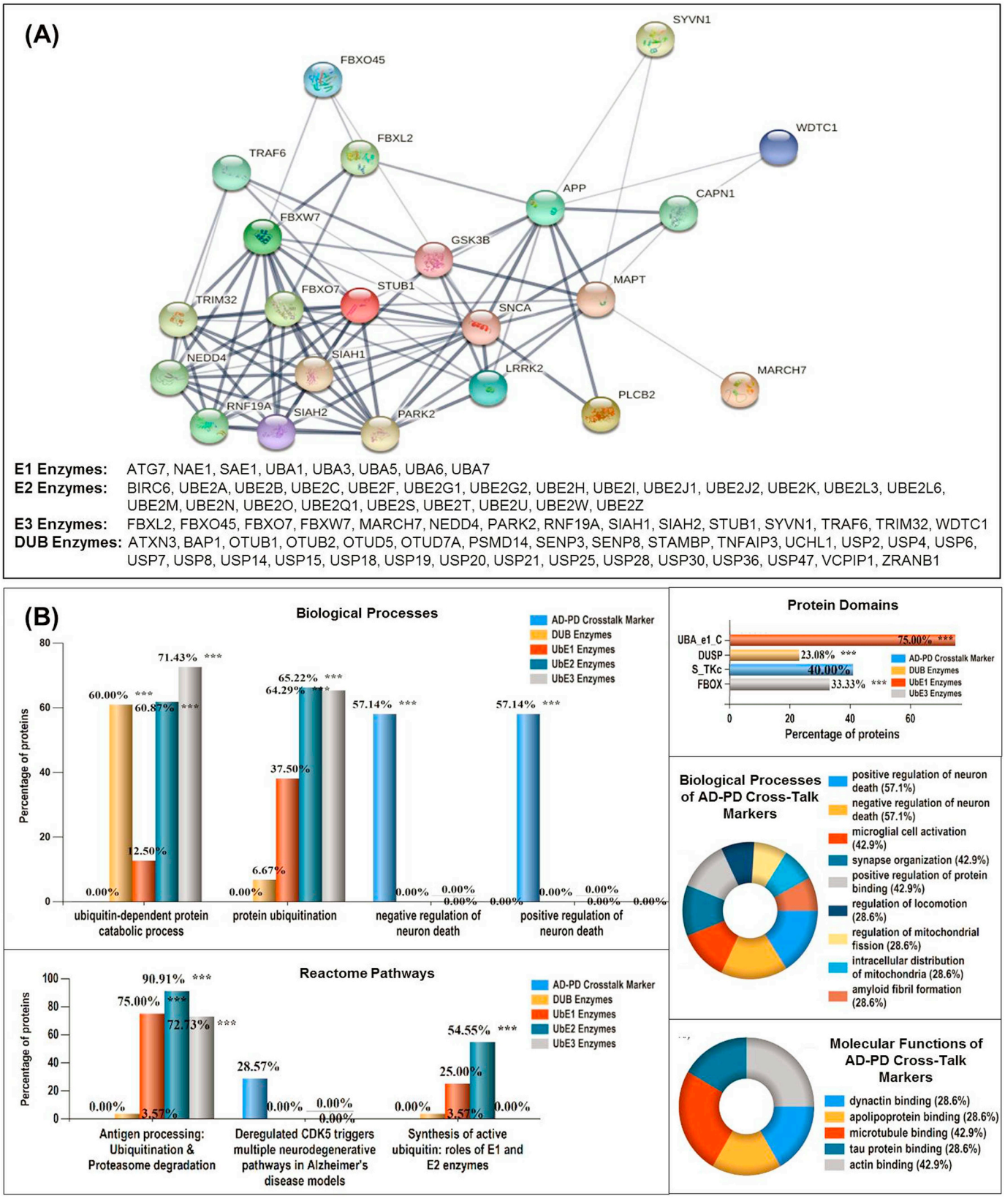

(caption on next page)

Fig. 6. (A) Ubiquitination enzyme interaction network for the clearance of AD-PD cross talk markers including Aβ, Tau and α-synuclein: - E1-activating enzymes: ATG7- Ubiquitin-like modifier-activating enzyme ATG7; NAE1- NEDD8-activating enzyme E1 regulatory subunit; SAE1- SUMO-activating enzyme subunit 1; UBA1/3/5/6/7- Ubiquitin-like modifier-activating enzyme 1/3/5/6/7. E2 conjugating enzymes: BIRC6- Baculoviral IAP repeat-containing protein 6; **UBE2A/B/C/F/G1/G2/H/I/J1/J2/K/L3/L6/M/N/O/Q1/S/T/U/W/Z-** Ubiquitin Conjugating Enzyme E2 A/B/C/F/G1/G2/H/I/J1/J2/K/L3/L6/M/N/O/Q1/S/T/U/W/Z. E3-ligases: FBXL2- F-box/LRR-repeat protein 2; FBXO45- F-box/SPRY domain-containing protein 1; FBXO7- F-box only protein 7; FBXW7- F-box/WD repeat-containing protein 7; MARCH7- Membrane Associated Ring-CH-Type Finger 7; NEDD4- Neural precursor cell expressed developmentally down-regulated protein 4; PARK2- Parkin; RNF19A- Ring finger protein19A; SIAH1/2- Siah E3 Ubiquitin Protein Ligase 1/2; STUB1- Ubiquitin-protein ligase CHIP; SYVN1- Synoviolin; TRAF6- TNF receptor-associated factor 6; TRIM32- Tripartite Motif Containing 32. Deubiquitinases: ATXN3- Ataxin-3; BAP1- Ubiquitin carboxyl-terminal hydrolase BAP1; OTUB1/2- OTU Deubiquitinase 1/2; OTUD5/7A- OTU domain-containing protein 5/7A; PSMD14- 26S proteasome non-ATPase regulatory subunit 14; SENP3/8- Sentrin-specific protease 3/8; STAMBP- STAM-binding protein; TNFAIP3- Tumor necrosis factor alpha-induced protein 3; UCHL1- Ubiquitin carboxyl-terminal hydrolase isozyme L1; USP2/4/6/7/8/14/15/18/19/20/21/25/28/30/36/47- Ubiquitin carboxyl-terminal hydrolase 2/4/6/7/8/14/15/18/19/20/21/25/28/30/36/47; VCPIP1- Valosin Containing Protein Interacting Protein 1; WDTC1- WD and tetratricopeptide repeats protein 1; ZRANB1- Zinc Finger RANBP2-Type Containing-1. (B) Functional enrichment analysis of AD-PD cross talk markers and the ubiquitination enzymes: - It has analysed the most important biological processes, reactome pathways, molecular functions, and protein domains at high significance *P*-values i.e. $P < .001$. The bar graph compares the percentage of input proteins with their associated top scoring biological processes, reactome pathways and protein domains. Biological processes: Ubiquitin-dependent protein catalytic process (UbE1s- UBA6; UbE2s- BIRC6, UBE2A/B/C/G1/G2/H/I/K/L3/L6/N/S/Z; UbE3s- FBXL2, FBXO7/45, NEDD4, RNF19A, SIAH1/2, STUB1, SYVN1, TRIM32; DUBs- ATXN3, BAP1, PSMD14, USP2/4/6/7/8/14/15/18/20/21/25/28/30/36/47), Protein ubiquitination (UbE1s- SAE1, UBA1/6; UbE2s- BIRC6, UBE2A/B/C/G1/G2/H/J2/K/L3/N/S/T/W/Z; UbE3s- FBXL2, FBXO7/45, FBXW7, NEDD4, PARK2, STUB1, SYVN1, TRIM32, WDTC1; DUBs- USP7, VCPIP1), Negative regulation of neuron death (AD-PD cross-talk markers- APP, GSK3B, LRRK2, SNCA), Positive regulation of neuron death (AD-PD cross-talk markers- APP, GSK3B, MAPT, SNCA). Reactome pathways: Antigen processing: Ubiquitination and Proteasome degradation (UbE1s- ATG7, UBA1/3/5/6/7; UbE2s- UBE2A/B/2C/F/G1/G2/H/J1/J2/K/L3/L6/M/N/O/Q1/S/U/W/Z; UbE3s- FBXO7, FBXW7, NEDD4, RNF19A, SIAH1/2, STUB1, TRIM32; DUBs- PSMD14), Deregulated CDK5 triggers multiple neurodegenerative pathways in Alzheimer's disease models (AD-PD cross-talk markers- APP, CAPN1), Synthesis of active ubiquitin: roles of E1 and E2 enzymes (UbE1s- UBA1/6; UbE2s- UBE2A/B/C/G1/G2/H/K/L3/S/T/W/Z; DUBs- USP7). Protein domains: UBA_e1_C (UbE1s- UBA1/6/7), DUSP (DUBs- USP4/15/20), S_TKc (AD-PD cross-talk markers- GSK3B, LRRK2), FBOX (UbE3s- FBXL2, FBXO7/45, FBXW7). The doughnut chart depicted the biological processes and molecular functions associated with the AD-PD cross talk markers. Biological processes: Positive regulation of neuron death (APP, GSK3B, MAPT, SNCA), Negative regulation of neuron death (APP, GSK3B, LRRK2, SNCA), Microglial cell activation (APP, MAPT, SNCA), Synapse organization (APP, MAPT, SNCA), Positive regulation of protein binding (APP, GSK3B, LRRK2), Regulation of locomotion (LRRK2, SNCA), Regulation of mitochondrial fission (MAPT, LRRK2), Intracellular distribution of mitochondria (MAPT, LRRK2), Amyloid fibril formation (APP, MAPT). Molecular functions: Dynactin binding (MAPT, GSK3B), Apolipoprotein binding (APP, MAPT), Microtubule binding (LRRK2, MAPT, SNCA), Tau protein binding (GSK3B, SNCA), Actin binding (LRRK2, MAPT, SNCA).

proteins were deduced and further iterated with another leading 100 interactors at high confidence, which revealed a set of 22 AβPP interacting proteins in AD while 6 in PD. Similarly, it identified 12 Tau interacting proteins in AD and 8 in PD. Likewise, six α-Synuclein interacting proteins were reported in AD and 10 in PD. In summary, the network identified 26 AD-related proteins, including ADAM10, APBB1, APH1A, APOE, APP, BACE1, BAD, CALM1, CAPN1, CAPN2, CASP3, CASSP8, CDK5, CDK5R1, GAPDH, GSK3B, MAPK1, MAPK3, MAPT, NAE1, NCSTN, PLCB2, PSEN1, PSEN2, PSENEN, and SNCA. However, it revealed 18 PD-related proteins, including PRKACB, PRKACG, PRKACA, GNAI3, TH, DRD2, GPR37, LRRK2, SNCA, SLC6A3, SNCAIP, PARK7, PARK2, CASP3, UBE2L6, UCHL1, PINK1, and UBB. The network maps of the functional partners are shown in Fig. 4, and their corresponding functions are summarized in Table 1. Altogether, these proteins were involved in the regulation of protein catalytic activity, amyloid fiber formation and associated signaling by receptor tyrosine kinases.

3.3. GSK3B and PARK2 are key markers for AD-PD crosstalk commonly interacting with Aβ, Tau, and α-Synuclein

The Venn diagram analysis of the top interacting partners reported only two proteins, including GSK3B and PARK2 to be commonly interacting with Aβ, Tau, and α-Synuclein. Instead other markers, found to interact either any of the two or any one of the Aβ, Tau, and α-Synuclein proteins. For instance, PSEN2, MAPK1, CDK5, SNCA, CASP3, MAPK3, APOE, and PSEN1 found to interact with AβPP and Tau, while PLCB2, CAPN1, and MAPT interacting with AβPP and α-Synuclein respectively. Likewise, UBB, APP, and LRRK2 observed to interact with Tau and α-Synuclein proteins. Moreover, their disease incidence analysis reported these eight key markers, including APP, CAPN1, GSK3B, LRRK2, MAPT, PARK2, PLCB2, and SNCA involved in the crosstalk of Alzheimer's and Parkinson's disease at the molecular level. While other markers, specific for AD and PD interacting with any of their pathological partners- Aβ, Tau and α-Synuclein is shown in Fig. 5. Here, only PARK2 and GSK3B found to interact commonly with all diseased proteins, including Aβ, Tau and α-synuclein. Since, PARK2 is a ubiquitin E3 ligase. Therefore, its interaction with Aβ, Tau and α-synuclein would certainly regulate their levels in our body.

3.4. PARK2 and STUB1 are the key ubiquitin E3 ligases regulating the clearance of pathological markers in AD and PD

The ubiquitin E3 ligases were identified against all the AD-PD cross talk markers and were classified as direct- and indirect-regulators depending on their potential interaction with Aβ, Tau and α-Synuclein. Those E3 ligases that were involved in the ubiquitination of Aβ, Tau and α-Synuclein is classified as direct-regulators, while those involved with other pathological markers classified as indirect-regulators. We reported only PARK2 and STUB1 to be commonly interacting with most of the AD-PD cross talk markers, including AβPP, MAPT, SNCA, and LRRK2. Instead, other E3 ligases found to regulate AβPP, Tau, and α-Synuclein ubiquitination individually or in different combinations. Likewise, we reported indirect-regulators that were involved with the ubiquitination of markers other than AβPP, Tau, and α-Synuclein, such as CAPN1, GSK3B, LRRK2, PARK2, and PLCB2. Among them, TRAF2 found to regulate GSK3B, LRRK2, and PARK2 markers commonly. Similarly, we defined a spectrum of E3 ligases involved in the ubiquitination of AD-PD cross talk markers that are summarized in Table 2. The comprehensive study reported 149 regulatory ubiquitin E3 ligases for the ubiquitination of PARK2 ubiquitin E3-ligase. It suggested the involvement of PARK2 in both the pathology and clearance biology, i.e. negative and positive role in neurodegenerative disorders like AD and PD.

3.5. Ubiquitination biology of toxic Aβ, Tau, and α-synuclein protein clearance

The ubiquitination reaction of Aβ, Tau, and α-synuclein clearance is a complex biology of interactions among a series of E1-activating, E2-conjugating, E3-ligating and deubiquitinating enzymes. Here, we reported the important ubiquitination markers, including the E3 ligases-PARK2, STUB1, FBXW7 SIAH1, FBXO7, WDTC1, SYVN1, TRAF6, RNF19A, SIAH2, TRIM32, NEDD4, FBXL2, MARCH7, and FBXO45, and

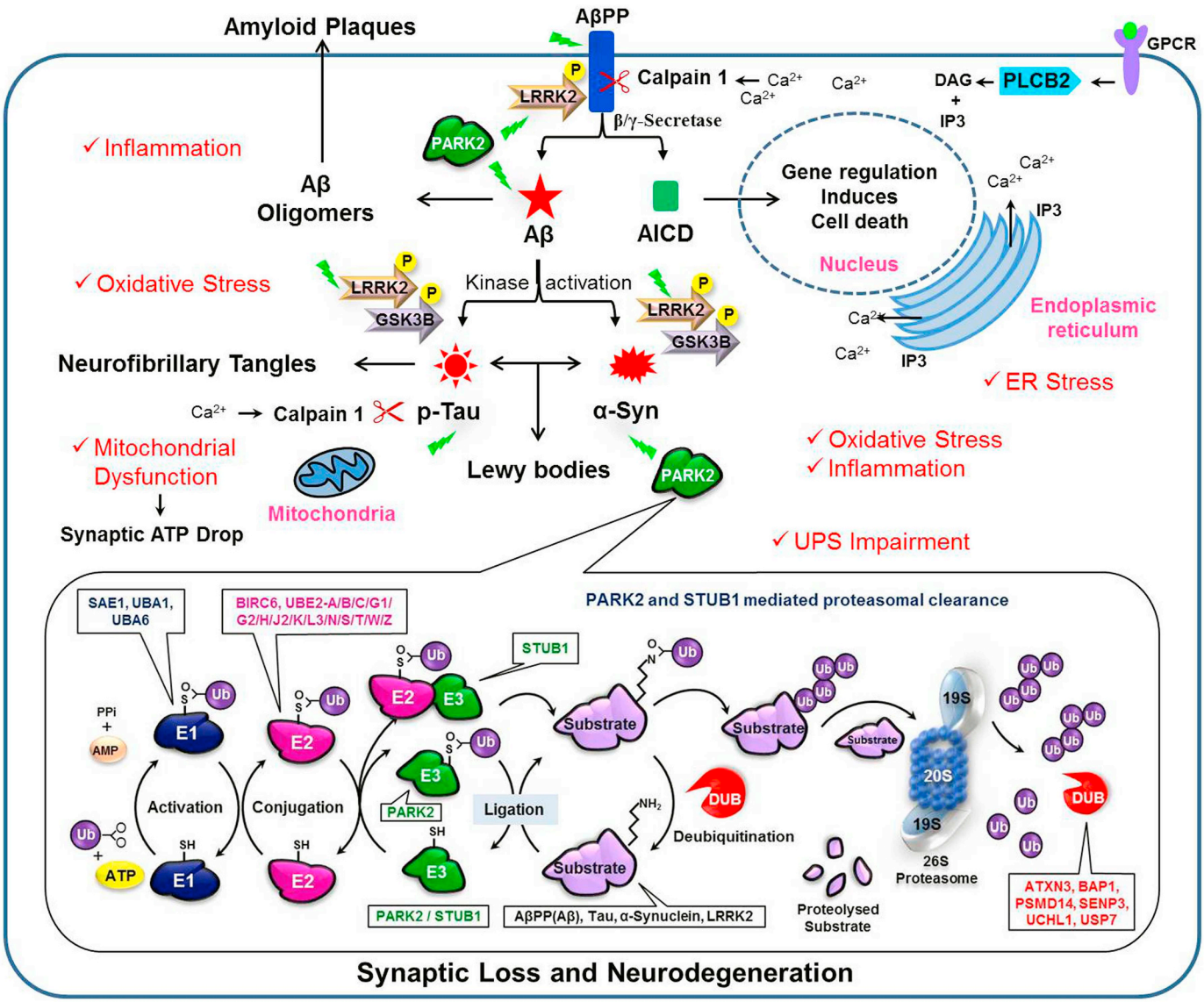

Fig. 7. Molecular mechanism of AD-PD crosstalk marker's associated neurodegeneration and their proteasomal clearance- In diseased state, proteolytic processing of AβPP leads to the production of Aβ and amyloid intracellular domain. Here, amyloid production activates the kinases like LRRK2 and GSK3B, which in turn accelerate the phosphorylation of Tau and α-Synuclein protein thereby resulting neurofibrillary tangles and lewy bodies. On the other side, AICD triggers the apoptotic gene regulation and induces cell death. Furthermore, G-protein coupled receptor activates phospholipase B (PLCB2) that triggers the calcium release from ER and consequent action of calpain 1 on their substrates, including AβPP and Tau. Here, calapin 1 mediated tau cleavage products, induces mitochondrial dysfunction and thus ATP loss. On the other side, Parkin (PARK2) as an E3 ligase acts on the pathogenic proteins- AβPP(Aβ), Tau, α-Synuclein, and LRRK2 to mark them for proteasomal degradation with the help of diverse ubiquitin activating enzymes, conjugating enzymes, and deubiquitinases. Altogether, these toxic proteins are associated with the ER stress, oxidative stress, mitochondrial dysfunction, inflammation, and UPS impairment in neurons thereby leading to synaptic loss and neurodegeneration. AICD- Amyloid intracellular domain; DAG- Diacylglycerol; PLCB2- Phospholipase B.

the deubiquitinases- ATXN3, USP8, PSMD14, and UCHL1 directly regulating the clearance of Aβ, Tau and α-synuclein. Furthermore, identified their corresponding ubiquitin E2-conjugating enzymes- UBE2A/B/C/F/G1/G2/H/J1/J2/K/L6/M/N/O/Q1/S/U/W/Z and ubiquitin E1-activating enzymes- ATG7, NAE1, SAE1, UBA1/3/5/6/7 involved in the ubiquitination biology of all these protein aggregates. In addition, we reported the majority with a similar set of E2s and E1s with crucial differences in their deubiquitinases. The important ubiquitination enzymes for the clearance of AD-PD cross talk markers are summarized in Table 3. Moreover, the enzymatic regulation of ubiquitination reaction for Aβ, Tau, and α-synuclein with their specific ubiquitin E3-ligases are mapped in Fig. 6A. These UPS enzymes along with their target AD-PD cross-talk markers were further investigated for their functional annotations, including the biological processes, reactome pathways, protein domains, and molecular functions (Fig. 6B). The biological process analysis revealed only the UPS enzymes including **UbE1s-***SAE1, UBA1/6;***UbE2s-***BIRC6, UBE2A/B/C/G1/G2/H/J2/K/L3/N/S/T/W/Z;***UbE3s-***FBXL2, FBXO7/45, FBXW7, NEDD4, PARK2, STUB1, SYVN1, TRIM32, WDTC1;* and **DUBs-***USP7, VCPIP1* to be associated with protein ubiquitination, while **UbE1s-***UBA6;***UbE2s-***BIRC6, UBE2A/B/C/G1/G2/H/I/K/L3/L6/N/S/Z;***UbE3s-***FBXL2, FBXO7/45, NEDD4, RNF19A, SIAH1/2, STUB1, SYVN1, TRIM32,* and **DUBs-***ATXN3, BAP1, PSMD14, USP2/4/6/7/8/14/15/18/20/21/25/28/30/36/47* to be linked with the ubiquitin dependent protein catabolic process. On the other hand, AD-PD cross-talk markers were reported to be linked with both positive (APP, GSK3B, MAPT, SNCA) and negative regulation (APP, GSK3B, LRRK2, SNCA) of neuronal death. The analysis revealed the peculiarity of LRRK2 in the pathogenesis of disease. Furthermore, the reactome pathway analysis identified three pathways with most significant scores, including i) UPS associated antigen processing (**UbE1s-***ATG7,*

*UBA1/3/5/6/7;***UbE2s-***UBE2A/B/2C/F/G1/G2/H/J1/J2/K/L3/L6/M/N/O/Q1/S/U/W/Z;***UbE3s-***FBXO7, FBXW7, NEDD4, RNF19A, SIAH1/2, STUB1, TRIM32; DUBs- PSMD14*), ii) CDK5 linked neurodegeneration (AD-PD cross-talk markers- APP, CAPN1), and iii) synthesis of active ubiquitin protein (**UbE1s-***UBA1/6*; **UbE2s-***UBE2A/B/C/G1/G2/H/K/L3/S/T/W/Z;***DUBs-***USP7*). In addition, the Protein domain analysis revealed the majority of ubiquitin E1 activating enzymes with UBA_e1_C domain, while ubiquitin E3 ligases with FBOX domain. Likewise, it reported DUSP domain in most of the deubiquitinases, while S_TKc domain in the majority of the AD-PD crosstalk markers. Moreover, the molecular functions and biological processes analysis of AD-PD crosstalk markers identified their roles in microglial activation, synapse organization, mitochondrial fission, amyloid fibril formation and binding with various cellular proteins, including actin, dynactin, apolipoprotein, tau and microtubule. Altogether, these findings have provided new insights into the molecular mechanisms for neurotoxic protein clearance in AD and PD.

3.6. Molecular cross talk among neurotoxic proteins and their clearance in Alzheimer's and Parkinson's disease

The functional enrichment analysis of the UPS enzymes has provided valuable insights for the choice of potential ubiquitination enzymes important for the proteasomal clearance of pathogenic proteins, while that of AD-PD cross talk markers revealed their role in protein aggregation. However, ubiquitination is a complex process of targeted protein degradation with the help of an array of ubiquitinational enzymes, especially the ubiquitin E3 ligases that are crucial for imparting the substrate specificity, but the obtained results have revealed the facts to a greater extent. Based on the evidence from our findings, we can hypothesize the molecular mechanism of the toxic protein aggregation and their clearance through the ubiquitination process for better understanding the medical state of Alzheimer's and Parkinson's disease (Fig. 7). The clinical reports suggest that the identified AD-PD cross-talk markers have their pathogenic role in both the diseases, but CAPN1 and PLCB2 are two novel markers whose roles need to be investigated in both diseases, although they are known to play some role in Alzheimer's disease. Moreover, future research is required to translate these findings to devise better diagnostic and therapeutic avenues for life management and care for the patients suffering with Alzheimer's and Parkinson's disease.

4. Discussion

The soluble forms of amyloid beta peptides- $A\beta_{40}$ and $A\beta_{42,}$ microtubule associated tau protein, and the α-synuclein protein is well evident to cause neurotoxicity in both Alzheimer's and Parkinson's disease pathology. Here, we studied their aggregation sites to analyze the protein folding dynamics in its diseased state. We found that these proteins transform their secondary structural helical conformations into beta strands upon their transition from monomer to fibrillar state. Recently, Balupuri et al. (2019) has also shown the occurrence of α-strand in the monomer to drive sheet formation in the oligomers that initiates and promotes α-synuclein aggregation and fibrillation (Balupuri et al., 2019). Moreover, the tertiary structures of amyloid beta have revealed the hydrobhobic sites HQKLVFFAEDV (14-24)/ GAIIGLMVGGVV (29-40) and HQKLVFFAEDVGS (14-26)/ GAIIGLMVGGVVI (29-41) in $A\beta_{40}$ and $A\beta_{42}$ respectively that are responsible for the intra- and inter-molecular interactions during protein aggregation. The hydrophobic residues at these sites rearrange their non-covalent interactions via disrupting their previous secondary structures and resulting in a seed-nucleus formation. It provides a surface for a series of misfolding events and molecular interactions with other proteins to form oligomers and consequent protofibrils (Marinko et al., 2019). Interestingly, Cox et al. (2018) also confirmed that protein aggregation is a biological driven process that evades out the intrinsic hydrophobic regions due to mutations or protein misfolding events (Cox et al., 2018). Moreover, Hao et al. (2010) demonstrated that $A\beta_{20–29}$ peptide blocks apoE-Aβ interaction through competitive binding at c-terminal domain of apoE and consequently, reduces full-length $A\beta_{40/42}$ fibril formation and cytotoxicity (Hao et al., 2010). This indicates that the proximal aggregation sites HQKLVFFAEDV (14-24) in $A\beta_{40}$ and HQKLVFFAEDVGS (14-26) in $A\beta_{42}$ as shown in our study has unique ability for self-aggregation as well as interaction with other proteins like apoE to facilitate its own aggregation.

Furthermore, the aggregation sites in amyloid beta peptides have revealed the spanning lysine residues that was also reported by Sinha et al. (2012) who have shown the role of lysine residues (K16) in amyloid beta folding, assembly and toxicity (Sinha et al., 2012). Moreover, the aggregation sequences in Aβ, Tau, and α-synuclein protein was highly populated with glycine and hydrophobic residues predominating alanine, valine, isoleucine and phenylalanine. Matsui et al. (2017) has also demonstrated the α-helix rules i.e. hydrophobicity of amino acids in the α-helix structure as a potential rationale for aggregation hotspot prediction (Matsui et al., 2017). Moreover, the arrangement of monomer in antiparallel fashion led to cooperative formation of β-sheet conformation (Lovas et al., 2013), and they attained different topologies based on the diversity of their intra- and inter-chain interactions. In fact, NMR studies have also shown the contribution of hydrophobic interaction and salt bridges in imparting the stability to beta-sheets and turns in protein folding and assembly (Petkova et al., 2002, 2006). However, their reverse transition from β-sheets to random coils is the governing principle for neuro-protection adopted by small peptides like NAP (NAPVSIPQ) and SAL (SALLRSIPA) in tau protein (Mokhtari et al., 2016). Interestingly, we identified VQIVYK (623–628) sequence in Tau protein responsible for its fibrillar state indicating their potential role in causing neurotoxicity that can be prevented by disrupting their specific interactions with help of certain short peptides. Moreove, the presence of glycine residue is also important for imparting flexibility to the protein structure, which can fit into both hydrophilic and hydrophobic environments due to its minimal side chain (Scott et al., 2007). Therefore, it sterically allows the protein aggregate to attain different conformations. In addition, hydrophobic regions are also responsible for the hydrophobic interactions among themselves that allow the protein to attain a variety of fibrillar forms with a common hydrophobic core (Kalinowska et al., 2017). On the other side, hydrophobic interactions with other proteins also trigger neuroinfammation. For instance, hydrophobic interactions of glycine zipper fragments of amyloid beta peptides with nitric oxide synthase facilitate the nitric oxide formation and consequent inflammation in neurons (Padayachee and Whiteley, 2013). Altogether, these findings enforce that the surface hydrophobicity guides the process of neurotoxic protein aggregation and consequent inflammation in different neurodegenerative disorders.

Alzheimer's and Parkinson's disease are two distinct neurodegenerative disorders with some pathological similarities. Therefore, numerous studies have investigated the links between them at protein level and found some protein aggregates /CSF peptides in common (Jolkkonen et al., 1991; Moskvina et al., 2013). The primary objective of this study was to investigate the shared pathogenic markers associated with Alzheimer's and Parkinson's disease. Since, the reported pathological proteins (Aβ, Tau and α-synuclein) interact synergistically to accelerate the neuropathology (Clinton et al., 2010); thus, we deduced the AD-PD cross-talk markers by identifying their functional interacting partners involved in the pathology of AD and PD. Altogether, we reported five markers apart from Aβ or AβPP, MAPT, and SNCA, including GSK3B, PARK2, LRRK2, PLCB2, and CAPN1 that are expressed in common during the diseased state. However, these markers have shown their involvement in either of the disease previously, but recent findings have shown their role in both diseases. For instance, LRRK2 variant R1628P increased the risk of AD in the population, and in-vitro findings suggested its predisposition to apoptosis (Zhao et al., 2011). On the other hand, LRRK2 mutation,

G2019S reported to promote AβPP phosphorylation and consequent AICD activity mediated neurotoxicity in PD (Chen et al., 2017). Likewise, apart from tau hyper-phosphorylation, it increased β-amyloid production and inflammatory responses in AD (Hooper et al., 2008). Moreover, GSK3B dysregulations, also contributed towards Parkinson's disease like pathology with induced phosphorylation and aggregation of Tau and α-synuclein (Credle et al., 2015), while it acts positively for neuronal growth in his health state (Yang et al., 2015). Similarly, PARK2 has shown their role in AD, since its enhancement has compensated mitophagic alterations in their pathology (Martin-Maestro et al., 2016). Here, CAPN1 and PLCB2 are two novel markers for AD-PD crosstalk whose roles are still illusive in both diseases, although they are known to play some role in Alzheimer's disease.

Interestingly, our study has reported GSK3B and PARK2 among the crosstalk markers commonly interacting with Aβ, Tau, and α-Synuclein signifying them as the potential candidates for regulating the pathophysiology of Alzheimer's and Parkinson's disease. Another objective of our study was to investigate the UPS markers crucial for the proteasomal clearance of toxic peptides from neurons. Here, we reported fifteen critical ubiquitin E3 ligases for the clearance of AD-PD crosstalk markers, including STUB1, PARK2, FBXW7, SIAH1, FBXO7, WDTC1, SYVN1, TRAF6, RNF19A, SIAH2, TRIM32, NEDD4, FBXL2, MARCH7, and FBXO45. Interestingly, only PARK2 and STUB1 are found to interact with all the key toxic proteins- Aβ, Tau, and α-Synuclein. It suggested the involvement of PARK2 in both the pathology and clearance biology, i.e. negative and positive role in neurodegenerative disorders like AD and PD. For instance, in the healthy state, HSPs, STUB1 and Parkin are known to play a critical role in refolding or targeting of these neurotoxic proteins to ubiquitin proteasome system for degradation (Yao, 2010), but the expression varies. However, in case of AD, Parkin's level is elevated along with HSPs and STUB1, but in case of PD, loss of parkin has been observed with high HSP and STUB1 level resulting in altered mitophagy and consequent pathologies (Kumar et al., 2012). Altogether, these findings reinstate that Parkin has a dual role, i.e. itself a molecular marker for AD-PD cross talk, and its role in the ubiquitination biology of toxic aggregates. Furthermore, AD-PD cross talk markers and their ubiquitination enzymes were extensively investigated for the precise molecular mechanism of Aβ, Tau, and α-Synuclein ubiquitination. It proposed the members from different classes of ubiquitination enzymes associated with the protein clearance in humans, including UbE1s- SAE1, UBA1/6; UbE2s- BIRC6, UBE2A/B/C/G1/G2/H/J2/K/L3/N/S/T/W/Z; UbE3s- FBXL2, FBXO7/45, FBXW7, NEDD4, PARK2, STUB1, SYVN1, TRIM32, WDTC1; and DUBs- USP7, VCPIP1. Moreover, the AD-PD cross talk markers are mapped on the reactome pathways and analysed for their biological functions in neurons. Based on the current findings, we hypothesized the molecular mechanism of neurotoxic protein aggregation and their proteasomal clearance in AD and PD. Overall, our study findings suggest a crucial role of PARK2 in the pathogenesis and therapeutics of neurodegenerative disorders like Alzheimer's and Parkinson's disease.

5. Conclusion

The formation of misfolded protein aggregates is the key hallmark of many neurodegenerative diseases that trigger the neurotoxicity and consequent proteostatic collapse. In addition, active research is going on to unravel the mechanism of protein folding and aggregation. Here, the distortion of helical conformation into beta-strands/bridges containing fibrils is the active principle for aggregation in amyloid-beta, Tau, and α-synuclein proteins. Moreover, aggregation sequences in $Aβ_{40/42}$: HQKLVFFAEDV (14-24), GAIIGLMVGGVV (29-40)/ HQKLVFFAEDVGS (14-26), GAIIGLMVGGVVI (29-41); Tau: GGG(650-652) and V630/G640 in paired and straight helical filaments, and VQI(I/V)(N/Y)K in amyloid-spines; α-Synuclein: GVVHGVATVAE (47-57) and GAVVTGVTAVA (68-78) was rich in glycine and hydrophobic residues-alanine, valine, isoleucine and phenylalanine. These hydrophobic residues were involved in the intra-chain and inter-chain interactions and reported to interact with other proteins involved in the pathogenesis of AD and PD. Therefore, the elucidation of aggregation sites in these pathological proteins and identification of their interacting partners would enable us to identify novel therapies for multiple disease states. Furthermore, the interactome analysis identified AβPP, CAPN1, GSK3B, LRRK2, MAPT, PARK2, PLCB2, and SNCA as key markers for AD-PD cross talk with GSK3B and PARK2 as common interactor of amyloid-beta, tau, and alpha synuclein. In addition, the identification of ubiquitinational markers, including E3 ligases- PARK2, STUB1, FBXW7, SIAH1, FBXO7, WDTC1, SYVN1, TRAF6, RNF19A, SIAH2, TRIM32, NEDD4, FBXL2, MARCH7, and FBXO45; and the deubiquitinases- ATXN3, USP8, PSMD14, and UCHL1 as direct-regulators of Aβ, Tau and α-synuclein ubiquitination, would help us to devise better therapeutic options for targeting misfolded proteins and large-scale rebalancing of proteostatic network. Moreover, the ubiquitination reaction is a complex biology of interactions among a series of E1-activating, E2-conjugating, E3-ligating and deubiquitinating enzymes that are addressed here for the clearance of AD-PD cross talk markers. Altogether, these key findings can help the scientists to accelerate the identification of novel therapeutic modalities for such age related incurable neurodegenerative pathologies, including AD and PD.

Declaration of Competing Interest

There is no conflict or competing interest declared by the authors.

Acknowledgments

We would like to thanks the senior management of Delhi Technological University for constant support and encouragement.

References

Bailey, R.M., Covy, J.P., Melrose, H.L., Rousseau, L., Watkinson, R., Knight, J., Miles, S., Farrer, M.J., Dickson, D.W., Giasson, B.I., Lewis, J., 2013. LRRK2 phosphorylates novel tau epitopes and promotes tauopathy. Acta Neuropathol. 126 (6), 809–827. https://doi.org/10.1007/s00401-013-1188-4.

Balupuri, A., Choi, K.E., Kang, N.S., 2019. Computational insights into the role of α-strand/sheet in aggregation of α-synuclein. Sci. Rep. 9 (1), 59. https://doi.org/10.1038/s41598-018-37276-1.

Barage, S.H., Sonawane, K.D., 2015. Amyloid cascade hypothesis: pathogenesis and therapeutic strategies in Alzheimer's disease. Neuropeptides 52, 1–18. https://doi.org/10.1016/j.npep.2015.06.008.

Berman, H.M., Westbrook, J., Feng, Z., Gilliland, G., Bhat, T.N., Weissig, H., Shindyalov, I.N., Bourne, P.E., 2000. The Protein Data Bank. Nucleic Acids Res. 28, 235–242.

Breydo, L., Uversky, V.N., 2014. Molecular mechanisms of protein misfolding. In: Bionanoimaging (Protein Misfolding and Aggregation). 2014. pp. 1–14.

Chen, Z.C., Zhang, W., Chua, L.L., Chai, C., Li, R., Lin, L., Cao, Z., Angeles, D.C., Stanton, L.W., Peng, J.H., Zhou, Z.D., Lim, K.L., Zeng, L., Tan, E.K., 2017. Phosphorylation of amyloid precursor protein by mutant LRRK2 promotes AICD activity and neurotoxicity in Parkinson's disease. Sci. Signal. 10 (488). https://doi.org/10.1126/scisignal.aam6790. pii: eaam6790.

Choi, B.K., Kim, J.Y., Cha, M.Y., Mook-Jung, I., Shin, Y.K., Lee, N.K., 2015. β-Amyloid and α-Synuclein cooperate to block SNARE-dependent vesicle fusion. Biochemistry 54 (9), 1831–1840.

Choong, C.J., Mochizuki, H., 2017. Inappropriate trafficking of damaged mitochondria in Parkinson's disease. Stem Cell Investig. 4, 17. https://doi.org/10.21037/sci.2017.02.07.

Ciechanover, A., Kwon, Y.T., 2015. Degradation of misfolded proteins in neurodegenerative diseases: therapeutic targets and strategies. Exp. Mol. Med. 47, e147. https://doi.org/10.1038/emm.2014.117.

Clinton, L.K., Blurton-Jones, M., Myczek, K., Trojanowski, J.Q., LaFerla, F.M., 2010. Synergistic interactions between Abeta, tau, and alpha-synuclein: acceleration of neuropathology and cognitive decline. J. Neurosci. 30 (21), 7281–7289. https://doi.org/10.1523/JNEUROSCI.0490-10.2010.

Cox, D., Raeburn, C., Sui, X., Hatters, D.M., 2018. Protein aggregation in cell biology: an aggregomics perspective of health and disease. Semin. Cell Dev. Biol. (17), 2–30393. https://doi.org/10.1016/j.semcdb.2018.05.003. pii: S1084-9521.

Credle, J.J., George, J.L., Wills, J., Duka, V., Shah, K., Lee, Y.C., Rodriguez, O., Simkins, T., Winter, M., Moechars, D., Steckler, T., Goudreau, J., Finkelstein, D.I., Sidhu, A., 2015. GSK-3β dysregulation contributes to parkinson's-like pathophysiology with associated region-specific phosphorylation and accumulation of tau and α-synuclein. Cell Death Differ. 22 (5), 838–851. https://doi.org/10.1038/cdd.2014.179.

Cuanalo-Contreras, K., Mukherjee, A., Soto, C., 2013. Role of protein misfolding and

proteostasis deficiency in protein misfolding diseases and aging. Int. J. Cell Biol. 2013, 638083. https://doi.org/10.1155/2013/638083.

DeLano, W.L., 2002. The PyMOL Molecular Graphics System. DeLano Scientific LLC, San CarlosCA, pp. 700.

Dunkelmann, T., Teichmann, K., Ziehm, T., Schemmert, S., Frenzel, D., Tusche, M., Dammers, C., Jurgens, D., Langen, K.J., Demuth, H.U., Shah, N.J., Kutzsche, J., Willuweit, A., Willbold, D., 2018. Aβ oligomer eliminating compounds interfere successfully with pEAβ(3-42) induced motor neurodegenerative phenotype in transgenic mice. Neuropeptides 67, 27–35. https://doi.org/10.1016/j.npep.2017.11.011.

Guo, J.L., Covell, D.J., Daniels, J.P., Iba, M., Stieber, A., Zhang, B., Riddle, D.M., Kwong, L.K., Xu, Y., Trojanowski, J.Q., Lee, V.M., 2013. Distinct α-synuclein strains differentially promote tau inclusions in neurons. Cell 154 (1), 103–117.

Hao, J., Zhang, W., Zhang, P., Liu, R., Liu, L., Lei, G., Su, C., Miao, J., Li, Z., 2010. Abeta20-29 peptide blocking apoE/Abeta interaction reduces full-length Abeta42/40 fibril formation and cytotoxicity in vitro. Neuropeptides 44 (4), 305–313. https://doi.org/10.1016/j.npep.2010.03.001.

Hooper, C., Killick, R., Lovestone, S., 2008. The GSK3 hypothesis of Alzheimer's disease. J. Neurochem. 104 (6), 1433–1439.

Ibanez, L., Dube, U., Davis, A.A., Fernandez, M.V., Budde, J., Cooper, B., Diez-Fairen, M., Ortega-Cubero, S., Pastor, P., Perlmutter, J.S., Cruchaga, C., Benitez, B.A., 2018. Pleiotropic effects of variants in dementia genes in Parkinson disease. Front. Neurosci. 12, 230. https://doi.org/10.3389/fnins.2018.00230.

Jellinger, K.A., 2010. Basic mechanisms of neurodegeneration: a critical update. J. Cell. Mol. Med. 14 (3), 457–487. https://doi.org/10.1111/j.1582-4934.2010.01010.x.

Jellinger, K.A., 2012. Interaction between pathogenic proteins in neurodegenerative disorders. J. Cell. Mol. Med. 16 (6), 1166–1183.

Jensen, L.J., Kuhn, M., Stark, M., Chaffron, S., Creevey, C., Muller, J., Doerks, T., Julien, P., Roth, A., Simonovic, M., Bork, P., von Mering, C., 2009. STRING 8–a global view on proteins and their functional interactions in 630 organisms. Nucleic Acids Res. 37, D412–D416. https://doi.org/10.1093/nar/gkn760. Database issue.

Jolkkonen, J., Hartikainen, P., Soikkeli, R., Bissette, G., Nemeroff, C., Riekkinen, P., 1991. A correlation study of CSF neuropeptides in Alzheimer's and Parkinson's disease. Neuropeptides 19 (2), 97–102. https://doi.org/10.1016/0143-4179(91)90138-9.

Kalinowska, B., Banach, M., Wiśniowski, Z., Konieczny, L., Roterman, I., 2017. Is the hydrophobic core a universal structural element in proteins? J. Mol. Model. 23 (7), 205. https://doi.org/10.1007/s00894-017-3367-z.

Kanehisa, M., Furumichi, M., Tanabe, M., Sato, Y., Morishima, K., 2017. KEGG: new perspectives on genomes, pathways, diseases and drugs. Nucleic Acids Res. 45 (D1), D353–D361. https://doi.org/10.1093/nar/gkw1092.

Kumar, P., Pradhan, K., Karunya, R., Ambasta, R.K., Querfurth, H.W., 2012. Cross-functional E3 ligases parkin and C-terminus Hsp70-interacting protein in neurodegenerative disorders. J. Neurochem. 120 (3), 350–370. https://doi.org/10.1111/j.1471-4159.2011.07588.x.

Lei, P., Ayton, S., Finkelstein, D.I., Adlard, P.A., Masters, C.L., Bush, A.I., 2010. Tau protein: relevance to Parkinson's disease. Int. J. Biochem. Cell Biol. 42 (11), 1775–1778.

Linse, S., 2019. Mechanism of amyloid protein aggregation and the role of inhibitors. Pure Appl. Chem. 91 (2), 211–229. https://doi.org/10.1515/pac-2018-1017.

Lovas, S., Zhang, Y., Yu, J., Lyubchenko, Y.L., 2013. Molecular mechanism of misfolding and aggregation of Aβ(13 − 23). J. Phys. Chem. B 117 (20), 6175–6186. https://doi.org/10.1021/jp402938p.

Marinko, J.T., Huang, H., Penn, W.D., Capra, J.A., Schlebach, J.P., Sanders, C.R., 2019. Folding and misfolding of human membrane proteins in health and disease: from single molecules to cellular proteostasis. Chem. Rev. 119 (9), 5537–5606. https://doi.org/10.1021/acs.chemrev.8b00532.

Marsh, S.E., Blurton-Jones, M., 2012. Examining the mechanisms that link β-amyloid and α-synuclein pathologies. Alzheimers Res. Ther. 4 (2), 11. https://doi.org/10.1186/alzrt109.

Martin-Maestro, P., Gargini, R., Perry, G., Avila, J., García-Escudero, V., 2016. PARK2 enhancement is able to compensate mitophagy alterations found in sporadic Alzheimer's disease. Hum. Mol. Genet. 25 (4), 792–806. https://doi.org/10.1093/hmg/ddv616.

Matsui, D., Nakano, S., Dadashipour, M., Asano, Y., 2017. Rational identification of aggregation hotspots based on secondary structure and amino acid hydrophobicity. Sci. Rep. 7 (1), 9558. https://doi.org/10.1038/s41598-017-09749-2.

Mokhtari, F., Riazi, G., Balalaie, S., Khodarahmi, R., Karima, S., Hemati, A., Bolouri, B., Katouli, F.H., Fathi, E., 2016. Peptides NAP and SAL attenuate human tau granular-shaped oligomers in vitro and in SH-SY5Y cells. Neuropeptides 59, 21–31. https://doi.org/10.1016/j.npep.2016.06.005.

Morimoto, R.I., 2008. Proteotoxic stress and inducible chaperone networks in neurodegenerative disease and aging. Genes Dev. 22, 1427–1438.

Moskvina, V., Harold, D., Russo, G., Vedernikov, A., Sharma, M., Saad, M., Holmans, P., Bras, J.M., Bettella, F., Keller, M.F., Nicolaou, N., Simón-Sánchez, J., Gibbs, J.R., Schulte, C., Durr, A., Guerreir, R., Hernandez, D., Brice, A., Stefánsson, H., Majamaa, K., Gasser, T., Heutink, P., Wood, N., Martinez, M., Singleton, A.B., Nalls, M.A., Hardy, J., Owen, M.J., O'Donovan, M.C., Williams, J., Morris, H.R., Williams, N.M., IPDGC., GERAD investigators, 2013. Analysis of genome-wide association studies of alzheimer disease and of parkinson disease to determine if these 2 diseases share a common genetic risk. JAMA Neurol. 70 (10), 1268–1276.

Padayachee, E.R., Whiteley, C.G., 2013. Interaction of glycine zipper fragments of Aβ-peptides with neuronal nitric oxide synthase: kinetic, thermodynamic and spectrofluorimetric analysis. Neuropeptides 47 (3), 171–178. https://doi.org/10.1016/j.npep.2012.12.006.

Pathan, M., Keerthikumar, S., Ang, C.S., Gangoda, L., Quek, C.M.J., Williamson, N.J., Mouradov, D., Sieber, O.M., Simpson, R.J., Salim, A., Bacic, A., Hill, A.F., Stroud, D.A., Ryan, M.T., Agbinya, J.A., Mariadasson, J.M., Burgess, A.W., Mathivanan, S., 2015. FunRich: a standalone tool for functional enrichment analysis. Proteomics 15, 2597–2601. https://doi.org/10.1002/pmic.201400515.

Petkova, A.T., Ishii, Y., Balbach, J.J., Antzutkin, O.N., Leapman, R.D., Delaglio, F., Tycko, R., 2002. A structural model for Alzheimer's β-amyloid fibrils based on experimental constraints from solid state NMR. Proc. Natl. Acad. Sci. U. S. A. 99, 16742–16747.

Petkova, A.T., Yau, W.M., Tycko, R., 2006. Experimental constraints on quaternary structure in Alzheimer's β-amyloid fibrils. Biochemistry 45, 498–512.

Relini, A., Marano, N., Gliozzi, A., 2013. Misfolding of amyloidogenic proteins and their interactions with membranes. Biomolecules 4 (1), 20–55. https://doi.org/10.3390/biom4010020.

Rose, A.S., Hildebrand, P.W., 2015. NGL viewer: a web application for molecular visualization. Nucleic Acids Res. 43, W576–W579. https://doi.org/10.1093/nar/gkv402. Web Server issue.

Rutkowski, D.T., Kaufman, R.J., 2004. A trip to the ER: coping with stress. Trends Cell Biol. 14, 20–28.

Sassone, J., Serratto, G., Valtorta, F., Silani, V., Passafaro, M., Ciammola, A., 2017. The synaptic function of parkin. Brain 140 (9), 2265–2272. https://doi.org/10.1093/brain/awx006.

Scott, K.A., Alonso, D.O., Sato, S., Fersht, A.R., Daggett, V., 2007. Conformational entropy of alanine versus glycine in protein denatured states. Proc. Natl. Acad. Sci. U. S. A. 104 (8), 2661–2666.

Singh, K., Han, K., Tilve, S., Wu, K., Geller, H.M., Sack, M.N., 2018. Parkin targets NOD2 to regulate astrocyte endoplasmic reticulum stress and inflammation. Glia 66 (11), 2427–2437. https://doi.org/10.1002/glia.23482.

Singleton, A., Hardy, J., 2016. The evolution of genetics: Alzheimer's and Parkinson's diseases. Neuron 90 (6), 1154–1163. https://doi.org/10.1016/j.neuron.2016.05.040.

Sinha, S., Lopes, D.H., Bitan, G., 2012. A key role for lysine residues in amyloid β-protein folding, assembly, and toxicity. ACS Chem. Neurosci. 3 (6), 473–481. https://doi.org/10.1021/cn3000247.

Sun, T., Ding, W., Xu, T., Ao, X., Yu, T., Li, M., Liu, Y., Zhang, X., Hou, L., Wang, J., 2019. Parkin regulates programmed necrosis and myocardial ischemia/reperfusion injury by targeting CypD. Antioxid. Redox Signal. https://doi.org/10.1089/ars.2019.7734. Epub ahead of print.

Szklarczyk, D., Franceschini, A., Wyder, S., Forslund, K., Heller, D., Huerta-Cepas, J., Simonovic, M., Roth, A., Santos, A., Tsafou, K.P., Kuhn, M., Bork, P., Jensen, L.J., von Mering, C., 2015. STRING v10: protein-protein interaction networks, integrated over the tree of life. Nucleic Acids Res. 43, D447–D452. https://doi.org/10.1093/nar/gku1003. Database issue.

Touw, W.G., Baakman, C., Black, J., te Beek, T.A.H., Krieger, E., Joosten, R.P., Vriend, G., 2015. A series of PDB-related databanks for everyday needs. Nucleic Acids Res. 43, D364–D368. https://doi.org/10.1093/nar/gku1028. Database issue.

Williams, E.T., Glauser, L., Tsika, E., Jiang, H., Islam, S., Moore, D.J., 2018. Parkin mediates the ubiquitination of VPS35 and modulates retromer-dependent endosomal sorting. Hum. Mol. Genet. 27 (18), 3189–3205. https://doi.org/10.1093/hmg/ddy224.

Yang, J.W., Ru, J., Ma, W., Gao, Y., Liang, Z., Liu, J., Guo, J.H., Li, L.Y., 2015. BDNF promotes the growth of human neurons through crosstalk with the Wnt/β-catenin signaling pathway via GSK-3β. Neuropeptides 54, 35–46. https://doi.org/10.1016/j.npep.2015.08.005.

Yao, T.P., 2010. The role of ubiquitin in autophagy-dependent protein aggregate processing. Genes Cancer 1 (7), 779–786.

Zeng, L., Chen, Z., Zhang, W., Chua, L.L., Chai, C., Li, R., Lin, L., Cao, Z., Angeles, D.C., Stanton, L.W., Peng, J., Zhou, Z.D., Lim, K.H., Tan, E.K., 2018. Neuropathophysiology cross-talk between Alzheimer's and Parkinson's disease. J. Alzheimers Dis. Parkinsonism 8, 43.

Zhang, C.W., Hang, L., Yao, T.P., Lim, K.L., 2016. Parkin regulation and neurodegenerative disorders. Front. Aging Neurosci. 7, 248. https://doi.org/10.3389/fnagi.2015.00248.

Zhao, Y., Ho, P., Yih, Y., Chen, C., Lee, W.L., Tan, E.K., 2011 Nov. LRRK2 variant associated with Alzheimer's disease. Neurobiol Aging 32 (11), 1990–1993. https://doi.org/10.1016/j.neurobiolaging.2009.11.019. Epub 2009 Dec 16. PubMed PMID: 20018409.

ResearchGate

See discussions, stats, and author profiles for this publication at: https://www.researchgate.net/publication/335527859

Design and Study of a Solar Thermal Syphon Pump

Article · September 2014

CITATIONS
0

READ
1

5 authors, including:

Md Zishan Akhter
United Arab Emirates University
5 PUBLICATIONS **4** CITATIONS

SEE PROFILE

All content following this page was uploaded by Md Zishan Akhter on 01 September 2019.

The user has requested enhancement of the downloaded file.

DESIGN AND STUDY OF A SOLAR THERMAL SYPHON PUMP

Md. Zishan Akhter[1], Md. Sarwar Khan[2], Md Sameer Farooque[3], Kaushalendra K. Dubey[4], Gopal P. Sinha[5]

[1,2,3]U.G.Student,Dept of M & AE, School of Engg & Tech, Sharda University,Gr Noida,U.P. India
[4] Research Scholar, Dept of Mechanical, Production, Industrial & Automobile Engg, Delhi Technological University, New Delhi, India
[5]Professor,Dept of M & AE, School of Engg & Tech, Sharda University,Gr Noida,U.P. India

ABSTRACT

This paper describes the idea and the development of a solar thermal energy driven pump for lifting of ground water for irrigation as well as for meeting urban supply system. This has the potential of saving over 93billion kWh of electrical energy and 3.3 billion litres of diesel (fossil fuel) per year, for India. The invention has been patented. The most attractive feature of the pump is the absence of any moving part, which makes it almost maintenance-free. Solar thermal energy is used to create a pressure higher than the atmospheric pressure, over the surface of liquid to be pumped to height H. The estimated thermal efficiency of solar thermal syphon pumping is four times of photovoltaic pumping system.

Keywords - Solar Thermal Energy, Syphon Pump, Overall Efficiency.

NOMENCLATURE

Aa = aperture area of PTC in m^2
Sc = solar constant in KW/m^2
Pc = pressure created by solar energy in Pascal,
P_A = Atmospheric pressure in Pascal
P = Mass density of liquid in kg /m^3.
g = acceleration due to gravity in m/s^2.
h = Enthalpy of steam.
H = Discharge height.
m_w = mass flow rate of water in m^3/s.
m_s = mass flow of steam in m^3/s.
V = flow velocity of water in m/s
Hs = friction loss in pipe.

ϕ = Latitude angle of location where system is installed in degree

β = Inclination angle of PTC system from horizontal in degree.

r_r = Rim Radius in meter.

ϕ_r = Rim Angle in degree

f = Focal Distance in meter.

h_p = Parabolic Height in meter.

D = Receiver or Boiler Diameter in meter.

C_R = Concentration Ratio

Θ = Incidence Angle in degree.

ω = Hour angle

γ = System Azimuth angle in degree

δ = Solar Incidence angle in degree.

n = Total no of day in month measured from 1st January.

$\eta_{opto\text{-}thermal}$ = Opto-Thermal efficiency of Syphon system

Ib = Solar Irradiation

q_u = Rate of use full energy in joule

U_L = heat loss co-efficient (W / m^2k)

Tc = Receiver Temperature in ^0C

Tr = Mean Receiver Temperature in ^0C

Ta = Ambient Temperature in ^0C

Rk = Thermal Resistance of Receiver or Boiler Tube

Acond = Effective area of conduction in m^2

ϵr = Non selective absorber parameter.

$\tau\alpha$ = Effective Transmission.

Qgen = Heat generated from PTC.

Qreq = Required Heat for steam generation.

$\eta_{thermo\text{-}syphon}$ = Thermal Efficiency of system.

ηo = Overall Efficiency.

η_{SPV} =Solar Photovoltaic panel Efficiency.

η_{pump} = Irrigation pump Efficiency.

η_{CC} = Charge-Controller Efficiency.

η_B = Battery Efficiency.

l = Length

b = Width

t = Thickness

PTC=Parabolic Through Collector.

STSP= Solar Thermal Syphon Pump.

SPVP= Solar Photovoltaic Pump System.

IJARSE

I. INTRODUCTION.

Most of the developing countries have large needs of irrigation for meeting their agricultural requirements for food-security. The drinking water requirement also necessitates lifting of ground water to a height ranging from 50 to 200 feet. This requires huge amount of energy which is currently supplied through electricity and fossil fuel based engines. For a country like India the energy consumed for lift irrigation has been 93225.28MU, (in the year 2011),1MU= 1M kWhr [6].In most of the cases the developing countries are endowed with rich solar energy. Some of it has been used for lift irrigation using photovoltaic panels electrically coupled to a conventional motor pump system, or Stirling cycle based engine coupled through a conventional pump. The potential number of SPV pumps is estimated at 70 million, with extending irrigation support to untapped markets [7]. This work reports the use of direct solar thermal energy for creating pumping action. The uniqueness of this development is that the pumping action requires no moving parts-reciprocating, rotating or expander action. Therefore there is no possibility of wear and tear or lubrication requirement or loss of energy due to friction between moving parts. Syphon action created by water vapour picked-up from the source, lifts the water from the reservoir through the delivery head. This is being demonstrated for the first time. The efficiency of the entire system is also high on account of no moving parts. An excellent review of the development of solar energy based pumps have been carried out by Y.Wong et al [11].The proposed thermo-syphon pump is a high pressure steam forced pump where there is no limitation of a suction head of less than 34 feet of water, the delivery head is unlimited based on the concentration of solar energy and the aperture area requirement of the solar collector has been worked out in subsequent paragraphs.

A model has been fabricated for proving the concept. This model demonstrates lifting of water through a head of nearly 5 to 10 feet Fig.2, shows a sketch of the parabolic trough collector (PTC) used for concentrating the solar thermal energy.

In most of the developing countries are endowed with rich solar energy. Some of it has been used for lift irrigation using photovoltaic panels electrically coupled to a conventional pump, or Stirling cycle based engine coupled through a conventional pump. The potential number of SPV pumps is estimated at 70 million, with extending irrigation support to untapped markets [7]. Total cost (before subsidy) for installation and commissioning of SPV water pump system varies from Rs. 190,000 to 290,000 or even Rs. 450,000/- [8][9].Capital cost of a 1.8 kWp solar PV pump is about Rs. 0.3 million. The payback period of solar PV pump (without subsidy) replacing a diesel pump is about 9 years (at a cost of diesel is Rs. 32/litre) [12].Purohit evaluated the financial attractiveness of different renewable energy technologies for irrigation water pumping in India. He calculated the following unit costs for water for SVP pumping systems [10]. The unique part of this development is that the pumping action requires no moving parts, reciprocating or rotating and therefore there is no possibility of wear and tear or lubrication requirement. A model has been fabricated for proving the concept as shown in Fig.1a and Fig.1b. This model demonstrates lifting of water through a head of nearly 5 to 10 feet.

II. WORKING OF SOLAR THERMAL SYPHON PUMP.

Solar Thermal Syphon pumping system (STSP) may be used to lift water from the ground or any liquid to a height without using any moving mechanical-part by pressurized steam through syphon action. The steam is generated by solar energy concentrator on a tube filled with the liquid. The concentration of solar energy can be

achieved by parabolic trough collector (PTC) / concave / plane mirrors type solar concentrator or through Fresnel lenses based solar thermal system.

Water liquid enters into a boiler cell, through an inlet regulated by a float valve action, for maintaining a uniform level. Steam generated in the boiler flows through a perfectly insulated and sealed pipe into an enclosures connected to ground water to be pumped. The discharge pipe is dipped below the ground water. The pressurized steam lifts the water to the delivery head H, through a syphon action. The conversion of water in to steam at boiling temperature of water depends upon the thermal energy obtained from the area of PTC (Aperture Area of concentrator).The heat raise the temperature of boiler and water gets converts into steam. The water feeding pipe use some amount of steam pressure feeding water to the boiler [8]. Fig.1a and Fig.1b, show the model and working set up of the thermo-syphon pump. This system has been developed in mechanical

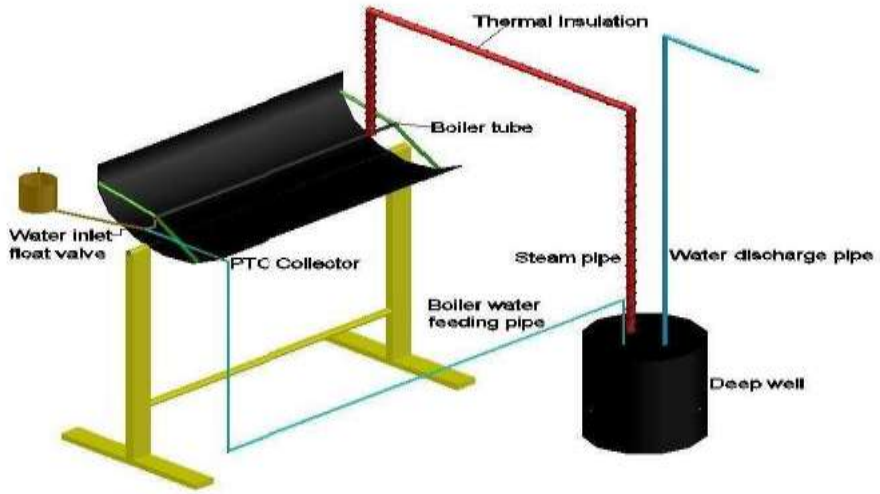

engineering department sharda university greater noida,u.p. state, India. Dimension of all parts of STSP listed in Table-1

Fig. 1a: Schematic of Solar thermal Syphon Pump.

Fig. 1b: Working set up of Solar thermal Syphon Pump at Sharda University Greater Noida campus.

III. PRINCIPLES OF THE SOLAR THERMAL SYPHON SYSTEM.

The solar thermal syphon pump derives its pumping action by putting additional pressure on the surface of the liquid, to be lifted. This additional pressure is obtained using solar thermal energy in concentrated form. The concentrated solar thermal energy obtained by a parabolic trough collector (PTC) is given by

[2]

$Q_{gen} = Aa\ Ib\ W$……..(1)

The useful solar gain by the collector $Qu = Aa\ (\tau\alpha)\ Ib\ W$

$\tau\alpha$ = Effective Transmission

The head of lifted water or liquid is given by

$H = (Pc - P_A)/ \beta g$ meters .Where Pc is pressure created by solar energy in Pascal, P_A is Atmospheric pressure in Pascal ,β is Mass density of liquid in kg /m^3 and g is acceleration due to gravity in m/s^2.

3.1 Collection and concentration of solar thermal energy using PTC.

For generating steam, whose pressure is used for pumping of liquid to a height, we require concentrated solar thermal energy for super heated high pressure steam at a high pressure. This is achieved by a PTC or a Fresnel lens or a combination of the two. The concentrated thermal energy obtained through PTC is given by Heat required for steam generation [4],

$Q_{reqired} = m_{water} [Cp_{water} (T_{boiling} - T_{ambient}) + LH_{water}] +$

$m_{steam} [Cp_{steam} (T_{sup} - T_{boiling}) + LH_{vaporisation}]$ KJ……..(2)

For system to work continuously

Qgen >. Qreq……..(3)

Boiling Temperature of water for the exerting the required steam pressure ($T_{boiling}$) is directly taken from steam table corresponding to the pressure Pc.This heat can generate steam at a pressure Pc is given by

Pressure required on water table for achieving the discharge head

$Pc = 10^5 + 10^4\ H$ Pa……..(4)

This pressure on the surface of the liquid can lift it by 'H' meter through syphon action is given by

$H = (Pc - Pa)/ \beta g$ meter……...(5)

3.2 Estimation of specified head H and flow rate Q.

Heat from PTC is mainly required to meet the heat loss occurring due to imperfect insulation and the temperature difference between the superheated steam and the ambient. It is given by,

Total energy in steam = Energy given to discharge

$m_s h = m_w g H + ½ m_w v^2 + hs$……..(6)

Conduction loss in pipe = Effective surface area for conduction (Acond) / thermal resistance (R_k).

$[\frac{(Tr-Ta)}{Rk} \times \frac{Acond}{Aa}]$……..……..(7)

3.3 Design parameters of PTC.

Parabolic through collector (PTC) are preferred for solar steam generation because high temperature can be obtained without any degradation of collector efficiency. The specifications of PTC shown in fig.2 of PTC design for steam generation. All design calculations provide by equations below.

Projected area for heat require = Aperture area of PTC = Aa m^2

Solar Constant [2] = 1000W/m^2 (Standard for India)

Solar radiation (Ib) = 750W/m^2. (Taken average value for month of April-May)

Parabolic Aperture area of PTC = Aa m^2 = 550 W / Q_{gen}.

Dimensions of PTC on the basis of aperture area, Aa = b × h.

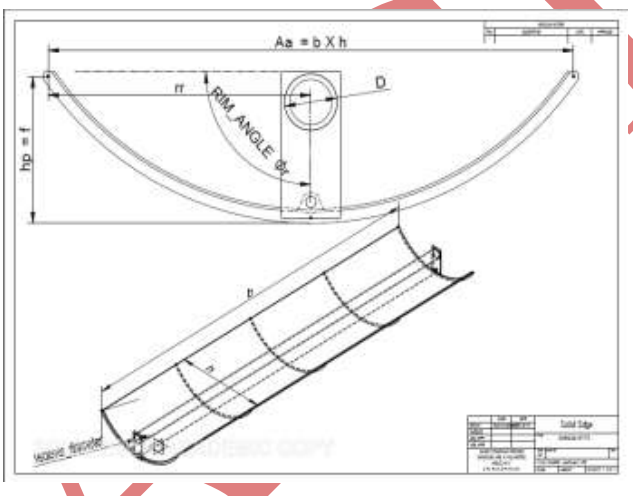

Fig. 2: Schematic of parabolic through collector.

Rim Angle [5] = ϕ_r = Sin^{-1} (Aa /2 r_r)……..……(8)

Focal Distance [5] = f = $\frac{Aa}{4\tan\frac{\varphi r}{2}}$……..……..(9)

Parabolic Height [5] = h_p = f

Receiver or Boiler Diameter [5] = D = $\sqrt{\frac{4}{1000\,\pi\,b}}$ m……..……(10)

Concentration Ratio [5] = C_R = $\frac{Aa-D}{\pi D}$……..……(11)

Incidence Angle (Θ) [2] = Cos Θ = Sin ϕ (Sin δ * Cos β + Cos δ* Cos γ * Cos ω * Sin β) + Cos ϕ (Cos δ * Cos ω * Cosβ – Sin δ * Cos γ * Sin β) + Cos δ * Sin γ * Sin ω * Sin β……..……(12)

ω = Hour angle [2] = (Solar Time – 12:00)15^0.

(Afternoon solar time taken as +ve hour angle, whereas forenoon solar time taken as –ve solar time.)

δ = Solar Incidence angle [2] = 23.45 × Sin [$\frac{360}{365}(n+284)$]……..……(13)

3.4 Dimensions of STSP parts.

Table-1 Dimensions of STSP

STSP Parts	Dimensions
Reflector	l = 2.44 m, b= 1.25 m, t= 0.4 m. Aperture Area = 2.44 m^2
G.I Sheet for reflector support.	l = 2.44 m, b= 1.25 m, t= 0.36 m.
Copper Water Tube	L = 2.44m,Diameter = 20mm, Volume = 7.6 ×10 $^{-5}$ m^3
PVC Steam Tube	Diameter =14mm, Thermally insulated with glass wool.
Supporting Iron Frame **Arc** **Rods** **Rivets** **Mounting Nut**	No. Of Arc = 5, No of Rods = 3 t = 3 mm, Arc length = 1.25 m t = 3mm, l = 2.44 m 10 (Aluminium with head), l = 10mm, diameter = 4mm. Diameter = 9mm (5mm from top and each side)
Iron Stand	l = 1.17 m, t = 5mm.

IV. EFFICIENCY INVOLVED.

4.1 Opto-Thermal Efficiency ($\eta_{opto\text{-}thermal}$)

$$\eta_{opto\text{-}thermal} = qu / Ib\ Aa = \eta_O - \frac{1}{Ib}\left[\frac{(Tr-Ta)}{Rk} \times \frac{Acond}{Aa}\right] + \epsilon r \left[\frac{Tr4-Tc4}{CR}\right] \quad \text{.....(14)}$$

$$\text{Rate of use full energy} = q_u = \eta o\ I_b\ Aa - U_L(Tr - Ta)Aa \quad \text{.....(15)}$$

Rk = Thermal Resistance of Receiver or Boiler Tube =

$$\frac{\text{Distence Travel by conductive heat in boiler tube or recevier } (x)}{\text{Thermal conductivity of recevier metal } (K) \times \text{Condution Area } (A)}$$

4.2 Thermal Efficiency ($\eta_{thermo\text{-}syphon}$)

$$\eta_{thermo\text{-}siphon} \text{ or } \eta_I = Q_{required} / Q_{gen} \quad \text{.....(16)}$$

4.3 Over All Efficiency (ηo)

$$\eta o = \eta_{opto\text{-}thermal} \times \eta_{thermo\text{-}syphon} \quad \text{.....(17)}$$

V. ESTIMATION OF STSP EFFICIENCY WITH PHOTOVOLTAIC PUMP EFFICIENCY.

Efficiency of Solar Photovoltaic Pump (η_{SPVP})

$$\eta_{SPVP} = \eta_{SPV} * \eta_B * \eta_{CC} * \eta_{pump}$$

η_{SPV} = 15%

η_{pump} = 50%

η_{CC} = 90%

η_B = 85%

Lead-acid batteries typically have columbic efficiency of 85% and energy efficiencies in order of 70 % [9]. Columbic efficiency is the ratio of number of charges that enter the battery during charging compared to the number that can be extracted from the battery during discharging [9].

η_{CC} depend on the input-output level of voltage-current. DC-AC conversion efficiency as 100% but practically it is not possible because some account of heat dissipated by the passive components. Therefore, there is no way to simulate 100% charge-controller efficiency. We can assume more than 90%.

Farm irrigation pumping is around 70 to 80% of total farm electricity usage [10].

η_{SPVP} = 15% * 85% * 90% * 70% = 8.08 %

VI. RESULTS AND DISCUSSION.

An experiment with the fabricated model was carried out in the month of April-May. In a mid day when the sun rays were focused on the copper boiler, the pump lifted the water from the down reservoir and sprayed a stream up to a height of 10 feet. This gave a feel that about 50% of energy was lost in reflector. A more reflective surface with better focussing power is recommended. The concept was clearly demonstrated.

The result of energy and exergy analysis of STSP shown in Table 2:

Table-2, STSP Efficiency results

System/Efficiency (%) → ↓	$\eta_{optical}$	$\eta_{thermal}$ or η_I	$\eta_{overall} = \eta_{optical} \times \eta_{thermal}$
STSP	75	46.6	34.9
SPV Pump			8.08

VII. CONCLUSION.

It is possible to use direct solar thermal energy for pumping action instead of going through the photovoltaic electrical route, where the SPV pumpinjg system overall efficiency comes to 8% against 35 % (η_{opt} and η_I comes 75% and 46% respectively) of solar thermal syphon pump system. Apart from this significant gain in utilisation of solar energy, there is further indirect savings in energy required for production of solar photovoltaic panel. The solar thermal syphon pump would be a significant environment friendly attempt for harnessing solar energy.

The unique part of this development is that the solar thermal syphon pump has no moving parts and it is thus maintenance free.

VIII. ACKNOWLEDGMENT

This project has been funded by Sharda University and we are very thankful for this.

REFERENCES.

[1] Principles of solar engineering by Frank Kreith, Jan F. Kreider, McGraw-Hill, 1981.

[2] Solar Energy: Principles of Thermal Collection and Storage By S.P. Sukhatme.Tata McGraw-Hill,2008.

[3] Introduction to Fluid Mechanics by Fox & McDonald,John Wiley & Sons,2008

[4] Basic and applied Thermodynamics by P.K.Nag,Tata McGraw-Hill, 2004

[5] Kalogirou, S.; and Lloyd, S.Use of solar parabolic trough collectors for hot water production in Cyprus. A feasibility study. Renewable Energy 2(2): 117-124.1992.

[6] State-wise Electricity Consumption & Conservation Potential in India. Bureau Of Energy Efficiency (BEE) Ministry of Power, Government of India, Report2009, www.emt india.net/eca2009/14Dec2009/CombinedSummaryReport.pdf.

[7] HWWI (2005): CDM potential of SPV pumps India. http://www.hwwi.org/uploads/tx_wilpubdb/HWWI_Research_Paper_4.pdf.

[8] "Solar Thermal Syphon pump System for Irrigation",Gopal P Sinha,Kaushalendra Kr Dubey, India Patent,Patent Docket No- 9684,Application No-1626/DEL/2013,Reference No- E-2/5773/2013-DEL, E-3/5571/2013-DEL, E-5/5240/2013-DEL,Date of Patent filied-30/05/2013.

[9] Cral John Rydh, BjornA. Sanden, Energy Analysis of batteries in photovoltaic syste,Part-ll, Energy return factors and overall efficiencies, Journal of energy conversion and management,Elsevier,46 (2005),1980-2000.

[10] Jamse Curaan, Agricultural Resource Management. Irrigation Pump Efficiency, www.farmpoint.tas.gov.au.

[11] Solar thermal water pumping systems-a review Y.W. Wong,K.Sumathy_ Department of Mechanical Engineering\ University of Hong Kong\ Hong Kong, August 1998.

IJARSE

Journal of Multi Disciplinary Engineering Technologies, Vol. 12, Issue 2

Design of Power Efficient 4:2 Compressors Using PFAL and Modified PFAL Adiabatic Logic Families

A. Mann[1], N. Malhotra[1], K. Gupta[2], N. Pandey[1,#]

[1]*Dept. of Electronics and Communication, Delhi Technological University*
[2]*Dept. of Electronics and Communication, Bharati Vidyapeeth's College of Engineering Delhi*

[#]Corresponding Author, Email: *n66pandey@rediffmail.com*

***Abstract*- Compressor is a crucial entity for all multiplier circuits, which influence the speed of operation of the circuit. This paper presents the low power design of a 4:2 compressor in adiabatic *logic* style. Two adiabatic logic families namely, positive feedback adiabatic logic (PFAL) and modified PFAL are chosen over the other adiabatic families due to their ease in CMOS integration in deep sub-micron technologies. The proposed compressor designs are implemented and their functionality is verified through simulations in Tanner EDA simulator using 180nm CMOS parameters. An investigation on the power consumption of the proposed compressor by varying the power supply, load capacitance and frequency of the signal is done. It is found that the modified PFAL based 4:2 compressor shows the best performance.**

***Keywords*- Adiabatic logic, PFAL, Modified PFAL, VLSI, Compressor, Power Efficient Circuits**

1. INTRODUCTION

In today's world, while moving towards digitalization of data and circuits, power consumption has become major concern in design of portable devices [1]. The digitization of data involves extensive processing resulting in power hungry devices. Portable devices like laptops, cell phones, therefore require the circuitries that consume low power. CMOS logic is generally employed in designing digital circuits due to design ease, high speed. But in relation to battery operated devices, there is a need to lower power consumption of devices. New methodologies have been developed in the past to reduce the losses in the CMOS circuits at various levels of abstraction such as voltage scaling, compact layout, clock gating etc. [2]. However, it has been proven that the circuit design using adiabatic logic has the potential to reduce power consumed per operation significantly [1].

Along with the low power requirement, now-a-days a majority of applications require high speed data computation units. High speed multipliers play a potent role in designing such digital circuits [3]. They are used in real time image and speech processing, mainly the fields where high speed and accuracy is required [4]. Consequently, many methods have been suggested to make multiplication fast and accurate [5]. It is noted that the partial product reduction stage is responsible for a significant portion of the total multiplication delay, power and area. To address this issue, compressors are usually employed since they reduce partial products thereby reducing the critical path to maintain the circuit's performance [6]. Today, majority of the multiplier designs use 4:2 compressors to speed up the partial product summation

tree [7]. In this paper, we propose compressor design in adiabatic logic style. As there are varieties of adiabatic logic families [8], the compressor design in positive feedback adiabatic logic (PFAL) is adopted due to its suitability to CMOS integration in deep sub-micron technologies. The power consumption is further lowered by designing the compressor using modified PFAL (MPFAL) style.

This paper is organized in five section including the introductory one. Section II briefly describes the adiabatic logic style and the two families. The compressor design is proposed in section III. The functional verification of the design and the performance comparison is presented section IV. The conclusions are drawn in the last section.

2.ADIABATIC LOGIC CIRCUITS

The schematic of a CMOS inverter consisting of NMOS (M1) and PMOS (M2) representing the pull-down and pull-up networks are shown in Fig. 1. Depending on the input either M1 or M2 is ON while the other remains OFF [9]. The inverter consumes power when the input switches from V_{DD} to 0 and charges the output capacitor C_1 whereas it dissipates the power via M1 in a discharging event initiated by the switching of the input from 0 to V_{DD}. The dynamic power consumption of the CMOS inverter is expressed as:

$$P_{dyn} = \alpha . C_1 . V_{DD}^2 . f \quad (1)$$

where, α, C_1, V_{DD} and f represents the switching activity, load capacitance, power supply and frequency of the input. Various methodologies to reduce the values of the factors are suggested as low power solutions for CMOS circuits. But adiabatic logic has been proven to be a potential solution over CMOS logic style when it comes to design of low power circuits [1]. In contrast to CMOS, adiabatic logic does not switch abruptly from 0 to V_{DD} or vice versa but employ a slow changing voltage to charge and recover the energy from the output.

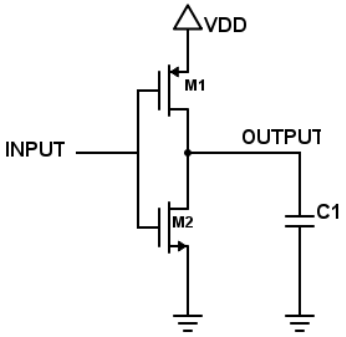

Fig.1: CMOS Inverter

Two adiabatic logic families namely positive feedback adiabatic logic (PFAL) [10,11] and modified positive feedback adiabatic logic (MPFAL) [12] are considered. The basic cell in PFAL is shown in Fig. 2. The logic function F and its complement Fbar are implemented using NMOS networks alongside the two cross coupled inverters as latch which drives the two complementary outputs of the circuit. It requires presence of dual nature of input and creates dual nature as well which increases its compatibility [11].

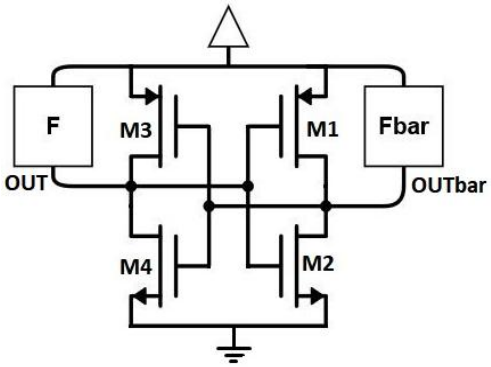

Fig.2: Basic Cell of PFAL [10]

Another enhanced version of the PFAL family is shown in Fig. 3 and is named as modified PFAL (MPFAL) [12]. A basic MPFAL gate has a latch with two cross

coupled inverters (M1-M4) similar to PFAL and an additional diode connected NMOS transistor M5, in between the source of PFAL cross coupled inverters and round terminal that helps in reducing power dissipation [13]. MPFAL is based on level shifting technique which has one power clock supply and a NMOS transistor. The logic function is realized in the similar manner as the PFAL thus the number of transistors remains same as that in PFAL for realizing the logic function.

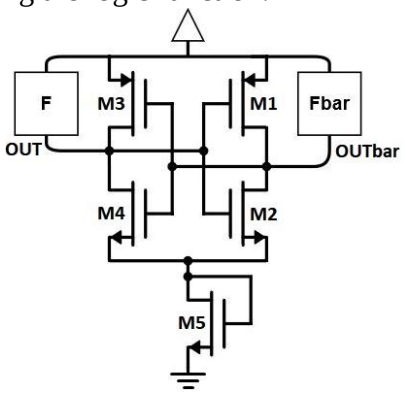

Fig.3: Basic Cell of MPFAL [12]

Both of these logics use four phase power supply (Fig. 4) with the phases as: evaluate, hold, recovery and wait state [1]. In the evaluate phase, the outputs are evaluated from the stable inputs while the outputs are kept stable for the evaluation of the next stage in the hold phase. The energy is recovered in the recovery phase and an extra wait phase has been added to maintain symmetry.

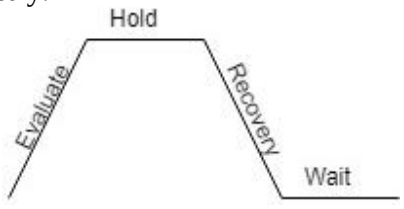

Fig.4: Four Phase Trapezoidal Power Supply [1]

3. PROPOSED COMPRESSOR

Major applications of electronics devices, today, desire high speed computation of data, which includes a multiplication unit [14]. An array multiplier is a fast multiplier architecture. It consists of three parts: a partial product summation tree, booth encoder and a final adder [15]. The partial product summation tree is responsible for total delay in multiplication procedure. Various techniques are available that helps in speeding up the partial product summation tree. One of these is column compressors since they simplify the interconnection circuitry [16]. The realization of a 4:2 compressor with five inputs (X1, X2, X3, X4, Cin) and three outputs (Sum, Carry, cout) is considered. The truth table of the compressor is listed in Table I [19]. The block diagrams of two compressors design (Compressor A [17] and Compressor B [18]) are depicted in Fig. 5 and Fig. 6. The functionality of 4:2 Compressor A can be expressed as:

$$\textbf{\textit{Sum}}=X1 \oplus X2 \oplus X3 \oplus X4 \oplus Cin \quad (2)$$

$$\textbf{\textit{Carry}}=(X1 \oplus X2 \oplus X3 \oplus X4).Cin+\overline{(X1 \oplus X2 \oplus X3 \oplus X4)}.X4 \quad (3)$$

$$\textbf{\textit{Cout}}= (X1 \oplus X2).X3 + \overline{(X1 \oplus X2)}.X1 \quad (4)$$

TABLE I: TRUTH TABLE OF 4:2 COMPRESSOR

C_{in}	X_4	X_3	X_2	X_1	C_{out}	Carry	Sum
0	0	0	0	0	0	0	0
0	0	0	0	1	0	0	1
0	0	0	1	0	0	0	1
0	0	0	1	1	1	0	0
0	0	1	0	0	0	0	1
0	0	1	0	1	1	0	0
0	0	1	1	0	1	0	0
0	0	1	1	1	1	0	1
0	1	0	0	0	0	0	1
0	1	0	0	1	0	1	0
0	1	0	1	0	0	1	0
0	1	0	1	1	1	0	1
0	1	1	0	0	0	1	0
0	1	1	0	1	1	0	1
0	1	1	1	0	1	0	1
0	1	1	1	1	1	1	0
1	0	0	0	0	0	0	1
1	0	0	0	1	0	1	0
1	0	0	1	0	0	1	0
1	0	0	1	1	1	0	1
1	0	1	0	0	0	1	0
1	0	1	0	1	1	0	1
1	0	1	1	0	1	0	1
1	0	1	1	1	1	1	0
1	1	0	0	0	0	1	0
1	1	0	0	1	0	1	1
1	1	0	1	0	0	1	1

1	1	0	1	1	1	1	0
1	1	1	0	0	0	1	1
1	1	1	0	1	1	1	0
1	1	1	1	0	1	1	0
1	1	1	1	1	1	1	1

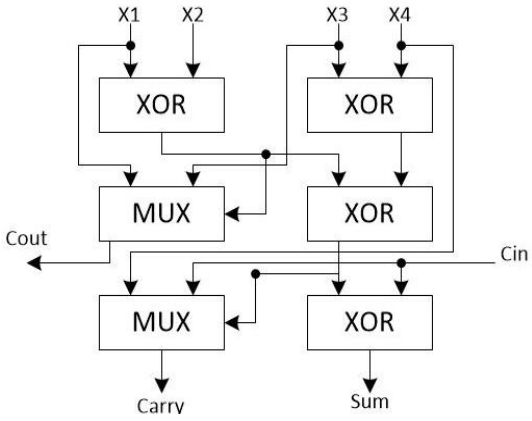

Fig. 5. Block Diagram of 4:2 Compressor A [17]

Similarly, the Boolean expression of the 4:2 Compressor B can be written as follows:

Sum=(X1 ⊕ X2). $\overline{(X3 \oplus X4)}$ + $\overline{(X1 \oplus X2)}$. (X3 ⊕ X4.Cin+(X1⊕X2). (X3⊕X4)+ X1⊕X2. X3⊕X4.Cin (5)

Carry= (X1⊕X2⊕ X3 ⊕ X4).Cin+$\overline{(X1 \oplus X2 \oplus X3 \oplus X4)}$. X4 (6)

Cout=(X1 ⊕ X2). X3 + $\overline{(X1 \oplus X2)}$. X1 (7)

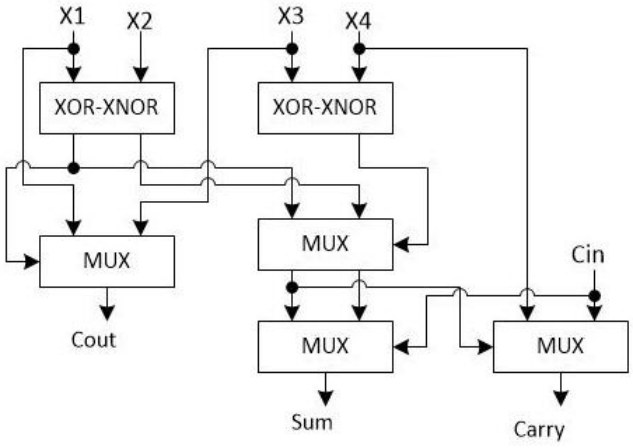

Fig.6: Block Diagram of 4:2 Compressor B [18]

It is clear from Figs. 5 and 6 that both the compressors use 2:1 multiplexer (MUX) [20] and exclusive-OR (XOR) gates as building blocks. The functionality of 2:1 MUX is expressed as:

OUT= A. Sbar + B.S (9)

The functionality of XOR gate is expressed as:

XOR= A ⊕ B = A.Bbar + Abar.B (10)

The functionality of XOR gate is expressed as:

XNOR = A ⊙ B = A.B + Abar.Bbar (11)

The Compressor A design consists of 2 MUX and 4 XOR blocks whereas the Compressor B design consists of 4 MUX and 2 XOR blocks. The PFAL based 2:1 MUX and XOR gate are shown in Figs. 7 and Fig. 8 respectively. A 2:1 multiplexer [21] contains two inputs A, B and one select line S and outputs OUT and OUTbar as shown in Fig. 7. The logic function has been realized using NMOS transistors only and both inputs and complemented inputs are applied. Similarly, XOR gate uses two inputs A and B supplied in true and complementary form to the NMOS network. The MPFAL based implementations of 2:1 MUX and XOR gate are shown in Fig. 9 and Fig. 10 respectively.

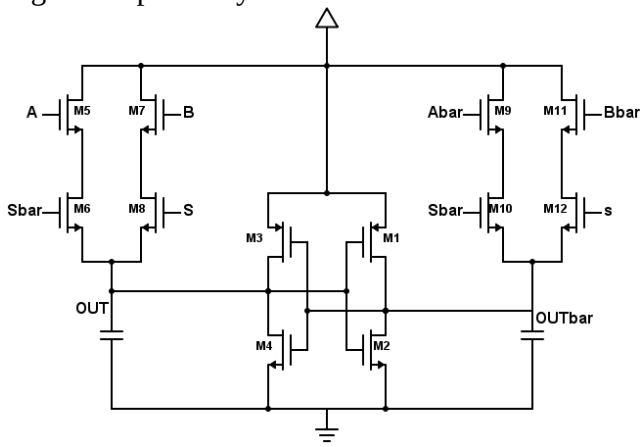

Fig.7: Proposed PFAL 2:1 MUX

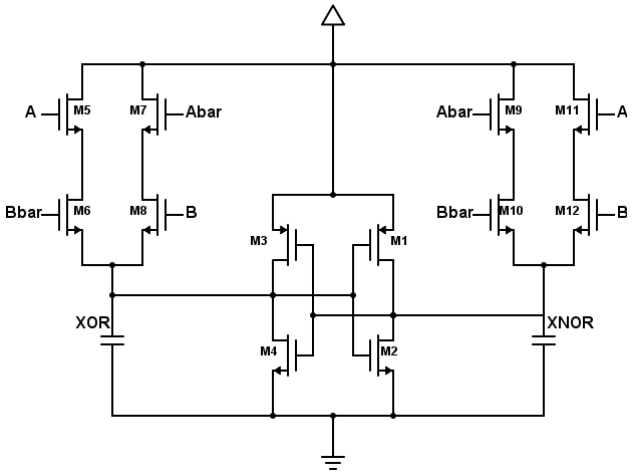

Fig.8: Proposed PFAL XOR gate

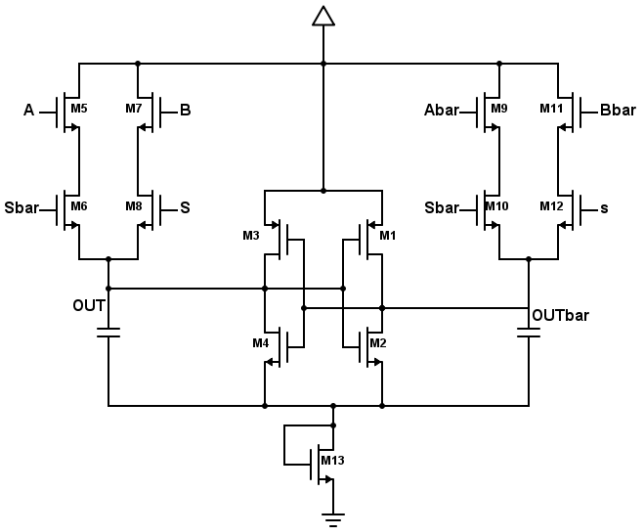

Fig.9: Proposed MPFAL 2:1 MUX

4. Simulation Results

The circuits for the 4:2 Compressor based on two designs Compressor A (Fig. 5) and Compressor B (Fig. 6) are designed in PFAL and MPFAL styles. Both the compressor designs are implemented and simulated in Tanner EDA using 180 nm CMOS technology parameters. For PFAL based design, the MUX and XOR gate circuits shown in Fig. 7 and Fig. 8 are used while for MPFAL, the circuits of Fig. 9 and Fig. 10 are employed. This section first presents the functional verification of the

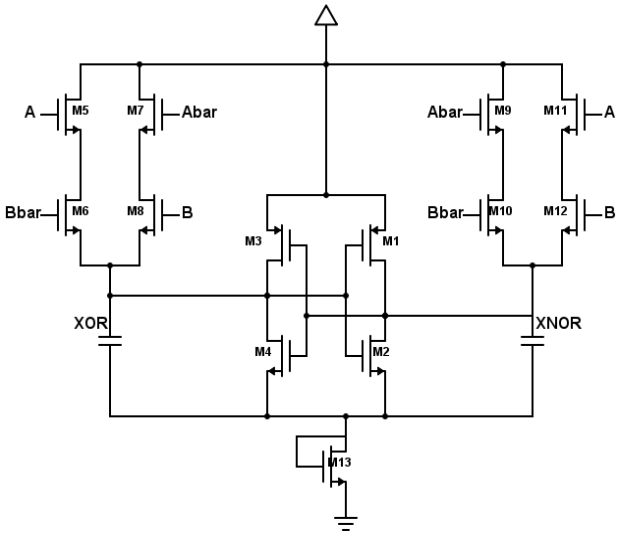

Fig.10: Proposed MPFAL XOR gate

compressors, thereafter their performance is compared with their CMOS counterparts, in terms of power for wide range of power supply, capacitance and input frequency value.

A. Verification of Compressor Functionality

The two compressors are implemented and simulated with a power supply, load capacitance, input frequency of 1.8 V, 10 fF and 25MHz respectively. The simulation waveforms for compressor A implemented in PFAL and MPFAL are plotted in Fig. 11 and Fig.12 respectively. Similar waveforms were obtained for compressor B and are not shown for the sake of brevity. It can be observed that the compressors exhibit the same functionality as predicted in Table I.

B. Power Dissipation Analysis With Power Supply

The power dissipation of the two proposed compressors A and B are measured by varying the supply voltages from 1V to 2V. The load capacitance and input frequency are maintained constant at 10fF and 25MHz respectively. The simulation results are plotted in Fig. 13 and

Fig. 14 for Compressor A and Compressor B respectively. The values of power consumption are listed in Table III. It can be observed that both the adiabatic implementation of the compressors consumes lesser power than the CMOS counterparts. Thus, identifying adiabatic logic as a low power style. Also, the power consumption in both the logic style increases with the increment in power supply. However, the increase in adiabatic family is not that sharp as observed in CMOS logic. Also, it may be observed that proposed Compressor B has a lower power dissipation compared to Compressor A. With respect to the logic family, MPFAL based compressor design show low power dissipation values than their PFAL implementations. Overall, Compressor B implemented using MPFAL had lowest power dissipation. CMOS circuits show the highest power consumption amongst the three logic families.

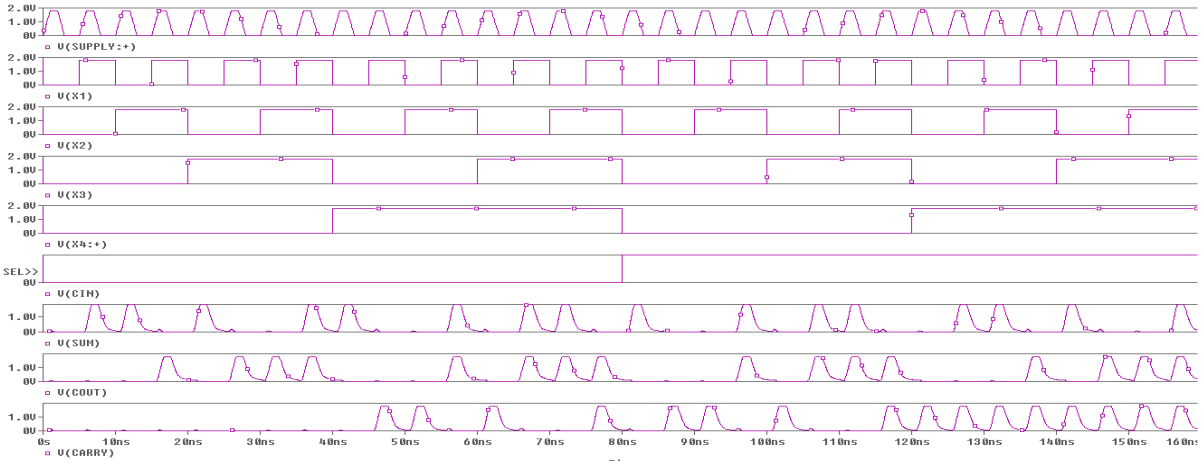

Fig.11: Simulation Waveform of PFAL Compressor A

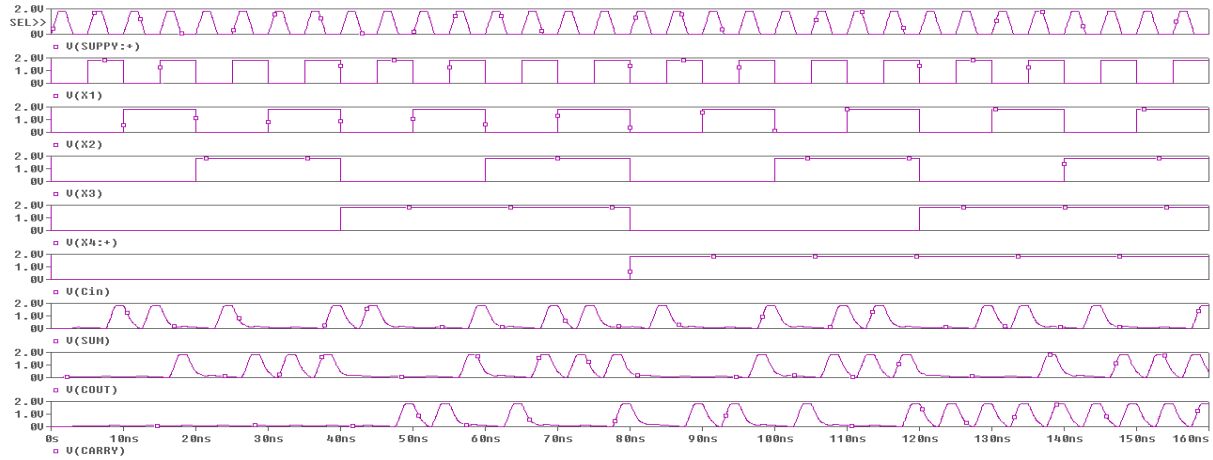

Fig.12: Simulation waveform of MPFAL Compressor A

TABLE III: POWER VS. POWER SUPPLY FOR PROPOSED COMPRESSORS A AND B

Supply Voltage (V)	COMPRESSOR A (µW)			COMPRESSOR B (µW)		
	PFAL	MPFAL	CMOS	PFAL	MPFAL	CMOS
1	0.61	0.51	0.98	0.58	0.52	0.93
1.1	0.64	0.57	1.61	0.61	0.54	1.13
1.2	0.68	0.61	2.25	0.69	0.61	1.35
1.3	0.78	0.64	2.23	0.72	0.62	2.08
1.4	0.83	0.70	3.62	0.83	0.76	2.65
1.5	0.93	0.76	3.83	0.94	0.82	3.62
1.6	1.09	0.92	4.46	1.05	0.94	4.13
1.7	1.28	1.06	5.23	1.17	1.02	4.57
1.8	1.58	1.22	5.86	1.43	1.18	4.91
1.9	1.83	1.36	6.53	1.59	1.33	5.48
2	1.02	1.52	7.54	1.91	1.58	5.89

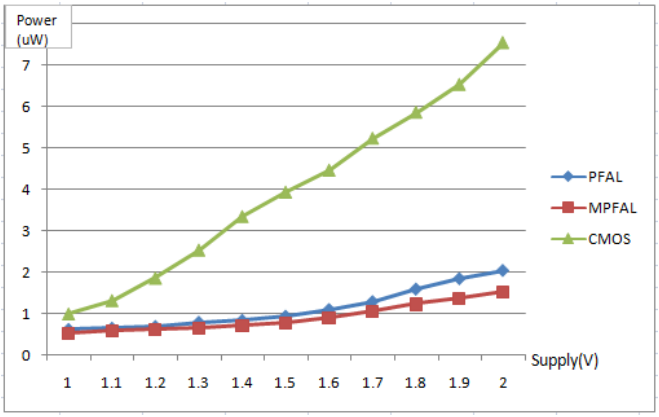

Fig.13: Power Dissipation vs. Power Supply for Proposed Compressor A

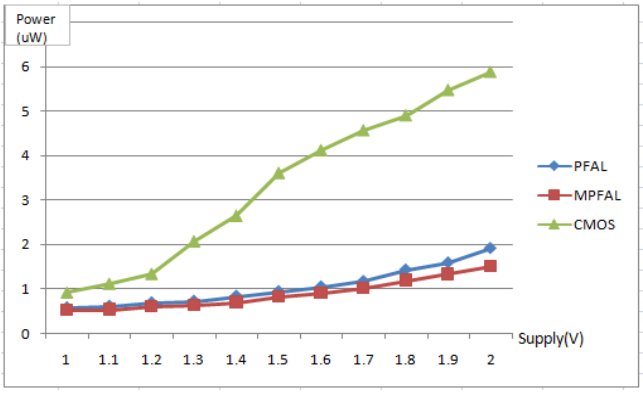

Fig.14: Power Dissipation vs. Power Supply for Proposed Compressor B

C. Power Dissipation Analysis With Varying Load Capacitances

The power dissipation of the proposed compressors A and B are measured for various load capacitances ranging from 1fF to 200fF while keeping the power supply voltage constant at 1.8 V. The simulation results are plotted for the compressors implemented in CMOS, PFAL and MPFAL are plotted in Fig. 15 and Fig. 16. It may be observed that compressor B consumes less power than the rest of the two circuits. The exact values are listed in Table IV. Initially, for capacitance values from 1fF to 40fF, all the four adiabatic compressors have almost same power dissipation but as the load capacitance increases, the proposed compressor B design using MPFAL shows the best performance amongst all the compressors. CMOS based compressors show highest power values at all values of load capacitance.

TABLE IV: POWER VS. LOAD CAPACITANCES FOR PROPOSED COMPRESSORS A AND B

Load Capacitance (fF)	COMPRESSOR A (µW)			COMPRESSOR B (µW)		
	PFAL	MPFAL	CMOS	PFAL	MPFAL	CMOS
1	1.23	1.35	3.49	1.19	1.36	2.56
2	1.22	1.21	3.74	1.98	1.32	2.80
5	1.27	1.12	4.46	1.49	1.21	4.01
10	1.38	1.02	5.66	1.93	1.23	4.11
20	2.07	1.87	8.03	2.26	1.62	7.02
30	3.25	2.81	10.44	3.29	2.68	8.91
40	4.64	3.85	12.83	4.46	3.83	11.31
50	6.19	4.89	15.26	6.47	4.86	13.73
60	7.86	6.06	17.71	7.99	6.23	16.14
80	10.85	8.59	22.56	11.41	8.57	20.93
100	16.32	11.39	27.42	14.91	11.81	31.73
150	24.67	19.62	39.53	24.72	19.54	40.78
200	36.01	29.21	51.66	36.34	28.83	49.69

D. Power Dissipation Analysis With Varying Frequency

The dependence of power dissipation on frequency is examined by simulating the compressor designs at supply voltage of 1.8

V and keeping load capacitance at 10 fF. The input frequency is varied from 12.5 MHz to 250 MHz. The simulation results are plotted in Fig. 17 and Fig. 18 for proposed Compressor A and B. It is observed from the graph that power dissipation is lower in Compressor B than Compressor A. At the beginning, at around 12.5MHz to 40MHZ, all the four adiabatic compressors have almost the same power dissipation. The exact values are listed in Table V. Here also, CMOS compressors show large power dissipation and it increases as the frequency value is increased. The adiabatic compressors show low power consumption than CMOS till 200MHZ after that gap between their power consumptions starts to decrease. Compressor B, designed using Modified PFAL shows the best performance amongst all the designed compressors.

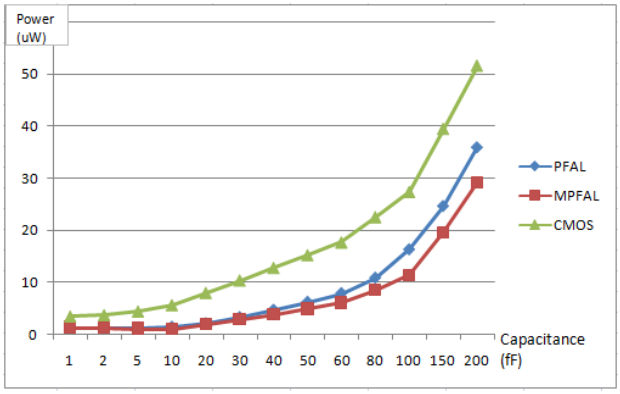

Fig.15: Power Dissipation vs. Load Capacitance for Proposed Compressor A

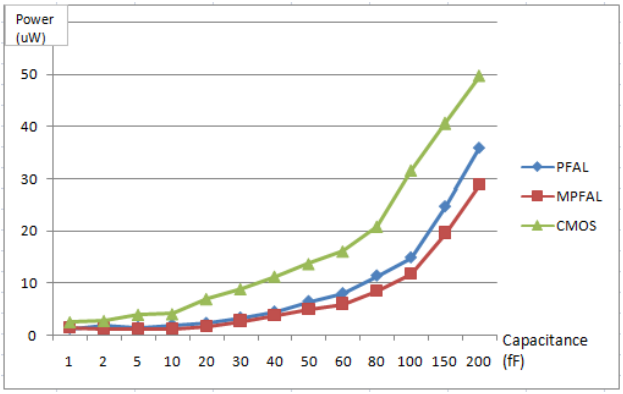

Fig.16: Power Dissipation vs. Load Capacitance for Proposed Compressor B

TABLE V: POWER VS. FREQUENCY FOR PROPOSED COMPRESSORS A AND B

Frequency (MHz)	COMPRESSOR A (µW)			COMPRESSOR B (µW)		
	PFAL	MPFAL	CMOS	PFAL	MPFAL	CMOS
12.5	0.99	0.38	3.97	0.84	0.59	1.59
25	2.38	0.72	5.66	1.66	1.26	3.91
50	6.25	2.76	9.05	5.42	2.91	9.04
100	9.53	5.12	15.83	10.99	6.86	15.62
125	13.34	8.22	20.48	12.71	8.74	23.48
200	23.61	17.87	29.27	21.98	16.43	28.48
250	34.44	27.13	38.06	31.94	23.50	37.72

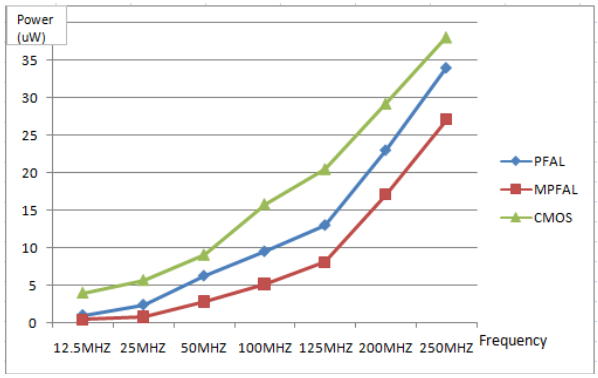

Fig.17: Power Dissipation vs. Input Frequency for Compressor A

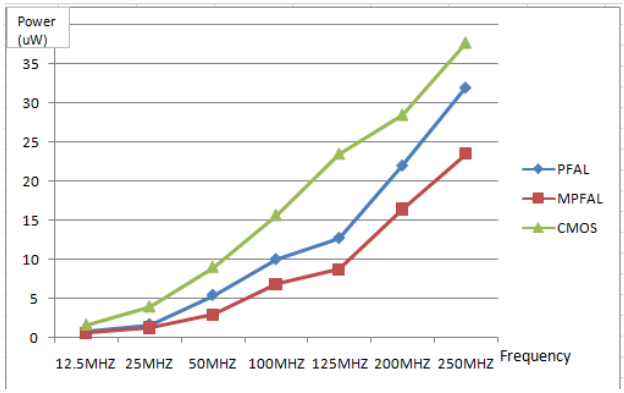

Fig.18: Power Dissipation vs. Input Frequency for proposed compressor B

5. CONCLUSION

In this paper, compressor designs in adiabatic logic style are proposed. The two adiabatic logic families, positive feedback adiabatic logic (PFAL) and it modified version (MPFAL) are adopted for their

realization. Two realization of 4:2 compressor for each logic family is proposed. The proposed compressor designs are simulated in Tanner EDA simulator using 180nm CMOS parameters. The performance between the circuits is made by varying the power supply, load capacitance and frequency of the signal. It is found that the adiabatic compressor consumes less power than the CMOS counterparts. Also, the modified PFAL based compressor design consumes the lowest power at all conditions.

REFERENCES

[1] Teichmann P. Adiabatic Logic in Future Trend and System Level Perspective. Springer Series in Advance Microelectronics, 2012.

[2] Teichmann P, Fischer J, Henzler S. Powerclock Gating in Adiabatic Logic Circuits. in Proc. PATMOS'05, 638– 646, 2005.

[3] Ravi N, Jayachandra Prasad T, Umamahesh M, Subba Rao T. Performance evaluation of high speed compressors for high speed multipliers using 90nm technology. Recent Advances in Space Technology Services and Climate Change, 2010

[4] Jou JM, Kuang SR, Chen RD. Design of Low-Error Fixed-Width Multipliers for DSP Applications. IEEE Transactions on Circuits And Systems—II: Analog And Digital Signal Processing, 46(6), 1999

[5] Gavali KR, Kadam P. VLSI design of high speed Vedic Multiplier for FPGA implementation. IEEE International Conference on Engineering and Technology (ICETECH), 2016

[6] Wang Y, DeBrunner LS, Zhou D, DeBrunner VE. A Multiplier Structure Based on a Novel Real-time CSD Recoding. IEEE International Symposium on Circuits and Systems, 2007

[7] Mokrian P, Howard GM, Jullien G, Ahmadi M. Use of 4:2 compressors for partial product reduction. IEEE International Symposium on Circuits and Systems, 2007

[8] Grover V, Gosain V, Pandey N, Gupta K. Arithmetic Logic Unit Using Diode Free Adiabatic Logic and Selection Unit for Adiabatic Logic Family. 5th International Conference on Signal Processing and Integrated Networks (SPIN), 2018.

[9] Rabaey JM, Chandrakasan A, Nikolic B. Digital Integrated Circuits. A Design Perspective, Second Edition, 2003.

[10] Bakshi A, Sharma M. Design of basic gates using ECRL and PFAL. International Conference on Advances in Computing, Communications and Informatics (ICACCI), 2013.

[11] Sowmiya M, Darwin S, Sindhuja D, Merlin S. Analysis and Design of Positive Feedback Adiabatic Logic (PFAL) Based Universal Gates. International Journal of Engineering Trends and Technology (IJETT), 33(1), 2016.

[12] Kushawaha SPS, Sasamal TN. Modified Positive Feedback Adiabatic Logic for Ultra Low Power VLSI. IEEE International Conference on Computer, Communication and Control, 2015.

[13] Sundar MS. Ultra Low Power Design of Combinational Logic Circuits. International Journal of Science and Research, 5(9), 2016.

[14] Chang CH, Gu J, Zhang M. Ultra low-voltage low-power CMOS 4-2 and 5-2 compressors for fast arithmetic circuits. IEEE Transactions on Circuits and Systems I: Regular Papers, 51(10), 2004.

[15] Ha M, Lee S. Multipliers with Approximate 4-2 Compressors and Error Recovery Modules. IEEE Embedded Systems Letters, 10(1), 6-9, 2018.

[16] Fonseca M, Martins J, Costa ED. Design of pipelined butterflies from radix-2 fft with decimation in time algorithm using efficient adder compressors. IEEE Second Latin American Symposium Circuits and Systems, 1-4, 2011.

[17] Tonfat J, Reis R. Low power 3–2 and 4–2 adder compressors implemented using ASTRAN. IEEE 3rd Latin American Symposium on Circuits and Systems (LASCAS), 2012.

[18] Kumar S, Kumar M. 4-2 Compressor Design with New XOR-XNOR Module. Fourth International Conference on Advanced Computing & Communication Technologies, 106–111, 2014

[19] Sowmiya S, Stella K, Senthilkumar VM. Design and Analysis of 4-2 Compressor for Arithmetic Application. Asian Journal of Applied Science and Technology (AJAST), 2017.

[20] Sharma A, Sohal H, Sharma K. Area and Power Analysis of Adiabatic 2x1 Multiplexer Design on 65nm CMOS Technology. 5th International Conference on Wireless Networks and Embedded Systems (WECON), 2016

[21] Mittal D, Niranjan A. Designing of Multiplexer and De-Multiplexer Using Different Adiabatic Logic in 90nm Technology. 9th International Conference on Computing, Communication and Networking Technologies (ICCCNT), 2018.

Genomics xxx (xxxx) xxx–xxx

Contents lists available at ScienceDirect

Genomics

journal homepage: www.elsevier.com/locate/ygeno

Original Article

Development and characterization of non-coding RNA based simple sequence repeat markers in *Capsicum* species

Vandana Jaiswal[a], Abdul Rawoof[a], Meenakshi Dubey[a,b], Sushil Satish Chhapekar[a], Vineet Sharma[a], Nirala Ramchiary[a,b,*]

[a] Translational and Evolutionary Genomics Lab, School of Life Sciences, Jawaharlal Nehru University, New Delhi 110067, India
[b] Department of Biotechnology, Delhi Technological University, Delhi 110042, India

ARTICLE INFO

Keywords:
Capsicum
miRNA
lncRNA
SSR
Polymorphism
Diversity
Molecular breeding

ABSTRACT

Plant growth and development are largely regulated by non-coding RNAs (ncRNA); thus ncRNA based markers would be rewarding in molecular breeding. In the present study, for the first time we developed total 623 ncRNA based SSRs including 119 microRNASSRs (miRNASSRs) and 504 long non-coding RNASSRs (lncRNASSRs) distributed across 12 *Capsicum* chromosomes. Out of 623 ncRNASSRs, 120 (including 60 each miRNASSRs and lncRNASSRs) were used for genotyping of 96 *Capsicum* accessions belonging to *C. annuum, C. chinense* and *C. frutescens*; and 75% SSRs were polymorphic. Model-based and distance-based cluster analyses identified three species specific clusters, i.e. cluster-I (*C. annuum*), cluster-II (*C. frutescens*) and cluster-III (*C. chinense*); therefore, these SSRs may have a potential role to play in interspecific *Capsicum* breeding. Tissue specific expression of SSR containing ncRNAs and versatile functions of their targets suggested the usefulness of SSRs for mapping of genes/QTLs and breeding of wide range of traits in *Capsicum*.

1. Introduction

The development of DNA based molecular markers is crucial for any plant species and they play a vital role in different molecular genetic studies such as gene tagging, QTL mapping, germplasm evaluation, population genetics and ultimately molecular breeding of crop plants for improvement of economically important traits [48]. During the last four decades, several marker systems have evolved starting from random amplified polymorphic DNA (RAPD), restriction fragment length polymorphism (RFLP), amplified fragment length polymorphism (AFLP), simple sequence repeats (SSR), single nucleotide polymorphism (SNP) etc. [7,29,31,59,61]. Although, SNPs are considered as the current generation markers, SSRs are still widely used and continuously being developed due to its reproducible and user friendly nature [10,23,47,68,78]. The co-dominant nature of SSRs is one of the most important reasons for their widespread application in molecular genetics and breeding.

Non-coding RNAs (ncRNAs), which are transcribed but unable to translate into proteins, are the key players of post transcriptional gene regulations. ncRNAs can be grouped into two- (i) small non-coding RNAs (sncRNAs) which are about 22 nucleotide long, and (ii) long non-coding RNAs (lncRNAs) which are > 200 nucleotide long. MicroRNAs (miRNAs) are major class of sncRNAs that involved in negative regulation of genes through either affecting mRNA stability or inhibiting translation [51]. Mostly miRNAs are transcribed from intergenic regions, but exonic miRNAs have also been reported [14,28,82]. On the other hand, lncRNAs are diverse class of ncRNAs which may be transcribed from different genomic regions like exon, intron, UTRs, promoter, intergenic regions etc. [45,50]. lncRNAs may regulate the gene expression in both the directions i.e. it may play down-regulatory and up-regulatory role [51].

Capsicum is one of the most important vegetable crops belonging to the family Solanaceae and mostly used as spice. Till now a total 5 cultivated and 32 wild *Capsicum species* is reported [24,65]. *Capsicum* fruits have several health benefits like it is rich in anti-oxidants and phenolic compounds besides having anti-inflammatory, anti-cancerous and anti-microbial properties [69]. As per genetic architecture is concerned, *Capsicum* is diploid crop with 12 chromosomes and upto 3.5 GB genome. *Capsicum* crop is also explored for the development of molecular markers and genetic dissection of important traits by several research groups [1,4,17,18,23,71,74,81]. Whole genome sequencing have also been done in two *Capsicum* spp. viz. *C. annuum* [33,62] and *C. chinense* [34]. However, only few studies are available which focused on exploration of ncRNAs in *Capsicum* [30,73,85,87]; and unfortunately

* Corresponding author: Translational and Evolutionary Genomics Lab, School of Life Sciences, Jawaharlal Nehru University, New Delhi 110067, India.
E-mail address: nrudsc@gmail.com (N. Ramchiary).

https://doi.org/10.1016/j.ygeno.2019.09.005
Received 18 June 2019; Received in revised form 30 August 2019; Accepted 6 September 2019
0888-7543/ © 2019 Elsevier Inc. All rights reserved.

none of the studies reported which explored the development ncRNAs based molecular markers so that these gene expression regulators could be exploited in breeding programs.

Therefore, in the present study we reported the successful development of ncRNA based, cost-effective, user friendly, co-dominant, PCR-based and highly reproducible SSR markers from miRNAs and lncRNAs (miRNA and lncRNA were identified in our laboratory, unpublished data) for the first time in *Capsicum*. Furthermore, we validated the ncRNASSRs in 96 *Capsicum* accessions belonging to different *Capsicum* species and found that these markers were highly polymorphic, transferable and stable across different *Capsicum* species which could be important asset for genetic studies and breeding programs.

2. Materials and methods

2.1. Plant material

A set of total 96 *Capsicum* accessions including 91 Indian (collected from Assam, Manipur, Nagaland, Uttarakhand, Jammu and Kashmir, Mirozum, Sikkim, Meghalaya and NBPGR- Delhi) and 5 exotic accessions were utilized during present study. Out of above mentioned 96 *Capsicum* accessions, majority were belonged to three *Capsicum* species- (i) *C. annuum* (53), (ii) *C. chinense* (26) and (iii) *C. frutescens* (8). However, one accession each belonged to *C. baccatum* and *C. pubescens*; and species of seven accessions were unknown (Supplementary Table S1). Seed of all the 96 *Capsicum* accessions were surface sterilized with 4% sodium hypochlorite solution and then sown in small pots in glass house (24–26 °C with 16 h light period). After one month (approx. 8–10 leaves stage), seedlings were transferred in the research field of Jawaharlal Nehru University, New Delhi, India.

2.2. Selection of miRNA and lncRNA

In the present study, in order to develop ncRNA based SSR markers, we used 1645 miRNAs and 15,450 lncRNAs (unpublished) identified from small RNA sequencing data (GSE112738) and transcriptome (PRJNA327797, PRJNA327800) data, respectively which were generated earlier in our laboratory. In brief, whole genome transcriptome was done using five tissues (three biological replicates) including leaf, flower, early fruit, breaker fruit and mature fruit in two *Capsicum* genotypes frutescens 4 (*C. frutescens;* PRJNA327800) and chinense 7 (*C. chinense;* PRJNA327797). For each the four different tissues, three biological replicates were pooled before sequencing. Quality check of raw RNAseq reads of each samples were performed and adaptor sequences were trimmed using TrimGalore (v0.4.4). The quality trimmed reads (with phred score > 20 following [39,70,86]) were aligned against the *C. annuum* zunla [62] reference genome using standard RNAseq pipeline [76] and final assembled transcripts were obtained after merging the total transcripts from each samples using cuffmerge. The identified transcripts were subjected for a series of filters including- (i) open reading frame (ORF) length (≤ 300 bp i.e. encoded ≤100 amino acid long peptide), (ii) coding potential calculator (CPC) score (< 0), (iii) Fragments Per Kilobase of transcript per Million mapped reads (FPKM) value (> 1), (iv) blastp against swiss-prot database (*p*-value < 0.01) and hmmscan filter (p-value < 0.01) to identify potential *Capsicum* lncRNAs.

Besides this, the miRNAs were identified using small RNA sequencing data of four tissues (with three biological replicates) including leaf, stem, flower and fruit in *C. chinense* and *C. frutescens* (GSE112738). Biological replicates were pooled before sequencing. Adapter and poly-A tail sequences were trimmed from the raw reads. Reads with length < 18 and > 30 nucleotide were removed. Filtered reads were then subjected to quality score and reads with phred score < 30 [22] were further removed. The resultant high quality filtered reads were mapped to *C. annuum* zunla reference genome using bowtie programs permitting with maximum two base pair mismatches. Then, 100 bp flanking regions of each aligned reads were extracted followed by removal of non-coding RNAs (tRNAs, rRNAs, snRNAs and snoRNAs) reads. The left-over reads were screened for potential miRNAs using blastn (*E*-value < 0.01, and allowing 1–2 mismatches); against all reported miRNAs from miRBase 21.0 database along with *Capsicum* miRNAs [30]. The precursor sequences of putative miRNAs were identified following Meyers et al. [46].

2.3. SSR mining and primer designing

In order to develop miRNA based SSRs, we selected matured miRNA sequences along with 500 bp sequences flanking either sides of miRNA sequence. Unlike miRNAs, SSRs in lncRNAs were explored only in lncRNA sequences (ranged 201–7150 bp). The SSRs were mined using online tool "WebSat" [44]. For SSRs mining, stretch with di, tri, tetra, penta and hexa nucleotides with minimum of six repeats were selected and mononucleotide repeats were excluded. A cutoff of 100 bp was set as minimum interval distance between two SSRs, and SSRs present within this range were considered as overlapping and thus excluded from further analysis. Using primer 3 software (Rozen and Skaletsky 2000) incorporated in WebSat tool, primers were designed with following criteria - (i) primer size: 18–27 bp with optimum 22 bp, (ii) melting temperature (Tm): 50–65 °C with optimum 60 °C, (iii) GC %: 40–80, (iv) amplicon size: 100–400 bp, (v) max Tm difference between forward and reverse primers: 1 °C, (vi) maximum 3′ stability: 250.

2.4. Expression analysis of SSR containing miRNAs and lncRNAs

For expression analysis of SSR containing ncRNAs, transcriptomes of only one species were used. In case of miRNAs, small RNAseq data of four tissues (including leaf, stem, flower and fruit) of *C. chinense* were used. Expression of miRNAs was measured in Reads Per Kilobase of transcript per Million mapped reads (RPKM). However, for expression analysis of lncRNAs we used transcriptome of five tissues (including leaf, flower, early fruit, breaker fruit and mature fruit) of *C. annuum* [62]. Expression of lncRNAs was measured in term of Fragments Per Kilobase of transcript per Million mapped reads (FPKM) as resulted from paired-end sequencing. Further, to obtain tissue specific expression, RPKM and FPKM values were converted into *Z*-score using the formula $(X - X_{av})/SD$, where X is the average RPKM/FPKM value in a particular tissue, and X_{av} and SD are the mean and standard deviation of the average RPKM/FPKM values across all the samples, respectively. ncRNAs showing *Z*-score > 0 (positive) in particular tissue, and < 0 (negative) in other tissues were considered as tissue specific [35].

2.5. Target prediction for miRNAs and lncRNA

For identification of miRNA targets we used psRNATarget server (http://plantgrn.nobel.org/psRNATarget/) with maximum expectation = 2.0, complementarity scoring length (HSP size) = 21–24, maximum allowed unpaired energy (UPE) = 25, the flanking length for target accessibility analysis was 17 nucleotide upstream and 13 nucleotide downstream along with 10–11 nucleotide for central mismatch range leading to translation inhibition [20]. Similarly, for lncRNA targets identification, mRNAs/genes located within 100 kb upstream and 100 kb downstream of lncRNAs were screened as candidate target gene. The LncTar tool was used to analyse potential mRNAs as lncRNA targets using normalized free energy (ndG) cutoff ≤ −0.1 [37]. Interaction networks for miRNA:mRNA and lncRNA:mRNAs were generated based on a binary matrix of 0 and 1 (where 0 represents not a target and 1 represent as target of miRNA/lncRNA) using *sna* package [12] in R statistical software (www.bioconductor.org).

2.6. DNA isolation and genotyping

Genomic DNA was extracted from leaf tissues of 96 *Capsicum* accessions using CTAB method [66] using following steps- approx. 100 mg leaf tissues (collected from one plant per accession) were homogenized using liquid nitrogen and transferred into CTAB buffer (CTAB 2%; 0.1 M Tris, pH 8; 0.02 M EDTA pH 8; 1.4 M NaCl) and incubated at 65 °C for 45 min. The mixture was then subjected to chloroform:isoamyl (24:1 *v*/v) treatment followed by precipitation using chilled isopropanol. DNA pellet was washed with 70% ethyl alcohol. The DNA pellets were suspended in TE (10 mM TrisBase and 1 mM EDTA) buffer after air dry. DNA integrity and quantity were checked on 1% agarose gel and Nanodrop, respectively. Using genomic DNA of 96 accession, polymerase chain reaction (PCR) was set up with composition- 25 ng of DNA, 1× PCR buffer (50 mM KCl, 20 mM Tris–HCl pH 8.4), 1.5 mM $MgCl_2$, 0.125 mM of each dNTPs, 0.5 mM of each primer, and 0.5 U of Taq DNA polymerase (iTaq); and amplification profile- denaturation 95 °C for 4 min, 35 cycles of denaturation (94 °C for 2 min), annealing (50-65 °C, as per SSR Tm, for 45 s), elongation (72 °C for 30 s), and final extension at 72 °C for 2 min and performed in Eppendorf Thermal Cycler (Germany). Amplicons were then resolved using 10X PAGE on vertical gel electrophoretic system (C.B·S Scientific Co.) at 250 V for six hrs. Followed by silver staining [75] for visualization. Genotyping data of each SSRs were recorded as presence/absence and/or length variation. Data was finally converted into allele size (bp) using fragment size calculator.

2.7. Genetic diversity analysis and population structure

The polymorphism information content (PIC) of SSRs was calculated [3,49] using formula in MS excel.

$$\mathbf{PIC} = 1 - \sum_{i=1}^{l} P_i^2 - \sum_{i=1}^{1-1} \sum_{j=i+1}^{l} 2P_i^2 P_j^2$$

Where, P_i and P_j are the population frequency of the ith and jth alleles.

Genetic diversity parameters including number of alleles (na), effective number of alleles (ne), Shannon's information index (I), and Nei's gene diversity index were calculated using POPGEN32 v1.32 [80]. The phylogenetic relationship between the accessions was estimated using DARwin 5 [56]. Genetic distances between the accessions were obtained by computing the usual Euclidean distance matrix. From this matrix, a dendrogram was constructed using the UPGMA method implemented in DARwin 5. The significance of each node was evaluated by bootstrapping data over a locus for 1000 replications of the original matrix. Model-based population structure analysis was performed using software STRUCTURE version 2.2 [60] assuming number of sub-populations (K) 2 to 10 with five iterations each. Burn-in and MCMC iterations were set to 50,000 and 100,000, respectively for each run; admixture and correlated allele frequencies model was used in model. The number of sub-populations was determined following delta K (ΔK) method [25] using online tool STRUCTURE harvester.

3. Result

3.1. Non-coding RNAs used to develop SSR markers

Using whole genome transcriptome data, a total of 17,095 ncRNAs were developed in our laboratory (unpublished) and used for SSR mining in the present study. These 17,095 ncRNAs includes 1645 miRNAs and 15,450 lncRNAs. For miRNAs development, small RNA sequencing was done and raw reads were developed (66,550,467 reads in *C. chinense* and 61,791,387 reads in *C. frutescens*) followed by adapter trimming. Raw reads were then filtered using the following criteria- (i) quality score; > 30, (ii) sequence length; between 18 and 30 nucleotide, and (iii) redundancy; remove redundant sequences; and 5,220,387 (*C. chinenese*) and 10,557,693 (*C. frutescence*) high quality reads were identified. 74–82% miRNAs with sequence length of 21–24 nucleotides lied within sRNAs processed by dicer-like (DCL) proteins. In order to develop mature miRNA sequences, we examined the GC composition (following Watson- Crick base pairing rule) and found that GC content ranged from 35% to 70%. To enhance the confidence, miRNAs with < 10 read counts were excluded and finally a total of 1645 miRNAs were developed; and used in the present study for SSR development.

Similarly, in order to identify lncRNAs, a total 448 million sequence reads were developed. After merging reads of each sample using cuffmerge, a total 2,28,806 transcripts were found. Transcripts were then filtered using two criteria- (i) sequence length, and (ii) ORF length. Reads longer than 200 nucleotides were selected. These reads (≥ 200 nucleotides) were then subjected for ORF identification and reads containing ORF length ≥ 300 nucleotides (i.e. encode ≥100 amino acid long peptide) were removed; and a total of 78,621 transcripts were selected for BLAST against SwissProt and hmmscan in Pfam databases in order to filter out protein coding genes. Transcript with coding potential calculator (CPC) score > 0 were further excluded; and finally a total of 24,205 lncRNAs were identified. Out of 24,205 lncRNAs, 15,450 showed expression with FPKM > 1.0, and thus selected for SSR development in the present study.

3.2. Distribution of ncRNAs (miRNA/lncRNA) across Capsicum genome

Out of 1645 miRNAs, 190 were mapped on scaffolds and remaining 1455 miRNAs were distributed on 12 chromosomes of *Capsicum* genome. On the individual chromosomes, the number of miRNAs distributed ranged from 84 (chromosome 11) to 190 (chromosome 3, Table 1). Similarly, 15,450 lncRNAs were distributed on 12 *Capsicum*

Table 1
The details of number of non-coding RNAs taken for study and ncRNA SSRs developed from different chromosomes of *Capsicum* species.

Chromosome	miRNA	lncRNA	Total ncRNA	miRNASSR	lncRNASSR	Total ncRNASSR
1	165	2666	2831	11	67	78
2	113	1460	1573	8	37	45
3	190	1346	1536	13	52	65
4	87	990	1077	8	33	41
5	111	1061	1172	6	26	32
6	150	1083	1233	16	30	46
7	114	959	1073	1	36	37
8	112	279	391	7	6	13
9	131	15	146	13	0	13
10	88	1914	2002	7	63	70
11	84	1693	1777	1	60	61
12	110	1984	2094	3	63	66
Scaffold	190	0	190	25	31	56
Total	1645	15,450	17,095	119	504	623

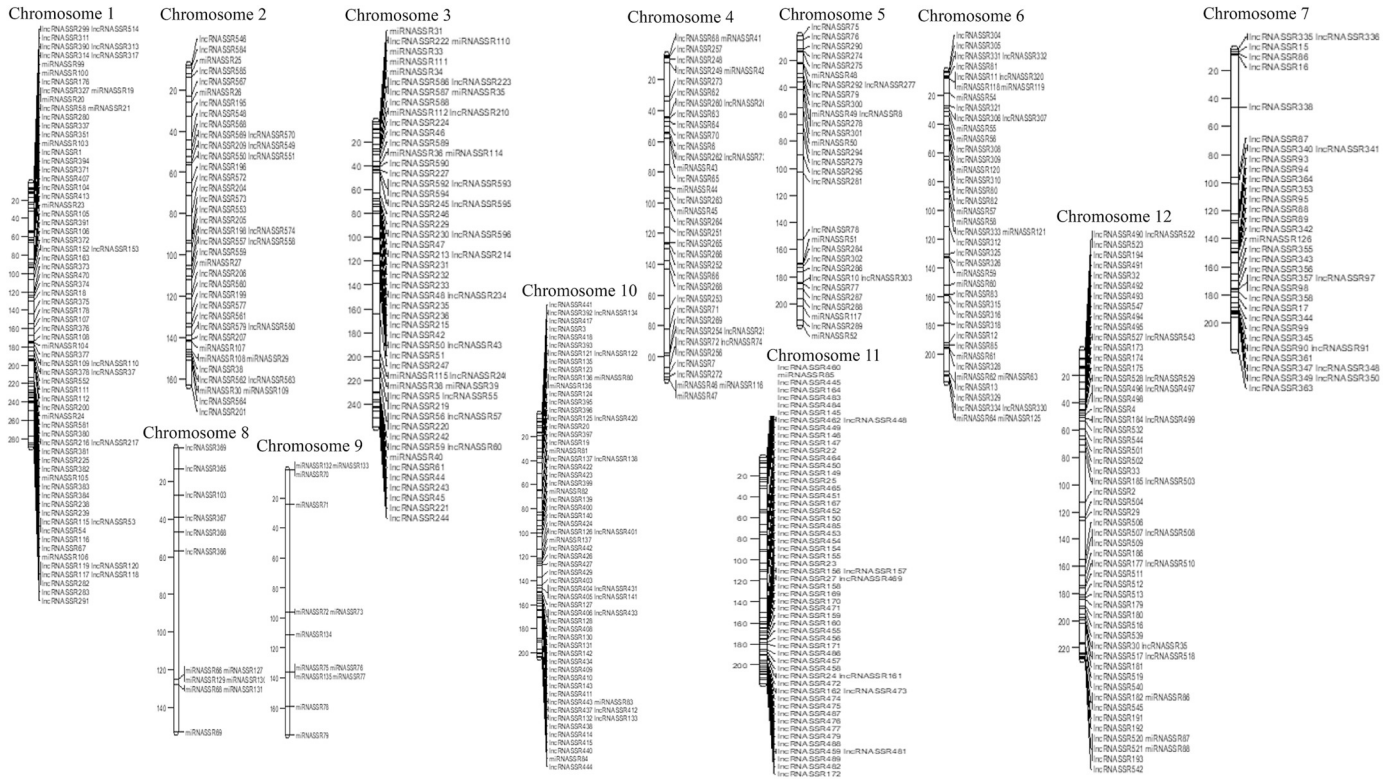

Fig. 1. The distribution of non-coding RNA based SSRs (ncRNASSRs) in 12 chromosomes of *Capsicum* genome.

chromosomes ranging from 15 on chromosome 9 to 2666 on chromosome 1 (Table 1).

3.3. miRNASSRs across Capsicum genome

Using 1645 mature miRNA along with 500 bp flanking sequences from both the sides, we identified a total of 119 SSRs (called as miRNASSR). Of these, 94 SSRs were distributed on 12 chromosomes of *Capsicum* genome which ranged from one (chromosomes 7 and 11) to 16 (on chromosome 6) on individual chromosomes (Table 1, Fig. 1). The remaining 25 SSRs were mapped on scaffolds. Out of 119 SSRs, 96 (80.67%) SSRs were dinucleotide repeats followed by tri- (20; 16.81%) and tetra (3; 2.52%) nucleotides. Among di-nucleotide SSRs, six different types of repeats i.e. AG/CT, AT/AT, CA/TG, GA/TC, GT/AC and TA/TA were identified including. Of these repeats, AT/AT repeats was found maximum (47) followed by TA/TA repeats [21, Fig. 2A]. Similarly, among tri- and tetra nucleotide SSRs, 10 and 2 types of repeats were identified, respectively (Fig. 2A). Further, the number of repeats in above mentioned 119 miRNASSRs was found up to 29 (miRNASSR41) (Supplementary Table S2). The details of 119 miRNASSR markers such as forward and reverse primer sequences, their melting temperatures and amplicon sizes is given in Supplementary Table S2. Sequence information of SSR containing miRNAs are given in Supplementary Table S3.

3.4. lncRNASSR in Capsicum genome

Similar to miRNASSR, using the 15,450 lncRNAs, we identified a total 504 SSRs (called as lncRNASSR). Of these, 473 SSRs were distributed on 11 *Capsicum* chromosomes (maximum of 67 SSRs found on chromosome 1; Table 1, Fig. 1). Surprisingly, none of the lncRNASSRs were mapped on chromosome 9. The remaining 31 SSRs were mapped on scaffolds. Out of total 504 SSRs, the maximum number of SSRs were (323, 64.09%) dinucleotide followed by tri- (149; 29.56%) and tetra (28; 5.56%) nucleotides. Two SSRs were identified under penta- and hexa-nucleotide categories (Fig. 2B). Similar to miRNASSR, among dinucleotide SSRs, six different type of repeats AG/CT, AT/AT, CA/TG, GA/TC, GT/AC and TA/TA were identified (Fig. 2B). Similarly, for tri- and tetra nucleotide SSRs, 15 and 7 types of repeats were identified (Fig. 2B). Further, the maximum number of repeats in above mentioned 504 lncRNASSRs were found up to 32 (lncRNASSR156; Supplementary Table S2). The details of 504 lncRNASSR markers, their forward and reverse primer sequences along with melting temperature and amplicon sizes are given in Supplementary Table S2. Sequence information of SSR containing lncRNAs are given in Supplementary Table S3.

3.5. SSR polymorphism and genetic diversity

In order to see the utility of SSR markers (developed during present study) in population genetics and trait mapping, we used randomly selected 120 SSR markers (60 each from miRNASSR and lncRNASSR) for genotyping of 96 *Capsicum* accessions belonging to *Capsicum annuum*, *C. chinense*, *C. frutescens*, *C. baccatum* and *C. pubescens* (Supplementary Table S1). Out of 120 SSR markers, 90 (75%) were found polymorphic. Among the 90 polymorphic SSRs, 49 were miRNASSRs and 41 were lncRNASSRs (Table 2). The representative gel image is given in Fig. 2. The 49 polymorphic miRNASSRs produced a total of 124 alleles ranging from 2 to 5 alleles per SSR markers with an average 2.5 alleles per locus; however, the effective number of alleles ranged from 1.38–3.87 with an average of 2.2. The polymorphic information content (PIC) of these miRNASSR markers ranged from 0.24 (miRNASSR84) to 0.70 (miRNASSR117) with an average of 0.43. Nei's gene diversity was observed from 0.28 (miRNASSR84) – 0.74 (miRNASSR117) with an average of 0.52. Shanon index (another diversity parameter) varied from 0.45 to 1.48 (average 0.82, Table 3). Similarly, in case of lncRNASSR markers a total of 103 alleles were observed for 41 polymorphic SSR markers, ranging from 2 to 4 (average 2.5) alleles per locus. However, the effective number of alleles ranged from 1.22 to 2.95 with an average of 2.0. PIC of these lncRNASSR markers ranged from 0.17 (lncRNASSR33) to 0.59 (lncRNASSR22) with an average of

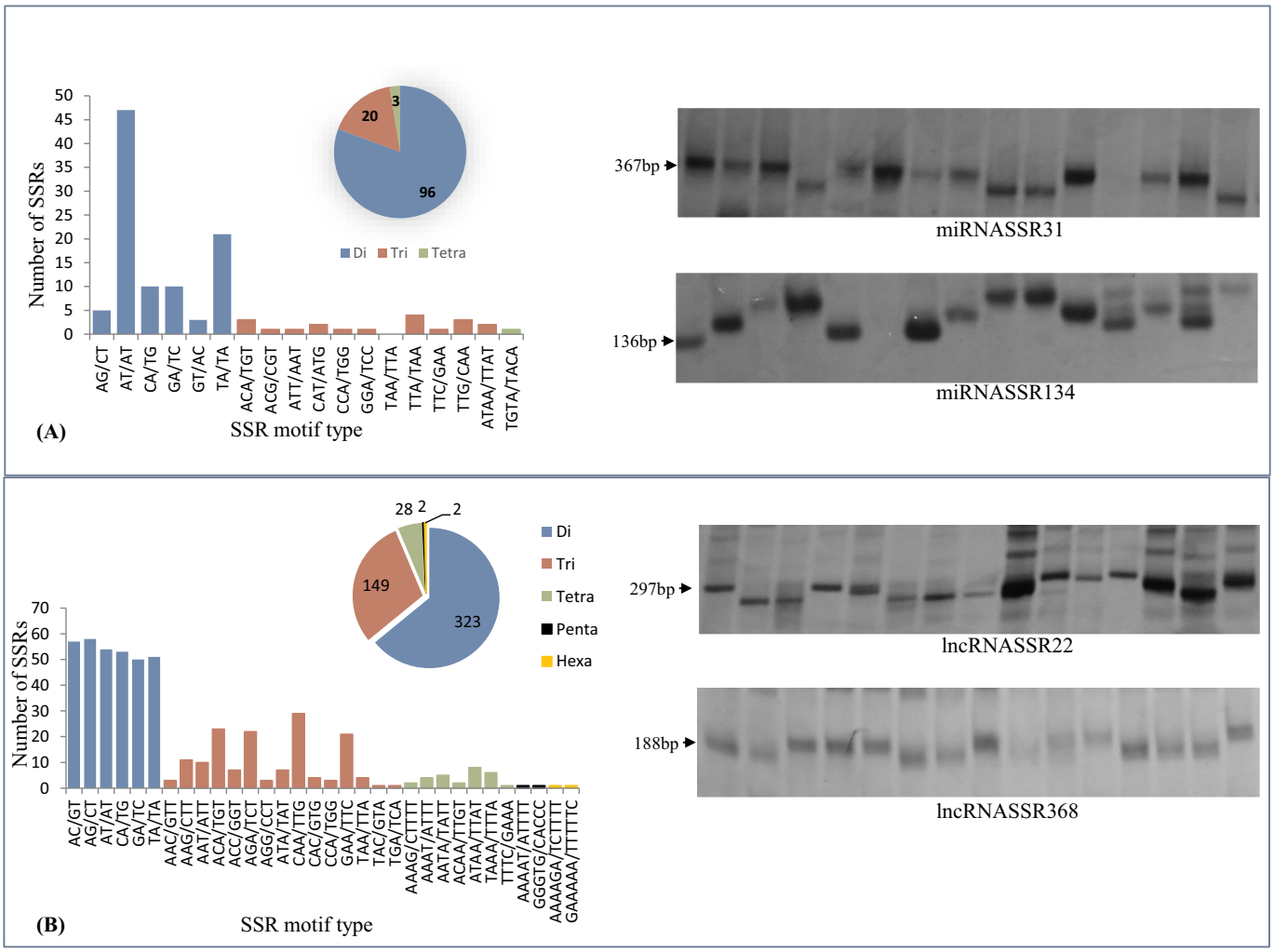

Fig. 2. Frequency of different types of non-coding RNA based simple sequence repeat (ncRNASSR) markers and representative gel image showing banding patterns of polymorphic ncRNASSRs. (A) miRNASSR markers and (B) lncRNASSR markers.

Table 2
Summary of ncRNAs examined and used for SSR marker development.

	miRNA	lncRNA	Total
Non-coding RNA examined	1645	15,450	17,095
SSR identified	119	504	623
SSR amplified	60	60	120
Polymorphic SSR	49	41	90
Percent polymorphism	81.7%	68.3%	75.0%

0.39. Nei's gene diversity was observed from 0.19 (lncRNASSR33) – 0.66 (lncRNASSR22) with an average of 0.48. Shanon index (I) varied from 0.33 to 1.13 (average $I = 0.75$, Table 3).

3.6. Distance based cluster analysis and population structure

To study the genetic distance among 96 *Capsicum* accessions, the total of 227 allelic data scored from 90 polymorphic SSR markers were used. The cluster analysis was done using two approaches- i) distance based and ii) model based. The distance based cluster analysis (UPGMA; Unweighted pair group method with arithmetic mean) identified a total of three clusters formed by 96 *Capsicum* accessions (Fig. 3A). The cluster I contain a total of 60 accessions; with majority of them being the *C. annuum* accessions (50 out of 60); four accessions from *C. chinense*; two from *C. frutescens*; and four accessions, with exact species category not known. Similarly, clusters II and III contained 15 (majorly *C. frutescens*; 6) and 21 (majorly *C. chinense*; 19) *Capsicum* accession, respectively.

Interestingly, the model based population structure analysis also divided whole panel into three subpopulations (identified through STRUCTURE harvester following Evano et al. 2005; Fig. 3B). Out of 96 accessions, 81 belonged to specific subpopulation, and remaining 15 accessions showed admixture (Fig. 3C). Of the 81 accessions, 19, 52, and 10 accessions belonged to subpopulation I, subpopulation II and subpopulation III, respectively. Further, out of 19 accessions categorized in subpopulation I, 18 were from *C. chinense*. Similarly, of the 52 accessions belonging to subpopulations II, 45 accessions were from *C. annuum*; and of the 10 accessions belonging to subpopulations III, five were from *C. frutescens*.

The results of both the cluster analyses (distance based and model based) showed similar pattern of grouping of 96 *Capsicum* accessions. Cluster I showed similarity with subpopulation II, similarly, Cluster II and III showed similarity with subpopulation III and subpopulation I, respectively.

3.7. Tissue specific expression of SSR containing ncRNA

In order to see the utility of developed SSRs, expression analysis of SSR containing ncRNAs were conducted using transcriptome data of different tissues. Interestingly, out of total 112 miRNAs (containing119

Table 3
The details of genetic diversity parameters observed in 96 *Capsicum* accessions using 90 polymorphic non-coding RNA based simple sequence repeats (ncRNASSRs).

SSR	Numebr of alleles	Effective number of alleles	Shanon Index	Gene diversity	PIC	SSR	Numebr of alleles	Effective number of alleles	Shanon Index	Gene diversity	PIC
miRNASSR100	2	1.98	0.69	0.49	0.37	lncRNASSR103	4	2.69	1.14	0.63	0.57
miRNASSR103	2	1.86	0.66	0.46	0.36	lncRNASSR11	2	1.84	0.65	0.46	0.35
miRNASSR105	3	1.70	0.71	0.41	0.36	lncRNASSR116	3	1.99	0.86	0.50	0.44
miRNAssr107	2	1.96	0.68	0.49	0.37	lncRNASSR13	2	1.95	0.68	0.49	0.37
miRNASSR108	2	1.99	0.69	0.50	0.37	lncRNASSR17	3	1.86	0.79	0.46	0.41
miRNASSR111	3	1.70	0.72	0.41	0.36	lncRNASSR18	2	1.79	0.63	0.44	0.34
miRNASSR117	5	3.87	1.48	0.74	0.70	lncRNASSR20	2	1.97	0.69	0.49	0.37
miRNASSR119	3	2.66	1.03	0.62	0.54	lncRNASSR205	2	1.68	0.59	0.40	0.32
miRNASSR127	3	2.77	1.06	0.64	0.57	lncRNASSR22	4	2.95	1.13	0.66	0.59
miRNASSR132	2	1.97	0.69	0.49	0.37	lncRNASSR25	2	1.77	0.63	0.44	0.34
miRNASSR134	3	2.98	1.10	0.66	0.59	lncRNASSR265	2	1.99	0.69	0.50	0.37
miRNASSR20	2	1.97	0.69	0.49	0.37	lncRNASSR27	4	2.32	0.99	0.57	0.49
miRNASSR21	2	1.77	0.63	0.44	0.34	lncRNASSR315	2	2.00	0.69	0.50	0.37
miRNASSR23	2	1.84	0.65	0.46	0.35	lncRNASSR32	4	2.67	1.11	0.62	0.56
miRNASSR24	3	2.25	0.94	0.56	0.49	lncRNASSR33	2	1.23	0.33	0.19	0.17
miRNASSR25	2	1.80	0.64	0.44	0.35	lncRNASSR333	2	1.73	0.61	0.42	0.33
miRNASSR26	2	1.91	0.67	0.48	0.36	lncRNASSR36	3	2.40	0.98	0.58	0.51
miRNASSR29	3	2.74	1.05	0.63	0.56	lncRNASSR365	2	1.99	0.69	0.50	0.37
miRNASSR30	2	1.99	0.69	0.50	0.37	lncRNASSR368	2	1.81	0.64	0.45	0.35
miRNASSR31	3	2.01	0.86	0.50	0.45	lncRNASSR37	2	1.94	0.68	0.48	0.37
miRNASSR35	3	2.86	1.07	0.65	0.58	lncRNASSR38	2	1.55	0.54	0.35	0.29
miRNASSR36	3	2.81	1.06	0.64	0.57	lncRNASSR4	3	2.71	1.04	0.63	0.55
miRNASSR38	3	2.82	1.07	0.65	0.57	lncRNASSR42	2	1.96	0.68	0.49	0.37
miRNASSR40	2	2.00	0.69	0.50	0.37	lncRNASSR443	2	1.55	0.54	0.35	0.29
miRNASSR41	4	2.34	1.08	0.57	0.53	lncRNASSR46	2	1.87	0.66	0.46	0.36
miRNASSR43	2	1.66	0.59	0.40	0.32	lncRNASSR47	3	2.26	0.93	0.56	0.49
miRNASSR44	3	2.64	1.03	0.62	0.55	lncRNASSR487	2	1.90	0.67	0.47	0.36
miRNASSR45	2	1.57	0.55	0.36	0.30	lncRNASSR5	2	1.97	0.69	0.49	0.37
miRNASSR50	2	2.00	0.69	0.50	0.37	lncRNASSR512	2	1.86	0.66	0.46	0.36
miRNASSR51	3	1.53	0.64	0.35	0.32	lncRNASSR517	2	1.99	0.69	0.50	0.37
miRNASSR54	2	1.90	0.67	0.47	0.36	lncRNASSR546	3	2.28	0.93	0.56	0.49
miRNASSR57	2	1.86	0.66	0.46	0.36	lncRNASSR551	4	2.69	1.08	0.63	0.56
miRNASSR61	3	2.83	1.07	0.65	0.57	lncRNASSR7	2	1.76	0.62	0.43	0.34
miRNASSR62	3	2.91	1.08	0.66	0.58	lncRNASSR71	3	1.95	0.72	0.49	0.38
miRNASSR68	2	2.00	0.69	0.50	0.38	lncRNASSR73	3	2.59	1.02	0.61	0.54
miRNASSR69	2	1.95	0.68	0.49	0.37	lncRNASSR78	2	1.97	0.69	0.49	0.37
miRNASSR71	2	1.90	0.67	0.47	0.36	lncRNASSR81	3	1.76	0.74	0.43	0.38
miRNASSR76	3	2.82	1.07	0.65	0.57	lncRNASSR85	3	1.79	0.67	0.44	0.35
miRNASSR78	2	1.96	0.68	0.49	0.37	lncRNASSR87	2	1.63	0.57	0.39	0.31
miRNASSR79	3	2.21	0.93	0.55	0.49	lncRNASSR89	3	1.42	0.56	0.29	0.27
miRNASSR80	2	1.86	0.66	0.46	0.36	lncRNASSR164	2	1.96	0.68	0.49	0.37
miRNASSR81	3	2.08	0.83	0.52	0.43						
miRNASSR82	3	2.97	1.09	0.66	0.59						
miRNASSR83	2	1.87	0.66	0.46	0.36						
miRNASSR84	2	1.38	0.45	0.28	0.24						
miRNASSR86	2	2.00	0.69	0.50	0.37						
miRNASSR87	2	1.95	0.68	0.49	0.37						
miRNASSR88	3	2.51	1.00	0.60	0.53						
miRNASSR99	3	2.71	1.04	0.63	0.55						

SSR markers), 47 miRNAs showed tissue specific expression (Fig. 4A, Supplementary Table S4A). Among the 47 miRNAs, five (5) miRNAs were differentially expressed in leaf, 25 in flower, 11 in fruit, and eight (8) in stem tissues (Fig. 4A, Supplementary Table S4A). Similarly, out of 479 lncRNAs (containing 504 SSR markers), 86 lncRNAs showed tissue specific expression (Fig. 4B, Supplementary Table S4B). Out of 86 differentially expressed lncRNA, 20 showed differential expression in leaf, 11 in flower, 13 in early fruit, 18 in breaker fruit and 24 in mature fruit (Fig. 4B, Supplementary Table S4B).

3.8. Target genes of SSR containing tissue specific ncRNAs

A total of 161 targets genes were identified for 38 SSR containing tissue specific miRNAs (out of above mentioned 47 miRNAs), and for the remaining nine miRNAs we could not identify any target genes (Fig. 5A). Maximum 62 targets were identified for miRNA-CHR10:94196531-94,196,547 followed by 20 targets for miRNA-CHR10:202986126-202,986,150; and a single target gene was identified for 10 miRNAs (Fig. 5B). Likewise, total 120 genes (51 were in upstream and 69 were in downstrem regions of lncRNAs) were identified as potential targets for 38 lncRNAs (Fig. 5C and 5D). Maximum 22 target genes were identified for C_lncRNA_2004, followed by 15 targets for C_lncRNA_438; and single target gene was identified for 11 lncRNAs.

Gene ontology of above mentioned target genes suggested that these genes are involved in different biological processes like metabolism, hormone signalling, cellular component, enzymatic reaction, elements, nucleic acid, extracellular activities, vitamins, ligase activity etc. (Supplementary Tables S5 and S6). Surprisingly, all of the above mentioned target genes were only predicted in case of *Capsicum*, none was characterized. However, in case of model plant *Arabidopsis*, most of them are well characterized for different traits. For example, gene *guanine nucleotide exchange factor SPIKE 1* (LOC107846697 in *Capsicum*) play important role in cytoskeleton organization and trichome development and cotyledon shape [6,63]. Another gene, *Cyclin-Dependent Kinase C* (LOC107850317 in *Capsicum*) was shown to provide resistance

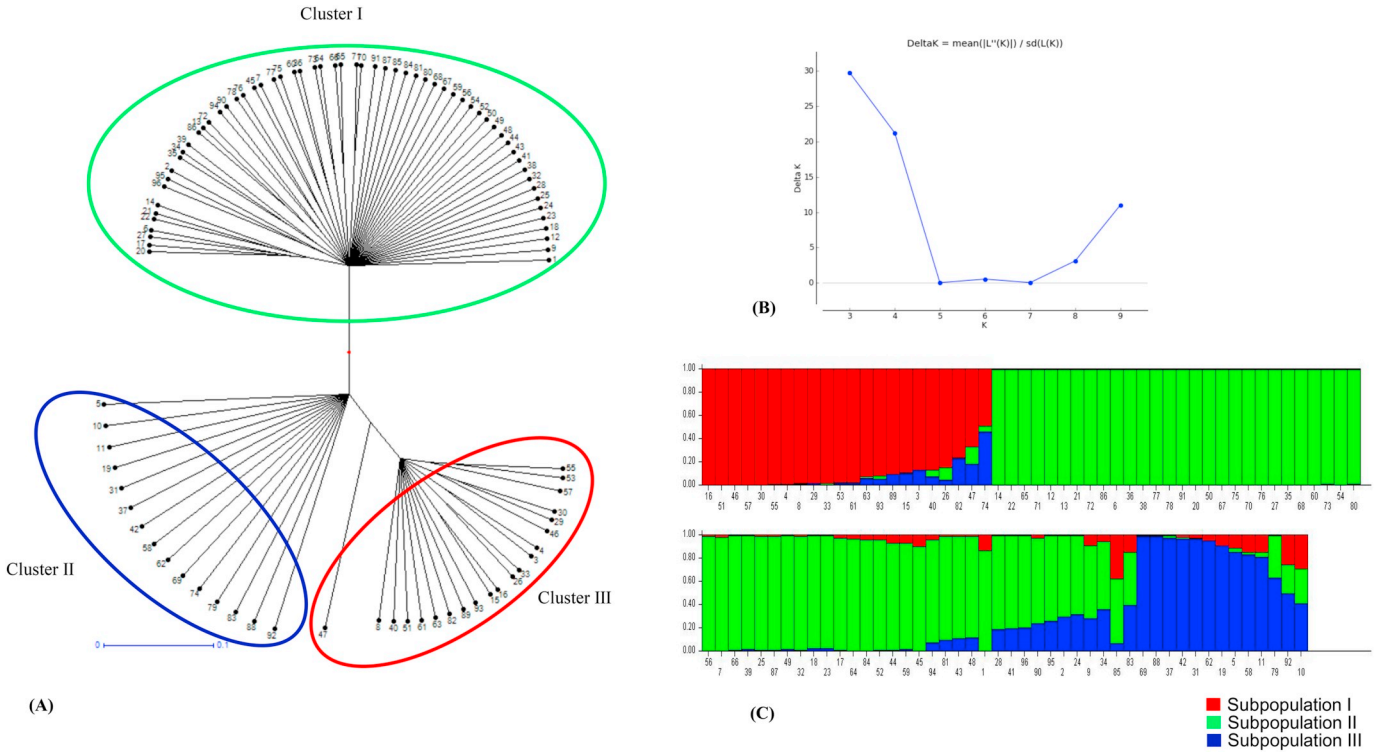

Fig. 3. Custer analysis using polymorphic non-coding RNA based simple sequence repeat (ncRNASSR) markers. (A) UPGMA dendogram showing three major cluster, (B) delta K plot suggesting three sub-populations, and (C) three subpopulations represented by three colours (each bar represents individual accession).

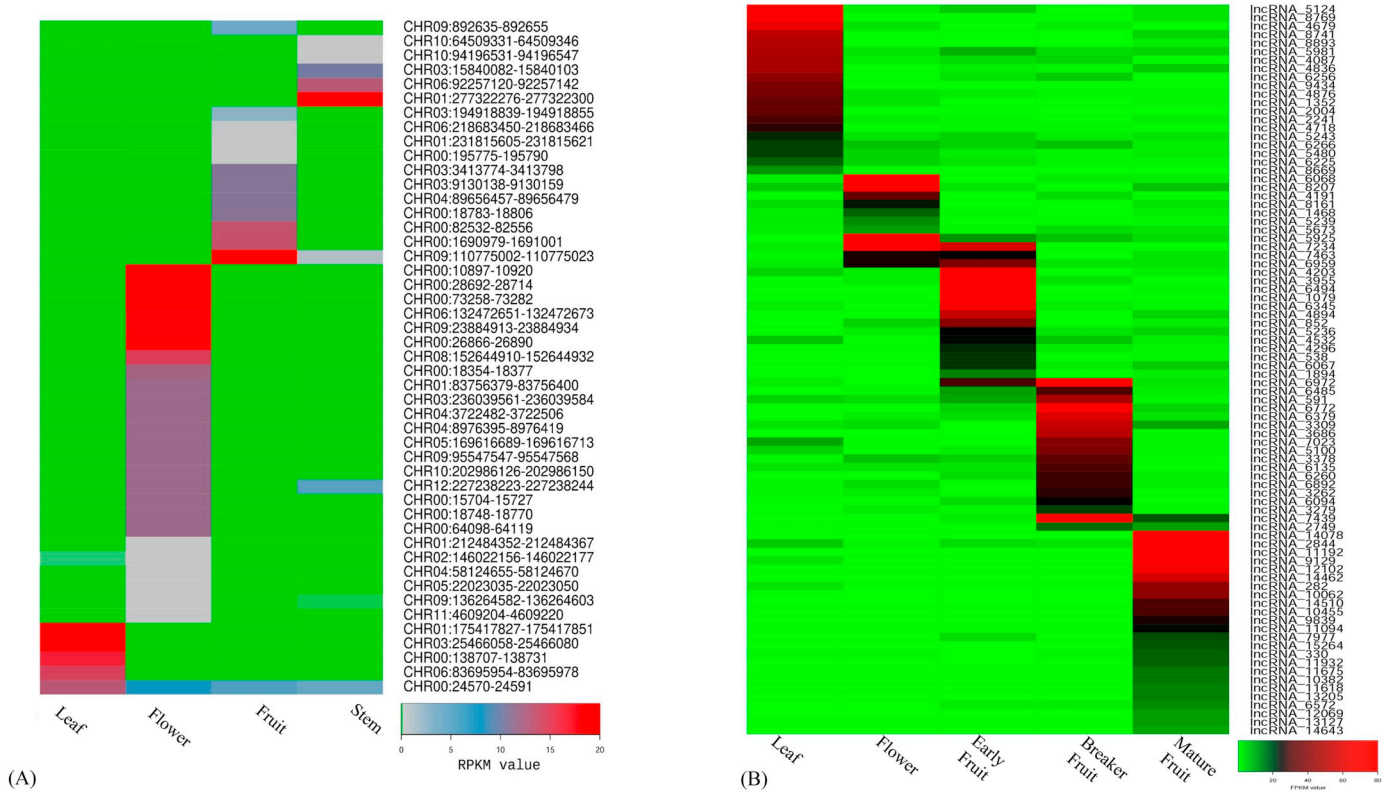

Fig. 4. Tissue specific expression of SSR containing non-coding RNAs (ncRNAs) in different plant tissues (A) miRNAs, (B) lncRNAs.

against Cauliflower mosaic virus (CaMV,[19]). *ATP-dependent DNA helicase Q-like 5* (LOC107847390 in *Capsicum*) suggested to be involved in DNA repair, genome stability and maintenance [5]. Similarly, *probable prolyl 4-hydroxylase 9* gene (LOC107858632 in *Capsicum*) was found to provide resistance against low oxygen conditions (like hypoxia, anoxia) and wounding [77]. Some target genes were also found to involve in carbohydrate metabolism. For example, *UDP-galactose/UDP-glucose transporter 5* gene (LOC107847908 in *Capsicum*) suggested

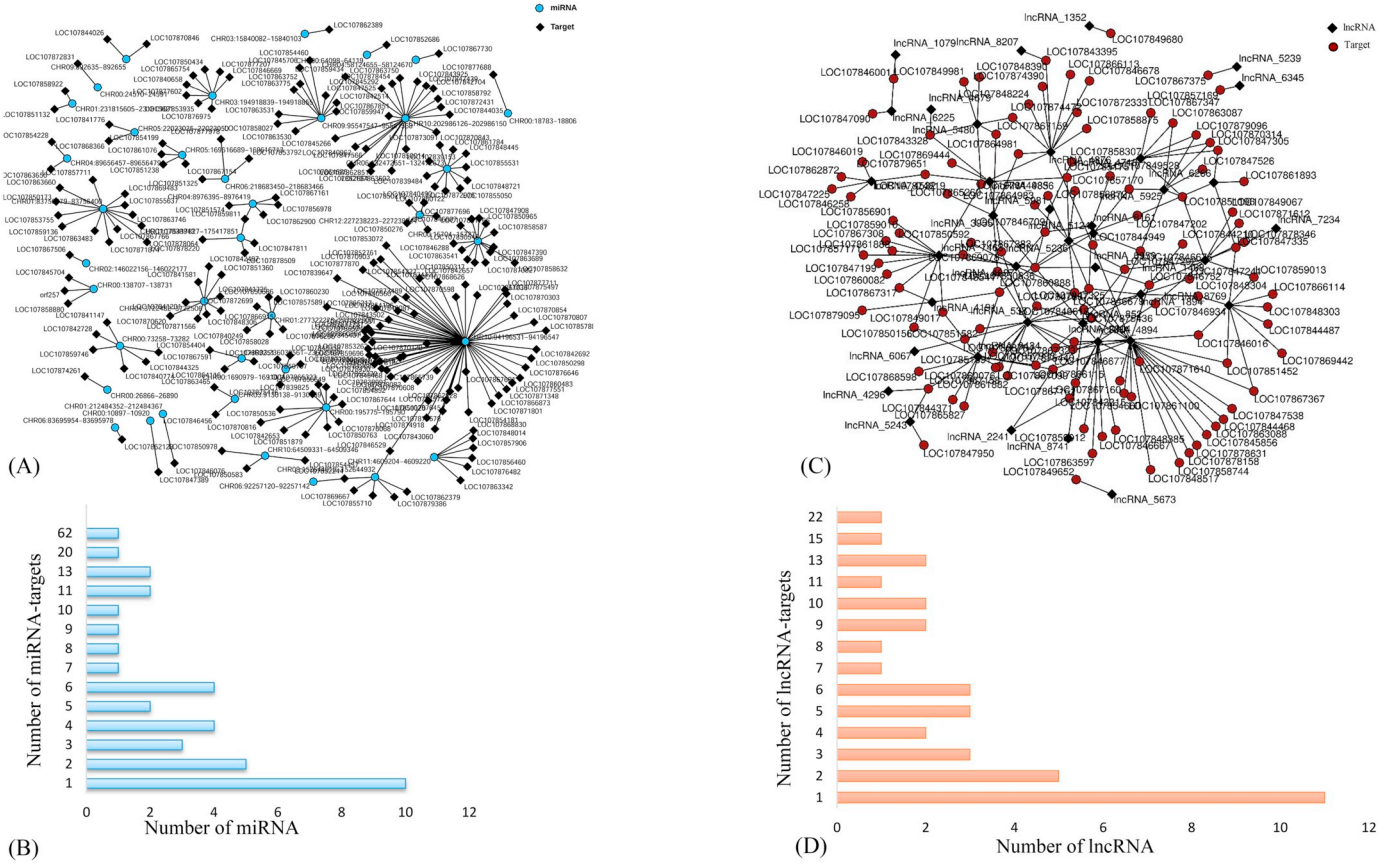

Fig. 5. Networking of SSR containing tissue specific non-coding RNAs (ncRNAs) and their target mRNAs. (A) miRNAs and targets, (B) frequency of miRNAs and miRNA targets, (C) lncRNAs and targets, (D) frequency of lncRNAs and their targets.

as the key player of glycoconjugates biosynthesis in *Arabidopsis* [52].

4. Discussion

The non-coding RNAs are widely known as key players of gene regulation at transcriptional and post transcriptional level [51]. Among the ncRNAs, miRNAs (~22 nucleotide long) and lncRNAs (> 200 nucleotide long) are found to be the most important abundantly found non-coding RNAs regulating growth and development of plants [21,51,79]. The miRNAs, are reported to mainly down regulate gene expression either through affecting the mRNA stability or by inhibiting the translation [51]. On the other hand, lncRNAs may regulate gene expression in both the directions i.e. up-regulation as well as down-regulation [51]. As they regulate overall gene expression resulting into plant phenotypes, the development of molecular markers based on non-coding RNAs would be very much helpful in breeding programs. In several crop plants, non-coding RNAs based molecular markers have been developed [26,27,47,78]. However, till now there is no report of development of non-coding RNAs based molecular markers in *Capsicum* species. Therefore, in the present study for the first time we have developed a total of 623 ncRNA based SSRs which includes 119 miRNASSRs and 504 lncRNASSRs in *Capsicum* species since SSR markers are one of the most widely used DNA based marker due to its co-dominant, robust, high reproducibility and simple PCR based user-friendly marker. For this purpose, we have utilized 1645 miRNAs and 15,450 lncRNAs that were developed in our laboratory. In earlier studies, the number of miRNAs reported in *Capsicum* ranged from 176 to 369 [30,42,62]; however, the number of miRNAs (1645) identified in our laboratory was higher which were used to develop SSRs in this study. Similarly, the number of lncRNAs identified and used in the present study (15450) were more compared to earlier reports (6527; [62]). The identification of a large number of ncRNAs in our laboratory may be either due to utilization of- (i) more number of tissue samples, and (ii) more than one *Capsicum* spp. compared to the previously reported studies.

Several studies have reported the development of miRNA based markers in many crop plants including jute (Saha et al. 2017), rice [27], Brassica [26], lotus [78], and Medicago [47]. It has been suggested that flanking sequences (0.3-1Kb) of pre-miRNA sequences are found to be important to understand the origin and evolution of miRNAs [53]. In rice, in order to develop SSR markers 500 bp flanking sequences of either side of the genes were taken along with pre-miRNA sequences [27]. Similarly, in another study of rice, 1 Kb flanking sequences were utilized for marker development [40]. We believe that the use of 500 bp flanking sequences along with miRNA sequence for SSR mining in the present study is completely justified and as per standard method. However, till date, no study is reported where long non-coding RNA is used for the development of molecular markers, and therefore the present study is the first to develop lncRNA based markers in plant.

In this study, the lower frequency (3.26% to 7.23%) of SSR containing ncRNAs (119 miRNASSR using 1645 miRNAs and 504 lncRNA SSRs from 15,450 lncRNAs) were observed. The less frequency of SSRs (1.5% - 11.9%) in coding regions were also observed in several crops like maize, rice, barley, *Sorghum*, bean, *Brassica* spp. [2,8,32]. The lower frequency of miRNASSRs was also reported in rice [27]. We found that the identified ncRNASSRs were distributed on all the 12 chromosomes of *Capsicum* genome. Furthermore, we observed that the frequency is inversely proportional to SSR motif length, i.e. frequency of dinucleotide SSRs were the highest followed by tri-, tetra, penta, and hexa nucleotide SSR motifs. Similar pattern was also observed in rice [15,27].

The direct correlation of number of repeats and polymorphism of

SSR markers has also been suggested [27,36]. In the present study, the number of repeats were found upto 32 times (average repeats 7.6 times) which suggested that the high level of possibility of getting polymorphisms with ncSSRs. The high polymorphism level of ncSSR markers were also confirmed by the genotyping of 96 *Capsicum* accessions using randomly selected 120 ncSSR markers. Among miRNASSRs 81.7% (49 markers out of 60) and among lncRNASSRs 68.3% (41 markers out of 60) were found to be polymorphic. Present study suggested the percent polymorphisms of ncRNA based SSR markers in *Capsicum* are higher or at par to other crops. For example, in pigeonpea, the per cent polymorphism reported ranged from 15 to 54.11% ([9,10,54,55,64]). Similarly, in jute the percent polymorphism ranged from 53.9–83.6% [41,68,83,84]; and it was 44–73% in *Brassica* [16,26,43,58] etc. The level of polymorphism may also be determined on the basis of PIC values which are grouped as low = below 0.25, medium = 0.25–0.50 and high = above 0.50 [11,26,57]. The non-coding RNA SSRs developed in the present study mostly lied under medium (72.2%; 65 out of 90 markers) and high (25.6%; 23 out of 90 markers) level of polymorphism and suggested their potential application in population genetic, QTL mapping, genetic diversity studies and *Capsicum* breeding programme.

The, ncRNA based SSR markers are also found to be extremely reliable for genetic diversity studies [26]. The UPGMA dendrogram analysis using 90 polymorphic ncRNASSR markers grouped three *Capsicum* spp. i.e. *C. annuum*, *C. frutescens* and *C. chinense* in three different clusters- Cluster I, cluster II and cluster III, respectively; suggesting their potential role in cross species genetic studies. In spite of distance based cluster analysis, the model based population structure analysis also showed similar kind of results where population of 96 accessions were divided into three subpopulations representing three different spp. of *Capsicum* (*C. annuum*, *C. frutescens* and *C. chinense*); Similar kind of observation was also suggested in *Brassica* crop where miRNA-based markers were found to produce more reliable estimates of genetic divergence than other marker system [26].

The ncRNA based markers also have high level of transferability across different species and may be potentially useful to develop markers in case where genome sequence is not available in a particular species [26]. For example, in the present study, we used transcriptome data of *C. chinense* and *C. frutescens* for miRNA and lncRNA identification and finally developed SSR markers. Due to highly conserved nature, ncRNAs were physically mapped on chromosomes using available *C. annuum* (Zulna-1) reference genome ([33]. The successful amplification of ncSSRs in all the three spp. along with some other spp. (like *C. pubescens*, *C. baccatum*) suggested the high transferability of these SSRs across the *Capsicum* species; and may found important to establish marker system in species which are unexploited like *frutescens, baccatum* and *pubescens*.

Marker systems may be categorized as functional markers if they are part of the genes; and it is widely known that functional markers (perfect markers) are more important in breeding programs and genetic studies. Several functional marker systems have been developed in plants which include EST-SSRs [13], gene-SSRs [38], inter-retro transposon amplified polymorphism (IRAPs; [67]), target region amplification polymorphism (TRAPs) and sequence-related amplification polymorphism (SRAPs) [72] etc. The ncRNASSRs are also another kind of potential functional markers which are very important as they play a key role in gene regulations. Further, the tissue specific expression of SSR containing ncRNAs suggested that SSRs developed in this study may found useful in mapping of QTLs/genes for different traits related to fruit, flower, leaf, and plant architecture. Similarly, the targets of ncRNAs we identified in the present study are those genes which are involved DNA repair, resistance against stresses, metabolism, genome stability, cytoskeleton organization, cell shape etc. This adds up the potential utility of associated SSRs of ncRNAs in different study and breeding program.

In summary, for the first time, in this study we report the development of cost effective, user friendly ncRNA based SSRs which includes 119 miRNASSRs and 504 lncRNASSRs in *Capsicum* species. These ncRNASSRs were distributed on all 12 *Capsicum* chromosomes and were highly polymorphic. Due to the conserved nature of ncRNAs, SSRs developed were found highly transferable and stable across different species of *Capsicum*, and may prove potential resource to develop marker system in orphan species of *Capsicum*. Furthermore, the UPGMA and population structure analyses suggested suitability of developed ncRNASSR markers for genetic diversity studies across *Capsicum* spp. ncRNASSR markers may serve as functional marker, and would be useful in *Capsicum* genetic studies for gene/QTL mapping and in overall in *Capsicum* breeding programs.

Supplementary data to this article can be found online at https://doi.org/10.1016/j.ygeno.2019.09.005.

Author's contribution

NR and VJ conceived and designed research. VJ and MD conducted experiments. AR performed bioinformatics analysis. VJ developed SSRs and analysed the data. SSC provide miRNA sequences, VS provided lncRNA sequences. VJ and AR wrote the manuscript. NR finalized the manuscript and gave critical suggestions. All authors read and approved the manuscript.

Authors declare no conflict of interest

Acknowledgement

This work was supported by the Department of Biotechnology, Government of India, in the form of Ramalingaswami *Re*-Entry Fellowship cum Research Grant, and Science and Engineering Research Board (SB/EMEQ-086/2014), Department of Science and Technology Govt. of India to Dr. Nirala Ramchiary. MD acknowledges WOS-A (SR/WOS-A/LS/1339/2015), VJ acknowledges the DST-INSPIRE faculty (DST/INSPIRE/04/2016/001189) award received from the Department of Science and Technology, Ministry of Science and Technology, Government of India and Early Career Research Award received from Science and Engineering Research Board, Government of India for supporting grant to carry out research work. AR acknowledges Senior Research Fellowship received from Council of Scientific & Industrial Research.

References

[1] Y.K. Ahn, S. Tripathi, J.H. Kim, Y.I. Cho, H.E. Lee, et al., Transcriptome analysis of *Capsicum* annuum varieties mandarin and Blackcluster: assembly, annotation and molecular marker discovery, Gene 533 (2014) 494–499.
[2] Z. An, C. Gao, J. Li, D. Fu, Z. Tang, O. Ortegon, Large-scale development of functional markers in *Brassica* species, Genome 54 (2011) 763–770.
[3] P.A. Anderson, G.J. Lawrence, B.C. Morrish, M.A. Ayliffe, E.J. Finnegan, J.G. Ellis, Inactivation of the flax rust resistance gene M associated with loss of a repeated unit within the leucine rich repeat coding region, Plant Cell 9 (1997) 641–651.
[4] H. Ashrafi, T. Hill, K. Stoffel, A. Kozik, J. Yao, et al., De novo assembly of the pepper transcriptome (*Capsicum* annuum): a benchmark for in silico discovery of SNPs, SSRs and candidate genes, BMC Genomics 13 (2012) 571.
[5] M.B. Bagherieh-Najjar, O.M.H. deVries, J.T.M. Kroon, E.L. Wright, K.M. Elborough, J. Hille, P.P. Dijkwe, *Arabidopsis* RecQsim, a plant-specific member of the *RecQ helicase* family, can suppress the MMS hypersensitivity of the yeast *sgs1* mutant, Plant Mol. Biol. 52 (2003) 273–284.
[6] D. Basu, J. Le, T. Zakharova, E.L. Mallery, D.B. Szymanski, A SPIKE1 signaling complex controls actin-dependent cell morphogenesis through the heteromeric *WAVE* and *ARP2/3* complexes, Proc. Natl. Acad. Sci. USA. 105 (2008) 4044–4049.
[7] J. Becker, P. Vos, M. Kuiper, F. Salamini, M. Heun, Combined mapping of AFLP and RFLP markers in barley, Mol. Gen. Genet. 249 (1995) 65–73.
[8] M.W. Blair, N. Hurtado, C.M. Chavarro, M.C. Munoz-Torres, M.C. Giraldo, F. Pedraza, J. Tomkins, R. Wing, Gene-based SSR markers for common bean (*Phaseolus vulgaris* L.) derived from root and leaf tissue ESTs, BMC Plant Biol. 11 (2011) 50.
[9] A. Bohra, I.P. Singh, A.K. Yadav, A. Pathak, K.R. Soren, S.K. Chaturvedi, et al., Utility of informative SSR markers in the molecular characterization of cytoplasmic genetic male sterility-based hybrid and its parents in pigeonpea, Natl. Acad. Sci. Lett. 38 (2015) 13–19.
[10] A. Bohra, R. Jha, G. Pandey, P.G. Patil, R.K. Saxena, I.P. Singh, D. Singh,

R.K. Mishra, A. Mishra, F. Singh, R.K. Varshney, N.P. Singh, New hypervariable SSR markers for diversity analysis, hybrid purity testing and trait mapping in pigeonpea [*Cajanus cajan* (L.) Millspaugh], Front. Plant Sci. 8 (2017) 377.
[11] D. Botstein, R.L. White, M. Skolnick, R.W. Davis, Construction of a genetic linkage map in man using restriction fragment length polymorphisms, Am. J. Hum. Genet. 32 (1980) 314.
[12] C.T. Butts, sna: Tools for Social Network Analysis, R Package Version 2.4, 2016 available at: https://cran.r-project.org/package=sna.
[13] K. Cai, L. Zhu, K. Zhang, L. Li, Z. Zhao, W. Zeng, X. Lin, Development and characterization of EST-SSR markers from RNA-Seq data in phyllostachys violascens, Front. Plant Sci. 10 (2019) 50.
[14] J.C. Carrington, V. Ambros, Role of microRNAs in plant and animal development, Science 301 (2003) 336–338.
[15] M. Chen, Z. Tan, G. Zeng, J. Peng, Comprehensive analysis of simple sequence repeats in pre-miRNAs, Mol. Biol. Evol. 2710 (2010) 2227–2232.
[16] X. Cheng, J. Xu, S. Xia, J. Gu, Y. Yang, J. Fu, X. Qian, S. Zhang, J. Wu, K. Liu, Development and genetic mapping of microsatellite markers from genome survey sequences in *Brassica napus*, Theor. Appl. Genet. 118 (2009) 1121–1131.
[17] J. Cheng, C. Qin, X. Tang, H. Zhou, Y. Hu, Z. Zhai, J. Cui, B. Li, Z. Wu, J. Yu, K. Hu, Development of a SNP array and its application to genetic mapping and diversity assessment in pepper (*Capsicum* spp.), Sci. Rep. 6 (2016) 33293.
[18] J. Cheng, Z. Zhao, B. Li, C. Qin, Z. Wu, et al., A comprehensive characterization of simple sequence repeats in pepper genomes provides valuable resources for marker development in *Capsicum*, Sci. Rep. 6 (2016) 18919.
[19] X. Cui, B. Fan, J. Scholz, Z. Chen, Roles of *Arabidopsis cyclin-dependent kinase C* complexes in cauliflower mosaic virus infection, plant growth, and development, Plant Cell 19 (2007) 1388–1402.
[20] X.B. Dai, P.X. Zhao, psRNATarge: a plant small RNA target analysis server, Nucleic Acids Res. 39 (2011) W155–W159.
[21] P. Deng, S. Liu, X. Nie, S. Weining, L. Wu, Conservation analysis of long non-coding RNAs in plants, Sci. China Life Sci. 61 (2018) 190–198.
[22] K.M. Dimitrov, P. Sharma, J.D. Volkening, I.V. Goraichuk, A. Wajid, S.F. Rehmani, A. Basharat, I. Shittu, T.M. Joannis, P.J. Miller, C.L. Afonso, A robust and cost-effective approach to sequence and analyze complete genomes of small RNA viruses, Virol. J. 14 (2017) 72.
[23] M. Dubey, V. Jaiswal, A. Rawoof, A. Kumar, M. Nitin, S.S. Chhapekar, et al., Identification of genes involved in fruit development/ripening in *Capsicum* and development of functional markers, Genomics (2019), https://doi.org/10.1016/j.ygeno.2019.01.002.
[24] W.H. Eshbaugh, The taxonomy of the genus *Capsicum*, Peppers: Botany, Production and Uses, CAB international, 2012, pp. 14–28.
[25] G. Evanno, S. Regnaut, J. Goudet, Detecting the number of clusters of individuals using the software STRUCTURE: a simulation study, Mol. Ecol. 14 (2005) 2611–2620.
[26] D. Fu, B. Ma, A.L. Mason, M. Xiao, L. Wei, Z. An, MicroRNA-based molecular markers: a novel PCR-based genotyping technique in *Brassica* species, Plant Breed. 132 (2013) 375–381.
[27] S.A. Ganie, T.K. Mondal, Genome-wide development of novel miRNA-based microsatellite markers of rice (*Oryza sativa*) for genotyping applications, Mol. Breed. 35 (2015) 51.
[28] S. Griffiths-Jones, H.K. Saini, S. van Dongen, A.J. Enright, miRBase: tools for microRNA genomics, Nucleic Acids Res. 36 (2008) D154–D158.
[29] J. Hormaza, L. Dollo, V. Polito, Identification of a RAPD marker linked to sex determination in Pistacia vera using bulked segregant analysis, Theor. Appl. Genet. 89 (1994) 9–13.
[30] D.-G. Hwang, J.H. Park, J.Y. Lim, D. Kim, Y. Choi, S. Kim, et al., The hot pepper (*Capsicum annuum*) MicroRNA transcriptome reveals novel and conserved targets: a foundation for understanding microRNA functional roles in hot pepper, PLoS One 8 (2013) e64238.
[31] Q. Jin, D. Waters, G.M. Cordeiro, R.J. Henry, R.F. Reinke, A single nucleotide polymorphism (SNP) marker linked to the fragrance gene in rice (*Oryza sativa* L.), Plant Sci. 165 (2003) 359–364.
[32] R.V. Kantety, M. La Rota, D.E. Matthews, M.E. Sorrells, Data mining for simple sequence repeats in expressed sequence tags from barley, maize, rice, sorghum and wheat, Plant Mol. Biol. 48 (2002) 501–510.
[33] S. Kim, M. Park, S.I. Yeom, Y.M. Kim, J.M. Lee, H.A. Lee, et al., Genome sequence of the hot pepper provides insights into the evolution of pungency in *Capsicum* species, Nat. Genet. 46 (2014) 270–278.
[34] S. Kim, J. Park, S.I. Yeom, Y.M. Kim, E. Seo, K.T. Kim, M.S. Kim, J.M. Lee, K. Cheong, H.S. Shin, S.B. Kim, K. Han, J. Lee, M. Park, H.A. Lee, H.Y. Lee, Y. Lee, S. Oh, J.H. Lee, E. Choi, E. Choi, Lee SEet al., New reference genome sequence of hot pepper reveal the massive evolution of plant disease-resistance genes by retroduplication, Genome Biol. 18 (2017) 210.
[35] Y. Lai, F. Zhang, T.K. Nayak, R. Modarres, N.H. Lee, T.A. McCaffrey, Detecting discordance enrichment among a series of two-sample genome-wide expression data sets, BMC Genomics 18 (2017) 1050.
[36] Y.C. Li, A.B. Korol, T. Fahima, Microsatellites: genomic distribution, putative functions and mutational mechanisms: a review, Mol. Ecol. 11 (2002) 2453–2465.
[37] J. Li, W. Ma, P. Zeng, J. Wang, B. Geng, J. Yang, Q. Cui, LncTar: a tool for predicting the RNA targets of long noncoding RNAs, Brief Bioinform 16 (2014) 806–812.
[38] J. Li, R. Zhou, T.R. Endo, N. Stein, High-throughput development of SSR marker candidates and their chromosomal assignment in rye (*Secale cereale* L.), Plant Breed. 137 (2018) 561–572.
[39] X. Li, X. Xing, S. Xu, M. Zhang, Y. Wang, H. Wu, Z. Sun, Z. Huo, F. Chen, T. Yang, Genome-wide identification and functional prediction of tobacco lncRNAs responsive to root-knot nematode stress, PLoS One 13 (2018) e0204506.
[40] Q. Liu, H. Wang, L. Zhu, H. Hu, Y. Sun, Genome-wide identification and analysis of miRNA-related single nucleotide polymorphisms (SNPs) in rice, Rice 6 (2013) 10–20.
[41] T.M. Liu, S.Y. Zhu, L.L. Fu, Q.M. Tang, Y.T. Yu, P. Chen, M.B. Luan, C.B. Wang, S.W. Wang, Development and characterization of 1,827 expressed sequence tag-derived simple sequence repeat markers for ramie (*Boehmeria nivea* L. Gaud), PLoS One 8 (2013) e60346.
[42] Z. Liu, Y. Zhang, L. Ou, L. Kang, Y. Liu, J. Lv, G. Wei, B. Yang, S. Yang, W. Chen, X. Dai, X. Li, S. Zhou, Z. Zhang, Y. Ma, X. Zou, Identification and characterization of novel microRNAs for fruit development and quality in hot pepper (*Capsicum annuum* L.), Gene. 608 (2017) 66–72.
[43] A.J. Lowe, C. Moule, M. Trick, K.J. Edwards, Efficient large-scale development of microsatellites for marker and mapping applications in *Brassica* crop species, Theor. Appl. Genet. 108 (2004) 1103–1112.
[44] W.S. Martins, D.C.S. Lucas, K.F.S. Neves, D.J. Bertioli, WebSat - a web software for microsatellite marker development, Bioinformation 3 (2009) 282–283.
[45] J.S. Mattick, J.L. Rinn, Discovery and annotation of long noncoding RNAs, Nat. Struct. Mol. Biol. 22 (2015) 5–7.
[46] B.C. Meyers, M.J. Axtell, B. Bartel, D.P. Bartel, D. Baulcombe, J.L. Bowman, X. Cao, J.C. Carrington, X. Chen, P.J. Green, S. Griffiths-Jones, S.E. Jacobsen, A.C. Mallory, R.A. Martienssen, et al., Criteria for annotation of plant microRNAs, Plant Cell 20 (2008) 3189–3190.
[47] X. Min, Z. Zhang, Y. Liu, X. Wei, Z. Liu, Y. Wang, W. Liu, Genome-wide development of microRNA-based SSR markers in *Medicago truncatula* with their transferability analysis and utilization in related legume species, Int. J. Mol. Sci. 18 (2017) 2440.
[48] M.A. Nadeem, M.A. Nawaz, M.Q. Shahid, et al., DNA molecular markers in plant breeding: current status and recent advancements in genomic selection and genome editing, Biotechnol. Biotechnol. Equip. 32 (2018) 261–285.
[49] S. Nagy, P. Poczai, I. Cernak, A.M. Gorji, G. Hegedus, J. Taller, PICcalc: an online program to calculate polymorphic information content for molecular genetic studies, Biochem. Genet. 50 (2012) 670–672.
[50] L. Nie, H.J. Wu, J.M. Hsu, S.S. Chang, A.M. Labaff, C.W. Li, Y. Wang, J.L. Hsu, M.C. Hung, Long non-coding RNAs: versatile master regulators of gene expression and crucial players in cancer, Am. J. Transl. Res. 4 (2012) 127–150.
[51] C. Nithin, A. Thomas, J. Basak, R.P. Bahadur, Genome-wide identification of miRNAs and lncRNAs in *Cajanus cajan*, BMC Genom. 18 (2017) 878.
[52] L. Norambuena, L. Marchant, P. Berninsone, C.B. Hirschberg, H. Silva, A. Orellana, Transport of UDP-galactose in plants. Identification and functional characterization of *AtUTr1*, an Arabidopsis thaliana UDP-galactose/UDP-glucose transporter, J. Biol. Chem. 277 (2002) 32923–32929.
[53] M. Nozawa, S. Miura, M. Nei, Origins and evolution of miRNA genes in plant species, Genome Biol. Evol. 4 (2012) 230–239.
[54] D.A. Odeny, B. Jayashree, M. Ferguson, D. Hoisington, L.J. Cry, C. Gebhardt, Development, characterization and utilization of microsatellite markers in pigeonpea, Plant Breed. 126 (2007) 130–136.
[55] D.A. Odeny, B. Jayashree, C. Gebhardt, J. Crouch, New microsatellite markers for pigeonpea (*Cajanus cajan (L.)Millsp.)*, BMC Res. Notes 2 (2009) 35.
[56] X. Perrier, J.P. Jacquemoud-Collet, DARwin Software, Centre de Cooperation Internationale en Recherche Agronomique Pour leDe'veloppement (CIRAD), Paris, 2006.
[57] Z.H. Pervaiz, M.A. Rabbani, S.R. Pearce, S.A. Malik, Determination of genetic variability of Asian rice (*Oryza sativa* L.) varieties using microsatellite markers, Afr. J. Biotechnol. 8 (2011) 5641–5651.
[58] J.E. Piquemal, C.F. Couton, C. Rondeau, E. Seignoret, I. Doucet, D. Perret, M.J. Villeger, P. Vincourt, P. Blanchard, Construction of an oilseed rape (*Brassica napus* L.) genetic map with SSR markers, Theor. Appl. Genet. 111 (2005) 1514–1523.
[59] W. Powell, G.C. Machray, J. Provan, Polymorphism revealed by simple sequence repeats, Trends Plant Sci. 1 (1996) 215–222.
[60] J.K. Pritchard, M. Stephens, P. Donnelly, Inference of population structure using multilocus genotype data, Genetics 155 (2000) 945–959.
[61] X. Qi, P. Lindhout, Development of AFLP markers in barley, Mol. Gen. Genet. 254 (1997) 330–336.
[62] C. Qin, C. Yu, Y. Shen, X. Fang, L. Chen, J. Min, J. Cheng, S. Zhao, M. Xu, Y. Luo, Y. Yang, et al., Whole-genome sequencing of cultivated and wild peppers provides insights into Capsicum domestication and specialization, Proc. Natl. Acad. Sci. USA 111 (2014) 5135–5140.
[63] J.-L. Qiu, R. Jilk, M.D. Marks, D.B. Szymanski, The Arabidopsis *SPIKE1* gene is required for normal cell shape control and tissue development, Plant Cell 14 (2002) 101–118.
[64] N.L. Raju, B.N. Gnanesh, P.T. Lekha, B. Jayashree, S. Pande, P. Hiremath, et al., The first set of EST resource for gene discovery and marker development in pigeonpea (*Cajanus cajan* L.), BMC Plant Biol. 10 (2010) 45.
[65] N. Ramchiary, M. Kehie, V. Brahma, S. Kumaria, P. Tandon, Application of genetics and genomics towards *Capsicum* translational research, Plant Biotechnol. Rep. 8 (2014) 101–123.
[66] S.O. Rogers, A.J. Bendich, Extraction of DNA from milligram amounts of fresh herbarium and mummified plant tissues, Plant Mol. Biol. 5 (1985) 69–76.
[67] H. Saeidi, M.R. Rahiminejad, J.S. Heslopherrison, Retroelement insertional polymorphisms, diversity and phylogeography within diploid, D-genome *Aegilops tauschii* (*Triticeae, Poaceae*) sub-taxa in Iran, Ann. Bot. 101 (2008) 855–861.
[68] D. Saha, R.K. Rana, S. Chakraborty, S. Datta, A.A. Kumar, A.K. Chakraborty, P.G. Karmakar, Development of a set of SSR markers for genetic polymorphism detection and interspecific hybrid jute breeding, Crop J. 5 (2017) 416–429.
[69] M. Sarpras, R. Gaur, V. Sharma, S.S. Chhapekar, J. Das, et al., Comparative analysis

of fruit metabolites and pungency candidate genes expression between Bhut jolokia and other *Capsicum* species, PLoS One 11 (2016) e0167791.
[70] Q. Sheng, K. Vickers, S. Zhao, J. Wang, D.C. Samuels, O. Koues, Y. Shyr, Y. Guo, Multi-perspective quality control of Illumina RNA sequencing data analysis, Brief Funct. Genom. 16 (2017) 194–204.
[71] K. Shirasawa, K. Ishii, C. Kim, T. Ban, M. Suzuki, et al., Development of *Capsicum* EST–SSR markers for species identification and in silico mapping onto the tomato genome sequence, Mol. Breed. 31 (2013) 101–110.
[72] E.F. Silva, S.B. Sousa, G.F. Silva, N.R. Sousa, F.J.N. Filho, R.E. Hanada, TRAP and SRAP markers to find genetic variability in complex polyploid Paullinia cupana var. sorbilis, Plant Gene 6 (2016) 43–47.
[73] D. Taller, J. Balint, P. Gyula, T. Nagy, E. Barta, et al., Correction: expansion of *Capsicum annum* fruit is linked to dynamic tissue-specific differential expression of miRNA and siRNA profiles, PLoS One 13 (2018) e0203582.
[74] F. Taranto, N. D'Agostino, B. Greco, T. Cardi, P. Tripodi, Genome-wide SNP discovery and population structure analysis in pepper (*Capsicum annuum*) using genotyping by sequencing, BMC Genomics 17 (2016) 943.
[75] H. Tegelstrom, Detection of mitochondrial DNA fragments, in: A.R. Hoelzel (Ed.), Molecular Genetic Analysis of Populations: A Practical Approach, IRL Press, Oxford, 1992, pp. 89–114.
[76] C. Trapnell, A. Roberts, L. Goff, G. Pertea, D. Kim, D.R. Kelley, H. Pimentel, S.L. Salzberg, J.L. Rinn, L. Pachter, Differential gene and transcript expression analysis of RNA-Seq experiments with TopHat and Cufflinks, Nat. Prot. 7 (2012) 562–578.
[77] F. Vlad, T. Spano, D. Vlad, F. Bou Daher, A. Ouelhadj, P. Kalaitzis, Arabidopsis prolyl 4-hydroxylases are differentially expressed in response to hypoxia, anoxia and mechanical wounding, Physiol. Plantarum 130 (2007) 471–483.
[78] X. Wang, S. Gui, L. Pan, J. Hu, Y. Ding, Development and characterization of polymorphic microrna-based microsatellite markers in *Nelumbo nucifera* (Nelumbonaceae), Appl. Plant Sci. 4 (2016) 1500091.
[79] J. Wang, X. Meng, O.B. Dobrovolskaya, Y.L. Orlov, M. Chen, Non-coding RNAs and their roles in stress response in plants, Genom. Proteom. Bioinform. 15 (2017) 301–312.
[80] F.C. Yeh, R.C. Yang, T.B.J. Boyel, Z.H. Ye, J.X. Mao, POPGENE, the User-Friendly Shareware for Population Genetic Analysis, Molecular Biology and Biotechnology Centre, University of Alberta, Canada, 1997.
[81] G. Yi, J.M. Lee, S. Lee, D. Choi, B.D. Kim, Exploitation of pepper EST-SSRs and an SSR-based linkage map, Theor. Appl. Genet. 114 (2006) 113–130.
[82] L. Zhang, J.M. Chia, S. Kumari, J.C. Stein, Z. Liu, A. Narechania, C.A. Maher, K. Guill, M.D. McMullen, D. Ware, A genome-wide characterization of microRNA genes in maize, PLoS Genet. 5 (2009) e1000716.
[83] L.W. Zhang, Y.R. Li, A.F. Tao, P.P. Fang, J.M. Qi, Development and characterization of 1,906 EST-SSR markers from unigenes in jute (*Corchorus* spp.), PLoS One 10 (2015) e0140861.
[84] L.W. Zhang, X.B. Wan, J.T. Xu, L.H. Lin, J.M. Qi, De novo assembly of kenaf (*Hibiscus cannabinus*) transcriptome using Illumina sequencing for gene discovery and marker identification, Mol. Breed. 35 (2015) 192.
[85] L. Zhang, C. Qin, J. Mei, X. Chen, Z. Wu, X. Luo, J. Chen, X. Tang, K. Hu, S.C. Li, Identification of microRNA targets of *Capsicum* spp. using MiRTrans—a trans-omics approach. Front, Plant Sci. 8 (2017) 495.
[86] X. Zhao, J. Li, B. Lian, H. Gu, Y. Li, Y. Qi, Global identification of ArabidopsislncRNAs reveals the regulation of MAF4 by a natural antisense RNA, Nat. Commun. 9 (2018) 5056.
[87] J. Zuo, Y. Wang, B. Zhu, Y. Luo, Q. Wang, L. Gao, Analysis of the coding and non-coding RNA transcriptomes in response to bell pepper chilling, Int. J. Mol. Sci. 19 (2018) 2001.

International Journal of Precision Engineering and Manufacturing-Green Technology
https://doi.org/10.1007/s40684-019-00151-z

Online ISSN 2198-0810
Print ISSN 2288-6206

REGULAR PAPER

Elucidations on the Effect of Lanthanum Doping in ZnO Towards Enhanced Performance Nanogenerators

Pandey Rajagopalan[1] · Pramila Jakhar[2] · I. A. Palani[1,3] · Vipul Singh[2] · Sang Jae Kim[4]

Received: 22 January 2019 / Revised: 6 August 2019 / Accepted: 19 August 2019
© Korean Society for Precision Engineering 2019

Abstract

Energy harvesting using semiconducting piezoelectric materials is one of the key areas of current research due to its high biocompatibility, low impedance, and high temperature workable range. In this work, we have optimized the doping of Lanthanum in ZnO towards the realization of enhanced output nanogenerator. We have varied the percentage of lanthanum (0, 1, 2.5, 5 and 7.5%) in the ZnO and systematically studied the piezoelectric response of each device. The piezoelectric output improved three to fourfolds by the incorporation of Lanthanum above 2.5%. The voltage response was further escalated by the controlled annealing in an oxygen environment. The doped and annealed device show eight to ninefolds improved output (~ 13.5 V) compared to the intrinsic device (~ 1.6 V). Material properties were investigated thoroughly along with the piezoelectric using various characterization tools. The device show a high maximum power density (~ 2.5 mW/m^2) and was used to charge several commercial capacitors. Finally, the device was demonstrated to work in intruder-safety alarm system application as low-cost device.

Keywords Piezoelectric energy · Zinc oxide · Doping · Sensor

Abbreviations

ZnO	Zinc oxide
La	Lanthanum
ITO	Indium tin oxide
PET	Polyethylene terephthalate
PVA	Polyvinyl alcohol
PDMS	Polydimethylsiloxane

List of Symbols

K	Shape factor
Λ	Wavelength of X-ray
D	Crystallite size
Θ	Braggs diffraction angle
V_{p-p}	Peak to peak voltage
A	Active area of the device
R	Load resistance

Electronic supplementary material The online version of this article (https://doi.org/10.1007/s40684-019-00151-z) contains supplementary material, which is available to authorized users.

✉ I. A. Palani
palaniia@iiti.ac.in

✉ Sang Jae Kim
kimsangj@jejunu.ac.kr

[1] Mechatronics and Instrumentation Lab, Discipline of Metallurgy Engineering and Materials Science, Indian Institute of Technology Indore, Indore 453552, India

[2] Molecular and Nano-electronics Research Group (MNRG), Discipline of Electrical Engineering, Indian Institute of Technology Indore, Indore 453552, India

[3] Mechatronics and Instrumentation Lab, Discipline of Mechanical Engineering, Indian Institute of Technology Indore, Indore 453552, India

[4] Nano Materials and Systems Lab, Department of Mechatronics Engineering, Jeju National University, Jeju 63243, South Korea

1 Introduction

Energy scavenging using unconventional sources like piezoelectricity have taken the strides in the last decade [1–12]. Moreover, with the advancements in the area of flexible and wearable devices, these is a need of biocompatible energy harvesting source which is lightweight and portable [13–15]. Piezoelectric materials show a linear mechano-electrical phenomenon which turns strain into the useful electric output. Among many piezoelectric materials, available zinc oxide (ZnO) is a material of interest in past decades because of its high piezoelectricity and high order of biocompatibility. Moreover, its vivid nanostructures, versatile

Published online: 10 September 2019

semiconducting properties and low impedance compared to conventional materials make it a unique candidate [9, 16]. When compared to the other semiconductors like aluminum nitride, gallium nitride, etc. it shows high piezoelectric coefficient however compared to conventional piezoelectric materials like lead zirconia titanate, its property is insignificant. Hence, researchers have opted to enhance the piezoelectric property of ZnO by different methods doping and interfacing. Doping is one of the easiest ways to alter the lattice parameter resulting in the change in piezoelectric output. However, all elemental doping does not improve the piezoelectric output. Transitional metal doping has been investigated in depth in the past [17]. Few transition metals like copper, cobalt, vanadium, and iron improved the response of the intrinsic ZnO however others like silver, Nickel, etc. proved to further deplete the response [2, 18–20]. Rare earth metals have been recently investigated and found to be effective in enhancing the piezoelectric output of ZnO [21–24]. The fabrication strategy commonly used is the low temperature chemical route method. However, it often results in the intermediate compounds in the lattice [25]. Moreover, the precipitates of basic salts on the surface go away after multiple washes of the sample which increases the process complexity. Recently Sinha et al. have studied the effect of lanthanum (La) on the ZnO using co-precipitation method towards the application of dye-sensitized solar cells [23]. However, the detailed analysis and optimization towards the piezoelectric device were not studied. Hence, here we have performed a detailed analysis in which different doping concentration of La in the ZnO (1, 2.5, 5 and 7.5%) were studied towards the improved piezoelectric output. The best performing concentrations were improved further by the effect of oxygen annealing in the samples. The piezoelectric response (voltage, current and power density, etc.) was studied in details. The increase in piezoelectric response was correlated with other characterization techniques like IV and Raman. Further, the device was used to charge the commercial capacitors of different capacity to ensure the practical use of the device.

2 Experimental Techniques

2.1 Doping, Fabrication and Packaging of Device

Intrinsic zinc oxide powder and lanthanum oxide used from high purity chemicals, Japan. Both oxide materials were mixed in different weight percentages viz. 1, 2.5, 5 and 7.5%. In a typical synthesis, the oxides were ground together using a minuscule amount of ethyl alcohol for 30 min. Then the resulting powder was placed in the tube furnace and heated to 1000 °C at the heating rate of 3 °C per minute [26]. The samples kept at this elevated temperature for 10 h, and the furnace was allowed to cool down naturally. Further, the powder was ground again for the subsequent use. For the fabrication of the device, indium tin oxide (ITO) coated polyethylene terephthalate (PET) substrate was cleaned with acetone and ethanol. The powder was deposited using a slurry coating method reported earlier [27]. In a typical coating, 100 mg of ZnO was ground with 100 µL of water for some time. Then 100 µL of 5 wt% polyvinyl alcohol (PVA) aqua solution was injected into the slurry. PVA acts as a binder to hold the particles together. Later the slurry was drop cast onto the ITO coated PET sheet. Then, the samples were heated in hot air oven at 70° for 2 h to dry the slurry. It was observed that the amount of material coated was around 50 mg. After complete drying, a thin layer of PDMS was coated to passivate the layer and the top electrode. PDMS layer was coated at 2500 rpm using a spin coating method for 30 s. PDMS was cured at recommended 70° for 2 h. Later the top electrode was coated using silver paste (Dupont). Copper leads (0.1 mm) were connected using silver epoxy. Finally, the device was packed using anti-static tape from both the sides to avoid the incorporation of triboelectric charges. This extra layer also provides structural stability and electrical shielding from external charges. For application as an intruder alarm system, ITO coated PET was used as a top electrode to give extra structural safety to the device. The schematic diagram of the entire fabrication process is shown in Fig. 1.

2.2 Characterization

The FESEM examination was completed on MIRA3 TESCAN FESEM combined with oxford instrument EDS detector. The crystallinity studies were performed by powder XRD (Rigaku Smart Lab system). Vibrational modes were studied using Raman spectra (LabRAM HR Evolution; Horiba, Japan) with an excitation wavelength of 514 nm. Piezoelectric characterization was done using Keithley electrometer 6514b with internal input impedance: > 200 TΩ). To produce a persistent mechanical input force, a linear motor (model HF01-37; LinMot) having a shaft mass of 2 kg was used. For the IV_{dark} measurement, 0.25 g powder was ground with polyvinyl alcohol (PVA) as a binder. The pellets were then sintered at 425 °C for 1 h (to remove PVA from pellets) and cooled down using natural convection. Later, planner copper electrode was evaporated for contacts. Keithley 2612 SMU was used to measure the IV characteristics.

3 Results and Discussion

3.1 Structural and Morphological Studies

Figure 2 shows the HR-XRD diffraction data for all the samples. The sample shows the high crystallinity phase with the least peak broadening. The intrinsic sample shows the

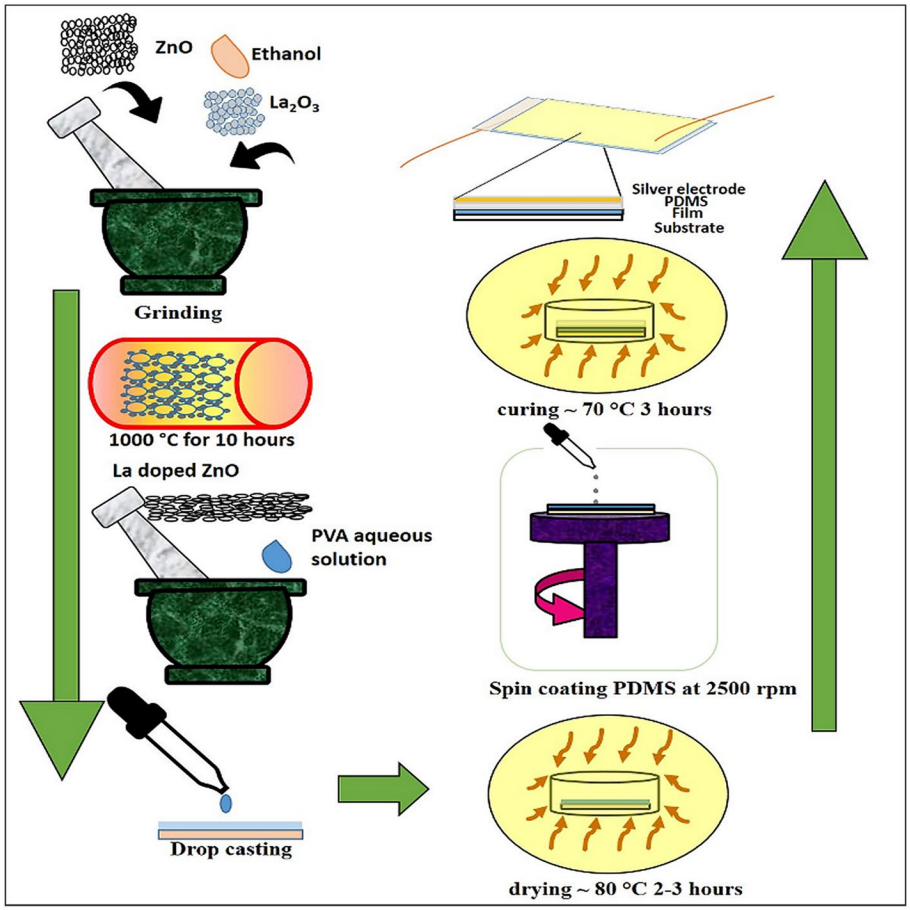

Fig. 1 Schematic diagram of synthesis, fabrication and packaging of device

extremely pure hexagonal wurtzite phase. All the peaks characterized by different phases are marked in Fig. 2a.

As the doping increases the intensity of the peaks increases and finally decreases with 7.5% doping as shown in the inset. Figure 2 b reveals the impurity phase formation at 29° and 30° in case of the sample with 7.5% doped samples which corresponds to 002 and 101 phase of lanthanum oxide (JCPDS 05 0602). Figure 2b also reveals the shifting of peaks towards lower theta signifying the increase in lattice parameters [28]. This is owing to the larger ionic radii of La^{3+} ions (104 pm) compared to Zn^{2+} ions (74 pm). Further, a plot of FWHM and relative intensity with respect to doping concentration suggested the successful incorporation of La inside the ZnO lattice inducing the highest broadening of (002) peak and the lowest relative intensity (I002/I101) as compared to other samples as shown in Fig. 2c. Beyond 5% doping, it has also been observed that lattice distortion (in terms of FWHM) was reduced in increasing relative intensity which is associated phase separation as shown in Fig. 2b (at $2\theta = \sim 30°$). Scherer's equation is commonly used for size broadening and Wilson equation for strain broadening. The equation is as follows

$$\beta cos\theta = \frac{k * \lambda}{D} + (4sin\theta * \varepsilon) \quad (1)$$

where k is the shape factor, λ is the wavelength of x-ray used, D is the crystallite size, and θ is the Braggs diffraction angle. The intercept from the above equation can be put into the Scherer's equation to estimate the crystallite size. This tells that the crystallite size decreases with the increase in doping. These results are in consistency with previously published reports in this direction [29, 30].

Raman spectrometer is a versatile vibrational spectroscopy tool to identify the crystal structure and throw some light on vibrational modes and behavior. Figure 2c shows the results of Raman spectroscopy of as prepared samples. Theoretical calculation predicts six different zone center optical phonons modes, which can be denoted by the: $\Gamma = A_1 + 2B_1 + E_1 + 2E_2$. The polar E_1 and A_1 modes are infrared and Raman active modes while the B_1 mode is the silent mode and is the Raman inactive. The main peak at 435 cm^{-1} is denoted as the E_2^{High} mode, and it is linked to oxygen sub-lattice [31].

A sharp E_2^{High} optical mode indicates the hexagonal wurtzite phase of Zinc Oxide with excellent crystallinity. The other minor peaks observed are at 326, 378, 526 and 585 cm^{-1}. The peak at 326 cm^{-1} is a second order peak and denoted as $E_2^{high} - E_2^{low}$ corresponding to multiphonon process. The other peaks at 378 cm^{-1} is denoted as a

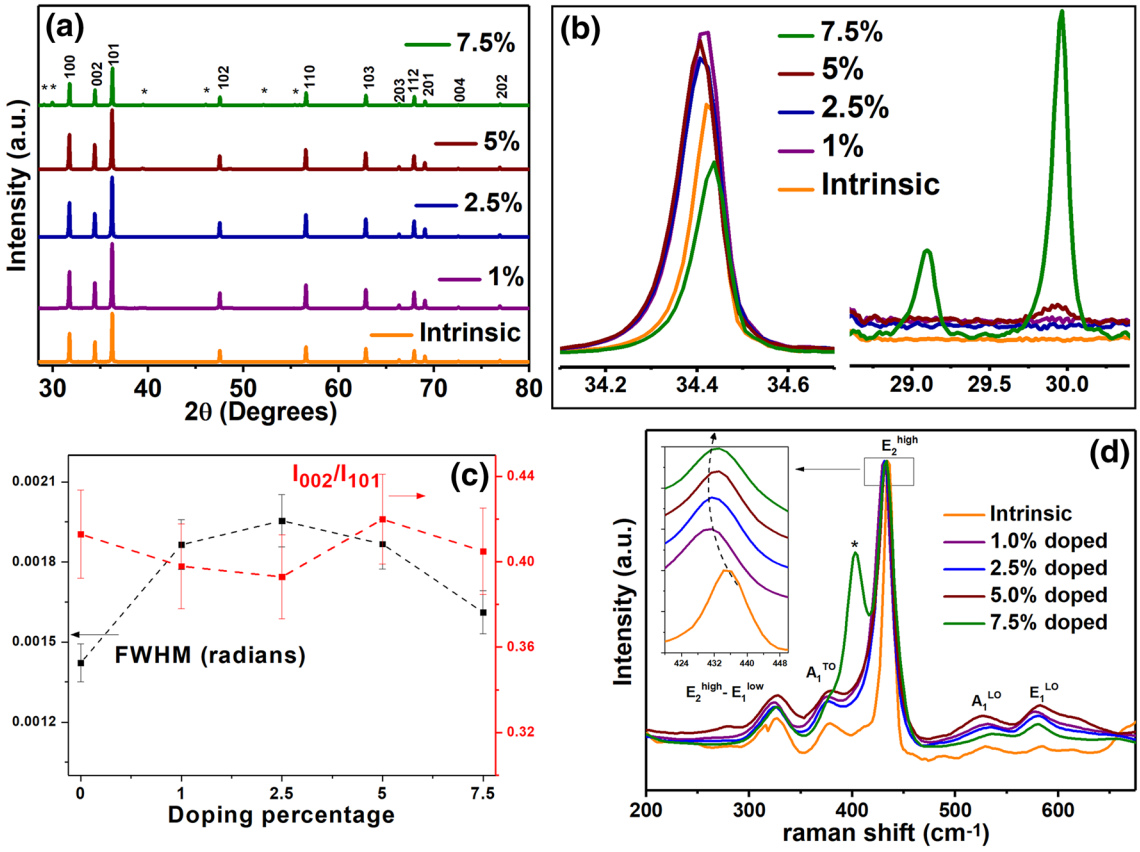

Fig. 2 **a** X-Ray diffraction of intrinsic and doped ZnO, **b** magnified 002 phase peaks of XRD shows shifting, the image on right shows the impurity phase formation in samples doped with 7.5 wt%, **c** Raman spectra of intrinsic and doped samples

transverse optics A_1 mode. The minor broad peaks at 526 and 585 cm^{-1} corresponds to longitudinal optics mode of A_1 and E_1 respectively. All the samples show the corresponding peaks of only ZnO except the samples doped with 7.5% La. The peak at 403 cm^{-1} corresponds to La–O stretching of E_g mode suggesting a separate phase [32]. Thus, the results in Raman is consistent with XRD results presented above. The inset shows the magnified E_2^{High} mode demonstrating the shifting to lower wavenumber. The shifting in the peaks suggests the red-shift in the lattice which reveals the presence of tensile stress in the lattice due to the incorporation of dopant. These results are in conformance with the XRD results discussed previously.

Figure 3 shows the FE-SEM results of all the samples. It also shows the elemental analysis of the compounds present in the sample. The average size of ZnO particles was around 650 nm. The particle size slightly decreases with increasing the dopant concentration which is in conformance with the variation of crystallite size discussed previously. The elemental analysis shows the presence of Lanthanum ions which again confirms the successful doping along with XRD and Raman spectroscopy results. The weight percentage of dopant analyzed from EDS was in close conformance with the original sample. The EDS shown 1.2, 2.3–2.8 and 4.4–5.5% for the samples doped with 1, 2.5 and 5%.

3.2 Piezoelectric Studies on the Effect of Dopant

The device was mounted on the rigid base, and a 2 N of force was applied using a linear motor separated by 125 mm (base 2 kg, acceleration 1 m/s^2). The potential was measured across 1000 MΩ resistance using electrometer. Figure 4a, b shows the electrical performance of intrinsic and doped devices. The frequency of the applied load is roughly equal to 0.75 Hz. It is observable that the doping enhanced the output of the device. The intrinsic device showed the potential of 1.6 V and current of about 28 nA. As the dopant concentration was increased by merely 1%, there was the enhancement in the current as well as the potential of the device. The device potential reached about 2.5 V with the current around 36 nA. Upon further increasing the concentration to 2.5% the electrical output was further increased by threefolds. The device potential was further increased to 5 V with the current value reached around 75 nA. Later, further increasing the concentration of dopant the performance saturates with

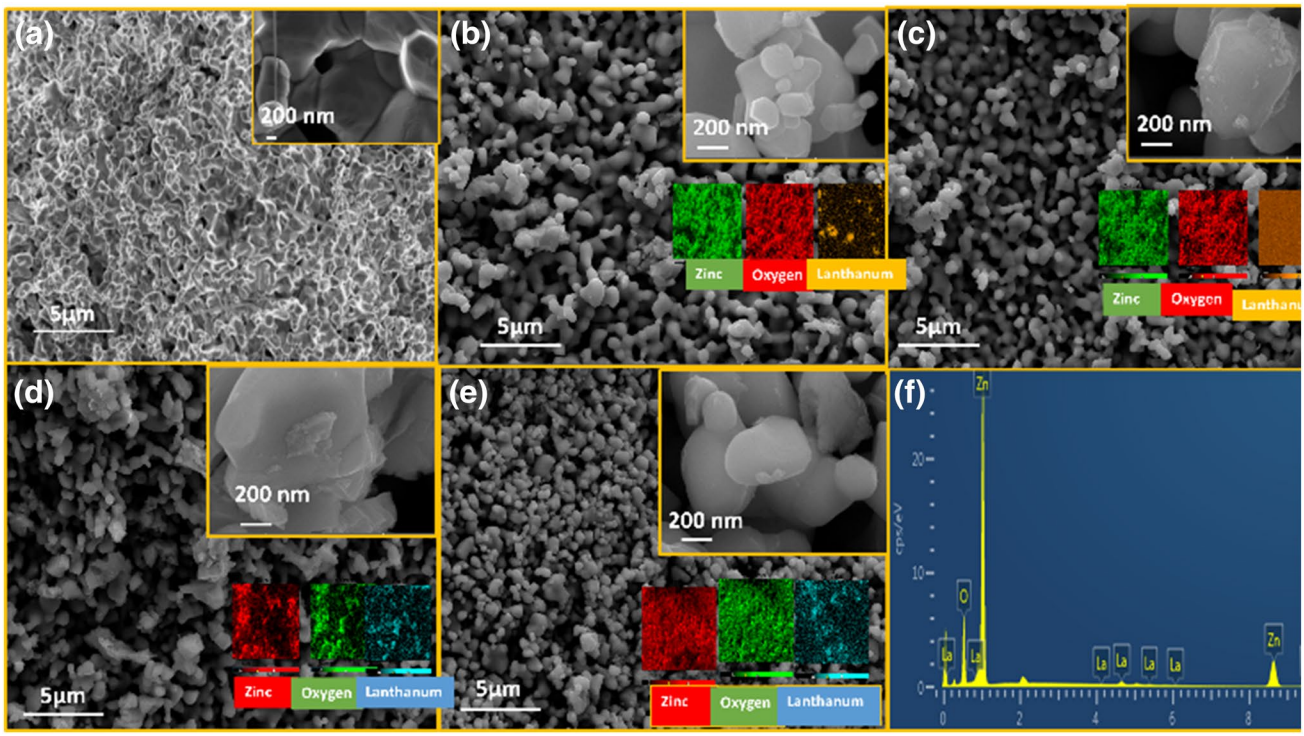

Fig. 3 **a** FESEM analysis of intrinsic samples, **b** 1 wt%, **c** 2.5 wt%, **d** 5 wt%, **e** 7.5 wt% and **f** EDS results of 5 wt% doped sample. The inset in each figure shows the magnified image as well as the elemental analysis

a slight improvement in the current. Upon increasing the concentration to 7.5% results in the slight reduction in the performance. A similar response in the current was also shown. Figure 4c presents the bar graph of the output of all the samples. Piezoelectric devices are high impedance devices which offers high voltage and low current. Moreover, the device impedance further increases by the addition of binder in the material in our case. Due to these reasons the device offers high voltage and lower current value. To ensure the repeatability we fabricated 2 devices of each and corresponding response is shown in the Fig. 4d. Previous studies have shown a strong dependence of ionic radii of dopant on the piezoelectric properties [2, 18, 19, 33]. It was observed that ionic radii smaller than Zinc lattice improved the performance of ZnO lattice. This was reflected in the shifting of XRD peaks to a higher angle. However, it was not universal as there are many reports where the larger ionic reported tends to increase the performance of the nanogenerator [21, 22, 24, 34]. Hence, ionic radii worked well for many materials but not for all. To reduce the discrepancy recently, Sinha et al. [24] gave the concept of ionic charge/crystal radii for benchmark improvement in the piezoelectric property of ZnO. This concept worked well for most of the dopant however we observed that it has a limitation. The ratio does not reflect the linear relationship of d_{33} improvement. For e.g., the ratio for intrinsic ZnO (2.70) was larger than the La-doped ZnO (2.56), however, La-doped ZnO shows a 10 times better d_{33} coefficient [23].

Though the concept was novel and worked pretty well for many of the materials hence can't be ruled out. However, the synthesis technique which directly affects the morphology, crystallinity and defect emission also plays an important role [1, 35–37]. In the wake of different ideas of enhancement in the piezoelectric response, one such idea is the charge screening phenomenon which has been supported by several researchers [2, 38–40]. Zinc oxide being semiconductor contains a large number of free electrons. When the material is strained, a dipole is generated which is readily depleted by these free electrons thus reducing the piezoelectric response. As the carrier concentration of the material increase the piezoelectric response of the material decreases [2, 39–41].

Lanthanum induces the doping impurity which reduces the carrier concentration of ZnO and induces a large number of holes [42]. These holes act as a trap for the free charge carriers in ZnO thus increasing the resistivity of the samples [2]. Additionally, the presence of extra positive charge on La^{3+} compared to Zn^{2+} results in the stronger polarity of La–O bonds hence easy rotation under strain [23, 43]. To check the feasibility, we also took the Dark IV response of the powders pressed into pellets with planar electrodes separated by a gap of 500 µm. It is clearly

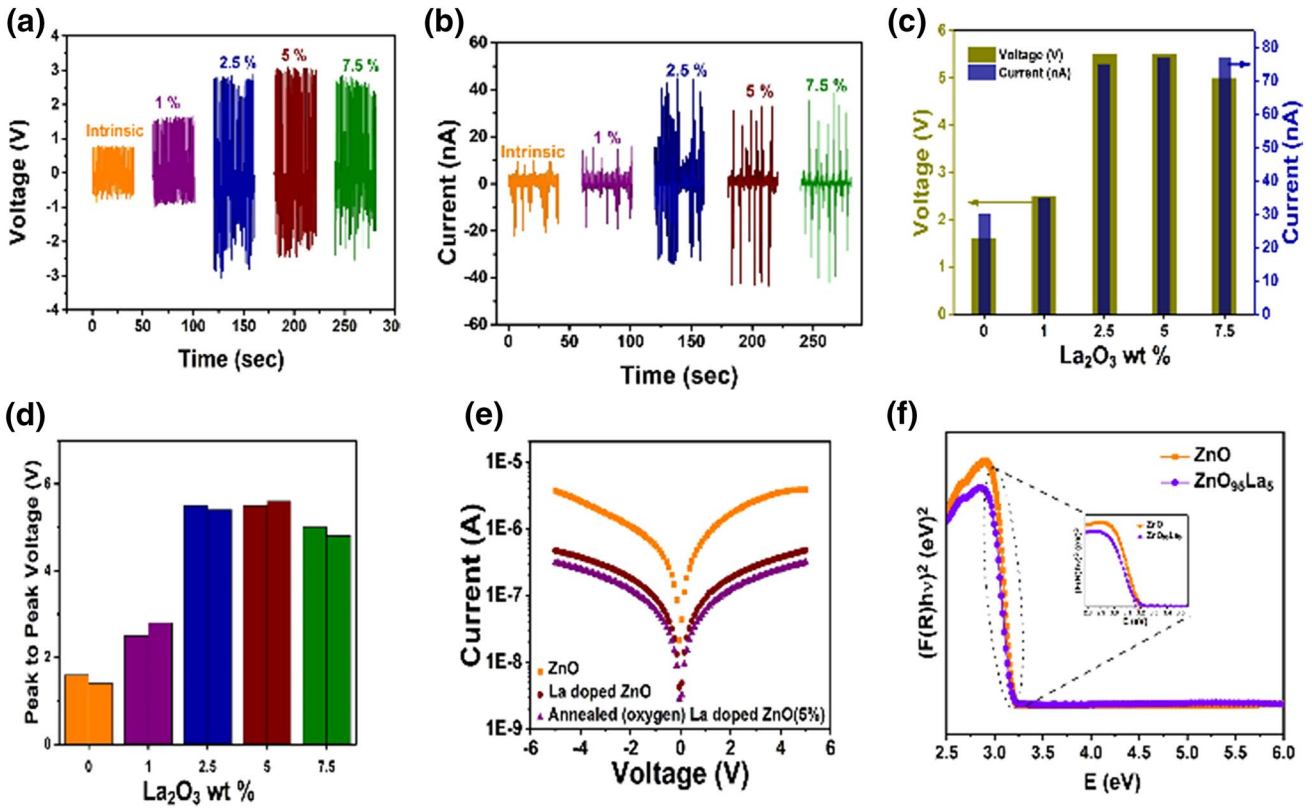

Fig. 4 **a** Piezoelectric voltage response of intrinsic and doped samples, **b** Piezoelectric current response of intrinsic and doped samples, **c** graphical representation of p–p voltage and p–p current of intrinsic and doped samples, **d** reliability of different devices, **e** IV_{dark} of intrinsic, 5 wt% doped and annealed samples and **f** DRS studied of intrinsic and doped samples

visible that the doping increases the resistivity and thus reducing the carrier concentration. The data is shown in Fig. 4e. To support this statement, Mott–Schottky analysis was performed. It was found that the carrier concentration decreased with doping and further reduced by annealing (8×10^{15}, 1.2×10^{15}, 4.14×10^{14}/cm^3). This reduction of dark current can indirectly elevate the potential produced in the device by reducing the charge screening phenomenon [2, 44]. The above point can be further proved by the UV–Vis data. The bandgap was calculated for ZnO and 5% doped ZnO using Diffused Reflectance spectroscopy. For this analysis, Kubelka–Munks function F(R) was calculated by the relation

$$F(R) = \frac{(1-R)^2}{2R} \tag{2}$$

To calculate the bandgap $(F(R)*h\upsilon)^2$, is plotted against the energy and extrapolating the curve to $F(R)=0$. The intercept gives the value of bandgap. It is detected that the band gap of the La-doped samples is slightly less than the intrinsic samples similar to earlier literatures on La-doped ZnO [45, 46]. Moreover, the lanthanum 5*d* orbital generates impurity bands above the ZnO valance band which reduces the band gap. The shift may also indicate the reduction in change in the carrier concentration due to hole impurities [47]. The graph is plotted and shown in Fig. 4f.

3.3 Piezoelectric Studies Improvement via Annealing and Other Device Performance

To further escalate the energy harvesting capability of piezoelectric nanogenerator the samples were annealed in the oxygen environment at 600 °C for 1 h. Oxygen environment has been shown to augment piezoelectric/ferroelectric property in zinc oxide [19, 33, 48]. Nevertheless, the consequence of annealing in oxygen on the defects states has been a tremendously arguable subject of interest. Annealing in oxygen verified to incorporate Arsenic type acceptor linked signatures [49]. Such defects are proved to be related to be beneficial for the piezoelectric property of ZnO [3, 18, 48]. Here, the sample 2.5 and 5% doped samples which showed the highest response were chosen and were annealed and a similar device was made out of it. The device 7.5% was discarded because of the high impurity phase as revealed in XRD and Raman studies. The

annealed devices showed an improved response. The p–p voltage response of 2.5% doped samples increased from 5 V to around 9 V. Additionally; the 5% doped samples showed even better response where the p–p voltage crossed more than 12 V. Thus the sample annealed in the oxygen showed significant improvement. Hence, in this work lanthanum doping and annealing in oxygen environment enhanced the piezoelectric response of the device by seven to eightfolds. This is a significant improvement in the property of the intrinsic device. To validate the piezoelectric response of the device, we have performed the dark current IV analysis [2]. The response is plotted in the Fig. 5a, b. The results clearly support the reduction of majority carriers upon doping and annealing and thus increasing the piezoelectric output of the device.

Finally, the device capability was measured by calculating the maximum instantaneous power density. It is an important tool to measure the effectiveness of the device and can be calculated using the following equation

$$P_{p-p} = \frac{V_{p-p}^2}{A * R} \tag{3}$$

where V_{p-p} is the peak to peak voltage, A is the active area of the device and R is the load resistance. The peak to peak voltage increases with the increasing the load resistance in accordance with Ohm's law. The data is plotted and shown in Fig. 5c. The maximum power density was found to around 2.5 mW/m^2 at 100 MΩ resistance which is very high and comparable to PZT based devices [52]. Table 1 gives the comparative analysis of the various device. Finally, the device capability can be figured out by its ability to charge the commercial capacitor. Here we used ceramic capacitors of different capacity and ran for 100 s. The device can charge even high capacity (400 nF) capacitor. The data is plotted and shown in Fig. 5d. Hence, the device can be used for practical applications.

Here we demonstrate the security and safety alarm system applications. We mounted our device below the doormat which could sense the intruder's presence if someone steps on the carpet/mat. Figure 6 shows the schematic of the diagram for the proposed application. Traditionally, IR based sensors are employed in such applications however these devices are prone to several conditions like a change in light, wind, shadow and often gives false signals. However, the

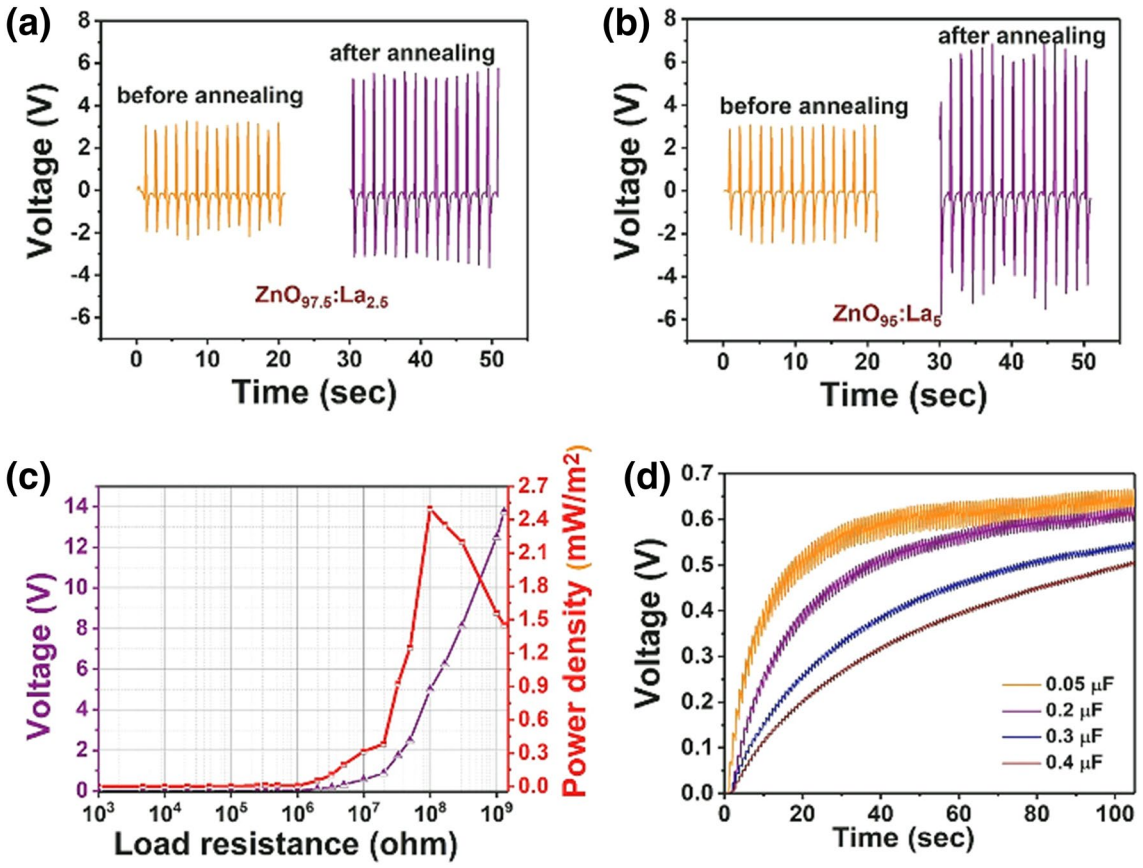

Fig. 5 **a** Piezoelectric response of 2.5 wt% doped sample before and after annealing, **b** Piezoelectric response of 5 wt% doped sample before and after annealing, **c** max power density curve of 5 wt% doped and annealed sample and **d** capacitance charging curves when charged for 100 s

Table 1 The comparative analysis of this work with other related works

Sr no	V_{p-p}	I_{p-p}/current density	Area	Force used	Material	Reference
1	–	1 μA/cm^2	~6 cm^2	5 N	V doped ZnO	[37]
2	1.5 V	–	6.25	34 N	Sb doped ZnO	[3]
3	5 V	2.5 μA/cm^2	~1 cm^2	~100 N	Halogens doped ZnO	[50]
4	–	1 μA/cm^2	–	5 N	Ga doped ZnO	[51]
5	15 V	7 μA	12.25 cm^2	Bending	Li doped ZnO	[48]
6	1 V	–	–	Finger force	PZT nanofiber	[52]
7	13 V	70 nA	1 cm^2	2 N	Lanthanum	This work

chances of false signals are less in piezoelectric devices. The device is connected to an alarm system connected through an Arduino circuit which activates the alarm upon receiving the signal. The device acts as a sensor whereas the alarm module is powered by an external battery. The video of the experiment is provided as the supplementary data.

We believe that our simple method for fabrication and doping opens up a new pathway for the enhancement of the piezoelectric output of ZnO cheaply and efficiently.

4 Conclusion

In summary, the consequence of La doping on the piezoelectric output of intrinsic ZnO was studied in details. The piezoelectric output was enhanced by 4–5 times with 5% doping of La. The intrinsic device gave an output around 1.5 V however the doped device gave an output around 5.5 V. The output was further improved by annealing of doped ZnO in oxygen, and the device gave an output close to 13 V. IV_{dark} measurement reveals the increasing trend of resistance with the increase in the output, thus confirming the reduction in charge screening phenomenon. The maximum power density obtained for best performing device was around 2.5 mW/m^2. Additionally, different capacity capacitors were charged using the device to check the feasibility of the device in practical energy harvesting application. Finally, the device was used for burglary alert sensor using highly cost-effective tools. We believe that our simple method for fabrication and doping opens up a new pathway towards the enhancement of the piezoelectric output of ZnO cheaply and efficiently.

Acknowledgements The author Pandey R is grateful to Research Instrument Center, JNU Jeju for providing characterization facilities. Pandey R. would further like to thank the (MHRD), India, for providing the Teaching Assistantship (TA). Pandey R is also Thankful to Indo Korea Research Internship by DST, India and NRF, Korea. Pandey R is thankful to Prof Kim Sang Jae for IKRI. Pandey R is grateful to Prof P M Shirage, Dr Prateek bhojane, Ms Lichhavi Sinha, Mr Aayush Gupta and Mr. S S Mani Prabhu for helping and improving in the content of the manuscript. A part of the research was supported by the Basic Science Research Program through the National Research Foundation of Korea (NRF) grant funded by the Korea government (MSIT) (2019R1A2C3009747, 2018R1A4A1025998).

Compliance with Ethical Standards

Conflict of interest On behalf of all authors, the corresponding author states that there is no conflict of interest.

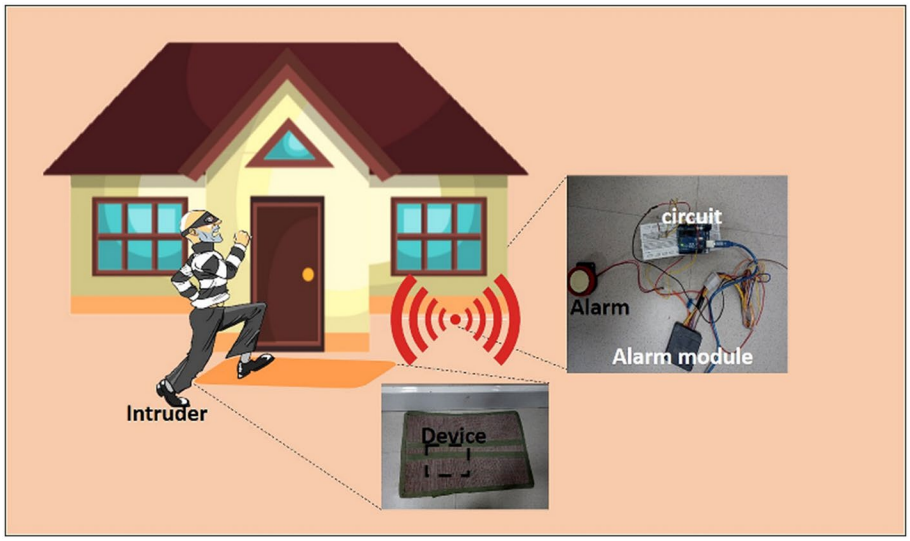

Fig. 6 Schematic diagram for the intruder-safety alarm system

References

1. Rajagopalan, P., Singh, V., & Palani, I. A. (2016). Investigations on the influence of substrate temperature in developing enhanced response ZnO nano generators on flexible polyimide using spray pyrolysis technique. *Materials Research Bulletin, 84,* 340–345. https://doi.org/10.1016/j.materresbull.2016.08.025.
2. Rajagopalan, P., Singh, V., & Palani, I. A. (2018). Enhancement of ZnO-based flexible nano generators via a sol–gel technique for sensing and energy harvesting applications. *Nanotechnology, 29*(10), 105406. https://doi.org/10.1088/1361-6528/aaa6bd.
3. Zhu, Y., Li, Q., Wang, P., Zang, W., Xing, L., & Xue, X. (2015). Enhanced piezo-humidity sensing of Sb-doped ZnO nanowire arrays as self-powered/active humidity sensor. *Materials Letters, 154,* 77–80. https://doi.org/10.1016/j.matlet.2015.04.060.
4. Khandelwal, G., Chandrasekhar, A., Pandey, R., Maria Joseph Raj, N. P., & Kim, S.-J. (2018). Phase inversion enabled energy scavenger: A multifunctional triboelectric nanogenerator as benzene monitoring system. *Sensors and Actuators B: Chemical*. https://doi.org/10.1016/j.snb.2018.11.110.
5. Rajagopalan, P., Singh, V., Palani, I. A., & Kim, S. J. (2018). Superior response in ZnO nanogenerator via interfaced heterojunction for novel smart gas purging system. *Extreme Mechanics Letters, 26,* 18–25. **(in press)**.
6. Turkmen, A. C., & Celik, C. (2018). Energy harvesting with the piezoelectric material integrated shoe. *Energy, 150,* 556–564. https://doi.org/10.1016/j.energy.2017.12.159.
7. Kim, J. E., Kim, H., Yoon, H., Kim, Y. Y., & Youn, B. D. (2015). An Energy conversion model for cantilevered piezoelectric vibration energy harvesters using only measurable parameters. *International Journal of Precision Engineering and Manufacturing-Green Technology, 2*(1), 51–57. https://doi.org/10.1007/s40684-015-0007-x.
8. Park, J.-H., Lim, T.-W., Kim, S.-D., & Park, S.-H. (2016). Design and experimental verification of flexible plate-type piezoelectric vibrator for energy harvesting system. *International Journal of Precision Engineering and Manufacturing-Green Technology, 3*(3), 253–259. https://doi.org/10.1007/s40684-016-0033-3.
9. Pandey, R., Maria Joseph Raj, N. P., Singh, V., Iyamperumal Anand, P., & Kim, S.-J. (2019). Novel interfacial bulk heterojunction technique for enhanced response in ZnO nanogenerator. *ACS Applied Materials & Interfaces, 1,* 2. https://doi.org/10.1021/acsami.8b19321.
10. Cui, J., Yoon, H., & Youn, B. D. (2018). An omnidirectional biomechanical energy harvesting (OBEH) sidewalk block for a self-generative power grid in a smart city. *International Journal of Precision Engineering and Manufacturing-Green Technology, 5*(4), 507–517.
11. Ghemari, Z., Saad, S., & Khettab, K. (2019). Improvement of the vibratory diagnostic method by evolution of the piezoelectric sensor performances. *International Journal of Precision Engineering and Manufacturing*, *20*(8), 1361–1369.
12. Cao, L.-M., Li, Z.-X., Guo, C., Li, P.-P., Meng, X.-Q., & Wang, T.-M. (2019). Design and test of the MEMS coupled piezoelectric-electromagnetic energy harvester. *International Journal of Precision Engineering and Manufacturing, 20*(4), 673–686.
13. Banerjee, S., & Roy, S. (2018). A dimensionally reduced order piezoelectric energy harvester model. *Energy, 148,* 112–122. https://doi.org/10.1016/j.energy.2018.01.116.
14. Sultana, A., Alam, M. M., Ghosh, S. K., Middya, T. R., & Mandal, D. (2019). Energy harvesting and self-powered microphone application on multifunctional inorganic-organic hybrid nanogenerator. *Energy, 166,* 963–971. https://doi.org/10.1016/j.energy.2018.10.124.
15. Kim, K.-B., Cho, J. Y., Jeon, D. H., Ahn, J. H., Hong, S. D., Jeong, Y.-H., et al. (2018). Enhanced flexible piezoelectric generating performance via high energy composite for wireless sensor network. *Energy, 159,* 196–202. https://doi.org/10.1016/j.energy.2018.06.048.
16. Yin, B., Qiu, Y., Zhang, H., Lei, J., Chang, Y., Ji, J., et al. (2015). Piezoelectric performance enhancement of ZnO flexible nanogenerator by a NiO–ZnO p–n junction formation. *Nano Energy, 14,* 95–101. https://doi.org/10.1016/j.nanoen.2015.01.032.
17. Wang, X. B., Song, C., Li, D. M., Geng, K. W., Zeng, F., & Pan, F. (2005). The influence of different doping elements on microstructure, piezoelectric coefficient and resistivity of sputtered ZnO film. *Applied Surface Science, 253,* 1639–1643. https://doi.org/10.1016/j.apsusc.2006.02.059.
18. Yang, Y. C., Song, C., Wang, X. H., Zeng, F., & Pan, F. (2008). Giant piezoelectric d_{33} coefficient in ferroelectric vanadium doped ZnO films. *Applied Physics Letters, 92*(1), 012907. https://doi.org/10.1063/1.2830663.
19. Laurenti, M., Castellino, M., Perrone, D., Asvarov, A., Canavese, G., & Chiolerio, A. (2017). Lead-free piezoelectrics: V(3+) to V(5+) ion conversion promoting the performances of V-doped Zinc Oxide. *Scientific Reports, 7,* 41957. https://doi.org/10.1038/srep41957.
20. Nour, E. S., Echresh, A., Liu, X., Broitman, E., Willander, M., & Nur, O. (2015). Piezoelectric and opto-electrical properties of silver-doped ZnO nanorods synthesized by low temperature aqueous chemical method. *AIP Advances, 5*(7), 077163. https://doi.org/10.1063/1.4927510.
21. Yadav, H., Sinha, N., Goel, S., & Kumar, B. (2016). Eu-doped ZnO nanoparticles for dielectric, ferroelectric and piezoelectric applications. *Journal of Alloys and Compounds, 689,* 333–341. https://doi.org/10.1016/j.jallcom.2016.07.329.
22. Goel, S., Sinha, N., Yadav, H., Godara, S., Joseph, A. J., & Kumar, B. (2017). Ferroelectric Gd-doped ZnO nanostructures: Enhanced dielectric, ferroelectric and piezoelectric properties. *Materials Chemistry and Physics, 202,* 56–64. https://doi.org/10.1016/j.matchemphys.2017.08.067.
23. Goel, S., Sinha, N., Yadav, H., Joseph, A. J., & Kumar, B. (2017). Experimental investigation on the structural, dielectric, ferroelectric and piezoelectric properties of La doped ZnO nanoparticles and their application in dye-sensitized solar cells. *Physica E: Low-dimensional Systems and Nanostructures, 91,* 72–81. https://doi.org/10.1016/j.physe.2017.04.010.
24. Sinha, N., Goel, S., Joseph, A. J., Yadav, H., Batra, K., Gupta, M. K., et al. (2018). Y-doped ZnO nanosheets: Gigantic piezoelectric response for an ultra-sensitive flexible piezoelectric nanogenerator. *Ceramics International, 44*(7), 8582–8590. https://doi.org/10.1016/j.ceramint.2018.02.066.
25. Uddin, M. T., Nicolas, Y., Olivier, C., Toupance, T., Servant, L., Muller, M. M., et al. (2012). Nanostructured SnO_2–ZnO heterojunction photocatalysts showing enhanced photocatalytic activity for the degradation of organic dyes. *Inorganic Chemistry, 51*(14), 7764–7773. https://doi.org/10.1021/ic300794j.
26. Kumar, A., Herng, T. S., Zeng, K., & Ding, J. (2012). Bipolar charge storage characteristics in copper and cobalt co-doped zinc oxide (ZnO) thin film. *ACS Applied Materials & Interfaces, 4*(10), 5276–5280. https://doi.org/10.1021/am301220h.
27. Krishnamoorthy, K., Pazhamalai, P., & Kim, S. J. (2017). Ruthenium sulfide nanoparticles as a new pseudocapacitive material for supercapacitor. *Electrochimica Acta, 227,* 85–94. https://doi.org/10.1016/j.electacta.2016.12.171.
28. Li, D., Huang, J.-F., Cao, L.-Y., Li, J.-Y., OuYang, H.-B., & Yao, C.-Y. (2014). Microwave hydrothermal synthesis of Sr^{2+} doped ZnO crystallites with enhanced photocatalytic properties. *Ceramics International, 40*(2), 2647–2653. https://doi.org/10.1016/j.ceramint.2013.10.061.

29. Anandan, S., Vinu, A., Sheeja Lovely, K. L. P., Gokulakrishnan, N., Srinivasu, P., Mori, T., et al. (2007). Photocatalytic activity of La-doped ZnO for the degradation of monocrotophos in aqueous suspension. *Journal of Molecular Catalysis A: Chemical, 266*(1–2), 149–157. https://doi.org/10.1016/j.molcata.2006.11.008.
30. Chen, J. T., Wang, J., Zhang, F., Zhang, G. A., Wu, Z. G., & Yan, P. X. (2008). The effect of La doping concentration on the properties of zinc oxide films prepared by the sol–gel method. *Journal of Crystal Growth, 310*(10), 2627–2632. https://doi.org/10.1016/j.jcrysgro.2008.01.011.
31. Sahoo, S., Sharma, G. L., & Katiyar, R. S. (2012). Raman spectroscopy to probe residual stress in ZnO nanowire. *Journal of Raman Spectroscopy, 43*(1), 72–75. https://doi.org/10.1002/jrs.3004.
32. Wang, N., Liu, J., Gu, W., Song, Y., & Wang, F. (2016). Toward synergy of carbon and La_2O_3 in their hybrid as an efficient catalyst for the oxygen reduction reaction. *RSC Advances, 6*(81), 77786–77795. https://doi.org/10.1039/c6ra17104d.
33. Luo, J. T., Yang, Y. C., Zhu, X. Y., Chen, G., Zeng, F., & Pan, F. (2010). Enhanced electromechanical response of Fe-doped ZnO films by modulating the chemical state and ionic size of the Fe dopant. *Physical Review B*. https://doi.org/10.1103/physrevb.82.014116.
34. Sinha, N., Ray, G., Bhandari, S., Godara, S., & Kumar, B. (2014). Synthesis and enhanced properties of cerium doped ZnO nanorods. *Ceramics International, 40*(8, Part A), 12337–12342. https://doi.org/10.1016/j.ceramint.2014.04.079.
35. Cardoso, J., Oliveira, F. F., Proenca, M. P., & Ventura, J. (2018). The influence of shape on the output potential of ZnO nanostructures: Sensitivity to parallel versus perpendicular forces. *Nanomaterials (Basel)*. https://doi.org/10.3390/nano8050354.
36. Saravanakumar, B., & Kim, S.-J. (2014). Growth of 2D ZnO nanowall for energy harvesting application. *The Journal of Physical Chemistry C, 118*(17), 8831–8836. https://doi.org/10.1021/jp502057p.
37. Gupta, M. K., Lee, J.-H., Lee, K. Y., & Kim, S.-W. (2013). Two-dimensional vanadium-doped ZnO nanosheet-based flexible direct current nanogenerator. *ACS Nano, 7*(10), 8932–8939.
38. Shin, S.-H., Lee, M. H., Jung, J.-Y., Seol, J. H., & Nah, J. (2013). Piezoelectric performance enhancement of ZnO flexible nanogenerator by a CuO–ZnO p–n junction formation. *Journal of Materials Chemistry C, 1*(48), 8103–8107. https://doi.org/10.1039/c3tc31664e.
39. Xue, X., Nie, Y., He, B., Xing, L., Zhang, Y., & Wang, Z. L. (2013). Surface free-carrier screening effect on the output of a ZnO nanowire nanogenerator and its potential as a self-powered active gas sensor. *IOP Nanotechnology, 24,* 225501. https://doi.org/10.1088/0957-4484/24/22/225501.
40. Baek, S. K., Kwak, S. S., Kim, J. S., Kim, S. W., & Cho, H. K. (2016). Binary oxide p–n heterojunction piezoelectric nanogenerators with an electrochemically deposited high p-type Cu_2O layer. *ACS Applied Materials & Interfaces, 8*(34), 22135–22141. https://doi.org/10.1021/acsami.6b03649.
41. Ong, W. L., Huang, H., Xiao, J., Zeng, K., & Ho, G. W. (2014). Tuning of multifunctional Cu-doped ZnO films and nanowires for enhanced piezo/ferroelectric-like and gas/photoresponse properties. *Nanoscale, 6,* 1680. https://doi.org/10.1039/c3nr05034c.
42. Hsu, C. L., Li, H. H., & Hsueh, T. J. (2013). Water- and humidity-enhanced UV detector by using p-type La-doped ZnO nanowires on flexible polyimide substrate. *ACS Applied Materials & Interfaces, 5*(21), 11142–11151. https://doi.org/10.1021/am403364r.
43. Tian, S., Zhang, Y., Zeng, D., Wang, H., Li, N., Xie, C., et al. (2015). Surface doping of La ions into ZnO nanocrystals to lower the optimal working temperature for HCHO sensing properties. *Physical Chemistry Chemical Physics, 17*(41), 27437–27445. https://doi.org/10.1039/c5cp04816h.
44. Jeong, D. K., Kang, J.-H., Ha, J.-S., & Ryu, S.-W. (2017). Enhanced piezoelectric operation of NiO/GaN heterojunction generator by suppressed internal carrier screening. *Journal of Physics. D. Applied Physics, 50*(42), 425101. https://doi.org/10.1088/1361-6463/aa882a.
45. Mrabet, C., Kamoun, O., Boukhachem, A., Amlouk, M., & Manoubi, T. (2015). Some physical investigations on hexagonal-shaped nanorods of lanthanum-doped ZnO. *Journal of Alloys and Compounds, 648,* 826–837. https://doi.org/10.1016/j.jallcom.2015.07.009.
46. Korake, P. V., Dhabbe, R. S., Kadam, A. N., Gaikwad, Y. B., & Garadkar, K. M. (2014). Highly active lanthanum doped ZnO nanorods for photodegradation of metasystox. *Journal of Photochemistry and Photobiology B: Biology, 130,* 11–19. https://doi.org/10.1016/j.jphotobiol.2013.10.012.
47. Shet, S., Ahn, K.-S., Yan, Y., Deutsch, T., Chrustowski, K. M., Turner, J., et al. (2008). Carrier concentration tuning of bandgap-reduced p-type ZnO films by codoping of Cu and Ga for improving photoelectrochemical response. *Journal of Applied Physics, 103,* 073504. https://doi.org/10.1063/1.2888578.
48. Shin, S.-H., Kim, Y.-H., Lee, M. H., Jung, J.-Y., Seol, J. H., & Nah, J. (2014). Lithium-doped zinc oxide nanowires–polymer composite for high performance flexible piezoelectric nanogenerator. *ACS Nano, 8*(10), 10844–10850.
49. Dangbegnon, J. K., Roro, K. T., & Botha, J. R. (2008). Towards p-type ZnO using post-growth annealing. *Physica Status Solidi (a), 205*(1), 155–158. https://doi.org/10.1002/pssa.200776828.
50. Zhang, Y., Liu, C., Liu, J., Xiong, J., Liu, J., Zhang, K., et al. (2016). Lattice strain induced remarkable enhancement in piezoelectric performance of ZnO-based flexible nanogenerators. *ACS Applied Materials & Interfaces, 8,* 1381–1387. https://doi.org/10.1021/acsami.5b10345.
51. Lee, J.-H., Lee, K. Y., Kumar, B., & Kim, S.-W. (2012). Synthesis of Ga-doped ZnO nanorods using an aqueous solution method for a piezoelectric nanogenerator. *Journal of Nanoscience and Nanotechnology, 12*(4), 3430–3433. https://doi.org/10.1166/jnn.2012.5632.
52. Chen, X., Xu, S., Yao, N., & Shi, Y. (2010). 1.6 V nanogenerator for mechanical energy harvesting using PZT nanofibers. *Nano Letters, 10*(6), 2133–2137. https://doi.org/10.1021/nl100812k.

Publisher's Note Springer Nature remains neutral with regard to jurisdictional claims in published maps and institutional affiliations.

Pandey Rajagopalan is a Ph.D. Research Fellow at Indian Institute of Technology, Indore, and was an Exchange Student at Jeju National University, Jeju, South Korea. He completed his undergraduate in Aerospace Engineering with Honors. He is passionate about energy and sustainable research. His hobbies include Reading, video games and football.

Pramila Jakhar received her M.Tech. degree in 2013; from Delhi Technological University, Delhi, India. Currently, she is pursuing her Ph.D. degree in the Discipline of Electrical Engineering at Indian Institute of Technology Indore (India). Her research work focuses on electrochemical growth of conducting polymer nanostructures and nanocomposites towards enzymatic glucose biosensors.

I. A. Palani is working as an Associate Professor in the Department of Mechanical Engineering at Indian Institute of Technology (IIT) Indore. He is head of the Discipline Mechanical Engineering, IIT Indore, Broad of Governors Member, IIT Indore. He obtained his Ph.D. from Precision Engineering lab, Department of Mechanical Engineering, IIT Madras, India. His research interest includes Smart Materials and Structures, Shape memory alloy, Laser assisted Surface processing, Mechatronics system design and optical Instrumentation.

Vipul Singh is working as an Associate Professor in the Department of Electrical Engineering at Indian Institute of Technology (IIT) Indore. He obtained his Bachelor degree in Electronics and Communication Engineering from Delhi College of Engineering (under University of Delhi) and MS from Kyushu Institute of Technology, Japan. His interest in the area of organic electronics ranges from device applications viz. OFETs, OSCs and OLEDs to the study of charge carrier transport or photo carrier generation in various organic materials.

Sang Jae Kim is a professor in the Department of Mechatronics Engineering and the Department of Advanced Convergence Technology and Science in Jeju National University, Republic of Korea. He received his Ph.D. degree in Electrical Communication Engineering from Tohoku University, Japan. He was a visiting research scholar in Materials Science Department at the University of Cambridge, UK and at the Georgia Institute of Technology, USA as well as a senior researcher at the National Institute of Materials Science (NIMS), Japan. His research disciplines are based on nanomaterials and systems for energy and electronics applications, covering Josephson devices, MEMS, and nano-bio sensors.

Available online at www.worldscientificnews.com

World Scientific News

An International Scientific Journal

WSN 135 (2019) 227-248 EISSN 2392-2192

Forecasting Landslide in Chukha from Index Properties of Soil-Research to Policy Making

Nimesh Chettri[1,*], Raju Sarkar[2], Kirtan Adhikari[1], Indra Bdr Chettri[3]

[1] Civil Engineering and Architecture Department, College of Science and Technology, Royal University of Bhutan, Phuentsholing, Bhutan

[2] Department of Civil Engineering, Delhi Technological University, Delhi, India

[3] Department of Civil Engineering and Surveying, Jigme Namgyel Engineering College, Samdrup Jongkhar, Bhutan

*E-mail address: nimeshchhetri.cst@rub.edu.bt

ABSTRACT

The Kingdom of Bhutan is located in the eastern Himalayas approximately between latitudes 26° 41'52" N to 28° 14' 52" N and longitudes 88° 44' 54" E to 92° 41' 7" E. The 38,686 square kilometers of landlocked and isolated mountain country has elevations ranging from about 160 meters in the southern part to more than 7500 meters in the northern part. People habituating along the steep slope valleys with river flowing at the foot of gorges are the finest epitome of exquisite scenery for outside world. However, such slopes particularly the unstable and loose ones pose greatest threat to the mankind and the development of the country. The complex arrangement of topography, constant tectonic movement and others human induced activities accelerate the landslide which are already active. The landslide problems in Bhutan dates back to 1960s when first road construction took place in the country. Every monsoon season is marked with countless landslide across the country, among which the landslide between Phuntsholing to Thimphu highway is the most frequent and disparaging. Many people lose their valuables and lives during the summer season every year due to landslides and falling stones on the highway. This research will help in bettering the knowledge in landslides and also combating it with necessary means. The main objective of this study is to comprehend the activating processes and mechanism of the landslide as well as examine to predict the possibility of another landslide by seeking natural causes and anthropogenic factors.

***Keywords*:** Dzongkhag, human-induced, AH48, soil profiling, factor of safety, slip, mud flow, landslide, Chhukha, Bhutan Himalayas

(Received 28 August 2019; Accepted 14 September 2019; Date of Publication 15 September 2019)

1. INTRODUCTION

Landslide problem has become one of the undeniable hurdles when one talks about developmental activities in the Himalayan regions. Every year Bhutan is facing numerous landslides or geohazards related activities which are making lacunae in gross economic development of the entire country. The fragile geology of the Himalayan area is prone to landslides and soil erosions especially during the monsoon season

. As the summer season approaches, the area along the Pasakha highway in Phuentsholing outnumbers the frequency of landslide compared to any other region in the country, therefore alarming the local municipal authority. Soil erosion during monsoon and fragile geology of the region are the main causes of landslides. In 1999, a slope failure occurred in Balujhora, Pasakha which consequently caused significant damage to agricultural lands, transportations and to the localities. Around 39 people died due to the landslide.

Figure 1. Some of the Active landslide of Chukha, Bhutan.

At present in Bhutan, ground reality survey adjudged that landslides are the result of heavy rain-falls and anthropogenic activities in mountain climate change also increasing landslide risk in this region. So, an urgent need has come up for the theoretical and empirical bases for this assertion to identify through the mechanisms by which climate can induce land

sliding and examines the manner in which these mechanisms may respond areas. Apart from it, human-induced to changes in a range of climatic and soil parameters. It is argued that inherent limiting stability factors, which vary with different terrain conditions and landslide types, ultimately govern the nature of response to changing climate. Several modelling approaches are needed to be evaluated on the basis of their potential to predict landslide response to climate projections. Given reliable input data of appropriate form and resolution, the existing slope stability, hydrological, and statistical models are for the most part capable of yielding useful prognoses on occurrence, reactivation, magnitude and frequency of land sliding

2. METHODLOGY

2. 1. Approach

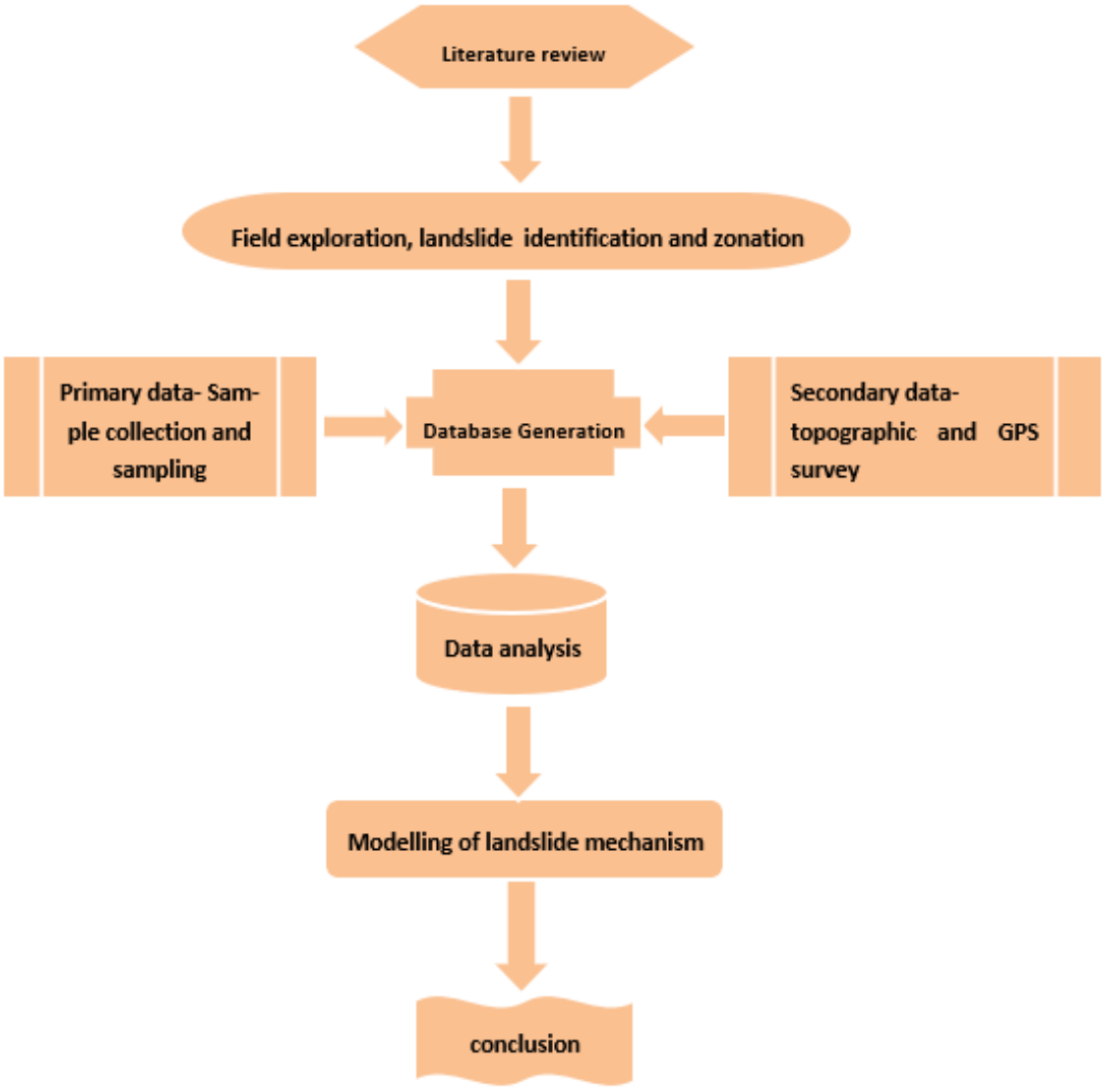

Figure 1. Methodology.

The sequential and processes of research philosophy to identity the governing factors that causes landslides are shown in Figure 2. The copious studies were made before the site visit and valuable information on past landslide were collected from various scholars. All the stretches along Phuentsholing – Thimphu which is approximately 98 km was visually investigated and demarcated into 16 zones. Soil samples are collected from each of these active landslide zones and analyzed for various mechanical properties. On contrary GPS coordinate were collected and topographical survey was done to quantify the extend of slope failure. DHMS, satellite images and Topographical Map (78F/05) were collected from Department of geology and mines and Ministry of work and human settlement which are the paramount entity for future research work of landslide zonation and soil map formulation using GIS. Soil samplings, shallow pitting and various engineering soil properties were determined in the lab. A partial hypothesis was drawn on the mechanism of landslide pattern occurring in study area. Finally, the result obtained shall be validated and verified in an engineering modeling. Mechanical and various Index properties such as water content, density, specific gravity, grains size distribution, permeability, shear strength parameters of soil obtained are used as an input parameter for landslide model analysis.

2. 2. Study Area

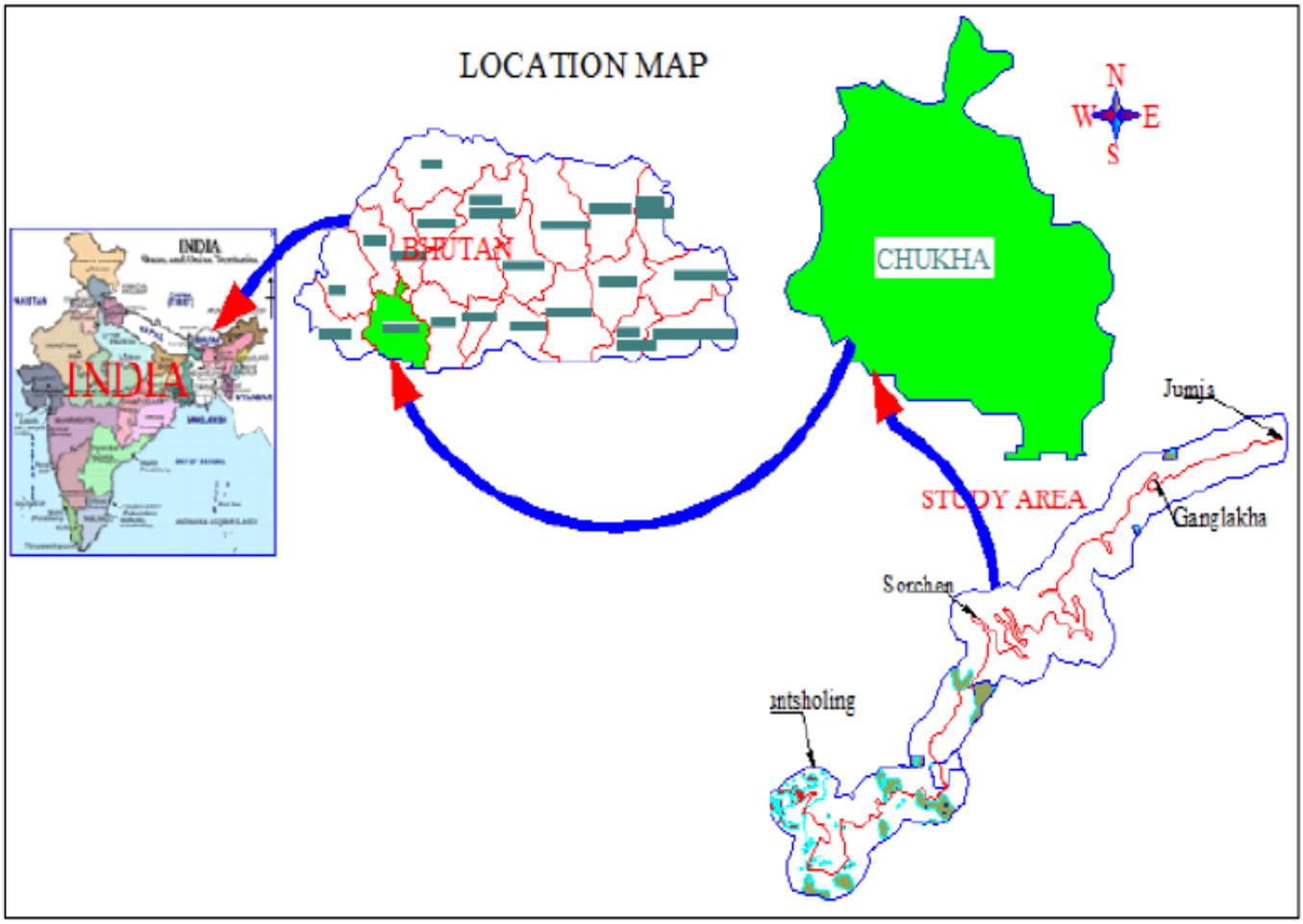

Figure 2. Study area along Asian Highway AH48

The study area stretches 98 km from the college of science and technology towards Thimphu Phuentsholing highway. Some stretches are chosen along Pasakha road since it comprises of some critical landslides. The entire study areas are divided into sixteen (16) zones as shown in the Figure 3 and 4 and soil sampling has been done for each zone. One of the active landslides included in the study is the Rinchending landslide below the college of science and technology. It is boarding India in south and lies on the southern part of Bhutan and has hampered society around for past decade. Another critical landslide included in this study is in Pasakha, adjacent to Rinchending is one of the major areas selected for industrial development in Bhutan. The only route connecting India and Pasakha is via Rinchending. Food supply for the people of Bhutan is transported from India through Asian Highway 47, along which Rinchending is situated. The route through Rinchending connecting India and Bhutan is considered as one of the shortest motorable road that connects the two countries. The blockage of the road along Thimphu - Phuentsholing highway for a considerable period of time can cause major shortage of ration to Bhutan. Hence, it is of utmost importance for the country to protect the region from major natural hazards.

ZONE NUMBER	DISTANCE FROM CST (KM)
ZONE 1	75.8km
ZONE 2	74.2km
ZONE 3	70.2km
ZONE 4	59.1km
ZONE 5	51.3km
ZONE 6	47.09km
ZONE 7	42.8km
ZONE 8	32km
ZONE 9	34.7km
ZONE 10	Balojora (10 km)
ZONE 11	Reldi (1.5 km)
ZONE 12	CST Goenpa (1.5 km)
ZONE 13	Sorchen(21.2km)
ZONE 14	Sorchen II (17km)
ZONE 15	Sorchen III (16.02km)
ZONE 16	Sorchen IV (11.5km)

Figure 3. Distance of Each study zone from College of Science and Technology, Phuentsholing.

Field data were also collected from landslide of Shorchen area, Jumja slide, Kamji and Gedu and analyzed in the lab. Jumja slide has always been threat to the travelers via it in every monsoon. The details of the analyzed results are presented in the report.

2. 3. Data Collection

Landslide prone regions along Thimphu-Phuentsholing highway till Chukha check post were identified and the coordinates were noted with the help of GPS on Android phone. In total, 16 active landslides were identified of which, Bhalujhora and Reldri are on the way to Pasakha. Pasakha bypass road departs from Rinchending check post and joints back to AH-48 on Gedu via Manitar. This route is occasionally used as and when AH-48 suffers major landslides and other land related disasters especially during monsoon.

Figure 4. Sample collection and topographic survey

Soil samples were collected from all the 16 zones and analysis were done for the mechanical and index properties of soils responsible for landslides. Moreover, topographic survey was conducted for all 16 critical landslides zone and the area affected and slope angle are quantified.

2. 4. Soil sampling and Analysis

Soil sample collected from site consists foreign partials which should be segregated and the sample should be oven dried for at least 24 hours. Mechanical characteristics such as water content, density, specific gravity, grains size distribution, infiltration test and Atterberg limits are conducted on samples collected from the study area. Test for consolidation parameters and shear strength parameters are also conducted in laboratory.

The analysis result of grain size of the sample collected is represented in Figure 7. The predominant soil type found in the study area is gravely sand with less than 10% fines. The physical visualization confirms that these are sandy loam which is vulnerable to slope movement.

Figure 5. Drying of soil sample.

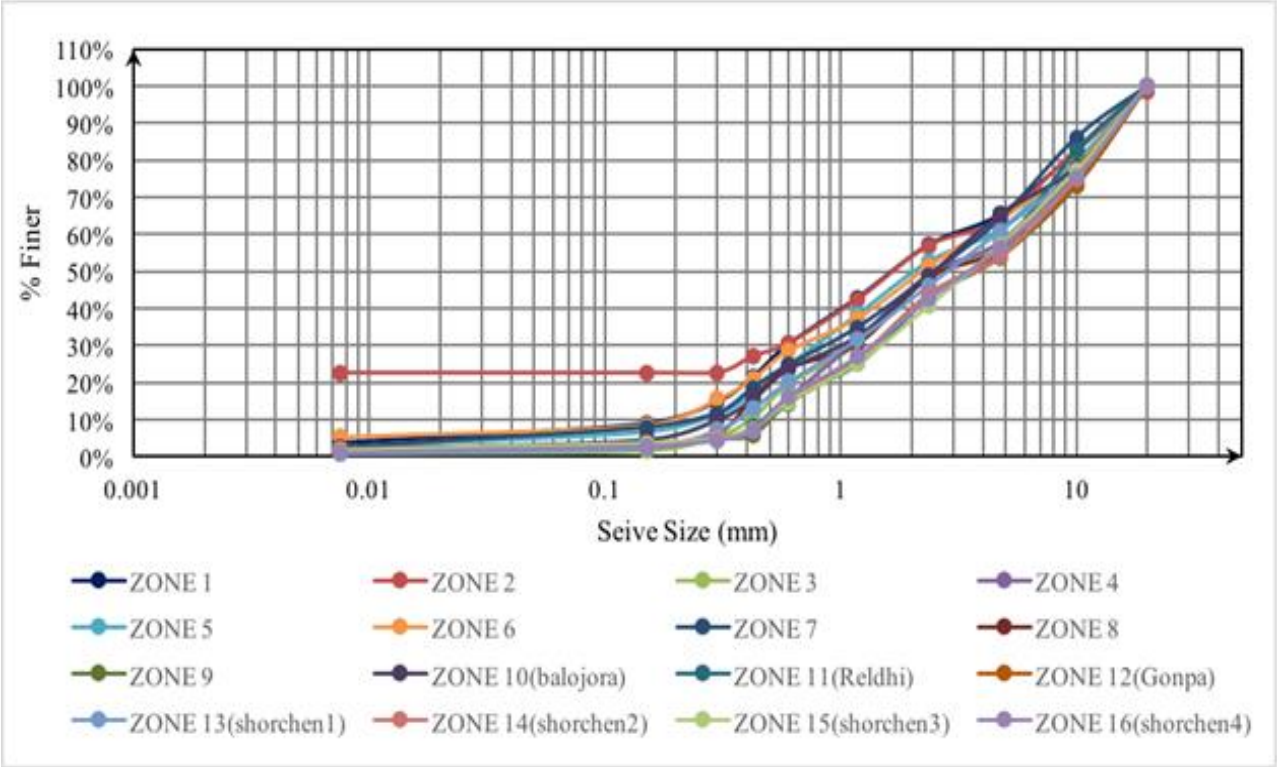

Figure 6. Sieve analysis result.

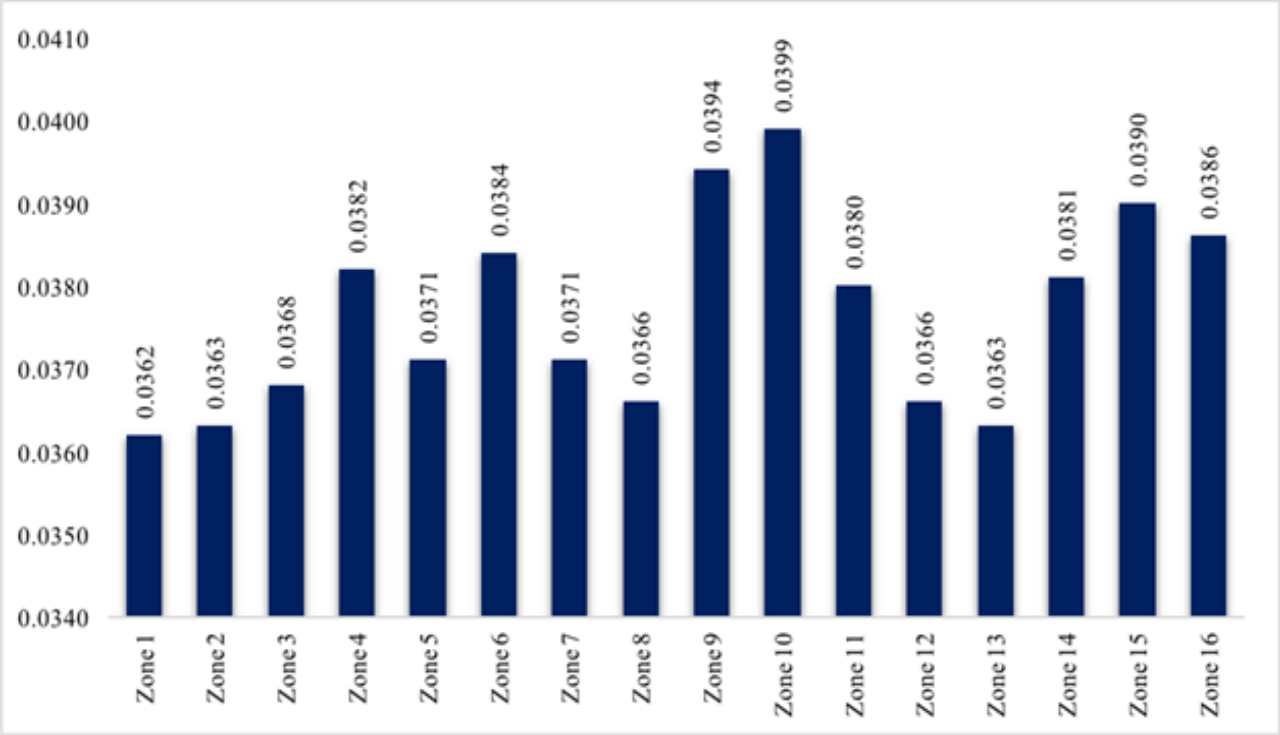

Figure 7. Permeability.

The hydraulic permeability of zone1 is 0.0363cm/sec and that of zone 10 is 0.0399 cm/sec which are lowest and highest data obtained from the study area respectively. These particular value is graded a contributing agent to accelerate the slope failure. The specific gravity results for zone 1 which indicate the mixture of sandy clay. However, for zone4 value is 3.09. This is the indispensable findings which indicate the presence of heavier particles along with the coarse sand. This condition leads to the instability of the slope. The predominant rock strata found across the study area is phyllite which is the sedimentary work. The phyllite forms the weak strata which erodes with rain and also forms the plane of failure with its adjacent soil mass at its surface.

2. 5. Field survey Data

Figure 9 shows active landslide of zone 4 which is located at a distance of 59.1 km from Rinchending. This is a classic example of landslide where surface mass loses its shear strength with its adjacent layer and then moves by sliding along a rupture or slip surface. This is also known as landslip. It is indispensable to note that visual observation of the failed slope depicts that majority of the slip/slide are translational movement and not the rotational. Since its translation movement the debris flows to the greater distance hence increasing its destruction action.

As seen in the Figure 9 the exposed surface consist of phyllite strata which poorly binds with the surface mass. Hence, in most of the zones failure planes has been identified as either subsurface phyllite rock or surface between artificial fill and cohesionless layer.

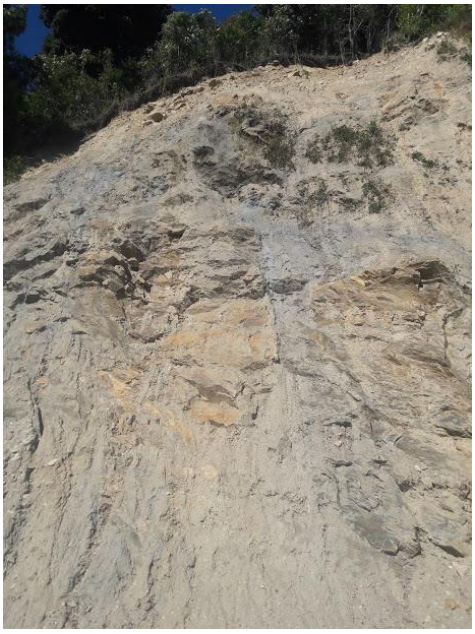

Sl. No.	Parameters	Data
1	Length	267.62m
2	Width	90.67(max) 36.54(min)
3	Area	1055.95m^2
4	Slope	26.24°
5	Casualties	• Frequent road blocks • Damages to retaining structures • Possible threats to travelers.

Figure 8. Failure plane (slip) - Phyllite strata

Active failed slope of zone 5 is shown in Figure 10. This is a very good example of mud flows. Flows involve the deformation of an entire soil mass that then flows downslope as a viscous or sticky fluid. Deformation may be due to a high soil water content or seismic shaking that leads to liquefaction and thus generates such a fluid flow. The slopes need not be very steep as shown in Figure. 9.

Sl. No.	Parameters	Data
1	Length	159.611m
2	Width	45.561(max),37.651 (min)
3	Area	6331.98m^2
4	Slope	25.19°, 17.63°
5	Casualties	• Frequent road blocks • Damages to retaining structures • Possible threats to travelers.

Figure 9. Collection of samples from landslide site

2. 6. Soil profiling

Figure 10. Trial pits (from left zone 12, 13, 14 and 16)

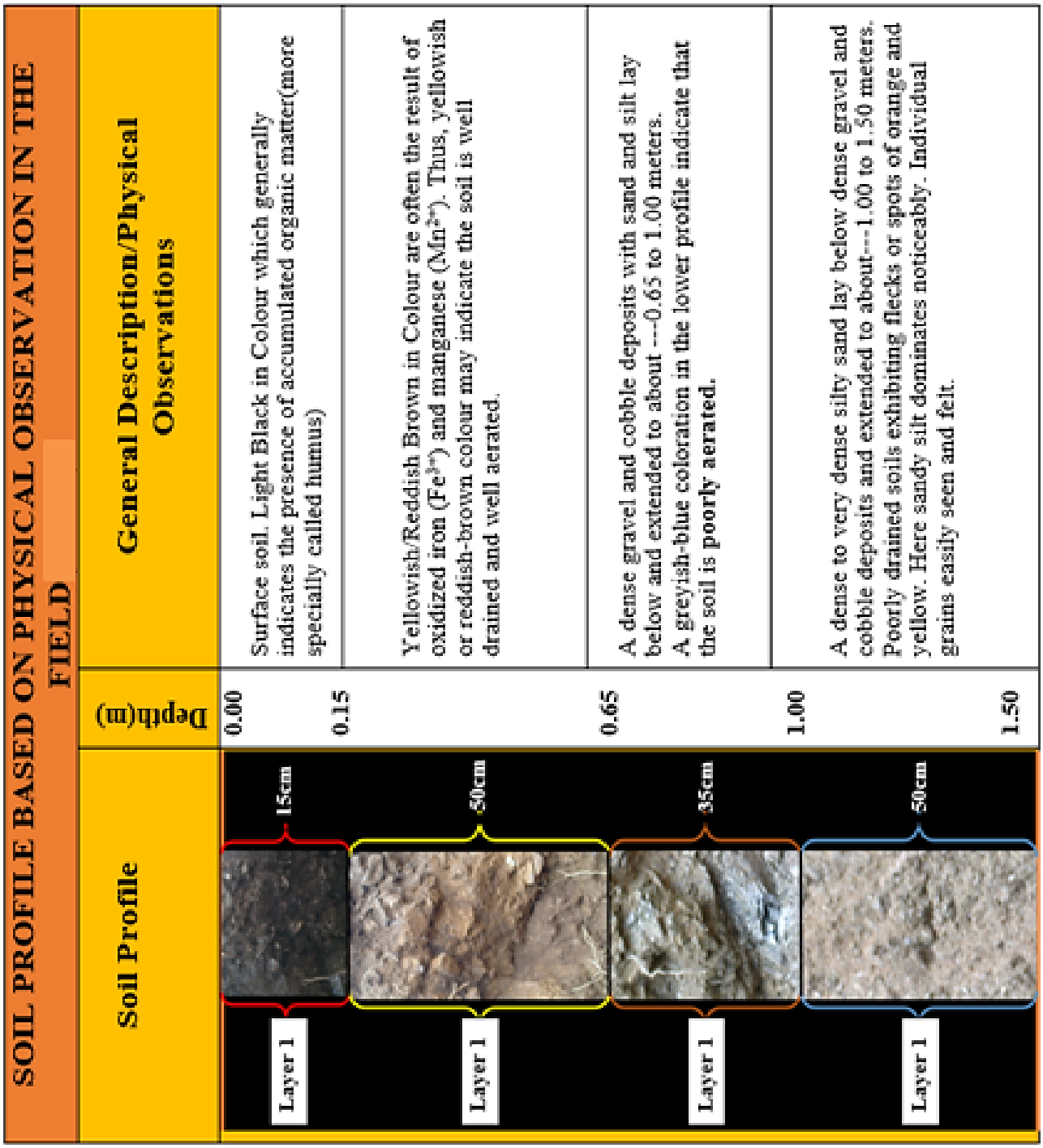

Figure 11. Soil profile with its physical properties-zone 13

Figure 12. Soil profile with its physical properties-zone 14

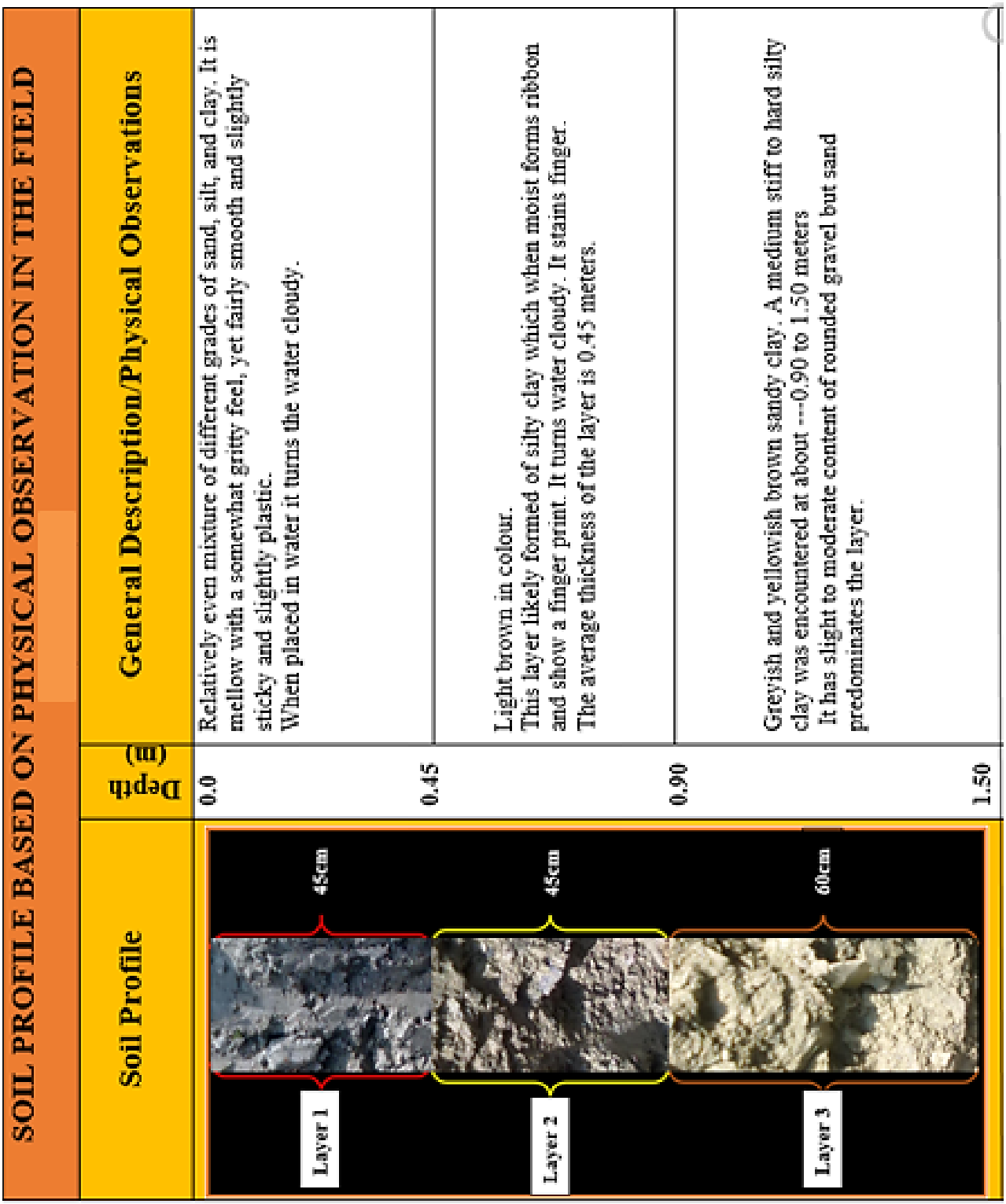

Figure 13. Soil profile with its physical properties-zone 16

SOIL PROFILE BASED ON LABORATORY TEST RESULT

Soil Profile	Layer Depth(m)	Lab investigation	Soil Description
	0-0.15	Mechanical Sieve Analysis Test Results Boulder = 0%, Cobbles = 0%, Gravel = 36.46%, Sand = 50.80%, Silt/Clay = 10.30% Atterberg Limit Liquid Limit = 37% , PI = NP	Coarse Grained; SP-SM (Poorly graded sand with silt and gravel). Cohesive less soil, non-plastic.
	0.15-0.65	Mechanical Sieve Analysis Test Results Boulder = 0% , Cobbles = 6.4%, Gravel = 33.2%, Sand = 53.8%, Silt/Clay = 5.4% Atterberg Limit Liquid Limit = 22%, PI = NP	Coarse Grained; SP-SM (Poorly graded sand with silt and gravel).
	0.65-1.00	Mechanical Sieve Analysis Test Results Boulder = 0%, Cobbles = 4.2%, Gravel = 24.7%, Sand = 62.4%, Silt/Clay = 8.2% Atterberg Limit Liquid Limit = 27%, PI = NP	Coarse Grained; SP-SM (Poorly graded sand with silt and gravel).
	1-1.50	Mechanical Sieve Analysis Test Results Boulder = 0%, Cobbles = 0%, Gravel = 35.8%, Sand = 58.5%, Silt/Clay = 5.3% Atterberg Limit Liquid Limit = 28%, PI = NP	Coarse Grained; SP-SM (Poorly graded sand with silt and gravel).

Figure 14. Soil profile with its mechanical properties-zone 13

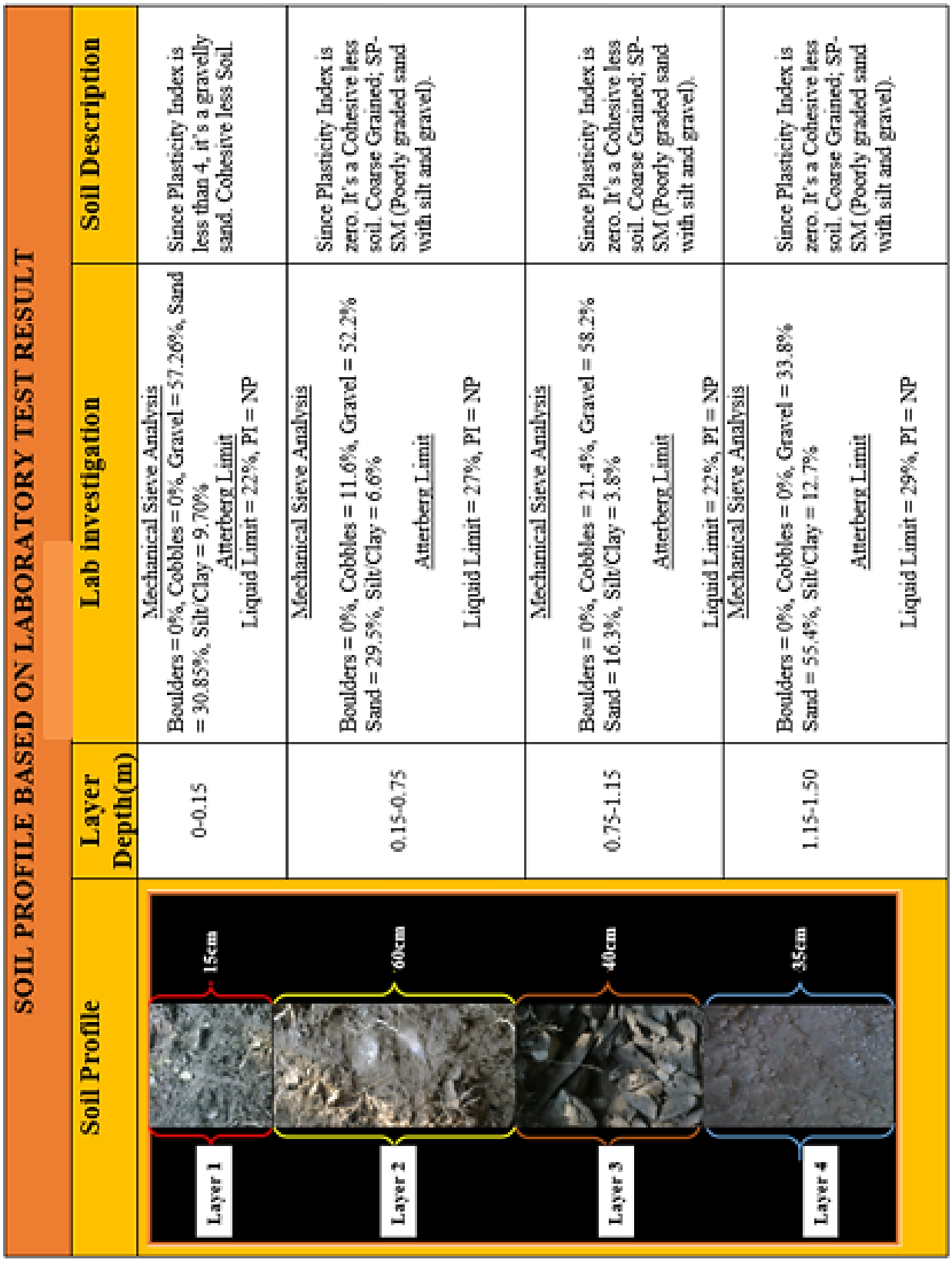

Figure 15. Soil profile with its mechanical properties-zone 14

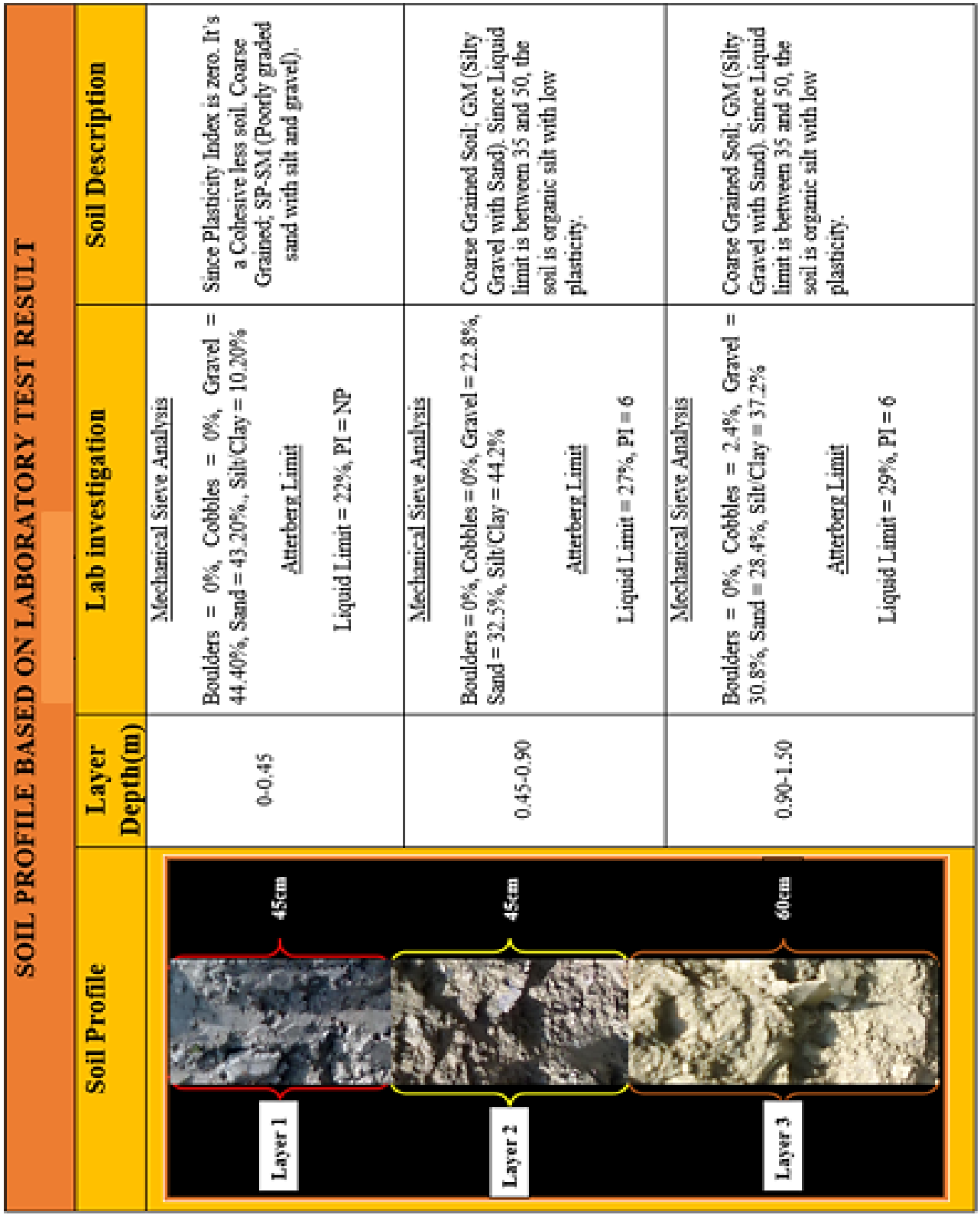

Figure 16. Soil profile with its mechanical properties-zone 16

Shallow Soil Profiling was done through pitting and based on Physical Observations in the Field and Based on Laboratory Test Results. Field tests looks for soil morphological properties in the pits like color, texture, structure, humus content and particle size which are used for soil profiling on the basis of visual observation. This are presented in Figure 12, 13 and 14.

The collected soil sample from different layers of pit is tested in the laboratory to determine the engineering properties of the soil such as mechanical sieve analysis, relative density, direct shear test, and specific gravity tests. In situ permeability test was also conducted through double ring infiltrometer at all the four zones in the study area. As discussed above the high permeability was the causative agents to slope movement worsened by other poor condition of the subsurface soil take from each layer of trial pits.

The physical properties of the soil at each layer beneath the surface is presented along the Figure 12, 13 and 14. The trial pit analysis shows that the soil present within the depth of 2 m below the ground is essentially coarse grained gravely sand similar to the surface. However, the gravel content is found excessively more below the surface in some zones.

2. 7. Strategic modelling and interpretation of landslide phenomenon

The physical investigation and soil parameters analysis of the study sites reveal that the landslide occurs in two different patterns namely the flow of the mud mass and the slipping/sliding of the surface mass from the subsurface strata. These two failures are explained by the following two models.

Mud flow is the commonly occurring landslide. It has been observed in several study zones. Small package or heap of soil mass creeps down the slope when the driving forces exceeds its restoring force. Mud flows is characterized by washing of topsoil during the rainy season. The weak topsoil loses its cohesion with the contact surface and gets eroded to the base as indicated in Figure 18. This phenomenon occurs annually, increases the slope angle and thus worsening the landslide problems. Moreover, it's not only rain that induces the mud flow. The seismic tremor or the movement of heavy vehicles liquefies the weaker package of surface soil. It loses its shear strength and gets detached from the adjacent layers. It has been noted from the study area that the distance travelled by mud flow is limited by slope angle and the density of the soil. The mass of the soil package is comparatively less.

Landslip is very common around Shorchen and Kamji area. Since phyllite is very common in these areas they form the weak layer beneath the surface. Due to the extreme degree of heat and pressure sedimentary rock like shale metamorphizes into slippery and weak Phyllite rock. It's difficult for surface soil to bind with phyllite strata and as a result the upper layer slides down the plane due to gravity. As indicated in Figure 19, entire strata above phyllite slips down to the toe of the slope. The entire soil mass loses the cohesion with the adjacent surface when disturbed by external agencies and thus slips down. However, the process of slips/slide occurs are categorized into two, namely translation and rotation. If the failure plane is free of irregularities and material present in debris doesn't contain boulder then translation slip occurs.

This is dangerous as seen in zone 10 and travels greater distance as the debris are pushed with greater force by following debris. On contrary, if the slip plane has curvature and the debris consist of boulder then the earth rolls down the plane and travels until the debris are scattered sideways of the slip plane. Therefore, the accelerating force diminishes and mass travels to short distance.

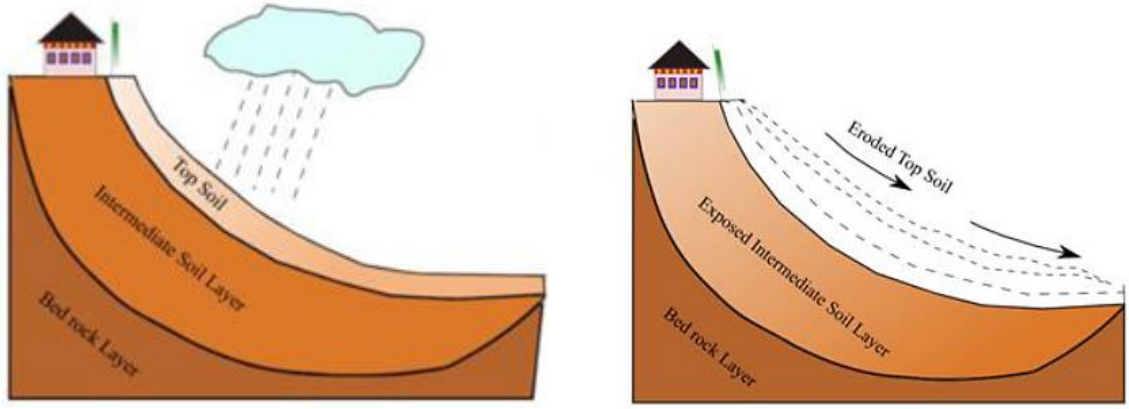

Figure 17. First failure type-mud flow

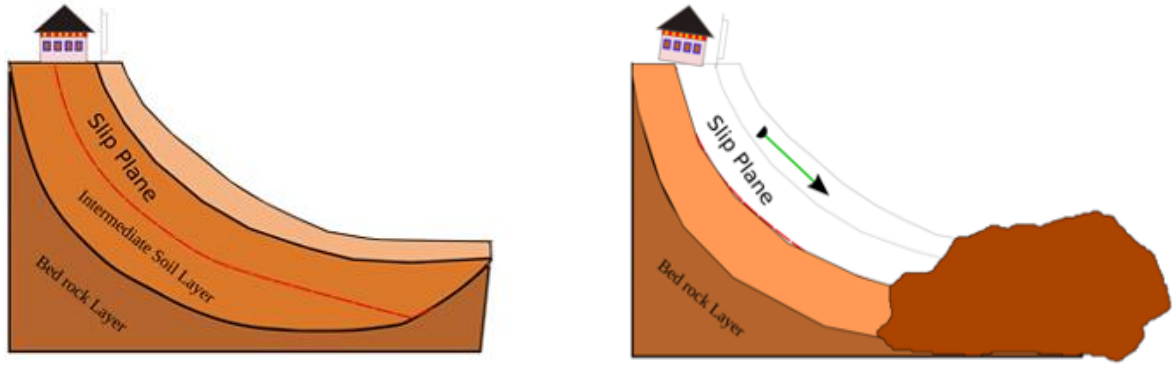

Figure 18. Second failure pattern-land slip

The model mainly focuses on the type of failure from the above two paradigms dominating the study area and the occurrence of the future landslide is prognosticated. The areal image of the sites revealed that the overall surface area of the landslide has not significantly increased in the decade 2004 to 2014. However, the slope has drastically increased. This is possible when the topsoil on the slope is eroded every rainy season. Figure 18 shows the initial gentle slope, which was eroded in due course of time, exposing the underlying layer. The erosion has led to significant increase in the slope of the landslide increasing the probability of slope failure. During monsoon, huge amount of exposed soil are being transported along with rainwater and saturated soils become highly susceptible to landslide. One made the basic calibration among slope angle, soil parameters and instability of the slope in their study of landslide of Nepal. It is the matter of serious concern looking in the slope angle and various soil parameters of study area that criticality of the landslide will remain for some more years to come until various mitigation measures like soil stabilization and slope angle reduction are carried out. The main focus has to be made towards precautionary measures travelers and inhabitants of the locality. All major zones are still active and will remain same until those unstable lump of soil creeps down and reduces the slope angle. Manually replacing the unstable soil will be of great help to solve the problem.

3. CONCLUSIONS

The preliminary survey for the assessment of Landslide along the Phuentsholing – Thimphu highway at Sorchen has shown sixteen zones. These zones are seen to be temporarily maintained through normal practice of retaining structure and bioengineering techniques however, the problem of landslide remains unsolved for the past last decades. To further assess the site characteristics of the critical landslide zones were conducted. The geotechnical site investigation was carried out through physical observation at the site, laboratory test and field exploration in each zone. Based on those tests, the shallow soil profiling and classification were carried out. The majority of the zones contain coarse grained gravely sand soil with little fine content of less than 10 %. The outcome of the soil sampling and analysis indicated the presence of fine gravely and different grains of sand which are mechanically weak. To verify these results, trial pits of 2m deep was dug which confirms the result obtained at the surface. Since the sandy soil has larger pores their water holding capacity is very less. They are cohesionless and doesn't not bind with adjacent surfaces like finer soil. Hence, with little rain or movement by heavy vehicles or tremors these weak loose gravely sand gets detached from its adjacent layers and flows down the slope as landslide. This is the driving force of landslide which is more than the restoring force. Technically, Factor of safety (FOS) is less than 1. Their higher permeability value leads the passage of water to deeper strata weakening their shear strength as well. The field data collected for Topography of the area, geological characteristics of the slope and slope angle was for sure the most confirming to the decade long landslide problem. The slope angle for all active landslide areas were more than 57°. This depicts the instability of the topography. The cause of slope failure in this project has been explained as non-homogeneity of soil stratum for different layers and its permeability. The activity of landslide seems to remain for some more years until it stabilizes its slope after sufficient fall of its top mass. However, there are many artificial means to solve the problem as explained above. Other factors such as ground water table, seismic activity, and rainfall may be considered for future researchers. Further, GIS will be used to demark the hazard zonation after the quantitative analysis in the future studies.

ACKNOWLEDGEMENT

The authors of research project entitled "Forecasting Landslide in Chukha from Index Properties of Soil – Research to Policy Making" would like to extend heartfelt gratitude to Royal University of Bhutan (RUB) and College of Science and Technology (CST) for providing a platform to do research project and financially supporting through Annual University Research Grand (AURG).
Immense gratitude to Department of Hydro-met services and Department of Geology and Mines, Ministry of Economic Affairs for providing us with various data and information.

References

[1] Abhirup Dikshit, Raju Sarkar, Biswajeet Pradhan, Saroj Acharya and Kelzang Dorji. Estimating Rainfall Thresholds for Landslide Occurrence in the Bhutan Himalayas. *Water* 2019, 11(8), 1616. https://doi.org/10.3390/w11081616

[2] Petley, D. Global patterns of loss of life from landslides. *Geology* 2010, 40, 927–930.

[3] Rosi, A.; Peternel, T.; Jemec-Auflič, M.; Komac, M.; Segoni, S.; Casagli, N. Rainfall thresholds for rainfall-induced landslides in Slovenia. *Landslides* 2016, 13, 1571–1577.

[4] Gariano, S.L.; Brunetti, M.; Iovine, G.; Melillo, M.; Peruccacci, S.; Terranova, O.; Vennari, C.; Guzzetti, F. Calibration and validation of rainfall thresholds for shallow landslide forecasting in Sicily, southern Italy. *Geomorphology* 2015, 228, 653–665.

[5] Segoni, S.; Piciullo, L.; Gariano, S.L. A review of the recent literature on rainfall thresholds for landslide occurrence. *Landslides* 2018, 15, 1483–1501.

[6] Lagomarsino, D.; Segoni, S.; Rosi, A.; Rossi, G.; Battistini, A.; Catani, F.; Casagli, N. Quantitative comparison between two different methodologies to define rainfall thresholds for landslide forecasting. *Nat. Hazards Earth Syst. Sci.* 2015, 15, 2413–2423.

[7] Melillo, M.; Brunetti, M.T.; Peruccacci, S.; Gariano, S.L.; Guzzetti, F. An algorithm for the objective reconstruction of rainfall events responsible for landslides. *Landslides* 2015, 12, 311–320.

[8] Iadanza, C.; Trigila, A.; Napolitano, F. Identification and characterization of rainfall events responsible for triggering of debris flows and shallow landslides. *J. Hydrol.* 2016, 541, 230–245.

[9] Staley, D.M.; Kean, J.W.; Cannon, S.H.; Schmidt, K.M.; Laber, J.L. Objective definition of rainfall intensity–duration thresholds for the initiation of post-fire debris flows in southern California. *Landslides* 2013, 10, 547–562.

[10] Piciullo, L.; Calvello, M.; Cepeda, J.M. Territorial early warning systems for rainfall-induced landslides. *Earth Sci. Rev.* 2018, 179, 228–247. [Google Scholar] [CrossRef]

[11] Gariano, S.L.; Sarkar, R.; Dikshit, A.; Dorji, K.; Brunetti, M.T.; Peruccacci, S.; Melillo, M. Automatic calculation of rainfall thresholds for landslide occurrence in Chukha Dzongkhag, Bhutan. *Bull. Eng. Geol. Environ.* September 2019, Volume 78, Issue 6, pp 4325–4332. https://doi.org/10.1007/s10064-018-1415-2

[12] Sengupta, A.; Gupta, S.; Anbarasu, K. Rainfall thresholds for the initiation of landslide at Lanta Khola in North Sikkim, India. *Nat. Hazards* 2010, 52, 31–42.

[13] Kanungo, D.P.; Sharma, S. Rainfall thresholds for prediction of shallow landslides around Chamoli-Joshimath region, Garhwal Himalayas, India. *Landslides* 2014, 11, 629–638.

[14] Dikshit, A.; Sarkar, R.; Satyam, N. Probabilistic approach toward Darjeeling Himalayas landslides - A case study. *Cogent Eng.* 2018, 5, 1537539.

[15] Gabet, E.J.; Burbank, D.W.; Putkonen, J.K.; Pratt-Sitaula, B.A.; Oiha, T. Rainfall thresholds for landsliding in the Himalayas of Nepal. *Geomorphology* 2004, 63, 131–143.

[16] Peruccacci, S.; Brunetti, M.T.; Luciani, S.; Vennari, C.; Guzzetti, F. Lithological and seasonal control of rainfall thresholds for the possible initiation of landslides in central Italy. *Geomorphology* 2012, 139–140, 79–90.

[17] Peruccacci, S.; Brunetti, M.T.; Gariano, S.L.; Melillo, M.; Rossi, M.; Guzzetti, F. Rainfall thresholds for possible landslide occurrence in Italy. *Geomorphology* 2017, 290, 39–57.

[18] Segoni, S.; Rosi, A.; Lagomarsino, D.; Fanti, R.; Casagli, N. Brief communication: Using averaged soil moisture estimates to improve the performances of a regional-scale landslide early warning system. *Nat. Hazards Earth Syst. Sci.* 2018, 18, 807–812.

[19] Polemio, M.; Sdao, F. The role of rainfall in the landslide hazard: The case of the Avigliano urban area (Southern Apennines, Italy). *Eng. Geol.* 1999, 53, 297–309.

[20] Terlien, M.T.J. The determination of statistical and deterministic hydrological landslide-triggering thresholds. *Environ. Geol.* 1998, 35, 124–130.

[21] Pagano, L.; Picarelli, L.; Rianna, G.; Urciuoli, G. A simple numerical procedure for timely prediction of precipitation-induced landslides in unsaturated pyroclastic soils. *Landslides* 2010, 7, 273.

[22] Marques, R.; Zêzere, J.; Trigo, R.; Gaspar, J.; Trigo, I. Rainfall patterns and critical values associated with landslides in Povoação County (São Miguel Island, Azores): Relationships with the North Atlantic Oscillation. *Hydrol. Proc.* 2008, 22, 478–494.

[23] Corominas, J.; van Westen, C.; Frattini, P.; Cascini, L.; Malet, J.P.; Fotopoulou, S.; Catani, F.; Van Den Eeckhaut, M.; Mavrouli, O.; Agliardi, F.; et al. Recommendations for the quantitative analysis of landslide risk. *Bull. Eng. Geol. Environ.* 2014, 73, 209–263.

[24] Froude, M.J.; Petley, D.N. Global fatal landslide occurrence from 2004 to 2016. *Nat. Hazards Earth Syst. Sci*. 2018, 18, 2161–2181.

[25] Sarkar, R.; Dorji, K. Determination of the Probabilities of Landslide Events - A Case Study of Bhutan. *Hydrology* 2019, 6, 52.

[26] Brunetti, M.T.; Peruccacci, S.; Rossi, M.; Luciani, S.; Valigi, D.; Guzzetti, F. Rainfall thresholds for the possible occurrence of landslides in Italy. *Nat. Hazards Earth Syst. Sci.* 2010, 10, 447–458.

[27] Guzzetti, F.; Peruccacci, S.; Rossi, M.; Stark, C.P. Rainfall thresholds for the initiation of landslides in central and southern Europe. *Meteorol. Atmos. Phys.* 2007, 98, 239–267.

[28] Mercogliano, P.; Segoni, S.; Rossi, G.; Sikorsky, B.; Tofani, V.; Schiano, P.; Catani, F.; Casagli, N. Brief communication: A prototype forecasting chain for rainfall induced shallow landslides. *Nat. Hazards Earth Syst. Sci.* 2013, 13, 771–777.

[29] Thiebes, B.; Bell, R.; Glade, T.; Jäger, S.; Mayer, J.; Anderson, M.; Holcombe, L. Integration of a limit-equilibrium model into a landslide early warning system. *Landslides* 2014, 11, 859–875.

[30] Huggel, C.; Khabarov, N.; Obersteiner, M.; Ramírez, J.M. Implementation and integrated numerical modeling of a landslide early warning system: A pilot study in Colombia. *Nat. Hazards* 2010, 52, 501–518.

[31] Dikshit, A.; Satyam, D.N. Estimation of rainfall thresholds for landslide occurrences in Kalimpong, India. *Innov. Infrastruct. Solut.* 2018, 3, 24.

[32] Segoni, S.; Rosi, A.; Fanti, R.; Gallucci, A.; Monni, A.; Casagli, N. A Regional-Scale Landslide Warning System Based on 20 Years of Operational Experience. *Water* 2018, 10, 1297.

[33] Reichenbach, P.; Cardinali, M.; De Vita, P.; Guzzetti, F. Regional hydrological thresholds for landslides and floods in the Tiber River Basin (Central Italy). *Environ. Geol.* 1998, 35, 146–159.

[34] Aleotti, P. A warning system for rainfall-induced shallow failures. *Eng. Geol.* 2004, 73, 247–265.

[35] Rosi, A.; Canavesi, V.; Segoni, S.; Nery, T.D.; Catani, F.; Casagli, N. Landslides in the Mountain Region of Rio de Janeiro: A Proposal for the Semi-Automated Definition of Multiple Rainfall Thresholds. *Geosciences* 2019, 9, 203.

[36] Segoni, S.; Rossi, G.; Rosi, A.; Catani, F. Landslides triggered by rainfall: A semiautomated procedure to define consistent intensity-duration thresholds. *Comput. Geosci.* 2014, 63, 123–131.

[37] Anbalagan, R., Kumar, R., Lakshmanan, K., Parida, S., & Neethu, S. (2015). Landslide hazard zonation mapping using frequency ratio and fuzzy logic approach, a case study of Lachung Valley, Sikkim. *Geoenvironmental Disasters*, 2(1), 11. https://doi.org/10.1186/s40677-014-0009-y

[38] Epada, P. D., Sylvestre, G., & Tabod, T. C. (2012). Geophysical and Geotechnical Investigations of a Landslide in Kekem Area, Western Cameroon. *International Journal of Geosciences*, 03(04), 780–789. https://doi.org/10.4236/ijg.2012.34079

[39] J Satheesh, L., & B.L, D. (2016). Investigation of Geotechnical Properties of the Soil Susceptible to Landslide. *International Journal of Engineering Trends and Technology*, 36(9), 477–480. https://doi.org/10.14445/22315381/ijett-v36p2

[40] Jeong, S., Lee, K., Kim, J., & Kim, Y. (2017). Analysis of rainfall-induced landslide on unsaturated soil slopes. *Sustainability* 9(7), 1–20. https://doi.org/10.3390/su9071280

[41] Kitutu, M. G., Muwanga, A., Poesen, J., & Deckers, J. A. (2009). Influence of soil properties on landslide occurrences in Bududa district, Eastern Uganda. *African Journal of Agricultural Research*, 4(7), 611–620.

[42] Mugagga, F., Kakembo, V., & Buyinza, M. (2012). A characterisation of the physical properties of soil and the implications for landslide occurrence on the slopes of Mount Elgon, Eastern Uganda. *Natural Hazards*, 60(3), 1113–1131. https://doi.org/10.1007/s11069-011-9896-3

[43] Sharma, L. P., Patel, N., Debnath, P., & Ghose, M. K. (2012). Assessing landslide vulnerability from soil characteristics-a GIS-based analysis. *Arabian Journal of Geosciences*, 5(4), 789–796. https://doi.org/10.1007/s12517-010-0272

This article has been accepted for publication in a future issue of this journal, but has not been fully edited. Content may change prior to final publication. Citation information: DOI 10.1109/TIA.2019.2932696, IEEE Transactions on Industry Applications

High Gain Quasi Mutually Coupled Active Impedance Source Converter Utilizing Reduced Components Count

Avneet Kumar *Member, IEEE*, Sajid Kamal, M Raghuram *Student Member, IEEE*, Deepankar, Santosh K. Singh *Senior Member, IEEE* and Xiaogang Xiong *Member, IEEE*

***Abstract*—High voltage gain using a mutually coupled inductor network is quite popular in recent years for Z source converters. To achieve high gain, reduced number of components used is a prime challenge to improve efficiency and reduce the cost and size. In the coupled inductor network, the energy stored is two-fold, hence, the effective number of components is reduced. Moreover, the boosting factor is also governed by the number of turns which again helps in reducing the number of components. In general, coupled inductor network is based on two winding transformers. However, to increase the effective number of turns, an autotransformer principle may be used where turns ratio is increased by one as compared to two winding transformers. Therefore, in this paper, a coupled inductor network is proposed which is based on the autotransformer concept. The proposed converter is called as quasi mutually coupled active impedance source converter. The proposed converter has a continuous input current which is helpful in reducing the current stress on the source. The operation, steady-state analysis and its comparison with the existing topology are discussed. Moreover, the developed topology is extended for hybrid topology. Furthermore, the converter is validated using experiment to prove its feasibility.**

***Index Terms*—Mutual Coupling, Auto-Transformer, Continuous input current, Boost**

I. Introduction

For the Buck-Boost operation of voltage source inverter(VSI), cascading of VSI and DC-DC converter is a traditional solution. Though cascading of these two serves the above purpose but it has got few issues a) Double stage conversion b) Boosting is limited due to non-linearities present in the system c) Required DC link Capacitor is large in size c) dead time requirement which poorer the AC voltage profile e) Prone to EMI problem which causes the inverter leg short-circuiting due to which a huge amount of current flows through them. To ameliorate this, an extra circuit needs to placed in the inverter which increases the cost of the converter.

Z source inverter invented by Peng in 2003 [1] is an attractive solution to address these issues. The Z source inverter inherently has shoot through state for charging the inductor, therefore, the problem of EMI and dead time requirement are eliminated. Moreover, Z source inverter does not require DC link capacitor and has a single stage conversion [2]. Z source inverter is quite suitable for a variety of appications [3]. Despite several merits, it has a discontinuous input current. Moreover, since Z source inverter utilizes zero state for boosting purpose, so the control is restricted in the range $m+d<1$ [4]. So, for a higher duty cycle, modulation index should be low which worsen the output voltage profile. On the flip side, if the modulation index is high than the duty cycle will be low which means that the gain is reduced.

Tang et al. modified the Z source network and placed the Z network after the inverter configuration to limit the inrush current drawn by the capacitors present in the Z network [5]. Nevertheless, still the current drawn from the source is discontinuous in nature. Anderson et al. developed four quasi Z source network to improve the profile of the input current [6]. But the voltage gain produced by these networks is similar to the Z source network. To improve this, the different arrangement like diode assisted and capacitor assisted network are reported [7]. These networks although having a higher number of passive elements but the voltage stress across them is reduced [8] [9]. The switched inductor network is also utilized to increase the gain of Z source converter [10]. Based on the switched inductor configuration, two generalized configurations are reported for CSI and VSI respectively [11]. Fathi et al. proposed an enhanced Z source converter by utilizing the switched Z network [12]. However, these converters have a trade-off between the gain and number of components. As compared to the conventional Z source network, a switched boost inverter(SBI) configuration is reported which has lower number of passive elements, consequently, the effective size of the converter is reduced [13]. To improve the gain of the SBI, different arrangement of elements [14] such as switched inductor network, diode assisted and capacitor assisted network may be used. However, the size of the converter is a matter of concern.

The coupled inductor network is another category to achieve higher voltage gain which has gained interest from researchers in recent years. The beauty of the coupled inductor network

Manuscript received July xx, xxxx; revised August xx, xxxx; accepted September xx, xxxx. Date of publication September xx, xxxx;date of current version January x, xxxx.(Corresponding author: Xiaogang Xiong)

Avneet Kumar, M Raghuram, Deepankar and S K Singh are with the Department of Electrical Engineering, Indian Institute of Technology, Varanasi 221005, India (e-mail: avneet.kumar.eee13@iitbhu.ac.in, raghuram.rs.eee14@iitbhu.ac.in; deepankar.eee15@iitbhu.ac.in ; sksingh.eee@iitbhu.ac.in).

Sajid Kamal and Xiaogang Xiong are with the Department of Mechanical and Automation, Harbin Institute of Technology, Shenzhen, P.R. China (e-mail: kamal.sajid93@gmail.com; xiongxg@hit.edu.cn).

Color versions of one or more of the figures in this letter are available onlineat http://ieeexplore.ieee.org.

Digital Object Identifier xxxx.

0093-9994 (c) 2019 IEEE. Personal use is permitted, but republication/redistribution requires IEEE permission. See http://www.ieee.org/publications_standards/publications/rights/index.html for more information.

This article has been accepted for publication in a future issue of this journal, but has not been fully edited. Content may change prior to final publication. Citation information: DOI 10.1109/TIA.2019.2932696, IEEE Transactions on Industry Applications

is to produce better gain at reduced components [15]. A magnetically coupled inductor network is reported to lift the voltage gain which utilizes single coupled inductor and single capacitor [16], [17]. However, they are having discontinuous input current. To improve the profile of input current, Qian et al. developed a Trans qZSI [18]. Based on the philosophy of coupled inductor, several coupled inductor networks had been reported. Few of them are Improved Trans-qZSI Asymmetrical [19], Y-source [20], T-ZSI [21], LCCT-ZSI [22] , T-ZSI [23], Quasi-Y source [24], and T-qZSI [25].

In 2016, Siwakoti et al. proposed an A source converter which has higher gain than the existing coupled inductor with reduced component count [26]. Contrary to earlier converters, A source converter integrates the concept of an autotransformer rather two winding transformers. This peculiar concept increase the effective turns ratio to $(1 + \frac{n_2}{n_1})$. At similar turns ratio, the voltage gain achieved by the reported converter is higher as compared to two winding transformers. Therefore, to obtain a similar gain at the AC terminal, the duty cycle in the A source converter is reduced which implies the reduction in voltage stress across the inverter switches. Furthermore, a new topology based on the switched inductor and coupled inductor concept is reported by Wang et al [27]. The reported converter is called as an SL-Y source converter which has a higher number of components count. This ultimately affects the size and cost of the system. Moreover, SL-Y source converter has higher input ripple current due to the presence of switched inductor network at the input.

This paper proposes a modified A-source topology which has even higher overall gain than SL-Y source converter with reduced components count which was presented in [28]. The proposed topology has zero start-up current, continuous input current which is suitable for industrial application such as lightning and motor drive purpose specifically powered by Fuel Cell or PV panels. The proposed topology is developed for DC-DC and Hybrid applications. The hybrid application includes where both DC and AC loads are present. The proposed hybrid converter produces two distinct output (DC and AC) simultaneously. The key feature of the hybrid converter includes single stage conversion, compactness, and better efficiency. To achieve similar gain as compared to the existing hybrid converter, the duty cycle in the proposed hybrid converter is further reduced which ultimately results in lower voltage stress across inverter switches. Due to operation at higher modulation index, the proposed hybrid converter will have better output voltage profile. Moreover, reduced voltage stress across the switches will result in reducing the cost of the converter. Furthermore, the inductor is directly connected in series with the source, so the input current has lower ripple and therefore, the current stress at the source is reduced as compared to SL-Y source converter. The proposed topology is named as quasi mutually coupled Active impedance source(QMCAIS).

The rest of the paper is organized as follows: section II elaborates the principle of the proposed converter and its operating modes with steady-state analysis. Section III is focused on the extension of the proposed topology for the hybrid and inverter configuration. The comparative analysis of the proposed converter is detailed in section IV which is followed by the discussion on experimental results in section V. Finally, the paper is concluded in section VI.

II. Working Principle and Analysis of Proposed Converter

The motivation of the proposed converter is based on switched boost inverter configuration. The placing of input inductor and capacitor is arranged such that the input inductor charges by the sum of the input voltage and capacitor voltage. This arrangement is implemented by bringing a diode and a switch in the circuit. In the proposed converter, the boosting network switches between Active and shoot through period, therefore, the converter is coined as active impedance source converter. Since it also employs the coupled inductor network, the proposed converter is called as quasi mutually coupled active impedance source converter (QMCAIS). It consists of an inductor, two capacitor, a mutually coupled inductor, diodes D_{in}, D_2 and a switch as shown in Fig-1.

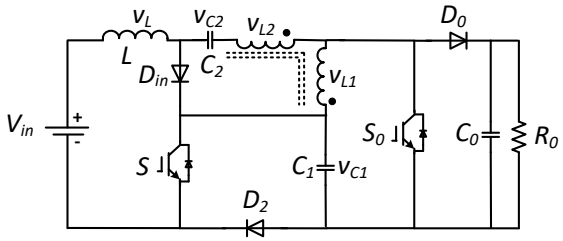

Fig. 1: Quasi mutually coupled active impendence source converter

A. Operation and Steady State Analysis of the Converter

For operation and steady-state analysis, the converter parameters are assumed to be ideal. The diodes and switches voltage drop is equal to zero. Furthermore, the internal resistance of the active and passive components are assumed zero and all the non-linearities present in the circuit are neglected. The mutually coupled inductor is assumed to be sufficiently tight so that leakage inductance is zero. Hence the voltage and number of turns relation hold tightly i.e. $(V_{L2} = \frac{n_2}{n_1} V_{L1})$.

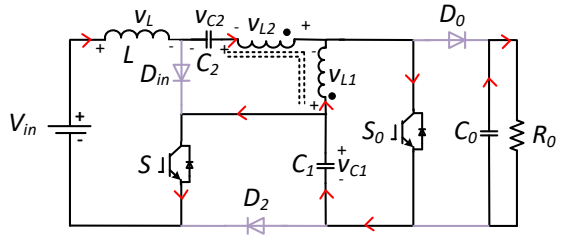

Fig. 2: Shoot through state

1) Shoot through state: In shoot through state, the switch S_0 and S are triggered, consequently the diode D_0 is reverse biased. Due to the polarity of inductor L, the diode D_{in} is also reverse biased. The inductor L and L_2 are charged through summation of V_{in}, V_{L2} and V_{C1}. However, L_1 is charged through V_{C1} and coupling effect. The capacitor C_0 supplies

0093-9994 (c) 2019 IEEE. Personal use is permitted, but republication/redistribution requires IEEE permission. See http://www.ieee.org/publications_standards/publications/rights/index.html for more information.

This article has been accepted for publication in a future issue of this journal, but has not been fully edited. Content may change prior to final publication. Citation information: DOI 10.1109/TIA.2019.2932696, IEEE Transactions on Industry Applications

the power to DC load and maintains a constant voltage across it.

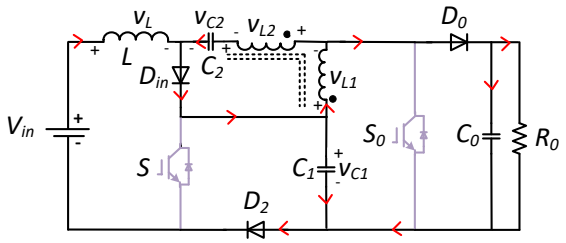

Fig. 3: Non shoot through state

2) Non shoot through state: During this state, the switch S_0 and S are turned off simultaneously, therefore, diode D_0 is forward biased. The inductor starts discharging its energy into the DC load. Due to this, diodes D_{in} and D_2 are forward biased. The capacitor C_1 and C_2 are charged by the source voltage via inductor L and coupled inductors, respectively.

B. Steady State Analysis

For steady state analysis, shoot through and non shoot through analysis is considered.

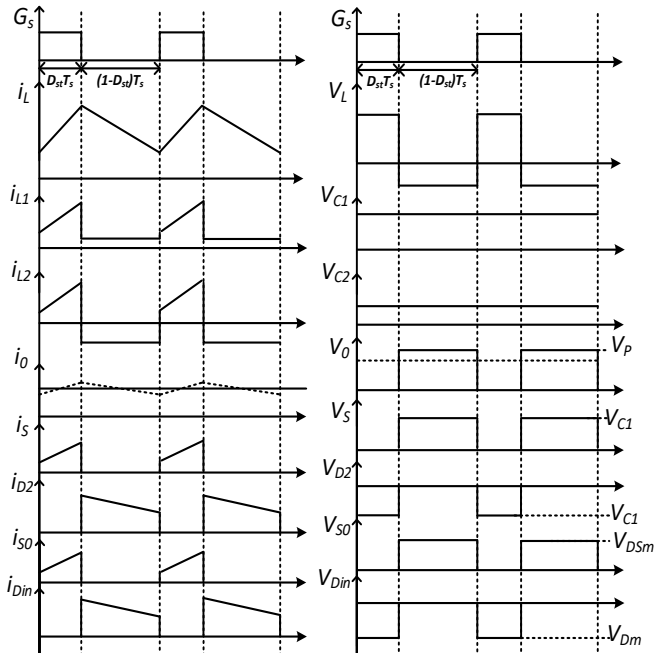

Fig. 4: Steady state waveforms

Shoot through interval: The switches S and S_0 are on and diode D_{in} and D_2 is in reverse bias condition. Applying KVL in the circuit shown in Fig-2, the voltage across input inductor is given as

$$V_{in} - V_L + V_{C2} + V_{L1} + V_{L2} = 0 \tag{1}$$

Voltage V_{L2} in terms of V_{L1} is given by

$$V_{L2} = \frac{n_2}{n_1} V_{L1} \tag{2}$$

Voltage V_{L1} in terms of capacitor voltage V_{C1} is

$$V_{L1} = V_{C1} \tag{3}$$

Combining Equ-(1), Equ-(2), and Equ-(3) , the inductor voltage is

$$V_L = V_{in} + V_{C2} + V_{C1} N \tag{4}$$

where

$$N = 1 + \frac{n_2}{n_1}$$

The inductor current L is given as

$$\begin{aligned} i_L &= \tfrac{1}{L} \int_0^t V_L dt + i_L(0) \\ &= \tfrac{1}{L} (V_{in} + V_{C2} + N V_{C1})\, t + i_L(0) \end{aligned} \tag{5}$$

At time $D_{st}T_s$, the current i_L is given by

$$i_L(D_{st}T_s) = \frac{1}{L}(V_{in} + V_{C2} + N V_{C1})\, D_{st}T_s + i_L(0) \tag{6}$$

So, peak to peak ripple current in inductor is given as

$$\Delta i_L = i_L(D_{st}T_s) - i_L(0) = \frac{D_{st}T_s}{L}(V_{in} + V_{C2} + N V_{C1}) \tag{7}$$

Non-shoot through interval: In this period the diode D_{in} and D_2 are in forward bias condition while switches S and S_0 are off. Similar to the earlier case, using KVL in the circuit indicated in Fig-3, the voltage across input inductor is given as

$$V_L = V_{in} - V_{C1} \tag{8}$$

The voltage across inductor can also be written as

$$V_{L2} + V_{C2} + V_{L1} = 0 \tag{9}$$

Equ-(9) results into

$$V_{L1} = -\frac{V_{C2}}{\left(1 + \frac{n_2}{n_1}\right)} \tag{10}$$

During this period, the inductor current is given by

$$\begin{aligned} i_L &= \tfrac{1}{L} \int_0^t V_L dt + i_L(D_{st}T_s) \\ &= \tfrac{1}{L} (V_{in} - V_{C1})\, t + i_L(D_{st}T_s) \end{aligned} \tag{11}$$

Thus, the peak to peak ripple current in inductor is

$$\Delta i_L = i_L(T_s) - i_L(D_{st}T_s) = \frac{T_s}{L}(V_{in} - V_{C1}) \tag{12}$$

By applying the energy balance theory, the equation across inductor L_1 is given by

$$\int_0^{D_{st}T_s} V_{L1} dt + \int_{D_{st}T_s}^{T_s} V_{L1} dt = 0 \tag{13}$$

Combining Equ-(3), Equ-(10) and Equ-(13) yield

$$V_{C1} D_{st} T_s - \frac{V_{C2}}{\left(1 + \frac{n_2}{n_1}\right)} (1 - D_{st})\, T_s = 0 \tag{14}$$

By rearranging, V_{C2} in terms of V_{C1} is written as

$$\frac{V_{C1}}{V_{C2}} = \frac{1 - D_{st}}{D_{st} N} \tag{15}$$

0093-9994 (c) 2019 IEEE. Personal use is permitted, but republication/redistribution requires IEEE permission. See http://www.ieee.org/publications_standards/publications/rights/index.html for more information.

This article has been accepted for publication in a future issue of this journal, but has not been fully edited. Content may change prior to final publication. Citation information: DOI 10.1109/TIA.2019.2932696, IEEE Transactions on Industry Applications

Similarly, by applying energy balance theory across input inductor L, the equation is written as

$$\int_{0}^{D_{st}T_s} V_L dt + \int_{D_{st}T_s}^{T_s} V_L dt = 0 \tag{16}$$

Combining Equ-(4), Equ-(8) and Equ-(16)

$$\left(V_{in} + V_{C2} + V_{C1}\left(1 + \frac{n_2}{n_1}\right)\right) D_{st} + (V_{in} - V_{C1})(1 - D_{st}) = 0 \tag{17}$$

The capacitor voltage V_{C2} is

$$m_{C2} = \frac{V_{C2}}{V_{in}} = \frac{D_{st}N}{1 + D_{st}^2 - D_{st}(2+N)} \tag{18}$$

and capacitor voltage V_{C1} is

$$m_{C1} = \frac{V_{C1}}{V_{in}} = \frac{1 - D_{st}}{1 + D_{st}^2 - D_{st}(2+N)} \tag{19}$$

Since the voltage across the switch is zero during shoot through state, so the output voltage (V_P) will be given by non shoot through interval as

$$V_P = V_{C1} - V_{L1} \tag{20}$$

Putting the value V_{L2} from non shoot through interval and substituting V_{C2} results, maximum voltage gain of the proposed converter which is given by

$$m_V = \frac{V_P}{V_{in}} = \frac{1}{1 + D_{st}^2 - D_{st}(2+N)} \tag{21}$$

For the different number of turns, the voltage gain of the proposed converter is presented in Fig-5a. Moreover, the voltage stress across the capacitors present in the boosting network is shown in Fig-5b for unity turns ratio. From the above equation, it is evident that the voltage gain of the proposed converter is a function of a square of D_{st}. Since in lower duty cycle region the term D_{st}^2 is quite low, so the impact of this can be neglected. However, when the duty cycle is higher than the $D_{st} > 0.2$, its impact is pronounced. Therefore, it is mandatory to have a non-linear dynamic controller with high precision at a higher duty cycle operation. The requirement these controllers can be fulfilled by advance controllers such as sliding mode control, output feedback control, state feedback control, etc.

Moreover, for the derivation of gain given by Equ-(21), all the diodes and switches are assumed ideal and parasitic present such as internal resistance of inductor and capacitor, the leakage inductance of coupled are also neglected. These non-idealities present in the circuit decreases the voltage gain, in particular, the impact of the leakage inductance of the coupled inductor is very high. Therefore, it is important that the switches and diodes must be selected with low voltage drop and internal resistance. Moreover, the passive elements should have low internal resistance. The voltage of the proposed QMCAIS in terms of leakage factor is given as

$$\frac{V_P}{V_{in}} = \frac{1 - \frac{3}{4}D_{st}(1-K)}{1 - D_{st}(3+K) + \frac{3}{2}D_{st}^2 - \frac{K}{2}D_{st}^2} \tag{22}$$

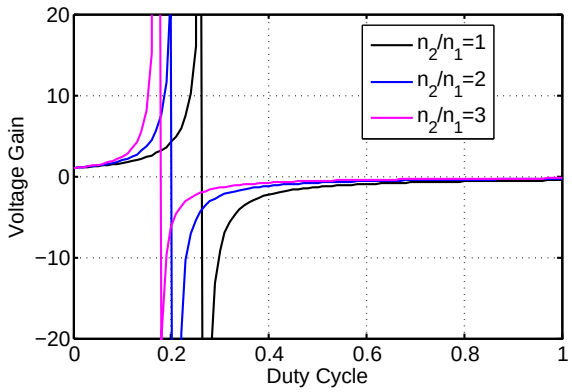

(a) Voltage Gain vs Duty Cycle at different number of turns

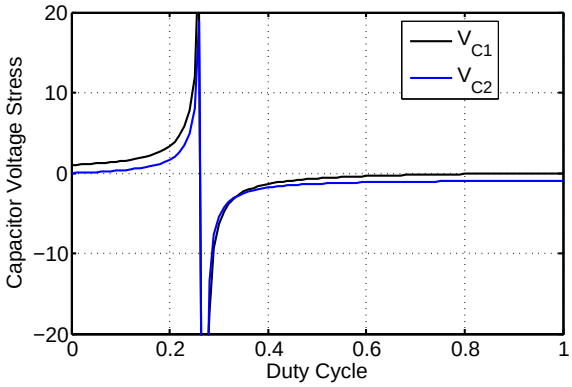

(b) Capacitor Voltage Stress as a function of duty cycle at equal number of turns

Fig. 5

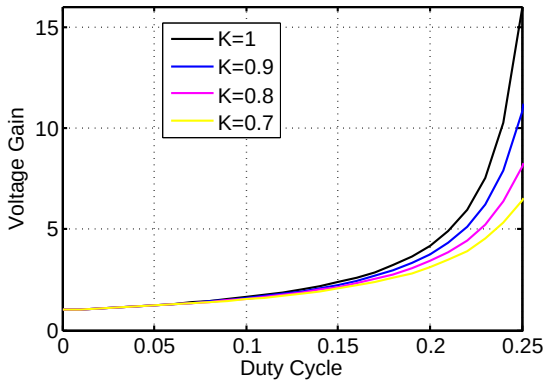

Fig. 6: Effect of leakage on voltage gain

where K is the leakage factor. For quantitative analysis, the voltage gain for different leakage factor is shown in Fig-6. It is to be note that with decrease in leakage factor i.e. increase in leakage inductance, the voltage gain of the converter decreases substantially. Therefore, for the coupled inductor design, a high flux core (CH777125) is selected and bifilar winding is used to reduce the leakage inductance.

In this paper, the number of turns for both the windings are equal to 20. However, they can be increased to reduce the peak current flowing through the windings but it will lead to higher

0093-9994 (c) 2019 IEEE. Personal use is permitted, but republication/redistribution requires IEEE permission. See http://www.ieee.org/publications_standards/publications/rights/index.html for more information.

This article has been accepted for publication in a future issue of this journal, but has not been fully edited. Content may change prior to final publication. Citation information: DOI 10.1109/TIA.2019.2932696, IEEE Transactions on Industry Applications

internal resistance and therefore higher loss. Therefore, there is always a trade off between number of turns and losses.

The current gain of the converter is inversely dependent on the voltage gain of the converter. Therefore, the maximum current gain of the converter is given as

$$m_i = \frac{I_{om}}{I_{im}} = \frac{1}{m_V} = 1 - (2+N)\,D_{st} + {D_{st}}^2 \tag{23}$$

where I_{om} is maximum current gain during non shoot through period.

The average output voltage is calculated as

$$V_0 = \frac{1}{T}\int_{D_{st}T_s}^{T_s} V_P dt = (1 - D_{st})\,V_P \tag{24}$$

Putting the value of V_P from Equ-(21) into Equ-(24) and hence, the V_0 is given as

$$V_0 = \frac{1 - D_{st}}{1 + D_{st}^2 - D_{st}\,(2+N)} V_{in} \tag{25}$$

From Equ-(24), it can be seen that the average output voltage is equal to the voltage across capacitor C_1. Since the average output voltage is inversely dependent on the load current, therefore, the average current is given as

$$\frac{I_o}{I_{in}} = \frac{1 - (2+N)\,D_{st} + {D_{st}}^2}{1 - D_{st}} \tag{26}$$

1) Calculation of minimum Inductance for CCM: Since at the boundary of CCM and DCM, the minimum value of inductor current is zero, therefore, the inductor current $i_L(T_s)$=0. Using Equ-(15), Equ-(18) and Equ-(19) in Equ-(12), the following peak to peak to ripple current is obtained:

$$\Delta i_L = i_L\,(T_s) - i_L\,(D_{st}T_s) = \frac{D_{st}Nm_V V_{in}}{2f_s L} \tag{27}$$

Moreover, at the boundary of CCM and DCM, the peak to peak ripple current is

$$\Delta i_L = 2I_L \tag{28}$$

With the help of Equ-(27) and Equ-(28), the average inductor current at the boundary of CCM and DCM is given as

$$I_L = \frac{D_{st}Nm_V V_{in}}{2f_s L} \tag{29}$$

At the boundary of CCM and DCM, the average inductor current is equal to the DC input current. Hence, input current is also given by Equ-(29).

Using Equ-(23), the maximum load current at the boundary of CCM and DCM is

$$I_{omB} = \frac{I_{im}}{m_V} = \frac{D_{st}NV_{in}}{2f_s L} = \frac{D_{st}NV_{om}}{2f_s L m_V} \tag{30}$$

which is simplified to

$$I_{omB} = \frac{D_{st}NV_{om}}{2f_s L}\left[1 - (2+N)\,D_{st} + {D_{st}}^2\right] \tag{31}$$

For determining the DCM boundary, it is required to plot the normalized current versus duty cycle plot. From Equ-(31), it is evident that normalized input current is $I_{omB}/(V_P/2f_sL)$, if number of turns are varied. For different turns ratio, normalized input current versus duty cycle is plotted in Fig-7. The enclosed region indicates the DCM region. For a higher turns ratio, the DCM region is narrowed. The maximum output current at the CCM and DCM boundary is calculated by differentiating the current with respect to duty cycle and putting it equal to zero. Hence,

$$\frac{dI_{omB}}{dD_{st}} = \frac{d}{dD_{st}}\left[\frac{D_{st}NV_{om}}{2f_s L}\left[1 - (2+N)\,D_{st} + {D_{st}}^2\right]\right] = 0 \tag{32}$$

which gives duty cycle equal to

$$D_{stB} = \frac{1}{2\,(2+N)} \tag{33}$$

Substituting the value D_{stB} from Equ-(33) into Equ-(31) gives the minimum value of inductance equal to

$$L_{\min} = \frac{NV_{om}\left[1 + 2(2+N)^2\right]}{16f_s(2+N)^3 I_{omB}} \tag{34}$$

So, in order to ensure CCM the value of inductance L should be greater than L_{min}.

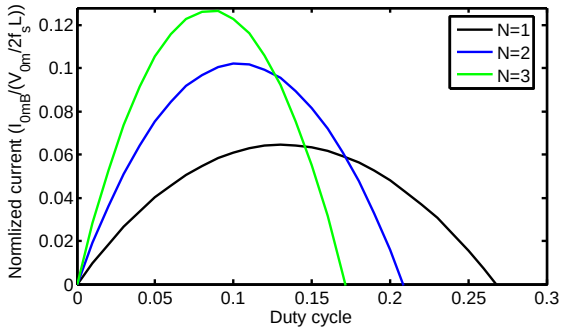

Fig. 7: Normalized load current versus duty cycle demarcating boundary between CCM/DCM

2) Calculation of Capacitance: The design of capacitance is based on the current flowing through the capacitor and percent of ripple allowed in the capacitor voltage. Based on this, the current flowing through the capacitor C_2 during shoot through period is equal to input inductor current. Therefore,

$$C_2\frac{dv_{C2}}{dt} = I_L \tag{35}$$

Since, I_L=$\frac{P_0}{V_{in}}$, the above equation can be written as

$$C_2\frac{\Delta V_{C2}}{D_{st}T_s} = \frac{P_0}{V_{in}} \tag{36}$$

which can simplified to

$$C_2 = \frac{D_{st}T_s\left[1 + D_{st}^2 - D_{st}\,(2+N)\right]P_0}{\%r_{v2}D_{st}V_{in}} \tag{37}$$

where r_{v2} is ripple in capacitor voltage C_2.

For capacitor C_1, the magnitude of current flowing through it equals to NI_L during shoot through. Hence, the current equation for capacitor C_1 is

$$C_1\frac{dv_{C1}}{dt} = NI_L \tag{38}$$

0093-9994 (c) 2019 IEEE. Personal use is permitted, but republication/redistribution requires IEEE permission. See http://www.ieee.org/publications_standards/publications/rights/index.html for more information.

This article has been accepted for publication in a future issue of this journal, but has not been fully edited. Content may change prior to final publication. Citation information: DOI 10.1109/TIA.2019.2932696, IEEE Transactions on Industry Applications

Substituting the value of I_L, the capacitor C_1 can be calculated as

$$C_1 = \frac{ND_{st}T_s\left[1 + D_{st}^2 - D_{st}\left(2 + N\right)\right]P_0}{\%r_{v1}\left(1 - D_{st}\right)V_{in}} \tag{39}$$

where r_{v1} is ripple in capacitor voltage C_1.

Similarly for capacitor C_0, I_0 is the current flowing through it during non shoot through. Therefore, the current equation for capacitor C_0 is given as

$$C_0\frac{dv_{C0}}{dt} = I_0 \tag{40}$$

which is simplified to

$$C_0 = \frac{(1 - D_{st})T_s\left[1 + D_{st}^2 - D_{st}\left(2 + N\right)\right]^2 P_0}{\%r_{v0}V_{in}^2} \tag{41}$$

where r_{v01} is ripple in capacitor voltage C_0.

III. Extension to Hybrid Topology

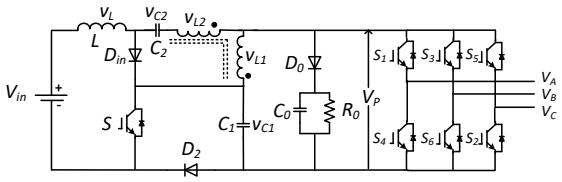

Fig. 8: Extended QMCAIS for hybrid outputs

The proposed topology can be extended for hybrid output application [29] and standalone AC application [30]. For standalone AC application, a snubber circuit (which consists of series connected resistor and capacitor) is required to avoid the spikes at the DC link which otherwise may damage the inverter switches. But there is a loss of energy in the snubber circuit which reduces the efficiency. However, in hybrid output applications, as shown in Fig-8, both DC load (represented by the arrangement of R_0 and C_0) and AC loads are present, therefore, the snubber circuit is not required and efficiency of the converter is improved. The operation for the hybrid application is as follows:

A. Operation

The operation of the extended QMCAIS for hybrid outputs is divided into three parts namely Shoot through state, Active State and Zero state. Dark lines are showing the current flow path while light lines indicate no current flow.

Shoot through state: Shoot through state is governed by charging of the inductor. During this state the inductor charges through the short circuit path provided by inserting shoot through pulses in the inverter operation. Charging is initiated by providing shoot through pulses which turn on both the switches of the same leg (like S_1 & S_4) and switch S as shown in Fig-9. If the duty cycle is defined as D_{st} then the time period for which shoot through pulses are given is $D_{st}T_s$.

Active state: This state is similar to the inverter operation for supplying the power to the load. The inverter is operated

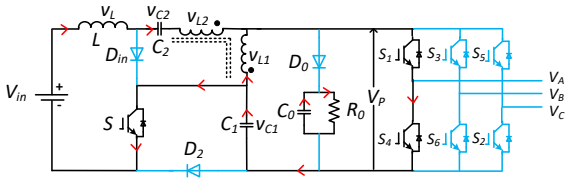

Fig. 9: Shoot through state for hybrid outputs

in its usual meaning. The energy stored during the shoot through interval now freewheels through the load. In the Active impedance network, diode D_{in} and D_2 comes into the conduction and switch S is in its off position. The current flow path is indicated in Fig-10.

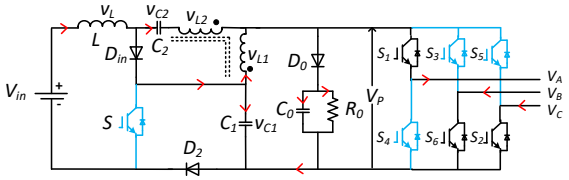

Fig. 10: Active state for hybrid outputs

Zero state: This state is also known as the AC load freewheel period. In this state, the AC load is disconnected from the supply and freewheel through the diode connected in parallel across the inverter switches and DC load receives power from the input. Diode D_{in} and D_2 still remains on while switch S is in off position. The equivalent circuit showing the current flow is indicated in Fig-11. In case of the inverter, if the zero

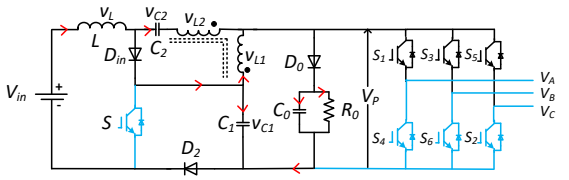

Fig. 11: Zero state for hybrid outputs

state is neglected that is full states are utilized as an active state then the inverter has only shoot through state and non shoot through state similar to a DC-DC converter. Hence, the steady state voltage and current equation are valid which will appear at the input of the inverter. Therefore, the voltage at the input of the inverter is given as V_P. Since this voltage is available across the inverter switches, the output AC peak voltage per phase for three phase inverter in terms of dc link voltage is written as

$$\hat{V}_{ac} = \frac{m.V_P}{2} \tag{42}$$

where m is the modulation index of the inverter. In case of a three-phase inverter, low-frequency harmonics are absent, therefore, it behaves like a DC load. Hence, the boundary equations for CCM and DCM can be determined by the earlier equation and subsequently the minimum value of inductance can be calculated.

0093-9994 (c) 2019 IEEE. Personal use is permitted, but republication/redistribution requires IEEE permission. See http://www.ieee.org/publications_standards/publications/rights/index.html for more information.

This article has been accepted for publication in a future issue of this journal, but has not been fully edited. Content may change prior to final publication. Citation information: DOI 10.1109/TIA.2019.2932696, IEEE Transactions on Industry Applications

TABLE I: Voltage stress across different elements

	Y-source	**Quasi Y-source**	**A-source**	**SL Y-source**	**Proposed**
S_0, D_0, C_0	$\frac{V_{in}}{1-KD_{st}}$	$\frac{V_{in}}{1-\delta D_{st}}$	$\frac{V_{in}}{1-(1+N)D_{st}}$	$\frac{(1+D_{st})V_{in}}{1-(1+K)D_{st}-KD_{st}^2}$	$\frac{V_{in}}{1-(2+N)D_{st}+D_{st}^2}$
D_{in}	$\frac{(K-1)V_{in}}{1-KD_{st}}$	$\frac{(\delta-1)V_{in}}{1-\delta D_{st}}$	$\frac{NV_{in}}{1-(1+N)D_{st}}$	$\frac{K(1+D_{st})V_{in}}{1-(1+K)D_{st}-KD_{st}^2}$	$\frac{(1+N)V_{in}}{1-(2+N)D_{st}+D_{st}^2}$
C_1	$\frac{(1-D_{st})V_{in}}{1-KD_{st}}$	$\frac{(1-D_{st})V_{in}}{1-\delta D_{st}}$	$\frac{(1-D_{st})V_{in}}{1-(1+N)D_{st}}$	$\frac{(1+D_{st})(1-D_{st})V_{in}}{1-(1+K)D_{st}-KD_{st}^2}$	$\frac{(1-D_{st})V_{in}}{1-(2+N)D_{st}+D_{st}^2}$
C_2	NA	$\frac{(\delta-1)D_{st}V_{in}}{1-\delta D_{st}}$	$\frac{ND_{st}V_{in}}{1-(1+N)D_{st}}$	$\frac{D_{st}K(1+D_{st})V_{in}}{1-(1+K)D_{st}-KD_{st}^2}$	$\frac{ND_{st}V_{in}}{1-(2+N)D_{st}+D_{st}^2}$
Remaining components	NA	NA	NA	$V_{D1,3}=\frac{D_{st}V_{in}}{1-(1+K)D_{st}-KD_{st}^2}$ $V_{D2}=\frac{(1-D_{st})V_{in}}{1-(1+K)D_{st}-KD_{st}^2}$	$V_{S1}=\frac{(1-D_{st})V_{in}}{1-(2+N)D_{st}+D_{st}^2}$ $V_{D2}=\frac{(1-D_{st})V_{in}}{1-(2+N)D_{st}+D_{st}^2}$

IV. Comparison with Existing Topology

To justify the novelty and importance of the proposed converter, an important aspect is to compare the proposed converter with the existing topologies. To compare QMCAIS, Y source [20], Quasi Y source [31], A source [26] and SL-Y source [27] are considered. The winding factors N, K and δ, for coupled inductor networks are considered as three.

A. Voltage stress across each components

The voltage stress across each component is an important factor that needs to be compared. The voltage stress for DC-DC topologies is compared which is listed in Table-I. Similarly, it can be extended for inverter configuration. The voltage stress across S_0, D_0 and C_0 is directly dependent on the boost factor. For example, for two times boost, the voltage stress will be twice across each of them. The voltage stress across C_1 is calculated for QMCAIS as per the Equ-(19). From Fig-12a, it is evident that for same voltage gain G, the proposed converter is having higher stress due to its parallel connection across the switch S_0. For capacitor C_2, the voltage stress is given by Equ-(18) and plotted in Fig-12b. The voltage stress across the capacitor C_2 is minimum in the proposed converter to achieve similar gain as compared to all the topologies. The voltage stress across D_{in} is calculated as

$$V_{Din} = V_{L1} + V_{L2} + V_{C2} \tag{43}$$

Substituting the values of V_{L1}, V_{L2}, V_{C1} and V_{C2}, the voltage across diode D_{in} is given as

$$V_{Din} = \frac{(1+N)\,V_{in}}{1-(2+N)\,D_{st}+D_{st}^2} \tag{44}$$

For achieving the same voltage gain, the voltage stress across input diode will be same for A source, SL-Y source and proposed converter which is higher than the Y source and Quasi Y source as shown in Fig-12c.
The voltage stress across the remaining components is plotted in Fig-12d. The diode and switch present in the proposed converter have voltage stress equal to the voltage across capacitor C_1 while for SL-Y source components, the voltage stress is considered as per Table-I.

B. Current Stress

The current stress in different compared topologies is calculated using PSIM. The output load and other parasitics are kept at a constant value for all the converters. The current stress in

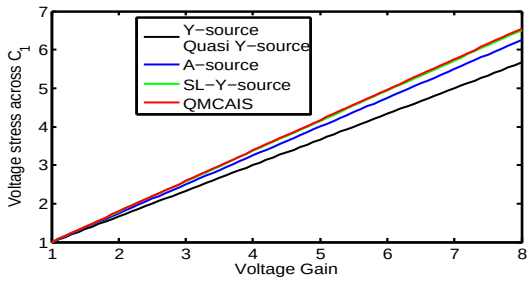

(a)

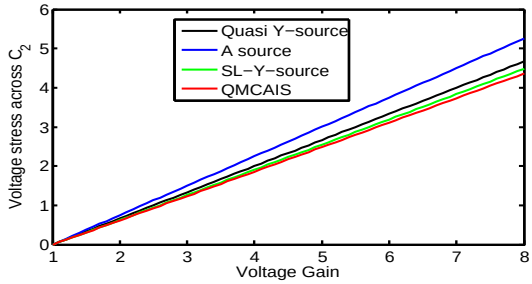

(b)

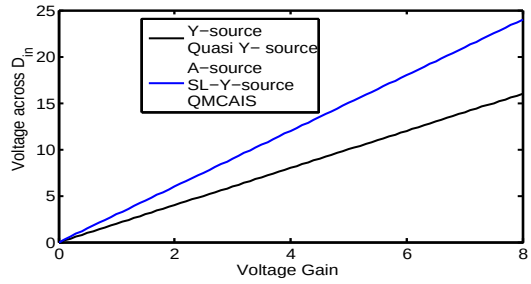

(c)

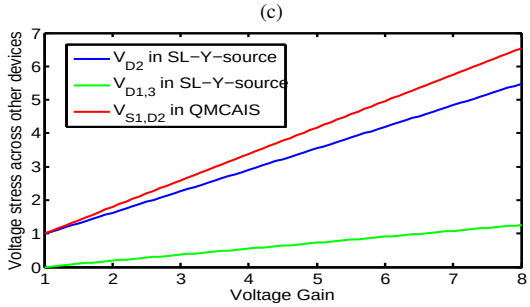

(d)

Fig. 12: Voltage stress across different components in per unit

0093-9994 (c) 2019 IEEE. Personal use is permitted, but republication/redistribution requires IEEE permission. See http://www.ieee.org/publications_standards/publications/rights/index.html for more information.

This article has been accepted for publication in a future issue of this journal, but has not been fully edited. Content may change prior to final publication. Citation information: DOI 10.1109/TIA.2019.2932696, IEEE Transactions on Industry Applications

TABLE II: Comparison among different topologies

	Y-source	**Quasi Y-source**	**A-source**	**SL Y-source**	**Proposed**
Inductor	NA	1	1	2	1
Coupled inductor	1	1	1	1	1
Capacitor	2	2	2	3	3
Diode	2	2	2	5	3
Switch	1	1	1	1	2
Boost factor	$\frac{1}{1-KD_{st}}$	$\frac{1}{1-\delta D_{st}}$	$\frac{1}{1-(1+N)D_{st}}$	$\frac{(1+D_{st})}{1-(1+K)D_{st}-KD_{st}^2}$	$\frac{1}{1-(2+N)D_{st}+D_{st}^2}$
Start up inrush current	Yes	No	No	No	No
Continuous input current	No	Yes	Yes	Yes(high ripple)	Yes

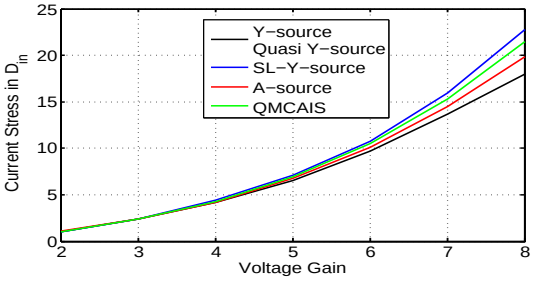

(a) Current Stress in D_{in} (A)

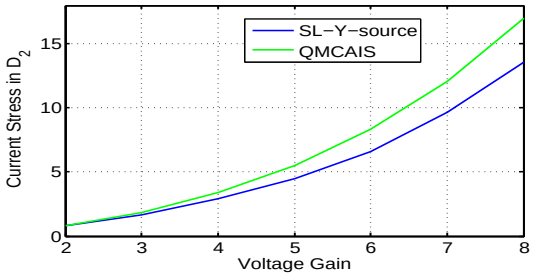

(b) Current Stress in D_2 (A)

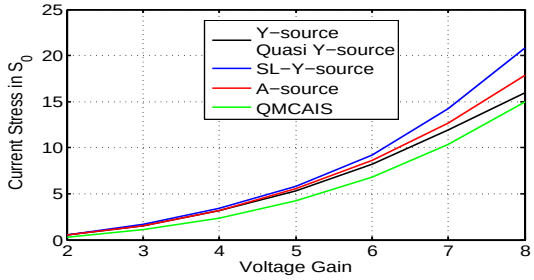

(c) Current Stress in S_0 (A)

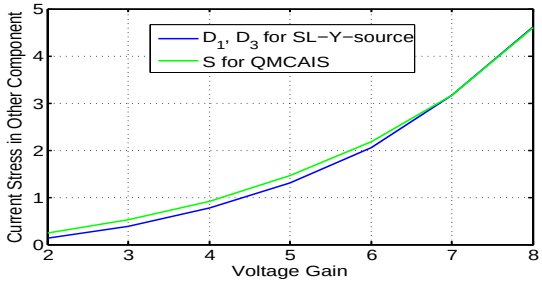

(d) Current Stress in Other Components (A)

Fig. 13: Current stress in different components

switches and diodes are calculated for different voltage gain factor. The current stress for the input diode D_{in} is presented in Fig-13a which indicates that QMCAIS has lower current stress as compared to SL Y-source converter. The current stress in diode D_2 is more in case of QMCAIS as compared to SL Y-source as shown in Fig-13b. For output switch S_0, the QMCAIS has the lowest current stress as compared to other topologies as shown in Fig-13c. Moreover, from Fig-13d, it evident that the current stress in remaining components is almost same as SL Y-source but it is also noted that the SL Y-source converter has more number of devices. Therefore, it can be concluded that the proposed converter is a better candidate as compared to SL Y-source.

C. Voltage gain

The voltage gain of the different topologies with duty cycle is plotted in Fig-14. It is evident that the voltage gain of the proposed converter is higher than the most recent converter SL-Y source [27], Y-source, Quasi Y source, and A source. The proposed converter can achieve a higher gain at a lower duty cycle which is beneficial in two ways: 1) Conduction period of the switch is reduced which helps in reducing the conduction loss. 2) For inverter operation, the modulation index can be varied in a wider range as D is varied in the range $0 < D < 1/4$: This features improves the output voltage profile and also reduces the voltage stress across the switches of the inverter for similar AC gain as achieved in existing topologies.

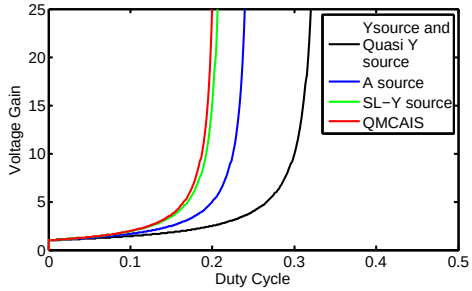

Fig. 14: Comparison of voltage gain

D. Comparison of other factors

There are a few other factors which are advantageous in the proposed topology:

- Due to the presence of input inductor, there is no start-up current in the proposed topology contrary to Y-source

0093-9994 (c) 2019 IEEE. Personal use is permitted, but republication/redistribution requires IEEE permission. See http://www.ieee.org/publications_standards/publications/rights/index.html for more information.

This article has been accepted for publication in a future issue of this journal, but has not been fully edited. Content may change prior to final publication. Citation information: DOI 10.1109/TIA.2019.2932696, IEEE Transactions on Industry Applications

converter where the input capacitor draws high current at the starting.

- In the proposed topology, contrary to SL-Y source converter, only two winding coupled inductor is used which reduces the size of the converter.
- It has a lower number of components count as compared to SL-Y source (switched inductor).
- Due to the presence of single inductor at the input in the proposed converter, it has lower input ripple current as compared to SL-Y source converter where switched inductor is present at the input.
- Since the inductor is directly connected to the source in the proposed converter, therefore, the input current is continuous.

Therefore, the proposed converter has the merits of zero start-up current, low cost, lower size and the lower maximum value of current stress on the source. The comparison of various factors is presented in Table-II.

E. Efficiency

To calculate the efficiency of the proposed converter and the converter reported in [20], [31], [26] and [27], method proposed in [32] is considered. The measured parasitic resistance of inductors and capacitors is 0.225 Ω and 30 $m\Omega$, respectively. The semiconductor switches and diodes used are IRFP4668PbF and STPS60SM200C, respectively for all the topologies. The internal resistance of the switch is r_{dson}= 8 $m\Omega$ and forward voltage drop of antiparallel diode is V_{sd}= 1.3 V. For diode, the forward voltage drop is V_f= 0.75 V and internal resistance is r_{don}= 0.1 Ω. The input voltage V_{in} is kept at 50 V while the output voltage is kept at 250 V. Considering these details, all the converters are simulated in PSIM 11.0 for efficiency calculation at distinct power which is shown in Fig-15. The Y-source, Quasi Y-source, and A-source converter have almost similar efficiency due to the presence of same number of passive elements which is slightly higher than the proposed converter. On the other hand, the proposed converter has quite better efficiency than the SL-Y-source converter due to the lower number of passive elements. The loss distribution chart is shown in Fig-16 which indicates that the contribution to the losses by diodes is more.

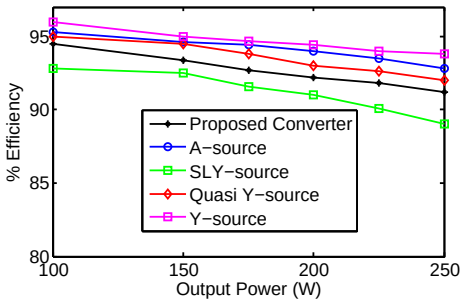

Fig. 15: Efficiency Comparison

V. Experimental Results and their Analysis

To verify the effectiveness of the proposed converters, the converters are validated experimentally. The hardware is designed on a PCB prototype board using Proteus software. The switching frequency for the boosting stage is selected 20 kHz. For control pulse generation, field programmable array gate(FPGA) is used. The experimental setup for testing DC-DC and hybrid converter is shown in Fig-17 separately.

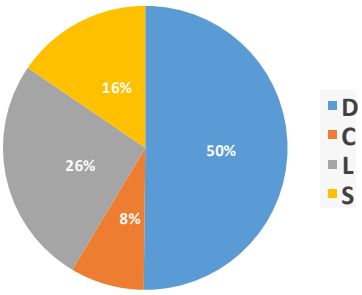

Fig. 16: Loss Distribution

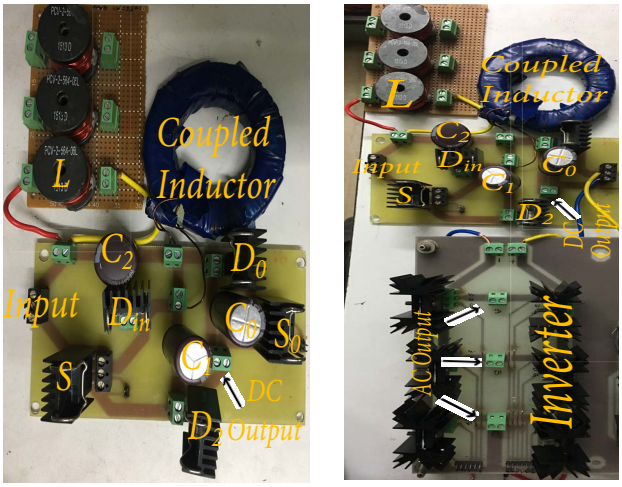

(a) DC-DC Topology (b) Hybrid Topology

Fig. 17

A. DC-DC Converter

For the DC-DC converter, the converter is designed for the 110 W power rating. For 110 W power rating, the parameters selected for the DC-DC converter are presented in Table-III.

TABLE III: DC-DC converter Parameters

Parameter	Rating
Power P	110 W
Input voltage V_{in}	40 V
Inductor L_1	1.12 mH
Capacitor C_1	110 μF
Capacitor C_2	220 μF
Capacitor C_0	110 μF
Switching frequency f_s	20 kHz
DC load resistance R_{dc}	100 Ω

The DC-DC converter is validated at 0.16 duty cycle. The inductor current profile L_1 is shown in Fig-18. The nature of inductor current L_1 ensures the CCM operation of the converter. During this, the voltage across the capacitor C_1 and

0093-9994 (c) 2019 IEEE. Personal use is permitted, but republication/redistribution requires IEEE permission. See http://www.ieee.org/publications_standards/publications/rights/index.html for more information.

This article has been accepted for publication in a future issue of this journal, but has not been fully edited. Content may change prior to final publication. Citation information: DOI 10.1109/TIA.2019.2932696, IEEE Transactions on Industry Applications

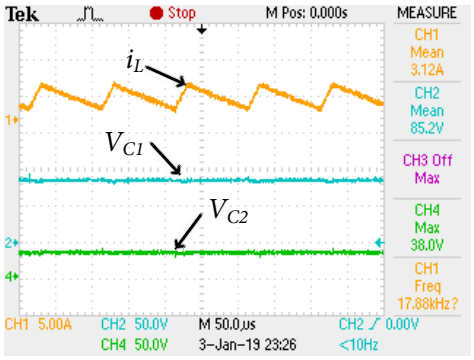

Fig. 18: Inductor current, Capacitor voltages C_1 and C_2 for DC-DC converter

C_2 is 88 V and 35.7 V, respectively which is shown in Fig-18. The coupled inductor current profile is shown in Fig-19. Both the coupled inductor winding charge during the shoot through period which is evident from the peaky nature. However, unlike the profile of coupled inductors current shown in Fig-4, the experimental waveforms exhibit finite slope which is due to non-ideal nature of coupled inductor.

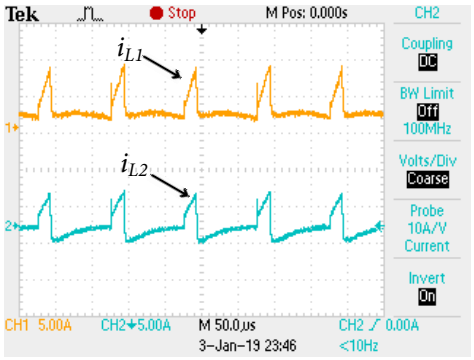

Fig. 19: Coupled inductor currents L_1 and L_2 for DC-DC converter

The experimental voltage stress across different diodes and switch is presented in Fig-20, which verifies the theoretical analysis.

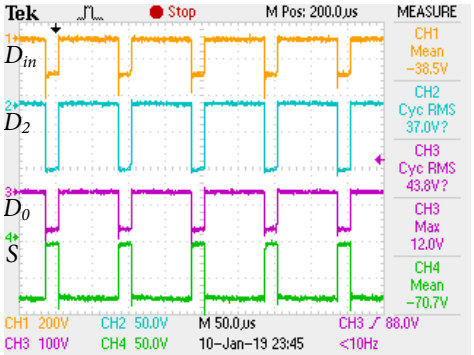

Fig. 20: Voltages across diodes and switch for DC-DC converter

Finally, the output voltage and current for the proposed converter is presented in Fig-21. The output voltage is equal to 105 V and current drawn by the load is 1.05 A, thus verifies that power rating is 110 W.

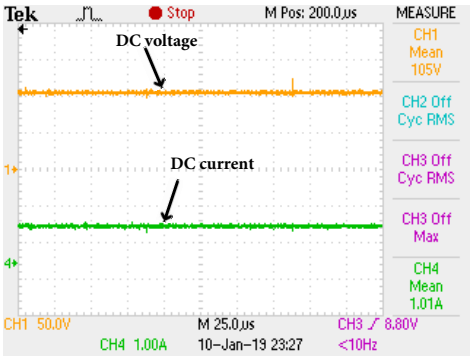

Fig. 21: output voltage and current for DC-DC converter

1) Hybrid converter: For validation of hybrid converter, the converter is designed for 270 W power rating. The simple boost control technique is selected for hybrid converter validation which is indicated in Fig-22 and Fig-23. The distribution of DC and AC power is 125 W and 145 W, respectively for validation purpose. However, this power rating can be configured according to a certain application. The other parameters considered for the hybrid converter are listed in Table-IV.

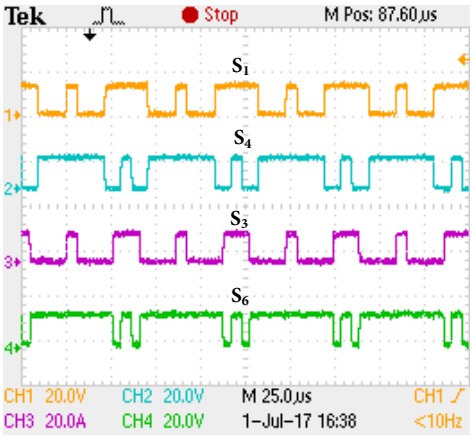

Fig. 22: Control pulses for S_1, S_4, S_3, S_6

TABLE IV: Hybrid converter Parameters

Parameter	Rating
Power P	270 W
Input voltage V_{in}	60 V
Inductor L_1	1.12 mH
Capacitor C_1	110 μF
Capacitor C_2	220 μF
Capacitor C_3	110 μF
Switching frequency f_s	20 kHz
DC load resistance R_{dc}	200 Ω
AC load resistance R_{ac}	40 Ω

The profile of inductor current and DC link voltage are depicted in Fig-24. The converter is operated in CCM which is evident from the inductor current profile. The DC link voltage is having zero voltage during shoot through and 105 voltage

0093-9994 (c) 2019 IEEE. Personal use is permitted, but republication/redistribution requires IEEE permission. See http://www.ieee.org/publications_standards/publications/rights/index.html for more information.

This article has been accepted for publication in a future issue of this journal, but has not been fully edited. Content may change prior to final publication. Citation information: DOI 10.1109/TIA.2019.2932696, IEEE Transactions on Industry Applications

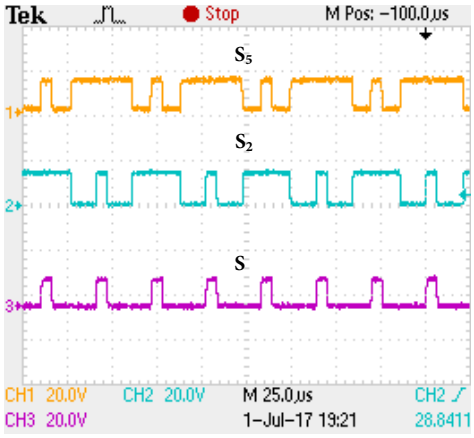

Fig. 23: Control pulses for S_5, S_2, S

during non-shoot through which verifies the theoretical analysis. The voltage across the capacitors C_1 and C_2 is presented in Fig-25 which is equal to 130 V and 53 V, respectively. The coupled inductor current profile is also presented in Fig-25 which has peaky nature in shoot through while almost flat nature during non-shoot through period. In addition, the voltage across the different devices is also presented in Fig-26.

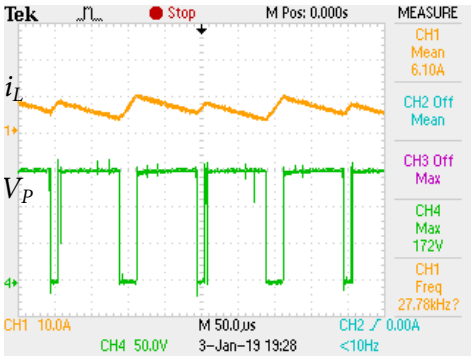

Fig. 24: Inductor current and DC link voltage for Hybrid converter

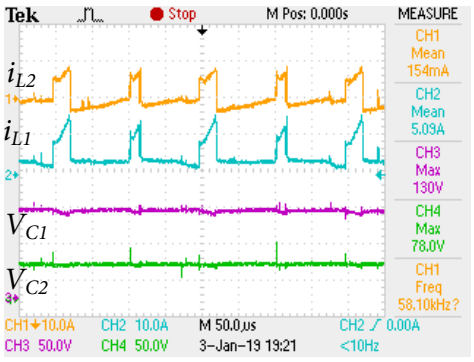

Fig. 25: Coupled inductor currents L_1, L_2 and Capacitor voltages C_1, C_2 for Hybrid converter

The DC output of the hybrid converter is shown in Fig-27. For a duty cycle of 0.16 and 60 V input voltage, the DC

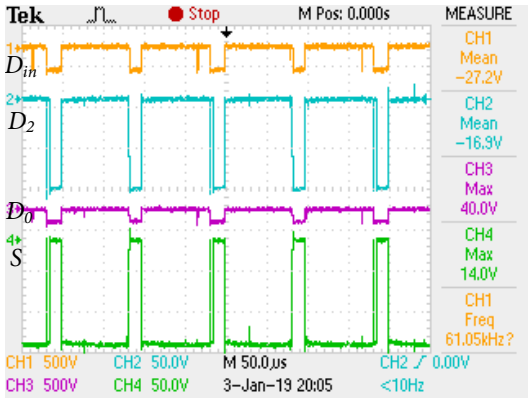

Fig. 26: Voltages across diodes and switch for Hybrid converter

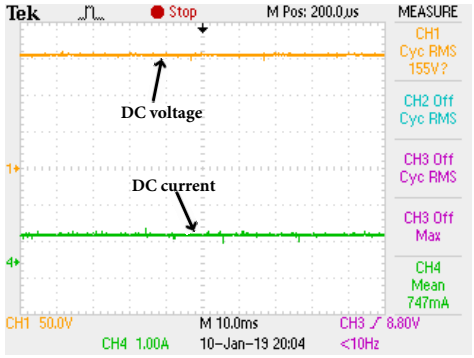

Fig. 27: DC voltage and DC current for Hybrid converter

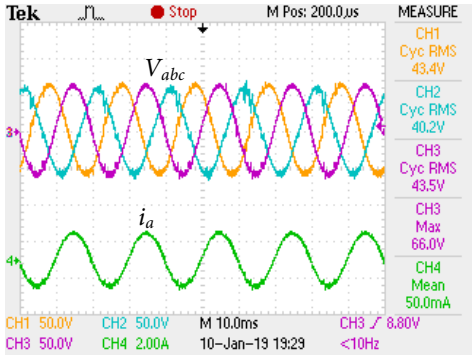

Fig. 28: AC voltage and AC current for Hybrid converter

voltage is equal to 156 V and the current is equal to 0.78 A. The AC output for the hybrid converter is presented in Fig-28. For 156 V dc output and modulation index 0.8, the peak value of per phase AC load voltage and current is 63 V and 1.5 A, respectively. The total harmonic distortion presents in the AC load current lower than 5% which satisfies the IEEE standards.

VI. Conclusion

In this paper, a coupled inductor network based on the concept of the autotransformer is validated. The key benefit of the proposed converter is, maximum gain can be achieved in the range of duty cycle $0 < D < 1/4$. This feature is

0093-9994 (c) 2019 IEEE. Personal use is permitted, but republication/redistribution requires IEEE permission. See http://www.ieee.org/publications_standards/publications/rights/index.html for more information.

This article has been accepted for publication in a future issue of this journal, but has not been fully edited. Content may change prior to final publication. Citation information: DOI 10.1109/TIA.2019.2932696, IEEE Transactions on Industry Applications

particularly important to reduce conduction loss and improves the output voltage profile. The proposed converter is a better candidate as compared to SL-Y source converter due to its lower components utilization. Moreover, the input current is continuous in nature and having lower input current ripple as compared to SL-Y source, therefore, reduces the current stress on the battery. The proposed configuration is validated for DC-DC topology at 110 W and hybrid topology at 270 W in the experiment which proves its effectiveness.

REFERENCES

[1] F. Z. Peng, "Z-source inverter," *IEEE Transactions on industry applications*, vol. 39, no. 2, pp. 504–510, 2003.

[2] A. Kumar, V. V. Ratnam, M. Reza, M. Raghuram, and S. K. Singh, "Modified boost derived hybrid converter: Redemption using fcm," *IEEE Transactions on Industry Applications*, 2017.

[3] F. Z. Peng, X. Yuan, X. Fang, and Z. Qian, "Z-source inverter for adjustable speed drives," *IEEE power electronics letters*, vol. 1, no. 2, pp. 33–35, 2003.

[4] A. Gambhir, S. K. Mishra, and A. Joshi, "A modified pwm scheme to improve performance of a single-phase active-front-end impedance source inverter," *IEEE Transactions on Industry Applications*, vol. 55, no. 1, pp. 928–942, 2019.

[5] Y. Tang, S. Xie, and C. Zhang, "An improved-source inverter," *IEEE transactions on power electronics*, vol. 26, no. 12, pp. 3865–3868, 2011.

[6] J. Anderson and F. Z. Peng, "Four quasi-z-source inverters," in *2008 IEEE Power Electronics Specialists Conference*. IEEE, 2008, pp. 2743–2749.

[7] C. J. Gajanayake, F. L. Luo, H. B. Gooi, P. L. So, and L. K. Siow, "Extended-boost-source inverters," *IEEE Transactions on Power Electronics*, vol. 25, no. 10, pp. 2642–2652, 2010.

[8] F. Gao, P. C. Loh, R. Teodorescu, and F. Blaabjerg, "Diode-assisted buck–boost voltage-source inverters," *IEEE Transactions on Power Electronics*, vol. 24, no. 9, pp. 2057–2064, 2009.

[9] Y. Zhang, J. Liu, and C. Zhang, "Improved pulse-width modulation strategies for diode-assisted buck–boost voltage source inverter," *IEEE Transactions on Power Electronics*, vol. 28, no. 8, pp. 3675–3688, 2013.

[10] M.-K. Nguyen, Y.-C. Lim, and G.-B. Cho, "Switched-inductor quasi-z-source inverter," *IEEE Transactions on Power Electronics*, vol. 26, no. 11, pp. 3183–3191, 2011.

[11] D. Li, P. C. Loh, M. Zhu, F. Gao, and F. Blaabjerg, "Cascaded multicell trans-z-source inverters," *IEEE Transactions on Power Electronics*, vol. 28, no. 2, pp. 826–836, 2013.

[12] H. Fathi and H. Madadi, "Enhanced-boost z-source inverters with switched z-impedance," *IEEE Transactions on Industrial Electronics*, vol. 63, no. 2, pp. 691–703, 2016.

[13] A. Ravindranath, S. K. Mishra, and A. Joshi, "Analysis and pwm control of switched boost inverter," *IEEE Transactions on industrial electronics*, vol. 60, no. 12, pp. 5593–5602, 2013.

[14] S. S. Nag and S. Mishra, "Current-fed switched inverter," *IEEE Transactions on Industrial Electronics*, vol. 61, no. 9, pp. 4680–4690, 2014.

[15] A. K. Chauhan, S. K. Singh *et al.*, "Integrated dual output lz source inverter for hybrid electric vehicle," *IEEE Transactions on Transportation Electrification*, 2018.

[16] M. Adamowicz and N. Strzelecka, "T-source inverter," *Przegl Elektrotechniczny*, vol. 85, no. 10, pp. 233–238, 2009.

[17] R. Strzelecki, M. Adamowicz, N. Strzelecka, and W. Bury, "New type t-source inverter," in *2009 Compatibility and Power Electronics*. IEEE, 2009, pp. 191–195.

[18] W. Qian, F. Z. Peng, and H. Cha, "Trans-z-source inverters," *IEEE transactions on power electronics*, vol. 26, no. 12, pp. 3453–3463, 2011.

[19] M.-K. Nguyen, Y.-C. Lim, and S.-J. Park, "Improved trans-z-source inverter with continuous input current and boost inversion capability," *IEEE Transactions on Power Electronics*, vol. 28, no. 10, pp. 4500–4510, 2013.

[20] Y. P. Siwakoti, P. C. Loh, F. Blaabjerg, and G. Town, "Y-source impedance network," in *2014 IEEE Applied Power Electronics Conference and Exposition-APEC 2014*. IEEE, 2014, pp. 3362–3366.

[21] W. Mo, P. C. Loh, and F. Blaabjerg, "Asymmetrical-source inverters," *IEEE Transactions on Industrial Electronics*, vol. 61, no. 2, pp. 637–647, 2014.

[22] M. Adamowicz, R. Strzelecki, F. Z. Peng, J. Guzinski, and H. A. Rub, "New type lcct-z-source inverters," in *Power Electronics and Applications (EPE 2011), Proceedings of the 2011-14th European Conference on*. IEEE, 2011, pp. 1–10.

[23] Y. P. Siwakoti, P. C. Loh, F. Blaabjerg, and G. E. Town, "T-z-source inverters," *IEEE Transactions on Power Electronics*, vol. 28, no. 11, pp. 4880–4884, 2013.

[24] Y. P. Siwakoti, F. Blaabjerg, and P. C. Loh, "Quasi-y-source boost dc–dc converter," *IEEE Transactions on Power Electronics*, vol. 30, no. 12, pp. 6514–6519, 2015.

[25] M.-K. Nguyen, Y.-C. Lim, and Y.-G. Kim, "Tz-source inverters," *IEEE Transactions on Industrial Electronics*, vol. 60, no. 12, pp. 5686–5695, 2013.

[26] Y. P. Siwakoti, F. Blaabjerg, V. P. Galigekere, A. Ayachit, and M. K. Kazimierczuk, "A-source impedance network," *IEEE Transactions on Power Electronics*, vol. 31, no. 12, pp. 8081–8087, 2016.

[27] Y. Wang, W. Jing, Y. Qiu, Y. Wang, X. Deng, K. Hua, B. Hu, and D. Xu, "Y-source boost a family of y-source dc/dc converter based on switched inductor," *IEEE Transactions on Industry Applications*, 2018.

[28] A. K. Chauhan, M. Raghuram, S. K. Singh *et al.*, "Quasi mutually coupled active impedance source converterautotransformer type turns ratio," in *Transportation Electrification Conference (ITEC-India), 2017 IEEE*. IEEE, 2017, pp. 1–5.

[29] A. K. Chauhan, V. R. Vakacharla, M. Reza, M. Raghuram, and S. K. Singh, "Modified boost derived hybrid converter: Redemption using fcm," *IEEE Transactions on Industry Applications*, vol. 53, no. 6, pp. 5893–5904, 2017.

[30] A. K. Chauhan, M. S. Teja, M. Jain, and S. K. Singh, "A cross regulated closed loop control for hybrid lz source inverter," *IEEE Transactions on Industry Applications*, 2018.

[31] Y. P. Siwakoti, F. Z. Peng, F. Blaabjerg, P. C. Loh, and G. E. Town, "Impedance-source networks for electric power conversion part i: a topological review," *IEEE Transactions on Power Electronics*, vol. 30, no. 2, pp. 699–716, 2015.

[32] X. Zhu, B. Zhang, and D. Qiu, "Enhanced boost quasi-z-source inverters with active switched-inductor boost network," *IET Power Electronics*, vol. 11, no. 11, pp. 1774–1787, 2018.

Avneet K Chauhan (S'15 M'19) received his B.Tech. in Electrical Engineering from Maharana Pratap Engineering College, Kanpur,(Affiliated from AKTU, Lucknow) India, in 2010. He received his Ph.D. degree from the Department of Electrical Engineering, IIT(BHU), Varanasi, India. From 2010 to 2013, he worked as Assistant Professor in the Department of Electrical Engineering, MPGI, Kanpur, India. He has received second Best Paper Award from IAS annual meeting in 2017.

His research interests include power converter modeling and control, digital control in power electronics, z-source converters and their applications, sliding mode control and electrical drives. He is frequent reviewer of several renowned conferences and IEEE Transaction.

Sajid Kamal received his B.E. in Electrical Engineering from University of Pune in 2015. Currently, he is working towards his Masters degree in the School of Mechanical Engineering and Automation from the Harbin Institute of Technology Shenzhen P.R. China. His research interests include digital control in power electronics, impedance source converters and sliding mode control.

0093-9994 (c) 2019 IEEE. Personal use is permitted, but republication/redistribution requires IEEE permission. See http://www.ieee.org/publications_standards/publications/rights/index.html for more information.

This article has been accepted for publication in a future issue of this journal, but has not been fully edited. Content may change prior to final publication. Citation information: DOI 10.1109/TIA.2019.2932696, IEEE Transactions on Industry Applications

M Raghuram (S'15) is currently working towards his Ph.D. degree in the Department of Electrical Engineering, from the Indian Institute of Technology BHU, Varanasi, India

His research interests include digital control in power electronics, matrix converter, impedance source converters.

Deepankar received the B.Tech degree in Electrical and Electronics Engineering from Delhi Technological University (DTU), India, in 2014 and M.Tech degree in Power Electronics from Indian Institute of Technology (BHU), Varanasi, in 2017. His research interests includes Power Converter Modelling and Digital Control, Impedance Source Converters and Electrical Drives.

Santosh Kumar Singh (S'09 M'12 SM'18) is Assistant Professor in the Department of Electrical Engineering at Indian Institute of Technology(BHU) Varanasi, India. He did his Ph.D. degree in the Engineering Department, University of Cambridge, U.K.

His research interests include Silicon carbide converters, Power electronic topologies, Electric drives and Permanent magnet generators.

Xiaogang Xiong received his PhD (Eng.) degrees from Kyushu University, Fukuoka, Japan, in 2014, in Mechanical and Science Engineering. From 2014 to 2015, he was a Researcher with Kyushu Institute of Technology, Iizuka, Japan. From 2015 to 2016, he was a Research Fellow with Singapore Institute of Manufacturing Technology, Singapore. He is currently an Assistant Professor with the Department of Mechanical Engineering and Automation, Harbin Institute of Technology (Shenzhen), Shenzhen, China. His research interests include human-robot coordination, nonsmooth systems such as multibody dynamics and DC-DC converter, human-robot coordination, intelligent robots and robot real-time control.

0093-9994 (c) 2019 IEEE. Personal use is permitted, but republication/redistribution requires IEEE permission. See http://www.ieee.org/publications_standards/publications/rights/index.html for more information.

I.J. Image, Graphics and Signal Processing, **2019, 9, 34-43**
Published Online September 2019 in MECS (http://www.mecs-press.org/)
DOI: 10.5815/ijigsp.2019.09.04

Human Action Recognition Using Modified Bag of Visual Word based on Spectral Perception

Om Mishra
Department of Electronics & Communication, Delhi Technological University, Delhi-110042, India
Email: om.mishra83@gmail.com

Rajiv Kapoor
Department of Electronics & Communication, Delhi Technological University, Delhi-110042, India
Email: rajivkapoor@dce.ac.in

M.M. Tripathi
Department of Electrical Engineering, Delhi Technological University, Delhi-110042, India
Email: mmtripathi@dce.ac.in

Received: 02 May 2019; Accepted: 25 June 2019; Published: 08 September 2019

Abstract—Human action recognition has a very vast application such as security, patient care, etc. Background cluttering, appearance change due to variation in viewpoint and occlusion are the prominent hurdles that can reduce the recognition rate significantly. Methodologies based on Bag-of-visual-words are very popular because they do not require accurate background subtraction. But the main disadvantage with these methods is that they do not retain the geometrical structural information of the clusters that they form. As a result, they show intra-class mismatching. Furthermore, these methods are very sensitive to noise. Addition of noise in the cluster also results in the misclassification of the action. To overcome these problems we proposed a new approach based on modified Bag-of-visual-word. Proposed methodology retains the geometrical structural information of the cluster based on the calculation of contextual distance among the points of the cluster. Normally contextual distance based on Euclidean measure cannot deal with the noise but in the proposed methodology contextual distance is calculated on the basis of a difference between the contributions of cluster points to maintain its geometrical structure. Later directed graphs of all clusters are formed and these directed graphs are described by the Laplacian. Then the feature vectors representing Laplacian are fed to the Radial Basis Function based Support Vector Machine (RBF-SVM) classifier.

Index Terms—Bag-of-visual-word, Contextual distance, Directed graph, Laplacian of directed graph, SVM.

I. Introduction

Human action recognition from a video is the most promising research area of computer vision and pattern analysis. It has vast applications including surveillance, human-computer interaction, video content analysis, patient care, etc. [1, 2]. Background cluttering, noise, variation in viewpoint, variation in illumination, occlusion are the major challenges for human action recognition in a video. The actions are described by the global and local feature descriptors. The global feature descriptor gives shape as well as the motion information of the person who is performing an action. These are not invariant to the appearance change, shape changes, etc. Whereas local descriptor such as spatio-temporal points shows invariance in appearance change, background change, etc. Local features based on Bag-of-visual–words have been very popular among the researchers. The disadvantage of these methods is that they do not retain the structural information of the clusters formed in Bag-of Visual words based methodology. The proposed method overcomes the limitation of the Bag-of-visual-word methodology. The proposed methodology contributed in the following manner:

1. The contextual distance among the points of a cluster is calculated on the basis of the difference between the contributions of points to maintain the geometrical structure of the cluster, unlike the contextual distance calculated on basis of Euclidean measure among the points in a cluster.
2. The contextual distance among any two points of the contextual set of a cluster, calculated as mentioned above may show asymmetry. So to deal with this asymmetry issue, we used the concept of the directed graph. Thus, a cluster is represented using contextual distance and directed graph together in a robust way.

The rest of the paper is discussed as follows: literature review has been discussed in section 2, section 3 deals with the proposed methodology. Section 4 deals with the experimental results. In this section, the proposed

Copyright © 2019 MECS

methodology is applied to challenging public datasets such as KTH, Ballet, and IXMAS. The accuracy of the proposed methodology and its comparison with other state-of-the-art methodologies are also discussed in this section. The conclusion part is discussed in section 5.

II. Literature Review

Many methodologies have been proposed by researchers to describe an action. Global features [3, 4, 5, 6, 7 and 8] require the detection of the human body whose action is to be recognized. Background subtraction or human body tracking is used to represent the human body. These methodologies used two-dimensional template matching. The silhouette of the human body detected from the frames is represented globally. The descriptors like Hu moments, Radon transform, etc. are used to describe these actions. Actions are also represented as spatiotemporal volumes [9, 10, 11 and 12]. The silhouettes are stacked together on a temporal axis to make spatiotemporal volume. The disadvantage of these methodologies is that it requires accurate background subtraction to create a 2-D template and spatiotemporal volume. These global features can only give shape information but fail to provide motion information. Some global features based on the optical flow [13, 14] are used to eliminate this problem but the disadvantage of this method is that they are very sensitive to noise.

Recently, local feature descriptions [15, 16, 17, 18, 19, 20, 21, 22, 23, 24 and 26] are used more often. These methodologies do not require accurate background subtraction. They also show invariance against the viewpoint and appearance of the object. This is represented in local patches formed around spatiotemporal interest points. Local spatiotemporal descriptors are based on the bag-of-words model. HOG/HOF, HOG3D, SURF, and MoSIFT are some major descriptors [27-29]. The main disadvantage with these methodologies is that it cannot hold the shape information of the clusters. This results in the same description for different actions.

In recent years, deep learning techniques are also getting famous in researchers for human action recognition [30, 31]. These techniques are completely automated. They require large datasets and the efficiency of these methods is based on the design of networks. These networks are made up of a huge number of data and parameters that makes the structure very complex. So it takes more time to train a model. Moreover, less availability of large datasets makes this method less generalized for action recognition. Researchers are working on deep learning techniques to overcome these problems**.**

Among all these above-discussed methodologies, spatiotemporal features points-based bag-of-word are very popular because they do not require important preprocessing like background subtraction, tracking of an object, etc. This makes it robust to the challenges like background cluttering, variation in viewpoint and illumination change. The major disadvantage of this methodology is that it cannot depict the structural relationship among spatiotemporal feature points. Due to this problem, the spatiotemporal features based on a bag-of-word methodology are not able to differentiate the similar type of actions often. Fig.1. illustrates the problem wherein a person on the left side of the figure is running while a person on the right is jogging. The traditional

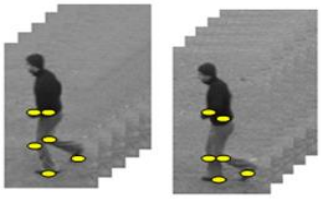

Fig.1. Similar activities (a person on the left side is running; a person on the right side is jogging)

Bag-of-words based methodology often treats them as the same action which is wrong. To overcome this limitation researchers have used the spatiotemporal contextual information [32, 33, 34]. But the limitation of these methods is that they are still weak in noise tolerance. When the noise is added, the representation of the interest points of action might be recognized as other activities. Moreover, the measures of contextual distance between spatiotemporal points traditionally use Euclidean distances among these points but this distance cannot hold the structural information of clusters. The proposed methodology is capable to overcome these limitations.

III. Proposed Methodology

Local features such as spatiotemporal points are most popularly used to represent an action. Spatiotemporal interest points such as Harris 3D detectors and SIFT detectors [43] are used to detect the interest points. We used the Harris 3D detector to extract the spatio-temporal interest points. These interest points are described locally by the descriptors such as HOG [27] and HOF [28]. The HOG and HOF are used in the proposed method to describe the interest points detected by Harris 3D detector. These local descriptors represent the feature vectors of each frame of the action video. A bag-of-visual-word of spatiotemporal interest points is formed to represent an action efficiently. The codebook is created by performing vector quantization through clustering. The K-means clustering [32] is popularly used. In K-means clustering clusters are placed near to most frequently occurring feature vectors. These most frequently occurring feature vectors are used as the discriminative features of action. But for certain actions, these most frequently occurring features are not capable enough to show the discriminative nature of an action. Further quantization error may also occur due to the assignment of a single cluster to feature vector. To avoid this we used the soft assigning technique [15] where Gaussian kernel is used in which feature vectors and cluster are represented by the normal distribution. Equation (1) defines the visual word $V_{i,t}$

$$V_{i,t} = \exp^{\left(-\frac{\|f_t - C_i\|^2}{2\theta^2}\right)} \quad (1)$$

where, f_t is the feature vector and C_i is the i^{th} cluster where $i=1, 2, 3\ldots N$ and θ is the smoothing parameter. We used the cross-validation to find out the size of the Gaussian kernel. In the proposed method we used this soft assigning technique and we get the codebook $\{C_1, C_2 \ldots C_N\}$ where C_i is the i^{th} cluster and the total number of the cluster is N. Fig. 2. shows the proposed methodology for codebook creation. Let the spatiotemporal feature points be represented in the form of tuple $X = (L, r)$ where L is local descriptor (appearance) of the interest points and $r = (x, y, t)$ is the spatial location of the interest points. The horizontal, vertical and temporal coordinates of interest points are represented by x, y, and t respectively. As discussed above, in the traditional bag-of-visual-word based methodology, the geometrical structure of the cluster cannot be maintained because of the introduction of noise. This results in the reduction of the recognition rate. Thus, to maintain the geometrical structure of the clusters, we propose a new methodology where we calculate the contextual distance among the points of the cluster on the basis of the difference between the contributions of points in a cluster to maintain its geometrical structure. The Methodology can be understood by the block diagram in fig. 2.

The spatiotemporal points are detected from the input action video by using Harris 3D corner detector. These points are described by the descriptors HOG and HOF. Using soft assigning technique we created the codebook having N no. of clusters. The traditional bag-of-visual-word technique is modified through the proposed methodology. Using the geometrical descriptor, the contextual distance among the points of the cluster is calculated. The directed graph of the cluster points is then created with the help of contextual distance between the points. These directed graphs are described by Laplacian.

A. Geometrical Description of a Cluster

As discussed above, among the N clusters formed, let us select the i[th] cluster C_i. The cluster C_i is represented by the set I_c. The set I_c is represented by (2) where i_c is a mean point of the cluster C_i having m nearest neighboring points.

$$\mathrm{I}_c = \left(i_{c0}, i_{c1}, i_{c2}, ..., i_{cm}\right) \quad (2)$$

We used centroid as the geometrical structure descriptor of set I_c denoted by (3) as shown below

$$\mathrm{M}\left(\mathrm{I}_c\right) = \frac{1}{m+1}\sum_{j=0}^{m} i_{ck} \,. \quad (3)$$

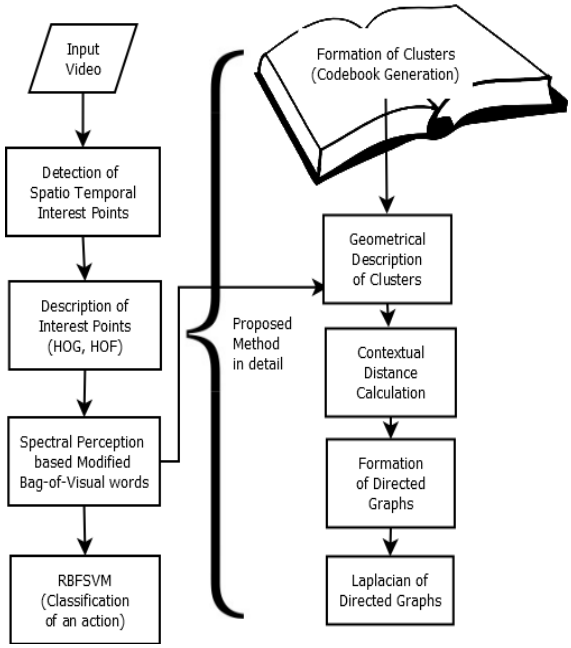

Fig.2. Detail process flow diagram of the proposed methodology

To calculate the contribution of each point in the set I_c, we removed one point at a time and recalculated the centroid using (3). Thus we get the contribution of all points in the set I_c that forms the geometrical structure of the cluster. The contribution of point i_{ck} can be found out by (4).

$$\delta\left(i_{ck}\right) = \left|\mathrm{M}\left(\mathrm{I}_c\right) - \mathrm{M}\left(\mathrm{I}_c \big/ i_{ck}\right)\right| \quad (4)$$

where $\delta(i_{ck})$ is the contribution of the point i_{ck} in the cluster set I_c. $M(I_c)$ is the complete descriptor of I_c and $M(I_c/i_{ck})$ is the description of set I_c after removing the point i_{ck} from the set. In a similar manner contribution of all the points in a cluster's set is found out. If the value of $\delta(i_{ck})$ is very small then the contribution of the point i_{ck} is not significant in maintaining the geometrical structure of the cluster and if the value of $\delta(i_{ck})$ is high then we can conclude that the point i_{ck} has a significant effect in retaining the geometrical structure of the set I_c.

B. Contextual Distance Among the Points of a Cluster

Fig. 3 describes the geometrical description of the cluster and the contextual distance among the points of the clusters. Once the contribution of points of a cluster to maintain its geometrical structure has been obtained, the contextual distance among these points is calculated by taking the difference between their contributions. This can be calculated from (5).

$$\Psi\left(i_{c0}, i_{c1}\right) = \left\{\delta\left(i_{c0}\right) - \delta\left(i_{c1}\right)\right\} \quad (5)$$

Copyright © 2019 MECS

where $\Psi(i_{c0},i_{c1})$ is the contextual distance between interest points i_{c0} to i_{c1} and $\delta(i_{c0})$ *and* $\delta(i_{c1})$ are the contribution of the points i_{c0} and i_{c1}. After calculating the contextual distances among the points of the cluster set I_c the set I_c is represented in the form of their contextual distances. This representation of the cluster set creates asymmetry among the points of the set I_c because the contextual distance between i_{c0} to i_{c1} may not be equal to the contextual distance between i_{c1} to i_{c0}. To deal with this naturally occurred asymmetry in the cluster set I_c, the directed graph has been used to make the cluster more informative as it introduced direction also.

C. Formation of the Directed Graph of a Cluster on the Basis of Contextual Distance

The cluster set I_c can be represented by the directed graph where the points of set are treated as the nodes/vertices of the graph as shown in fig. 4. Let the edge from the points i_{c0} to i_{c1} is defined by the weight $\lambda(i_{c0},i_{c1})$ as given by (6).

$$\lambda\left(i_{c0},i_{c1}\right)=e^{\left[\frac{\Psi\left(i_{c0},i_{c1}\right)}{\mu}\right]^2} \tag{6}$$

where $\lambda(i_{c0},i_{c1})$ is the weight of the edge from point i_{c0} to i_{c1}, $\Psi(i_{c0},i_{c1})$ is the contextual distance from i_{c0} to i_{c1}, μ is a free parameter and i_{c0} and i_{c1} are the neighborhood points of the cluster set I_c. Thus, in the cluster set I_c a point i_c is connected to its m neighborhood points through m edges as shown in fig. 4.

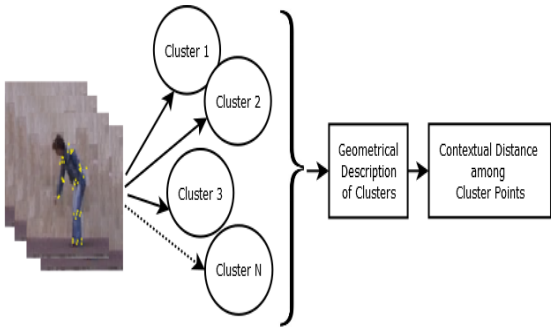

Fig.3. Geometrical description of a cluster and contextual distance among the cluster points

The directed graph of cluster set can be represented through weighted edge matrix W. The weighted edge matrix W carries the geometrical structural information of the cluster set I_c. Similarly, directed graphs have been applied on other contextual cluster sets also. The weighted edge matrix is created for a single cluster as shown below:

$$\begin{bmatrix} & i_{c0} & i_{c1} & i_{c2} & \cdots & i_{cm} \\ i_{c0} & \lambda(i_{c0},i_{c0}) & \lambda(i_{c0},i_{c1}) & \lambda(i_{c0},i_{c2}) & \dots & \lambda(i_{c0},i_{cm}) \\ i_{c1} & \lambda(i_{c1},i_{c0}) & \lambda(i_{c1},i_{c1}) & \lambda(i_{c1},i_{c2}) & \dots & \lambda(i_{c1},i_{cm}) \\ i_{c2} & \lambda(i_{c2},i_{c0}) & \lambda(i_{c2},i_{c1}) & \lambda(i_{c2},i_{c2}) & \dots & \lambda(i_{c2},i_{cm}) \\ \vdots & \dots & \dots & \dots & \ddots & \vdots \\ i_{cm} & \lambda(i_{cm},i_{c0}) & \lambda(i_{cm},i_{c1}) & \lambda(i_{cm},i_{c2}) & \cdots & \lambda(i_{cm},i_{cm}) \end{bmatrix}$$

Further to describe the weighted directed graph Laplacian of the directed graph has been used.

D. Laplacian of the Directed Graph of a Cluster

Suppose $G(i_{cj},\lambda)$, where $j=0\dots m$, is the directed graph of the set I_c and the directed edge (i_c, i_d) is the edge directed from vertex i_c to vertex i_d. A walk from one vertex to other is represented by the transition probability matrix O. If $O(i_c, i_d)$ is the transition probability of moving from point i_c to i_d, it is obvious that $O(i_c, i_d)>0$ only if there is an edge between i_c to i_d. Further for the weighted directed graph, the transition probability matrix is given by (7).

$$O\left(i_c,i_d\right)=\frac{\lambda_{(i_c,i_d)}}{\sum_m \lambda_{(i_c,i_m)}} \tag{7}$$

wherein, equation $\lambda(i_c, i_d)$ is the weight of the edge from point i_c to i_d and denominator in the right-hand side of the equation represents the total weighted sum of all the edges from point i_c to all its neighboring points.

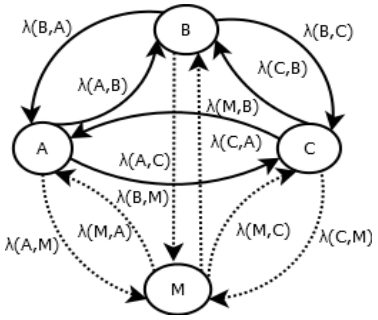

Fig.4. A cluster set I_c of m points where A=i_{c0}, B=i_{c1} and λ (A, B) = (i_{c0},i_{c1})

According to (7) transition probability matrix of the directed graph has a unique left Eigenvectors ε with all positive values and the Laplacian of the transition probability matrix Φ is defined by the (8).

$$\Phi=\mathrm{I}-\frac{\epsilon^{\frac{1}{2}}\,O\,\epsilon^{-\frac{1}{2}}+\epsilon^{-\frac{1}{2}}\,O\,\epsilon^{\frac{1}{2}}}{2} \tag{8}$$

where O is the transition probability matrix and ε is the Eigenvector. Equation (8) gives the Laplacian of the transition probability matrix for a cluster C_i. This Laplacian of the transition probability matrix is converted to a vector having dimension by scanning the matrix from the top-left element to bottom right element. Thus, the Laplacian of the transition probability matrix for N clusters has N feature vectors. These feature vectors are fed to RBF-SVM classifier. Fig. 5 shows the formation of N clusters and their Laplacian descriptors.

Copyright © 2019 MECS

IV. Experimental Results

The proposed method has been implemented in MATLAB R2013a having hardware configuration processor Intel(R) Core (TM) i5-6200U CPU @2.30GHz 2.40 GHz with 12 GB RAM and 64-bit operating system. For evaluation of the performance of proposed methodology two evaluation factors, accuracy and the equal error rate is used. Accuracy gives the correct prediction of the action out of all the predictions. Three standard datasets KTH [35], IXMAS[36] and Ballet[20] have been used to validate the proposed methodology. IXMAS dataset has been used for parameter settings and the same setting is applied to other datasets. For cross-validation, leave one actor out strategy has been adopted.

A. Parameter Settings

There are two parameters that can affect the proposed methodology. The First parameter is the size of the codebook using the soft assigning strategy and second is the number of nearest neighbors of a cluster. In most of the bag-of-visual-word based methods, the size of the codebook is around 1000. But in the proposed method cross-validation optimization has been done to find out the size of codebook. Fig. 6.a shows the codebook size 25, 30, 35 40, 45 and 50. The codebook size of 35 has been opted, because if the size of the cluster is greater than 30 then the accuracy varies only 2-3%. Another parameter is the number of nearest neighbor in the cluster. Different values such as 100, 120, 140, 160, 180, 200 and 220 have been taken. The size of nearest neighbor 160 has been taken because other than this value the accuracy varies only 1-2% as shown in fig. 6.b. Similar setting is used for KTH and Ballet datasets.

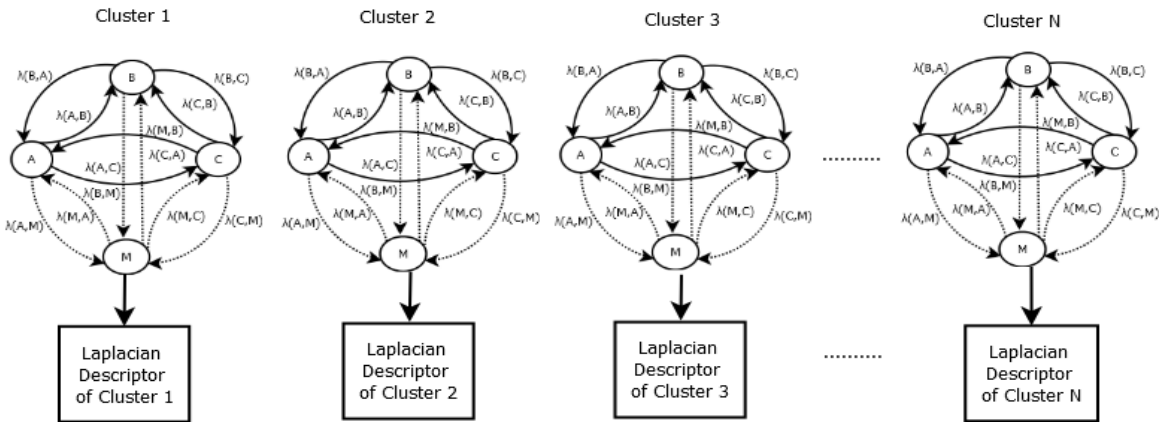

Fig.5. Formation of N clusters and their Laplacian descriptors

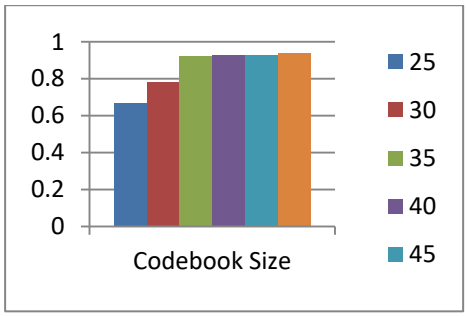

(a)

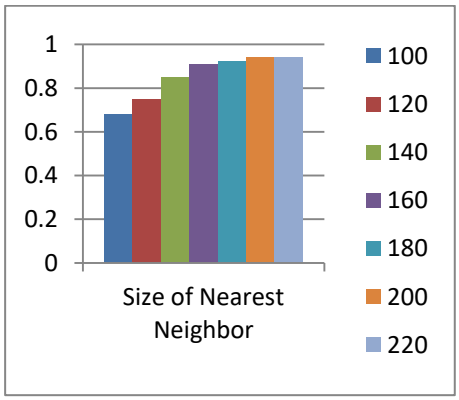

(b)

Fig.6. (a). Selection of codebook size (b) Selection of nearest neighbor size

B. Analysis and Discussion on KTH Dataset

The KTH dataset [35] comprises of six actions such as hand-applauding, waving, boxing, walking, jogging and running shown in fig. 7.a. Every activity has 100 recordings for four unique situations in various light conditions, indoor and open-air conditions.

Fig. 8 shows the confusion matrix where the proposed methodology gets the appreciable result for differentiating different actions. Similar types of actions like jogging and running are also very well classified. Only 5% jogging action is wrongly classified as running and running is only 3% confused with the jogging. The proposed method classifies hand waving action accurately, but it gets 7% confused with the action waving while classifying the boxing action.

The proposed methodology has been compared with the other state-of-the-art methods for KTH dataset in Table 1. Sadek et.al [10] uses the affine moment invariants of 3D action volume where they get the average accuracy of 93.3%. But to create the 3D volume of action there is a requirement of a sophisticated approach of background subtraction to detect the object.

Copyright © 2019 MECS

The action is represented with the combination of pose descriptors and negative space descriptor of each frame [16]. They get higher accuracy of 94.4% but still, there is also required to have a very good background subtraction technique. Furthermore, [18] and [19] are getting very high accuracies of 95.8% and 96% respectively wherein [18] proposed a new feature Hanklets which are view-invariant features and makes the accuracy higher and [19] is traditional deep learning-based methodology for action recognition that is presently used more popularly. The proposed methodology is outperforming these methodologies on KTH dataset as it is robust to view change, illumination change, and noise also. Table 1 shows that 98.2% of action samples are correctly classified which is a very high accuracy as compared to other prominent methods of Table 1.

Table 1. Comparison among other state-of-the-art methods for KTH dataset

Method	Year	EER	Accuracy
[30]	2015	5.8	94.2
[31]	2015	6.8	93.1
[10]	2012	6.7	93.3
[15]	2013	7.4	92.6
[16]	2014	5.6	94.4
[17]	2015	8.7	91.3
[18]	2012	4.2	95.8
[19]	2017	3.2	96.8
Proposed Method		**1.8**	**98.2**

In Table 2 comparison among the similar state-of-the-art methods is shown. The methodologies [32, 37-41] are based on the spatiotemporal features interest points. The disadvantage of these methodologies is that they do not show the relationship between the interest points and also the structural information of the clusters is missing. Although [32] retains the relationship among the spatiotemporal interest point, it is immune to noise. The proposed method shows the superior accuracy of 98.2% because it deals with these issues efficiently as discussed in the previous sections.

C. Analysis and Discussion on Ballet Dataset

The Second dataset that has been used is Ballet dance [20] shown in fig. 7.b. It is a typical dance dataset where different expressive dance steps. A single artist is performing the dance act. The dataset contains distinctive acts in Ballet dance such as hopping, jumping, standing still, left to right-hand opening, right to left-hand opening, leg swinging and turning right. This dataset has a total of 44 numbers of videos.

Proposed methodology maintains the structural information of the clusters and thus classifies similar actions better than other methods as summarized in Table 3. Fig. 9 shows the confusion matrix for actions in Ballet dataset. It is clear from the matrix that actions such as standing still, leg swinging and turning right are accurately classified by the proposed method. Whereas hopping is 5% confused with jumping and jumping action is 8% confused with hopping. Similarly, Left to right-hand opening is 10% confused with right-hand opening and right to left-hand opening is 12% confused with the left to right-hand opening. Table 3 shows the comparison of the proposed method with some very efficient methods when they tested on Ballet datasets. Vishwakarma et.al [5] uses the silhouettes as the key poses that can express the actions. These silhouettes are represented into grids and cells. A fusion of classifier is used to recognize the actions. They achieved an accuracy of 94.2%. Their only disadvantage is that to represent poses the accurate silhouettes are required. Methods [22] and [32] represented the action with the set of spatiotemporal descriptors. Where [22] uses the dictionary learning approach and [32] uses the contextual constraint linear coding for action recognition. They showed 94.2% and 91.2% accuracy respectively. These methods are not robust to the data tempered by the noise. But as the proposed method is robust to noise that makes its accuracy comparable to these methods. The accuracy and the equal error rate of the proposed methodology are compared with other promising state-of-the-art methodologies in Table 3. The proposed methodology achieved 96.2% accuracy and 3.8% equal error rate.

Table 2. Comparison among similar state-of-the-art methods for KTH dataset

Method	Year	EER	Accuracy
[37]	2014	5.8	95.0
[38]	2005	6.8	76.4
[39]	2011	6.7	84.1
[40]	2012	7.4	93.6
[41]	2013	7.5	92.5
[32]	2012	5.7	94.3
Proposed Method		**1.8**	**98.2**

D. Analysis and Discussion on IXMAS dataset

The third dataset that the proposed methodology experimented on is IXMAS. There are five different cameras used for the videos in IXMAS dataset. For IXMAS dataset [36] five camera views are taken. The proposed methodology has been compared with some latest prominent methodologies in Table 4. In Table 3 the methodologies [23] and [26] achieved the average accuracy of 87.6% and 87.1% on IXMAS dataset. [23] is based on the multi-view human action recognition where several cameras are observing a scene and features from each camera are considered for recognition. It makes the system complex. In [26] a statistical translation framework is used where the cross-view approach is applied. The proposed methodology achieved 90% accuracy for all five camera views. In the proposed method the camera view 3 shows the highest accuracy of 92.4%. The overall accuracy computed by taking an average of all camera views is 90.5%.

Copyright © 2019 MECS

Table 3. Illustration of EER and Accuracy for various approaches on Ballet dataset

Method	Year	EER	Accuracy
[20]	2008	48.7	51.3
[27]	2009	8.7	91.3
[21]	2014	9.2	90.8
[28]	2014	8.8	91.2
[32]	2012	5.5	94.5
[5]	2015	5.8	94.2
[22]	2012	8.8	91.2
Proposed Method		**3.8**	**96.2**

Table 4. Accuracy for various approaches from 5 different cameras

Method	[23]	[29]	[24]	[25]	[26]	**Proposed Method**
Year	2011	2010	2012	2013	2016	
C1	89.1	84.2	86.5	91.3	88.4	**90.8**
C2	83.4	85.2	83.8	85.7	85.3	**90.6**
C3	89.3	84.1	86.1	89.3	88.3	**92.4**
C4	87.2	81.5	84.5	90.2	86.5	**88.5**
C5	89.2	82.6	87.4	86.5	87.2	**90.6**
Overall Accuracy	87.6	83.5	85.6	88.6	87.1	**90.5**

(a)

(b)

Fig.7. (a). KTH dataset; (b). Ballet dataset

	Applauding	**Waving**	**Boxing**	**Walking**	**Jogging**	**Running**
Applauding	**1.00**	0.00	0.00	0.00	0.00	0.00
Waving	0.00	**1.00**	0.00	0.00	0.00	0.00
Boxing	0.00	0.07	**0.93**	0.00	0.00	0.00
Walking	0.00	0.00	0.00	**1.00**	0.00	0.00
Jogging	0.00	0.00	0.00	0.00	**0.95**	0.05
Running	0.00	0.00	0.00	0.00	0.03	**0.97**

Fig.8. Confusion Matrix for actions in KTH dataset

	Hopping	**Jumping**	**Standing Still**	**LR Hand Opening**	**RL Hand Opening**	**Leg Swinging**	**Turning Right**
Hopping	**0.95**	0.05	0.00	0.00	0.00	0.00	0.00
Jumping	0.08	**0.92**	0.00	0.00	0.00	0.00	0.00
Standing Still	0.00	0.00	**1.00**	0.00	0.00	0.00	0.00
LR Hand Opening	0.00	0.00	0.00	**0.90**	0.10	0.00	0.00
RL Hand Opening	0.00	0.00	0.00	0.12	**0.88**	0.00	0.00
Leg Swinging	0.00	0.00	0.00	0.00	0.00	**1.00**	0.00
Turning Right	0.00	0.00	0.00	0.00	0.00	0.00	**1.00**

Fig.9. Confusion Matrix for actions in Ballet dataset

	Check Watch	**Cross Arms**	**Scratch Head**	**Get Up**	**Turn Around**	**Walk**	**Wave**	**Punch**	**Kick**	**Pick Up**
Check Watch	**1.00**	0.00	0.00	0.00	0.00	0.00	0.00	0.00	0.00	0.00
Cross Arms	0.00	**1.00**	0.00	0.00	0.00	0.00	0.00	0.00	0.00	0.00
Scratch Head	0.00	0.00	**0.95**	0.00	0.00	0.00	0.05	0.00	0.00	0.00
Get Up	0.00	0.00	0.00	**0.93**	0.00	0.00	0.00	0.00	0.00	0.07
Turn Around	0.00	0.00	0.00	0.00	**1.00**	0.00	0.00	0.00	0.00	0.00
Walk	0.00	0.00	0.00	0.00	0.00	**1.00**	0.00	0.00	0.00	0.00
Wave	0.00	0.00	0.08	0.00	0.00	0.00	**0.92**	0.00	0.00	0.00
Punch	0.00	0.00	0.00	0.00	0.00	0.00	0.00	**1.00**	0.00	0.00
Kick	0.00	0.00	0.00	0.00	0.00	0.00	0.00	0.00	**1.00**	0.00
Pick Up	0.00	0.00	0.00	0.10	0.00	0.00	0.00	0.00	0.00	**0.90**

Fig.10. Confusion Matrix for actions in IXMAS dataset

There are different challenges included in this dataset that can reduce the recognition such as appearance change due to change in viewpoint and numbers of similar types of activities. Fig. 10 depicts the overall confusion matrix where the action scratching head is only 5% confused with the action wave. Wave is 8% confused with the action scratching head. Getting up is 7% confused with the action picking up and picking up is 10% confused with the getting up. The confusion percentage is very less for these similar activities shows the dominance of the proposed methodology in the case of interclass similarity. Other actions are clearly classified with 100% classification.

To summarize, the overall performance of the proposed method shows that this is a very effective method for human action recognition. The three action datasets comprise of several challenges for human action recognition. The proposed method achieved 98.2% accuracy for KTH dataset, 96.2% accuracy for Ballet dataset and the average accuracy for all five camera views of the IXMAS datasets is 90.5%.

V. Conclusion

In this research paper, a new methodology that is the modified version of the bag-of-visual-word has been proposed. The limitation of the traditional codebook based method where the geometrical structural information of the clusters was missing has been overcome in the proposed methodology. Moreover, a new methodology for calculating the contextual distance among the points of the cluster has been used for action recognition. The proposed methodology has been validated on the challenging public dataset such as KTH, Ballet, and IXMAS where it shows its superiority as compared to other existing methods.

Acknowledgment

The authors wish to thank the Department of Electronics and Communication Engineering of Delhi Technological University, Delhi India for their support.

References

[1] J. Aggrawal, and M. Rayoo, “Human Activity Analysis: A Review,” *Journal of ACM Computing Survey*, vol. 43(3), pp. 16-43, 2011.

[2] J. Dou, and J. Li, "Robust human action recognition based on spatiotemporal descriptors and motion temporal templates," *Optik*, vol.125(7), pp. 1891-1896, 2014.

[3] D.K. Vishwakarma, R. Kapoor, and A. Dhiman, “A proposed unified framework for the recognition of human activity by exploiting the characteristics of action dynamics,” *Journal of robotics and autonomous system*, vol. 77, pp. 25-28, 2016.

[4] D. Zhao, L. Shao, X. Zhen, and Y. Liu, “Combining appearance and structural features for human action recognition,” *Neurocomputing*, vol. 113(3), pp. 88-96, 2013.

[5] D.K. Vishwakarma, and R. Kapoor, “Hybrid classifier based human activity recognition using the silhouette and cells,” *Expert Systems with Applications*, vol. 42(20), pp. 6957-6965, 2015.

[6] C. Achar, X. Qu, A. Mokhber, and M. Milgram, “A novel approach for action recognition of human actions with semi-global features,” *Journal of machine vision and application*, vol. 19 (1), pp.27-34, 2008.

[7] C. Lin, F. Hsu, and W. Lin, “Recognizing human actions using NWFE-based histogram vectors,” *EURASIP Journal of Advances in Signal Processing*, vol. 9, 2010.

[8] J. Gu, X. Ding, and S. Wang, “Action recognition from arbitrary views using 3D-key-pose set,”*Frontiers of Electrical and Electronic Engineering*, vol. 7(2), pp.224-241, 2012.

[9] L.Gorelick, M. Blank, E. Shechtman, M. Irani, and R. Basri, “Actions as Space-Time Shapes,” *IEEE Transactions on Pattern Analysis and Machine Intelligence*, vol. 29(12), pp.2247-2253, 2007.

[10] S. Sadek, A. Hamadi, M. Elmezain, B. Michaelis, and U. Sayed, “Human action recognition via affine moment invariants,” *International Conference on Pattern Recognition, Tsukuba*, pp. 218-221,2012.

[11] L. Presti, M. Cascia, S. Sclaroff, and O. Camps, “Hanklet-based dynamical systems modeling for 3-D action recognition,” *Journal Image and Vision Computing*, vol. 44(C), pp.29-43, 2015.

[12] A. Yilmaz, and M. Shah, “A differential geometric approach to representing the human actions,” *Computer Vision and Image Understanding (CVIU)*, pp .335-351 2008.

[13] K. Guo, P. Ishwar, and J. Konrad, “Action recognition from video using feature covariance matrices,” *IEEE Transaction on Image Processing*, vol. 22(6), pp. 2479-2494, 2013.

[14] Q. Li, H. Cheng, Y. Zhou, and G. Huo, “Human Action Recognition Using Improved Salient Dense Trajectories,” *Computational Intelligence and Neuroscience*, vol.5,pp.1-11, 2016.

[15] D. Wu, and L. Shao, “Silhouette analysis-based action recognition via exploiting human poses,” *IEEE transaction on circuits and systems for video technology*, vol. 23(2), pp. 236-243, 2013.

[16] S. A. Rahman, I. Song, M.K.H. Leung, I. Lee, and K. Lee, “Fast action recognition using negative space features,” *Expert System and Applications*, vol. 41(2), pp.574-587, 2014.

[17] I.G. Conde, and D.N Olivieri, “A KPCA spatiotemporal differential geometric trajectory cloud classifier for recognizing human actions in a CBVR system,” *Expert System and Applications*, vol. 42(13), pp.5472-5490,2015.

[18] B. Li, O.I. Camps, and M. Sznaier, “Cross-view activity recognition using Hanklets,” *International Conference on Computer Vision and Pattern Recognition, Providence*, 2012.

[19] Y. Shi, Y. Tian, Y. Wang, and T. Huang, “Sequential deep trajectory descriptor for action recognition with three-stream CNN,” *IEEE Transaction of Multimedia*, vol. 19(7), pp.1510-1520, 2017.

[20] A. Fathi, and G. Mori, “Action recognition by learning mid-level motion features,” *International Conference on Computer Vision and Pattern Recognition (CVPR), Anchorage*, 2008.

[21] X.L. Min, H.J. Xia, and T.L. Zheng, “Human action recognition based on chaotic invariants,”*Journal of South Central University*, pp. 3171-3179, 2014.

[22] Guha, T. and Ward, R.K., “Learning sparse representations for human action recognition,” IEEE

Transaction of Pattern Analysis and Machine Intelligence, 34(8), pp. 1576-1588, 2012.
[23] X. Wu, D. Xu, L. Duan, and J. Luo, "Action recognition using con-text and appearance distribution features," *International IEEE Conference on Computer Vision and Pattern Recognition (CVPR), Providence*, 2011.
[24] X. Wu and Y. Jia, "View-invariant action recognition using latent kernelized structural SVM," *Proceedings of the 12th European Conference on Computer Vision (ECCV), Florence, Italy*, 2012.
[25] E.A. Mosabbeb, K. Raahemifar, and M. Fathy, "Multi-view human activity recognition in distributed camera," *Sensors*, vol. 13(7), pp. 8750-8770, 2013.
[26] J. Wang, H. Zheng, J. Gao, and J. Cen, "Cross-view action recognition based on a statistical translation framework," *IEEE Transaction of Circuits Systems for Video Technology*, vol. 26(8), pp.1461-1475, 2016.
[27] Y. Wang, and G. Mori, "Human action recognition using semi-latent topic model," *IEEE Transactional of Pattern Analysis and Machine Intelligence*, vol. 31(10), pp. 1762-1764, 2009.
[28] A. Iosifidis, A. Tefas, and I. Pitas, "Discriminant bag of words based representation for human action recognition," *Pattern Recognition Letters*, vol. 49(C), pp. 185-192, 2014.
[29] D. Weinland, M. Özuysal, and P. Fua, "Making action recognition robust to occlusions and viewpoint changes," *European Conference on Computer Vision (ECCV), Crete, Greece*, 2010.
[30] L. Wang, Y. Qiao and X. Tang, "Action recognition with trajectory pooled deep-convolutional descriptors," *IEEE Conference on Computer Vision and Pattern Recognition*, pp. 4305-4314, 2015.
[31] L. Sun, K. Jia, D-Y. Yeung, and B.E. Shi, "Human action recognition using factorized spatiotemporal convolutional networks," *IEEE International Conference on Computer Vision (ICCV)*, pp. 4597-4605, 2015.
[32] Z. Zhang, W. Chunheng, X. Baihua, Z. Wen, and L. Shuang, "Action Recognition Using Context-Constrained Linear Coding," *IEEE Signal Processing Letters*, vol. 19(7), pp. 439-442, 2012.
[33] A. Kovashka, and K. Grauman, "Learning a hierarchy of discriminative space-time neighborhood features for human action recognition," *Proceedings of IEEE Computer Society Conference on Computer Vision and Pattern Recognition*, pp. 2046-2053, 2010.
[34] I. Laptev, M. Marszalek, C. Schmid, and B. Rozenfield, "Learning realistic human actions from movies," *Proceedings of IEEE Computer Society Conference on Computer Vision and Pattern Recognition*, pp.1-8, Jun.2008.
[35] C. Schuldt, I. Laptev, and B. Caputo, "Recognizing human actions: a local SVM approach," *Proceedings of the 17th International Conference on Pattern Recognition, Cambridge*, 2004.
[36] D. Weinland, R. Ronfard, and E. Boyer, "Free viewpoint action recognition using motion history volumes," *Computer Vision and Image Understanding*, vol. 104(2-3), pp. 249-257, 2006.
[37] H. Liu, M. Liu, and Q. Sun, "Learning directional co-occurrence for human action classification," *IEEE International Conference on Acoustics, Speech, and Signal Processing (ICASSP)*, pp. 1235-1239, 2014.
[38] P. Dollar, V. Rabaud, G. Cottrell, and S. Belongie, "Behavior recognition via sparse spatiotemporal features," *IEEE International Workshop on Visual Surveillance and Performance Evaluation of Tracking and Surveillance*, pp. 65-72, 2005.
[39] M. Ryoo, "Human activity prediction: Early recognition of ongoing activities from streaming videos," *IEEE International Conference on Computer Vision (ICCV)*, pp. 1036-1043, 2011.
[40] Q. Sun, and H. Liu, "Action disambiguation analysis using normalized Google-like distance correlogram," *Springer Asian Conference on Computer Vision (ACCV)*, pp. 425-437, 2012.
[41] Q. Sun, and H. Liu, "Learning spatiotemporal co-occurrence correlograms for efficient human action classification," *IEEE International Conference on Image Processing (ICIP)*, pp. 3220-3224, 2013.
[42] J. Wang, J. Yang, K. Yu, F. Lv, T. Huang, and Y. Gong, "Locality constrained linear coding for image classification," *Proc. CVPR*, pp. 3360-3367, Jun. 2010.
[43] I. Laptev, "On space-time interest points," *International Journal of Computer Vision*, vol. 64(2-3), pp. 107-123, Sep.2005.

Authors' Profiles

Mr. Om Mishra is a research scholar in Department of Electronics & Communication, Delhi Technological University, Delhi, India. He has worked as an Assistant Professor in G.B. Pant Government Engineering College, New Delhi, India. He received Master of Engineering in Electronics & Communication Engineering from Delhi College of Engineering (Presently DTU), Delhi, India. His Research interest includes Vision based Activity Recognition, Signal Processing, Pattern Recognition.

Dr. Rajiv Kapoor is a Professor in Delhi Technological University, Delhi, India. He worked as Principal in AIACTR, Delhi, India in diverted capacity. He is Ph.D. in Electronics and Communication Engineering from Punjab Engineering College, India. His Research interest include Vision/Speech based Tracking, Activity Recognition Vision/Speech based, Signal Processing, Pattern Recognition. He has published more than 100 research papers in International Journals and Conferences. He is also an author of books published in IGI Global and Springer. He has been a Principal Investigator of sponsored projects, Government of India.

Dr. M.M. Tripathi is a Professor in Electrical Engineering Department of Delhi Technological University, Delhi, India. He has also worked as Scientist with the Institute for Plasma Research, India and National Institute of Electronics & Information Technology, India. He is Ph.D. in Electrical Engineering from G. B. Technical University, India. His research interests include Artificial Intelligence applications, Renewable energy and Power system

restructuring. He has published more than 30 research papers in International Journal and Conferences. Presently, he is Director, IQAC, Delhi Technological University, Delhi.

How to cite this paper: Om Mishra, Rajiv Kapoor, M.M. Tripathi, "Human Action Recognition Using Modified Bag of Visual Word based on Spectral Perception", International Journal of Image, Graphics and Signal Processing(IJIGSP), Vol.11, No.9, pp. 34-43, 2019.DOI: 10.5815/ijigsp.2019.09.04

Copyright © 2019 MECS

Impact of cryogenic cooling during machining: A Literature Review

Anurag Sharma1, R.C. Singh2, Ranganath M.Singari3
[1,2,3]Department Mechanical of Engineering, Delhi Technological University, Delhi, India

Abstract- Evolution in new engineering materials like difficult to cut materials, super alloys & composites materials and following of strict international norms during machining the use of conventional cutting fluids are unsatisfactory. Liquid nitrogen is better eco friendly and efficient coolant available. This is a step forward towards green machining. Direct supply of LN2 at the interface of tool and workpiece removes heat fast and make the temperature low. Co- efficient of friction, cutting force, cutting temperature, tool wear and surface roughness between tool and workpiece are reduced by 20-35%, 50-75%, 60-82%, 50-60% and 35-50% in comparison to dry machining respectively.
Keywords – Cryogenic cooling, Liquid nitrogen, cutting insert, dry machining, cutting fluid

I. INTRODUCTION

Dry machining is non polluting but it is restricted to low cutting parameters. This results in low manufacturing rate. Conventional cutting fluids can no longer be used during machining due to the development of new engineering materials to fulfill the ever rising demand of world and community [1-4]. Cryogenic cooling with LN2 is better available alternate. This is eco friendly and operator friendly. LN2 is colorless, odorless, tasteless and do not produce any toxic fumes. The boiling point of LN2 is -196°C. The high rate of heat transfer makes it efficient coolant for removing heat [5-7]. It is shown in Fig. 1 that during turning LN2 is directly supplied at the rake face of cutting tool and workpiece. LN2 is stored in Dewar container and passed through insulated pipes at the specified position. Compressor is used to supply compressed air in the container. Pressure regulator is used to keep the supply constant. Flow meter is used for measuring the flow rate.

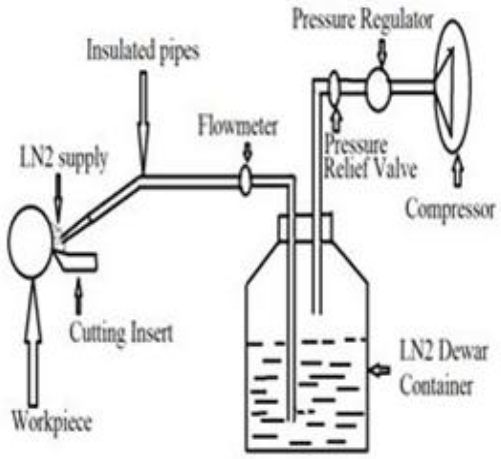

Fig.1. Schematic process of cryogenic machining

II. LITERATURE REVIEW:

2.1 Work done by researchers in Cryogenic Cooling

Cryogenic cooling means cooling the surface below 0°C to - 196°C. At low temperature the metallurgical properties of materials get changed e.g. porous materials become hard. This cooling is done by liquid nitrogen, solid carbon dioxide or other refrigerated non toxic gas and chilled air. The cutting temperature reduced by 60-70%.

Sno.	Author, Year, Reference No., Title of paper	Work Done	Results/ Findings

1	Mputz et al. 2016 [1]: Investigation of turning elastomers assisted cryogenic cooling.	Investigated approach to enhance machinability with cryogenic cooling during cutting elastomer components	Liquid Nitrogen used to cool down elastomers before machining. The surface quality was improved.
2	M.J. Bermingham et al. 2011 [2]:New observation on tool life, cutting forces and chip morphology in cryogenic machining Ti-6Al-4V	Investigated the effectiveness of cryogenic coolant during turning of Ti-6AI-4V at constant speed and material removal rate (125m/min, 48.5cm3/min) with different combinations of feed rate and depth of cut	Cryogenic coolant was effective in extending tool life compared to dry cutting for all machining parameters
3	Xinda Huang et al. 2014[3]: The influence of cryogenic cooling on milling stability.	Experimental studied the effect of cryogenic cooling on milling stability using a dedicated cryogenic cooling system for applying liquid nitrogen (LN2) jet to cutting zone.	Cryogenic cooling was enhanced the stability limits in end milling by 50-100%
4	N Yuvaraj et al. 2016 [4]: Cutting aluminium alloy with abrasive water jet and cryogenic assisted abrasive water jet: A comparative study of the surface integrity approach.	Cutting aluminium alloy with abrasive water jet and cryogenic assisted abrasive water jet: A comparative study of the surface integrity approach	CAAW Cutting process enhanced the functional performance of cut surface and uniform surface roughness pattern.
5	J.Schoop et al. 2013[5]:The effects of depth of cut pre cooling on surface porosity in cryogenic machining of porous tungsten.	Investigated the influence of cryogenic pre-cooling time and depth of cut on the attainable surface morphology of porous tungsten.	Result showed that increased pre-cooling significantly altered the deformation mechanism during machining.
6	Aman Aggarwal et al. 2008 [6]: Optimization of multiple quality characteristics for CNC turning under cryogenic cutting environment during desirability function	Optimized multiple characteristics (tool life, cutting force, surface roughness and power consumption) in CNC turning of AISP-20 tool steel using nitrogen as coolant.	Models developed were adequate in explaining the effect of independent parameters on responses.
7	Shane Y. Hong et al. 2001[7]: Cooling approaches and cutting temperature in cryogenic machining of Ti-6Al-4V	Introduced an innovative and economical dispensing method that directed LN2 through microjets to the flank, rake or both near the cutting edge in the turning of Ti6A1-4V alloy	Results showed that small amount of liquid nitrogen applied locally to the cutting edge was superior to emulsion cutting in lowering the temperature.
8	K.Aslantas et al. 2016[8]: Performance evaluation of a hybrid cooling lubrication system in micro - milling of Ti6Al4Valloy	Presented a hybrid system for cooling and lubrication in micro-milling of Ti6A14V alloy. Hybrid system was based on mixing oil with chilled air	Result showed that hybrid system gave minimum tool wear and burr size.
9	Nabil Ben Fredj et al. 2006[9]: Ground surface improvement of the austenitic stainless steel AISI 304 using cryogenic cooling	Presented evaluation of ground surface quality improvements of the austenitic stainless steel AISI 304 resulting from the application of cryogenic cooling.	Due to cryogenic cooling surface roughness reduced by 40%.
10	Le De Chiffre et al.	Investigated efficiency of cryogenic	Results showed that cryogenic

	2007[10]:Performance testing of cryogenic CO2 as cutting fluid in parting/ grooving and threading austenitic stainless steel.	CO2 and compared a commercial water based cutting fluid in terms of tool life, surface finish, chips disposal etc.	CO2 was an alternative as compared to water based cutting fluid
11	Weiwei Wu et al. 2017 [11]: The reinforcing effect of graphene nano platelets on the cryogenic mechanical properties of GNPs/Al2O3 composites	Presented the GNPs/Al2O3 (Graphene nano platelets reinforced alumina) fabricated by colloidal process. The optimum content of GNPs in GNPs/Al2O3 composite was 1.0 vol%.	Presented the GNPs/Al2O3 (Graphene nano platelets reinforced alumina) fabricated by colloidal process. The optimum content of GNPs in GNPs/Al2O3 composite was 1.0 vol%.
12	Y. Kayank et al. 2013 [12]: Tool-wear analysis in cryogenic machining of NiTi shape memory alloys: A comparison of tool-wear performance with dry and MQL machining	Examined the effets of cryogenic cooling on tool-wear rate and progressive tool-wear by comparing new findings from cryogenic machining with MQL and dry machining.	Cryogenic cooling was effective on reducing tool-wear rate at high cutting speeds and reducing flank wear and notch wear.
13	Satish et al. 2015 [13]: Machining of hardened steel - experimental investigations, performance modeling and cooling techniques: A review	Presented a comprehensive literature review on marching of hardened steels using coated tools, studies related to hard turning, different cooling method and attempt so far to machining performance	Optimal combination of low feed and low depth of cut with higher cutting speed was beneficial for reducing machining force and surface roughness.
14	E.M. Rubio et al. 2015[14]: Cooling systems based on cold compressed air a review of the applications in machining process.	Collected the review and analysised the cooling systems based on cold compressed	Results showed that cold compressed air is a real environmental friendly alternative to other conventional lubrication / cooling systems
15	Vishal S.Sharma et al. 2009[15]:Cooling techniques for improved productivity in turning.	Presented an overview of major advances in techniques as minimum quantity lubrication (MQL) / near dry machining (NDM), high pressure coolant (HPC) cryogenic cooling, compressed air cooling and used of solid lubricants coolants.	Result showed that coconut oil as coolant was encouraging at lower speeds. All types of cooling techniques gave good response with almost all tool material, particular with carbide (coated/uncoated) and PCBN.
16	C.Courbon et al. 2013[16]:Tribological behaviour of Ti6 Al4V and Inconel 718 under dry and cryogenic conditions application to the context of marching with carbide tools	Investigated the cooling and lubrication capabilities of nitrogen jet under extreme contact conditions using a dedicated tribometer..	Neither liquid nor gas nitrogen was able to decrease the co-efficient of friction and material transfer when Ti6Al4V and uncoated carbide pins were used, but a significant improvement was noted for Inconel 718 and TiN coated pins
17	Yang Gao et al. 2016[17]:Effects of keep cryogenic treatment on the microstructure and properties of WC-Fe-Ni cemented carbides.	Investigated the effects of deep cryogenic treatment on microstructure and properties of WC-Fe-Ni cemented carbides. The specimens were treated about -196° C for 2,12 and 24 hours.	The mastensite transformation temperature for WC-Fe-Ni cemented carbide was approximately - 23.28°C. The hardness and TRS of WC-FE-Ni cemented carbides after deep cryogenic treatment was higher

			than untreated ones.
18	A.I. Tyshchenko et al. 2010 [18]: Low-temperature martensitic transformation and deep cryogenic treatment of a tool steel.	The tool steel X220 CrV Mo 13-14 (DIN 1.2380) containing (mass%) 2.2C, 13 Cr, 4V,1Mo and the binary alloy Fe2 O3 mass%C were studied using transmission electron microscopy. It was cryogenically cooled to - 50°C	he results showed that , there was an increase in the density of dislocations, captured of immobile carbon atoms by moving dislocations and strain induced partial dissolution of carbide phase.
19	Alborz Shokrani et al. 2016[19]: Investigation of the effects of cryogenic machining on surface integrity in CNC end milling of Ti-6Al- 4Vi titanium alloy	Presented first comprehensive investigation on the effects of cryogenic cooling using liquid nitrogen on surface integrity of Ti-6Al-4V titanium alloy workpiece in milling operations	Results showed that 39% and 31% lower surface roughness when compared to dry and flood cooling methods respectively.
20	J. Schoop et al. 2016[20]: Cryogenic machining of porous tungsten for enchanced surface integrity.	Investigated cryogenic machining of porous tungsten was developed as alternative sustainable process to current industry practice of machining plastic infiltrated workpieces.	Results showed that by using modified polycrystalline diamond cutting tool, high speed cryogenic machining of porous tunsten by ductile shear was achieved. Cutting speed of 400m/min and low surface roughness Ra ~ 0.4 µm
21	B. Podgernik et al. 2012[21]: Improving tribological properties of tool steels through combination of deep - cryogenic treatment and plasma nitriding	Investigated the effect of deep cryogenic treatment parameters (time and temperature) in combination with plasma nitriding on the tribological performance of powder - metallurgy (P/M) high speed steel.	Results showed that deep cryogenic treatment contributed to improved abrasive wear resistance plasma nitriding improved tribological properties of P/M high speed steel and reduced the effect of austenzing temperature
22	Shaohong Li et al. [2013], [22]. Experimental verification of segregation of carbon and precipitation of carbides due to steel by internal friction method.	Presented an internal frictional behaviour of cold work tool steel subjected to different heat treatment schedules to get insight to segregation of carbon and refinement of carbide particles due to deep cryogenic treatment.	Results showed that interstitial carbon atoms migrated and segregated near by dislocations of shrinking strain energy during deep cryogenic treatment.
23	Shane Y. Hong et al. 2001[23]: Micro temperature manipulation in cryogenic machining of low carbon steel	Presented an environmentally safe approach of micro manipulation of cutting temperature in machining AISI /SAE 1008 low carbon steel.	Results showed that chip breaking was improved by cryogenic cooling the chip to below the embrittlemnt temperature -55°C the tool wear decreased and increased tool life..
24	F. Pusavec 2012 [24]: Porous tungsten machining under cryogenic conditions.	Experimentally studied on high performance machining of porous tungsten under cryogenic conditions	Cryogenic method was compared with traditional carbide tools PCD, CBN, ceramic etc. Results showed cryogenic was capable of producing unsemeared surfaces. The surface finish was improved.
25	Vojteh Leshovsek et al. 2012[25]: Vaccum heat treatment deep cryogenic treatment and simultaneous pulse plasma nitriding and tempering of	Presented vaccum heat treatment deep cryogenic treatment and pulse plasma nitriding were efficient techniques to improve properties of tool and high speed steels.	Results showed that deep cryogenic treatment improved the micro structure of investigated P/M high speed steel.

	P/M 5390 MC Steel.		
26	V.G. Dhokia et al. 2011[26]: A process control system for cryogenic CNC elastomer.	Presented the novel concept of cryogenic CNC maching of elastomers and development of a process control system for cryogenic CNC machining.	Results showed that the surface finish was very good as compared to other conventional methods.
27	Shaohong Li et al. 2010[27]: Influence of deep cryogenic treatment of microstructure and evaluation by internal friction of a tool steel.	Studied deep cryogenic treatment (DCT) on microstructure of tool steel.	Results showed that retained austenite was present in a thin film between laths of martensite and stably existed even during prolonged soaking time in liquid nitrogen. Hardness and wear resistance on tool steel increased.

III.CONCLUSION

1. The liquid nitrogen is an efficient and eco friendly coolant during machining.
2. It leaves no residue after applying at the interface of tool and workpiece.
3. The metal scrap after machining do not require any treatment for removing any oil deposits or toxic elements and can be readily available as a source of recycling material for further industrial use.
4. The tool life during cryogenic cooling is increased by 70-80% as compared to dry machining and 30-50% in wet machining using conventional cutting fluids.
5. Co- efficient of friction, cutting force, cutting temperature, tool wear and surface roughness between tool and workpiece are reduced by 20-35%, 50-75%, 60-82%, 50-60% and 35-50% in comparison to dry machining respectively.

IV. REFERENCES

[1] M. Putz, M. Dix, M. Neubert, G. Schmidt, R. Wertheim, "Investigation of turning Elastomers Assisted with cryogenic cooling," Procedia CIRP, vol. 401, pp. 631-636, 2016.

[2] M. J. Bermingham, J Kirsch, S. Sun, S. Palanisamy, M.S. Dargusch, "New Observations on tool life cutting forces and chip morphology in cryogenic machining Ti - 6Al - 4V", International Journal of Machine Tools & Manufacture,vol. 51, pp. 500-511, 2011.

[3] N. Huang, X. H. Ding,H. Mou, X. Zhang, H. Ding, " The influence of cryogenic coolingon milling stability", Journal of Material Processing Techonolgy, vol. 214, pp. 3169-3178, 2014.

[4] N. Yuvaraj, M. Pradeep Kumar, "Cutting of aluminum alloy with abrasive water jet and cryogenic abrasive water jet: A comparative study of the surface", Wear, vol. 362-363, pp.18-32, 2016.

[5] J. Schoop, M. Effgen, J. J. Balk, I. J. Jawahir, "The effects of depth in of cut and pre cooling on surface porosity in cryogenic machining of porous tungsten", Procedia CIRP, vol. 8, pp. 357-362, 2013.

[6] A. Aggarwal, H. Singh, P. Kumar, M. Singh, "Optimization of multiple quality characteristics for CNC turning under cryogenic cutting environment using desirability function", Journal of Materiasl Processing Technology, vol. 205, pp. 42-52, 2008.

[7] S. Y. Hong,Y. Ding, "Cooling approaches and cutting temperatures in cryogenic machining of Ti - 6Al - 4V", International Journal of Machine Tools and Manufacture, vol. 41, pp. 1417-1437, 2001.

[8] K. Aslantas, A. Cicek, I. Ucum, M. Percin, H.E. Hopa, "Performance evaluation of a hybrid cooling lubrication system in micro milling of Ti6Al4V alloy", Procedia CIRP, vol. 46,pp. 492-495, 2016.

[9] N. B. Fredj, H. Sidhem, C. Braham, "Ground surface improvement of the austentitic stainless steel AISI 304 using cryogenic cooling", Surface & Coatings Technology, vol. 200, pp. 4846-4860, 2006.

[10] L. De Chiffre, J. L. Andreasen, S. Lagerberg, I. B. Thesken, "Performance testing of cryogenic CO2 as cutting fluid in parting /grooving and threading austenitic stainless steel", Annals of CIRP, vol. 56, No.1, pp.101-104, 2007.

[11] W. Wu, J. Gui, W. Sai, Z. Xie, "The reinforcing effect of graphene nano platelets on the cryogenic mechanical properties of GNPs/Al2O3 composites", Journal of Alloys and compounds, vol.691,pp. 778-785, 2017.

[12] Y. Kayank, H. E. Karaca, R. D. Noebe, I. S. Jawahir, "Tool – wear analysis in cryogenic machining of NiTi shape memory alloys: A comparison of tool- wear performance with dry and MQL machining",Wear, vol.306, pp.51-63, 2013.

[13] S. Chinchanikar, S. K. Chaudhary,"Machining of hardened steel - Experimental investigations, performance modeling and cooling techniques: A review", International Journal of machine Tools & Manufacture, vol. 89, pp. 95-109, 2015.

[14] E. M. Rubio, B. Agustina, M. Marin, A. Bericua, "Cooling Systems based on cold compressed air: A review of the applications in machining processes", Procedia Engineering, vol. 132, pp. 413-418, 2015.

[15] V. S. Sharma, M. Dogra, N. M. Suri, "Cooling techniques for improved productivity in turning, International Journal of Machine Tools & Manufacture", vol. 49, pp.435-453, 2009.

[16] C. Courbon, F. Pursavec, F. Dumont, J. Rech, J. Kopac, "Tribological behaviour of Ti6Al4V and Inconel 718 under dry and cryogenic conditions - Application to the context of machining with carbide tools ", Tribology Inernational, vol. 66, pp. 72-82, 2013.

[17] Y. Gao, B. H. Lo, Z. Bai, Z. S. Ouyang, "Effects of deep cryogenic treatment on the microstructure and properties of Wc- Fe - Ni cemented carbides", Int. Journal of Refractory Metals and Hard Materials, vol. 58, pp. 42-50, 2016.

[18] M. Anthony Xavior, M. Adithan, "Determing the influence of cutting fluids on tool wear and surface roughness during turning of AISI 304 austentic stainless steel", Journal of Material Processing Technology, vol. 209, pp. 900-909, 2009.

[19] A.I.Tyshchenko, W. Theisen, A. Oppenkowski, S. Siebert, O. N. Razumov, A. P. Shoblik, V. A. Sirosh, Y. N. Petra, V.G. Gavriljuk, "Low temperature martensitc transformation and deep cryogenic treatment of a tool steel", Materials Science and Engineering A, vol. 527, pp. 7027-7039, 2010.
[20] A. Shokrani, V. Dhokia, S. T. Newman, "Investigation of the effects of cryogenic machining on surface integrity in CNC end milling of Ti - 6Al - 4V titanium alloy", Journal of Manufacturing Processes, vol. 21, pp. 172-179, 2016.
[21] J. Schoop, F. Ambrosy, F. Zanger, V. Schelze T. J. Balk, I.S. Jawahir, "Cryogenic machining of porous tungsten for enhanced surface ", Journal of Material Processing Technology, vol. 229, pp. 614-621, 2016.
[22] B. Podgornik, F. Majdic, V. Leskovsek, J. Vizinth, "Improving tribological properties of tool steels through combination of deep cryogenic treatment and plasma nitriding ", Wear, vol. 288, pp. 88-93, 2012.
[23] L. Shaohong, Namin, L. Junwan, W. Xiaochun, L. Chentui, T. Leilei, "Experimental verification of segregation of carbon and precipitation of carbide due to deep cryogenic treatment for steel by internal friction method", Materials Science & Engineering A, vol. 575, pp. 51-60, 2013.
[24] S. Y. Hong, Y. Ding, "Micro Temperature manipulation in cryogenic machining of low carbon steel", Journal of Material Processing Technology, vol. 116, pp. 22-30, 2001.
[25] F. Pusavec, "Porous tungsten machining under cryogenic conditions", Int. Journal of Refractory Metals and Hard Haterial, vol. 35, pp. 84-89,2012.
[26] V. Leskovsek, B. Podgornik, "Vacuum heat treatment deep cryogenic treatment and simultaneous pulse plasma nitriting and tempering of P/M S390MC steel", Material Science and Engineering A, vol. 531, pp. 119-129, 2012.
[27] V.G. Dhokia, S. T. Newman, P. Crabtree, M.P. Ansell, "A process control system for cryogenic CNC elastomer machining", Robotics and Computer Integrated Manufacturing, vol. 27,pp. 779-784, 2011.

ResearchGate

See discussions, stats, and author profiles for this publication at: https://www.researchgate.net/publication/335715807

Inverse Band Reject and All Pass Filter Structure Employing CMOS CDBAs

Article · September 2019

CITATIONS
0

READS
46

3 authors, including:

Ram Bhagat
Delhi Technological University
6 PUBLICATIONS **5** CITATIONS
SEE PROFILE

Data Ram Bhaskar
Delhi Technological University
5 PUBLICATIONS **3** CITATIONS
SEE PROFILE

Some of the authors of this publication are also working on these related projects:

Novel OTA based inductorless realisation of Chaos's circuit View project

All content following this page was uploaded by Ram Bhagat on 10 September 2019.

The user has requested enhancement of the downloaded file.

Published by :
http://www.ijert.org

International Journal of Engineering Research & Technology (IJERT)
ISSN: 2278-0181
Vol. 8 Issue 09, September-2019

Inverse Band Reject and All Pass Filter Structure Employing CMOS CDBAs

Ram Bhagat
Department of Electrical Engineering
Delhi Technological university
Delhi, India

D. R. Bhaskar
Department of Electronics and Communication Engineering
Delhi Technological university
Delhi, India

Pragati Kumar
Department of Electrical Engineering
Delhi Technological university
Delhi, India

***Abstract*— In this paper a new voltage-mode (VM) circuit for the realization of second order tuneable inverse band reject filter (IBRF) and inverse all pass filter (IAPF) have been introduced. The proposed circuit uses two current differencing buffered amplifiers (CDBA), two capacitors and four/five resistors. PSPICE simulation results employing CMOS CDBA implemented in 0.18µm CMOS TSMC technology have been presented to validate the workability of the configuration.**

Keywords*— *Analog Inverse Filters, Current Differencing Buffered Amplifier, Analog Signal Processing

I. INTRODUCTION

An analog inverse filter provides frequency selective characteristics which are opposite to those of the corresponding analog filter. These inverse filters are used to remove the effect of distortion introduced in the signal while it is processed through a system. Inverse filters find applications in control, instrumentation and communication systems [1]. Recently, a number of analog inverse active filterswith different properties have been realised with different active building blocks(ABB) like operational amplifiers (op-amps) [2], current feedback operational amplifiers (CFOAs) [3]-[7], second generation current conveyors CCIIs [8], [9], four terminal floating nullors (FTFNs) [10], [11], operational transresistance amplifiers (OTRAs) [13], [14] current differencing buffered amplifiers (CDBAs) [15], [16], current differencing transconductance amplifiers CDTAs [17], [18], operational transconductance amplifiers OTAs [19], differential difference current conveyors (DDCCs) [20] and voltage differencing transconductance amplifiers (VDTAs) [21]. However, there are few number of research publications for realising second order IBRF [3], [4], [7], [12], [14], [16] and IAPF [11], [12] and [14].

The CDBA has received prominent attention in analog signal processing and signal generation circuits due to its important property of providing at its input terminals virtual ground, which eliminates the effect of parasitic at the input terminals. Apart from this, its low output impedance enables the CDBA based circuit configurations to be cascaded easily.

From existing literature survey, it has been observed that only two circuit structures have been reported so far to realize second-order inverse active filters employing CDBAs [15], [16]. [15] has reported two CDBA based second order inverse low pass filter (ILPF) with four resistors and two capacitrs, inverse high pass filters (IHPF) using two resistors and four capacitors and inverse band pass filter (IBPF) with three resistors and three capacitors whereas in [16] the ILPF circuit is realized with four resistors and two capacitors the other four circuits namely, IHPF, IBPF, IBRF and IAPF have been realised with 3-4 capacitors and 2-4 resistors. Also none of these two reported inverse filters have utilized the intrinsic (current differencing) property of the CDBA, as n-terminal of one of the CDBA has been left open resulting into employment of more than two capacitors for realization of second order inverse filters of different types in many cases (IBPF, IHPF, IBRF and IAPF).

Therefore, the purpose of this communication is to present a new inverse filter circuit configuration employing two CDBAs with their intrinsic (current differencing) property fully utilized, four/five resistors and only two capacitors along with a switch. The realised second order IBRF has independent control of cut-off frequency and bandwidth while IAPF has independent tunability of cut-off frequency. The workability of the presented inverse filters has been verified using PSPICE simulations implemented in TSMC 0.18µm CMOS technology.

II. THE PROPOSED CONFIGURATION

The symbolic representation of the CDBA is shown in Fig.1, where p and n are current input terminals (with ideally zero input impedances), w is the voltage output terminal (ideally zero output impedance) and z is the current output terminal (ideally infinite output impedance).

The characterising terminal equations of an ideal CDBA are given by:

$$I_z = (I_p - I_n),\ V_p = 0 = V_n \text{ and } V_w = V_z \qquad (1)$$

The proposed configuration for the realization of IBRF and IAPF with two capacitors and four/five resistors is shown in Fig. 2.

(This work is licensed under a Creative Commons Attribution 4.0 International License.)

International Journal of Engineering Research & Technology (IJERT)
ISSN: 2278-0181
Vol. 8 Issue 09, September-2019

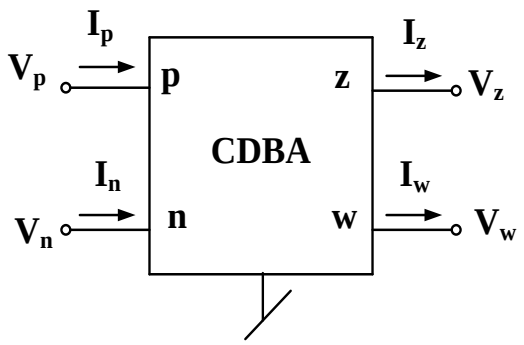

Fig. 1 Symbolic representation of CDBA

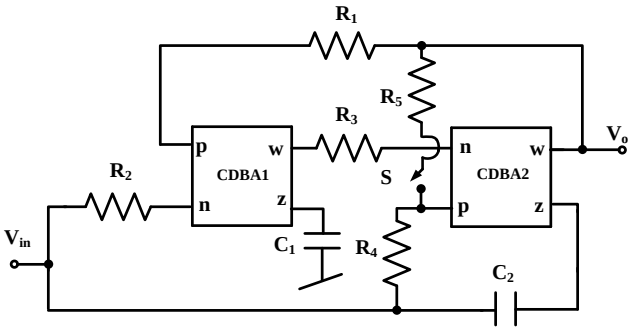

Fig. 2. The proposed inverse filer structure

Realization of IBRF and IAPF responses from Fig. 2 is as follows:

Case I: When switch 'S' is open the resulting transfer function becomes

$$\frac{V_o(s)}{V_{in}(s)} = \frac{1}{s^2 + \frac{1}{R_1R_3C_1C_2}} \Big/ \frac{s^2 + \frac{1}{R_4C_2}s + \frac{1}{R_2R_3C_1C_6}} \quad (2)$$

which represents an IBRF with cut-off frequency (ω_0) and bandwidth (BW) given by:

$$\omega_o = \frac{1}{\sqrt{R_2R_3C_1C_2}} \quad \text{For} R_1 = R_2 \text{ and}$$
$$BW = \frac{1}{R_4C_2} \quad (3)$$

Case II: When switch 'S' is closed the resulting transfer function will be given by:

$$\frac{V_o(s)}{V_{in}(s)} = \frac{1}{s^2 - \frac{1}{R_7C_6}s + \frac{1}{R_1R_3C_1C_2}} \Big/ \frac{s^2 + \frac{1}{R_4C_2}s + \frac{1}{R_2R_3C_1C_2}} \quad (4)$$

which realizes an IAPF with ω_0 and *BW* given by:

$$\omega_o = \frac{1}{\sqrt{R_2R_3C_1C_2}} \quad \text{For} R_1 = R_2 \text{ and}$$
$$BW = \frac{1}{R_4C_2} \text{For} R_4 = R_5 \quad (5)$$

Thus, it is clear that from equation (3), both ω_0 and *BW* can be tuned independently i.e. ω_0 through R_3/C_4 and *BW* through R_4

III. NON-IDEAL ANALYSIS

The non-ideal representation of the CDBA taking into account the parasitic at various terminals is shown in Fig.3, where parallel combination of R_z and 1/sCz is the parasitic impedance at port z, R_p and R_n are the parasitic resistances at terminals p and n respectively and R_o is the parasitic output resistance at terminal w.

A practical CDBA can be described [22] by the following relationships that take into account the non-idealities of the device:

$$V_P = V_n = 0, I_Z = \beta_P I_P - \beta_n I_n \text{and} V_W = \alpha V_Z \quad (6)$$

where $\beta_P = (1-\varepsilon_P)$ and $\varepsilon_p(|\varepsilon_p| \ll 1)$ is the current tracking error from p-terminal to z-terminal, $\beta_n = (1-\varepsilon_n)$ where $\varepsilon_n(|\varepsilon_n| \ll 1)$ is the current tracking error from n-terminal to z-terminal, and $\alpha = (1-\varepsilon_v)$ with $\varepsilon_v(|\varepsilon_v| \ll 1)$ is the voltage tracking error from *z*-terminal to w-terminal of the CDBA. In addition to the above, if we also consider parasitic impedances at z-terminal and parasitic resistances at p, n and w terminals of CDBA as shown in Fig. 3 and reanalyze the circuits of Fig. 2, we get the following non-ideal transfer functions of inverse active filters:

The non-ideal expression of IBRF is given by

$$\left.\frac{V_o(s)}{V_{in}(s)}\right|_{IBRF} = \frac{1}{\frac{1}{\alpha_2}s^2 + Bs + C} \Big/ \frac{s^2 + Ms + N}{} \quad (7)$$

where

$$B = \frac{1}{\alpha_2C_1(C_2 + C_{Z2}) + \alpha_2C_{Z1}(C_2 + C_{Z2})}\left(\frac{C_1}{R_{z2}} + \frac{C_{z1}}{R_{z2}} + \frac{C_2}{R_{z1}} + \frac{C_{z2}}{R_{Z1}}\right)$$

$$C = \frac{1}{\alpha_2C_1(C_2 + C_{Z2}) + \alpha_2C_{Z1}(C_2 + C_{Z2})}\left(\frac{\alpha_1\alpha_2\beta_{n1}\beta_{P2}}{R_1R_3}\right)$$

$$M = \frac{1}{\alpha_2C_1(C_2 + C_{Z2}) + \alpha_2C_{Z1}(C_2 + C_{Z2})}\left(\frac{\alpha_2C_1}{R_{z2}} + \frac{\alpha_2C_{z1}}{R_{z2}} + \frac{\alpha_2C_2}{R_{z1}} + \frac{\alpha_2C_{Z2}}{R_{Z1}} + \frac{C_4\beta_{P2}}{R_4} + \frac{C_{z1}\beta_{P2}}{R_4}\right)$$

$$N = \frac{1}{\alpha_2C_1(C_2 + C_{Z2}) + \alpha_2C_{Z1}(C_2 + C_{Z2})}\left(\frac{\alpha_1\alpha_2\beta_{n1}\beta_{n2}}{R_2R_3} + \frac{\alpha_2}{R_{Z2}R_{z1}}\right)$$

The non-ideal expressions of IAPF when switch 'S' is closed:

(This work is licensed under a Creative Commons Attribution 4.0 International License.)

International Journal of Engineering Research & Technology (IJERT)
ISSN: 2278-0181
Vol. 8 Issue 09, September-2019

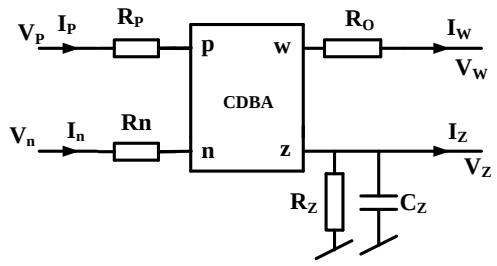

Fig. 3. Non-ideal CDBA with Parasitic elements

$$\left.\frac{V_O(s)}{V_{in}(s)}\right|_{IAPF} = \frac{\dfrac{1}{\alpha_2}s^2 + Bs + C}{s^2 + Ms + N} \tag{8}$$

where

$$B = \frac{1}{\alpha_2 C_1(C_2 + C_{Z2}) + \alpha_2 C_{Z1}(C_2 + C_{Z2})}\left(\frac{C_1}{R_{z2}} + \frac{C_{Z1}}{R_{z2}} + \frac{C_2}{R_{z1}} + \frac{C_{Z2}}{R_{Z1}} - \frac{\alpha_2\beta_{P2}(C_4 + C_{Z1})}{R_4}\right)$$

$$C = \frac{1}{\alpha_2 C_1(C_2 + C_{Z2}) + \alpha_2 C_{Z1}(C_2 + C_{Z2})}\left(\frac{\alpha_1\alpha_2\beta_{n1}\beta_{P2}}{R_1R_3} - \frac{\alpha_2\beta_{P2}}{R_{z1}R_4}\right)$$

$$M = \frac{1}{\alpha_2 C_1(C_2 + C_{Z2}) + \alpha_2 C_{Z1}(C_2 + C_{Z2})}\left(\frac{\alpha_2 C_4}{R_{z2}} + \frac{\alpha_2 C_{Z1}}{R_{z2}} + \frac{\alpha_2 C_6}{R_{z1}} + \frac{\alpha_2 C_{Z2}}{R_{Z1}} + \frac{C_4\beta_{P2}}{R_4} + \frac{C_{Z1}\beta_{P2}}{R_4}\right)$$

$$N = \frac{1}{\alpha_2 C_1(C_2 + C_{Z2}) + \alpha_2 C_{Z1}(C_2 + C_{Z2})}\left(\frac{\alpha_1\alpha_2\beta_{n1}\beta_{n2}}{R_2R_3} + \frac{\alpha_2}{R_{Z2}R_{z1}}\right)$$

Since the value of R_z is very high and the value of C_z is very low, therefore, the inverse filter transfer functions can be approximated as:

$$\left.\frac{V_0(s)}{V_{in}(s)}\right|_{IBRF} \cong \frac{1}{\dfrac{s^2}{\alpha_2} + \dfrac{\alpha_1\beta_{n1}\beta_{P2}}{R_1R_3C_1C_2}}{s^2 + \dfrac{\beta_{p2}}{C_2R_4}s + \dfrac{\alpha_1\alpha_2\beta_{n1}\beta_{P2}}{C_1C_2R_2R_3}} \tag{9}$$

which realizes IBRF with cut-off frequency ($\overline{\omega_0}$) and bandwidth ($\overline{BW}$) given by:

$$\overline{\omega_0} = \sqrt{\frac{\alpha_1\alpha_2\beta_{n1}\beta_{n2}}{C_1C_{24}R_2R_3}} = \omega_O\sqrt{\alpha_1\alpha_2\beta_{n1}\beta_{n2}} \quad \text{For } R_1 = R_2$$

$$\overline{BW} = \frac{\beta_{p2}}{C_2R_4} = \beta_{p2}BW \tag{10}$$

and

$$\left.\frac{V_0(s)}{V_{in}(s)}\right|_{IAPF} \cong \frac{1}{\dfrac{1}{\alpha_2}s^2 - \dfrac{\beta_{p2}}{\alpha_2C_2R_5}s + \dfrac{\alpha_1\alpha_2\beta_{n1}\beta_{P2}}{C_2C_4R_1R_3}}{s^2 + \dfrac{\beta_{p2}}{C_2R_4}s + \dfrac{\alpha_1\alpha_2\beta_{n1}\beta_{n2}}{C_1C_2R_2R_3}} \tag{11}$$

which realizes IAPF for with $\overline{\omega_0}$, and $\overline{BW}$ given by:

$$\overline{\omega_0} = \sqrt{\frac{\alpha_1\alpha_2\beta_{n1}\beta_{n2}}{C_1C_2(1+\beta_{n_1})R_2R_3}}$$

$$= \omega_O\sqrt{\frac{\alpha_1\alpha_2\beta_{n1}\beta_{n2}}{(1+\beta_{n_1})}} \quad \text{For } R_1 = R_2$$

$$\overline{BW} = \frac{\beta_{p2}}{C_2R_4} = \beta_{P2}BW \quad \text{For } R_5 = R_4 \tag{12}$$

Equations (10) and (12) reveal that the cut-off frequency, and bandwidth of the IBRF and IAPF are dependent on voltage/current tracking error coefficients of the CDBA terminals, hence subsequently introduce errors in the ω_0 and BW of the inverse filters.

IV. SENSITIVITY ANALYSIS

The active and passive sensitivities of ω_0 and *BW* of inverse active filters (IBRF and IAPF) are tabulated in Table 1 which shows that the sensitivities with respect to active and passive components are small.

Table-1 Sensitivity analysis of inverse filters

Filter	Sensitivity
IBRF	$S_{R_2}^{\omega_O} = S_{R3}^{\omega_O} = -\frac{1}{2}, S_{C1}^{\omega_0} = S_{C2}^{\omega_O} = -\frac{1}{2}, S_{R_1}^{\omega_0} = S_{R4}^{\omega_0} = 0$ $S_{\alpha1}^{\omega_O} = S_{\alpha2}^{\omega_0} = S_{\beta_{n2}}^{\omega_O} = \frac{1}{2}, S_{\beta_{p1}}^{\omega_0} = S_{\beta p2}^{\omega_0} = 0$ $S_{R4}^{BW} = S_{C2}^{BW} = -1, S_{R2}^{BW} = S_{R3}^{BW} = S_{C4}^{BW} = 0$ $S_{\beta_{p1}}^{BW} = 0, S_{\beta p2}^{BW} = 1, S_{\alpha1}^{BW} = S_{\alpha2}^{BW} = S_{\beta_{n2}}^{BW} = 0$
IAPF	$S_{R_2}^{\omega_O} = S_{R3}^{\omega_O} = -\frac{1}{2}, S_{C1}^{\omega_0} = S_{C2}^{\omega_O} = -\frac{1}{2},$ $S_{R_1}^{\omega_0} = S_{R_4}^{\omega_0} = S_{R5}^{\omega_O} = 0$ $S_{\alpha1}^{\omega_O} = S_{\alpha2}^{\omega_0} = S_{\beta_{n2}}^{\omega_O} = \frac{1}{2}, S_{\beta_{p1}}^{\omega_0} = S_{\beta p2}^{\omega_0} = 0$

V. SIMULATION RESULTS

The validity of the proposed inverse filters has been examined through PSPICE simulations using an exemplary CMOS CDBA architecture derived from [23], shown here in Fig. 4. The DC power supplies used were ± 2.5V and the bias current was taken 40µA.The aspect ratios used for implementation of CDBA are given in Table 2. The inverse filters were designed for a nominal value of the cut-off frequency of 159 kHz and quality factor Q = 1. The passive components were selected as $C_1 = C_2 = 100$pF, $R_1 = R_2 = R_3$ $R_4 = R_5 = 10$kΩ. Fig. 5 displays the frequency responses of IBRF and Fig. 6 shows the gain and phase responses of IAPF. The tunability of cut-off frequency and quality factor

(This work is licensed under a Creative Commons Attribution 4.0 International License.)

International Journal of Engineering Research & Technology (IJERT)
ISSN: 2278-0181
Vol. 8 Issue 09, September-2019

of the IBRF have been shown in Fig. 7 and Fig. 8 respectively. The input signal level during PSPICE simulations were kept at 1 V_{PP}.

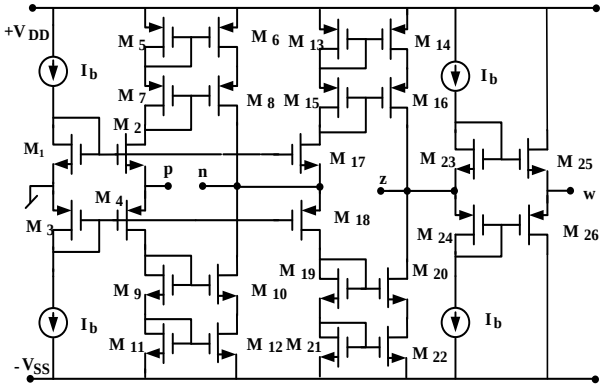

Fig.4 CMOS realization of CDBA derived from [23]

TABLE -2. Aspect ratios of MOSFETs used for realization of CDBA

MOSFETS	$\frac{W}{L}$ratios
M_1,M_2,M_{17},M_{23},M_{25}	50/0.5
M_3,M_4,M_{18},M_{24},M_{26}	100/0.5
M_5-M_{16},M_{19}-M_{22}	3.33/0.5

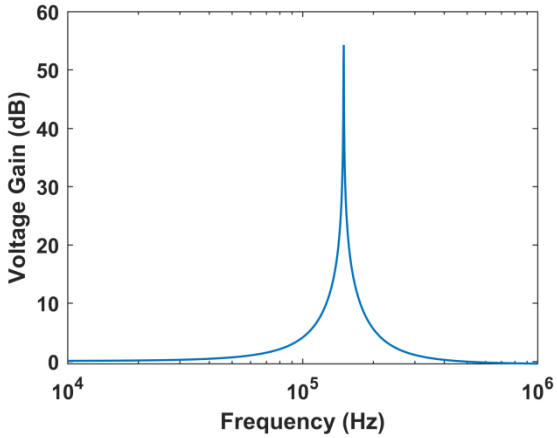

Fig. 5. Frequency responses of IBRF

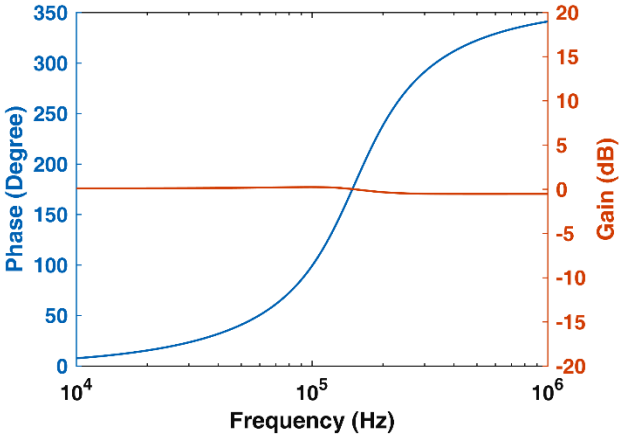

Fig. 6. Gain and phase responses of IAPF

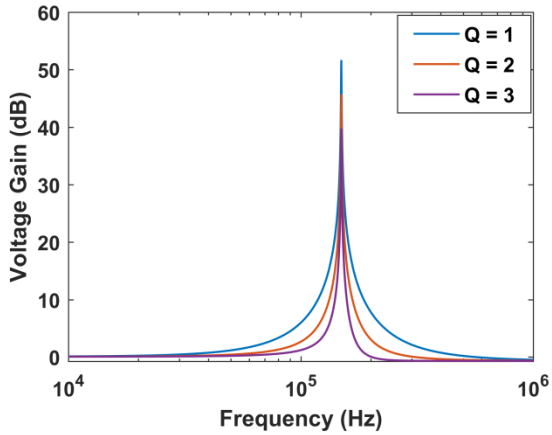

Fig. 7. Tunability of bandwidth for different value of Q for IBRF

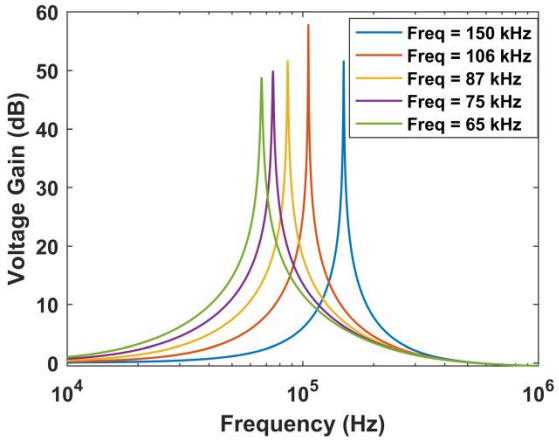

Fig. 8. Tunability of cut-off frequency for IBRF

The Monte Carlo simulation results of the inverse active filters showing variation of gain and cut-off frequency for 5% variation in resistance and capacitance values and have been displayed in Fig. 9 and Fig. 10 respectively. For IBRF the cut-off frequency obtained from the simulations was found to be 150 kHz while Monte Carlo analysis shows that median value of cut-off frequency as 152.148 kHz and similarly for IAPF corresponding to a simulated gain of 0 dB, the Monte Carlo analysis shows that median value of gain as 0.3 dB which shows that the mismatch in the passive component values do not have large effect on the cut-off frequency and gain.

(This work is licensed under a Creative Commons Attribution 4.0 International License.)

International Journal of Engineering Research & Technology (IJERT)
ISSN: 2278-0181
Vol. 8 Issue 09, September-2019

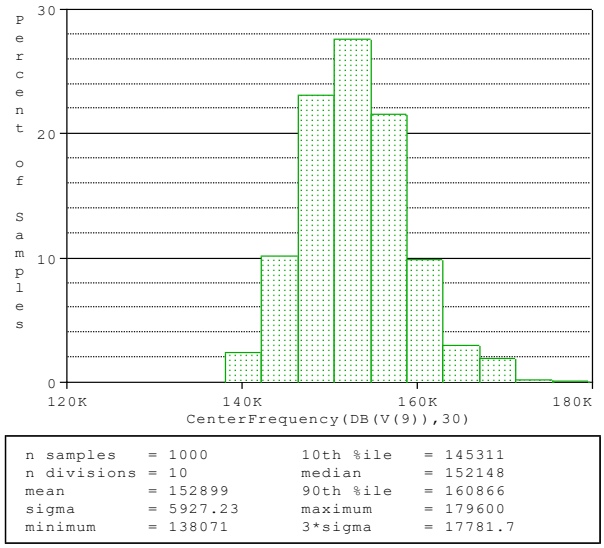

(a)

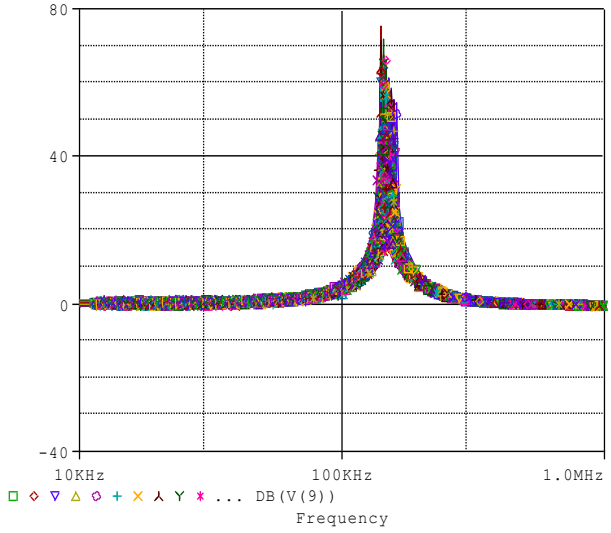

(b)

Fig. 9. Monte-Carlo analysis of IBRF showing variation of cut-off frequency for 5% variation in resistance and capacitance (a) Histogram (b) frequency response.

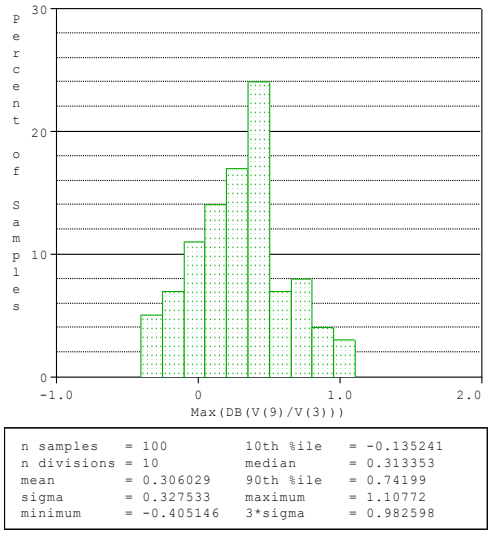

(a)

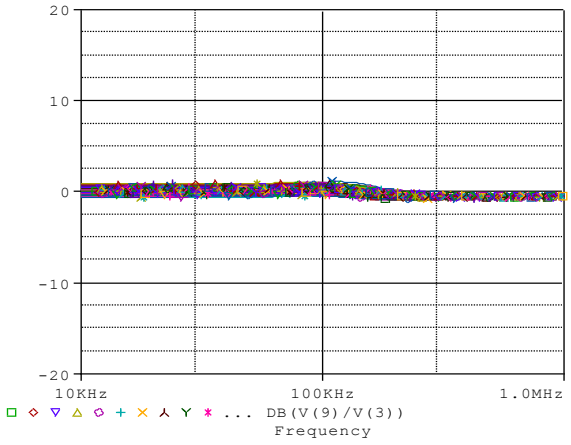

(b)

Fig. 10. Monte-Carlo analysis of IAPF showing variation of gain for 5% variation in resistance and capacitance (a) Histogram (b) frequency response.

VI. CONCLUSIONS

A new VM analog circuit for realizing IBRF and IAPF response has been proposed employing two fully utilised CDBAs, two capacitors, four/five resistors and a switch. The proposed IBRF offers independent tunability of cut-off frequency and quality factor whereas, the IAPF has independent control of cut-off frequency Non-ideal analysis of both the inverse filters has revealed that there is a little error in the cut-off frequency due to inclusion of the parasitic of the CDBAs. The active and passive sensitivities of presented inverse filters are low. The validity of inverse filters has been confirmed through PSPICE simulations using an exemplary CMOS CDBA architecture implemented in TSMC 0.18µm CMOS technology. These simulation results have been found to be in good agreement with the theoretical results.

REFERENCES

[1] Leuciuc, “Using nullors for realization of inverse transfer functions and characteristics”, Electro. Lett., 33(11) (1997), 949–951.
[2] D. R. Bhaskar, M. Kumar, and P. Kumar, “Fractional order inverse filters using operational amplifier”, Analog Integr. Circuits and Signal Process., 97(2018), 149-158.
[3] S. S. Gupta, D. R. Bhaskar, and R. Senani, A.K. Singh, “ Inverse active filters employing CFOA”, Elect. Eng. 1(2009), 23-26.
[4] S. S. Gupta, D.R. Bhaskar, and R. Senani, “New analogue inverse filters realized with current feedback op-amp”, Int. j. of Electro.9(2011),1103–1113.
[5] H. Y. Wang, S.H. Chang, T.Y. Yang, and P.Y. Tsai, “A novel multifunction CFOA based inverse filter”, Circuits and Syst.2(2011),14–17.
[6] K. Garg, R. Bhagat, and B. Jaint, “A novel multifunction modified CFOA based inverse filter”, In Power Electronics (IICPE), IEEE 5th India International Conference. (2012), 1-5.
[7] V. N. Patil, and R. K. Sharma, “Novel inverse active filters employing CFOA”, Int. J. for Scientific Research & Develop. 3(2015), 359–360.
[8] N. A. Shah, and M. F. Rather, “Realization of voltage-mode CCII-based all pass filter and its inversion version”, Indian J. Pure & Applied Physics, 44(2006), 269–271.
[9] T. Tsukutani, Y. Kunugasa, and N. Yabuki, “CCII-Based Inverse Active Filters with Grounded Passive Components”, J. Electr. Eng. 6(2018):212-215.
[10] B. Chipipop, and W. Surakampontorn, “Realization of current-mode FTFN-based inverse filter”, Electron. Lett. 35(1999), 690–692.
[11] H. Y. Wang, and C.T. Lee, “Using nullors for realisation of current-mode FTFN based inverse filters”, Electron. Lett. 35(1999),1889–1890.

(This work is licensed under a Creative Commons Attribution 4.0 International License.)

International Journal of Engineering Research & Technology (IJERT)
ISSN: 2278-0181
Vol. 8 Issue 09, September-2019

[12] M. T. Abuelma'atti, "Identification of cascadable current-mode filters and inverse-filters using single FTFN", Frequenz , 54(11–12)(2000), 284–289.
[13] A. K. Singh, A. Gupta, and R. Senani, "OTRA-based multi-function inverse filter configuration", Adv. in Elect. and Electron. Eng. 15(2018), 846-856.
[14] A. Pradhan, and R. K. Sharma, "Generation of OTRA-Based Inverse All Pass and Inverse Band Reject Filters", Proceedings of the National Acad. of Sci. India Section A: Physical Sciences, 1-11 (2019)https://doi.org/10.1007/s40010-019-00603-w
[15] A. R. Nasir, and S. N. Ahmad, "A new current mode multifunction inverse filter using CDBA", Int. J. of Comp. Sc. and Info. Security,11(2013),50-52.
[16] R. Pandey, N. Pandey, and T. Negi, V. Garg, "CDBA based universal inverse filter", ISRN Electronics, (2013), 1-6.
[17] A. Sharma, A. Kumar, and P. Whig, "On performance of CDTA based novel analog inverse low pass filter using 0.35 µm CMOS parameter", Int. J. of Sc., Tech. & Manag.4(2015), 594–601.
[18] N. A. Shah, M. Quadri, and S. Z. Iqbal, "High output impedance current-mode all pass inverse filter using CDTA", Indian J. of pure and app. physics,46(2018), 893–896.
[19] T. Tsukutani , Y. Sumi, and N. Yabuki, "Electronically tunable inverse active filters employing OTAs and grounded capacitors", Int. J. of Electron. Lett.4(2016), 166–176.
[20] N. Herencsar , A. Lahiri, J. Koton, and K. Vrba, "Realizations of second-order inverse active filters using minimum passive components and DDCCs", In Proceedings of 33rd Int. Conference on Telecomm. and Signal Proc.-TSP, (2010), 38-41.
[21] P. Kumar, N. Pandey, and S.K. Paul, "Realization of Resistor less and Electronically Tunable Inverse Filters Using VDTA", J. Circuits, Syst. Comp. (2018),1950143.
[22] J.K. Pathak, A. K. Singh, and R. Senani, "Systematic realisation of quadrature oscillators using current differencing buffered amplifiers", IET Circuits, Devices & Syst., 5(2011), 203-211.
[23] A.K. Singh, P. Kumar, "A novel fully differential current mode universal filter", In Circuits and Systems (MWSCAS),2014 IEEE 57th International Midwest Symposium, 579-582(2014).

(This work is licensed under a Creative Commons Attribution 4.0 International License.)

View publication stats

The current issue and full text archive of this journal is available on Emerald Insight at:
www.emeraldinsight.com/0368-492X.htm

Linking knowledge management practices to organizational performance using the balanced scorecard approach

Meenu Chopra and Vikas Gupta
Delhi School of Management, Delhi Technological University, Delhi, India

Received 30 April 2019
Revised 27 June 2019
Accepted 19 July 2019

Abstract

Purpose – The purpose of this study is to develop a decomposed model to inspect the effect of knowledge management practices (knowledge sharing culture [KSC], knowledge-based human resource management [KHRM], strategy and leadership [S&L], information and communication technology [ICT] on organizational performance [OP]) by using the four balanced scorecard outcomes (BSC) (learning and growth [L&G], internal process [IP] perspective, customer satisfaction [CS] perspective and financial performance [FP]).

Design/methodology/approach – The research methodology included development of a research model based on comprehensive literature review followed by survey of knowledge-intensive organizations. A sample of 277 employees was obtained and structured equation modeling analysis using SPSS AMOS was conducted to test the proposed hypotheses.

Findings – The study shows that KSC and KHRM have a highly significant effect on all the four aspects of OP; S&L positively and significantly affects only L&G and IP but does not have any significant effect on the other two, i.e. CS and FP, while ICT practices did not affect any of the measures significantly.

Research limitations/implications – The data are limited to 277 middle and senior level managers of Indian firms, which may be a limiting factor for generalizability.

Originality/value – The proposed model uncovers the dynamics of individual relationships between KM practices and measures of performance (proposed by BSC) in comparison to existing models which have mainly focused on the overall effect.

Keywords Balanced scorecard, Performance measures, Knowledge management practices, Information and communication technology, Knowledge sharing culture, Knowledge-based human resource management, Strategy and leadership

Paper type Research paper

1. Introduction

Gaining sustainable competitive advantage is based on the possession of knowledge by an organization, how it puts this set to use and how quickly can it upgrade itself by learning something new (Grant, 1996; Spender and Grant, 1996; Roth, 1996; Prusak, 1996). Indeed, the most powerful way to succeed in the current times is the possession and timely use of organizational knowledge (Prahalad and Hamel, 1997). The focus has metamorphosized from 'what an organization owns' to 'what an organization knows' (Vătămănescu *et al.*, 2016; Greco *et al.*, 2013). According to Kianto *et al.* (2014) 'knowledge' is a core business activity for standing out in the global economy and is fast evolving as the major differentiator. Bennett and Gabriel (1999) state that KM is capturing, storing, disseminating and using knowledge. KM is the process that facilitates creation and dissemination of knowledge for easy accessibility and use within organizations (Darroch, 2003). Sabherwal and Becerra-Fernandez (2010) define KM as doing what needs to be done to optimally utilize an

Kybernetes
© Emerald Publishing Limited
0368-492X
DOI 10.1108/K-04-2019-0295

organization's knowledge resources. According to American Productivity and Quality Centre (APQC), 1999 KM is "the systematic process of identifying, capturing and transferring information and knowledge people can use to improve."

Knowledge resource in an organization may be classified as explicit or tacit. Explicit knowledge can be captured, stored and retrieved for future use whereas tacit knowledge can neither be captured easily nor stored. It is inherently present in procedures/processes and it is generally not recognizable (Andreeva and Kianto, 2012). It can only be used when the individual possessing it chooses to do so and may be completely lost with the employee moving to another organization.

Creation of KM practices in the organization that boosts knowledge creation and sharing, and helps retain these practices in the organization, even after employees, customers, suppliers etc. are not associated with the organization, is the real challenge. Alongside creation and utilization, this knowledge has to be measured and stored in a manner that it is accessible, understandable and reusable by members of the organization in the future.

KM is strategically important for any competitive organization and hence it is imperative to align it with the overall business strategy. A pre-requisite for implementation of these strategies is to gauge their effect through the use of an integrated system of measurement that possesses the capability to capture financial as well as non-financial aspects of performance. Since most KM benefits are intangible in nature, balanced scorecard outcomes (BSC) is one method of measurement (Lee *et al.*, 2005) that may be employed to gauge the overall effect. Gupta and Chopra (2017) have proposed and developed a conceptual framework for integrating BSC in the measurement of KM performance. BSC is a strong and comprehensive metric program that can help an organization quantify the amount of effort and returns generated by different units of a business. The measures of BSC focus on both financial and non-financial perspectives of business performance. Complex business situations at a micro and macro level require organizations to take stock of various dimensions of performance at the same time. BSC enables them to do this and focus attention on the crucial areas (Moore *et al.*, 2001).

The main objective of this paper is to propose a decomposed model in order to analyze the effect of four KM practices namely, knowledge sharing culture (KSC), knowledge based HRM (KHRM), strategy and leadership (S&L) and information and communication technology (ICT) on BSC outcomes namely learning and growth (L&G), internal process perspective (IP), customer satisfaction perspective (CS) and financial performance (FP) of an organization using survey data of 277 subjects. To meet this objective, the paper is systematized in the following sections. In the first section, the theoretical model linking KM practices and BSC outcomes have been developed followed by research design and presentation of results. Discussion of empirical findings and implications for managers are presented in the next section followed by limitations and directions for future research.

2. Literature review

KM as a concept has been there for ages. As Hansen *et al.* (1999) has put it – 'knowledge has existed for a long time, businessmen have taught commercial skills to their heirs, craftsmen and workers pass on their skill set to apprentices too. From an organizational context, Grant (1996) proposed the knowledge-based view of the firm according to which performance of a firm depends on stocks of knowledge the firm has accumulated and its capability to use these stocks from time to time. KM starts with the development of a business vision about what an organization wishes to achieve over the long run, it adopts an integrated approach to identify, capture, evaluate, store and retrieve information assets of an organization.

One of the pioneering studies that measured the effect of KM on various aspects of performance of an organization was Gold *et al.* (2001) which concluded that management of knowledge assets positively affects innovation, opportunity identification, helps in coordinating efforts of different units, adapting to unanticipated changes and become responsive to new market demands. Since then the study on KM has come a long way. The knowledge possessed by an organization, its management and effects on performance have been under study for quite some time. Empirical research on the link between KM and organizational performance (OP) has developed along two lines - KM processes and KM practices. Literature on KM processes and OP discusses the role of knowledge processes such as acquisition, utilization and sharing on performance, these processes are broad knowledge-based activities in an organization and exist without active managerial control (Hussinki *et al.*, 2017), while Andreev and Kianto (2012) defined KM practices as a set of thoughtfully undertaken management processes and activities that are instrumental in enhancing the overall effectiveness of knowledge resources of the organization. These practices have been addressed as critical success factors, enablers or initiatives for KM and research has shown that their implementation affects various aspects of OP (Table I).

So as to ascertain success in implementation of KM practices, continuous measurement of performance related measures is essential. A number of research studies have tried to analyze the effects of KM on various OP measures. Some of them are stated below:

- competitiveness (Allard and Holsapple, 2002; Rodriguez Perez and Ordóñez de Pablos, 2003; Choy Chong, 2006; Wang *et al.*, 2012);
- market share (Andreeva and Kianto, 2012; Zheng *et al.*, 2010; Lee and Choi, 2003);
- growth rate (Andreeva and Kianto, 2012; Lee and Choi, 2003);
- innovativeness (Sinha *et al.*, 2015; Zheng *et al.*, 2010; Zack *et al.*, 2009; Lu *et al.*, 2008; Choy Chong, 2006; Darroch, 2005; Gloet and Terziovski, 2004);
- profitability (Andreeva and Kianto, 2012; Zheng *et al.*, 2010; Zack *et al.*, 2009; Lee and Choi, 2003);
- research and development performance (Lee *et al.*, 2005);
- better training (Choy Chong, 2006);
- enhanced OP (Wu and Chen, 2014; Wang *et al.*, 2012; Mills and Smith, 2011; Starns and Odom, 2006);
- customer performance (Han and Anantamula, 2007; Zack *et al.*, 2009; Wu and Chen, 2014);
- FP (Jain and Moreno, 2015; Wu and Chen, 2014; Andreeva and Kianto, 2012; Vaccaro *et al.*, 2010; Zack *et al.*, 2009);
- employee creativity (Kianto, 2011);
- commercialization of creative ideas (Kianto, 2011); and
- balanced scorecard (Gonzalez-Padron *et al.*, 2010; Chen and Mohamed, 2008; Arora, 2002).

BSC has been established as a powerful tool for strategic planning and successful communication of strategy across all levels of an organization. Kaplan and Norton (1992, 1996a, 1996b) used as a combination of measures to align departmental, organizational and individual initiatives with the overall organizational mission (Chen and Huang, 2009). BSC is an effective strategy performance management tool that provides managers a quick and comprehensive view of business (Chopra *et al.*, 2017). The BSC has revolutionized the

Knowledge management practices (independent variable)	Effect on business (dependent variable)	Literature support
Technology Structure Culture KM processes	Organizational effectiveness: measures Innovate new products/services Identify new opportunities Coordinate the development efforts of different units Anticipate market opportunities Rapidly commercialize innovations Adapt quickly to unanticipated changes Anticipate crises and surprises Quickly adapt its goals and objectives React to new information Be responsive to new market demands Streamlining internal processes Coordinate the development efforts of different units Anticipate market opportunities Rapidly commercialize innovations Adapt quickly to unanticipated changes Anticipate crises and surprises Quickly adapt its goals and objectives React to new information Be responsive to new market demands Streamlining internal processes	Gold *et al.* (2001)
Knowledge processes KM leadership Assessment of knowledge initiatives Knowledge integration	Organizational competitiveness	Allard and Holsapple (2002)
Knowledge processes	Innovation	Darroch and McNaughton (2002)
Knowledge processes	Innovation Compared with industry average, company is more profitable Increased market share and sales growth	Darroch and McNaughton (2003)
Technology Structure Culture People – integration of HRM and KM	Positively affect knowledge creation Knowledge creation positively affects OP in terms of: Market Share Profitability Growth rate Innovativeness Successfulness Increased size of business in comparison to competitors	Lee and Choi (2003)
People – integration of HRM and KM	Competitiveness	Jesus Rodriguez Perez, Patricia Ordóñez de Pablos, (2003)

Table I.
Linking knowledge management practices and organizational performance measures

(*continued*)

Knowledge management practices (independent variable)	Effect on business (dependent variable)	Literature support
Technology	Positively affects Innovation performance	Gloet and Terziovski (2004)
People – integration of HRM and KM	Better performance of an organization	
Knowledge processes	Improved ability to sustain the competitive advantage of an organization Immediate results in solving Improved organizational productivity in delivering services to clients Development and constant improvement of competitive long-range service and technology strategies Improvements in the quality of an organization's workforce, through capacity building and upskilling Stimulation and motivation of employees Formalized knowledge transfer system Improved knowledge acquisition and absorption from sources outside the firm Improved integration of knowledge within the firm Better on-the-job training of employees Enhanced client relations – better client interaction Development of culture for organizational growth and success Improved employee retention Enhanced business development and the creation of opportunities for organizations Enhanced and streamlined internal administrative processes	Charles *et al.* (2005)
Knowledge processes	Stock price R&D expenditure Performance	Lee *et al.* (2005)
Knowledge processes	Innovation Profitability Better knowledge dissemination Better knowledge responsiveness Greater market share More growth Better performance Better achievement of objectives	Darroch (2005)
Knowledge processes	Capital profitability	Palacios Marqués and José Garrigós Simón (2006)
Culture	Growth	
People – integration of HRM and KM	Operational and financial efficiency	
KM strategy	Stakeholder satisfaction Competitive position	

(*continued*)

Table I.

Knowledge management practices (independent variable)	Effect on business (dependent variable)	Literature support
Degree of importance and implementation of:	Knowledge management competitiveness	
Leadership and policy	Better on-the-job training for employees	Choy Chong (2006)
Performance measurement	Enhanced company innovation and creativity	
Knowledge sharing and acquisition	Means to identify industry best practices	
Information systems infrastructure	Enhance client interaction – better client interaction	
Benchmarking and training	Development of business strategies	
Teamworking and environment	Improve employee retention	
	Overall company performance	
Technology	Enhanced organizational performance	Starns and Odom (2006)
Structure		
Culture		
Resources for KM		
People	Customer performance	
Structure	FP	Young-Chan Lee Sun-Kyu Lee (2007)
Culture		
Information technology		
KM Process		
KM leadership	Learning environment	Han and Anantatmula (2007)
Knowledge from, about and for the customer	Employee development (Effective communication tools and KM tools)	
	Critical process skills	
	Customer service through new products and services	
	Customer Service through enhanced product/ service Quality	
Human issue	Innovation	Lu *et al.* (2008)
Process issue		
Structural issue – infrastructure leadership		
KM processes	Organizational performance	Zack *et al.* (2009)
People – integration of HRM and KM	Product leadership	
KM strategy	Innovation	
KM leadership	Quality	
Assessment of knowledge initiatives	CS	
	Customer retention	
	Operational excellence	
	Operating costs	
	FP	
	ROA/ROE	
	Profitability	
KM	Knowledge management effectiveness	Zheng *et al.* (2010)
Knowledge generation	Acquiring,	
Knowledge sharing	Creating,	
Knowledge utilization	Storing,	

Table I.

(*continued*)

Knowledge management practices (independent variable)	Effect on business (dependent variable)	Literature support
Organizational culture Adaptability Consistency Mission Involvement Organizational structure Centralization Organizational strategy Analysis Defensiveness Futurity Proactiveness	Sharing, Diffusing, Developing, Deploying Organizational effectiveness Overall success, Market share, Profitability, Growth rate, and Innovativeness	
Knowledge infrastructure capability Technology Culture Structure KM processes	Organizational performance	Mills and Smith (2011)
Knowledge processes	Employee creativity Commercialization of creative ideas (innovation) Strategic flexibility	Kianto (2011)
Technology	Greater market share	Andreeva and Kianto (2012)
People – integration of HRM and KM	Growing faster Innovative More profitable Better FP	
Knowledge acquisition Knowledge creation Knowledge dissemination Knowledge accumulation	Competitive advantage Enhanced organizational performance	Wang *et al.* (2012)
Technology Culture People Knowledge processes	OP in terms of financial and non-financial measures	Rašula *et al.* (2012)
Knowledge from, about and for the customer	Innovation speed Innovation quality which leads to business performance Operational performance FP	Taherparvar *et al.* (2014)
Technology Culture Structure People Network and alliances	Operational excellence CS Product leadership Financial achievement	Wu and Chen (2014)

(*continued*)

Table I.

Knowledge management practices (independent variable)	Effect on business (dependent variable)	Literature support
Knowledge from, about and for the customer Knowledge processes		
Knowledge processes	Positive effect on the four BSC measures Higher KMO-enabled L&G Drives higher IP CS FP (indirect effect)	Chang and Lin (2015)
Technology Structure Culture People KM strategy KM leadership Network and alliances Assessment of knowledge initiatives Knowledge processes	Innovation	Sinha *et al.* (2015)
Technology	Strongly affects L&G	Valmohammadi and Ahmadi (2015).
Culture People KM strategy KM leadership Resources for KM Knowledge processes	Effect on IP Customer perspective Financial perspective	
Knowledge processes	Financial measures Customer/market measures Process measures People development measures Preparing for future measures	Tubigi and Alshawi (2015)
Technology Culture People Network and alliances Knowledge from, about and for the customer Knowledge processes	Better communication and participation Increased CS Improved efficiency Improved effectiveness Increased sales Increased share price Improvement of strategy quality Better decision-making Shorter problem-solving time Increased innovation Fewer mistakes Rework reduction Improved business processes Improved ability to sustain the competitive advantage of an organization	Yahyapour *et al.* (2015)

Table I.

(*continued*)

Knowledge management practices (independent variable)	Effect on business (dependent variable)	Literature support
Organizational learning	Knowledge creation	
Collaboration and team working,	FP	Jain and Moreno (2015)
Performance management,	Km process and leadership	
Autonomy and freedom	KM technology and measurement	
Reward and recognition,	KM culture	
Achievement orientation		
KM practices	Innovation	Roldán *et al.* (2018)
Knowledge maintenance and protection	Productivity	
External knowledge capturing	Competitive position	
Knowledge codification	Profitability	
Knowledge practices focused on the human factor.	Revenues	
IT infrastructure	Overall performance	
Communication and collaboration technologies	FP	
Business intelligence applications	Sales growth	
	Profitability	
Knowledge creation process	Human capital	Gholamhossein *et al.* (2018)
Socialization	Innovation and creativity	
Combination	Experience and expertise	
Internalization	Learning and education	
Externalization	Structural capital	
	Systems and programs	
	Research and development	
	IPR	
	Relational capital	
	BSC	
	FP	
	Customer perspective	
	IP perspective	
	L&G	

Source: Adapted from Gupta and Chopra (2017)

Table I.

conventional thought process about performance metrics (Farzaneh *et al.*, 2018). The major benefit of the tool is its capability to assess via the use of financial and non- FP indicators, namely,

L&G – studies effect on an organization's intangible assets like employee skill set and competencies for organization's overall development;

IP – analyses the organizational operations and processes that help in creation and delivery of customer value;

CS – focusses on the value of relationship and in-time service delivery to the customer;

FP – focuses on the more tangible aspects such as increase in market share, return on investment.

The tool is helpful to analyze whether the current level of performance is in line with the expected performance. Keeping in mind the comprehensiveness and wide acceptance of the

tool, the authors have integrated it into the process of KM performance measurement. Table I presents a thorough literature review on the various KM practices and measures of OP.

2.1 Research gap

Despite the presence of this literature, a cross country study (conducted on more than 200 KM experts) concluded that one of the major shortages in KM literature is the lack of understanding about the linkage between KM and performance of an organization (Perez-Arrau *et al.*, 2014). This paper is an endeavor to address this gap by integrating significant KM practices and measures of BSC to help draw an overall picture of the magnitude and type of effects KM implementation has on an organization. This analysis carries significance for researchers, academicians and companies. The research is deeply rooted in the KM literature and provides structure and meaning to the current set of literature for reference and research in future. For organizations, it offers empirical evidence about the cause and effect relationships that exist between KM practices and OP measures.

2.2 The research framework

While exploring literature on KM practices and OP (Table I), generally studies have found that KM positively affects performance (Gold *et al.*, 2001; Lee and Choi, 2003; Palacios Marqués and José Garrigós Simón, 2006; Rasula *et al.*, 2012; Jain and Moreno, 2015), though some could not establish a significant direct relationship between the two (Mills and Smith, 2011; Abualoush *et al.*, 2018). The paper proposes to take this forward and explore the effect of four KM practices that have achieved notable support theoretically and empirically viz. KSC, knowledge-based human resource management (KHRM), S&L, ICT on the four BSC items in a decomposed model.

2.2.1 Knowledge sharing culture. Culture refers to the values and norms existing in an organization, which have been developed, shared and passed on from one to another (Davenport and Klahr, 1998). Research has proven time and again that creating a knowledge-friendly culture is imperative for smooth flow of information essential for knowledge-based value creation (Moffett *et al.*, 2003; Lee and Choi, 2003; Wong and Aspinwall, 2005; Hung *et al.*, 2005; Al-Busaidi and Olfman,2005; Akhavan and Jafari, 2006; Choy Chong, 2006; du Plessis, 2007; Tunc Bozbura, 2007; Basu and Kumar Ray, 2014; Palacios Marqués and José Garrigós Simón, 2006; Zaim *et al.*, 2007; Valmohammadi and Ahmadi, 2015; Appelbaum *et al.*, 2014; Vanhala and Ritala, 2016; Lee *et al.*, 2016; Gupta and Chopra, 2017). Development of an environment of mutual trust and collaboration positively affects inter-personal interaction, facilitates knowledge sharing, leading to better yielding knowledge processes and organizational effort. No organization can create 'knowledge workers' in the true sense of the word until the organization has been successful in creating an environment of support and collaboration. Existence of a culture of mutual trust, free flow of information and a clear focus on learning and innovation are requisites for promoting effective KM in the organization. So, it is expected that:

H1. KSC in an organization will positively affect

H1a. L&G perspective

H1b. IP perspective

H1c. CS perspective

H1d. FP perspective

2.2.2 Knowledge based human resource management. People i.e. human resource management is the fulcrum for all KM activity in an organization since it is this resource which is going to use and implement all these practices. HRM includes important people functions like recruitment, compensation, training and development. The aim is to hire talented people, train and develop them and enable them to reach their potential. The interaction of HRM and KM has been analyzed by practitioners and researchers (Yahya and Goh, 2002; Hwang, 2003; Moffett *et al.*, 2003; Hung *et al.*, 2005; Chong and Choi, 2005; Wong and Aspinwall, 2005; Akhavan and Jafari, 2006; Choy Chong, 2006; Soto-Acosta *et al.*, 2014; Jain and Moreno, 2015; Inkinen, 2015; Hussinki *et al.*, 2017; Ardito and Petruzzelli, 2017; Gupta and Chopra, 2017). It is well established that on one hand where technology can provide an impetus to KM, it cannot replace human contribution in the process. Empirical research points out that technology is weak in interpreting information (knowledge), which is the keystone of knowledge creation, whereas, high-level communication amongst individuals leads to transfer of knowledge and information (Yahya and Goh, 2002). The 'people' factor in an organization is the major force of KM (De Gooijer, 2000) and has been identified to play an important role in creation of a culture where it is understood that the use and implementation of KM practices can act as a pivotal tool and provide a foundation of competitive advantage (Singh and Soltani, 2010). Thus, it is expected that:

H2. KHRM practices will positively affect

H2a. L&G of an organization

H2b. IP perspective

H2c. CS

H2d. FP

2.2.3 Strategy and leadership. Effective S&L are key to set up the right environment for KM in an organization. Empirical research has proven that good leaders and managers who participate, inspire and support their team members are invariably able to produce better results (Holsapple and Joshi, 2000; Civi, 2000; Choi, 2000; Ryan and Prybutok, 2001; Pemberton *et al.*, 2002; Kalling, 2003; Moffett *et al.*, 2003; Ribiere and Sitar, 2003; Chong and Choi, 2005; Hung *et al.*, 2005; Wong and Aspinwall, 2005; Al-Busaidi and Olfman, 2005; Choy Chong, 2006; Akhavan and Jafari, 2006; Akhavan and Jafari, 2006; du Plessis, 2007; Anantatmula, 2007; Valmohammadi and Ahmadi (2015); Birasnav, 2014; Donate and de Pablo, 2015). A leader has a strong influence on the organization as they create, communicate and build the knowledge vision of the organization that determines the treatment of data, information and knowledge as assets in the organization. They are the ones responsible for creating an atmosphere of mutual trust and cooperation, and motivate employees to tread new paths and reach higher levels of excellence. Establishing a vision and taking the organization in the desired direction by listening, learning, teaching and sharing knowledge is a leader's task (Holsapple and Singh, 2000). Taken together, it is expected that:

H3. S&L for KM will positively affect.

H3a. L&G of an organization.

H3b. IP perspective.

H3c. CS.

H3d. FP.

2.2.4 Information and communication technology. The use of technology in the spread and use of knowledge is important to appreciate in an intra-organizational setup. If organizations have to be benefitted and become more effective, a very important contributing factor will be setting up of solid technological information infrastructure capable of knowledge sharing. Organizations have been keen on developing systems and technologies to capture and use internal and external knowledge strategically (Del Giudice and Della Peruta, 2016). There is a clear focus on ICT practices in organizations (Davenport and Klahr, 1998; Choi, 2000; Gold *et al.*, 2001; Hsieh *et al.*, 2002; Lee and Choi, 2003; Moffett *et al.*, 2003; Chong and Choi, 2005; Wong and Aspinwall, 2005; Zaim *et al.*, 2007; Valmohammadi and Ahmadi (2015); Andreeva and Kianto, 2012; Cohen and Olsen, 2015; Hussinki *et al.*, 2017; Sumbal *et al.*, 2017; Inkinen *et al.*, 2017; Gupta and Chopra, 2017). Use of ICT for gathering internal and external information and using this information for creating seamless communication systems and making better decisions is a significant practice which helps leverage other KM resources optimally. Proper and smooth functioning requires identification, codification and communication of knowledge workers spread across different locations (Zack *et al.*, 2009). Managers need to easily manageable information that assists in decision-making (Walsh and Ungson, 1991). Thus, it is expected that:

H4. ICT for KM will positively affect

H3a. L&G of an organization

H3b. IP perspective

H3c. CS

H3d. FP

3. Methodology

Decomposed models are put to use in research in order to examine complex relationships (Mills and Smith, 2011). The overall construct is formed by its underlying dimensions and a change in these dimensions causes a change in the construct too. An individual dimension may have a negative, neutral or positive effect on the dependent variable, this relationship won't surface and stay underneath and uncovered in case of a composite model and will only come to light if a decomposed model is analyzed (Petter *et al.*, 2007; Mills and Smith, 2011). Although a flip side of the use of decomposed models is loss of parsimony as these models are bulky and may uncover relationships which may not be true at higher level and vice-versa (Petter *et al.*, 2007). However, since the objective of this paper is to uncover cause and effect individual level relationships between KM practices and measures of OP, a decomposed model has been employed (refer Figure 1).

3.1 Data collection and sample

In order to examine the research hypotheses, a questionnaire on KM practices and OP measures was developed. The measures consisted of multi-item constructs from a range of studies adapted according to the need of the current study (presented in Table II). A seven-point scale anchored with 'Strongly disagree' to 'Strongly agree' was employed to measure all items. The questionnaire was checked for content validity by five experts followed by pilot testing on a sample of 50 respondents. The reliability for each construct was above 0.7; hence, final data collection was undertaken.

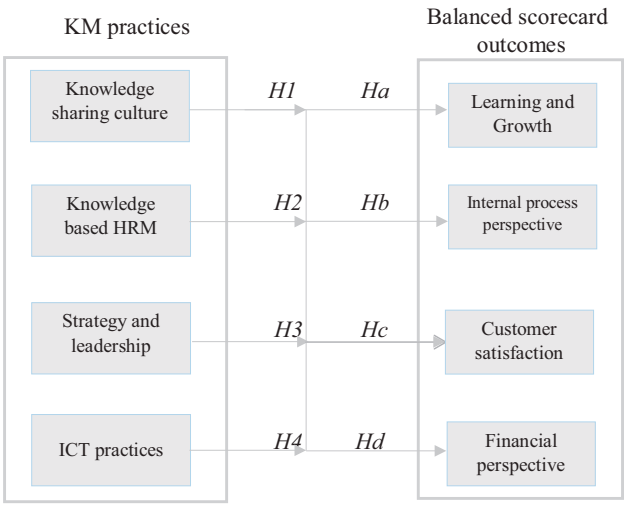

Source: Author

Figure 1.
Research framework

Since the main focus of this research is to analyze the effect of KM practices on BSC outcomes, the firms that qualify for the study have to be essentially focused on the development of KM infrastructure and possess rich experience in KM projects. Assuming that knowledge is an inevitable resource for any large and successful business organization, the Fortune India 500, a list of top 500 Indian companies, compiled annually by Fortune magazine, on the basis of sales and gross revenue figures, was considered as the sampling frame for the study.

Data was collected by administering questionnaires in both online and offline mode. For some organizations with offices in Delhi-NCR, data was collected personally by visiting with prior appointment. For others, participants were invited via e-mail by including the link to a web-based survey designed through Google form. Follow-up visits and emails were done to increase the response rate. The exercise of data collection spanned over a period of five months from September 2018 to January 2019. Approximately 974 questionnaires were distributed and 289 responses were received, out of which 277 were used for the study, 12 could not be used as they were found to be incomplete (response rate – 29.36 per cent). Respondent profile is presented in Table III.

4. Data analysis and result

AMOS SEM and IBM SPSS version 22.0 have been used to assess the linkage between KM practices and OP measures.

4.1 Measurement model

As depicted in Table IV, the measurement model is a good fit for data –

χ^2 value = 517.869,
degree of freedom(df) = 373,
χ^2/df = 1.388,
comparative fit index (CFI) = 0.936,
Standardized root mean squared residual (SRMR) = 0.061,
Root mean square of approximation (RMSEA) = 0.052, p close = 0.356).

KSC	
the organization has a supportive and collaborative culture	Lee and Choi, 2003; Wong and Aspinwall, 2005; Al-Busaidi and Olfman, 2005; Hung *et al.*, 2005; Akhavan and Jafari, 2006; Choy Chong, 2006; Tunc Bozbura, 2007; du Plessis, 2007; Han and Anantamula, 2007; Basu and Kumar Ray, 2014; Appelbaum *et al.*, 2014; Jain and Moreno, 2015; Lee, Shiue and Chen, 2016
there is an environment of participation and team spirit in the organization	
there is a clear focus on learning and innovation in the organization	
the organization has a value system tdat promotes knowledge creation and sharing	
there is stress on the development of an innovative environment tdat encourages R&D projects	
Experienced workers or managers transfer their knowledge to new or less experienced workers	
the organization has an encouraging environment to develop and implement ideas and express opinions	
KHRM	
Our organization lays a lot of stress on recruitment practices and policies	Bontis and Giradi, 2000; Garavan *et al.*, 2007; Mentzas *et al.*, 2001; Horak, 2001; Yahya and Goh, 2002; Hwang, 2003; Moffett *et al.*, 2003; Hung *et al.*, 2005; Chong and Choi, 2005; Wong and Aspinwall, 2005; Akhavan and Jafari, 2006; Choy Chong, 2006; Akhavan and Jafari, 2006; Tunc Bozbura, 2007; du Plessis, 2007; Priesto -Pastor *et al.*, 2010; Andreeva and Kianto, 2012
there is a system of mentoring and training in the organization	
Our organization rewards knowledge creation witd incentives	
Our organization rewards knowledge sharing witd incentives	
S&L	
Top Management has developed an environment of responsible employee behavior and teamwork	Bollinger and Smith, 2001; Chong and Choi, 2005; Hung *et al.*, 2005; Wong and Aspinwall, 2005; Al-Busaidi and Olfman, 2005; Akhavan and Jafari, 2006; Akhavan and Jafari, 2006; du Plessis, 2007; Choy Chong, 2006; Han and Anantamula, 2007; Donate and de Pablo, 2015
Management provides wholehearted support to KM initiatives	
Managers show tolerance for mistakes and encourage employee creativity	
KM policy of the organization is clearly documented	
ICT	
Our organization's ICT is capable of supporting management decisions and knowledge work	Davenport and Klahr, 1998; Greco *et al.*, 2013; Wenger and Snyder, 2000; Choi, 2000; Alavi and Leidner (2001), Gold *et al.*, 2001; Hsieh *et al.*, 2002; Lee and Choi, 2003; Moffett *et al.*, 2003; Chong and Choi, 2005; Wong and Aspinwall, 2005; Andreeva and Kianto, 2012
Our organization's KM systems and tools are widely accepted, regularly monitored and updated	
Our organization's ICT architecture is capable of timely sharing of information witd all stakeholders in the organization	
L&G	
Professional ability of employees	Kaplan and Norton, 1996; Kaplan, 2009; Punniyamoortdy and Murali, 2008; Chen and Huang, 2009; Chen *et al.*, 2011.
Productivity of employees	
Knowledge sharing behavior of employees	
Ability of the employees to handle emergency situations	
Ability of the employees to effectively use an organization's IT resources	

Table II.
Measures

(*continued*)

IP
Ability of the employees to retain existing customers
Ability of the employees to effectively use an organization's IT resources
Time reduction in handling customer inquiries and complaints
Time reduction in commercializing innovations
Rework reduction
Effective problem-solving percentage
Customer perspective
Better customer service tdrough new products and services
Customer intimacy
Increase in market share
Customer retention
Increase in service quality
Increase in rate of acquisition of new customers
Financial perspective
Increase in size of business
Return on investment
Return on assets
Average profit
Revenue growtd rate

Table II.

Gender		
Male	194	70.04
Female	83	29.96
	277	100.00
Educational qualification:		
Graduate	128	46.21
Post graduate	148	53.43
PhD	1	0.36
	277	100.00
Position		
Entry level	0	0.00
Middle level	190	68.59
Senior level	87	31.41
	277	100.00
Total experience		
5-10 years	22	7.94
11-20 years	168	60.65
21-30years	78	28.16
31 years and above	9	3.25
	277	100.00
Experience with the existing organization		
less than 5 years	64	23.10
5-10 years	107	38.63
more than 10 years	106	38.27
	277	100.00

Table III.
Respondent profile

Type	Index	Measurement model	Structural model	Recommended value for satisfactory fit for a model to data
χ^2 test	χ^2	517.869	576.737	
	df	373	379	
	χ^2/df	1.388	1.522	Between 1 and 3
Absolute fit index	CFI	0.936	0.913	>0.95
	SRMR	0.061	0.067	<0.08
	RMSEA	0.052	0.061	<0.06
	PClose	0.356	0.043	>0.05

Source: Hu and Bentler (1999); Gaskin and Lim, (2016)

Table IV.
Measurement model and structural model

Clearing this level of check, the instrument could be checked for psychometric properties i.e. construct reliability, convergent and discriminant reliability. With the use of Cronbach's alpha, internal reliability was ascertained. As presented in Table V, all Cronbach alpha values exceeded 0.70 as suggested by Nunnally and Bernstein, 1994 (pp. 264-265). Anderson and Gerbing (1988) recommended three criteria for checking convergent validity:

(1) all standardized factor loading should be significant ($p < 0.01$) (Gefen *et al.*, 2000);

(2) composite reliability (CR) > 0.70 (Hair *et al.*, 1998); and

(3) average variance extracted (AVE) >0.5 (Fornell and Larcker, 1981).

Table V presents the values for these measures and shows that all values fulfill the said criteria (All standardized factor loadings were significant at $p < 0.01$; Composite reliability ranges from 0.773-0.881; AVE ranges between 0.504 and 0.682).

Table V also depicts that AVE of every construct > squared correlation among constructs, proving discriminant validity (Fornell and Larcker, 1981). Hence, the measurement model cleared all checks for reliability and validity.

4.2 Hypothesis testing

Similar indices were used for the structural model (Table IV).

The ratio of χ^2 to degrees of freedom (df) = 1.522 (χ^2 = 576.737, degree of freedom(df) = 379, χ^2/df = 1.522),
comparative fit index (CFI) = 0.913,
Standardized root mean squared residual (SRMR) = 0.067,
Root mean square of approximation (RMSEA) = 0.061,
p close = 0.043.

Since the model was a good fit, the study could move forward to check the path coefficients of the structural model. The path analysis coefficients and verification of research hypothesis is presented in Table VI.

Turning to the structural model for hypothesis testing, the results show that out of a total of sixteen hypotheses, ten hypotheses were supported by the data. The study of the decomposed model helped uncover individual connections between the constructs and lead to a deeper understanding of the dynamics of their relationship.

5. Conclusion

The study tests the decomposed model that examines the effect of KM practices on four BSC outcomes. The empirical analysis throws light on several major findings. Since this study

	Cronbach's α	CR	AVE	MSV	MaxR (H)	1	2	3	4	5	6	7	8
1	0.880	0.881	0.515	0.379	0.885	0.717							
2	0.836	0.839	0.636	0.458	0.847	0.510***	0.798						
3	0.884	0.885	0.659	0.346	0.889	0.504***	0.588***	0.812					
4	0.797	0.801	0.504	0.369	0.809	0.607***	0.452***	0.481***	0.71				
5	0.859	0.865	0.682	0.385	0.87	0.616***	0.286**	0.414***	0.600***	0.826			
6	0.776	0.789	0.562	0.308	0.843	0.269*	0.386**	0.428***	0.219*	0.278*	0.749		
7	0.850	0.852	0.659	0.385	0.866	0.559***	0.376***	0.385***	0.582***	0.620***	0.202*	0.812	
8	0.772	0.773	0.533	0.458	0.784	0.563***	0.677***	0.565***	0.432***	0.470***	0.555***	0.418***	0.73

Notes: Significance of correlations: †$p < 0.100$; *$p < 0.050$; **$p < 0.010$; ***$p < 0.001$
Sources: Hu and Bentler (1999); Gaskin and Lim (2016)

Table V.
Results of measurement model

Table VI.
Path analysis and verification of research hypothesis

Hypothesis			β	t	p	Supported
H1a	KSC	L&G	0.431	3.346	***	S
H1b		IP	0.338	4.028	***	S
H1c		CS	0.387	7.24	***	S
H1d		FP	0.197	2.141	0.033	S
H2a	HRM for KM	L&G	0.276	3.072	0.002	S
H2b		IP	0.223	3.212	***	S
H2c		CS	0.174	4.343	***	S
H2d		FP	0.164	2.235	0.027	S
H3a	S&L	L&G	0.403	2.2	0.031	S
H3b		IP	0.416	2.104	0.035	S
H3c		CS	0.217	1.496	0.066	NS
H3d		FP	0.154	1.103	0.079	NS
H4a	ICT	L&G	0.062	0.401	0.689	NS
H4b		IP	0.13	0.785	0.432	NS
H4c		CS	0.094	0.647	0.517	NS
H4d		FP	0.128	0.944	0.345	NS

Note: Significant at $p < 0.05$

has measured independent relationships through a decomposed model, the paper has been able to uncover underlying relationships between constructs. Interpretations based on these findings are presented below.

KSC has emerged as a strong positive influencer affecting all the measures of OP significantly, proving *H1a* ($\beta = 0.431$, $p = 0.000$), b ($\beta = 0.338$, $p = 0.000$), c ($\beta = 0.387$, $p = 0.000$) and d ($\beta = 197$, $p = 0.033$). KM literature has generally accepted that culture of the work environment has a significant influence on OP (Gold *et al.*, 2001; Lee and Choi, 2003; Lee and Lee, 2007; Zheng *et al.*, 2010; Mills and Smith, 2011; Jain and Moreno, 2015). The respondents felt that the presence of an environment of collaboration, support, participation and team spirit in the organization serve as key underlying success factors. When there is a clear focus on development through learning and innovation, the employees find themselves placed in comfortable spots to develop new skills and hone current ones. This constant quest for new knowledge and application of the current set has shown to affect not only learning processes of the organization but also improve the IP, CS and most importantly the financial aspect of performance too (Figure 2).

The effect of KHRM practices on the OP measures, i.e. *H2a* ($\beta = 0.276$, $p = 0.002$), b ($\beta = 0.223$, $p = 0.000$), c ($\beta = 0.174$, $p = 0.000$) and d ($\beta = 0.164$, $p = 0.027$) is strongly supported. It is interesting to note that KHRM practices have shown a positive direct effect on L&G, IP, CS and FP. Literature endorses that an organization's focus on the management of the human resource in line with knowledge has proved to be advantageous for the organization (Lee and Choi, 2003; Palacios Marqués and José Garrigos Simon, 2006; Lu *et al.*, 2008; Andreeva and Kianto, 2012; Wu and Chen, 2014). The "people" factor in organizations has garnered immense importance. With the advent of intangibles in product portfolios and service industry becoming a major contributor to an organization's bottom line, knowledge has become an indispensable resource for organizations and people being creators, users and disseminators of the same have become the fulcrum of all activity. While there is theoretical evidence from previous research that HRM contributes to knowledge performance and FP (Foss *et al.*, 2009), very little empirical research has proven this link before. This research is a definitive step in this direction (Figure 3).

H3a ($\beta = 403$, $p = 0.031$) – "S&L" – has a positive and significant effect on L&G is supported. This is in concurrence with previous research "S&L" has a profound effect on knowledge processes in the organization (Chong and Choi, 2005; Hung *et al.*, 2005;

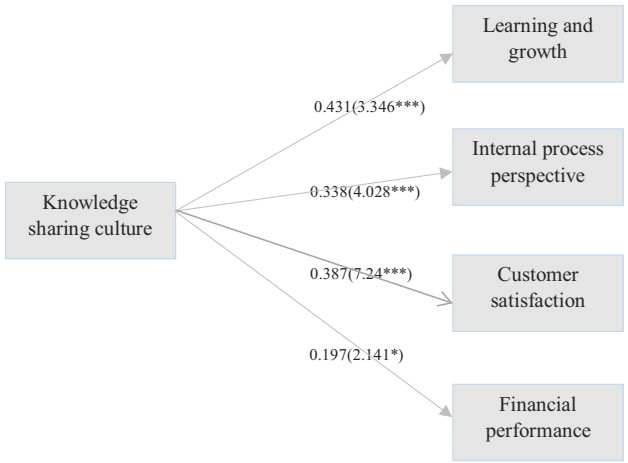

Source: Author

Figure 2.
Results – KSC and BSC measures

Ananatamulla, 2007; Donate and de Pablo, 2015). This is evident and endorsed that it is the responsibility of the top management to develop an environment of teamwork and mutual trust in the organization. When the organization leaders express their confidence in the employee skills and are instrumental in the development of an atmosphere where creativity is valued and nurtured, employee L&G grows by leaps and bounds. The data also support *H3b* ($\beta = 0.416$, $p = 0.035$) i.e. S&L positively affect IP. Whole-hearted support to KM initiatives and removal of factors that constraint-free flow of knowledge leads to inefficiency and ineffectiveness. Rigidity in organizational procedures can create long chains of command and slow response time. Management's resolve to curtail these processes and procedures contributes massively to the improvement of IP. However, *H3c* ($\beta = 0.217$, $p = 0.066$) and *H3d* ($\beta = 0.154$, $p = 0.079$) i.e. the effect of 'S&L' on CS and FP were found to be insignificant. This hints to the fact that there are other factors at play that affect CS and FP of an organization and the benefits of good leadership do not percolate to the customer and FP of an organization directly (Figure 4).

H4a ($\beta = 0.062$, $p = 0.689$), *H4b* ($\beta = 13$, $p = 0.432$), c ($\beta = 0.094$, $p = 0.647$) and *H4d* ($\beta = 0.128$, $p = 0.345$) were not supported by the data i.e. ICT does not have a significant effect on any of the measures of OP. These findings are in support of the earlier views that ICT

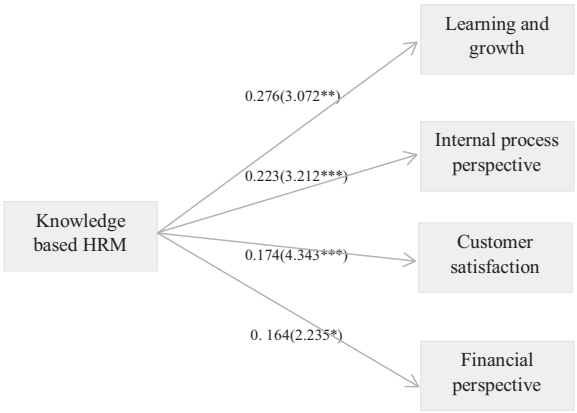

Figure 3.
Results –HRM for KM and BSC measures

Source: Author

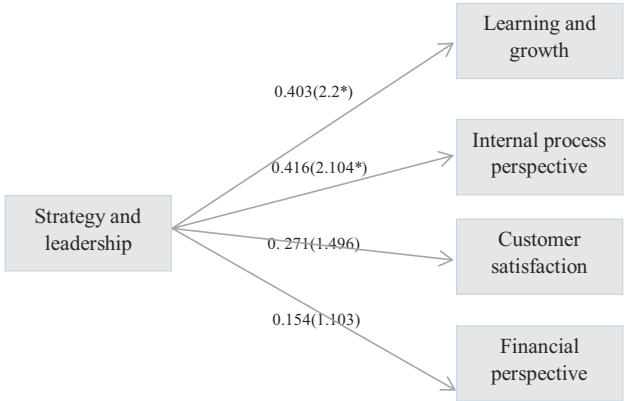

Figure 4.
Results – S&L and BSC measures

Source: Author

practices acted as enablers and facilitators and could only produce results when coupled with HRM (Andreeva and Kianto, 2012; Chong and Choi, 2005); effective knowledge processes (Kamhawi, 2012); strategic intent (Cao *et al.*, 2013). This is of significance as there needs to a deep and thorough sense of understanding that mere possession of up-to-date and capable ICT systems do not guarantee the development of an organization where knowledge creation and sharing processes would flourish; instead ICT has to be looked upon as a resource just like any other which has to be put to good use for gaining competitive advantage. It has been observed that although previous studies also endorsed this point of view, notwithstanding this, most KM implementation project managers lay a lot of focus on the use of high- tech equipment. One important take away from this is that presence of high-tech modern ICT does not act as a motivator for creating or sharing organizational knowledge and contribute positively to performance directly but the absence of these technologies will surely be a limiting factor. It is important to suit these KM systems to the needs of their internal and external customers i.e. employees and customers (Tiwana, 2002) (Figure 5).

6. Implications

6.1 Implications for research

By studying the decomposed relationships that exist between individual KM practices and OP, many important implications for KM in organizations have been highlighted. First, the research results have thread bared individual relationships and shown that KM, when implemented in thought and spirit in organizations affects all the aspects of performance percolating down to FP also.

Second, KSC and KHRM have a significant positive effect on all the measures of OP. This highlights that development of highly comparative, breakneck competition is not required for organizations to perform well. This is of significance since the findings are based on the Indian sample. Due to various historical, demographic and economic factors, India has faced enormous pressure on resources, there exists huge competition for even small means. This has led to a common belief in India that competition is all pervasive. It is extremely heartening to see through this study that Indian organizations are now working towards the development of a culture of collaboration and cooperation and believing and experiencing *that this is in the best interest of the company.*

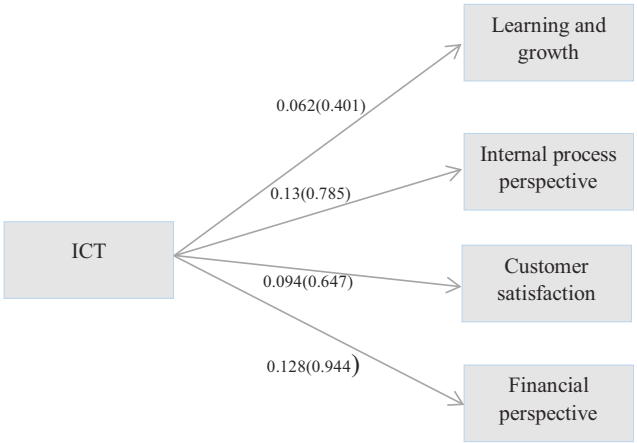

Source: Author

Figure 5.
Results – ICT and BSC measures

When compared to composite models, this research is a step forward, as it has been able to identify and quantify the effect and contribution of individual KM practices to performance of an organization. There exists a gap in the literature linking specific KM practices with OP (Mills and Smith, 2011), the current research helps bridge this gap.

6.2 Implications for practice

Association of KM practices with BSC has major implications for organizations. Generally, OP has been measured as a single construct in previous research. The measures used for gauging OP have been limited to innovation (Darroch, 2003; Gloet and Terziovski, 2004; Zheng *et al.*, 2010); competitiveness (Allard and Holsapple, 2002; Choy Chong, 2006); market share and profitability (Lee and Choi, 2003; Palacios Marqués and José Garrigós Simón, 2006); stock price and FP (Lee *et al.*, 2005; Jain and Moreno, 2015). Also, the KM practices analyzed vary from one research to another. Due to this, the development of an overall understanding of the relationship between KM practices and OP is difficult to draw from the current set of literature.

This research has not only integrated KM practices with financial and non-financial measures of OP, but it also exhibits individual relationships between them. The study shows that KSC and KHRM practices when implemented in an organization will lead to better L&G of the organization, efficiency in the IP, better customer service and also positively affect the FP of the organization. While S&L affect L&G and IP positively, there is no significant effect exhibited on CS and FP of an organization. These are important KM-performance links that have been uncovered by means of this research. This is an in-depth study and stands in stark comparison to the current set of literature on KM and OP which focusses on the overall effects.

7. Research limitations and future research

Despite its contributions, there are some limitations, which if addressed in future studies, can help add more robustness to the study. First, the current paper has a limited scope as it uses an Indian sample to study the effect of KM practices on the performance of organizations. This adversely affects the generalizability of the study. Second, the data used for analysis is perceptual, self-reported data. Future studies could measure these constructs using more objective data instead of perceptual data. Subjective data can be reliable and used for research in the absence of objective data (Delaney and Huselid, 1996). Another change could be made in the method of data collection, structured interviews could be used instead of a questionnaire so as to overcome misinterpretations of questions if any. Future research could also integrate more KM practices like KM structure and decentralization to develop a more comprehensive model.

References

Abualoush, S., Masa'deh, R.E., Bataineh, K. and Alrowwad, A. (2018), "The role of knowledge management process and intellectual capital as intermediary variables between knowledge management infrastructure and organization performance", *Interdisciplinary Journal of Information, Knowledge, and Management*, Vol. 13, pp. 279-309.

Akhavan, P. and Jafari, M. (2006), "Critical issues for knowledge management implementation at a national level", *VINE*, Vol. 36 No. 1, pp. 52-66.

Alavi, M. and Leidner, D.E. (2001), "Knowledge management and knowledge management systems: conceptual foundations and research issues", *MIS Quarterly*, Vol. 25, pp. 107-136.

Al-Busaidi, K.A. and Olfman, L. (2005), "An investigation of the determinants of knowledge management systems success in Omani organizations", *Journal of Global Information Technology Management*, Vol. 8 No. 3, pp. 6-27.

Allard, S. and Holsapple, C.W. (2002), "Knowledge management as a key for e-business competitiveness: from the knowledge chain to KM audits", *Journal of Computer Information Systems*, Vol. 4 No. 5, pp. 19-25, doi: 10.1080/08874417.2002.11647606.

American Productivity and Quality Center (APQC) (1999), *Knowledge Management: Executive Summary, Consortium Benchmarking Study Best-Practice Report*, APQC, Houston, TX, available at: www.apqc.org (accessed 7 April 2018).

Anderson, J. and Gerbing, D.W. (1988), "Structural equation modeling in practice: a review and recommended two-step approach", *Psychological Bulletin*, Vol. 103 No. 3, pp. 411-423, available at: https://doi.org/10.1037/0033-2909.103.3.411

Andreeva, T. and Kianto, A. (2012), "Does knowledge management really matter? Linking knowledge management practices, competitiveness and economic performance", *Journal of Knowledge Management*, Vol. 16 No. 4, pp. 617-636.

Appelbaum, S., Karasek, R., Lapointe, F. and Quelch, K. (2014), "Employee empowerment: factors affecting the consequent success or failure – part I", *Industrial and Commercial Training*, Vol. 46 No. 7, pp. 379-386.

Ardito, L. and Petruzzelli, A.M. (2017), "Breadth of external knowledge sourcing and product innovation: the moderating role of strategic human resource practices", *European Management Journal*, Vol. 35 No. 2, pp. 261-272.

Arora, R. (2002), "Implementing KM–a balanced score card approach", *Journal of Knowledge Management*, Vol. 6 No. 3, pp. 240-249.

Basu, B. and Kumar Ray, P. (2014), "Measuring and evaluating KM capability in an organization: an exploratory case study", *VINE*, Vol. 44 No. 2, pp. 267-294.

Bennett, R. and Gabriel, H. (1999), "Organisational factors and knowledge management within large marketing departments: an empirical study", *Journal of Knowledge Management*, Vol. 3 No. 3, pp. 212-225.

Birasnav, M. (2014), "Knowledge management and organizational performance in the service industry: the role of transformational leadership beyond the effects of transactional leadership", *Journal of Business Research*, Vol. 67 No. 8, pp. 1622-1629.

Bollinger, A. and Smith, R. (2001), "Managing organizational knowledge as a strategic asset", *Journal of Knowledge Management*, Vol. 5 No. 1, pp. 8-18.

Bontis, N and Giradi, J. (2000), "Teaching knowledge management and intellectual capital lessons: an empirical examination of TANGO situation", *Journal of Technology Management*, Vol. 20 Nos 5/8, pp. 545-555.

Cao, Q., Thompson, M.A. and Triche, J. (2013), "Investigating the role of business processes and knowledge management systems on performance: a multi-case study approach", *International Journal of Production Research*, Vol. 51 No. 18, pp. 5565-5575.

Chang, C. and Lin, T. (2015), "The role of organizational culture in the knowledge management process", *Journal of Knowledge Management*, Vol. 19 No. 3, pp. 433-455.

Chen, C.-J. and Huang, J.-W. (2009), "Strategic human resource practices and innovation performance – the mediating role of knowledge management capacity", *Journal of Business Research*, Vol. 62 No. 1, pp. 104-114.

Chen, L. and Mohamed, S. (2008), "Contribution of knowledge management activities to organisational business performance", *Journal of Engineering, Design and Technology*, Vol. 6 No. 3, pp. 269-285.

Chen, F.H., Hsu, T.S. and Tzeng, G.H. (2011), "A balanced scorecard approach to establish a performance evaluation and relationship model for hot spring hotels based on a hybrid MCDM

model combining DEMATEL and ANP", *International Journal of Hospitality Management*, Vol. 30 No. 4, pp. 908-932.

Choi, Y.S. (2000), "An empirical study of factors affecting successful implementation of knowledge management", (Doctoral dissertation), University of Nebraska, Lincoln.

Chong, S.C. and Choi, Y.S. (2005), "Critical factors of knowledge management implementation success", *Journal of Knowledge Management Practice*, Vol. 6 No. 3, pp. 21-37.

Chopra, M., Gupta, V. and Chhabra, B. (2017), "Strategic management using balanced scorecard—a case study on tata power", *South Asian Journal of Business and Management Cases*, Vol. 6 No. 2, pp. 176-190, doi: 10.1177/2277977917730446.

Choy Chong, S. (2006), "KM critical success factors", *The Learning Organization*, Vol. 13 No. 3, pp. 230-256, available at: https://doi.org/10.1108/09696470610661108

Civi, E. (2000), "Knowledge management as a competitive asset: a review", *Marketing Intelligence and Planning*, Vol. 18 No. 4, pp. 166-174.

Cohen, J.F. and Olsen, K. (2015), "Knowledge management capabilities and firm performance: a test of universalistic, contingency and complementarity perspectives", *Expert Systems with Applications*, Vol. 42 No. 3, pp. 1178-1188.

Darroch, J. (2003), "Developing a measure of knowledge management behaviors and practices", *Journal of Knowledge Management*, Vol. 7 No. 5, pp. 41-54.

Darroch, J. (2005), "Knowledge management, innovation and firm performance", *Journal of Knowledge Management*, Vol. 9 No. 3, pp. 101-115.

Darroch, J. and McNaughton, R. (2002), "Examining the link between knowledge management practices and types of innovation." *Journal of Intellectual Capital*, Vol. 3 No. 3, pp. 210-222.

Darroch, J. and McNaughton, R. (2003), "Beyond market orientation", *European Journal of Marketing*, Vol. 37 Nos 3/4, pp. 572-593, available at: https://doi.org/10.1108/03090560310459096

Davenport, T.H. and Klahr, P. (1998), "Managing customer support knowledge", *California Management Review*, Vol. 40 No. 3, pp. 195-208.

De Gooijer, J. (2000), "Designing a knowledge management performance framework", *Journal of Knowledge Management*, Vol. 4 No. 4, pp. 303-310.

Del Giudice, M. and Della Peruta, M.R. (2016), "The impact of IT-based knowledge management systems on internal venturing and innovation: a structural equation modelling approach to corporate performance", *Journal of Knowledge Management*, Vol. 20 No. 3, pp. 484-498.

Delaney, J.T. and Huselid, M.A. (1996), "The impact of human resource management practices on perceptions of organizational performance", *Academy of Management Journal*, Vol. 39 No. 4, pp. 949-969.

Donate, M.J. and de Pablo, J.D.S. (2015), "The role of knowledge-oriented leadership in knowledge management practices and innovation", *Journal of Business Research*, Vol. 68 No. 2, pp. 360-370.

Du Plessis, M. (2007), "The role of knowledge management in innovation", *Journal of Knowledge Management*, Vol. 11 No. 4, pp. 20-29.

Farzaneh, M., Isaai, M.T., Arasti, M.R. and Mehralian, G. (2018), "A framework for developing business intelligence systems: a knowledge perspective", *Management Research Review*, Vol. 41 No. 12, pp. 1358-1374.

Fornell, C. and Larcker, D.F. (1981), "Evaluating structural equation models with unobservable variables and measurement error", *Journal of Marketing Research*, Vol. 18 No. 1, pp. 39-50.

Foss, N.J., Minbaeva, D.B., Pedersen, T. and Reinholt, M. (2009), "Encouraging knowledge sharing among employees: how job design matters", *Human Resource Management*, Vol. 48 No. 6, pp. 871-893.

Gaskin, J. and Lim, J. (2016), *Master Validity Tool: AMOS Plugin*, Gaskination's StatWiki.

Gloet, M. and Terziovski, M. (2004), "Exploring the relationship between knowledge management practices and innovation performance", *Journal of Manufacturing Technology Management*, Vol. 15 No. 5, pp. 402-409.

Gold, A.H., Malhotra, A. and Segars, A.H. (2001), "Knowledge management: an organizational capabilities perspective", *Journal of Management Information Systems*, Vol. 18 No. 1, pp. 185-214.

Gonzalez, -Padron, T.L., Chabowski, B.R., Hult, G.T.M. and Ketchen, Jr, D.J. (2010), "Knowledge management and balanced scorecard outcomes: exploring the importance of interpretation, learning and internationality", *British Journal of Management*, Vol. 21 No. 4, pp. 967-982.

Grant, R.M. (1996), "Toward a knowledge-based theory of the firm", *Strategic Management Journal*, Vol. 17 No. S2, pp. 109-122.

Greco, M., Grimaldi, M. and Hanandi, M. (2013), "How to select knowledge management systems: a framework to support managers", *International Journal of Engineering Business Management*, Vol. 5, p. 56.

Gupta, V. and Chopra, M. (2017), "Gauging the impact of knowledge management practices on organizational performance – a balanced scorecard perspective", *VINE Journal of Information and Knowledge Management Systems*, Vol. 48 No. 1, pp. 21-46.

Han, B. and Anantatmula, V. (2007), "Knowledge sharing in large IT organizations: a case study", *VINE*, Vol. 37 No. 4, pp. 421-439, available at: https://doi.org/10.1108/03055720710838506

Hansen, M.T., Nohria, N. and Tierney, T. (1999), "What's your strategy for managing knowledge", *The Knowledge Management Yearbook 2000–2001*, pp. 1-10.

Holsapple, C.W. and Joshi, K.D. (2000), "An investigation of factors that influence the management of knowledge in organizations", *The Journal of Strategic Information Systems*, Vol. 9 Nos 2/3, pp. 235-261.

Holsapple, C.W. and Singh, M. (2000), "Toward a unified view of electronic commerce, electronic business, and collaborative commerce: a knowledge management approach", *Knowledge and Process Management*, Vol. 7 No. 3, pp. 151-164.

Hsieh, C.T., Yang, H. and Lin, B. (2002), "Roles of knowledge management in online procurement systems", *Industrial Management and Data Systems*, Vol. 102 No. 7, pp. 365-370.

Hu, L.T. and Bentler, P.M. (1999), "Cutoff criteria for fit indexes in covariance structure analysis: conventional criteria versus new alternatives", *Structural Equation Modeling*, Vol. 6, pp. 1-55.

Hung, Y.C., Huang, S.M., Lin, Q.P. and Tsai, M.L. (2005), "Critical factors in adopting a knowledge management system for the pharmaceutical industry", *Industrial Management and Data Systems*, Vol. 105 No. 2, pp. 164-183.

Hussinki, H., Ritala, P., Vanhala, M. and Kianto, A. (2017), "Intellectual capital, knowledge management practices and firm performance", *Journal of Intellectual Capital*, Vol. 18 No. 4, pp. 904-922.

Hwang, A.S. (2003), "Training strategies in the management of knowledge", *Journal of Knowledge Management*, Vol. 7 No. 3, pp. 92-104.

Inkinen, H. (2015), "Review of empirical research on intellectual capital and firm performance", *Journal of Intellectual Capital*, Vol. 16 No. 3, pp. 518-565.

Inkinen, H., Kianto, A., Vanhala, M. and Ritala, P. (2017), "Structure of intellectual capital–an international comparison", *Accounting, Auditing and Accountability Journal*, Vol. 30 No. 5, pp. 1160-1183.

Jain, A.K. and Moreno, A. (2015), "Organizational learning, knowledge management practices and firm's performance: an empirical study of a heavy engineering firm in India", *The Learning Organization*, Vol. 22 No. 1, pp. 14-39.

Kalling, T. (2003), "Knowledge management and the occasional links with performance", *Journal of Knowledge Management*, Vol. 7 No. 3, pp. 67-81.

Kaplan, R.S. and Norton, D.P. (1992), "The balanced scorecard – measures that drive performance", *Harvard Business Review*, Vol. 70 Nos 7/8, pp. 172-180.

Kaplan, R.S. and Norton, D.P. (1996), "Linking the balanced scorecard to strategy", *California Management Review*, Vol. 39 No. 1, pp. 53-79.

Kaplan, R.S. and Norton, D.P. (1996a), "Linking the balanced scorecard to strategy", *California Management Review* , Vol. 39 No. 1, pp. 53-79.

Kaplan, R.S. and Norton, D.P. (1996b), "Strategic learning and the balanced scorecard", *Strategy and Leadership*, No. 5, pp. 18-24.

Kamhawi, E. (2012), "Knowledge management fishbone: a standard framework of organizational enablers", *Journal of Knowledge Management*, Vol. 16 No. 5, pp. 808-828, available at: https://doi.org/10.1108/13673271211262826

Kianto, A. (2011), "The influence of knowledge management on continuous innovation", *International Journal of Technology Management*, Vol. 55 Nos 1/2, pp. 110-121.

Kianto, A., Ritala, P., Spender, J.C. and Vanhala, M. (2014), "The interaction of intellectual capital assets and knowledge management practices in organizational value creation", *Journal of Intellectual Capital*, Vol. 15 No. 3, pp. 362-375.

Lee, H. and Choi, B. (2003), "Knowledge management enablers, processes, and organizational performance: an integrative view and empirical examination", *Journal of Management Information Systems*, Vol. 20 No. 1, pp. 179-228.

Lee, Y.-C. and Lee, S.-K. (2007), "Capabilities, processes, performance of knowledge management: a structural approach", *Human Factors and Ergonomics in Manufacturing*, Vol. 17 No. 1, pp. 21-41.

Lee, K.C., Lee, S. and Kang, I.W. (2005), "KMPI: measuring knowledge management performance", *Information and Management*, Vol. 42 No. 3, pp. 469-482.

Lee, J.C., Shiue, Y.C. and Chen, C.Y. (2016), "Examining the impacts of organizational culture and top management support of knowledge sharing on the success of software process improvement", *Computers in Human Behavior*, Vol. 54, pp. 462-474.

Lu, Y., Tsang, E.W. and Peng, M.W. (2008), *Knowledge Management and Innovation Strategy in the Asia Pacific: Toward an Institution-Based View*.

Mills, A.M. and Smith, T.A. (2011), "Knowledge management and organizational performance: a decomposed view", *Journal of Knowledge Management*, Vol. 15 No. 1, pp. 156-171.

Mohammed, T. and Alshawi, S. (2015), "The impact of knowledge management processes on organizational performance", *Journal of Enterprise Information Management*, Vol. 28 No. 2, pp. 167-185.

Moffett, S., McAdam, R. and Parkinson, S. (2003), "An empirical analysis of knowledge management applications", *Journal of Knowledge Management*, Vol. 7 No. 3, pp. 6-26.

Moore, C., Rowe, B.J. and Widener, S.K. (2001), "HCS: designing a balanced scorecard in a knowledge-based firm", *Issues in Accounting Education*, Vol. 16 No. 4, pp. 569--601.

Nunnally, J.C. and Bernstein, I.H. (1994), *Psychometric Theory*, 3rd ed., McGraw-Hill, New York, NY.

Palacios Marqués, D. and José Garrigós Simón, F. (2006), "The effect of knowledge management practices on firm performance", *Journal of Knowledge Management*, Vol. 10 No. 3, pp. 143-156.

Pemberton, J.D., Stonehouse, G.H. and Francis, M.S. (2002), "Black and decker – towards a knowledge-centric organization", *Knowledge and Process Management*, Vol. 9 No. 3, pp. 178-189.

Perez-Arrau, G., Suraj, O.A., Heisig, P., Kemboi, C., Easa, N. and Kianto, A. (2014), "Knowledge management and business outcome/performance: results from a review and global expert study with future research", *BAM2014-The Role of the Business School in Supporting Economic and Social Development, British Academy of Management Conference*, *Belfast*, 9-11 September.

Petter, S., Straub, D. and Rai, A. (2007), "Specifying formative constructs in information systems research", *MIS Quarterly*, Vol. 31 No. 4, pp. 623-656.

Prahalad, C.K. and Hamel, G. (1997), "The core competence of the corporation", *Strategische Unternehmungsplanung/Strategische Unternehmungsführung*, Physica, Heidelberg, pp. 969-987.

Prusak, L. (1996), "The knowledge advantage", *Planning Review*, Vol. 24, pp. 6-8.

Rasula, J., Vuksic, V.B. and Stemberger, M.I. (2012), "The impact of knowledge management on organisational performance", *Economic and Business Review*, Vol. 14 No. 2, pp. 147-168.

Ribiere, V.M. and Sitar, A.S. (2003), "Critical role of leadership in nurturing a knowledge-supporting culture", *Knowledge Management Research and Practice*, Vol. 1 No. 1, pp. 39-48.

Rodriguez Perez, J. and Ordóñez de Pablos, P. (2003), "Knowledge management and organizational competitiveness: a framework for human capital analysis", *Journal of Knowledge Management*, Vol. 7 No. 3, pp. 82-91.

Roth, A.V. (1996), "Achieving strategic agility through economies of knowledge", *Planning Review*, Vol. 24, pp. 30-37. (March-April).

Ryan, S.D. and Prybutok, V.R. (2001), "Factors affecting the adoption of knowledge management technologies: a discriminative approach", *Journal of Computer Information Systems*, Vol. 41 No. 4, pp. 31-37.

Sabherwal, R.A.J.I.V. and Becerra-Fernandez, I. (2010), "Knowledge management systems and processes", *ME Sharpe, New York, NY*.

Singh, A. and Soltani, E. (2010), "Knowledge management practices in Indian information technology companies", *Total Quality Management and Business Excellence*, Vol. 21 No. 2, pp. 145-157, doi: 10.1080/14783360903549832.

Sinha, N., Kakkar, N.K. and Gupta, V. (2015), "Harnessing the power of knowledge management for innovation", *International Journal of Knowledge and Learning*, Vol. 10 No. 2, pp. 124-146.

Soto-Acosta, P., Colomo-Palacios, R. and Popa, S. (2014), "Web knowledge sharing and its effect on innovation: an empirical investigation in SMEs", *Knowledge Management Research and Practice*, Vol. 12 No. 1, pp. 103-113.

Spender, J.C. and Grant, R.M. (1996), "Knowledge and the firm: overview", *Strategic Management Journal*, Vol. 17 No. S2, pp. 5-9.

Starns, J. and Odom, C. (2006), "Using knowledge management principles to solve organizational performance problems", *VINE*, Vol. 36 No. 2, pp. 186-198.

Sumbal, M.S., Tsui, E. and See-To, E.W.K. (2017), "Interrelationship between big data and knowledge management: an exploratory study in the oil and gas sector", *Journal of Knowledge Management*, Vol. 21 No. 1, pp. 180-196.

Taherparvar, N., Esmaeilpour, R. and Dostar, M. (2014), "Customer knowledge management, innovation capability and business performance: a case study of the banking industry", *Journal of Knowledge Management*, Vol. 18 No. 3, pp. 591-610.

Tiwana, A. (2002), *The Knowledge Management Toolkit: Orchestrating IT, Strategy, and Knowledge Platforms*, Prentice Hall PTR, Upper Saddle River, NJ.

Tunc Bozbura, F. (2007), "Knowledge management practices in Turkish SME", *Journal of Enterprise Information Management*, Vol. 20 No. 2, pp. 209-221.

Vaccaro, A., Parente, R. and Veloso, F.M. (2010), "Knowledge management tools, inter-organizational relationships, innovation and firm performance", *Technological Forecasting and Social Change*, Vol. 77 No. 7, pp. 1076-1089.

Valmohammadi, C. and Ahmadi, M. (2015), "The impact of knowledge management practices on organizational performance: a balanced scorecard approach", *Journal of Enterprise Information Management*, Vol. 28 No. 1, pp. 131-159.

Vanhala, M. and Ritala, P. (2016), "HRM practices, impersonal trust and organizational innovativeness", *Journal of Managerial Psychology*, Vol. 31 No. 1, pp. 95-109.

Vătămănescu, E.M., Andrei, A.G., Dumitriu, D.L. and Leovaridis, C. (2016), "Harnessing network-based intellectual capital in online academic networks. From the organizational policies and practices towards competitiveness", *Journal of Knowledge Management*, Vol. 20 No. 3, pp. 594-619.

Walsh, J.P. and Ungson, G.R. (1991), "Organizational memory", *The Academy of Management Review*, Vol. 16 No. 1, pp. 57-91.

Wang, K.L., Chiang, C. and Tung, C.M. (2012), "Integrating human resource management and knowledge management: from the viewpoint of core employees and organizational performance", *International Journal of Organizational Innovation (Online)*, Vol. 5 No. 1, p. 109.

Wenger, E.C. and Snyder, W.M. (2000), "Communities of practice: the organizational frontier", *Harvard Business Review*, Vol. 78 No. 1, pp. 139-146.

Wong, K.Y. and Aspinwall, E. (2005), "An empirical study of the important factors for knowledge-management adoption in the SME sector", *Journal of Knowledge Management*, Vol. 9 No. 3, pp. 64-82.

Wu, I.L. and Chen, J.L. (2014), "Knowledge management driven firm performance: the roles of business process capabilities and organizational learning", *Journal of Knowledge Management*, Vol. 18 No. 6, pp. 1141-1164.

Yahya, S. and Goh, W.K. (2002), "Managing human resources toward achieving knowledge management", *Journal of Knowledge Management*, Vol. 6 No. 5, pp. 457-468.

Yahyapour, S., Shamizanjani, M. and Mosakhani, M. (2015), "A conceptual breakdown structure for knowledge management benefits using meta-synthesis method", *Journal of Knowledge Management*, Vol. 19 No. 6, pp. 1295-1309.

Zack, M., McKeen, J. and Singh, S. (2009), "Knowledge management and organizational performance: an exploratory analysis", *Journal of Knowledge Management*, Vol. 13 No. 6, pp. 392-409.

Zaim, H., Tatoglu, E. and Zaim, S. (2007), "Performance of knowledge management practices: a causal analysis", *Journal of Knowledge Management*, Vol. 11 No. 6, pp. 54-67.

Zheng, W., Yang, B. and McLean, G.N. (2010), "Linking organizational culture, structure, strategy, and organizational effectiveness: mediating role of knowledge management", *Journal of Business Research*, Vol. 63 No. 7, pp. 763-771.

Further reading

Chen, M.Y., Huang, M.J. and Cheng, Y.C. (2009), "Measuring knowledge management performance using a competitive perspective: an empirical study", *Expert Systems with Applications*, Vol. 36 No. 4, pp. 8449-8459.

Churchill, G.A. Jr, (1979), "A paradigm for developing better measures of marketing constructs", *Journal of Marketing Research*, Vol. 16 No. 1, pp. 64-73.

Grimaldi, M. and Hanandi, M. (2013), "Evaluating the intellectual capital of technology transfer and learning public services", *International Journal of Engineering Business Management*, Vol. 5 No. 7, pp. 1-10.

Hair, J.F., Anderson, R.E., Tatham, R.L. and Black, W.C. (2005), "*Multivariate Data Analysis*", *Prentice-Hall, NJ*.

Heisig, P. (2009), "Harmonisation of knowledge management – comparing 160 KM frameworks around the globe", *Journal of Knowledge Management*, Vol. 13 No. 4, pp. 4-31.

Kaplan, R.S. (2009), "Conceptual foundations of the balanced scorecard", *Handbooks of Management Accounting Research*, pp. 1253-1269, doi: 10.1016/s1751-3243(07)03003-9.

Martí-de Castro, G., López-Sáez, P., Delgado-Verde, M., Andreeva, T. and Kianto, A. (2011), "Knowledge processes, knowledge-intensity and innovation: a moderated mediation analysis", *Journal of Knowledge Management*, Vol. 15 No. 6, pp. 1016-1034, available at: https://doi.org/10.1108/13673271111179343

Punniyamoorthy, M. and Murali, R. (2008), "Balanced score for the balanced scorecard: a benchmarking tool", *Benchmarking: An International Journal*, Vol. 15 No. 4, pp. 420-443.

Sinha, N., Kakkar, N.K. and Gupta, V. (2012), "Uncovering the secrets of the twenty-first-century organization", *Global Business and Organizational Excellence*, Vol. 31 No. 2, pp. 49-56.

Zhang, M. (2018), "Cross-cultural reliability and validity of a scale to measure international entrepreneurial capability in emerging markets", *Journal of Asia-Pacific Business*, Vol. 19 No. 1, pp. 23-35.

Corresponding author
Meenu Chopra can be contacted at: mchopra2002@gmail.com

For instructions on how to order reprints of this article, please visit our website:
www.emeraldgrouppublishing.com/licensing/reprints.htm
Or contact us for further details: **permissions@emeraldinsight.com**

ResearchGate

See discussions, stats, and author profiles for this publication at: https://www.researchgate.net/publication/327675035

Low power analog comb filter for biomedical applications

Article *in* Analog Integrated Circuits and Signal Processing · September 2018

DOI: 10.1007/s10470-018-1329-8

CITATIONS
0

READS
103

3 authors, including:

Gaurav Tiwari
Dr. D.Y. Patil School of Engineering, lohegaon ,pune
3 PUBLICATIONS **15** CITATIONS

SEE PROFILE

Some of the authors of this publication are also working on these related projects:

Realization of the function of intellegent smart sensor for IoT in WSN View project

All content following this page was uploaded by Gaurav Tiwari on 02 May 2019.

The user has requested enhancement of the downloaded file.

Low power analog comb filter for biomedical applications

Sajal K. Paul, Chandan Kumar Choubey & Gaurav Tiwari

Analog Integrated Circuits and Signal Processing
An International Journal

ISSN 0925-1030

Analog Integr Circ Sig Process
DOI 10.1007/s10470-018-1329-8

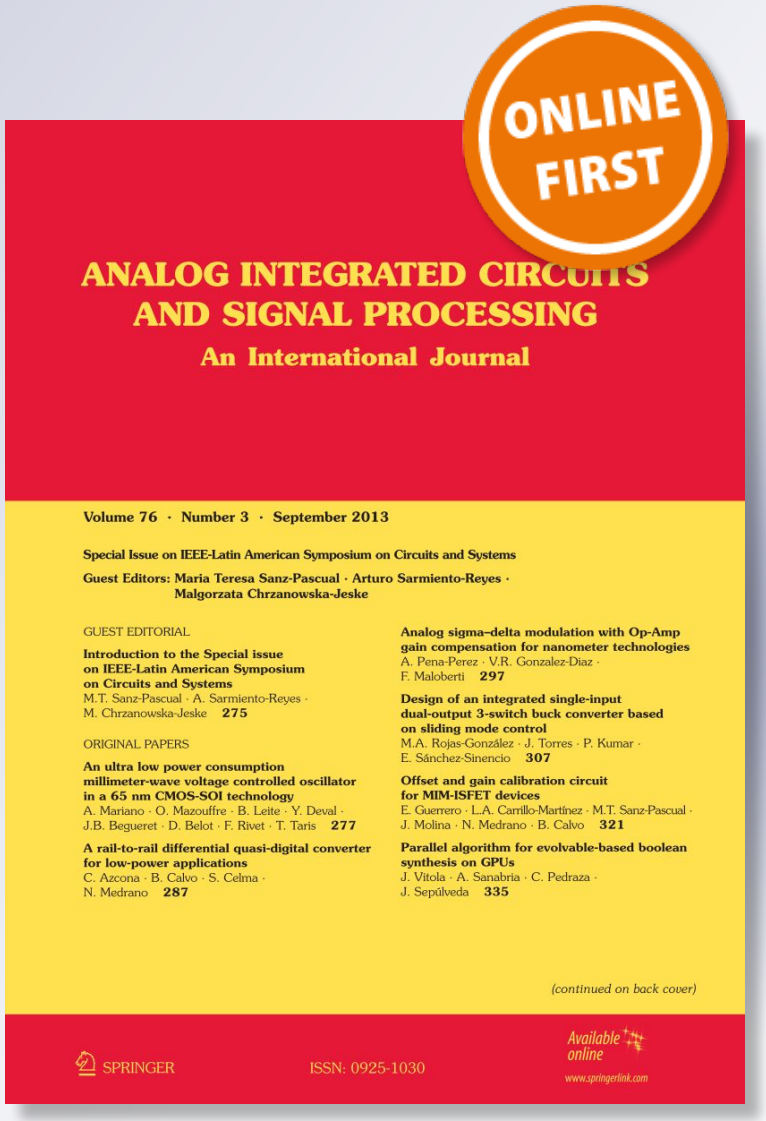

Springer

Your article is protected by copyright and all rights are held exclusively by Springer Science+Business Media, LLC, part of Springer Nature. This e-offprint is for personal use only and shall not be self-archived in electronic repositories. If you wish to self-archive your article, please use the accepted manuscript version for posting on your own website. You may further deposit the accepted manuscript version in any repository, provided it is only made publicly available 12 months after official publication or later and provided acknowledgement is given to the original source of publication and a link is inserted to the published article on Springer's website. The link must be accompanied by the following text: "The final publication is available at link.springer.com”.

Author's personal copy

Analog Integrated Circuits and Signal Processing
https://doi.org/10.1007/s10470-018-1329-8

MIXED SIGNAL LETTER

Low power analog comb filter for biomedical applications

Sajal K. Paul[1] · Chandan Kumar Choubey[2] · Gaurav Tiwari[3]

Received: 23 April 2018 / Revised: 17 July 2018 / Accepted: 6 September 2018
© Springer Science+Business Media, LLC, part of Springer Nature 2018

Abstract
An analog topology is proposed to implement a comb filter for removal of power-line interference from various low-amplitude biomedical signals. In this proposed methodology, an n-number of all-pass filters (APFs) and an adder circuit are used to suppress n-number of frequencies. All the APFs as well as the adder circuit are designed using a current conveyor to utilize the various properties of the current-mode circuits. The active and passive components used to design the comb filter include second-generation current conveyor (CCII±), resistor, and capacitor. The circuit is designed for n = 4 to remove the power-line frequency of 50 Hz, and its three odd harmonics such as 150 Hz, 250 Hz, and 350 Hz. A PSPICE simulation is done to verify the performance of the proposed circuit. In simulation, all CCII± are designed using macro model of commercially-available current feedback operational amplifier integrated circuit (IC) AD844 as well as dynamic threshold voltage metal oxide semiconductor technology. The proposed circuit is also implemented also using commercially available IC AD844 on breadboard for n = 3. The output result on digital storage oscilloscope confirm the effectiveness of the proposed comb filter circuit in removing the power line interference i.e. the power-line frequency and its odd harmonics.

Keywords Comb filter · APF · CCII± · DTMOS · Power line interference

1 Introduction

Power-line interference plays a major role in many low-frequency electronic instruments such as electrocardiogram (ECG) [1–3], electroencephalogram (EEG) [4] and magnetoencephalography (MEG) [5]. Usually, ECG and EEG signals may be contaminated by various noises such as power-line interference, base-line drift, motion artifacts, muscle contraction, electrode contact noise, electrosurgical noise, and instrumentation noise [6]. Among these noises, the power-line interference is one of the most common and easily recognizable [7]. Stray effect of the alternating current fields, loose contacts, dirty electrodes and improper grounding of the machine may be the causes behind power-line interference in ECG signal. Electromagnetic interference from the power lines also disturbs these low-frequency signals. Some heavy electrical equipment such as elevators, air conditioners and X-ray units draw large power-line current, which introduce 50 Hz noise signals in the input of these instruments. Generally, alternating current (AC) interferences have two components: (a) electric field interference (characterized by noise concentrated at the fundamental frequency) and (b) magnetic field interference (characterized by high harmonic contents) [8]. Various solutions have been proposed in literatures to remove the complete AC interference using both digital and analog filters [9–19]. Since analog filters are more suitable for real time processing, many researchers have reported a number of methods using various types of analog filters to remove/attenuate the 50 Hz signal as well as its odd harmonics [20–33]. These types of circuits are

✉ Sajal K. Paul
sajalkpaul@rediffmail.com

Chandan Kumar Choubey
chandan.ism@rediffmail.com

Gaurav Tiwari
gt1989s@gmail.com

[1] Indian Institute of Technology (ISM), Dhanbad, Jharkhand, India

[2] Department of Electronics and Communication Engineering, MLV Textile and Engineering College, Bhilwara, Rajasthan 311001, India

[3] Department of Electronics and Telecommunication Engineering, Dr. D. Y. Patil School of Engineering, Pune, Maharashtra 412105, India

Published online: 14 September 2018

Author's personal copy

known as a comb filter which may be defined as 'A filter, which notches more than one frequencies'.

In the past few decades, current mode circuits have attracted significant attention of many researchers [34–39] due to its inherent properties such as simpler architecture, wider bandwidth, greater linearity, larger dynamic range, higher slew rate, better accuracy, and capability to operate at low voltage [40]. The CCII is one of the most versatile and useful current-mode building block [41, 42]. The basic building block used for designing the proposed analog comb filter is CCII due to its versatile and efficient operation. Since CCII is commercially available as current feedback operational amplifier (CFOA)-integrated circuit AD844 [43], it is convenient to practically test the performance of the proposed analog comb filter.

In this work, an APF-based analog comb filter is designed using CCII, to eliminate or reduce power-line interference of the low frequency biomedical signal like ECG signal. However, the proposed circuit may be used also for other applications like pitch estimation of speech signal within noise [44], elimination of power line interference on telephone cables under frequency-varying condition [45], and canceling acoustic feedback oscillation in audio amplification system [46]. The proposed circuit is designed for 50 Hz fundamental frequency and its three odd harmonically frequencies. It has been simulated using PSPICE software. Moreover, a prototype of the circuit is designed on a breadboard using commercially available CFOA IC AD844 to experimentally check the effectiveness of the comb filter in removal of selective frequencies.

2 Comb filter methodology

The circuits reported in [8, 20–33] for analog comb filter realization use notch filter, low pass filter, band pass filter, inverted band pass filter and some other techniques. However an analog comb filter realization using all pass filter is not available in literature. It motivated the authors to make an attempt to realize an analog comb filter using an APF as basic circuit. The methods to realize a band-stop filter is shown in Fig. 1. An APF and an adder circuit are used in this method. The output of APF is added with input signal and scaled down by a factor of ½. If the quality factor (Q_O) of APF increases, the bandwidth decreases and behaves as a sharp notch filter. The Laplace transform of the output voltage of the notch filter, shown in Fig. 1, is given in (1) while the transfer function is given in (2).

$$V_{O(notch)}(s) = \frac{1}{2}\left\{\frac{s^2 - \left(\frac{\omega_0}{Q_0}\right)s + \omega_0^2}{s^2 + \left(\frac{\omega_0}{Q_0}\right)s + \omega_0^2} V_{in}(s) + V_{in}(s)\right\} \quad (1)$$

$$H(s) = \frac{V_{O(notch)}(s)}{V_{in}(s)} = \frac{s^2 + \omega_0^2}{s^2 + \left(\frac{\omega_0}{Q_0}\right)s + \omega_0^2} \quad (2)$$

The transfer function of a notch filter should satisfy the three main aspects: (a) The zeros should be at imaginary axis, (b) The poles should be closer to the zeros, and (c) The phase shift at pole frequency should be $-\pi/2$ or $\pi/2$.

The poles and zeros of the transfer function, given in (2), are presented below and the corresponding pole-zero locations are shown in Fig. 2

$$P_1 = -\frac{\omega_0}{2Q_0} + j\frac{\omega_0}{2Q_0}\sqrt{4Q_0^2 - 1},$$

$$P_2 = -\frac{\omega_0}{2Q_0} - j\frac{\omega_0}{2Q_0}\sqrt{4Q_0^2 - 1}, \quad \text{and} \quad Z_1 = j\omega_0;$$

$$Z_2 = -j\omega_0$$

The radius (r) and the angle (θ) of Fig. 2 are found as:

$$r = \omega_0, \quad \text{and} \quad \theta = \tan^{-1}\sqrt{4Q_0^2 - 1}$$

It shows that as Q_0 increases, the θ will increase and the poles approach towards the zeros.

Now, on putting $s = j\omega$ in (2) we get,

$$H(j\omega) = \frac{-\omega^2 + \omega_0^2}{-\omega^2 + \omega_0^2 + j\omega\left(\frac{\omega_0}{Q_0}\right)} \quad (3)$$

The phase expression of $H(j\omega)$ can be written as:

$$\angle H(j\omega) = -\tan^{-1}\frac{\omega\omega_0}{Q_0(\omega_0^2 - \omega^2)} \quad (4)$$

At $\omega = \omega_0$

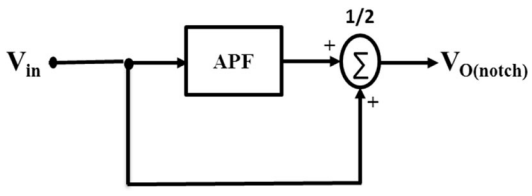

Fig. 1 Realization of notch filter using an APF

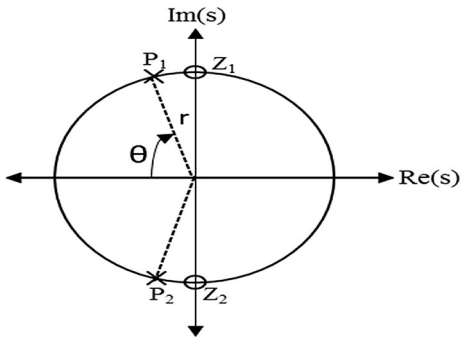

Fig. 2 Pole-zero plot of notch filter

Author's personal copy

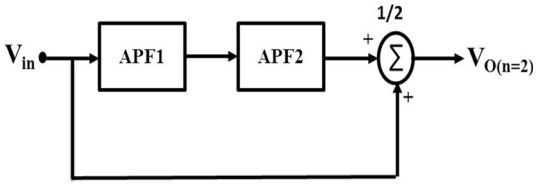

Fig. 3 Realization of comb filter using two APFs for n = 2

$$\angle H(j\omega) = -\tan^{-1}\infty = -\frac{\pi}{2} \tag{5}$$

It is clear that the filter, shown in Fig. 1, is acting as a notch filter for higher value of Q_0.

Now, we can design a comb filter to eliminate/suppress two frequencies by cascading two APFs as shown in Fig. 3.

The Laplace transform of the output voltage of the comb filter, shown in Fig. 3, is given in (6) while the transfer function is given in (7).

$$V_{O(n=2)}(s) = \frac{1}{2}\left\{V_{in}(s)\frac{\left(s^2-\left(\frac{\omega_1}{Q_1}\right)s+\omega_1^2\right)}{s^2+\left(\frac{\omega_1}{Q_1}\right)s+\omega_1^2}\frac{\left(s^2-\left(\frac{\omega_2}{Q_2}\right)s+\omega_2^2\right)}{s^2+\left(\frac{\omega_2}{Q_2}\right)s+\omega_2^2}+V_{in}(s)\right\} \tag{6}$$

$$H(s) = \frac{V_{O(n=2)}(s)}{V_{in}(s)} = \frac{S^4+\left(\omega_1^2+\omega_2^2+\frac{\omega_1\omega_2}{Q_1Q_2}\right)S^2+\omega_1^2\omega_2^2}{\left(S^2+\left(\frac{\omega_1}{Q_1}\right)S+\omega_1^2\right)\left(S^2+\left(\frac{\omega_2}{Q_2}\right)S+\omega_2^2\right)}$$

Since $\frac{\omega_1\omega_2}{Q_1Q_2} \ll \left(\omega_1^2+\omega_2^2\right)$ for higher values of Q_1 and Q_2, the transfer function $H(s)$ can be written as:

$$H(s) = \frac{S^4+\left(\omega_1^2+\omega_2^2\right)S^2+\omega_1^2\omega_2^2}{\left(S^2+\left(\frac{\omega_1}{Q_1}\right)S+\omega_1^2\right)\left(S^2+\left(\frac{\omega_2}{Q_2}\right)S+\omega_2^2\right)} \tag{7}$$

The poles and zeros of the transfer function, given in (7), are presented below and the corresponding pole-zero locations are shown in Fig. 4

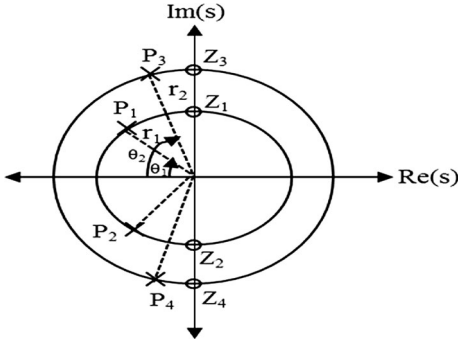

Fig. 4 Pole-zero plot of comb filter for n = 2

$$P_1 = -\frac{\omega_1}{2Q_1} + j\frac{\omega_1}{2Q_1}\sqrt{4Q_1^2-1},$$

$$P_2 = -\frac{\omega_1}{2Q_1} - j\frac{\omega_1}{2Q_1}\sqrt{4Q_1^2-1},$$

$$P_3 = -\frac{\omega_2}{2Q_2} + j\frac{\omega_2}{2Q_2}\sqrt{4Q_2^2-1} \quad \text{and}$$

$$P_4 = -\frac{\omega_2}{2Q_2} - j\frac{\omega_2}{2Q_2}\sqrt{4Q_2^2-1}$$

$$Z_1 = j\omega_1, \quad Z_2 = -j\omega_1, \quad Z_3 = j\omega_2, \quad \text{and} \quad Z_4 = -j\omega_2$$

By putting $s = j\omega$ in (7) we get,

$$H(j\omega) = \frac{\omega^4-\left(\omega_1^2+\omega_2^2\right)\omega^2+\omega_1^2\omega_2^2}{\left(\omega_1^2-\omega^2+j\omega\left(\frac{\omega_1}{Q_1}\right)\right)\left(\omega_2^2-\omega^2+j\omega\left(\frac{\omega_2}{Q_2}\right)\right)}$$

$$H(j\omega) = \frac{\omega^4-\left(\omega_1^2+\omega_2^2\right)\omega^2+\omega_1^2\omega_2^2}{\omega^4-\left(\omega_1^2+\omega_2^2+\frac{\omega_1\omega_2}{Q_1Q_2}\right)\omega^2+\omega_1^2\omega_2^2+j\left[\omega\left(\frac{\omega_1\omega_2^2}{Q_1}+\frac{\omega_1^2\omega_2}{Q_2}\right)-\omega^3\left(\frac{\omega_1}{Q_1}+\frac{\omega_2}{Q_2}\right)\right]}$$

Since $\frac{\omega_1\omega_2}{Q_1Q_2} \ll \left(\omega_1^2+\omega_2^2\right)$ for higher values of Q_1 and Q_2, $H(j\omega)$ can be written as:

$$H(j\omega) = \frac{\omega^4-\left(\omega_1^2+\omega_2^2\right)\omega^2+\omega_1^2\omega_2^2}{\omega^4-\left(\omega_1^2+\omega_2^2\right)\omega^2+\omega_1^2\omega_2^2+j\left[\omega\left(\frac{\omega_1\omega_2^2}{Q_1}+\frac{\omega_1^2\omega_2}{Q_2}\right)-\omega^3\left(\frac{\omega_1}{Q_1}+\frac{\omega_2}{Q_2}\right)\right]} \tag{8}$$

The phase expression of $H(j\omega)$ can be written as:

$$\angle H(j\omega) = -\tan^{-1}\left[\frac{\omega\left(\frac{\omega_1\omega_2^2}{Q_1}+\frac{\omega_1^2\omega_2}{Q_2}\right)-\omega^3\left(\frac{\omega_1}{Q_1}+\frac{\omega_2}{Q_2}\right)}{\omega^4-\left(\omega_1^2+\omega_2^2\right)\omega^2+\omega_1^2\omega_2^2}\right] \tag{9}$$

For $\omega = \omega_1$

$$\angle H(j\omega) = -\tan^{-1}\infty = -\frac{\pi}{2} \tag{10}$$

Similarly, for $\omega = \omega_2$

$$\angle H(j\omega) = -\tan^{-1}-\infty = \frac{\pi}{2} \tag{11}$$

From the above discussion, we can conclude that (a) The phase angles are $-\pi/2$ and $\pi/2$ at the pole frequencies ω_1 and ω_2, respectively (b) Zeros at imaginary axis (c) Poles are near to Zeros, which confirm the property of comb filter to attenuate two pole frequencies ω_1 and ω_2.

In a similar manner, a number of APFs having high quality factor are cascaded, as shown in Fig. 5, to design a comb filter for stopping n-number of pole frequencies. In this methodology, the output of cascaded APFs is added to the input signal V_{in}. An adder circuit is used to add these two signals. Further, it is scaled down by a factor of ½ to get the required output of the comb filter. The transfer function (T.F) of the comb filter as given in (12) may also be expressed as (13). The pole frequencies of APFs are set in such a way that the comb filter notches the frequency of

Author's personal copy

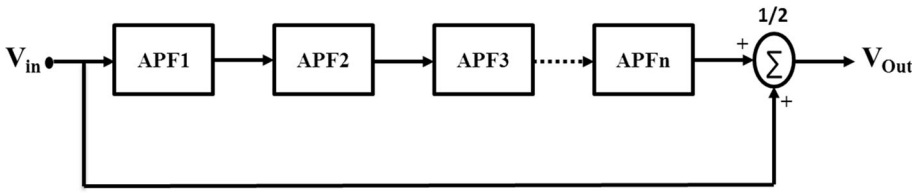

Fig. 5 Block diagram of the proposed comb filter

power-line as well as its odd harmonics. For example, let the comb filter be designed to remove the undesired power-line interference of frequency f_1 and its odd harmonics f_2, f_3 …f_n. The APF1, APF2, APF3… APFn are designed in such a way that they are set at pole frequencies f_1, f_2, f_3…f_n respectively. This gives an undistorted output signal V_{out} at the output of comb filter rejecting the undesired frequencies f_1, f_2, f_3…f_n.

$$H(s) = \frac{V_{Out}(s)}{V_{in}(s)} = \frac{1}{2}\{(T.F_{APF1})(T.F_{APF2})(T.F_{APF3}).....(T.F_{APFn}) + 1\} \tag{12}$$

$$H(s) = \frac{V_{Out}(s)}{V_{in}(s)} = \frac{1}{2}\left\{\frac{\left(S^2 - \left(\frac{w_1}{Q_1}\right)S + w_1^2\right)}{S^2 + \left(\frac{w_1}{Q_1}\right)S + w_1^2}\frac{\left(S^2 - \left(\frac{w_2}{Q_2}\right)S + w_2^2\right)}{S^2 + \left(\frac{w_2}{Q_2}\right)S + w_2^2}\frac{\left(S^2 - \left(\frac{w_3}{Q_3}\right)S + w_2^2\right)}{S^2 + \left(\frac{w_3}{Q_3}\right)S + w_2^2}.....\frac{\left(S^2 - \left(\frac{w_n}{Q_n}\right)S + w_2^2\right)}{S^2 + \left(\frac{w_n}{Q_n}\right)S + w_2^2} + 1\right\} \tag{13}$$

3 Second-generation current conveyor (CCII±)

The CCII± is a device with three or four terminals. The block diagram of CCII± is shown in Fig. 6. There are two input ports (Port x and Port y) and two output ports (Port z+ and Port z−).The relation between the voltages and currents of the ports of CCII± can be defined in a matrix form as given below.

$$\begin{bmatrix} i_y \\ v_x \\ i_z \end{bmatrix} = \begin{bmatrix} 0 & 0 & 0 \\ 1 & 0 & 0 \\ 0 & \pm 1 & 0 \end{bmatrix} \begin{bmatrix} v_y \\ i_x \\ v_z \end{bmatrix} \tag{14}$$

The impedance at Port y is ideally infinite to remove the loading effect of a device while impedance at Port x is low. From (14), we can see that the voltage at Port x follows the voltage at Port y. The current flowing into Port z is equal to the current flowing into Port x. The current flowing into Port y is zero due to ideally infinite impedance. The plus (+) and minus (−) signs denote the direction of the current into and out to the block respectively.

A closely-related building block to CCII is the CFOA. The CFOAs fabricated in the bipolar technology exhibits almost constant bandwidth and high slew rate. A commercially available CFOA is IC AD844. The IC AD844 is a four-terminal device. The internal architecture of CFOA is a translinear CCII+ followed by a translinear voltage buffer. The implementation of CCII+ and CCII− using IC AD844 is shown in the Figs. 7 and 8, respectively.

Power consumption plays an important role in analog circuit design for a long lifetime of battery in the biomedical systems [47, 48]. Since IC AD844 is a Bipolar Junction Transistor (BJT) based device and it consumes more power, there is a need to use a low-power technique to design a low-power comb filter circuit. Ideally, the power consumption of an electronic device should be negligible. Although some of the methods are emerging in the field of Complementary Metal Oxide Semiconductor (CMOS) technology [49–51], the use of dynamic threshold voltage metal oxide semiconductor (DTMOS) transistor in analog circuit is one of the most efficient techniques to minimize the power consumption [52, 53]. The DTMOS transistor can be realized by simply connecting the body terminal to the gate terminal as shown in Fig. 9, and it is applicable for P-channel Metal Oxide Semiconductor (PMOS) transistors only. It was first proposed by Assederaghi [54]. When the MOS circuit of CCII, as shown in the Fig. 10, is designed using the DTMOS transistor technique [55], the power consumption of the proposed comb filter circuit is drastically reduced.

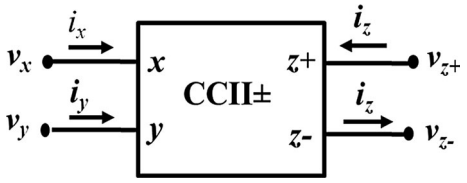

Fig. 6 Block diagram of CCII± with two outputs

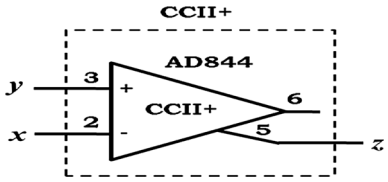

Fig. 7 Implementation of CCII+ using IC AD844

Author's personal copy

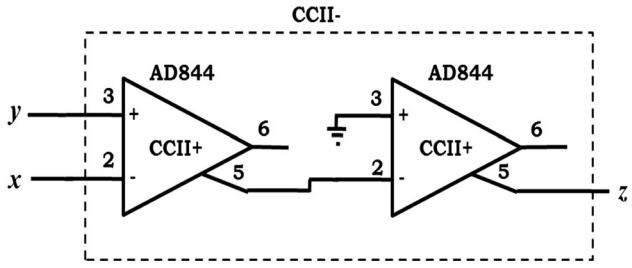

Fig. 8 Implementation of CCII− using IC AD844

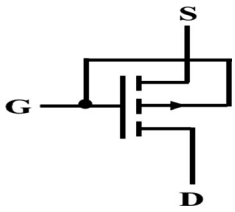

Fig. 9 Symbol of DT-MOS Transistor

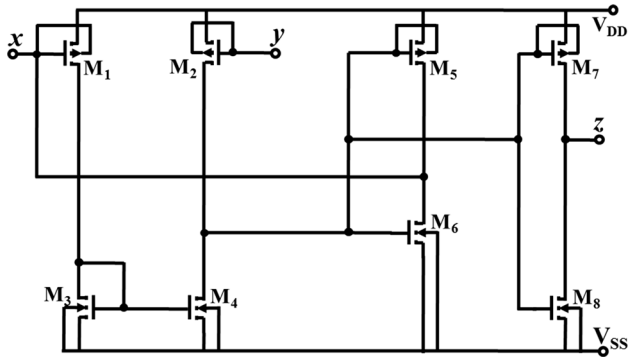

Fig. 10 Implementation of CCII using DTMOS transistor

4 Comb filter implementation

The implementation of the proposed comb filter as discussed in Sect. 2 is presented in this section. Section 4.1 discusses the all pass filter (APF) followed by adder circuit in Sect. 4.2. In Sect. 4.3 the complete comb filter circuit is presented and discussed its general expression.

4.1 An APF using CCII±

The APF, used to design the proposed comb filter, is shown in Fig. 11 [56]. It consists of four passive components (two resistors and two capacitors), two CCIIs (one CCII+ and one CCII−), and one inverted buffer. The routine analysis of the circuit yields a transfer function of APF, which is given as:

$$\frac{V_{O(APF)}}{V_{in}} = \frac{s^2 - \frac{s}{C_2R_1} + \frac{1}{C_1C_2R_1R_2}}{s^2 + \frac{s}{C_2R_1} + \frac{1}{C_1C_2R_1R_2}} \tag{15}$$

The pole frequency (f_0), and the quality factor (Q_0) of APF are obtained as:

$$f_0 = \frac{1}{2\pi\sqrt{C_1C_2R_1R_2}} \tag{16}$$

$$Q_0 = \sqrt{\frac{C_2R_1}{C_1R_2}} \tag{17}$$

It is clear from (16) and (17) that the pole frequency (f_0) of the APF can be adjusted independent of quality factor (Q_0) by varying R_1 and R_2 in such a way that the product R_1R_2 varies while the ratio R_1/R_2 remains fixed. Similarly Q_0 can be adjusted independent of f_0 by varying R_1 and R_2 in such a way that the ratio R_1/R_2 varies while the product R_1R_2 remains constant. It may also be noted that the circuit may be made resistor less by replacing CCII by CCCII. As a result of that the electronic tuning of f_0 and Q_0 can be achieved by varying bias current of CCCIIs.

4.2 Adder circuit using CCII±

Figure 12 shows the adder circuit, which is used to add two signals in the proposed comb filter design. The output of the cascaded APFs (say V_{in1}) and the input signal to the comb filter (say V_{in2}) are added as given in (18) and (19).

$$\frac{V_{O(Adder)}}{R_5} = \frac{V_{in1}}{R_3} + \frac{V_{in2}}{R_4} \tag{18}$$

If $R_3 = R_4 = R$,

$$V_{O(Adder)} = \frac{R_5}{R}(V_{in1} + V_{in2}) \tag{19}$$

where $V_{O(Adder)}$ is the output of the adder.It is seen that the gain of the adder can be adjusted by selecting proper value of R_5, R_3, and R_4. It may be noted that the output of the adder is actually the output of the comb filter.

4.3 Proposed comb filter

The proposed APF based comb filter, which is designed according to the methodology as shown in Fig. 5, is depicted in Fig. 13. It is used to eliminate the fundamental frequency of the power line and its odd harmonics from biomedical signal. The generalized voltage transfer function of the proposed comb filter is obtained by assuming $R_3 = R_4 = 2R_5$ for a gain of 0.5 of adder as:

$$\mathrm{T.F_{(COMB)}} = \frac{1}{2}\left[\prod_{k=1}^{n}\left\{\frac{s^2 - \frac{s}{C_{k2}R_{k1}} + \frac{1}{C_{k1}C_{k2}R_{k1}R_{k2}}}{s^2 + \frac{s}{C_{k2}R_{k1}} + \frac{1}{C_{k1}C_{k2}R_{k1}R_{k2}}}\right\} + 1\right] \tag{20}$$

The pole frequency and quality factor of Kth APF can be written as:

Author's personal copy

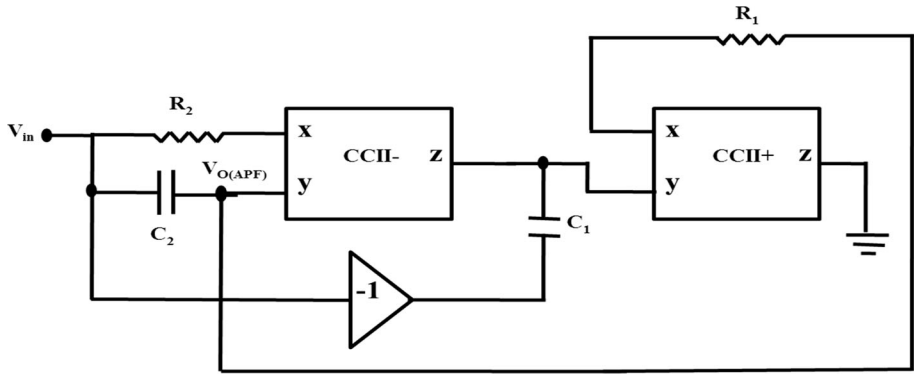

Fig. 11 APF using CCII±

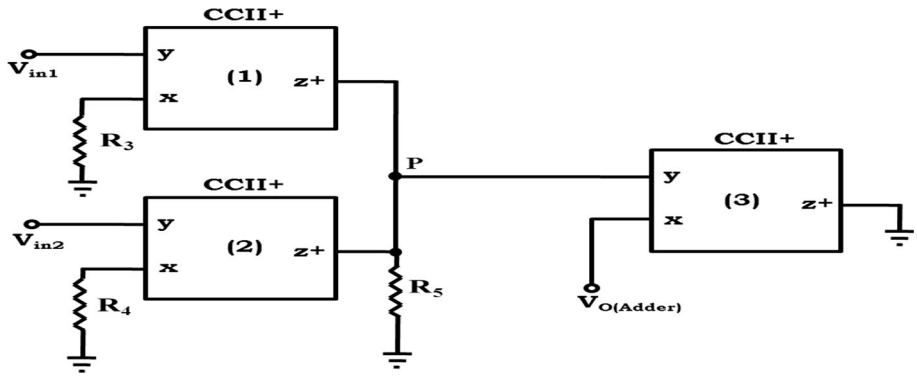

Fig. 12 Adder circuit using CCII±

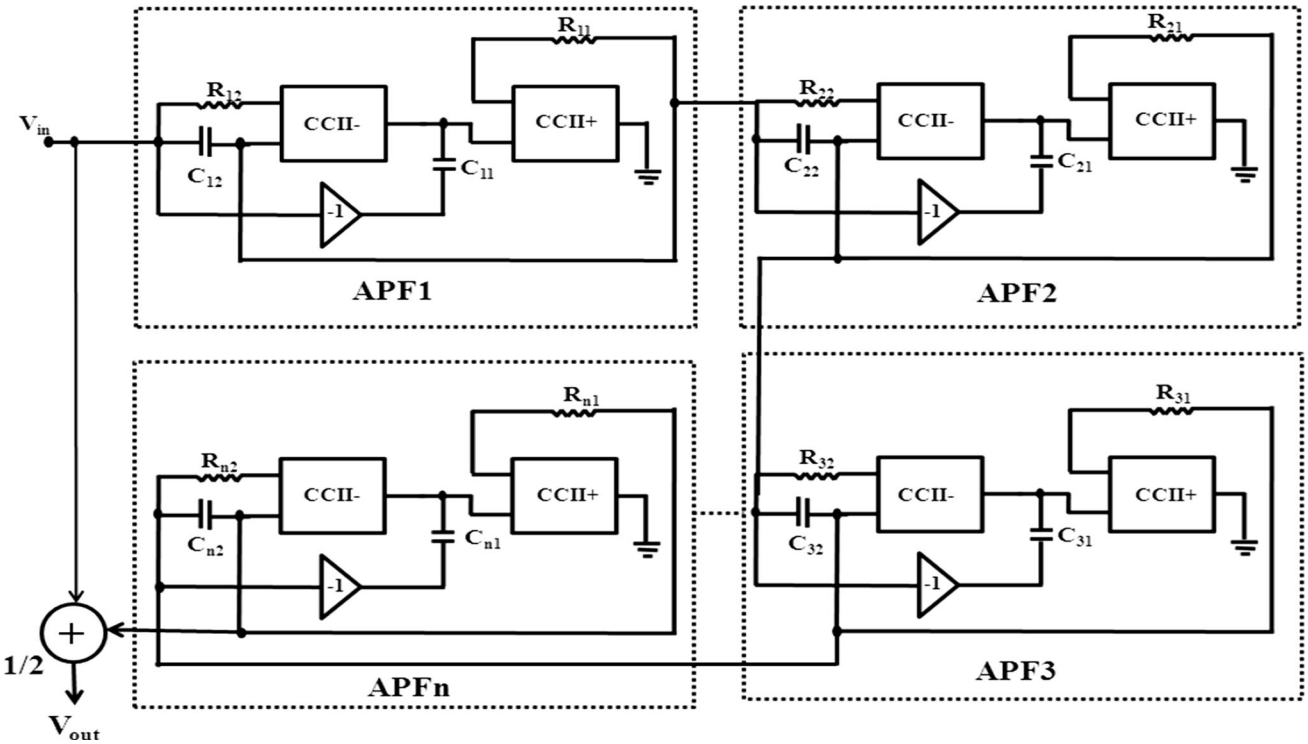

Fig. 13 Proposed comb filter using CCII± for n = 4

Author's personal copy

$$f_k = \frac{1}{2\pi\sqrt{C_{k1}C_{k2}R_{k1}R_{k2}}} \tag{21}$$

$$Q_k = \sqrt{\frac{C_{k2}R_{k1}}{C_{k1}R_{k2}}} \tag{22}$$

The adder circuit, shown in Fig. 12, is used to add the contaminated input signal $V_{in}(t)$ with the output of the cascaded APFs. A contamination free signal is found at the output of adder. We can amplify this signal to a desired level by varying the value of the resistors of adder circuit.

5 Simulation results

A SPICE simulation is performed to verify the effectiveness of the proposed analog approach shown in the Fig. 5. The APF based comb filter, shown in Fig. 13, has been simulated in PSPICE using macro model of CFOA IC AD844. Since the frequency of biomedical signal is low, the removal of power-line interference up to the third harmonics is found to be sufficient to obtain a contamination-free biomedical signal. Hence, the proposed comb filter is designed for n = 4 to check the performance in removing the undesired power-line interference (50 Hz) and its three odd harmonics (150 Hz, 250 Hz, 350 Hz). APFs used in the comb filter are realized with the circuit as shown in Fig. 11. The pole frequencies and the quality factors of the APFs are taken as 50 Hz, 150 Hz, 250 Hz, 350Hz and 10, 20, 30, 40, respectively. The values of the passive components used for the circuit for various frequencies as shown in Fig. 13 are given in Table 1. The value of the resistors R_3, R_4, and R_5 of the adder circuit is taken as 8 kΩ, 16 kΩ, and 16 kΩ, respectively. The simulated frequency response of the comb filter using macro model of CFOA IC AD844 is shown in Fig. 14, which verifies the effectiveness of the proposed analog approach.

The proposed comb filter has also been simulated using DTMOS-based low-power low-voltage CCII± circuit, as shown in Fig. 10, in 0.18 µm TSMC CMOS process technology. The values of the passive components used for the simulation of the circuit, as given in Fig. 13, using DTMOS for various frequencies are given in Table 2. The values of R_3, R_4, and R_5 of the adder circuit is taken as 8 kΩ, 16 kΩ, and 16 kΩ, respectively.

The aspect ratios of MOS transistors, used to design CCII± circuit, are given in Table 3 [55]. The supply voltage used is ± 0.2 V. All of the MOS transistors are operated in sub-threshold region. The bias currents and transconductances of MOS transitors of the circuit, shown in Fig. 10, are given in Table 4. The simulated frequency response of the comb filter circuit using DTMOS is shown in the Fig. 15. It shows that notch depth obtained using DTMOS is better than that using macro model of AD844.

To check the performance in time domain, sinusoidal wave of various frequencies (50 Hz, 150 Hz, 250 Hz and 350 Hz) are fed at the input of the proposed comb filter circuit. The circuit has been simulated using macro model of IC AD844. The input and output waveforms for sinusoidal input signals of frequency 50 Hz, 150 Hz, 250 Hz and 350 Hz are shown in Figs. 16, 17, 18, and 19, respectively. It is observed that the magnitude of the output waveforms of undesired signals is remarkably low. It shows that the fundamental and harmonically-related noises can be suppressed by the proposed comb filter circuit effectively.

Furthermore to validate the function of the proposed analog comb filter, a corrupted ECG signal is processed through comb filter in a similar manner as that of [57, 58]. An ECG signal from MIT-BIH arrhythmia database [59, 60] corrupted with powerline interference has been uploaded in PSPICE to see the performance of the comb filter. The result of the simulation is given in Fig. 20. The ECG signal as obtained from MIT-BIH arrhythmia database is shown in Fig. 20(a) followed by spectrum in Fig. 20(b). An artificial 50 Hz powerline interference of 0.4 mV_{P-P} is added to the ECG signal, as shown in Fig. 20(c). The FFT of the corrupted signal is shown in Fig. 20(d). To eliminate the powerline intereference, the corrupted ECG signal is processed through the proposed comb filter circuit. The output of ECG signal and FFT of the output, are shown in Fig. 20(e) and Fig. 20(f), respectively. It shows that the 50 Hz powerline interference has been attenuated remarkably. Similarly, an artificial 50 Hz powerline interference of 0.1 mV_{P-P} is added to the ECG signal, as shown in Fig. 20(g) and its FFT in Fig. 20(h). After filtering the corrupted signal, the outputs of ECG signal and its FFT are shown in Fig. 20(i) and Fig. 20(j), respectively.

Table 1 Values of passive components taken for comb filter of Fig. 13 using AD844 based CCII±

Sr. No.	Component values	Pole frequency f_0 in Hz	Quality factor Q_O
1	R_{11} = 5 kΩ, R_{12} = 500 Ω, C_{11} = 0.63 µF, C_{12} = 6.3 µF	50.52	10
2	R_{21} = 2 kΩ, R_{22} = 400 Ω, C_{21} = 132 nF, C_{22} = 10.56 µF	150.70	20
3	R_{31} = 2.1 kΩ, R_{32} = 350 Ω, C_{31} = 60.5 nF, C_{32} = 9.075 µF	250.54	30
4	R_{41} = 4.8 kΩ, R_{42} = 300 Ω, C_{41} = 37.8 nF, C_{42} = 3.78 µF	350.57	40

Author's personal copy

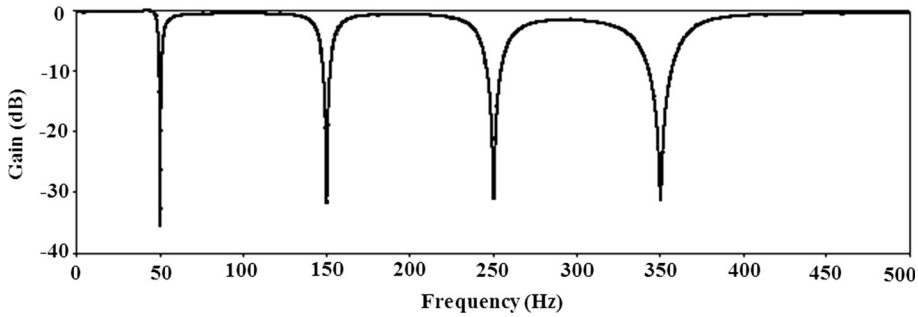

Fig. 14 Frequency response of the proposed comb filter using macro model of IC AD844

Table 2 Values of passive components taken for comb filter of Fig. 13 using DTMOS based CCII±

Sr. No.	Component values	Pole frequency f_0 in Hz	Quality factor Q_O
1	R_{11} = 7.5 kΩ, R_{12} = 1.8 kΩ, C_{11} = 175 nF, C_{12} = 4.2 μF	50.52	10
2	R_{21} = 11 kΩ, R_{22} = 2.2 kΩ, C_{21} = 24 nF, C_{22} = 1.92 μF	150.71	20
3	R_{31} = 16.8 kΩ, R_{32} = 2.4 kΩ, C_{31} = 8.8 nF, C_{32} = 1.14 μF	250.24	30
4	R_{41} = 56 kΩ, R_{42} = 3.5 kΩ, C_{41} = 3.24 nF, C_{42} = 324 nF	350.87	40

Table 3 Aspect ratios of MOS transistors used in CCII± [55]

Transistors	Width (μm)	Length (μm)
M1, M2, M5, M7	300	2
M3, M4	50	2
M6, M8	320	0.4

The quality of the output signal in a pass-band region has also been checked by obtaining the total harmonic distortion (THD) for a signal at 100 Hz as shown in Fig. 21. It shows that when the comb filter is designed using macro model of IC AD844, the THD is in the range of − 65 dB to − 75 dB up to 600 mV, and when it is designed for low-power comb filter using DTMOS technology, the THD is in the range of − 38 dB to − 58 dB up to 40 mV. It verifies that the quality of output is very good for both the cases.

6 Experimental results

The experimental demonstration of the proposed comb filter is done by using a prototype of the entire circuit for n = 3. It has been assembled on a breadboard using commercially available IC AD844 as shown in Fig. 22, and the values of passive components used are given in the Table 5.

Table 4 Bias current and transconductance of MOS transitors shown in Fig. 10

MOS Transistor	M_1	M_2	M_3	M_4	M_5	M_6	M_7	M_8
Bias current (nA)	284.5	281.4	284.7	281.6	243	243.2	243	243.1
Transconductance (g_m in μA/V)	1.416	1.407	1	0.99	1.245	1.187	1.245	1.187

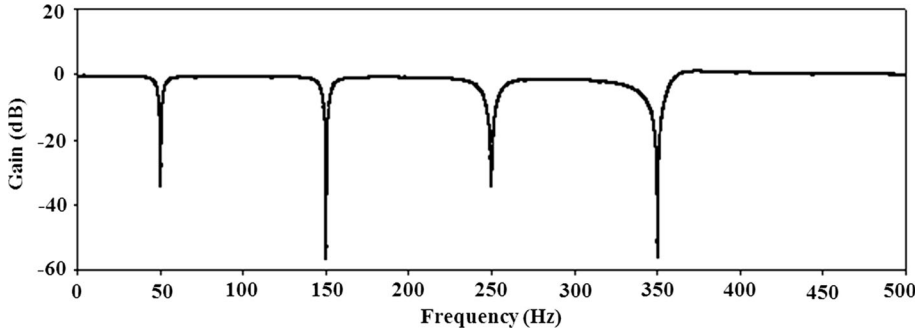

Fig. 15 Frequency response of the proposed comb filter using DTMOS technology

Author's personal copy

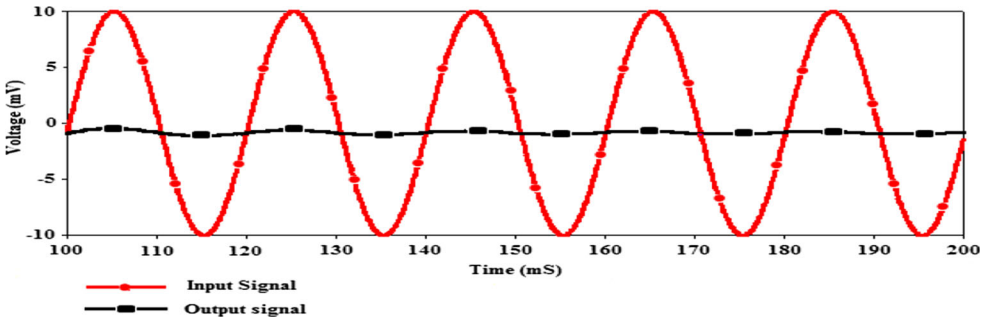

Fig. 16 Time domain response for 50 Hz Sinusoidal wave

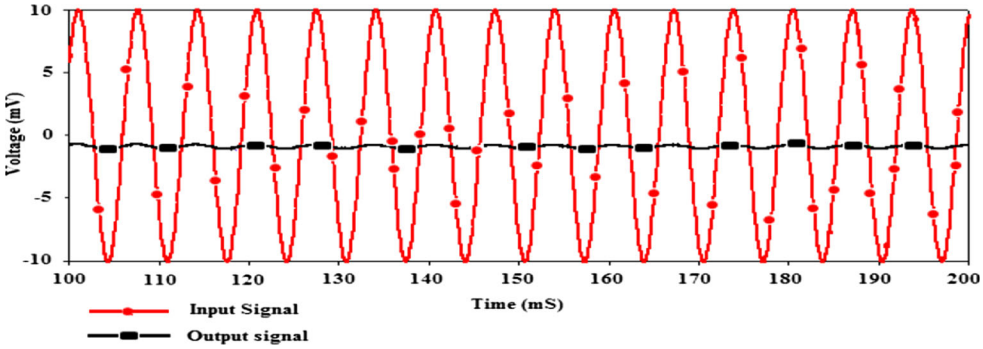

Fig. 17 Time domain response for 150 Hz Sinusoidal wave

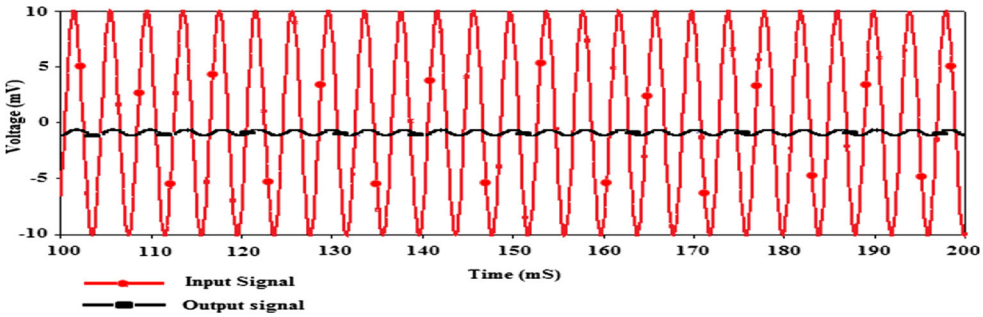

Fig. 18 Time domain response for 250 Hz sinusoidal wave

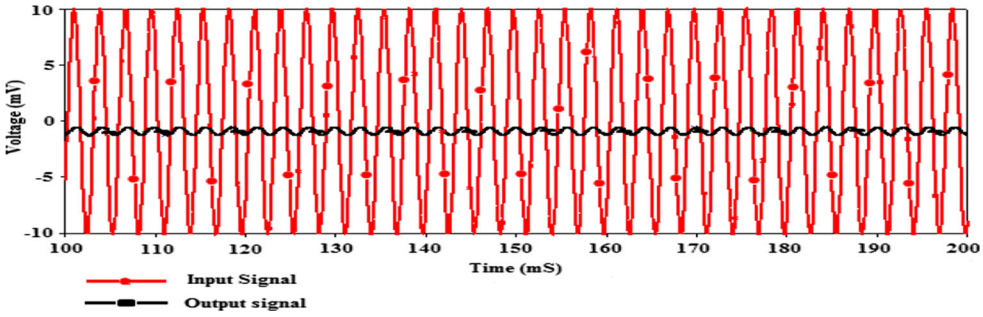

Fig. 19 Time domain response for 350 Hz sinusoidal wave

The complete experimental setup is shown in Fig. 23. Sinusoidal test signals of frequencies 50 Hz, 150 Hz, and 250 Hz are applied separately to examine the workability of the circuit. Resulting waveforms, shown in Figs. 24, 25, and 26, prove the effectiveness of the proposed circuit to remove/suppress the undesired power-line signals along with its two odd harmonics.

7 Comparison

Table 6 compares the effectiveness of the proposed comb filter with the available literatures. It is observed that the power consumption of the proposed circuit is high when it is designed with BJT-based IC AD844. However, when it is implemented with DTMOS technology, the power consumption is remarkably low. However, the power

Author's personal copy

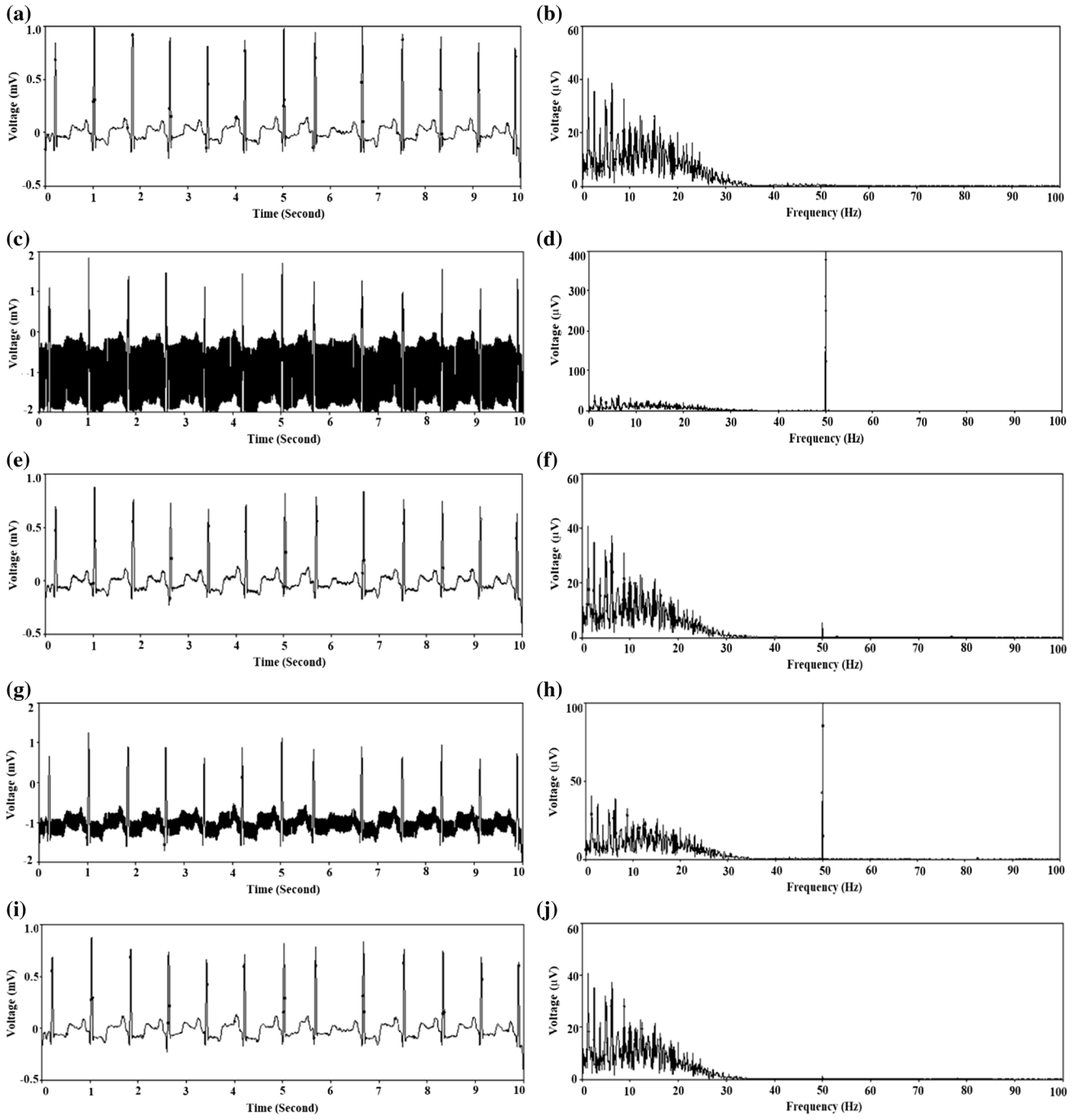

Fig. 20 A representative examples of filtering of ECG signal mixed with a 50 Hz power line interference **a** ECG signal generated from MIT-BIH arrhythmia database, **b** spectra of ECG signal shown in (**a**), **c** ECG signal mixed with artificial powerline interference (0.4 mV, 50 Hz), **d** spectra of corrupted ECG signal shown in (**c**), **e** filtered ECG signal by the proposed comb filter, **f** spectra of filtered ECG signal shown in (**e**), **g** ECG signal corrupted with artificial powerline interference (0.1 mV, 50 Hz), **h** spectra of corrupted ECG signal shown in (**g**), **i** filtered ECG signal by the proposed comb filter, and **j** spectra of filtered ECG signal shown in (**i**)

consumption is lesser in [33, 57]. The filter circuits given in [29, 33] have been designed for notching one frequency while in [57], a LPF has been designed. On comparing the number of passive components used for notching more than one frequencies [8, 20–22], it is found that the proposed comb filter uses lesser number of resistors except [21]. Since the filter used in [21] is g_m-C type, there is no need of external resistors in designing the circuit. The number of capacitors used is same as in [8, 20–22]. The notch depth is found to be satisfactory while the THD is very good for both the proposed implementations.

Author's personal copy

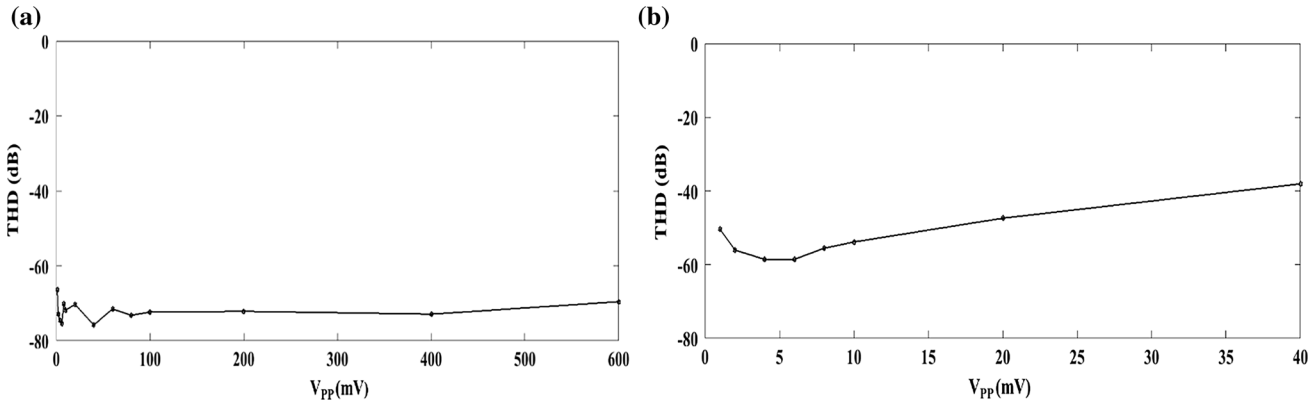

Fig. 21 THD of comb filter at 100 Hz using CCII± based on: **a** macro model of AD844, **b** DTMOS technology

Fig. 22 Circuit realization on breadboard using IC AD844

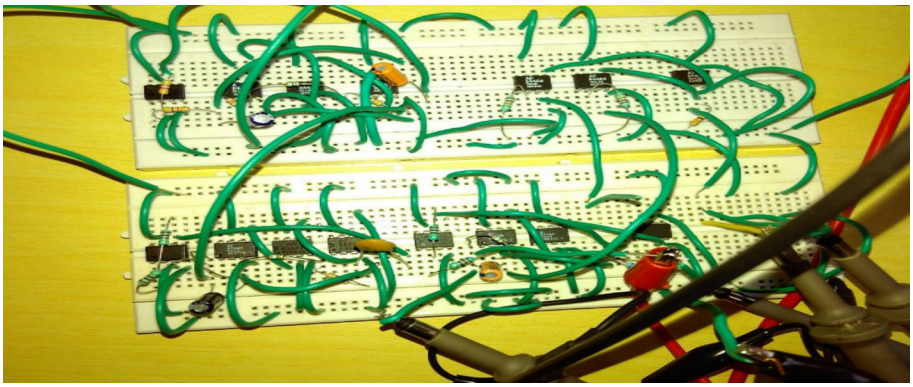

Table 5 Values of passive components for practical implementation of the circuit

Frequency	50 Hz	150 Hz	250 Hz
Component values	R_{11} = 4.7 kΩ	R_{21} = 4.5 kΩ	R_{31} = 3.4 kΩ
	R_{12} = 470 Ω	R_{22} = 440 Ω	R_{32} = 380 Ω
	C_{11} = 0.68 μF	C_{21} = 0.12 μF	C_{31} = 56 nF
	C_{12} = 6.8 μF	C_{22} = 4.7 μF	C_{32} = 5.6 μF

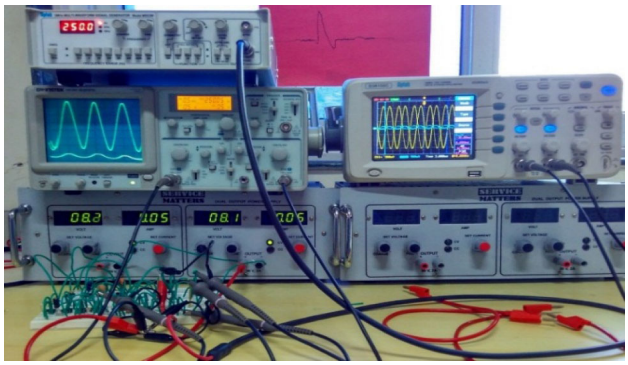

Fig. 23 Experimental setup

Moreover, the notch frequencies can be independently tuned through resistors without changing the quality factor. It means the circuit can be configured for other power line frequencies like 60 Hz and its odd harmonics (180 Hz, 300 Hz, 420 Hz, etc.) without disturbing the quality factor. Similarly quality factor may also be changed independent of frequency through resistor. Furthermore, the proposed circuit finds its applications in all low-amplitude low-frequency biomedical signals such as EEG, ECG, and EMG. The output of the proposed comb filter can also be amplified by adjusting resistors of the adder. Moreover it may be designed as a resistor less circuit by replacing CCII by CCCII. As a consequence it may be tuned electronically by the bias currents of CCCII.

8 Conclusion

This paper describes a new approach to design an analog comb filter using a number of APFs. The design of the comb filter is proposed using basic second generation current conveyor (CCII±). This comb filter finds applications in the biomedical instruments where very precise output with low power consumption is required. One of the applications is removal of the power-line interference from

Author's personal copy

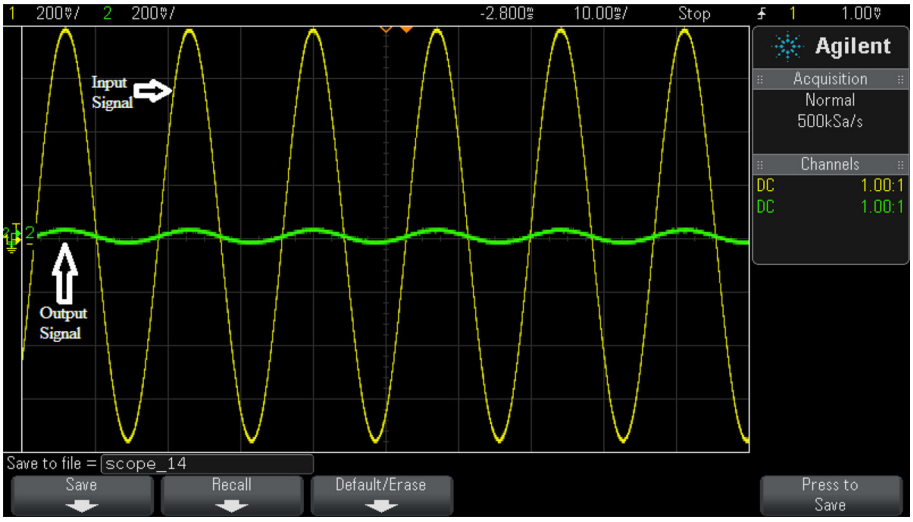

Fig. 24 Experimental result of sinusoidal wave of 50 Hz

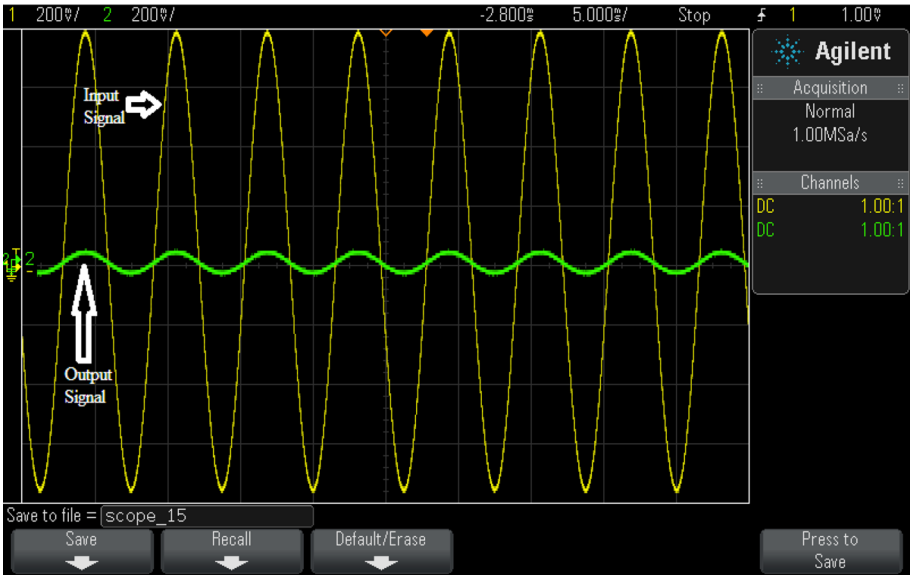

Fig. 25 Experimental result of sinusoidal wave of 150 Hz

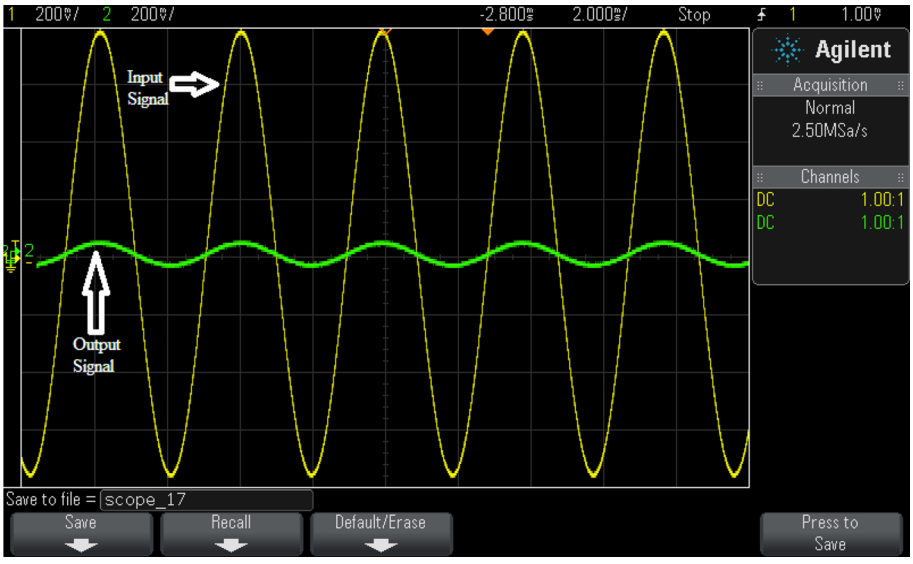

Fig. 26 Experimental result of sinusoidal wave of 250 Hz

Author's personal copy

Table 6 Comparison table

Reference	Active block	Techn.	Appl.	Rejection freq. (Hz)	Results	Power consumption/supply	No. of passive components used	Notch depth (dB)	THD (dB)
[8]	Op-amp	BJT	ECG	60, 180, 300, 420	Sim + Exp	–	Resistor-18 Capacitor-08	–	–
[20]	Op-amp	BJT	ECG	60, 180, 300, 420	Sim	–	Resistor-18 Capacitor-08	–	–
[21]	OTA	CMOS 0.5 µm	ECG	60, 180, 300, 420	Sim	21.5 mw/± 5 V	Capacitor-08	–	− 40
[22]	CCII	CMOS 0.18 µm	EEG, ECG, EMG	60, 180, 300, 420	Sim + Exp	10.2 µW/± 0.4 V	Resistor-19	− 61 to − 64	− 48
	AD844	BJT				289 mW/± 5 V	Capacitor-08	− 37 to − 50	− 43
[23]	CCII	CMOS 0.35 µm	EEG, ECG	–	Sim	28 µW/± 1.5 V	Resistor-10 Capacitor-02	–	–
[24]	OTA	CMOS 0.6 µm	EEG	50	Sim	–	–	− 58	–
[25]	OTA	CMOS 90 nm	EEG, ECG, EMG	50–60	Sim	75 µW/3 V	–	− 41	–
[26]	OTA	CMOS 0.5 µm	EEG, ECG, EMG	–	Exp	60 µW/± 1.5 V	–	− 41	− 45
[27]	Op-amp	BJT	ECG	60	–	–	Resistor-27 Capacitor-03	− 60	–
[28]	Op-amp	BJT	ECG	60	Sim + Exp	–	–	–	–
[29]	CCII	CMOS 0.35 µm	ECG	60	Sim	2.2 µW/± 1.5 V	Resistor-08	–	–
[30]	Op-amp	CMOS 0.18 µm	ECG	50	Sim	25.2 µW/± 1.8 V	Resistor-03 Capacitor-06	− 55.4	–
[31]	OTA	CMOS 0.35 µm	EEG	30–67	Exp	11 µW/± 1.5 V	Capacitor-07	− 66	− 50
[32]	OTA	CMOS 90 nm	EEG, ECG, EMG	50–60	Sim	75 µW/3 V	–	− 41	–
[33]	OTA	CMOS 0.18 µm	EEG, ECG, EMG	60	Exp	1.1 µW/1.5 V	Capacitor-05	− 60	− 60
[57]	Op-amp	CMOS 0.18 µm	EEG, ECG, EMG	40–80	Exp	150 nW/1.5 V	Resistor-06 Capacitor-03	− 43	− 70
Proposed circuit	AD844	BJT	EEG, ECG, EMG	50, 150, 250, 350	Sim + Exp	289 mW/± 5 V	Resistor-11	− 31 to − 36	− 65 to − 75
	CCII+	DTMOS 0.18 µm	EEG, ECG, EMG			2.5 µW/± 0.2 V	Capacitor-08	− 35 to − 58	− 40 to − 58

Author's personal copy

low-amplitude biomedical signal such as an ECG, EEG, and EMG. A number of APFs are cascaded followed by an adder circuit to design the presented comb filter. Each APF consists of one positive-type CCII, one negative-type CCII, two resistors and two capacitors. The adder circuit consists of three positive-type CCIIs and three grounded resistors. In order to verify the theoretical results, the circuit (shown in Fig. 13) has been simulated in PSPICE using both; a macro model of commercially-available IC AD844 and 0.18 μm DTMOS technology. The frequency domain and time domain representations of the simulated results for power-line frequency (50 Hz), and its three odd harmonics (150 Hz, 250 Hz and 350 Hz) agree well with the theory. An artificial power line interference is added with ECG signal and processed through the proposed filter. The output ECG signal verifies the effectiveness of the proposed comb filter in removal of power line interference from ECG signal. With DTMOS technology, the power consumption of the circuit is 2.5 μW and 6.16 μW for n = 1 and n = 4, respectively. The proposed circuit is also designed and verified experimentally. The experimental results confirms that the proposed comb filter circuit is very much effective in eliminating power-line harmonic interference from low-amplitude low-frequency biomedical signals.

References

1. Huhta, J. C., & Webster, J. G. (1973). 60-Hz interference in electrocardiography. *IEEE Transactions on Biomedical Engineering, 20*(2), 91–101.
2. Hamilton, P. S. (1996). A comparison of adaptive and nonadaptive filters for reduction of power line interference in the ECG. *IEEE Transactions on Biomedical Engineering, 43*(I), 105–109.
3. Van Alste, J. A., & Schilder, T. S. (1985). Removal of base-line wander and power-line interference from the ECG by an efficient FIR filter with a reduced number of taps. *IEEE Transactions on Biomedical Engineering, 32*(12), 1052–1059.
4. Mantri, S., Agrawal, P., Patil, D., & Wadhai, V. (2015). Non invasive EEG signal processing framework for real time depression analysis. In: *SAI intelligent systems conference* (pp. 10–11), London, UK.
5. Vigario, R., Sarela, J., Jousmaki, V., Hamalainen, M., & Oja, E. (2000). Independent component approach to the analysis of EEG and MEG recordings. *IEEE Transactions on Biomedical Engineering, 47*(5), 589–593.
6. Singh, B., Singh, P., & Budhiraja, S. (2015). Various approaches to minimise noises in ECG signal: A survey. In: *Fifth international conference on advanced computing & communication technologies* (pp. 131–137), London, UK.
7. Ziarani, A. K., & Konrad, A. A. (2002). Non-linear adaptive method of elimination of power line interference in ECG signals. *IEEE Transactions on Biomedical Engineering, 49*(6), 540–547.
8. Tsai, C., Chiou, D., Lin, Y., Chan, H., & Wu, C. (1998). An active comb filter design for harmonic interference removal. *Journal of the Chinese Institute of Engineers, 21*(5), 605–610.
9. Mishra, S., Das, D., Kumar, R., & Sumathi, P. (2015). A power-line interference canceler based on sliding DFT phase locking scheme for ECG signals. *IEEE Transactions on Instrumentation and Measurement, 64*(1), 132–142.
10. Tomasini, M., & Benatti, S. (2016). Power line interference removal for high-quality continuous biosignal monitoring with low-power wearable devices. *IEEE Sensors Journal, 16*(10), 3887–3895.
11. Dhillon, S. S., & Chakrabarti, S. (2001). Power line interference removal from electrocardiogram using a simplified lattice based adaptive IIR notch filter. In: *Proceedings—23rd annual conference—IEEE/EMBS* (pp. 25–28), Turkey.
12. Ziarani, A. K. (2002). A nonlinear adaptive method of elimination of power line interference in ECG signals. *IEEE Transactions on Biomedical Engineering, 49*(6), 540–547.
13. Chang, C. (2010). Cancellation of high-frequency noise in ECG signals using adaptive filter without external reference. In: *3rd international conference on biomedical engineering and informatics (BMEI)* (pp. 787–790), Yantai, China.
14. Gaikwad, K. M. (2014). Removal of high frequency noise from ECG signal using digital IIR butterworth filter. In: *IEEE global conference on wireless computing and networking (GCWCN)* (pp. 121–124), Lonavala, India.
15. Liu, Y., & Chang, N. (2004). An adaptive algorithm for canceling power-line interference in biopotential measurement. *Biomedical Engineering Applications. Basis & Communications, 16*(06), 350–354.
16. Martens, S. M. M. (2006). An improved adaptive power line interference canceller for electrocardiography. *IEEE Transactions on Biomedical Engineering, 53*(11), 2220–2231.
17. Yamamoto, Y. (1998). Elimination of power line interference in ECG signal using inverse loop. In: *Proceedings of the 20th annual international conference of the IEEE engineering in medicine and biology society* (pp. 3313–3314), Hong Kong, China.
18. Verma, A. R., & Singh, Y. (2015). Adaptive tunable notch filter for ECG signal enhancement. In: *3rd international conference on recent trends in computing (ICRTC-2015)* (pp. 332–337).
19. Zaitsev, E. V. (2015). Elimination on power line interference from ECG signal using combined bidirectional narrowband notch filter. *Biophysics, 60*(4), 656–658.
20. Tsai, C., Chan, H. (1994). Harmonic interference elimination by an active comb Filter. In: *Proceedings of 16th annual international conference on IEEE of engineering in medicine and biology society* (Vol. 2, pp. 964–965), Department of Electrical Engineering, Taiwan University, Baltimore, MD, USA.
21. Ranjan, R. K., Yalla, S. P., Sorya, S., & Paul, S. K. (2014). Active comb filter using operational transconductance amplifier. *Active and Passive Electronic Components, 2014,* 1–6.
22. Ranjan, R. K., Choubey, C. K., Nagar, B. C., & Paul, S. K. (2016). Comb filter for elimination of unwanted power line interference in biomedical signal. *Journal of Circuits, Systems, and Computers, 25*(6), 1–16.
23. Stornelli, V., & Ferri, G. (2014). A single current conveyor-based low voltage low power bootstrap circuit for ElectroCardioGraphy and ElectroEncephaloGraphy acquisition systems. *Analog Integrated Circuits and Signal Processing*. https://doi.org/10.1007/s10470-013-0252-2.
24. Ling, C., & Luo, M. (2008). Research of the ASIC used for EEG signal detecting. In: *2nd international conference on anti-counterfeiting, security and identification*, Guiyang, China.
25. Ma C., Mak, P., & Vai, M. (2009) A 90 nm CMOS bio-potential signal readout front-end with improved powerline interference rejection. In: *IEEE conference* (pp. 665–668), Taipei, Taiwan.

Author's personal copy

26. Yazicioglu, R. F., & Merken, P. (2007). A 60 μW 60 nV/$\sqrt{}$Hz readout front-end for portable biopotential acquisition systems. *IEEE Journal of Solid-State Circuits, 42*(5), 1100–1110.
27. Casper, B. K., & Comer, D. J. (1999). An integrable 60-Hz notch filter. *IEEE Transactions on Circuits and Systems: Analog and Digital Signal Processing, 46*(1), 74–77.
28. Bai, Y., & Chu, W. (2004). Adjustable 60 Hz noise reduction by a notch filter for ECG signals. In: *IEEE conference on instrumentation and measurement technology* (pp. 1706–1711), Como, Italy.
29. Ferri, G., & Stornelli, V. (2011). A CCII-based high impedance input stage for biomedical applications. *World Scientific Journal of Circuits, Systems, and Computers, 20*(8), 1441–1447.
30. Li, K. Xi., Zhang, J. Y., & Wang, L. (2011). A fully integrated continuous time 50 Hz notch filter with center frequency tenability. *Bulletin of Advance Technology Research, 5*(7), 24–28.
31. Qian, X., Xu, Y. P., & Li, X. (2005). A CMOS continuous-time low-pass notch filter for EEG systems. *Analog Integrated Circuits and Signal Processing, 44*(3), 231–238.
32. Ma, C., Mak, P., Vai, M., Mak, P., Pun, S., Feng, W., et al. (2009). Frequency-bandwidth-tunablepowerline notch filter for biopotentialacquisition systems. *Electronics Letters, 45*(4), 197–199.
33. Lee, S., & Cheng, C. (2009). Systematic design and modeling of a OTA-C filter for portable ECG detection. *IEEE Transactions on Biomedical Circuits and Systems, 3*(1), 53–64.
34. Frey, D. R. (1993). Log-domain filtering: an approach to current-mode filtering. *IEEE Proceedings-G, 140*(6), 406–416.
35. Prasada, D., & Bhaskara, D. R. (2009). Universal current-mode biquad filter using dual output current differencing transconductance amplifier. *AEU-International Journal of Electronics and Communications, 63*(6), 497–501.
36. Xu, J., & Wang, C. (2014). Low-voltage high-linearity wideband current differencing transconductance amplifier and its application on current-mode active filter. *Radio-engineering, 23*(1), 512–522.
37. Yucey, E., & Minaei, S. (2006). Full-wave rectifier realization using only two CCIIQs and NMOS transistors. *Taylor & Francis International Journal of Electronics, 93*(8), 533–541.
38. Jaikla, W., & Siripruchyanun, M. (2008). A simple current-mode quadrature oscillator using single CDTA. *Radioengineering, 17*(4), 33–40.
39. Khan, A. A. (1995). An improved current-mode instrumentation amplifier with bandwidth independent of gain. *IEEE Transacttons on Instrumentation and Measurement, 44*(4), 887–891.
40. Toumazou, C., Lidgcy, F. G., & Haigh, D. G. (1990). *Analogue IC design: the current mode approach*. London: Peter Peregrinus Ltd.
41. Sedra, A., & Smith, K. C. (1970). A second generation current conveyor and its applications. *IEEE Transactions on Circuit Theory, 17*(1), 132–134.
42. Alzaher, H. A., Elwan, H., & Ismail, M. (2003). A CMOS fully balanced second-generation current conveyor. *IEEE Transactions on Circuits and Systems-II: Analog and Digital Signal Processing, 50*(6), 278–287.
43. Analog Devices. (1990). *Linear products data book*. Norwood, Massachusetts, USA: Analog Devices.
44. Chang, J. H., Kimb, N. S., & Mitra, S. K. (2005). Pitch estimation of speech signal based on adaptive lattice notch filter. *Signal Processing, 85*(3), 637–641.
45. McNamara, D. M., Majo, J. P., & Ziarani, A. K. (2008). Elimination of power line interference on telephone cables under frequency-varying conditions. *IEEE Transactions on Instrumentation and Measurement, 57*(2), 321–331.
46. Parsa, V. (2006). Acoustic feedback and its reduction through digital signal processing. *The Hearing Journal, 59*(11), 16–23.
47. Baker, M. W., & Sarpeshkar, R. (2006). Low-power single-loop and dual-loop AGCs for bionic ears. *IEEE Journal of Solid-State Circuits, 41*(9), 1983–1996.
48. Chua, E., & Fang, W. C. (2011). Mixed bio-signal lossless data compressor for portable brain–heart monitoring systems. *IEEE Transactions on Consumer Electronics, 57*(1), 267–273.
49. Khateb, F., Khatib, N., Prommee, P., Jaikla, W., & Fujcik, L. (2013). Ultra-low voltage tunable transconductor based on bulk-driven quasi-floating-gate technique. *Journal of Circuits, Systems, and Computers, 22*(8), 1350073.
50. Kumngern, M., Khateb, F., Dejhan, K., Phasukkit, P., & Tungjitkusolmun, S. (2013). Voltage-mode multifunction biquadratic filters using new ultra-low-power differential difference current conveyors. *Radioengineering, 22*(2), 448–457.
51. Khateb, F., Kumngern, M., Spyridon, V., & Psychalinos, C. (2014). Differential difference current conveyor using bulk-driven technique for ultra-low-voltage applications. *Circuits, Systems and Signal Processing, 33*(1), 159–176.
52. Uygur, A., & Kuntman, H. (2013). DTMOS-based 0.4 V ultra low-voltage low-power VDTA design and its application to EEG data processing. *Radioengineering, 22*(2), 458–466.
53. Khateb, F., Kulej, T., & Kumnger, M. (2015). 0.5-V DTMOS median filter. *AEU-International Journal of Electronics and Communications, 69*(11), 1733–1736.
54. Assaderaghi, F., Sinitsky, D., Parke, S. A., Bokor, J., Ko, P. K., & Hu, C. (1997). Dynamic threshold-voltage MOSFET for ultra-lowvoltage VLSI. *IEEE Transactions on Electron Devices, 44*(3), 414–422.
55. Uygur, A., & Kuntman, H. (2014). A very compact, 0.4 V DTMOS CCII employed in an audio-frequency filter. *Analog Integrated Circuits and Signal Processing, 81*(1), 89–98.
56. Horng, J., Lee, M., Cheng, H., & Chang, C. (1997). New CCII-based voltage-mode universal biquadratic filter. *International Journal of Electronics, 82*(2), 151–155.
57. Alzaher, H. A., Tasadduq, N., & Mahnashi, Y. (2013). A highly linear fully integrated powerline filter for biopotential acquisition systems. *IEEE Transactions on Biomedical Circuits and Systems, 7*(5), 703–712.
58. Mahmoud, S. A., Bamakhramah, A., & Al-Tunaiji, S. A. (2013). Low-noise low-pass filter for ECG portable detection systems with digitally programmable range. *Circuits, Systems and Signal Processing, 32*(5), 2029–2045.
59. Moody, G. B., & Mark, R. G. (2001). The impact of the MIT-BIH arrhythmia database. *IEEE Engineering in Medicine and Biology, 20*(3), 45–50.
60. Goldberger, A. L., Amaral, L. A. N., Glass, L., Hausdorff, J. M., Ivanov, P. Ch., Mark, R. G., Mietus, J. E., Moody, G. B., Peng, C.-K., Stanley, H. E. (2000). PhysioBank, PhysioToolkit, and PhysioNet: components of a new research resource for complex physiologic signals. *Circulation*, *101*(23), e215–e220 [Circulation Electronic Pages; http://circ.ahajournals.org/content/101/23/e215.full].

Author's personal copy

Sajal K. Paul did his B.Tech., M.Tech., and Ph.D. in Radio Physics and Electronics from the Institute of Radio Physics and Electronics, University of Calcutta. He has served Webel Telecommunication Industries, Kolkata; Indira Gandhi National Open University (IGNOU), Kolkata; Advanced Training Institute for Electronics and Process Instrumentation (ATI-EPI), Hyderabad; North Eastern Regional Institute of Science and Technology(NERIST), Nirjuli and Delhi College of Engineering(DCE), Delhi in various capacities. He has served the Department of Electronics Engineering, Indian Institute of Technology (Indian School of Mines), Dhanbad as Head of the Department and at present Professor and Dean (Faculty) of the same institute. His research interest includes Microelectronic Devices, Electronic Properties of Semiconductor and Bipolar and MOS Analog Integrated Circuits. Dr. Paul has more than 115 research publications in International and National journals of repute and conferences.

Chandan Kumar Choubey received M.Tech degree in Electronics and Communication Engineering from IIT(ISM) Dhanbad, India in 2013. He is currently working as Assistant Professor in Electronics and Communication Engineering Department of M.L.V Textile and Engineering College Bhilwara, India. He is also part time research scholar in Electronics Engineering Department, IIT(-ISM) Dhanbad, India. His main research interests are current mode circuit design, CMOS analog circuits, and analog VLSI circuit design.

Gaurav Tiwari received B.E. degree from J.T.M College of Engineering (North Maharashtra University) in Electronics and Telecommunication Engineering in 2012. M.E degree from Dr. D Y Patil School of Engineering (Savitribai Phule, Pune University) in VLSI and Embedded Systems in 2015. His main research interests are analog VLSI circuit design and CMOS circuits.

View publication stats

The current issue and full text archive of this journal is available on Emerald Insight at:
www.emeraldinsight.com/2398-5364.htm

Measuring the flexibility index for a supply chain using graph theory matrix approach

Rajesh Kumar Singh
Management Development Institute, Gurgaon, India, and
Pravin Kumar
Department of Mechanical Engineering, Delhi Technological University, Delhi, India

Received 1 April 2019
Revised 5 May 2019
Accepted 16 May 2019

Abstract

Purpose – In complex business environment of today, organizations are trying to be flexible and agile for meeting dynamic demands of customers in terms of product variety, cost cutting and decreasing product life cycle. The main purpose of this paper is to identify different attributes of flexibility and to propose an approach for evaluating flexibility index of a supply chain.

Design/methodology/approach – Total 33 factors are identified from the literature and further clustered into six major groups. They are top management commitment, organizational factors, mutual understanding, flow of information, relationship and decision-making and responsiveness. On the basis of these factors, an index has been developed by using graph theory matrix approach to evaluate the flexibility intensity of the supply chain for the firm in consideration.

Findings – The proposed approach has been illustrated in context to an Indian automobile organization, and value of the flexibility index has been evaluated. Framework proposed will help the supply chain managers to evaluate the flexibility index of their respective organizations.

Research limitations/implications – As values taken for different flexibility sub-factors are based on inputs given by managers of case organization, chances of bias may be there. Therefore, a study may be validated with more case studies to validate the proposed framework. Based on the flexibility index, organizations can find their strong and weak areas for strategy development.

Originality/value – A firm can also compare the flexibility index of its own supply chain with other's supply chain or with the best in the industry for benchmarking purpose. Benchmarking of flexibility will help organizations in developing strategies to compete in dynamic market scenario.

Keywords Performance, Benchmarking, Supply chain, Flexibility, Graph theory matrix approach, Flexibility index

Paper type Research paper

1. Introduction

In the present business environment, firms are facing a lot of market uncertainties and disruptions (Tse *et al.*, 2016). With increasing competition in the market, a firm has to give its best performance to earn profit. Various techniques such as Just in time (JIT), six sigma, among others have been adopted by firms so as to keep up with the pace of the changing market needs and environment. A very important aspect of any firm is its supply chain that affects its efficiency to a large extent. Firm-level competition is replaced with competition

The authors would like to thank the reviewers and the editor of the journal for their valuable suggestions and comments to improve the quality and content of the paper.

Journal of Global Operations and Strategic Sourcing
© Emerald Publishing Limited
2398-5364
DOI 10.1108/JGOSS-04-2019-0027

among supply chains. The term supply chain, has already been defined by a number of researchers in their own ways. According to Ganesan and Harrison (1995), a supply chain involves all functions from procurement of materials to selling of finished products to end consumer. A supply chain is a network of facilities for procurement, transformation and distribution of products (Lee and Billington, 1995).

As business pressures intensify, supply chain managers should develop new capabilities, change interactions with customers and suppliers to improve firm performance (Kocabasogu *et al.*, 2007). Supply chains are becoming more complex and challenging to manage (Craighead *et al.*, 2007). To manage complexity in business, supply chains need to be flexible. Supply chain flexibility can be analyzed in terms of its responsiveness and coordination too. Responsiveness may be defined as the ease for the management to change the structure of the supply chain as per the demand of the market. Coordination may be defined as the ability of the supply chain staff that comprises almost everyone from the top-level management to lower-level employees, to interact in a proper manner and conclude with a unanimous and fruitful decision so as to bring about the change in an effective manner. Responsiveness and coordination are further dependent on another factor called flexibility. According to Sawhney (2006), flexibility in supply chains helps in reacting to demand with minimum cost. Flexibility determines the performance of supply chains.

Owing to the continuous increasing competition in the market, organizations are trying to shorten product life cycles, increase product variety and adopt the technological changes. Therefore, supply chains have become more complex and dynamic. To meet changing customers' requirements, organizations are trying to adopt new practices and technologies for making their supply chains flexible (Swafford *et al.*, 2006). A lot of cost and risk is involved in making supply chains flexible. Therefore, many a times, organizations hesitate in making investments for being flexible and continue with traditional supply chain practices. According to Pujawan (2004), firms should conduct a detailed analysis of market requirements and level of flexibility required.

Traditionally, flexibility has been considered as a reaction to uncertainties in market demands (Beach *et al.*, 2000). Nowadays, there is a need to develop flexible manufacturing systems to have sustainable competitiveness. An index could be constructed that accounts for all the variables that affects the supply chain, and this could be used to quantify the quality of the supply chain and hence, a means to measure it and compare it. This index is regarded as the flexibility index. From the literature review, it is observed that very limited research has been done in developing an index for flexibility of the supply chain. The main objectives of this study are as follows:

- to identify the factors of flexibility and propose an approach for evaluating the flexibility index of the supply chain; and
- to illustrate the proposed approach for evaluating the flexibility index with the help of an Indian case study from auto sector.

The remaining part of the paper is organized as follows: Section 2 deals with identification of factors for flexibility in supply chains, Section 3 deals with research methodology, Section 4 deals case illustration of proposed approach and finally, Section 5 is the conclusion.

2. Identification of factors for flexibility in supply chains

Kumar *et al.* (2008) defined the flexibility in global supply chain from three perspectives i.e. performance, operational and strategic. The influencing factors are logistics, sourcing,

manufacturing, supplier, location, volume, delivery, cultural and linguistic compatibility, information systems, rerouting, warehousing and distribution, delayed product differentiation, security and demand variation, among others. These areas of flexibility have been kept in mind to develop the flexibility index in the present research. Flexibility is an important characteristic of the supply chain to meet the uncertainty. According to Naim *et al.* (2006), flexibility may be analyzed in terms of new product development and ability to change volume, delivery lead time etc.

Fayezi *et al.* (2014) have mapped uncertainty – flexibility in supply chains. They focused their attention on improving the flexibility with an exposure of uncertainty in the supply chain. Soon and Udin (2010) investigated different supply chain management practices related to flexibility. Singh and Sharma (2014a) used analytic network process to prioritize the alternatives of flexibility in supply chain. These flexibility factors are further grouped into six clusters (Singh and Sharma, 2014b) as discussed in following section.

2.1 Top management commitment (F1)

A firm can take major decisions such as investment of time and money(Shin *et al.*, 2000), long-term goal for investment (Arshinder and Deshmukh, 2006), adoption of new technology (Arshinder and Deshmukh, 2006), better focused communication system and employee training and empowerment (Simatupang *et al.*, 2002) with the help of top management commitment, vision and support. The structure of the top management working corresponds to a firm, which is well established in the market. The working and strategies are well planned with proper layout and is not much favorable to change till the time a more profitable and better organized plan is offered. The firm is confident of meeting its commitment and strongly believes in proper training and empowerment of its employees so as meet the desired goals.

2.2 Organizational factors (F2)

The long and successful existence has created a strong integrated structure where various departments are well interconnected with each other and various important behavioral and cultural elements are well defined so as to facilitate the proper working of the unit. The second classification (into organizational factors) involves lean organization structure (Grittell and Weiss, 2004), JIT and lean practices, organizational behavior and culture for supply chain implementation (Grittell and Weiss, 2004; Arshinder and Deshmukh, 2006), role in the supply chain with respect to other members (Ramsay, 1996; Freathy and O'Connell, 1998) and integration of departments within the organization (Grittel and Weiss, 2004). These factors are important for better coordination of supply chain.

2.3 Mutual understanding (F3)

Mutual understanding includes factors which are agreed vision and goals of members of the supply chain (Arshinder and Deshmukh, 2006; Simatupang *et al.*, 2002), trust development in supply chain members (Arshinder and Deshmukh, 2006; Sahay, 2003), effective implementation of joint replenishment and forecasting decisions (Arshinder and Deshmukh, 2006; Aviv, 2001) and supply chain risk/reward sharing (Cachon and Lariviere, 2005; Lee, 2000). According to Chopra and Meindl (2001), trust is a favorable attitude that exists when one supply chain member has confidence in another supply chain member. It is necessary that all members of supply chains trust each other and share information across the value chain. Managing supply chains without trust and information sharing is challenging task. It affects the whole supply chain adversely. Trust also influences risk and award sharing mechanism of supply chains (Cachon and Lariviere, 2005). Mutual

understanding is a very important element in any organization to carry out the work functions smoothly.

2.4 Flow of information (F4)

For a business to run efficiently and smoothly proper communication between various channels is required so as to have a trouble-free flow of information. The flow of information is classified into the use of information technology (IT)tools and techniques (Simatupang and Sridharan, 2002), information sharing/exchange, sharing of data related to purchasing and supplies (Lee *et al.*,1997), inventory tracking at supply chain linkage, knowledge sharing and design data sharing. Information sharing between various departments is done in a planned manner and it is taken care that the transparency is maintained by providing information flow among various departments regarding various elements such as raw material purchasing and inventory tracking.

2.5 Relationship and decision-making (F5)

A firm, to be successful, needs to maintain healthy relationships, both with its suppliers and consumers. Long-term relationship among members of supply chains reduces conflicts and increases collaboration among members of supply chains. Members are able to take collaborative decision in the interest of supply chain (Simatupang and Sridharan, 2002). It also helps in supply chain integration (Arshinder and Deshmukh, 2006), rationalization of suppliers (Jain *et al.*, 2009), logistics synchronization, vendor-managed inventory and bullwhip effect reduction.

2.6 Responsiveness (F6)

The response of a firm toward the external stimuli is an indicator of how much the firm is dedicated toward the consumer side. Responsiveness in a supply chain is a cluster that involves flexibility in supply chain (Koh *et al.*, 2007), delivery on time (Lee *et al.*, 1997), service reliability (Fisher, 1997) and increased ability to adopt process changes (Zhao and Wang, 2002).

The 33 factors identified from literature are grouped into six clusters as discussed above. Sub-factors considered under each cluster are summarized in Table I.

3. Research methodology – Graph theory matrix approach

The graph theory matrix (digraph) approach has been used here for evaluating a flexibility value of a supply chain using the permanent matrix. The use of digraph methodology is not new and has been used in various cases. A similar approach was used to develop the machinability index for different materials (Rao and Gandhi, 2002. Grover *et al.* (2006) have used this approach in the field of quality management. Malhotra *et al.* (2012) used the graph theory matrix approach to evaluate the barriers in reconfigurable manufacturing systems. Apart from the field of mechanical and industrial engineering, digraphs have found a common use to deal with problems in fault reduction and various other analyses. Computer analysis of general linear network using a digraph (McClenahan and Chan, 2004), system fault diagnostics (Kelly and Bartlett, 2006) for finding out the causes of failure and using a backward approach to reduce them, and hence making the system safer and various other such uses have been seen. Agrawal *et al.* (2016) have applied graph theory and matrix approach for analyzing disposition decisions in reverse logistics. Kumar *et al.* (2017) have used diagraph approach to evaluate agility index. Bhandari *et al.* (2019) have used graph theory matrix approach for quantifying the barriers in implementation of cleaner

Table I. Factors considered for evaluating flexibility index

S. N.	Clusters of flexibility sub factors	References
1.	*Top management commitment (F1)*	
	Allocation of resources for flexible production systems	Shin *et al.* (2000), Kumar and Singh (2017), Gupta *et al.* (2019)
	Flexible communication system	Narasimhan and Kim (2002), Stank *et al.* (1999), Simchi-Levis *et al.* (1999), Singh *et al.* (2017), Gupta *et al.* (2019)
	Long-term goals for flexible production systems	Kumar *et al.* (2013), Singh *et al.* (2019b) Chiang *et al.* (2012), Arshinder and Deshmukh (2006), Ganesan (1994), Morgan and Hunt(1994)
	Flexible service quality	Fisher (1997), Kumar and Singh (2017)
	Application of new technologies for flexible systems	Arshinder and Deshmukh (2006), Chiang *et al.* (2012)
	Training of workforce for flexible manufacturing systems	Simatupang *et al.* (2002), Efstathiades *et al.* (2002)
2.	*Organizational factors (F2)*	
	Lean and flexible organization structure	Grittell and Weiss (2004), Kumar *et al.* (2013),
	Application of flexible supply chain practices	Kumar *et al.* (2017), Arshinder and Deshmukh (2006), Grittell and Weiss (2004)
	Organizational behavior for flexibility in supply chains	Arshinder and Deshmukh (2006), Grittel and Weiss (2004)
	Organizational culture for supply chain coordination	Arshinder and Deshmukh (2006), Grittel and Weiss (2004), Singh *et al.* (2019b)
	Role in supply chain with respect to other members	Ramsay (1996), Freathy and O'Connell (1998)
	Integration of departments within the organization	Grittel and Weiss (2004), Kumar *et al.* (2017),
3.	*Mutual understanding (F3)*	
	Agreed vision and goals for flexibility in supply chain	Arshinder and Deshmukh (2006), Simatupang *et al.* (2002)
	Trust development in the supply chain members	Arshinder and Deshmukh (2006), Sahay (2003), Kumar *et al.* (2013),
	Effective implementation of joint replenishment and forecasting decisions	Arshinder and Deshmukh (2006), Aviv (2001), Haque and Islam (2018)
	Supply chain risk/reward sharing for ensuring flexibility	Cachon and Lariviere (2005), Lee (2000), Singh *et al.* (2017)
4.	*Flow of information (F4)*	
	Use of IT tools and techniques	Simatupang and Sridharan (2002), Lee *et al.* (1997), Singh *et al.* (2019a, 2019b)
	Information sharing among members of supply chain	Arshinder and Deshmukh (2006), Ozer (2003), Sachan *et al.* (2018), Haque and Islam (2018)
	Inventory tracking at supply chain linkage	Mentzer *et al.* (2001), Gupta *et al.* (2019)
	Sharing of data related to purchasing and supplies	Simatupang and Sridharan (2002), Lee *et al.* (1997), Moinzadeh (2002)
	Knowledge management	Pyke *et al.* (2000), Simatupang *et al.* (2002), Singh *et al.* (2019a, 2019b)
	Design data sharing for flexible manufacturing systems	Narus and Anderson (1996),Lambert *et al.* (1999)

(*continued*)

Table I.

S. N.	Clusters of flexibility sub factors	References
5.	*Relationship and decision making (F5)*	
	Long-term relationships with suppliers	Jain *et al.* (2009), Olorunniwo and Hartfield (2001)
	Long-term relationship with customers	Jain *et al.* (2009), Olorunniwo and Hartfield (2001)
	Collaborative decision-making for flexibility	Tsay (1999), Cachon and Fisher (2000), Disny and Towill (2003)
	Logistics synchronization for flexibility	Simatupang and Sridharan(2002), Bowersox (1990), Simatupang *et al.* (2002)
	Supply chain integration for flexibility	Arshinder and Deshmukh (2006), Lee (2000),Chan *et al.* (2009)
	Rationalization and development of flexible suppliers	Jain *et al.* (2009), Simchi-Levis *et al.* (1999)
6.	*Responsiveness (F6)*	
	Flexibility in production system	Koh *et al.* (2007), Arshinder and Deshmukh (2006), Kumar *et al.* (2008)
	Flexible delivery time	Lee *et al.* (1997), Fisher (1997)
	Service flexibility	Konijnendijk (1994), Fisher (1997)
	Flexibility in adopting process change	Zhao and Wang (2002)

technologies. Digraph approach is a very important tool, as it helps in correlation and evaluation by forming an index. Based on the literature review, six clusters comprising of 33 factors of supply chain flexibility are identified in this study.

The various steps in the proposed methodology consist of developing diagraph between factors depending upon their mutual relationship as shown in Figure 2. Permanent function of the factors' permanent matrix at system level is evaluated using the equation (1).

3.1 Variables digraph

The variable's digraph is prepared to represent the variables of the flexibility in supply chain in terms of nodes and edges. Let the nodes represent the variables and the edges represent their interactions. F_i indicates the inheritance of factors and f_{ij} indicates the degree of dependence of *jth* factor on *ith* factor. In the digraph, f_{ij} is represented as a directed edge from node i to node j. The interactions among clusters of factors considered for this study are shown in Figure 1. Detailed linkage can be also understood from the diagraph given in Figure 2.

3.2 Variables' permanent matrix

Overall variables' effect is maximum when the variables' effect of all the factors is the maximum. The permanent matrix for the system in general (assuming interactions among all factors) can be shown as:

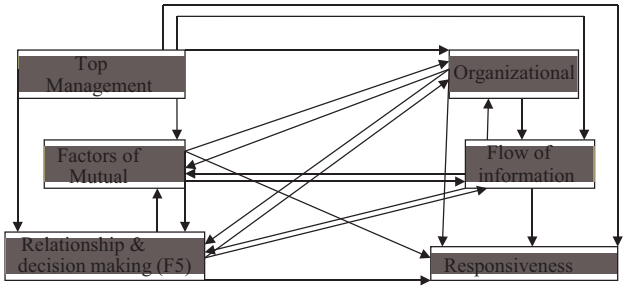

Figure 1.
Interactions among clusters of factors of flexibility index

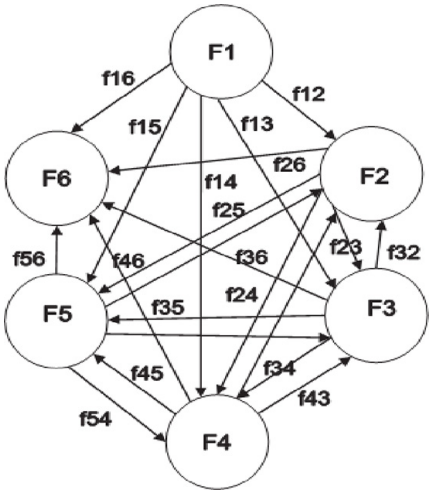

Figure 2.
Diagraph representation of elements of permanent matrix

$$permF = \begin{vmatrix} F1 & f_{12} & f_{13} & f_{14} & f_{15} & f_{16} \\ 0 & F2 & f_{23} & f_{24} & f_{25} & f_{26} \\ 0 & f_{32} & F3 & f_{34} & f_{35} & f_{36} \\ 0 & f_{42} & f_{43} & F4 & f_{45} & f_{46} \\ 0 & f_{52} & f_{53} & f_{54} & F5 & f_{56} \\ 0 & 0 & 0 & 0 & 0 & F6 \end{vmatrix}$$

The linkage of f_{ij} can be understood using diagraph as shown in Figure 2.

The permanent of a matrix, given by equation (1), is multinomial and is known as permanent of F (per F). This is evaluated by standard procedures and is the same as the determinant of EVCM but with all signs positive. The permanent for matrix equation (6) in the general form is written as:

$$\begin{aligned} permF = & \prod_{i=1}^{6} F_i + \sum_{i=1}^{5}\sum_{j=i+1}^{6}\sum_{k=1}^{3}\sum_{l=k+1}^{4}\sum_{m=l+1}^{5}\sum_{n=m+1}^{6} (f_{ij}f_{ji})F_kF_lF_mF_n \\ & + \sum_{i=1}^{4}\sum_{j=i+1}^{5}\sum_{k=j+1}^{6}\sum_{l=1}^{4}\sum_{m=l+1}^{5}\sum_{n=m+1}^{6} (f_{ij}f_{jk}f_{ki} + f_{ik}f_{kj}f_{ji})F_lF_mF_n \\ & + \left[\begin{array}{l} \sum_{i=1}^{3}\sum_{j=i+1}^{6}\sum_{k=j+1}^{5}\sum_{l=i+2}^{6}\sum_{m=1}^{5}\sum_{n=m+1}^{6} (f_{ij}f_{jk})(f_{kl}f_{lk})_lF_mF_n \\ + \sum_{i=1}^{3}\sum_{j=i+1}^{5}\sum_{k=i+1}^{6}\sum_{l=j+1}^{6}\sum_{m=1}^{5}\sum_{n=m+1}^{6} (f_{ij}f_{jk}f_{kl}f_{li} + f_{il}f_{lk}f_{kj}f_{ji})_l F_mF_n \end{array} \right] \\ & + \left[\begin{array}{l} \sum_{i=1}^{4}\sum_{j=i+1}^{5}\sum_{k=j+1}^{6}\sum_{l=1}^{5}\sum_{m=l+1}^{6}\sum_{n=1}^{6} (f_{ij}f_{jk}f_{ki} + f_{ik}f_{kj}f_{ji})(f_{lm}f_{ml})_lF_m \\ + \sum_{i=1}^{2}\sum_{j=i+1}^{5}\sum_{k=i+1}^{6}\sum_{l=i+1}^{6}\sum_{m=j+1}^{6}\sum_{n=1}^{6} (f_{ij}f_{jk}f_{kl}f_{lm}f_{mi} + f_{im}f_{ml}f_{lk}f_{kj}f_{ji})F_n \end{array} \right] \\ & + \left[\begin{array}{l} \sum_{i=1}^{3}\sum_{j=i+1}^{5}\sum_{k=i+1}^{6}\sum_{l=i+1}^{6}\sum_{m=1}^{6}\sum_{n=m+1}^{6} (f_{ij}f_{jk}f_{kl}f_{li} + f_{il}f_{lk}f_{kj}f_{ji})(f_{mn}f_{nm}) \\ + \sum_{i=1}^{1}\sum_{j=i+1}^{5}\sum_{k=j+1}^{6}\sum_{l=1}^{4}\sum_{m=l+1}^{5}\sum_{n=m+1}^{6} (f_{ij}f_{jk}f_{ki} + f_{ik}f_{kj}f_{ji})(f_{lm}f_{mn}f_{nl} + f_{ln}f_{nm}f_{ml}) \\ + \sum_{i=1}^{1}\sum_{j=i+1}^{6}\sum_{k=i+1}^{3}\sum_{l=i+2}^{6}\sum_{m=k+1}^{5}\sum_{n=k+2}^{6} (f_{ij}f_{ji})(f_{kl}f_{lk})(f_{mn}f_{nm}) \\ + \sum_{i=1}^{1}\sum_{j=i+1}^{5}\sum_{k=i+1}^{6}\sum_{l=i+1}^{6}\sum_{m=i+1}^{6}\sum_{n=j+1}^{6} (f_{ij}f_{jk}f_{kl}f_{lm}f_{mn}f_{ni} + f_{in}f_{nm}f_{ml}f_{lk}f_{kj}f_{ji}) \end{array} \right] \end{aligned} \tag{1}$$

4. Case illustration

In this research paper, a case study of organization ABC Ltd. is considered, which is a wholly-owned subsidiary of world's fifth largest automobile company, XYZ of South Korea,

and is the largest passenger car exporter and the second largest car manufacturer of India. ABC Ltd. presently markets 49 variants of passenger cars across segments. ABC Ltd. is continuing its tradition of being the fastest growing passenger car manufacturer. ABC Ltd. currently exports cars to more than 110 countries across the European Union, Africa, Middle East, Latin America and Asia. It has been the number one exporter of passenger car of the country for the sixth year in a row.

4.1 Production statistics

ABC Ltd., the country's second largest car manufacturer and the largest passenger car exporter achieved record sales of 31,501 units for the month of March 2010 in the domestic market, registering 27.3 per cent growth over the same month last year. In September 2017, ABC Ltd.'s exports grew by 3.9 per cent to 22,707 units, whereas the company exported 21,849 vehicles in September 2016.

This study includes inputs from supply chain managers, top management members, marketing and vendor development managers. For the survey, two well-structured, multi-choice questionnaires were sent to professionals of ABC Ltd. The first questionnaire was designed to collect the response on the importance of sub-factors of six main factors of cluster (F1 to F6). Second questionnaire was prepared to find the influence of the main factors of the cluster on each other (i.e F12 – relationship/influence of top management commitment (F1) with organizational factors (F2), similarly F23 – relationship between organizational factors (F2) on mutual understanding (F3) and so on).

The putting values of the variables in the equation i.e. variables' variable permanent matrix (VPM):

$$permF = \begin{vmatrix} F1 & f_{12} & f_{13} & f_{14} & f_{15} & f_{16} \\ 0 & F2 & f_{23} & f_{24} & f_{25} & f_{26} \\ 0 & f_{32} & F3 & f_{34} & f_{35} & f_{36} \\ 0 & f_{42} & f_{43} & F4 & f_{45} & f_{46} \\ 0 & f_{52} & f_{53} & f_{54} & F5 & f_{56} \\ 0 & 0 & 0 & 0 & 0 & F6 \end{vmatrix} = \begin{vmatrix} 3.6 & 4 & 3 & 3 & 3 & 3 \\ 0 & 3.6 & 2 & 3 & 3 & 4 \\ 0 & 3 & 4 & 4 & 4 & 4 \\ 0 & 3 & 3 & 2.9 & 4 & 4 \\ 0 & 3 & 3 & 3 & 3.4 & 3 \\ 0 & 0 & 0 & 0 & 0 & 4 \end{vmatrix}$$

$$permF^* = 37,578.3$$

The maximum value of the index is achieved when all the parameters have highest rating, and this could be set as the maximum on a reference scale. Putting all the parameters in the matrix equations, we have the following:

$$\text{Per}\, F^* = F^*_{\max} = 3,75,000.$$

F^* is the flexibility index of the supply chain of company ABC Ltd. Now, this value of flexibility index can be used to compare the index of flexibility of any other organization's supply chain. The comparison procedure helps the organization to compare different groups, based on which weak link in the flexibility in the supply chain can be analyzed and improved. The maximum value, $F^*_{\max}$ defines the maximum flexibility when all the factors are fulfilled with maximum satisfaction (each factor awarded score of 5-very high).

The various shortcomings of the supply chain of a particular organization can be analyzed from the approach illustrated in the study. It can lead to improve the flexibility in the supply chain.

5. Conclusion, managerial implications and future scope

In dynamic markets of today, organizations need to improve flexibility of their respective supply chains on a continuous basis. Supply chain flexibility depends on many factors. In this study, a total of 33 factors are considered. These factors, directly or indirectly, influence flexibility of supply chains. These factors are further categorized into six major groups. They are top management commitment, organizational factors, mutual understanding, flow of information, relationship and decision-making and responsiveness. The flexibility index of a given supply chain has been evaluated in terms of scores of these factors for the corresponding supply chain. The graph theory approach has been used to evaluate flexibility index of this supply chain.

The proposed framework in this study will help the supply chain managers to evaluate the flexibility index of their respective organizations. It will also help managers in benchmarking their respective performance and thereby taking corrective measures. Flexible organizations can easily cope up the required changes in practices being followed. Organizations having less flexibility score may find weak areas to improve upon. As values taken for different factors are based on inputs given by managers of case organization, chances of bias may be there. Managers need to be careful while considering flexibility sub-factors and rating them for evaluating the flexibility index. Therefore, findings may be further validated with more case studies. As a future scope, framework may be applied for supply chains of different sectors. Apart from it, different factors considered in this study may be further prioritized by using different multi-criteria decision-making tools or empirical studies. Proposed framework may be further modified in context to emerging business environment of circular economy and Industry 4.0.

References

Agrawal, S., Singh, R.K. and Murtaza, Q. (2016), "Disposition decisions in reverse logistics: graph theory and matrix approach", *Journal of Cleaner Production*, Vol. 137, pp. 93-104.

Arshinder and Deshmukh, S.G. (2006), "Supply chain coordination issues: an SAP-LAP framework", *Asia Pacific Journal of Marketing and Logistics*, Vol. 19 No. 3, pp. 240-264. 2007,

Aviv, Y. (2001), "The effect of collaborative forecasting on supply chain performance", *Management Science*, Vol. 47 No. 10, pp. 1326-1343.

Beach, R., Muhlemann, A.P., Price, D.H.R., Paterson, A. and Sharp, A. (2000), "A review of manufacturing flexibility", *European Journal of Operational Research*, Vol. 122 No. 1, pp. 41-57.

Bhandari, D., Singh, R.K. and Garg, S.K. (2019), "Prioritisation and evaluation of barriers intensity for implementation of cleaner technologies: framework for sustainable production", *Resources, Conservation and Recycling*, Vol. 146, pp. 156-167.

Bowersox, D.J. (1990), "The strategic benefits of logistics alliances", *Harvard Business Review*, Vol. 68 No. 4, pp. 36-43.

Cachon, G.P. and Fisher, M. (2000), "Supply chain inventory management and value of shared information", *Management Science*, Vol. 46 No. 8, pp. 1032-1048.

Cachon, G.P. and Lariviere, M.A. (2005), "Supply chain coordination with revenue sharing contracts: strengths and limitations", *Management Science*, Vol. 51 No. 1, pp. 30-44.

Chan, H.K., Wang, W.Y.C., Luong, L.H.S. and Chan, F.T.S. (2009), "Flexibility and adaptability in supply chains: a lesson learnt from a practitioner", *Supply Chain Management: An International Journal*, Vol. 14 No. 6, pp. 407-410.

Chiang, C.Y., Hillmer, C.K. and Suresh, N. (2012), "An empirical investigation of the impact of strategic sourcing and flexibility on firm's supply chain agility", *International Journal of Operations and Production Management*, Vol. 32 No. 1, pp. 49-78.

Chopra, S. and Meindl, P. (2001), "Supply chain management: strategy, planning, and operation", Prentice-Hall, Upper Saddle River, NJ.

Craighead, C.W., Blackhurst, J., Rungtusanatham, M.J. and Handfield, R.B. (2007), "The severity of supply chain disruptions: design characteristics and mitigation capabilities", *Decision Sciences*, Vol. 38 No. 1, pp. 131-156.

Disny, S.M. and Towill, D.R. (2003), "Vendor managed inventory and bullwhip effect reduction in a two level supply chain", *International Journal of Operations and Production Management*, Vol. 23 No. 6, pp. 625-651.

Efstathiades, A., Tassou, S.A. and Antoniou, A. (2002), "Strategic planning, transfer and implementation of advanced manufacturing technologies (AMT), development of an integrated process plan", *Technovation*, Vol. 22 No. 4, pp. 201-212.

Fayezi, S., Zutshi, A. and O'Loughlin, A. (2014), "Developing an analytical framework to assess the uncertainty and flexibility mismatches across the supply chain", *Business Process Management Journal*, Vol. 20 No. 3, pp. 362-391.

Fisher, M.L. (1997), "What is right supply chain for your product", *Harvard Business Review*, Vol. 75 No. 2, pp. 105-116.

Freathy, P. and O'Connell, F. (1998), "Supply chain relationships within airport retailing", *International Journal of Physical Distribution and Logistics Management*, Vol. 28 No. 6, pp. 451-462.

Ganesan, S. (1994), "Determinants of long-term orientation in buyer-supplier relationships", *Journal of Marketing*, Vol. 58 No. 2, pp. 1-19.

Ganesan, R. and Harrison, T. (1995), "An introduction to supply chain management", *Department of Management Science and Information Systems*, 303 Beam Business Building Penn State University University Park, PA 16802 USA.

Grittell, J.H. and Weiss, L. (2004), "Coordination networks within and across organizations: a multi-level framework", *Journal of Management Studies*, Vol. 41 No. 1, pp. 127-153.

Grover, S., Agrawal, V.P. and Khan, I. (2006), "Digraph and matrix method for the performance evaluation of carbide compacting die manufactured by wire EDM", *International Journal of Advanced Manufacturing Technology*, Vol. 42 No. 19, pp. 4031-4041.

Gupta, A., Suri, P. and Singh, R.K. (2019), "Analyzing the interaction of barriers in e-governance implementation for effective service quality: interpretive structural modeling approach", *Business Perspectives and Research*, Vol. 7 No. 1, pp. 59-75.

Haque, M. and Islam, R. (2018), "Impact of supply chain collaboration and knowledge sharing on organizational outcomes in pharmaceutical industry of Bangladesh", *Journal of Global Operations and Strategic Sourcing*, Vol. 11 No. 3, pp. 301-320.

Jain, V., Wadhwa, S. and Deshmukh, S.G. (2009), "Select supplier related issues in modeling a dynamic supply chain: potential, challenges and direction for future research", *International Journal of Production Research*, Vol. 47 No. 11, pp. 3013-3039.

Kelly, E.M. and Bartlett, L.M. (2006), "Application of the digraph method in system fault diagnostics", *First International Conference on Availability, Reliability and Security (ARES'06), 2006, Ares*, pp. 693-700.

Kocabasogu, C., Prahinski, C. and Klassen, R.D. (2007), "Linking forward and reverse supply chain investments: the role of business uncertainty", *Journal of Operations Management*, Vol. 25 No. 6, pp. 1141-1160.

Koh, L.S.C., Mehmet, D., Erkan, B., Ekrem, T. and Selim, Z. (2007), "The impact of supply chain management practices on performance of SMEs", *Industrial Management and Data Systems*, Vol. 107 No. 1, pp. 103-124.

Konijnendijk, P.A. (1994), "Coordinating marketing and manufacturing in ETO companies", *International Journal of Production Economics*, Vol. 37 No. 1, pp. 19-26.

Kumar, P., Shankar, R. and Yadav, S.S. (2008), "Flexibility in global supply chain: modeling the enablers", *Journal of Modelling in Management*, Vol. 3 No. 3, pp. 277-297.

Kumar, R. and Singh, R.K. (2017), "Coordination and responsiveness issues in SMEs supply chains: a review", *Benchmarking: An International Journal*, Vol. 24 No. 3, pp. 635-650.

Kumar, P., Singh, R.K. and Kumar, R. (2017), "An integrated framework of interpretive structural modeling and graph theory matrix approach to fix the agility index of an automobile manufacturing organization", *International Journal of System Assurance Engineering and Management*, Vol. 8 No. S1, pp. 342-352.

Kumar, R., Singh, R.K. and Shankar, R. (2013), "Study on coordination issues for flexibility in supply chain of SMEs: a case study", *Global Journal of Flexible Systems Management*, Vol. 14 No. 2, pp. 81-92.

Lambert, D.M., Emmelhainz, M.A. and Gardner, J.T. (1999), "Building successful partnership", *Journal of Business Logistics*, Vol. 16 No. 1, pp. 165-181.

Lee, H.L. (2000), "Creating value through supply chain integration", *Supply Chain Management Review*, Vol. 4 No. 4, pp. 30-36.

Lee, H.L. and Billington, C. (1995), "The evolution of supply-chain-management models and practice at Hewlett-Packard", *Interfaces*, Vol. 25 No. 5, pp. 42-63.

Lee, H.L., Padmanabhan, P. and Whang, S. (1997), "The bullwhip effect in supply chains", *Sloan Management Review*, Vol. 38, pp. 93-102.

McClenahan, J.O. and Chan, S.P. (2004), "Computer analysis of general linear networks using digraphs", *International Journal of Electronics*, Vol. 33 No. 2, pp. 153-191.

Malhotra, V., Raj, T. and Arora, A. (2012), "Evaluation of barriers affecting reconfigurable manufacturing systems with graph theory and matrix approach", *Materials and Manufacturing Processes*, Vol. 27 No. 1, pp. 88-94.

Mentzer, J.T., DeWitt, W., Keebler, J.S., Min, S., Nix, N.W., Smith, C.D. and Zacharia, G.Z. (2001), "Defining supply chain management", *Journal of Business Logistics*, Vol. 22 No. 2, pp. 1-25.

Moinzadeh, K. (2002), "A multi-echelon inventory system with information exchange", *Management Science*, Vol. 48 No. 3, pp. 414-426.

Morgan, R.M. and Hunt, S.D. (1994), "The commitment-trust theory of relationship marketing", *Journal of Marketing*, Vol. 58 No. 3, pp. 20-38.

Naim, M., Potter, A., Mason, R. and Bateman, N. (2006), "The role of transport flexibility in logistics provision", *International Journal of Logistics Management*, Vol. 17 No. 3, pp. 297-311.

Narasimhan, R. and Kim, S. (2002), "Effect of supply chain integration on the relationship between diversification and performance: evidence from Japanese and Korean firms", *Journal of Operations Management*, Vol. 20 No. 3, pp. 303-323.

Narus, J.A. and Anderson, J.C. (1996), "Rethinking distribution: adaptive channels", *Harvard Business Review*, Vol. 74, pp. 112-120.

Olorunniwo, P. and Hartfield, J. (2001), "The knowledge of coordination of supply chain integration", *Business Process Management jJournal*, Vol. 8 No. 3, pp. 289-308.

Ozer, O. (2003), "Replenishment strategies for distribution system under advanced demand information", *Management Science*, Vol. 49No No. 3, pp. 255-272.

Pujawan, I.N. (2004), "Assessing supply chain flexibility: a conceptual framework and case study", *International Journal of Integrated Supply Management*, Vol. 1 No. 1, pp. 79-97.

Pyke, D., Robb, D. and Farley, J. (2000), "Manufacturing and supply chain management in China: a survey of states, collective and privately-owned enterprises", *European Management Journal*, Vol. 8 No. 6, pp. 577-589.

Ramsay, J. (1996), "The case against purchasing partnerships", *International Journal of Purchasing and Materials Management*, pp. 13-19.

Rao, R.V. and Gandhi, O.P. (2002), "Machinability evaluation of work materials using a combined multiple attribute decision-making method", *International Journal of Advanced Manufacturing Technology*, Vol. 28 Nos 3/4, pp. 221-227.

Sachan, A., Kumar, R. and Kumar, R. (2018), "Examining the impact of e-government service process on user satisfaction", *Journal of Global Operations and Strategic Sourcing*, Vol. 11 No. 3, pp. 321-336.

Sahay, B.S. (2003), "Understanding trust in supply chain relationships", *Industrial Management and Data Systems*, Vol. 103 No. 8, pp. 553-563.

Sawhney, R. (2006), "Interplay between uncertainty and flexibility across the value-chain: towards a transformation model of manufacturing flexibility", *Journal of Operations Management*, Vol. 24 No. 5, pp. 476-493.

Shin, H., Collier, D.A. and Wilson, D.D. (2000), "Supply management orientation and supplier/buyer performance", *Journal of Operations Management*, Vol. 18 No. 3, pp. 317-333.

Simatupang, T.M. and Sridharan, R. (2002), "The collaborative supply chain", *The International Journal of Logistics Management*, Vol. 13 No. 1, pp. 15-30.

Simatupang, T.M., Wright, A.C. and Sridharan, R. (2002), "The knowledge of coordination for supply chain integration", *Business Process Management Journal*, Vol. 8 No. 3, pp. 289-308.

Simchi-Levis, D., Kaminsky, P. and Simchi-Levis, E. (1999), "Designing and managing the supply chain", Mc Graw -Kill, London.

Singh, R.K., Koul, S. and Kumar, P. (2017), "Analyzing the interaction of factors for flexibility in supply chains", *Journal of Modelling in Management*, Vol. 12 No. 4, pp. 671-689.

Singh, R.K., Kumar, P. and Chand, M. (2019b), "Evaluation of coordination and responsiveness index for supply chain using graph theoretic approach", *Benchmarking: An International Journal*, (In press)

Singh, R.K., Luthra, S., Mangla, S.K. and Uniyal, S. (2019a), "Applications of information and communication technology for sustainable growth of SMEs in India food industry", *Resources, Conservation and Recycling*, Vol. 147, pp. 10-18.

Singh, R.K. and Sharma, M.K. (2014a), "Prioritising the alternatives for flexibility in supply chains", *Production Planning and Control*, Vol. 25 No. 2, pp. 176-192.

Singh, R.K. and Sharma, P.B. (2014b), "Development of framework for analizing flexibility in supply chain", *Organizational Flexibility and Competitiveness*, Springer, New Delhi, pp. 273-283.

Soon, Q.H. and Udin, Z.M. (2010), "Supply chain management from the perspective of value chain flexibility: an exploratory study", *Journal of Manufacturing Technology Management*, Vol. 22 No. 4, pp. 506-526.

Stank, T., Michael, C. and Miren, A. (1999), "Benefits of interfirm coordination in food industry supply chains", *Journal of Business Logistics*, Vol. 20 No. 2, pp. 21-41.

Swafford, P.M., Ghosh, S. and Murthy, N.N. (2006), "The antecedents of supply chain agility of a firm: scale development and model testing", *Journal of Operations Management*, Vol. 24 No. 2, pp. 170-188.

Tsay, A. (1999), "The quantity flexibility contract and supplier customer incentives", *Management Science*, Vol. 45 No. 10, pp. 1339-1358.

Tse, Y.K., Matthews, R.L., Tan, K.H., Sato, Y. and Pongpanich, C. (2016), "Unlocking supply chain disruption risk within the Thai beverage industry", *Industrial Management and Data Systems*, Vol. 116 No. 1, pp. 21-42.

Zhao, W. and Wang, Y. (2002), "Coordination of joint pricing-production decisions in a supply chain", *IIE Transactions*, Vol. 34 No. 8, pp. 701-715.

Further reading

Chatterjee, A., Cohen, M., Maxwell, W. and Miller, L. (1984), *"Proceedings of the 1st ORSA/TIMS Special Interest Conference on FMS", MI, Ann Arbor*, pp. 49-64.

Mandelbaum, M. and Buzzacott, J.A. (1990), "Flexibility and decision making", *European Journal of Operations Research*, Vol. 44 No. 1, pp. 17-27.

Meyer, L.H. (1999), "Market discipline as a complement to bank supervision and regulation", *Speech before the Conference on Reforming Bank Capital Standards, New York, NY*.

About the authors

Dr Rajesh Kumar Singh is a Professor in Operations Management Area at Management Development Institute (MDI), Gurgaon, India. His areas of interest include competitiveness, small business management, quality management and supply chain management. He has about 160 research papers published in reputed international/national journals and conferences. He has published papers in journals such as *Resources, Conservation and Recycling, Journal of Cleaner Production, Industrial Management and Data Systems, Production planning and Control, Annals of Operations Research, International Journal of Production Research, Singapore Management Review, International Journal of Productivity and Performance Management, Benchmarking: An International Journal, Journal of Modelling in Management, Competitiveness Review: An International Business Journal, Global Journal of Flexible Systems and Management, International Journals of Productivity and Quality Management, International Journal of Services and Operations Management, International Journal of Automotive Industry and Management, International Journal of Logistic Systems Management, IIMB Management Review and Productivity Promotion*. Rajesh Kumar Singh is the corresponding author and can be contacted at: rksdce@yahoo.com

Dr Pravin Kumar is working as an Associate Professor in the Department of Mechanical Engineering, Delhi Technological University, Delhi. He has more than 18 years of teaching and research experience. He obtained a PhD in Supply Chain Management from IIT Delhi and an MTech in Industrial Management from IIT (Banaras Hindu University), Varanasi. His research area is supply chain and operations management. He has authored a book on engineering economy and management, Wiley India Pvt. Ltd., and a book on industrial engineering and management from Pearson learning, India. He has also published more than 50 research papers in international journals and conferences. His research articles have been published in the journals such as *Applied Soft Computing*; *Annals of Operations Research*; *Clean Technology and Environmental Policy*; *Environment, Development and Sustainability*; *International Journal of System Assurance Engineering and Management; Journal of Modelling in Management; International Journal of Mobile Communications; International Journal of Business Excellence*, among others.

For instructions on how to order reprints of this article, please visit our website:
www.emeraldgrouppublishing.com/licensing/reprints.htm
Or contact us for further details: **permissions@emeraldinsight.com**

arXiv:1909.11890v1 [cs.NE] 26 Sep 2019

Military Dog Based Optimizer and its Application to Fake Review Detection

Ashish Kumar Tripathi
Jaypee Institute of Information Technology, Noida
mail2ashish07@gmail.com

Kapil Sharma
Delhi Technological University, New Delhi
kapil@ieee.org

Manju Bala
IP College of Women, New Delhi
manjugpm@gmail.com

Abstract

Over the last three decades more then sixty meta-heuristic algorithms have been proposed by the various authors. Such algorithms are inspired from physical phenomena, animal behavior or evolutionary concepts. These algorithms have been widely used for solving the various real world optimization problems. Researchers are continuously working to improve the existing algorithms and also proposing new algorithms that are giving competitive results as compared to the existing algorithms present in the literature. In this paper a novel meta heuristic algorithm based on military dogs squad is introduced. The proposed algorithm mimics the searching capability of the trained military dogs. Military dogs have strong smell senses by which they are able to search the suspicious objects like bombs, wildlife scats, currency, or blood as well as they can communicate with each other by their barking. The performance of the proposed algorithm is tested on 17 benchmark functions and compared with five other meta-heuristics namely particle swarm optimization (PSO), multi-verse optimizer (MVO), genetic algorithm (GA), probability based learning (PBIL) and evolutionary strategy (ES). The results are validated in terms of mean and standard deviation of the fitness value. The convergence behavior and consistency of the results have been also validated by plotting convergence graphs and BoxPlots. Further the, proposed algorithm is successfully utilized to solve the real world fake review detection problem. The experimental results demonstrate that the

proposed algorithm outperforms the other considered algorithms on the majority of performance parameters.

Keywords: **Optimization, benchmark, clustering, fake reviews.**

1. Introduction

Meta-heuristic algorithm are gaining more and more popularity in the engineering domain due to their ability to bypass local optima and applicability across different disciplines, whereas the classical optimization algorithms are not able to provide a suitable solution for solving the optimization problems of high dimensionality. Since, the search space increases exponentially with the problem size, therefore solving these problems with the techniques like exhaustive search is impractical. Various heuristic approaches have been developed by the researchers to solve the global optimization problems such as Genetic algorithm (GA) [1], Particle swarm Optimization (PSO) [2], Gravitational search algorithm (GSA) [3], central force optimization (CFO) [4], Colliding Bodies optimization (CBO) [5], Magnetic charged system search (MCS) [5], Ray optimization [6], Cuckoo optimization (CO) [7], Firefly algorithm (FA) [8], etc. Meta-heuristics are the population based algorithms inspired from the nature. Each algorithms starts with the random set of solution called population. What makes the difference is the way of movements of population towards the global optima during the optimization process. These algorithms are tested and analyzed in the different domains of engineering. As No Free Lunch theorem clearly obviates the claim of an optimization algorithm for all optimization problems [9]. Thus, the urge of new meta-heuristic algorithm is standstill. Therefore, in this paper, a new meta-heuristic algorithm is proposed which leverages the searching ability of the trained military dogs. Dogs are trained by the humans for object detecting and tracking purposes. They train them especially as military dogs, sniffer dogs, hunting dogs, police dogs, search dogs, and detector dogs. Military dogs are the category of dogs, especially trained for detecting substances like bombs, illegal drugs, wildlife scats, currency, or blood [10]. Mostly, military dogs work in groups called military dog squad to detect the object. They use the barking sound to locate or signal other dogs. Coren and Hodgson [11] studied that each sound of the military dog have some meaning associated with it. For example, loud sound of dog indicates insecurity. Baying sound indicates a call from the military dog to assure that his mates are alerted [11]. Generally, the smelling power of the dog is 1,000 to 10,000 times more than the humans or other species [11]. Table 1 shows the number of scent receptors in the various species. Moreover,

Table 1: Number of Scent Receptors for different Species

Species	Number of Scent Receptors
Humans	5 million
Dachshund	125 million
Fox Terrier	147 million
Beagle	225 million
German Shepherd	225 million
Bloodhound	300 million

the military dogs have the capability of deducing the direction of smell by moving their nostrils. Also, they have ability of storing meaningful information about the object in the form of scent while searching, which helps them in reaching to the desired object.

Furthermore, united states war dogs association studies stated that the smelling power of dogs is effected by the wind. A dog may detect the suspected object up to 200 meters by the smell power if there is no wind. However, with the greater wind factor, the same can detect up to 1000 meters. Moreover, the factors like smoke and heavy vegetation are the confusing factors for a dog, as it confuse them in sensing the direction of actual smell or sound. This paper mimics the searching process of trained military dog squad to introduce a novel military dog based optimizer for finding the global optima. The overall contribution of this paper has three folds. First, a new military dog based optimization has been presented. Second, the mathematical model of the proposed algorithm has been detailed. The validation of the proposed algorithm has been done against 17 benchmark functions and performance is measured in term of 4 parameters namely: fitness value, standard deviation, convergence behavior, and consistency in the results. The efficiency of the algorithm is compared with 5 existing meta-heuristics. Third, the real-world problem of fake review detection has been unfolded using the proposed algorithm.

Rest of the paper is organized as follows. Section II discusses the related work. Section III presents the mathematical model of the military dog based optimizer. Section IV provides the experimental results. Section V details the fake review detection problem and how it can be solved using MDBO. Conclusion and future work is elucidated in section VI.

2. Related Work

Nature-inspired meta-heuristic algorithms mimics the optimization behavior of the nature. Generally, these algorithms are population-based and start with a population of random solutions to

obtain the global best solution. In contrast to this, there exists single-solution based algorithms like hill climbing [12] and simulated annealing [13], which initiates the optimization process with a single solution. However, these algorithms suffer with the problem of local trap and premature convergence as they do not share any kind of information. On the contrary, population-based algorithms improve the solution over the iterations by information sharing. Two common aspects of the population-based algorithms are exploration and exploitation. Exploration represents the diversification in the search space, while exploitation corresponds to the intensification of the current solution. All population based algorithm tries to attain an equilibrium between exploration and exploitation to achieve the global best solution. Every agent of the meta-heuristic tries to improve its performance by sharing its fitness value with other agents at each iteration. The meta-heuristic can be broadly classified into three categories namely; physics-based, swarm-behavior based and evolutionary-based.

The physics-based algorithm optimizes the problem by imitating the physics based phenomenon. Gravitational search algorithm, proposed by Rashedi et al. [3], is one such algorithm which is based on Newtonian laws of gravity and motion. Hosseini [14] proposed an intelligent water drop algorithm which was inspired from the flow of rivers, as rivers often follow shortest path while flowing from source to destination. Further, Birbil [15] proposed an algorithm based on the concept of electromagnetism in which the properties of attraction and repulsion is used to attain a balanced trade-off between exploration and exploitation. Moreover, Mirjalili et al. [16] proposed multi-verse optimizer (MVO) in 2015, which is based on the notion of cosmology i.e white hole, black hole and wormhole. Some other physics based algorithms are Galaxy-based Search Algorithm (GbSA) [17], Black Hole (BH) [18] algorithm, Small-World Optimization Algorithm (SWOA) [19], Ray Optimization (RO) [20], Curved Space Optimization (CSO) [21].

Swarm-based algorithms behave like the swarm of agents such as fishes or birds to achieve optimization results. Eberhart et al. [22] proposed the particle swarm optimization (PSO) which was inspired from the swarming behavior of fish or birds in search of food. Gandomi [23] presented an algorithm based on the simulation of the krill individuals. Mirjalili [24] proposed an ant-lion based optimizer that mimics the hunting mechanism of ant-lions. Moreover, Mirjalili [25]also introduced the moth-flame optimization, which simulates the death behavior of moths, in which the movement of agent is based on the transverse orientation based navigation of moths. Further, Wang et al. [26]

proposed the hybrid krill heard algorithm to overcome the problem of poor exploitation capability of the krill herd algorithm. Ant colony optimization is another swarm based algorithm, which imitates the path finding behavior of ants [27]. Some other swarm based algorithm proposed in the literature are Cuckko search, Bat algorithm, Firefly optimization, Spider monkey optimization and Artificial bee colony optimization [28].

Evolution based algorithm are inspired from the biological evolution phenomena such as Darvin evolutionary theory. The evolutionary algorithms work on the principle of generating better individuals with the course of iterations by combining best individuals of the current generation. The popular genetic algorithm (GA) is an evolutionary algorithm based on the evolution of natural species. It maintains the balance between exploration and exploitation through the mutation and crossover operators. Another biological process based evolutionary algorithm is ES which gives almost equal importance to recombination and mutation, and it uses more than two parents to accord to an offspring. Baluja [29] proposed the probability-based incremental learning algorithm (PBIL) which manages only statics of the population rather than managing the complete population. Simon presented bio-geography based optimizer which is based on the immigration and emigration of the species between the islands of natural bio-geography. Differential evolution is another popular evolutionary algorithmic introduced by storm et al. [30].

3. Military Dog Optimizer

In this section, a new optimization algorithm based on the behavior of military dog's squad is introduced. Military dogs are the special trained dogs who go through a special training to search any specific type object, where they learn to identify thousands of scents. Moreover, military dogs undergo intense one on one training where they learn to work as a team to find the particular suspicious object for which they are trained. All these military dogs can communicate with each other by passing their message via barking. Hence dogs can cooperate with each other directly by passing message via the way of barking and its loudness. The loudness of barking indicates its closeness with the target object. When, a group of military dogs are left out for searching of a target object hidden in an open ground. The military dogs randomly start searching the area. With smelling sensation, the military dogs analyze a particular location and they define the fitness of the location in terms of loudness. The highest loudness indicates the best location among them. Military dog takes small step based on the scent smell in a particular location to exploit the local

search area and it moves to explore the search space based on the loudness of barking. The smelling sensation analysis of the military dogs help them to take a move closer towards the target object and exploit the current location. Military dogs diverge from each other to search for the target object and converge to indicate that the target object is close.

3.1. MDBO Definitions and Algorithm

In this subsection the behavior of military dogs is mathematically simulated and explained. First, some definitions for formalizing the MDBO are explained. Thereafter, the whole procedure of the MDBO is outlined. In the given definitions R is used to refer the set of real numbers, ϕ is used to refer an empty set, while Z is used to denote the set of integers.

$Definition1$: A military dog squad MDS^m is a set of m trained military dogs. The size m of the military dog squad remains constant. Future work could allow variable size military dog squad.
$Definition2$: The feasible solution vector FSV^d, represents the position of a military dog in MDS. $FSV \in R^d$ is a set of all real numbers that represents the urine marking of a MDS.
$Definition3$: A military dog smell index $MDSI : MD \rightarrow R$ is a measure of goodness of the solution that is represented by a MD. In most of the population based algorithm, this $MDSI$ is called fitness of the individual.
$Definition4$: Sniffing movement $\delta(p, P_m,) : MD \rightarrow MD$ is a probabilistic operator that randomly modifies the military dogs FSV^d based on the fitness of the loudest barking MD and movement probability P_m. Sniffing movement takes place using the following equation.

$$FSV_i^j(t+1) = \begin{cases} FSV_{lodest}^j, \ p \leq P_m \\ FSV_i^j + R(0,1) \times step(i), \ p > P_m \end{cases} \tag{1}$$

where,
$step(i) = w \times K(0,1) \times (FSV_i^j - FSV_{loudest}^j)$
$K(0,1)$ is any randomly chosen number between 0 and 1. w is wind constant and p is any random number between 0,1.

$Definition5$: Barking movement $\omega(p, q, \alpha) : MD^n \rightarrow$ MD is a probabilistic operator that adjusts position of a military dog based on FSV^d of loudest barking and any randomly chosen Military Dog. The probability p, that position of MD is modified is constant and $q \in (1, 2, 3..., d)$ is the randomly chosen index. *alpha* is the smog or vegetation constant that effects the sound coming from the other military dog.

The feasible solution vector (FSV^d) modification of a military dog is defined by:

$$FSV_i^j(t+1) = \begin{cases} FSV_i^j(t),\ p \leq \alpha \\ FSV_i^j(t) + B_m \times R(0,1),\ p > \alpha \end{cases} \tag{2}$$

where $B_m = (FSV_{loudest} - FSV_q)$ and $R(0,1)$ is any random number between (0,1).

$Definition 6$: The MDS transition function $\phi = (m, d, \delta, \omega, P_m) : MD^m \rightarrow MD^m$ is a 5-tuple that modifies the MDS from one iteration to the next iteration. The MDS transition function begins by computing the feasible solution vector FSV^d and military dog smell index $MDSI$. Further, the MDS modification is performed on each military dog MD followed by $MDSI$ recalculation for each military dog.

$Definition 7$: A MDBO algorithm $MDBO = (H, \phi, T)$ is a three tuple that finds the solution for an optimization problem. $H :\rightarrow \{MD^n, MDSI^n\}$ is a function that creates an initial MDS and computes the corresponding $MDSI$. ϕ is a MDS transition function defined earlier. H is implemented using the random number generators inside the urine marking area of the military dog. $T : MD^n \rightarrow \{true, false\}$ is a termination criterion.

The MDBO algorithm can be informally described as follows:

1. The MDBO algorithm starts with the initialization of the MDBO parameters. In this step the method is derived for mapping the problem solution to FSV^d and MDS as described in definition 1 and 2, which are problem dependent. Also the maximum number of military dogs, sniff movement probability P_m, smoke or vegetation constant α, wind factor K are initialized according to the nature of the optimization problem.
2. Initialize the position of each military dog in the search space corresponding to the potential solution given in the problem. This is defined by the H operator described in definition 7.
3. Sniffing around current area (exploitation step): In this step, each MD modifies its FSV based on the information got from the loudest barking dog. While searching, the dogs take a random walk and steer around the new location. MD searches around the target object and may either move directly towards the military dog at best position with movement probability P_m or they may take random movements according to its own position and the position of the MD nearest to the target object as described in definition 4.

   The pseducode of the sniffing movement is described as follows

for $(i = 1\ to\ m)$ **do**

IF$(K < P_m)$

$FSV_i^j(t+1) = FSV_{loudest}^j$

$step(i) = w \times K(0,1) \times (FSV_i^j - FSV_{loudest}^j)$;

$FSV_i^j(t+1) = FSV_i^j + R(0,1) \times step(i)$

end for

Table 2: Parameter values of algorithm of proposed and other algorithms

S. No.	Parameter	PSO	PBIL	GA	ES	MVO	MDBO
1.	Population Size (N)	50	50	50	50	50	50
2.	Number of Iterations (itr)	500	500	500	500	500	500
3.	Number of Dimensions (dim)	30	30	30	30	30	30
4.	Elite Size ($keep$)	2	2	2	2	2	2
5.	Inertial Constant (w)	1	0.3	−−	−−	−−	−−
6.	Congnitive Constant (c_1)	1	–	−−	−−	−−	−−
7.	Social Constant (c_2)	1	–	−−	−−	−−	−−
8.	Mutation Probability (P_{mutate})	−−	−−	.1	0.1		
9.	Smog or Vegetation factor (α)	–	–	–	–	–	.25
10.	Wind constant (w)	–	–	–	–	–	.25

4. Movement due to barking of other dogs(exploration step): It is the general nature of the military dogs that they bark loudly where they smell the suspected object. This creates a global movement of the military dogs. After a certain threshold of barking military dogs try to explore the search region with respect to the most loudly barking military dog. Each military dog takes a random move by considering the loudest barking military dog as global best and any randomly chosen barking military dog. The updated position is defined as per definition 5. The psedo-code of the barking movement is described as follows:

for $(i = 1\ to\ m)$ **do**

$K = rand(0,1)$

K=IF$(K < \alpha)$

$B_m = rand * (FSV_{loudest} - FSV_q)$;

$FSV_i^{(i+1)} = FSV_i(t) + B_m \times K$

end for

5. Go to step three for the next iteration. This loop continues till the predefined number of iterations, or the desired solution has been found . This is the implementation of the T operator described in definition 6.

Fig. **??**a and Fig. **??**b demonstrate the barking and sniffing movement of the MDs. It can be depicted from Fig. **??**a that the barking movement represents the exploration step of the MDBO. However, the barking movement corresponds to the exploration step, as its movement is influenced any randomly chosen MD.

4. Fake Review Detection

Nowadays, reviews play an important role in the sales of the products and services, thus ascertaining their authenticity is a challenging problem. For the same, fake review detection is one of the fundamental approach used to detect the fake reviews. In literature, the majority of the contemporary work is based on supervised learning models [31]. However, the supervised models require labeled datasets. Therefore, the applicability of the supervised models is limited, as labeled datasets of fake reviews are rarely available. On the contrary, unsupervised learning models work on unlabeled datasets to induce the learning model. Generally, these models explore hidden structures of the dataset with N data objects into K clusters such that the data objects within a cluster have maximum resemblance [32]. The traditional clustering methods, such as K-means and FCM, generally produce local optima in the presence of noise [33][34] [35] [18]. To alleviate this, the meta-heuristic algorithms have been proved to be efficient in performing clustering [36] [37]. Therefore, this paper leverages the strengths of MDBO to produce optimal cluster centroids for untangling the fake review detection problem.

4.1. MDBO based clustering for fake review detection

In the MDBO based clustering, the FSV of each military dog represents a set of cluster centroids, $C = \{C_1, C_2, \cdots, C_k\}$ for K clusters. The $MDSI$ value of each military dog corresponds to the sum of squired Euclidean distance as defined in Eq. (3).

$$MinD(Z, C) = \sum_{i=1}^{N} \sum_{j=1}^{k} w_{ij} \mid z_i - c_j \mid \tag{3}$$

Table 3: Benchmark Functions

Sr. No.	Function Name	Equation	Range	Optimal value	Optimal position values	Category
1	Ackley	$F_1(X) = -20e^{-0.02\sqrt{d^{-1}\sum_{i=1}^{d} x_i^2}} - e^{d^{-1}\sum_{i=1}^{d} cos(2\pi x_i)} + 20 + e$	-32,+32	0	$(0, \cdots, 0)$	Multi-Model
2	Alpine	$F_2(X) = \sum_{i=1}^{d} \lvert x_i \sin(x_i) + 0.1x_i \rvert$	-100,+100	0	$(0, \cdots, 0)$	Multi-Model
3	Dixon and Price	$F_3(X) = (x_1 - 1)^2 + \sum_{i=2}^{d} i(2x_i^2 - x_{i-1})^2$	-100,+100	0	$(0, \cdots, 0)$	Unimodal
4	Griewank	$F_4(X) = 1 + \sum_{i=1}^{d} \frac{x_i^2}{4000} - \prod_{i=1}^{d} \cos(\frac{x_i}{\sqrt{i}})$	-20,+20	0	$(0, \cdots, 0)$	Multi-model
5	Levy	$F_5(X) = \sin^2(\pi\omega_1) + \sum_{i=1}^{d-1}(\omega_i - 1)^2 \left[1 + 10\sin^2(\pi\omega_i + 1)\right] + (\omega_d - 1)^2 \left[1 + \sin^2(2\pi\omega_d) +\right], \omega_i = 1 + \frac{x_i - 1}{4}, for all i = 1, \cdots, d$	-50,+50	0	$(0, \cdots, 0)$	Multi-Model
6	Pathological	$F_6(X) = \sum_{i=1}^{d-1} \left(0.5 + \frac{\sin^2\sqrt{100x_i^2 + x_{i+1}^2} - 0.5}{1 + 0.001(x_i^2 - 2x_i x_{i+1} + x_{i+1}^2)^2}\right)$	-100,+100	0	$(0, \cdots, 0)$	Multi-model
7	Perm	$F_7(X) = \sum_{i=1}^{d} \left(\sum_{j=1}^{d} (j + \beta)\left(x_i^j - \frac{1}{j_i}\right)\right)^2$	-100,+100	0	$(1, 1/2, \cdots, 1/d)$	Multi-Model
8	Powell	$F_8(X) = \sum_{i=1}^{d/4} [(x_{4i-3} + 10x_{4i-2})^2 + 5(x_{4i-1} - x_{4i})^2 + (x_{4i-3} + 2x_{4i-2})^4 + 10(x_{4i-3} + x_{4i})^4]$	-10,10	0	$(0, \cdots, 0)$	Uni-model
9	PowellSum	$F_9(X) = \sum_{i=1}^{d} \lvert x_i \rvert^{i+1}$	-100,+100	0	$(0, \cdots, 0)$	Uni-Model
10	Rastrigin	$F_{10}(X) = 10d + \sum_{i=1}^{d}(x_i^2 - 10cos(2\pi x_i))$	-5.12,+5.12	0	$(0, \cdots, 0)$	Uni-Model
11	Rosenbrock's	$F_{11}(X) = \sum_{i=1}^{d-1}[100(x_{i+1} - x_i^2)^2 + (x_i - 1)^2]$	-30,+30	0	$(0, \cdots, 0)$	Multi-Model
12	Rotated Hyper-Ellipsoid	$F_{12}(X) = \sum_{i=1}^{d} \sum_{j=1}^{i} x_j^2$	-65.536,+65.536	0	$(0, \cdots, 0)$	Uni-Model
13	Schumer Steiglitz	$F_{13}(X) = \sum_{i=1}^{d} x_i^4$	-100,+100	0	$(0, \cdots, 0)$	Uni-model
14	Schwefel	$F_{14} = -\sum_{i=1}^{d} x_i \sin\sqrt{\lvert x_i \rvert}$	-500,+500	0	$(0, \cdots, 0)$	Multi-Model
15	Sphere	$F_{15}(X) = \sum_{i=1}^{d} x_i^2$	-100,+100	0	$(0, \cdots, 0)$	Uni-Model
16	Step	$F_{16}(X) = \sum_{i=1}^{d}(\lfloor \lvert x_i \rvert \rfloor)$	-100,+100	0	$(0, \cdots, 0)$	Uni-model
17	Trigonometric	$F_{17}(X) = \sum_{i=1}^{d}[d - \sum_{j=1}^{d} \cos x_j + i(1 - cos(x_i) - sin(x_i))]^2$	0,3.14	0	$(0, \cdots, 0)$	Uni-Model

Where N represents the number of data objects, $\mid z_i - c_j \mid$ is the Ecludian distance of I^{th} data object from the J^{th} centroid. Further, w_{ij} represents the association weight of i^{th} review vector in the j^{th} cluster, i.e. the value of w_{ij} is 1 if the data object i is allocated to the cluster j otherwise 0. For, the MDS of size N, the clustering process starts with N candidate solution and these solutions are optimized with the course of iterations to improve $MDSI$. Finally, the FSI of the MD with best $MDSI$ value are returned as the final cluster centroids.

4.2. Datasets

For performing the experiments, the real life dataset is collected from the Yelp [38], which has 142 million unique visitors from 31 countries. Yelp itself filters the reviews which are considered as highly reliable and accurate [39]. In this work, total of 6000 reviews are compiled from the Yelp recommended and non recommended section for genuine and fake reviews. The beautiful soup library of python for web scraping is used for crawling the data. The reviews are extracted pin code wise, starting from zip code 10000 and 10050, which corresponds to the restaurant pages of New York city. The complete block of the review is extracted consisting of review text, star rating by the reviewer to the restaurant, no of cool votes to the particular review, no of funny votes to the particular review, no of useful votes to the particular review, no of check-ins of reviewer in the hotel, no of photos uploaded by reviewer of the review on Yelp, no of friends of reviewer of the review on yelp, no of reviews till date of the reviewer of the review. Furthermore, the content analysis of the reviews has been performed using natural language tool kit (NLTK) to extract review centric features. NLTK provides an easy to use interface with rich set of lexical resources such as WordNet for the tokenization, parsing, semantic reasoning and tagging. Moreover, the feature extracted from the NLTK were also validated manually by randomly picking 30 reviews. Total 11 verbal and non verbal features has been used in the experiments based on the previous studies [40] [31] [39]. Table 4 contains the summary of the features used in the experiments. Each review represent a feature vector of length 11 and the numerical value of each feature is normalized between [0,1].

5. Experimental results

The performance of the proposed algorithm is evaluated in two folds, first the MDBO is validated on benchmark functions and results are are detailed in section 5.1. Second, the the effectiveness of the MDBO is vindicated on fake review detection problem and the results are presented in section

Table 4: Features taken for the clustering using MDBO

Sr. No.	Feature Name	Category	Definition
1	Nonverbal	Review count	It defines the total number of reviews posted by the reviewer.
2	Nonverbal	check-ins:	it represents the number of check-ins by the reviewer for the hotel
3	Nonverbal	Friend count:	It denotes the total number of friends of the person making review
4	Nonverbal	Vote count	it represents the count of votes on the review
5	Nonverbal	useful, cool, funny votes	count of useful, cool and funny votes
6	Nonverbal	Followers	it is the total number of followers of the reviewers
7	Nonverbal	Elite reviewer	it is the count of years for which reviewer has been a permanent yelp member
8	Nonverbal	Average posting rate:	it represents the total number of reviews posted per day
9	verbal	Review length	it is the total number of words per review
10	verbal	Average content similarity	It is defines as the average similarity in the reviews given by a single reviewer
11	Verbal	Average content similarity	It corresponds the average similarity in the text of the reviews posted by a particular reviewer

5.2. For fair comparison, each algorithms is rum on a computer with 2.8 Ghz Intel (R) Pentiam (R) core i3 processor and 8 GB RAM using Matlab 2015a.

5.1. Benchmark Function Results

In this section, the performance and uniqueness of the proposed MDBO is analyzed and compared with five recent population based algorithms. Seventeen standard benchmark functions given in Table 3 are used for comparison of algorithm based on mean and standard deviation. Convergence behavior of MDBO is analyzed and compared with other algorithms by plotting the convergence graph for each benchmark function. Box plots are employed to visualize and establish the consistency of the proposed MDBO algorithm. Box plots are non parametric methods to display variations in results of proposed MDBO algorithm, which are further compared with five other algorithms on seventeen benchmark functions. Moreover, Wilcoxon rank sum test is performed, which shows the dissimilarity of MDBO with other algorithms.

5.1.1. Comparison with existing algorithms

The proposed MDBO was tested on the minimization functions and the results were compared with five other algorithms namely MVO, ES, Pbil, GA as well as PSO. Table 2 contains the values of population size, number of dimensions, number of iterations, social constant, cognitive constant, mutation probability, wind factor and smog constant used in simulation. Table 3 contains the details of the seventeen benchmark functions including range values, optimal position values and categories upon which the proposed algorithm has been tested and compared. Each function either belongs to uni-model or multi-model class. Nine uni-model functions are used to test the convergence rate and eight multi-model functions are used to test the local optima avoidance capability of the algorithm. Further, each algorithm was run fifteen times on each benchmark function to get the mean and standard deviation. Table 5 shows the values of mean and the standard deviation of fitness values computed in fifteen rounds by each algorithm. From the comparison of mean and standard deviation of seventeen benchmark functions for six algorithms as given in Table 5, it is observed that proposed MDBO outperformed all five algorithms under comparison on sixteen benchmark functions in terms of mean fitness values. However, ES performed better than MDBO for only one benchmark functions i.e F6 with mean value 4.48 as compared to 4.68 mean value of proposed MDBO. Further, standard deviation of the proposed MDBO is minimum for sixteen benchmark functions while ES has given minimum value of the standard deviation for one function

i.e., F1. It can be observed that in all the nine uni-model functions proposed MDBO algorithm has beat all other algorithms showing stronger local search ability. However, proposed algorithm outperformed other algorithms in seven multi-model functions out of eight which confirms stronger exploration capability of the proposed algorithm.

5.1.2. Wilcoxon Test

The uniqueness of the proposed algorithms have been statistically validated using Wilcoxon rank sum test. NULL hypothesis assumes that the two algorithms are similar at the five percent significance level α for benchmark functions. p values has been computed for all the benchmark functions using the fitness values of compared and proposed algorithms. If the value of $p<0.05$ then null hypothesis is rejected and symbolized by '+' or '-', otherwise it is rejected and represented by symbol '='. However '+' indicates better result and '-' represents poor results of the proposed MDBO algorithm. Table 6 shows the results of Wilcoxon rank sum test for the NULL hypothesis over seventeen benchmark functions explained Table 3. The proposed MDBO algorithm is compared with ES, PSO, MVO, Pbil, and GA on the basis of p values value. The p value is computed by running fifteen iterations of each algorithm on all functions. A pair wise comparison of MDBO with other algorithms shows significant levels on the basis of p value, mean and standard deviation. Significant level is positive if p value is less than 0.05 and the value of mean and standard deviation are less than the compared algorithm. It is observed from the Table 6, that MDBO has outperformed ES on all the benchmark functions except F6 where ES has given competitive result. Further, MDBO has surpassed PSO for all the benchmark functions. When MDBO is compared with MVO it has beaten on sixteen benchmark function out of seventeen. However for one function i.e., F6, GA performed well. Moreover, MDBO has given positive significance on all the benchmark functions when compared with PBIL and GA except for F6 function. Hence is can be concluded that the proposed algorithm is significantly different and outperforms five existing algorithms i.e., MVO, ES, PBIL, GA as well as PSO on each benchmark function.

5.1.3. Convergence rate

The convergence behavior of the proposed MDBO algorithm is analyzed and compared with other five existing algorithms by plotting the convergence graph for each bench-mark function. Vertical axis of the graph represents the best of fitness value and the horizontal axis represents corresponding iteration number as depicted in Fig. ??. Further, Fig. ??a, ??b...??q, shows

Table 5: Comparison of mean fitness and standard deviation values for 15 runs on benchmark functions for existing and proposed algorithms

Fun	PBIL		PSO		GA		MVO		ES		MDBO	
	Mean	STD	Mean	STD	Mean	STD	Mean	STD	Mean	STD	Mean	STD
F_1	4.51E+00	0.19E+00	3.55E+00	0.30E+00	2.18E+00	4.32E-01	1.63E+00	4.50E-01	6.31E+00	**1.88E-01**	**9.71E-01**	7.39E-01
F_2	4.89E+02	3.54E+01	1.02E+00	5.01E+00	5.29E+01	1.15E+01	1.27E+02	3.42E+01	4.91E+02	3.67E+01	**2.34E+00**	**1.91E+00**
F_3	8.56E+09	1.84E+09	3.06E+08	3.03E+08	1.05E+06	1.06E+06	5.71E+03	5.32E+03	8.26E+09	2.54E+09	**1.90E+02**	**7.28E+02**
F_4	1.46E+00	0.06E+00	1.11E+00	0.04E+00	1.07E+00	2.57E-02	1.50E-02	1.25E-02	1.54E+00	4.98E-02	**2.79E-03**	**4.26E-03**
F_5	3.69E+03	5.89E+02	5.21E+02	2.13E+02	5.32E+01	1.86E+01	4.83E+02	3.14E+02	3.70E+03	3.60E+02	**2.22E+01**	**2.35E+01**
F_6	9.37E+00	0.66E+00	7.80E+00	0.52E+00	5.65E+00	4.94E-01	9.93E+00	3.62E-01	**4.48E+00**	**3.19E-01**	4.68E+00	8.03E-01
F_7	2.00E+117	3.60E+117	3.30E+98	1.20E+99	5.59E+58	2.15E+59	1.05E+17	4.05E+17	4.50E+117	6.50E+117	**1.00E+10**	**0.00E+00**
F_8	4.62E+04	93.54E+02	1.82E+04	7.40E+03	1.86E+02	1.22E+02	7.78E+00	5.49E+00	1.24E+05	2.91E+04	**9.65E-03**	**7.42E-03**
F_9	4.46E+41	4.99E+41	1.32E+54	4.80E+54	3.33E+16	1.20E+17	2.96E+11	4.10E+11	8.41E+43	1.70E+44	**1.00E+10**	**0.00E+00**
F_{10}	1.54E+02	1.17E+01	1.43E+00	3.94E+01	1.40E+01	6.49E+00	1.23E+02	3.56E+01	4.14E+02	1.96E+01	**2.07E+01**	**5.61E+00**
F_{11}	1.39E+08	3.50E+07	3.67E+06	3.10E+06	9.47E+03	1.03E+04	4.58E+02	5.30E+02	1.50E+08	2.87E+07	**1.02E+02**	**4.02E+01**
F_{12}	2.46E+01	1.99E+04	9.56E+04	7.77E+04	4.88E+03	2.50E+03	1.83E+01	1.31E+01	2.79E+05	2.70E+04	**8.89E-12**	**5.32E-12**
F_{13}	1.87E+08	3.56E+08	7.40E+06	6.77E+06	4.25E+04	3.49E+04	1.01E-01	5.52E-02	1.55E+08	4.13E+07	**3.55E-16**	**5.74E-16**
F_{14}	8.65E+00	3.32E+02	6.57E+03	1.07E+03	3.22E+03	6.44E+02	4.53E+03	7.70E+02	8.41E+03	3.79E+02	**5.48E+02**	**2.20E+02**
F_{15}	4.52E+00	4.14E+03	1.02E+04	2.70E+03	1.05E+03	4.98E+02	6.76E-01	1.91E-01	4.62E+04	4.21E+03	**2.07E-12**	**1.58E-12**
F_{16}	9.32E+02	6.70E+00	4.82E+02	7.82E+01	1.82E+02	5.65E+01	5.60E+00	4.73E+00	9.12E+02	5.87E+01	**2.67E-01**	**7.04E-01**
F_{17}	0.89E+00	2.36E+00	7.67E+03	6.86E+00	5.05E+00	1.96E+01	1.85E+00	9.18E-01	7.68E+03	2.36E+03	**2.74E-01**	**5.10E-01**

Table 6: wilcoxon test for statistically significance level at $\alpha = 0.05$ on benchmark functions

Function	MDBO-ES		MDBO-PSO		MDBO-MVO		MDBO-PBIL		MDBO-GA	
	p-value	SGFNT	p-value	SGFNT	p-value	SGFNT	p-value	SGFNT	p-value	SGFNT
F_1	3.27E-06	+	3.27E-06	+	3.27E-06	+	3.27E-06	+	3.27E-06	+
F_2	9.07E-06	+	3.39E-06	+	9.07E-06	+	9.07E-06	+	9.07E-06	+
F_3	3.39E-06	+	3.39E-06	+	3.39E-06	+	3.39E-06	+	3.39E-06	+
F_4	3.31E-06	+	3.31E-06	+	3.31E-06	+	3.31E-06	+	3.31E-06	+
F_5	3.39E-06	+	3.39E-06	+	3.39E-06	+	3.39E-06	+	3.39E-06	+
F_6	0.167962	=	3.39E-06	+	0.167962	=	0.167962	=	0.167962	=
F_7	6.87E-07	+	6.87E-07	+	6.87E-07	+	6.87E-07	+	6.87E-07	+
F_8	3.39E-06	+	3.39E-06	+	3.39E-06	+	3.39E-06	+	3.39E-06	+
F_9	6.87E-07	+	6.87E-07	+	6.87E-07	+	6.87E-07	+	6.87E-07	+
F_{10}	3.39E-06	+	3.39E-06	+	3.39E-06	+	3.39E-06	+	3.39E-06	+
F_{11}	3.39E-06	+	3.39E-06	+	3.39E-06	+	3.39E-06	+	3.39E-06	+
F_{12}	3.39E-06	+	3.39E-06	+	3.39E-06	+	3.39E-06	+	3.39E-06	+
F_{13}	3.39E-06	+	3.39E-06	+	3.39E-06	+	3.39E-06	+	3.39E-06	+
F_{14}	3.38E-06	+	3.38E-06	+	3.38E-06	+	3.38E-06	+	3.38E-06	+
F_{15}	3.39E-06	+	3.39E-06	+	3.39E-06	+	3.39E-06	+	3.39E-06	+
F_{16}	1.26E-06	+	1.26E-06	+	1.26E-06	+	1.26E-06	+	1.26E-06	+
F_{17}	1.90E-06	+	1.90E-06	+	1.90E-06	+	1.90E-06	+	1.90E-06	+

convergence trends of six algorithms under study for benchmark functions F1 to F17 respectively. It can be visualized from the figures that the proposed MDBO is converging with a faster rate for fourteen benchmark functions out of seventeen benchmark functions as compared to MVO, ES, GA, PBIL and PSO. However for function F11, PSO and GA has outperformed MDBO and for function F13, F17 GA and ES are showing faster convergence rate respectively. It can also be concluded that the proposed algorithm is beating eighty eight percent of the uni-model functions and seventy eight percent of the multi-model functions. The results shows that the proposed algorithm not only gives better fitness value but also shows good convergence rate for both the unimodal and multi-modal functions.

5.1.4. Box plots

Box plots are used to show the consistency in the final result values found for each compared and proposed algorithm over fifteen runs. Fig. **??** depicts groups of final best solution values through their quartiles. Further extending vertical lines from the boxes indicates variability outside the upper and lower quartiles of final best solution for all algorithms under comparison. Fig. **??** contains seventeen sub-figures a, b, c...q for seventeen benchmark functions F1, F2...F17 respectively as given in Table 3. Fig. **??**d, **??**e, **??**j and **??**p shows minimum spacing between the different parts of boxes as compared to ES, PSO, MVO, PBIL and GA that indicates the degree of dispersion and skewness in the final best solution. And hence the proposed MDBO has outperformed ES, PSO, MVO, PBIL and GA algorithms for functions F4, F5, F10 and F16. The proposed MDBO has beat ES, PSO and PBIL and tie with MVO and GA as observed from Fig. **??**c, **??**h, **??**k, **??**m. Fig. **??**i shows a tie for all algorithms under study. Further **??**g and **??**n depicts that MDBO beat ES and PBIL and tie with PSO, MVO and GA. Fig. **??**b depicts that MDBO beat ES, PSO, PBIL and GA and tie MVO. Fig. **??**q depicts MDBO beat ES, PSO and tie with MVO, PBIL and GA. The proposed MDBO is defeated by all algorithms under study as depicted in Fig. **??**a and **??**f. Further MDBO beat PSO, MVO, PBIL and GA except ES as shown in Fig. **??**e.

5.2. Fake Review Detection Results

This section, details the performance of the MDBO for fake review detection problem. The dataset used for evaluating the performance is explained in section 4.2. The proposed algorithm has been validated by comparing the results with K-means and 4 other meta-heuristic based algorithms proposed for the clustering. Table 7 presents the mean and best accuracy of the proposed and

Table 7: Best and average accuracy over 15 runs

Dataset Name	Criteria	K-Means	PSO	GSA	GA	GWO	MDBO
Yelp review	Best	50.24	54.32	57.60	53.46	62.32	**71.42**
	Mean	50.72	58.46	54.68	59.50	63.92	**71.52**

considered algorithms obtained by executing each algorithm 15 times in the same environment. It can be depicted from the table 7, that the proposed method has outperformed the K-means and other considered meta-heuristic based clustering methods for the fake review detection. Thus, it can be concluded that the proposed method can serve as a powerful tool for solving the fake review detection problem.

6. Conclusion

In last three decades more than sixty meta-heuristic algorithms have been proposed by the various authors. Some of them are inspired by physics based phenomena of nature like GSA, CFO and Black hole optimization and some are inspired by the swarm behavior and evolution of species. This paper proposed a new optimization algorithm called Military Dog Based Optimization (MDBO). MDBO utilizes the searching capability of the suspected objects by the trained military dogs. MDBO uses the tendency of military dogs to communicate with each other and move towards the suspected object by their smell power. Every Military Dog follow his companion which have the best fitness value. The overall contribution of the paper has been divided into four folds, (i) a novel algorithm has been proposed (ii) The proposed algorithm has been validated on 17 benchmark functions and compared with 5 other existing meta-heuristics(iii) The proposed algorithm is successfully utilized for the fake review detection problem. The proposed MDBO outperforms the other algorithms in terms of mean fitness, standard deviations and convergence behavior. The consistency in the results of the MDBO has been statistically validated using the Box-plots curves. The quality of the results and the uniqueness of the MDBO has been also verified by the Wilcoxon rank sum test. Further, the proposed algorithm has also surpassed the compared algorithm in detecting the fake reviews. Thus, it can be concluded that the proposed algorithm can be applied for the optimization problem and can also serve as an alternative tool for handling real word prob-

lems. The future work will include the applications of the proposed algorithm in various real world large datasets optimization problems. Moreover, it can also be tested for the big data problems by adopting it in parallel environment.

References

[1] D. E. Goldberg, J. H. Holland, Genetic algorithms and machine learning, Machine learning 3 (1988) 95–99.

[2] J. Kennedy, Particle swarm optimization, in: Encyclopedia of machine learning, Springer, 2011.

[3] E. Rashedi, H. Nezamabadi-Pour, S. Saryazdi, Gsa: a gravitational search algorithm, Information sciences 179 (2009) 2232–2248.

[4] R. A. Formato, Central force optimization: a new metaheuristic with applications in applied electromagnetics, Progress In Electromagnetics Research 77 (2007) 425–491.

[5] A. Kaveh, Advances in metaheuristic algorithms for optimal design of structures, Springer, 2014.

[6] A. Kaveh, M. Khayatazad, Ray optimization for size and shape optimization of truss structures, Computers & Structures 117 (2013) 82–94.

[7] R. Rajabioun, Cuckoo optimization algorithm, Applied soft computing 11 (2011) 5508–5518.

[8] X.-S. Yang, Firefly algorithm, levy flights and global optimization, in: Research and development in intelligent systems XXVI, Springer, 2010.

[9] D. H. Wolpert, W. G. Macready, No free lunch theorems for optimization, IEEE transactions on evolutionary computation 1 (1997) 67–82.

[10] Detection dog - wikipedia, the free encyclopedia, `https://en.wikipedia.org/wiki/Detection_dog`.

[11] Understanding a dog's senses, `http://www.dogbreedinfo.com/articles/dogsenses.htm`.

[12] M. Mitchell, J. H. Holland, When will a genetic algorithm outperform hill-climbing?

[13] S. Bandyopadhyay, S. Saha, U. Maulik, K. Deb, A simulated annealing-based multiobjective optimization algorithm: Amosa, IEEE transactions on evolutionary computation 12 (2008) 269–283.

[14] H. Shah-Hosseini, The intelligent water drops algorithm: a nature-inspired swarm-based optimization algorithm, International Journal of Bio-Inspired Computation 1 (2009) 71–79.

[15] Ş. İ. Birbil, S.-C. Fang, An electromagnetism-like mechanism for global optimization, Journal of global optimization 25 (2003) 263–282.

[16] S. Mirjalili, S. M. Mirjalili, A. Hatamlou, Multi-verse optimizer: a nature-inspired algorithm for global optimization, Neural Computing and Applications 27 (2) (2016) 495–513.

[17] H. Shah-Hosseini, Principal components analysis by the galaxy-based search algorithm: a novel metaheuristic for continuous optimisation, International Journal of Computational Science and Engineering 6 (1-2) (2011) 132–140.

[18] A. Hatamlou, Black hole: A new heuristic optimization approach for data clustering, Information sciences 222 (2013) 175–184.

[19] H. Du, X. Wu, J. Zhuang, Small-world optimization algorithm for function optimization, in: International Conference on Natural Computation, Springer, 2006, pp. 264–273.

[20] A. Kaveh, M. Khayatazad, A new meta-heuristic method: ray optimization, Computers & structures 112 (2012) 283–294.

[21] F. F. Moghaddam, R. F. Moghaddam, M. Cheriet, Curved space optimization: a random search based on general relativity theory, arXiv preprint arXiv:1208.2214.

[22] J. Kennedy, R. Eberhart, Particle swarm optimization, in: IEEE Internation Conference on Neural Networks, 1995.

[23] A. H. Gandomi, A. H. Alavi, Krill herd: a new bio-inspired optimization algorithm, Communications in Nonlinear Science and Numerical Simulation 17 (2012) 4831–4845.

[24] S. Mirjalili, The ant lion optimizer, Advances in Engineering Software 83 (2015) 80–98.

[25] S. Mirjalili, Moth-flame optimization algorithm: A novel nature-inspired heuristic paradigm, Knowledge-Based Systems 89 (2015) 228–249.

[26] G.-G. Wang, A. H. Gandomi, A. H. Alavi, G.-S. Hao, Hybrid krill herd algorithm with differential evolution for global numerical optimization, Neural Computing and Applications 25 (2) (2014) 297–308.

[27] M. Dorigo, M. Birattari, Ant colony optimization, in: Encyclopedia of machine learning, Springer, 2011, pp. 36–39.

[28] D. Karaboga, B. Basturk, A powerful and efficient algorithm for numerical function optimization: artificial bee colony (abc) algorithm, Journal of global optimization 39 (3) (2007) 459–471.

[29] D. Dasgupta, Z. Michalewicz, Evolutionary algorithms in engineering applications, Springer Science & Business Media, 2013.

[30] R. Storn, K. Price, Differential evolution–a simple and efficient heuristic for global optimization over continuous spaces, Journal of global optimization 11 (4) (1997) 341–359.

[31] M. Crawford, T. M. Khoshgoftaar, J. D. Prusa, A. N. Richter, H. Al Najada, Survey of review spam detection using machine learning techniques, Journal of Big Data 2 (1) (2015) 23.

[32] A. Kulhari, A. Pandey, R. Pal, H. Mittal, Unsupervised data classification using modified cuckoo search method, in: Contemporary Computing (IC3), 2016 Ninth International Conference on, IEEE, 2016, pp. 1–5.

[33] A. C. Pandey, R. Pal, A. Kulhari, Unsupervised data classification using improved biogeography based optimization, International Journal of System Assurance Engineering and Management 1–9.

[34] K. Sharma, R. Garg, C. Nagpal, R. Garg, Selection of optimal software reliability growth models using a distance based approach, IEEE Transactions on Reliability 59 (2) (2010) 266–276.

[35] A. K. Tripathi, K. Sharma, M. Bala, Dynamic frequency based parallel k-bat algorithm for massive data clustering (dfbpkba), International Journal of System Assurance Engineering and Management 1–9.

[36] A. C. Pandey, D. S. Rajpoot, M. Saraswat, Twitter sentiment analysis using hybrid cuckoo search method, Information Processing & Management 53 (4) (2017) 764–779.

[37] T. Ashish, S. Kapil, B. Manju, Parallel bat algorithm-based clustering using mapreduce, in: Networking Communication and Data Knowledge Engineering, Springer, 2018, pp. 73–82.

[38] Restaurants- yelp, `https://www.yelp.com/`, (Accessed on 06/17/2018).

[39] D. Zhang, L. Zhou, J. L. Kehoe, I. Y. Kilic, What online reviewer behaviors really matter? effects of verbal and nonverbal behaviors on detection of fake online reviews, Journal of Management Information Systems 33 (2) (2016) 456–481.

[40] J. K. Rout, S. Singh, S. K. Jena, S. Bakshi, Deceptive review detection using labeled and unlabeled data, Multimedia Tools and Applications 76 (3) (2017) 3187–3211.

REVIEW

Global Challenges

Conducting Paper

www.global-challenges.com

Nanomaterial-Modified Conducting Paper: Fabrication, Properties, and Emerging Biomedical Applications

Saurabh Kumar, Chandra Mouli Pandey, Amir Hatamie, Abdolreza Simchi, Magnus Willander, and Bansi D. Malhotra**

The emerging demand for wearable, lightweight portable devices has led to the development of new materials for flexible electronics using non-rigid substrates. In this context, nanomaterial-modified conducting paper (CP) represents a new concept that utilizes paper as a functional part in various devices. Paper has drawn significant interest among the research community because it is ubiquitous, cheap, and environmentally friendly. This review provides information on the basic characteristics of paper and its functionalization with nanomaterials, methodology for device fabrication, and their various applications. It also highlights some of the exciting applications of CP in point-of-care diagnostics for biomedical applications. Furthermore, recent challenges and opportunities in paper-based devices are summarized.

1. Introduction

Point-of-care (POC) devices are being widely explored for many clinical and analytical applications. POC devices are useful for speedy decision on additional testing or therapy as compared to conventional laboratory assay methods. Since the testing can be performed at resourceless area and/or near the patient, therefore POC has attracted much attention for health monitoring.[1] Currently, the majority of the POC devices are based on glass, ceramics, or semi-conducting substrates that are neither flexible nor biocompatible and are thus not helpful for the fabrication of advanced POC devices. Recently, research is being focused on the development of flexible sensors that have applications in healthcare. These POC devices are likely to be cost-effective, portable, flexible, and user-friendly with distinct advantages of safe disposal and biosafety management.[1c,2] Moreover, these devices can be interfaced with curved surfaces, complex geometries, soft and non-planar body surfaces.

Flexible devices are an interesting alternative to the bulky health-monitoring devices due to their inexpensiveness, excellent flexibility, and lower manufacturing cost. In recent years, many review articles have discussed the characteristics of the flexible devices such as functional textiles, wearable devices,[3] electronic skins,[4] flexible bio-devices and optoelectronics.[5] In the field of biosensors, many handy and wearable non-flexible biosensors have been reported, that are used for the measurement of biophysical parameters (heart rate, blood pressure, temperature, pH), and air quality.[6] Research has also been focused on the use of flexible devices for biosensor applications wherein the biological elements are used for the sensing of biological and chemical entities. In this context, CP can play an interesting role in the ongoing development toward the development of flexible, lightweight, portable, cost-effective, and disposable POC devices. There is also a possibility to enhance the properties of CP-based devices by modifying it with functional nanostructured materials that are known to exhibit unique physiochemical properties.[7] Nanomaterial modified CP can be utilized to improve the conduction of charges (electronic and ionic) within the 3D ordered structure of cellulose paper.[8] Several inorganic and organic nanomaterials have been reported for the fabrication of various CP-based devices.[9]

The performance of paper-based device depends on the various properties such as surface roughness, mechanical strength, ink absorbance, and composition.[10] Paper has a high surface-to-volume ratio that allows storage of increased amount of reagents. Their mesoporous structures provide faster transport of electrolytes and can be used to the ion diffusion in energy storage devices. Thus, paper with strong adsorption of desired electrolyte, favorable porous structure, and good

Dr. S. Kumar
Centre for Nano Science and Engineering (CeNSE)
Indian Institute of Science
Bengaluru 560012, India
E-mail: saurabh2203@iisc.ac.in

Dr. S. Kumar, Dr. C. M. Pandey, Prof. B. D. Malhotra
Department of Biotechnology
Delhi Technological University
Main Bawana Road, Delhi 110042, India
E-mail: bansi.malhotra@dce.ac.in

Dr. C. M. Pandey
Department of Applied Chemistry
Delhi Technological University
Main Bawana Road, Delhi 110042, India

Dr. A. Hatamie, Prof. M. Willander
Department of Science & Technology
Campus Norrkoping
Linkoping University
SE 60174 Norrkoping, Sweden

Dr. A. Hatamie, Prof. A. Simchi
Nanostructured & Advanced Materials Lab
Department of Materials Science and Engineering
Sharif University of Technology
Tehran 1458889694, Iran

The ORCID identification number(s) for the author(s) of this article can be found under https://doi.org/10.1002/gch2.201900041.

© 2019 The Authors. Published by WILEY-VCH Verlag GmbH & Co. KGaA, Weinheim. This is an open access article under the terms of the Creative Commons Attribution License, which permits use, distribution and reproduction in any medium, provided the original work is properly cited.

DOI: 10.1002/gch2.201900041

stability in electrochemical and mechanical performance are preferred for the various energy storage applications. However, for electronics application high surface roughness is a negative factor that adds to increased printing difficulty and can affect the electrical conductivity. A smooth surface and less/non-absorbent paper like photo-paper, parchment, and wax paper have been found suitable for electronics application. Such surfaces are made by an additional coating of pigment (containing sodium polyacrylate, carboxymethyl cellulose, and starch), treatment of paper pulp, and wax coating, respectively, followed by calendaring.[11] These steps make paper surface smooth and reduce the pore size. The strong absorbance, surface functionalization, biocompatiblity, and white background are some of the deciding factors for the various biomedical applications. In scaffolds and cell culturing experiment, biocompatibility is a major concern. However for measurement of physiological signal (ECG, pulse rate, etc.), strong and uniform attachment of interesting materials are important factors because they provide high surface area and low electrical impedance.[12] For biosensor application, it is recommended that paper should have properties to transport fluid flow, high surface to volume ratio, efficient conductivity, and mechanical strength during electrochemical measurements. The most commonly used paper is filter/chromatography paper #1 that consists of 98% of α-cellulose, uniformity on both sides, medium flow rate, and 0.18 mm thick.[10a] Further surface modification/treatment helps to attach desired biomolecules covalently on paper surface for enhanced biosensor performance. However, the aforementioned properties are dependent on a variety of environmental factors such as humidity, temperature, composition, etc. Therefore, a careful consideration is required prior to the selection of a suitable substrate. The paper has been mostly explored in microfludic-based devices for fluid handling and analysis. In these devices, it is important to direct the fluid flow within the confined channel. Various hydrophobic materials such as wax, photoresist, paraffin, etc., have been used to make a hydrophobic barrier. Later it was integrated with various detection methods to obtain analytical information. Microfludic-based paper devices are a separate study and various review articles are available in literature.[13]

This review explores the recent developments in nanomaterials modified CP for POC diagnostics. The significant characteristics and problems in the design and modification of flexible devices are discussed to highlight the features that affect the performance of CP-based devices. Besides this, overview of different types of materials and fabrication techniques used for the development of CP are presented. Efforts will also be made to summarize some of the other applications of conducting paper including energy storage, printable electronics.

1.1. Conducting Paper (CP)

Paper is a flexible, lightweight, low cost, recyclable, and biodegradable material. The cellulose fibers present in a paper have diameter of 10–50 μm and length up to a few millimeters (2–5 mm). The intra-intermolecular hydrogen bond leads to the formation of the microfibrillar structure that provides excellent mechanical properties to cellulose fibers. Cell walls of cellulose fibers consist of smaller fibrils. These smaller fibrils comprise of microfibril, hemicellulose, and lignin.[10c,11,14] The microfibrils are crystalline in nature and are mostly composed of cellulose ($(C_6H_{10}O_5)_n$) and cellulose molecules that consist of a linear chain of D-glucose units that are linked together by $\beta(1\rightarrow4)$ glycosidic bond. However, lignin (a hydrophobic and more crossed linked polymer) and hemicelluloses (a hydrophilic polymer of shorter chain of different sugar molecules) are amorphous in nature and provide rigidity, brittleness, and yellow color over time. The proportion of lignin, hemicellulose, and cellulose vary across different types of paper.

Paper was initially used for packaging, displaying, and storing information. However, in due course of time, mankind has discovered applications in filtration (Whatman paper), transformer (as a dielectric material), and has been used as an actuator. Recently filter paper has been utilized as a substrate for the development of low-cost, flexible sensor[11] since it is known to have sufficient roughness, poor chemical and

Saurabh Kumar received his Ph.D. in Biotechnology from Delhi Technological University in 2017 and then worked as a postdoctoral fellow in a functional nanomaterials and devices lab in the material science and engineering division of King Abdullah University of Science and Technology (KAUST) until July 2018. He is currently working as a DST INSPIRE faculty member at the Centre for Nanoscience and Engineering (CeNSE), Indian Institute of Science, Bangalore, India. His research interests include flexible nano-bioelectronics, printed/stretchable/transparent sensors, wearable medical devices, microfluidics, biosensors, nanomaterials, and cancer detection.

Bansi D. Malhotra received his Ph.D. from the University of Delhi in 1980. He is a fellow of the Indian National Science Academy; the National Academy of Sciences, India; and an academician of Asia Pacific Academy of Materials. His current research activities include nanobiomaterials, biosensors, biofuel cells, ordered molecular assemblies, conducting polymers, Langmuir–Blodgett Films, self-assembled monolayers, nano-biotechnology, biomedical engineering, and biomolecular electronics. He is currently a Science & Engineering Research Board (SERB), Govt. of India, Distinguished Fellow at the Department of Biotechnology, Delhi Technological University, Delhi, India.

© 2019 The Authors. Published by WILEY-VCH Verlag GmbH & Co. KGaA, Weinheim

mechanical barrier that enable it to absorb conducting materials into its porous structure. Moreover, the paper substrate can be chemically modified to incorporate a wide variety of favorable functional groups that can modulate the bulk and surface properties of paper.[2,15]

Since ancient times paper has been used for a number of analytical applications. The traditional paper tests are based on visual observation that mostly gives qualitative or semi-quantitative results. The change in color of paper is an indication of positive or negative result.[2,16] The first commercial paper test for blood glucose detection called Dextrostix was developed by Ames Private Ltd. followed by the launch of pregnancy test kit by Unipath.[2,17] A US patent was filed on laminated assay device for detection of cholesterol by modifying paper substrate with hydrophobic printing.[18] Recently, paper has been reintroduced as a promising substrate for fabrication of flexible, disposable, lightweight, cost-effective devices. Thanks to the advancement in technique and unusual properties of nanomaterial that may made it possible.[19]

Researchers have recently conceptualized a new dimension of paper-based electronics that can reduce the cost of device fabrication. Apart from this, its flexibility, light weight, and ease of availability and disposability may fulfill the increasing demand for smart electronic devices. CP has been found to be a promising substrate for transport of electronic as well as ionic charge carriers. CP has received enormous attention for various technological applications, i.e., energy storage (capacitors and batteries), electronics (displays, thin film transistors, and touch pads) to biomedical devices (ELISA, cell culture, and biosensors).[11,20]

1.2. Conducting Materials and Fabrication Methods

Many materials including both organic and inorganic have been used to fabricate CP. The inorganic materials (metal, metal oxide, etc.) provide better electrical signal but are costly, and difficult to process. Besides this, cracks may result in these films during bending/sintering. On the other hand organic materials (conducting polymer, carbon nanomaterials, etc.) provide excellent flexibility, low cost, and solution processability but suffer from poor conductivity and/or long-term stability. To overcome these limitations, a compromise can perhaps be made by using a composite material. Siegel et al. used a variety of metals (Al, Zn, Cu, Pb, Ni, Sb, Sn, Ti, Ag, Bi, In, Au, and Pt) to produce electrical conductive pathways on paper and studied its electrical conductivity, mechanical properties, melting point, and cost, etc.[21] Besides this, organic materials can be utilized to make paper conducting.[22] A variety of techniques (depending on the material behavior) have been used to deposit conducting materials over the paper. These include dip coating, printing, sputtering, spin-coating, etc. (**Figure 1**). Most of these processes require conducting materials or their templates.

Dip coating technique has often been employed to fabricate a CP using conducting ink or sol–gel precursors. In this method, the substrate is immersed and withdrawn

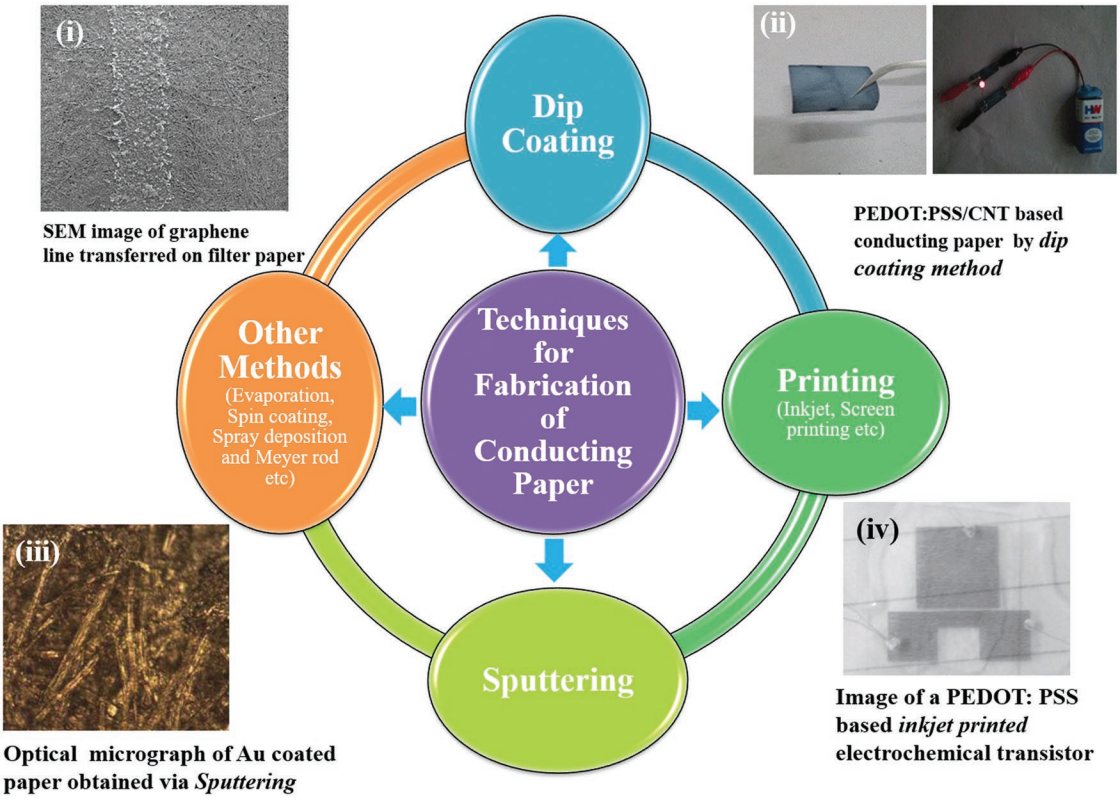

Figure 1. Fabrication of CP via different technique. Reproduced with permission.[23] a) Copyright 2016, AIP Publishing. b) Copyright 2017, IOP Publishing. c) Copyright 2013, Wiley-VCH. d) Copyright 2015, RSC Publishing.

© 2019 The Authors. Published by WILEY-VCH Verlag GmbH & Co. KGaA, Weinheim

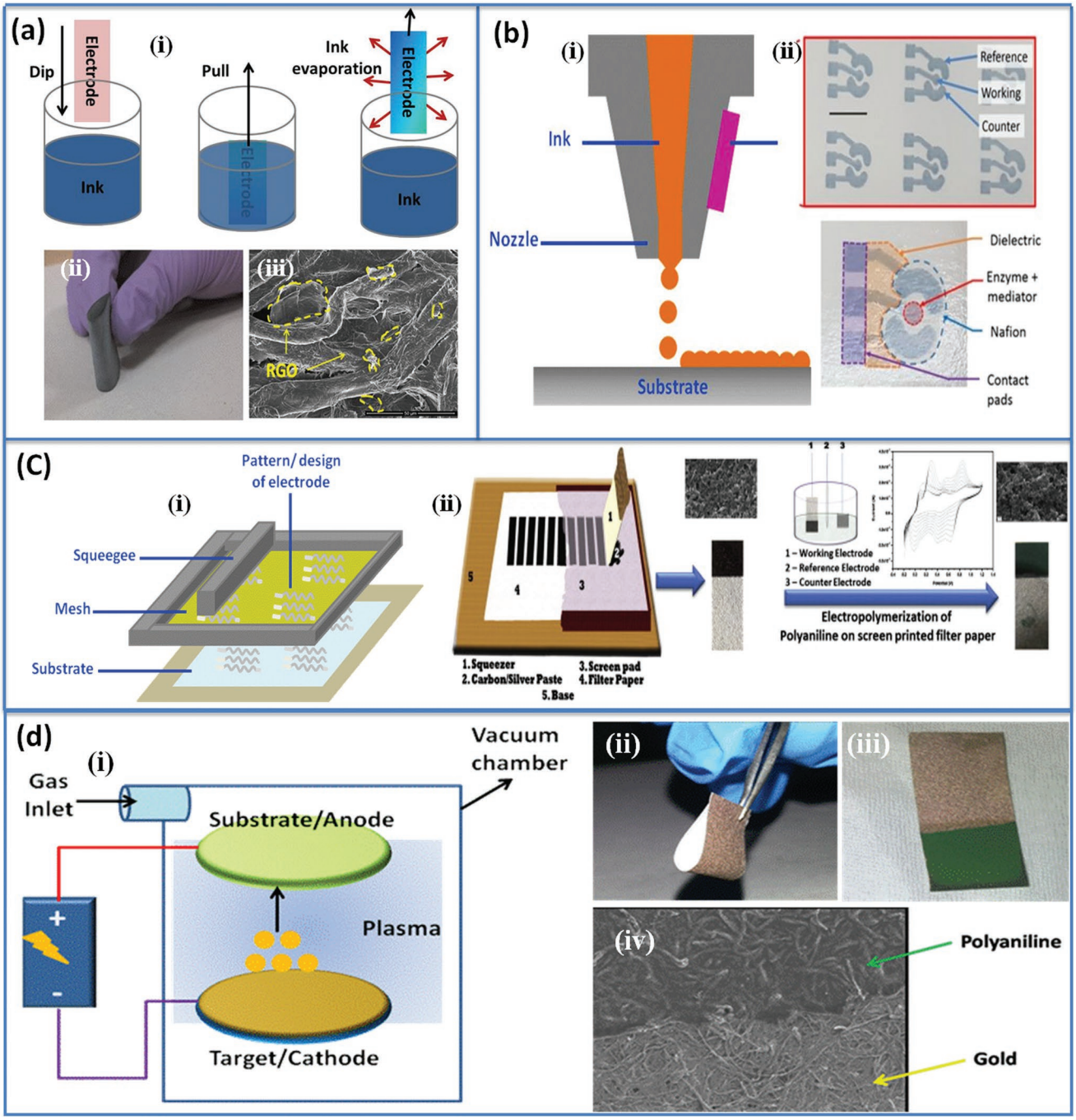

Figure 2. a) i) Schematic of dip-coating method. ii) An image of PEDOT:PSS and RGO-modified paper. This CP was fabricated by dip-coating. iii) SEM of PEDOT:PSS/RGO-coated filter paper. Reproduced with permission.[27] Copyright 2015, Elsevier. b) i) Schematic of inkjet printing method. ii) Image of a fully-inkjet-printed glucose sensor on paper. The device has been fabricated by printing of PEDOT:PSS, dielectric layer and biological components. Reproduced with permission.[24] Copyright 2018, Springer Nature. c) i) Schematic representation of screen-printing method. ii) A screen-printed CP electrode was fabricated using graphite and silver ink. Further, polyaniline was deposited on CP strips via electrochemical method to enhance electrochemical properties and anchoring of biomolecules. Reproduced with permission.[25] Copyright 2012, Elsevier. d) i) Schematic of sputtering technique. Target materials were deposited (from the cathode) on the substrate placed over the anode in a vacuum chamber filled with usually inert gases. The thickness of the deposited layer could be controlled by the duration and intensity of discharge. ii) Image of gold-sputtered filter paper. iii) Next, polyaniline was electrochemically deposited on gold-coated paper to prevent cracks in the film during bending. iv) SEM image of polyaniline-modified CP. Reproduced with permission.[26] Copyright 2016, AIP Publishing.

into a reservoir of liquid with precise control (**Figure 2**a). The thickness and reproduciblity of the film can be controlled by tuning the ink properties, functionality of the substrate, submersion time, dipping cycle, and humidity. Many materials such as carbon nanotubes, gold nanowires, PEDOT:PSS, and organic–inorganic nanostructured materials

© 2019 The Authors. Published by WILEY-VCH Verlag GmbH & Co. KGaA, Weinheim

(PEDOT:PSS-RGO, PEDOT:PSS-CNT, PEDOT:PSS-Fe_2O_3, etc.) have been employed to fabricate CP. Figure 2a (ii and iii) shows the optical and SEM image of a PEDOT:PSS-RGO nanocomposite–coated paper.

Printing technique widely used for fabrication of flexible electronic components is considered to be rapid and low-cost. Selection of paper substrate is essential to print suitable ink that can be easily adsorbed onto paper, and form uniform continuous layer. However, formulation of ink is a crucial step to print electronic component on a paper substrate. Properties of ink depend primarily on ink concentration, solvent used, and the presence of binders or additives, which define the viscosity, surface tension, and evaporation rate of ink. Usually binders or additives reduce the electrical performance of ink and choice of solvent is also limited in printing technique. The printing technique basically depends on the properties of ink and characteristics of substrate (surface energy, roughness, and porosity). The most common techniques are inkjet printing and screen printing. The advantage of using paper as a substrate is the fast drying of the ink, better adhesion of desired materials, homogenous printing, and large print thickness. Furthermore, low cost and environment friendly materials and solvent should be used in manufacturing process to obtain a recyclable and environment friendly product. Since the cellulose fibers are hygroscopic in nature and hence these may cause swelling of the substrate during the printing process that may affect the resolution of printing and adhesion of subsequent ink layers. Recently, a fully inkjet printed paper–based electrochemical device was fabricated for glucose detection (Figure 2b).[24] All the components (electrodes, dielectric layer, biological coating etc.) were fabricated by inkjet method. In the screen printing method, inks were squeezed through a patterned screen mesh using squeezer. The patterned screen mesh contains small size of pore through which conducting ink was patterned onto the substrate (Figure 2c). The thickness of ink deposited on the substrate and print resolution depends on ink properties and the density of pores on patterned mesh. Mostly silver, graphite, and their composites were used to render electrical conductivity to the paper. However, it is possible to further modify the surface of a CP strip. A polyaniline film was recently deposited onto CP strips via electrochemical method (Figure 2c, ii) to enhance electrochemical properties and anchoring of biomolecules.[1c,25]

Paper can be made conducting by directly depositing a uniform layer of metal via sputtering technique. The main advantage of sputter deposition is that it can be easily used for even those materials that have high melting points. The target material may be a metal, alloy, ceramic, or compound. In case of the metal target, atoms can be ejected by the ionized gas for deposition onto any surface within the coating unit including the specimen, paper (Figure 2d, i). By adjusting and tuning the vacuum and the time of sputtering, thick coatings of metal depositions can be achieved on a paper substrate. Siegel et al. fabricated paper-based printed circuit boards (PCBs) by sputtering silver and gold metals on the surface of a paper.[21] Similarly, gold was sputtered on filter paper and electrochemically coated with polyaniline to prevent cracks in the film during bending (Figure 2c, ii–iv).[26] Further, this surface was used to anchor protein and for the detection of cancer biomarker, CEA.

To introduce electrical conductivity in the paper, other methods like evaporation,[28] spin coating,[28] spray deposition,[29] and the Meyer rod[30]–based coating have been reported. Compared to sputtering technique, the thermal evaporation method requires expensive equipment and high vacuum condition. For example, deposition of Au and Ag can be done via thermal evaporation while spray deposition can be used to deposit Ni and Ag. Spray deposition is a fast and cheap method for deposition of a metal. This method does not require any vacuum condition and deposition can be performed at room temperature and can be utilized for testing a device/design before considering the expensive technique such as evaporation and sputtering. As compared to evaporation and sputtering, spray coating has been found to have poor resolution and lower conductivity. A Meyer rod–based method has also been used to coat CNT and Ag nanowire ink on commercial Xerox paper.[30] The Meyer-rod is made of a stainless steel and a groove of certain diameter is present on it. This helps in conformal coating of the slurry-based materials on a paper substrate. This technique is cheap, user-friendly, and maintenance-free. It is, however, difficult to get small size feature and the resolution is poor.

2. Application of Nanomaterial-Modified CP

The research and development of nanomaterial modified paper has dramatically intensified due to potential applications in electronics,[31] energy storage devices,[31a,32] and biomedical and biosensors devices (**Figure 3**). Integration of nanomaterials with paper is predicted to exhibit unique physical and chemical properties (i.e., thermal, electrical conductivity, optical properties, high mechanical strength, and electrochemical behavior) that may perhaps be due to the presence of a nanomaterial, flexibility, lightweight, low-cost, disposability, and environment friendliness of paper. In the next section, we discuss the different potential applications of nanomaterial-modified paper including electronics, energy, and medical diagnostics.

2.1. Electronic Applications

The recent developments in preparation of functional nanomaterials in the form of nanocrystals, nanowires, and nanotubes have led to the development of functional inks. These can be easily integrated with paper substrate and form a conductive layer. The CP can be used as a flexible platform onto which an electronic structure can be fabricated. For example, Lyth et al. reported homogenously coated paper substrate with multi-walled CNT for photodiode application.[34] Härting et al. demonstrated the use of a traditional screen printing approach for the fabrication of paper-based field effect transistor using interconnecting silicon nanoparticles.[35] Manekkathodi et al. deposited a thin film of ZnO onto paper substrate for the fabrication of the flexible diode and UV photodetectors.[36] Silver nanowire integrated paper was used to fabricate paper-based capacitive touch pads[33a] and polyimide-based printed circuit board (PCB) was replaced by paper-based flexible PCB by using silver and gold metals on the surface of a paper.[21] These unusual combinations of novel unique nanomaterials and paper indicate

© 2019 The Authors. Published by WILEY-VCH Verlag GmbH & Co. KGaA, Weinheim

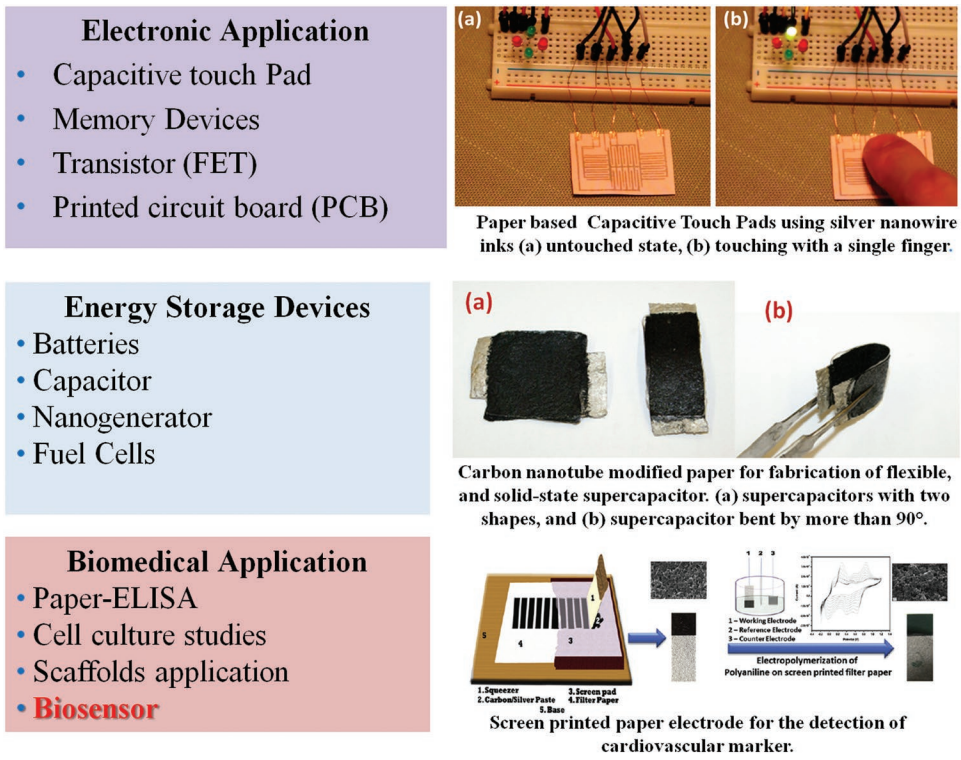

Figure 3. Application of CP in various fields. Reproduced with permission.[25,33] Copyright 2012, Elsevier. Copyright 2014, American Chemical Society. Copyright 2012, AIP Publishing.

that a wide variety of electronic devices can be fabricated. Morphology and composition of the paper substrate have also been found to play a key role to construct high efficient devices. Lee et al. reported a highly conductive paper via low temperature (110 °C) stamping process using aluminum precursor ink $[AlH_3\{O(C_4H_9)_2\}]$.[37] The observed conductivity was found to be as good as thermally evaporated aluminum film and displayed excellent flexibility. Further, aluminum ink was deposited on various paper substrates and showed different electrical and mechanical performance. This was attributed to the different morphology and composition of the paper substrate.

The efforts are being made to replace glass based thin film transistor (TFT) screens with a less expensive, lightweight, flexible, and thermally stable substrate. Fortunato et al. developed an oxide-based semiconductor thin film FET transistor wherein paper was used as a dielectric layer. Hybrid FETs with device on both sides of the paper were developed with excellent characteristics like high channel saturation mobility of >30 cm^2 Vs^{-1} and subthreshold swing of 0.8 V dec^{-1}.[38] With recent advancements in flexible electronics, printed paper–based memory devices (PPMDs) have gained much attention. Lien et al. at National Taiwan University (NTU) worked on PPMDs and successfully fabricated a printed paper–based resistive random access memory (RRAM) device on A4 sheet with storage capacity in gigabytes.[39] The PPMD showed excellent endurance, reliable retention, and operating capability under extreme bending condition. Unlike regular silicon-based storage devices, PPMDs showed excellent ease of data handling, disposability, switching endurance, and reliable retention. Gong et al. fabricated a highly sensitive pressure sensor based on gold nanowire integrated conductive tissue paper.[40] Conductive paper was sandwiched between PDMS and interdigited electrode integrated PDMS chip for fabrication of wearable sensor that easily monitored the blood pulse and could be used to measure small vibration forces originate from music.

There is a growing interest in exploiting the potential of paper as a substrate for ultrahigh frequency and microwave applications since these are inexpensive, reliable, and has durable wireless radio frequency identification (RFID) tags. RFID tags were used in logistics, monitoring of supply chain, healthcare, pharmaceutical, space, and anti-counterfeiting. Another work relating to RFID based on paper has been reported by Yang et al., integrated with silver nanoparticles.[41] This silver-modified paper-based RFID tags successfully reduced its cost and is eco-friendly. Transparent and conducting electrodes are major elements for various optoelectronics application such as solar cell, touch panel, electrochromics, etc. The conventional devices are based on rigid and brittle glass substrate that limits their application for fabrication of smart electronic devices. Kang et al. fabricated a conductive and transparent paper using nanocellulose and conducting materials, i.e., silver nanowire and carbon nanotube for fabrication of foldable electrochromics devices that showed strong endurance to deformation, good cycling stability, and improve coloration efficiency.[42]

The electrical conduction in a modified paper is due to the presence of charge carriers (ions and electrons), and their short range mobility. The charge carriers are believed to be heterogeneous, involving many species as the paper material is chemically heterogeneous.[43] Additionally paper is chemically and mechanically stable in normal atmospheric conditions and its

© 2019 The Authors. Published by WILEY-VCH Verlag GmbH & Co. KGaA, Weinheim

excellent ability to absorb ink makes it superior as compared to other substrates. Its bulk and surface properties can be easily tuned by modifying the fiber, adding chemical additives, and surface treatment.[44] Furthermore, the abundance of cellulosic material on this planet makes conductive paper a renewable and sustainable component for various electronic devices mentioned above such as circuit board, capacitive touch pad, memory devices, field effect transistor, frequency identification tags (FID), and electrochromic. However, humidity and temperature have been found to influence the properties of CP. Compared to traditional electronic devices, life span of CP-based devices is currently the major issue. Nevertheless, with advancement in manufacturing technique it should be possible to make paper fiber resistant to external factor up to a certain limit and improve the device characteristics for longer period.

2.2. Energy Storage Devices

The 3D hierarchical structure of cellulose paper has the ability to store and transport liquid electrolytes. Its interconnected pores allow fast movement of the ionic species. These properties were used as a key for development of paper-based energy storage devices. Further conducting paths were integrated into a paper using conducting materials such as metal oxides, nanowires, carbon nanomaterials, and conducting polymers.[11,45] These nanomaterial-based CP have been predicted to have applications in energy storage devices such as electrochemical batteries,[46] lithium-ion batteries,[47] supercapacitors,[48] biofuel cells,[49] and nanogenerators.[28] Lithium-ion batteries and supercapacitors are known to be excellent power sources for high power electronics whereas nanogenerators are useful for wearable electronics. Biofuel cells have proved handy for small power electronics such as microfluidics paper analytical devices (μPADs) and biosensors wherein the energy requirement is minimal.

Compared to other substrates, paper has exceptional properties to absorb conducting ink and form a stable film. It also minimizes the additional steps required for coating process and significantly reduces the device cost. The light weight of CP can be used as an excellent current collector in lithium-ion batteries to substitute the metallic chemical counterpart. Wang et al. developed a flexible single walled CNT/poly-cellulose paper for lithium-ion battery with first discharge capacity of 153.3 mA h g^{-1} at 0.1 C and discharge capacity of 102.6 mA h g^{-1} at 10 C.[47] Chou et al. integrated MnO_2 nanowires with CNT paper using cyclic voltammetry for demonstration of supercapacitor application.[48] The supercapacitor showed specific capacitance of 167.5 F g^{-1} at a current density of 77 mA g^{-1}. The composite paper retained 88% of the initial capacitance even after 3000 cycles of charge and discharge. Furthermore, CNT and silver nanowire composites were integrated with paper to fabricate a high efficient supercapacitor and lithium-ion battery.[30] The efforts are being made to fabricate small power devices that can utilize mechanical energy to convert it into electrical energy. Nanogenerators have proved to be an ideal power source for self-powered system as an energy source for application in micro-electro-mechanical systems (MEMS). Kim et al. fabricated the first paper-based mechanical nanogenerator.[50] In this work, a piezoelectric active layer of ZnO rods was introduced on cellulose substrate that produced a current density of 2 μA cm^{-2} and an output voltage of 75 mV with stable current output after 10 mechanical bending cycles. In another work Zhong et al. designed a paper-based nanogenerator using polytetrafluoroethylene (PTFE)–Ag–paper assembly.[28] By applying external mechanical force on PTFE–Ag–paper assembly (nanogenrator) a maximum instantaneous power of up to ≈90.6 μW cm^{-2} was generated, which is sufficient to glow 70 LEDs simultaneously. An environment friendly triboelectric nanogenerator comprising of cellulose nanofibers (CNF) and Ag nanowires (AgNW) were reported.[51] By contacting and moving apart two sheets of fabricated paper (AgNW/CNF) produced a power output of 693 mW m^{-2} against a 10 MΩ external resistance. The fabricated electrode (AgNW/CNF paper) could be easily decomposed into its constituents by simple sonication method and is hence, a clean energy source for low power devices. Microbial fuel cell (MFC) devices are using organic matter to generate electrical power. Here bacteria decomposed into organic matter and resultant chemical energy was used to generate electricity. Typically, MFCs are made up of two chambers (anode and cathode) that are separated by a membrane. During bacterial decomposition of organic matter H^+/positive ions release and migrate from anodic to cathode chamber and resulted into flow of electricity. Electrical power generated by MFC was very low (≈3–4 W m^{-2}) to meet the societal need. Fraiwan et al. developed the first paper-based microbial fuel cell (MFC) with rapid electricity generation, an improvement over the conventional MFCs with long startup time usually several days to a week.[49] Choi and coworkers developed battery stack using MFC that was able to glow a red LED for 30 min.[20a] This paper battery is simple, cost-effective, and is a user friendly power source. It could also a source of power for single time run of paper-based diagnostic devices. There is enough scope for MFCs since even O_2 could be used as electron acceptor instead of conventionally used toxic ferricyanide.

One of the major concerns in paper-based energy storage devices is the fast drying of electrolytes. Thus, sealing of device would be an alternative. Further, to increase the life span of these devices we can choose ionic electrolyte that could perhaps be utilized for longer duration. However, the transport of ions is usually low.

2.3. Biomedical Applications

The fluidic properties, 3D geometry, white background, biocompatible surface, ability to separate analyte, low cost, and easy to dispose off paper make them an ideal platform for biomedical applications.[2,52] Integration of a nanomaterial with paper may lead to improved quality of the paper-based devices such as enhanced separation, color contrast, and loading of the biomolecules, etc. The nanomaterial-modified paper has been predicted to have applications in bioassays,[53] drug screening,[54] ELISA,[55] cell culture studies,[56] scaffolds,[57] and biosensing[58] applications.

For electrocardiogram (ECG) recording, the wet gel adhesives are needed that make them inconvenient for long-term

© 2019 The Authors. Published by WILEY-VCH Verlag GmbH & Co. KGaA, Weinheim

monitoring. Mostafalu et al. fabricated a patterned paper electrode using platinum, nickel, and copper nanowire. This nanomaterial-modified flexible electrode can be utilized for recording of the ECG signal.[12] The paper-based electrodes provide high surface area and low impedance and can perhaps be helpful to record the signal even in dry attachment with skin. Similarly, Bihar et al. used PEDOT:PSS-coated paper electrode to measure ECG signal via a simple finger to electrode contact (**Figure 4**a) and electrode was stable for 3 months.[59] This work has the potential to minimize the manufacturing steps and is cost effective. Besides this, it provides a metal free medical electrode with large durability. Kuzmenko et al. fabricated scaffolds by modifying electrospun cellulose with MWCNT and carbon nanofiber for enhanced neural tissue growth.[57] It provides ideal feature similar to neural extracellular matrix that allows neural cell to grow, differentiate, and adhere to substrate. This kind of matrix is useful to regenerate neural tissue in vitro that will lead to increased understanding of the disease and will help to design new drug at laboratory scale. In another example, polydopamine-modified Fe_3O_4 nanoparticles were deposited on Whatman paper termed as "Magnetic paper," can be used for ELISA to detect dengue (Figure 4b).[60] The analytical performance of paper ELISA for IgM-dengue detection showed sensitivity (500 times lower detection limit) two order more than traditional ELISA method.

The surface modification of paper with nanomaterials reveals plasmonic behavior. Liu et al. fabricated a plasmonic filter paper by dipping paper in gold nanorods (GNRs) solution.[61] This platform was used to differentiate normal and cancerous cells using surface-enhanced Raman scattering (SERS) in which a diagnostic result based on the ratio of the spectral values was adopted to distinguish healthy and cancerous cells. Another

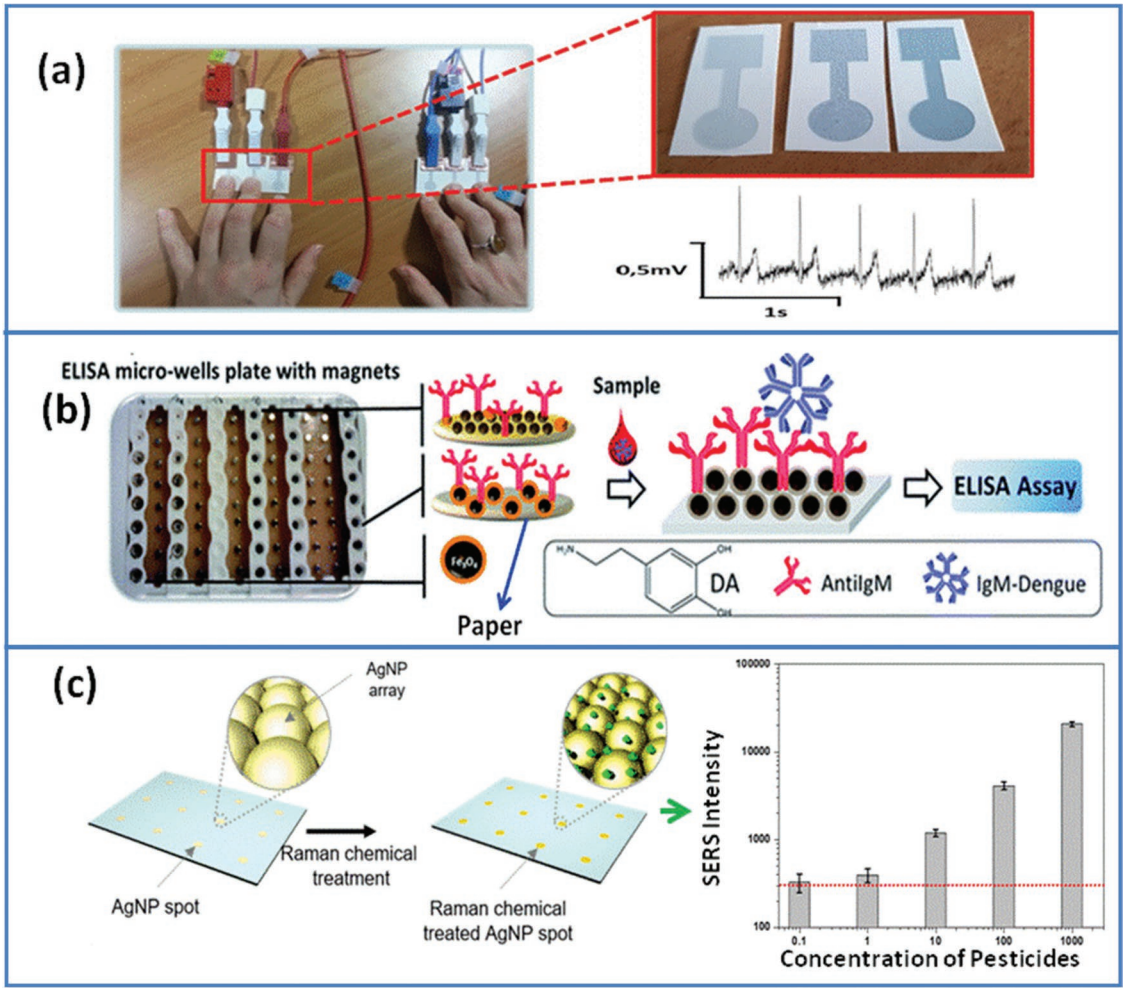

Figure 4. a) Electrophysiological signal measurement: A paper-based electrocardiography was recorded using a PEDOT:PSS-coated electrode via a simple finger-to-electrode contact. Reproduced with permission.[59] Copyright 2017, Wiley-VCH. b) ELISA: a polydopamine-modified Fe_3O_4 nanoparticle was deposited on Whatman paper. The modified paper was used in pristine microwells having 96 well plates that are coupled to a magnet. Further, Fe_3O_4-nanoparticle-modified paper was used for the ELISA assay to detect dengue. The analytical performance of paper ELISA for IgM-dengue detection shows two orders higher sensitivity (500 times lower detection limit) than traditional ELISA. Reproduced with permission.[60] Copyright 2017, Royal Society of Chemistry. c) Analyte assay: a paper-based SERS substrate was fabricated to detect pesticides (4-ATP, thiram, and ferbam). The paper was initially treated with alkyl ketene dimer (AKD) to modify its property from hydrophilic to hydrophobic. This treatment increased the density of AgNPs and retention time on paper (SERS substrate) and therefore consequently enhances the sensitivity and reproducibility. Reproduced with permission.[62] Copyright 2018, American Chemical Society.

© 2019 The Authors. Published by WILEY-VCH Verlag GmbH & Co. KGaA, Weinheim

work with paper-based SERS substrate was employed for pesticides detection (Figure 4c).[62] First, paper was chemically treated with alkyl ketene dimer to modify it from hydrophilic to hydrophobic. This treatment increased the density of AgNPs and retention time on paper and consequently enhanced the sensitivity and reproducibility. The electrocatlytic activity and functional group of nanomaterials were also taken as advantage for detection of various bioanalyte. Ornatska et al. modified the paper with ceria nanoparticles for naked-eye detection of glucose.[63] In this work, glucose oxidase was immobilized on the ceria nanoparticle-modified paper. In the presence of glucose, the hydrogen peroxide genrated during enzymatic reaction and ceria modified paper induced a visual color change from white-yellowish to dark orange. The change in the color intensity was directly proportional to glucose concentration. This assay utilized the redox behavior of cerium oxide as a colorimetric probe indicator and could be used for 10 consecutive cycles and stability of 79 d. In another work, zirconia nanotubes modified filter paper was utilized to bind oligonucleotides.[15] The co-ordination bond was formed between zirconia and the phosphate group present in probe DNAs. This platform (zirconia/paper) is highly sensitive and selective to detect complementary target DNA present at nanomolar concentration. Additionally, nanostructure ZnO-coated paper possessed antibacterial activity.[64] Besides this, CP can be used to culture other cells ranging from bacteria, fungi, plant to other human cells line such as primary, tumor, stem, osteoblasts, fibroblasts, and immune cells.[56b] These paper-based platforms are compatible with standard analytical procedure that are usually used to monitor cell response in stress condition.[56b] Thus, paper can be an interesting and easy substitute for existing assay platforms since this would open up new possibilities in the biomedical field. However, strong and uniform attachment of material on paper substrate is very crucial because it provides high surface-to-volume ratio and allows low impedance. During measurement of physiological signal, compatibility of materials with human skin is very important to prevent unwanted allergic reaction.

2.4. Biosensor Applications

The CP-based biosensors are recently gaining much interest for development of flexible, portable, low cost, power efficient, and environment friendly devices. These devices are known to have potential application in diagnostics, monitoring of analytes, and environmental studies. Wang et al. used single-walled CNT to modify filter paper for environmental toxin detection (microcystin-LR).[65] Carvalhal et al. sputtered gold on Whatman paper for fabrication of electrodes and further, this paper electrode was used for quantitative detection of electroactive compounds, such as ascorbic acid and uric acid.[66] Later these researchers used electrochemical method for detection of paracetamol and 4-aminophenol using patterned gold electrode in the paper-based microfluidic device.[67] In another work, a screen printed paper electrode was fabricated using graphite and silver ink on the paper substrate followed by electrochemical deposition of polyaniline for the detection of cardiac (cTnI) and cancer biomarkers (sIL2Rα).[1c,25] The conventional laboratory assay requires long time and expertise; whereas these devices are fast, low cost, and easy to handle. Additionally, it does not require any large infrastructure and hence testing can be performed near the vicinity of patient.[1] For the fabrication of an electrochemical biosensor, conducting electrodes such as glassy carbon, indium tin oxide, and gold-coated glass electrodes can be used.[68] These electrodes are rigid, brittle, and are costly which limit their applications for fabrication of smart, flexible, low cost, and wearable POC devices. In addition to these problems, conventional electrodes require high temperature for processing and expertise. On the other hand, CP-based biosensors have attracted significant interest due to their light weight, flexibility, portability, high sensitivity, fast response time, and disposibility.[20b,27,53] CP has many advantages such as cost, renewable material and has strong adsorption properties that can be useful for the modification of paper for efficient fabrication of the biosensing devices.[2] It has been considered to be an efficient platform that can conduct both electrons and ionic charge carriers. These two properties play a major role in electrochemical biosensor for communication with biomolecule during sensing process.[20b] The advantages and scope of CP as a sensor substrate are listed in **Table 1** and are compared with conventional electrodes.

Immobilization of bioreceptor on transducer surface is an important parameter for fabrication of efficient biosensing platform. For this purpose, an immobilization matrix can be used since it integrates and maintains the functionality of bioreceptor at one end and at the other end it binds with the

Table 1. Comparison between conventional electrode and CP electrode.

S.No.	Properties	Conventional electrodes (Indium tin oxide, gold coated glass, Glassy carbon)	CP
1	Cost	High	Low
2	Flexibility	No	Yes (Room for improvement)
3	Transparency	Only ITO	Room for development
4	Biocompatibility	No	Room for development
5	Modification/Functionalization	Difficult	Easy
6	Fluid flow	Forced	Capillary action
7	Surface by volume ratio	Low	High
8	Fabrication and high throughput production	No	Yes
9	Disposability	Complex	Simple

© 2019 The Authors. Published by WILEY-VCH Verlag GmbH & Co. KGaA, Weinheim

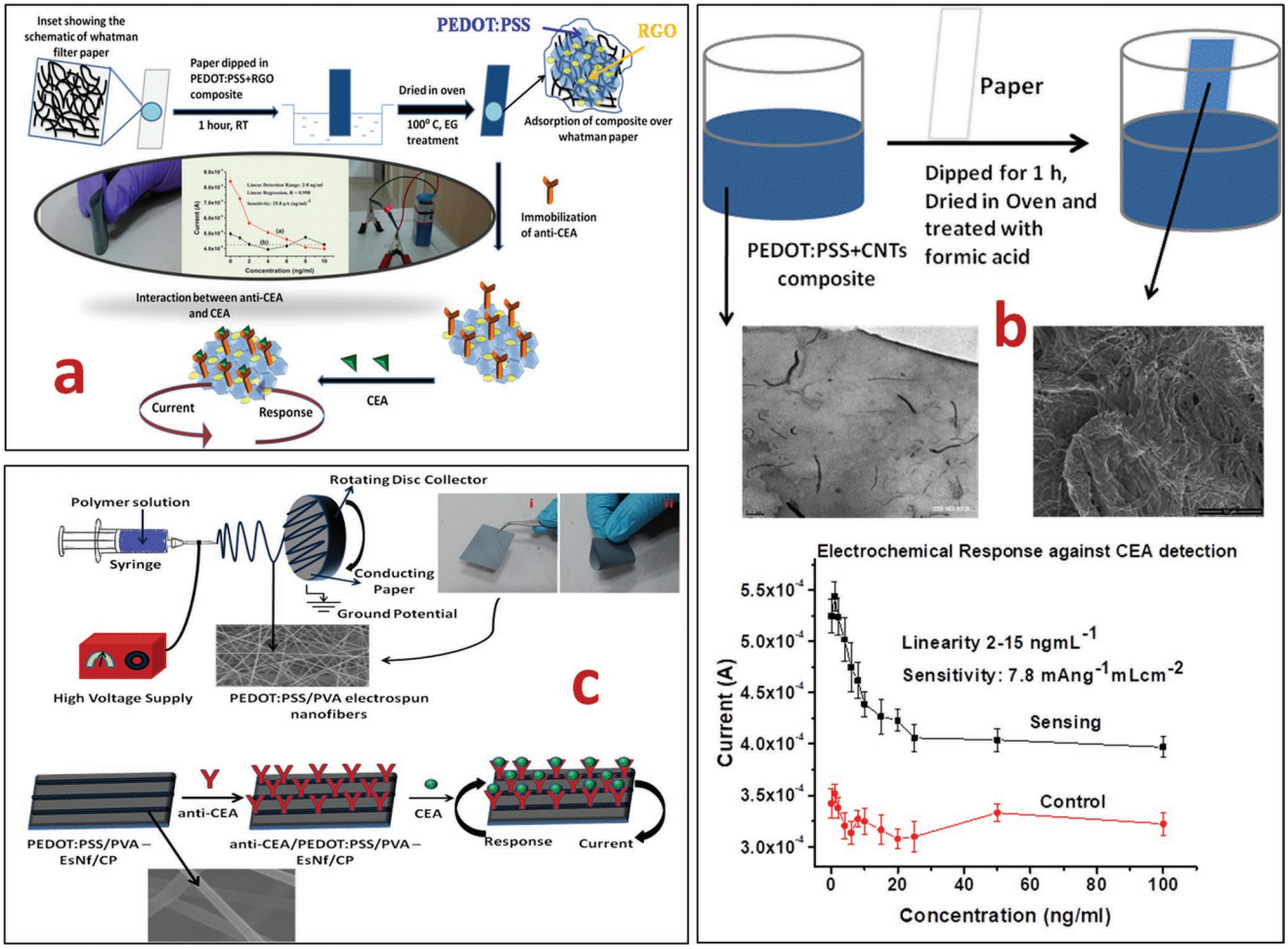

Figure 5. a) A graphic representation of PEDOT:PSS-RGO-modified CP. The fabricated CP shows excellent flexibility, electrochemical properties, and is used for CEA detection. Reproduced with permission.[27] Copyright 2015, Elsevier. b) The schematic representation of PEDOT:PSS-CNT paper by dip-coating method. The PEDOT:PSS-CNT paper electrode is further used for CEA detection. Reproduce with permission.[23d] Copyright 2015, Royal Society of Chemistry. c) CP modified by electrospinning of PEDOT:PSS/PVA-nanofibers. Reproduced with permission.[71] Copyright 2016, Wiley-VCH.

transducer surface. It provides the accessibility of analyte to bioreceptor and, thereafter, physiochemical changes are measured by transducer. In this context, the incorporation of a nanomaterial as an immobilization matrix improves the characteristics of the CP in terms of performance, signal stability, biomolecules loading, and sensitivity.[69] The large surface area of the nanomaterial-integrated paper is likely to provide a better matrix for the immobilization of desired biomolecules leading to increased loading. The effect of immobilization matrix on the sensing performance of CP has been shown and discussed in **Figure 5**. The solution processed CP comprising PEDOT:PSS-RGO (Figure 5a) and PEDOT:PSS-CNT (Figure 5b) was used to detect cancer biomarker, CEA in the range of 2–8 ng mL^{-1} with sensitivity of 25.8 mA ng^{-1} mL cm^{-2} and 2–15 ng mL^{-1} with sensitivity of 7.8 mA ng^{-1}mL cm^{-2}, respectively.[23a,27] These changes in sensing parameter relied on selection of the dopant (nanomaterials) and solvent. Conductivity of CP was found to be increased by two orders of magnitude (10^{-4} to 10^{-2} Scm^{-1}) by treatment with different solvents like ethylene glycol (EG), formic acid, and DMSO.[23a,27,70] Whereas nanomaterials such as RGO, CNT, and $n Fe_2O_3$ can be utilized to obtain improved electrochemical properties, signal stability, and enhanced mass loading of a bioreceptor. In another example, morphology of the CP was modified by electrospinning of PEDOT:PSS/PVA-nanofibers.[71] The outcome of the electrochemical response studies showed that the PEDO:PSS/PVA-EsNf modified CP could be used to estimate CEA in the range of 0.2 to 25 ng mL^{-1}, with sensitivity of 14.2 µA ng^{-1} mL cm^{-2} and shelf life of 22 d (Figure 5c). The resulting paper sensor covered the entire physiological range of CEA secreted in serum sample (<3 to 20 ng mL^{-1}) with acceptable lower detection limit. These nanomaterial-modified CP electrodes exhibited improved results as compared to conventional ITO, gold, and glassy carbon electrode. Next, these CP platforms could be easily decomposed by simple burning/incineration that are an additional advantage for biomedical waste management. **Table 2** summarizes the materials and techniques used for the fabrication of nanomaterials modified paper-based electrochemical biosensors and their characteristics as reported in the literature. In spite of

© 2019 The Authors. Published by WILEY-VCH Verlag GmbH & Co. KGaA, Weinheim

Table 2. CP-based electrochemical biosensors: fabrication and characteristics.

S.No.	Substrate	Materials	Fabrication method	Analyte	Detection technique	Sensing parameter	Refs.
1	Whatman filter paper #1	Screen printed carbon electrode	Drop casting	Glucose	Amperometry	[L] = 1–5 × 10^{-3} M [LOD] = 0.18 × 10^{-3} M [T] = 4 months	[72]
2	Whatman filter paper #1	Ag/AgCl ink, carbon ink, wax, graphene, AuNP	Wax printing, screen printing	DNA	Differential pulse voltammetry	[L] = 0.0008–500 × 10^{-12} M [LOD] = 0.2 × 10^{-15} M [T] = 4 months	[73]
3	Whatman filter paper #1	Ag/AgCl ink, carbon ink, SU-8	Photolithography, screen printing	Glucose Pb(II)	Chronoamperometry Anodic striping voltammetery	Glucose [L] = 0–22.2 × 10^{-3} M [LOD] = 0.22 × 10^{-3} M [S] = 0.43 µA mM^{-1} mm^{-2} Pb(II) [L] = 5–100 ppb [LOD] = 1 ppb [S] = 0.17 µA ppb^{-1}	[74]
4	Whatman filter paper #1	Graphene, polyvinyl pyrrolidone, polyaniline (G/PVP/PANI), carbon ink, Ag/AgCl ink	Electrospraying wax printing screen printing	Cholesterol	Amperometric	[L] = 0.05–10 × 10^{-3} M [LOD] = 1 × 10^{-6} M [S] = 34.77 µA mM^{-1} cm^{-2} [T] = 2 weeks	[75]
5	Platinum sputtered glass	Nitrocellulose paper, polyester cellulose blend	Drop casting	Glucose	Amperometric	–	[76]
6	Whatman paper #1	ITO coated glass wax, Prussian blue	Drop casting	Glucose	Electrochromic	–	[77]
7	Filter paper	Gold nanorods	Dip coating	Oral squamous cell carcinoma (OSCC) cell line CAL-27	Surface-enhanced Raman scattering (SERS)	Intensity ratio of particular Raman peak	[61]
8	Filter paper	Carbon nanotube (CNT)	Dip coating	Microcystin-LR (MC-LR)	Amperometry	[L] = 1–10 ng mL^{-1} [LOD] = 0.6 ng mL^{-1}	[65]
9	Whatman filter paper #1	Screen printed carbon electrode	Drop casting	Pb(III)	Anodic striping voltametry	[L] = 10–100 ppb [T] = 3 months	[78]
10	Whatman filter paper #1	Gold	Sputtering	Uric Acid (UA) Ascorbic Acid (AA)	Amperometry	[L] = 0–40 pmols [LOD] = 0.02 mmol L^{-1} AA [S] = 152 nA L $mmol^{-1}$ UA [S] = 64 nA L $mmol^{-1}$	[66]
11	Whatman filter paper #1	Carbon ink	Screen printing	Glucose lactate uric acid	Chronoamperometry	Glucose [L] = 0–100 × 10^{-3} M [LOD] = 0.21 ± 0.02 × 10^{-3} M [S] = 64 µA mM^{-1} Lactate [L] = 0–50 × 10^{-3} M [LOD] = 0.36 ± 0.03 × 10^{-3} M [S] = 40 µA mM^{-1} Uric acid [L] = 0–35 × 10^{-3} M [LOD] = 1.38 ± 0.13 × 10^{-3} M [S] = 6 µA mM^{-1}	[79]
12	Whatman filter paper #1	Carbon ink, prussian blue	Wax screen printing	Glucose	Chronoamperometry	[L] = 0.5–5 × 10^{-3} M [S] = 1 µA mM^{-1}	[80]
13	Whatman filter paper #1	Carbon ink	Solid wax printing screen printing	Glucose	Chronoamperometry	[L] = 0–20 × 10^{-3} M [LOD] = 0.35 × 10^{-3} M [S] = 0.041 µA mM^{-1}	[81]

© 2019 The Authors. Published by WILEY-VCH Verlag GmbH & Co. KGaA, Weinheim

Table 2. Continued.

S.No.	Substrate	Materials	Fabrication method	Analyte	Detection technique	Sensing parameter	Refs.
14	Whatman filter paper #1	Gold and platinum NPs on SPE	Wax printing	Single stranded DNA	Amperometry cyclic voltammetry	[L] = 10.0×10^{-15} M–100×10^{-9} M [LOD] = 6.3×10^{-15} M	[82]
15	Whatman filter paper #1	Pencil-drawn electrode, carbon paste	Wax printing	Ascorbic acid, dopamine, paracetamol	Amperometry	–	[83]
16	Whatman filter paper #1	Graphite pencil	Wax printing	Glucose	Chronoamperometry	[L] = 0.01–1.5×10^{-3} M [LOD] = 0.38×10^{-6} M [T] = 5 d	[84]
17	Whatman filter paper #1	CdS quantum dot and CNTs on SPE	Wax printing	Adenosine triphosphate (ATP)	Cyclic voltammetry	[L] = 1–1000×10^{-12} M [LOD] = 0.2×10^{-12} M [S] = 27 nA pM^{-1} [T] = 4 weeks	[85]
18	Whatman filter paper #1	Gold NPs on carbon	Wax printing, SlipPAD technique	Single stranded DNA, Thrombin	Alternating current voltammetry	ssDNA [LOD] = 30×10^{-9} M Thrombin [LOD] = 16×10^{-9} M [T] = 4 weeks	[86]
19	Japanese paper	Screen-printed electrode	Screen printing	Glucose	Amperometry	[L] = 10–100×10^{-3} M [S] = 0.055 µA mM^{-1}	[87]
20	Whatman filter paper #1	Gold NPs on SPE	Wax printing screen printing	Microcystin-LR	Differential pulse voltammetry	[L] = 0.01–200 µg mL^{-1} [LOD] = 0.004 µg mL^{-1} [T] = 2 months	[88]
21	Whatman filter paper #1	Carbon graphite ink on SPE	Screen printing	Nicotinamide adenine dinucleotide (NADH) Nitrite	Cyclic voltammetry	NADH [L] = 10–100×10^{-3} M [LOD] = 1.8×10^{-6} M Nitrite [L] = 10–100×10^{-3} M [LOD] = 15.1×10^{-3} M	[89]
22	Whatman filter paper #1	Chitosan–silver on SPE	Screen printing	Cancer antigen 125 (CA125) Carcinoma antigen (CA199)	Square wave voltammetry	CA125 [L] = 0.1–100 U mL^{-1} [LOD] = 0.02 mU mL^{-1} [S] = 2.56 µA mL U^{-1} [T] = 21 d CA 199 [L] = 0.1–100 U mL [LOD] = 0.04 mU mL^{-1} [S] = 0.91 µA mL U^{-1} [T] = 21 d	[33a]
23	Whatman filter paper #1	Gold–manganese oxide NPs on SPE	Wax printing screen printing	Prostate protein antigen (PSA)	Differential pulse voltammetry	[L] = 0.005–100 ng mL^{-1} [LOD] = 0.0012 ng mL^{-1} [T] = 4 weeks	[90]
24	Whatman filter paper #1	Polyaniline (PANI) on SPE, graphite and silver paste	Screen printing	Human troponin I	Cyclic voltammetry	[L] = 1–100 ng mL^{-1} [S] = 5.5 µA ngmL^{-1} cm^{-2}	[25]
25	Whatman filter paper #1	SPE, graphite, carbon, and silver paste	Screen printing	2-(dibutylamino) ethanol NADH	Cyclic voltammetry	DBAE [L] = 3–5000×10^{-6} M [LOD] = 0.9×10^{-6} M NADH [L] = 0.2–10×10^{-3} M [LOD] = 72×10^{-6} M	[91]
26	Whatman filter paper #1	Nafion/graphene oxide on SPE	Photolithography screen printing	DNA mismatches	Electro chemiluminescence	[L] = 10×10^{-9} M–5×10^{-6} M [LOD] = 1×10^{-9} M [T] = 3 months	[92]
27	Whatman filter paper #1	Tin oxide QDs/ RGO/gold NPs on SPE	Screen printing	ATP	Electrochemical impedence spectroscopy [EIS]	[L] = 0.1×10^{-12} M 100×10^{-9} M [LOD] = 0.025×10^{-12} M [T] = 5 weeks	[93]

© 2019 The Authors. Published by WILEY-VCH Verlag GmbH & Co. KGaA, Weinheim

Table 2. Continued.

S.No.	Substrate	Materials	Fabrication method	Analyte	Detection technique	Sensing parameter	Refs.
28	Filter paper	SWCNTs	CNT ink painting	Human immunoglobulinG (HIgG)	Amperometry	[L] = 6.3–62 × 10^{-12} M [S] = −70.8 pA $pmol^{-1}$ sL^{-1}	[94]
29	Whatman filter paper #1	PEDOT:PSS-RGO	Dip coating	CEA	Chronoamperometry	[L] = 2–8 ng mL^{-1} [S] = 25.8 μA ng^{-1} mL cm^{-2} [T] = 21 d	[27]
30	Whatman filter paper #1	PEDOT:PSS-CNT	Dip coating	CEA	Chronoamperometry	[L] = 2–15 ng mL^{-1} [S] = 7.8 μA ng^{-1} mL cm^{-2} [T] = 18 d	[23a]
31	Whatman filter paper #1	PEDOT:PSS-nFe_2O_3	Dip coating	CEA	Chronoamperometry	[L] = 4–25 ng mL^{-1} [S] = 10.2 μA ng^{-1} mL cm^{-2} [T] = 34 d	[70]
32	Whatman filter paper #1	Gold, PANI	Sputtering, electrochemical coating	CEA	Chronoamperometry	[L] = 2–20 ng mL^{-1} [S] = 13.9 μA ng^{-1} mL cm^{-2} [T] = 22 d	[26]
33	Whatman filter paper #1	PEDOT:PSS/PVA electrospun nanofiber	Dip coating	CEA	Chronoamperometry	[L] = 0.2–25 ng mL^{-1} [S] = 14.2 μA ng^{-1} mL cm^{-2} [T] = 22 d	[71]
34	Office paper (Fabriano, Italy, 80 and 100 gm/m^2)	Carbon black- Prussian blue nanocomposites (CB/PBNPs), Ag/AgCl ink, graphite ink, wax	Wax printing, screen printing	Ethanol	Amperometry	[L] = 0–10 × 10^{-3} M [LOD] = 0.52 × 10^{-3} M [S] = 9.13 μA mM^{-1} cm^2	[95]
35	Filter paper and nitrocellulose membrane	Ag/AgCl ink, carbon ink, wax, CB/PBNPs	Wax printing, screen printing	Nerve stimulant (Paraxon)	Amperometry	[L] = 5–25 μg L^{-1} [LOD] = 3 μg L^{-1} [T] = 15 d	[96]
36	Whatman filter paper #1	AuNP-modified Cu-based MOFs, Au-coated paper, carbon ink, Ag/AgCl ink, wax	Wax printing, screen printing	miRNA-155	DPV	[L] = 1 × 10^{-15} M–10 × 10^{-9} M [LOD] = 0.35 × 10^{-15} M	[97]
37	Filter paper (Cordenons, Italy, 67 g m^{-2})	Prussian blue nanoparticles (PBNPs), carbon ink, Ag/AgCl ink, wax	Wax printing, screen printing	Glucose	Amperometry	[L] = 0–30 × 10^{-3} M	[98]
38	Screen printed electrode (SPE)	Silane functionalized silica nanoparticles/ banana peel tissue (source of enzyme)/ mediator modified filter paper disc	Drop casting	L-tyrosine	DPV	[L] = 0.05–600 × 10^{-6} M [LOD] = 0.02 × 10^{-6} M	[99]
39	Whatman filter paper #1	Cyclodextrin functionalized AuNPs (CD@AuNPs), carbon ink, Ag/AgCl ink, wax	Wax printing, screen printing	CEA and PSA	DPV	CEA [L] = 0.005–100 ng mL^{-1} [LOD] = 0.002 ng mL^{-1} PSA [L] = 0.002–100 ng mL^{-1} [LOD] = 0.001 ng mL^{-1}	[100]

Abbreviations: [L] = linear detection range, [LOD] = lower detection limit; [S] = sensitivity; [T] = stability; Ag/AgCl = silver/silver chloride; SPE = screen-printed carbon electrode; ITO = indium tin oxide; NP = nanoparticle; CdS = cadmium sulfide; CNT = carbon nanotubes; SWCNT = single-walled carbon nanotubes; PAD = paper analytical device; QD = quantum dot; RGO = reduced graphene oxides; DNA = deoxyribose nucleic acid, PANI = polyaniline.

these interesting developments, there is a considerable scope for the development of simple, low cost, flexible, lightweight, and environment-friendly biosensors with improved sensing characteristics using nanomaterial-modified paper platform.

CP-based biosensor provides an interesting platform for simple, precise, and quick recognition of desired biomolecules. These CP-based devices can be used as cost-effective technology for the development of POC diagnostic systems that can be used in developing countries, where there is no availability of fully equipped facilities and trained human resources. The important benefit of using CP as a biosensing platform is their compatibility with chemicals and biochemicals.[101] Nowadays efforts are being made toward the fabrication of paper-based microfluidics devices that can be readily available and may play a crucial role in biomedical research.[102] Prior to commercialization of CP-based biosensors, many parameters such

© 2019 The Authors. Published by WILEY-VCH Verlag GmbH & Co. KGaA, Weinheim

as accuracy and sensitivity must be addressed. And addressing other issues such as nonspecific adsorption of biomolecules, reduction in surface roughness, mechanical and environmental stability are very important for commercialization of these biodevices. Moreover, the application of CP-based biosensors must not be limited to the detection and diagnosis of disease, the POC devices can also be used for the monitoring of toxins, and food quality, in environmental samples and agricultural applications. With advancement in fabrication techniques, novel nanomaterials, and structural design, it is anticipated that in the near future more exciting and innovative research in CP-based biosensors will be seen.

3. Conclusion and Outlook

The recent development in conducting paper-based devices has demonstrated exciting results ranging from electronics, energy storage to various biomedical applications. These conducting paper-based substrates are gaining more popularity than the conventional substrates in terms of their cost, flexibility, availability, ease of modification, disposability, and easy to use. Further, the desired properties of these paper-based devices can perhaps be achieved by specific modification of the paper substrate with nanomaterials. In spite of all these advantages, many fundamental and applied challenges hinder the commercialization of paper-based electronic devices. For example, stability and durability of conductive paper-based devices are currently lesser than those of traditional devices. Smooth surface, strong mechanical strength and novel unique materials may open the window for development of paper-based electronic devices that have a wide range of application. Sealing of energy storage devices may prevent fast drying of the electrolyte and effect of humidity and temperature to some extent. In this context, enhanced cooperation between scientific research community and industrial partner is essential to develop paper for long-term electronics application. Furthermore, controlled conditions are necessary for the fabrication of CP-based POC devices as the properties of paper gets altered with humidity and temperature. The porous structure and high absorbance of paper are beneficial for strong adhesion of nanomaterials and immobilization of bioreceptor. Besides this, paper may interfere with the electrical conductivity and non-specific adsorption of other analytes that can yield false signal during measurement. These intrinsic surface properties could perhaps be controlled during manufacturing process and an application-oriented paper may perhaps provide the desired solution. Besides this, in-depth analysis of paper composition with geometric structure may open door to control the surface architecture. For qualitative or yes/no screening test, paper-based devices are doing well. However, for quantitative detection poor sensitivity and lack of reproducibility are presently major concern. Thus, the development of more sensitive and accurate detection strategy would be very helpful to commercialize POC devices. The novel nanomaterials, advancement in fabrication technique and appropriate structural design may result in improved properties, accuracy, and sensitivity of the CP-based POC devices.

Acknowledgements

The authors (S.K., C.M.P., and B.D.M.) thank Prof. Yogesh Singh, Vice Chancellor, Delhi Technological University for providing the facilities. S.K. (DST/INSPIRE/04/2017/002750) and C.M.P. (DST/INSPIRE/04/2015/000932) acknowledges Department of Science and Technology, New Delhi, India, for DST-INSPIRE Faculty Award. B.D.M. thanks Science & Engineering Research Board (Govt. of India) for the award of a Distinguished Fellowship (SB/S9/YSCP/SERB-DF/2018).

Conflict of Interest

The authors declare no conflict of interest.

Keywords

conducting paper, deposition methods, nanomaterials, point-of-care devices

Received: May 5, 2019
Revised: August 9, 2019
Published online:

[1] a) P. B. Luppa, C. Müller, A. Schlichtiger, H. Schlebusch, *TrAC, Trends Anal. Chem.* **2011**, *30*, 887; b) L. Gervais, N. De Rooij, E. Delamarche, *Adv. Mater.* **2011**, *23*, H151; c) S. Kumar, K. K. Jagadeesan, A. G. Joshi, G. Sumana, *RSC Adv.* **2013**, *3*, 11846.
[2] E. W. Nery, L. T. Kubota, *Anal. Bioanal. Chem.* **2013**, *405*, 7573.
[3] a) M. Xu, D. Obodo, V. K. Yadavalli, *Biosens. Bioelectron.* **2019**, *124–125*, 96; b) A. J. Bandodkar, J. Wang, *Trends Biotechnol.* **2014**, *32*, 363.
[4] R. Feiner, T. Dvir, *Nat. Rev. Mater.* **2018**, *3*, 17076.
[5] a) D.-H. Kim, R. Ghaffari, N. Lu, J. A. Rogers, *Annu. Rev. Biomed. Eng.* **2012**, *14*, 113; b) L. Wang, D. Chen, K. Jiang, G. Shen, *Chem. Soc. Rev.* **2017**, *46*, 6764.
[6] a) G. Schwartz, B. C.-K. Tee, J. Mei, A. L. Appleton, D. H. Kim, H. Wang, Z. Bao, *Nat. Commun.* **2013**, *4*, 1859; b) J. Heikenfeld, A. Jajack, J. Rogers, P. Gutruf, L. Tian, T. Pan, R. Li, M. Khine, J. Kim, J. Wang, *Lab Chip* **2018**, *18*, 217.
[7] a) D. Quesada-González, A. Merkoçi, *Chem. Soc. Rev.* **2018**, *47*, 4697; b) F. Xu, W. Lu, Y. Zhu, *ACS Nano* **2011**, *5*, 672.
[8] M. Kaltenbrunner, T. Sekitani, J. Reeder, T. Yokota, K. Kuribara, T. Tokuhara, M. Drack, R. Schwödiauer, I. Graz, S. Bauer-Gogonea, *Nature* **2013**, *499*, 458.
[9] a) S.-K. Lee, B. J. Kim, H. Jang, S. C. Yoon, C. Lee, B. H. Hong, J. A. Rogers, J. H. Cho, J.-H. Ahn, *Nano Lett.* **2011**, *11*, 4642; b) S. Choi, H. Lee, R. Ghaffari, T. Hyeon, D. H. Kim, *Adv. Mater.* **2016**, *28*, 4203.
[10] a) W. J. Paschoalino, S. Kogikoski Jr., J. T. Barragan, J. F. Giarola, L. Cantelli, T. M. Rabelo, T. M. Pessanha, L. T. Kubota, *ChemElectroChem* **2019**, *6*, 10; b) Y. Zhang, L. Zhang, K. Cui, S. Ge, X. Cheng, M. Yan, J. Yu, H. Liu, *Adv. Mater.* **2018**, *30*, 1801588; c) D. Ha, Z. Fang, N. B. Zhitenev, *Adv. Electron. Mater.* **2018**, *4*, 1700593.
[11] D. Tobjörk, R. Österbacka, *Adv. Mater.* **2011**, *23*, 1935.
[12] P. Mostafalu, S. Sonkusale, *RSC Adv.* **2015**, *5*, 8680.
[13] a) D. M. Cate, J. A. Adkins, J. Mettakoonpitak, C. S. Henry, *Anal. Chem.* **2015**, *87*, 19; b) T. Akyazi, L. Basabe-Desmonts, F. Benito-Lopez, *Anal. Chim. Acta* **2018**, *1001*, 1; c) C. M. Pandey, S. Augustine, S. Kumar, S. Kumar, S. Nara, S. Srivastava, B. D. Malhotra, *Biotechnol. J.* **2018**, *13*, 1700047.

© 2019 The Authors. Published by WILEY-VCH Verlag GmbH & Co. KGaA, Weinheim

[14] C. Hagiopol, J. W. Johnston, *Chemistry of Modern Papermaking*, CRC Press, Boca Raton, FL **2011**.
[15] W. Xiao, J. Huang, *Langmuir* **2011**, *27*, 12284.
[16] a) D. D. Liana, B. Raguse, J. J. Gooding, E. Chow, *Sensors* **2012**, *12*, 11505; b) E. Morgan, I. Wilson, *Chromatographia* **2004**, *60*, 135; c) R. M. Rocco, *Landmark Papers in Clinical Chemistry*, Elsevier, Amsterdam/New York **2005**; d) H. G. Kunkel, A. Tiselius, *J. Gen. Physiol.* **1951**, *35*, 89.
[17] H. Liu, Y. Xiang, Y. Lu, R. M. Crooks, *Angew. Chem.* **2012**, *124*, 7031.
[18] M. P. Allen, Google Patents, **1995**.
[19] a) A. W. Martinez, S. T. Phillips, M. J. Butte, G. M. Whitesides, *Angew. Chem., Int. Ed.* **2007**, *46*, 1318; b) B. Liu, D. Du, X. Hua, X. Y. Yu, Y. Lin, *Electroanalysis* **2014**, *26*, 1214.
[20] a) T. H. Nguyen, A. Fraiwan, S. Choi, *Biosens. Bioelectron.* **2014**, *54*, 640; b) C. Desmet, C. A. Marquette, L. J. Blum, B. Doumèche, *Biosens. Bioelectron.* **2016**, *76*, 145.
[21] A. C. Siegel, S. T. Phillips, M. D. Dickey, N. Lu, Z. Suo, G. M. Whitesides, *Adv. Funct. Mater.* **2010**, *20*, 28.
[22] a) J. Zhou, T. Fukawa, H. Shirai, M. Kimura, *Macromol. Mater. Eng.* **2010**, *295*, 671; b) T. Mäkelä, S. Jussila, M. Vilkman, H. Kosonen, R. Korhonen, *Synth. Met.* **2003**, *135–136*, 41.
[23] a) M. Afonso, J. Morgado, L. Alcácer, *J. Appl. Phys.* **2016**, *120*, 165502; b) A. Kaidatzis, V. Psycharis, M. G. Sagardoy, J. G. Martín, D. Niarchos, presented at *6th Int. Conf. on Materials and Applications for Sensors and Transducers - IC-MAST*, Athens, Greece, September **2016**; c) W. J. Hyun, O. O. Park, B. D. Chin, *Adv. Mater.* **2013**, *25*, 4729; d) S. Kumar, M. Willander, J. G. Sharma, B. D. Malhotra, *J. Mater. Chem. B* **2015**, *3*, 9305.
[24] E. Bihar, S. Wustoni, A. M. Pappa, K. N. Salama, D. Baran, S. Inal, *NPJ Flexible Electron.* **2018**, *2*, 30.
[25] K. K. Jagadeesan, S. Kumar, G. Sumana, *Electrochem. Commun.* **2012**, *20*, 71.
[26] S. Kumar, A. Sen, S. Kumar, S. Augustine, B. K. Yadav, S. Mishra, B. D. Malhotra, *Appl. Phys. Lett.* **2016**, *108*, 203702.
[27] S. Kumar, S. Kumar, S. Srivastava, B. K. Yadav, S. H. Lee, J. G. Sharma, D. C. Doval, B. D. Malhotra, *Biosens. Bioelectron.* **2015**, *73*, 114.
[28] Q. Zhong, J. Zhong, B. Hu, Q. Hu, J. Zhou, Z. L. Wang, *Energy Environ. Sci.* **2013**, *6*, 1779.
[29] H. Ogihara, J. Xie, J. Okagaki, T. Saji, *Langmuir* **2012**, *28*, 4605.
[30] L. Hu, J. W. Choi, Y. Yang, S. Jeong, F. La Mantia, L.-F. Cui, Y. Cui, *Proc. Natl. Acad. Sci. USA* **2009**, *106*, 21490.
[31] a) Y.-Z. Chen, X.-Y. Zhang, J.-J. Xu, N. Zhao, J.-Y. Wu, T. Zhang, *Surf. Coat. Technol.* **2019**, *360*, 87; b) R. Martins, D. Gaspar, M. J. Mendes, L. Pereira, J. Martins, P. Bahubalindruni, P. Barquinha, E. Fortunato, *Appl. Mater. Today* **2018**, *12*, 402.
[32] Z. Wang, R. Pan, C. Xu, C. Ruan, K. Edström, M. Strømme, L. Nyholm, *Energy Storage Mater.* **2018**, *13*, 283.
[33] a) R.-Z. Li, A. Hu, T. Zhang, K. D. Oakes, *ACS Appl. Mater. Interfaces* **2014**, *6*, 21721; b) S. Hu, R. Rajamani, X. Yu, *Appl. Phys. Lett.* **2012**, *100*, 104103.
[34] S. Lyth, S. Silva, *Appl. Phys. Lett.* **2007**, *90*, 173124.
[35] M. Härting, J. Zhang, D. Gamota, D. Britton, *Appl. Phys. Lett.* **2009**, *94*, 193509.
[36] A. Manekkathodi, M. Y. Lu, C. W. Wang, L. J. Chen, *Adv. Mater.* **2010**, *22*, 4059.
[37] H. M. Lee, H. B. Lee, D. S. Jung, J.-Y. Yun, S. H. Ko, S. B. Park, *Langmuir* **2012**, *28*, 13127.
[38] E. Fortunato, N. Correia, P. Barquinha, L. Pereira, G. Gonçalves, R. Martins, *IEEE Electron Device Lett.* **2008**, *29*, 988.
[39] D.-H. Lien, Z.-K. Kao, T.-H. Huang, Y.-C. Liao, S.-C. Lee, J.-H. He, *ACS Nano* **2014**, *8*, 7613.
[40] S. Gong, W. Schwalb, Y. Wang, Y. Chen, Y. Tang, J. Si, B. Shirinzadeh, W. Cheng, *Nat. Commun.* **2014**, *5*, 3132.
[41] L. Yang, A. Rida, R. Vyas, M. M. Tentzeris, *IEEE Trans. Microw. Theory Tech.* **2007**, *55*, 2894.
[42] a) W. Kang, C. Yan, C. Y. Foo, P. S. Lee, *Adv. Funct. Mater.* **2015**, *25*, 4203; b) W. Kang, M. F. Lin, J. Chen, P. S. Lee, *Small* **2016**, *12*, 6370.
[43] a) E. Montibon, M. Lestelius, L. Järnström, K. T. Love, *Nord. Pulp Pap. Res. J.* **2010**, *25*, 473; b) L. Zhang, P. Zhu, F. Zhou, W. Zeng, H. Su, G. Li, J. Gao, R. Sun, C.-p. Wong, *ACS Nano* **2015**, *10*, 1273.
[44] a) S. Song, M. Zhang, Z. He, J. Z. Li, Y. Ni, *Ind. Eng. Chem. Res.* **2012**, *51*, 16377; b) A. Baptista, I. Ferreira, J. Borges, *Cellulose: Medical, Pharmaceutical and Electronic Applications* (Ed: T. Van De Ven), InTech, **2013**; c) A. Barhoum, H. Rahier, R. E. Abou-Zaied, M. Rehan, T. Dufour, G. Hill, A. Dufresne, *ACS Appl. Mater. Interfaces* **2014**, *6*, 2734.
[45] G. Zheng, Y. Cui, E. Karabulut, L. Wågberg, H. Zhu, L. Hu, *MRS Bull.* **2013**, *38*, 320.
[46] G. Nyström, A. Razaq, M. Strømme, L. Nyholm, A. Mihranyan, *Nano Lett.* **2009**, *9*, 3635.
[47] J. Wang, L. Li, C. L. Wong, S. Madhavi, *Nanotechnology* **2012**, *23*, 495401.
[48] S.-L. Chou, J.-Z. Wang, S.-Y. Chew, H.-K. Liu, S.-X. Dou, *Electrochem. Commun.* **2008**, *10*, 1724.
[49] A. Fraiwan, S. Mukherjee, S. Sundermier, H.-S. Lee, S. Choi, *Biosens. Bioelectron.* **2013**, *49*, 410.
[50] K. H. Kim, K. Y. Lee, J. S. Seo, B. Kumar, S. W. Kim, *Small* **2011**, *7*, 2577.
[51] I. Kim, H. Jeon, D. Kim, J. You, D. Kim, *Nano Energy* **2018**, *53*, 975.
[52] A. W. Martinez, S. T. Phillips, G. M. Whitesides, *Proc. Natl. Acad. Sci. USA* **2008**, *105*, 19606.
[53] Y.-H. Chen, Z.-K. Kuo, C.-M. Cheng, *Trends Biotechnol.* **2015**, *33*, 4.
[54] Z. Zhang, W. Xu, N. E. Manicke, R. G. Cooks, Z. Ouyang, *Anal. Chem.* **2012**, *84*, 931.
[55] M.-Y. Hsu, C.-Y. Yang, W.-H. Hsu, K.-H. Lin, C.-Y. Wang, Y.-C. Shen, Y.-C. Chen, S.-F. Chau, H.-Y. Tsai, C.-M. Cheng, *Biomaterials* **2014**, *35*, 3729.
[56] a) R. Derda, S. K. Tang, A. Laromaine, B. Mosadegh, E. Hong, M. Mwangi, A. Mammoto, D. E. Ingber, G. M. Whitesides, *PLoS One* **2011**, *6*, e18940; b) K. Ng, B. Gao, K. W. Yong, Y. Li, M. Shi, X. Zhao, Z. Li, X. Zhang, B. Pingguan-Murphy, H. Yang, F. Xu, *Mater. Today* **2017**, *20*, 32.
[57] V. Kuzmenko, T. Kalogeropoulos, J. Thunberg, S. Johannesson, D. Hägg, P. Enoksson, P. Gatenholm, *Mater. Sci. Eng., C* **2016**, *58*, 14.
[58] X. Ge, A. M. Asiri, D. Du, W. Wen, S. Wang, Y. Lin, *TrAC, Trends Anal. Chem.* **2014**, *58*, 31.
[59] E. Bihar, T. Roberts, M. Saadaoui, T. Hervé, J. B. De Graaf, G. G. Malliaras, *Adv. Healthcare Mater.* **2017**, *6*, 1601167.
[60] G. Ortega, S. Pérez-Rodríguez, E. Reguera, *RSC Adv.* **2017**, *7*, 4921.
[61] Q. Liu, J. Wang, B. Wang, Z. Li, H. Huang, C. Li, X. Yu, P. K. Chu, *Biosens. Bioelectron.* **2014**, *54*, 128.
[62] M. Lee, K. Oh, H.-K. Choi, S. G. Lee, H. J. Youn, H. L. Lee, D. H. Jeong, *ACS Sens.* **2018**, *3*, 151.
[63] M. Ornatska, E. Sharpe, D. Andreescu, S. Andreescu, *Anal. Chem.* **2011**, *83*, 4273.
[64] K. Ghule, A. V. Ghule, B.-J. Chen, Y.-C. Ling, *Green Chem.* **2006**, *8*, 1034.
[65] L. Wang, W. Chen, D. Xu, B. S. Shim, Y. Zhu, F. Sun, L. Liu, C. Peng, Z. Jin, C. Xu, *Nano Lett.* **2009**, *9*, 4147.
[66] R. F. Carvalhal, M. Simão Kfouri, M. H. de Oliveira Piazetta, A. L. Gobbi, L. T. Kubota, *Anal. Chem.* **2010**, *82*, 1162.
[67] L. Y. Shiroma, M. Santhiago, A. L. Gobbi, L. T. Kubota, *Anal. Chim. Acta* **2012**, *725*, 44.

© 2019 The Authors. Published by WILEY-VCH Verlag GmbH & Co. KGaA, Weinheim

[68] a) S. Kumar, S. Kumar, S. Tiwari, S. Srivastava, M. Srivastava, B. K. Yadav, S. Kumar, T. T. Tran, A. K. Dewan, A. Mulchandani, *Adv. Sci.* **2015**, *2*, 1500048; b) Z. Liu, Z. Ma, *Biosens. Bioelectron.* **2013**, *46*, 1; c) K.-J. Huang, D.-J. Niu, W.-Z. Xie, W. Wang, *Anal. Chim. Acta* **2010**, *659*, 102; d) S. W. Lee, K. Hosokawa, S. Kim, O. C. Jeong, H. Lilja, T. Laurell, M. Maeda, *Sensors* **2015**, *15*, 11972.
[69] a) N. J. Ronkainen, S. L. Okon, *Materials* **2014**, *7*, 4669; b) J. Wang, *Analyst* **2005**, *130*, 421.
[70] S. Kumar, M. Umar, A. Saifi, S. Kumar, S. Augustine, S. Srivastava, B. D. Malhotra, *Anal. Chim. Acta* **2019**.
[71] S. Kumar, P. Rai, J. G. Sharma, A. Sharma, B. D. Malhotra, *Adv. Mater. Technol.* **2016**, *1*, 1600056.
[72] C. S. K. Lawrence, S. N. Tan, C. Z. Floresca, *Sens. Actuators, B* **2014**, *193*, 536.
[73] J. Lu, S. Ge, L. Ge, M. Yan, J. Yu, *Electrochim. Acta* **2012**, *80*, 334.
[74] Z. Nie, C. A. Nijhuis, J. Gong, X. Chen, A. Kumachev, A. W. Martinez, M. Narovlyansky, G. M. Whitesides, *Lab Chip* **2010**, *10*, 477.
[75] N. Ruecha, R. Rangkupan, N. Rodthongkum, O. Chailapakul, *Biosens. Bioelectron.* **2014**, *52*, 13.
[76] J. Lankelma, Z. Nie, E. Carrilho, G. M. Whitesides, *Anal. Chem.* **2012**, *84*, 4147.
[77] H. Liu, R. M. Crooks, *Anal. Chem.* **2012**, *84*, 2528.
[78] S. N. Tan, L. Ge, W. Wang, *Anal. Chem.* **2010**, *82*, 8844.
[79] W. Dungchai, O. Chailapakul, C. S. Henry, *Anal. Chem.* **2009**, *81*, 5821.
[80] W. Dungchai, O. Chailapakul, C. S. Henry, *Analyst* **2011**, *136*, 77.
[81] C. Zhao, M. M. Thuo, X. Liu, *Sci. Technol. Adv. Mater.* **2016**, *14*, 054402.
[82] Y. Wang, L. Ge, C. Ma, Q. Kong, M. Yan, S. Ge, J. Yu, *Chem. - Eur. J.* **2014**, *20*, 12453.
[83] N. Dossi, R. Toniolo, E. Piccin, S. Susmel, A. Pizzariello, G. Bontempelli, *Electroanalysis* **2013**, *25*, 2515.
[84] M. Santhiago, L. T. Kubota, *Sens. Actuators, B* **2013**, *177*, 224.
[85] L. Ge, P. Wang, S. Ge, N. Li, J. Yu, M. Yan, J. Huang, *Anal. Chem.* **2013**, *85*, 3961.
[86] J. C. Cunningham, N. J. Brenes, R. M. Crooks, *Anal. Chem.* **2014**, *86*, 6166.
[87] I. Shitanda, T. Yamaguchi, Y. Hoshi, M. Itagaki, *Chem. Lett.* **2013**, *42*, 1369.
[88] S. Ge, W. Liu, L. Ge, M. Yan, J. Yan, J. Huang, J. Yu, *Biosens. Bioelectron.* **2013**, *49*, 111.
[89] J. P. Metters, S. M. Houssein, D. K. Kampouris, C. E. Banks, *Anal. Methods* **2013**, *5*, 103.
[90] P. Rai, S. Oh, P. Shyamkumar, M. Ramasamy, R. E. Harbaugh, V. K. Varadan, *J. Electrochem. Soc.* **2014**, *161*, B3116.
[91] J. L. Delaney, C. F. Hogan, J. Tian, W. Shen, *Anal. Chem.* **2011**, *83*, 1300.
[92] Y. Xu, B. Lou, Z. Lv, Z. Zhou, L. Zhang, E. Wang, *Anal. Chim. Acta* **2013**, *763*, 20.
[93] Y. Wang, J. Xu, C. Ma, S. Li, J. Yu, S. Ge, M. Yan, *J. Mater. Chem. B* **2014**, *2*, 3462.
[94] M. Pozuelo, P. Blondeau, M. Novell, F. J. Andrade, F. X. Rius, J. Riu, *Biosens. Bioelectron.* **2013**, *49*, 462.
[95] S. Cinti, M. Basso, D. Moscone, F. Arduini, *Anal. Chim. Acta* **2017**, *960*, 123.
[96] S. Cinti, C. Minotti, D. Moscone, G. Palleschi, F. Arduini, *Biosens. Bioelectron.* **2017**, *93*, 46.
[97] H. Wang, Y. Jian, Q. Kong, H. Liu, F. Lan, L. Liang, S. Ge, J. Yu, *Sens. Actuators, B* **2018**, *257*, 561.
[98] S. Cinti, R. Cusenza, D. Moscone, F. Arduini, *Talanta* **2018**, *187*, 59.
[99] M. Rahimi-Mohseni, J. B. Raoof, R. Ojani, T. A. Aghajanzadeh, A. B. Hashkavayi, *Int. J. Biol. Macromol.* **2018**, *113*, 648.
[100] X. Zheng, L. Li, K. Cui, Y. Zhang, L. Zhang, S. Ge, J. Yu, *ACS Appl. Mater. Interfaces* **2018**, *10*, 3333.
[101] V. B. C. Lee, N. F. MOHD-NAIM, E. Tamiya, M. U. Ahmed, *Anal. Sci.* **2018**, *34*, 7.
[102] A. W. Martinez, S. T. Phillips, G. M. Whitesides, E. Carrilho, *Anal. Chem.* **2010**, *82*, 3.

© 2019 The Authors. Published by WILEY-VCH Verlag GmbH & Co. KGaA, Weinheim

MUNINDRA
Deva Nand
Delhi Technological University, Shahbad Daulatpur Delhi-India, 110042
kumar.munindra90@gmail.com

Non-linearity of the Single Layer Graphene Field Effect Transistors

Graphene nanoscale ballistic transport FETs (GFETs) is the new emerging and promising technology, which is ready to add new dimension to the nanoelectronics world and egger for replacement of conventional silicon technology. thus, study of characteristic behaviour of the GFET models at radio (GHz) frequency especially static linearity and nonlinearity performance potential. In this work static nonlinearity behaviour of graphene FET under the ballistic transport approach will be elaborate with help of the close mathematic expression for Harmonic distortion and intermodulation distortion and interception points. The second and third order harmonic and intermodulation distortion are studied with help of mathematical analysis of drain current equation formulated using Mckelvey's flux theory (MFT). The presented close expressions are validated through nonlinear large and small signal circuit models as they have been illustrated in literature.

References

[1] S. Rodriguez, A. Smith, S. Vaziri, M. Ostling, M. C. Lemme and A. Rusu, IEEE Transactions on Electron Devices, Vol. 61. No. 8, pp. 3001-3003, 2014.
[2] A. Ul Alam, K. D. Holland, M. Wong, S. Ahmed, D. Kienle, and M. Vaidyanathan, IEEE Transactions on Microwave Theory and Techniques, Vol. 63. No. 12, pp. 3874-3887, 2015.
[3] K. A. Jenkins, D. B. Farmer, S.-J. Han, C. Dimitrakopoulos, S. Oida, and A. Valdes-Garcia, APPLIED PHYSICS LETTERS 103, 173115, 2013.
[4] G. Vincenzi, G. Deligeorgis, F. Coccetti, M. Dragoman, L. Pierantoni, D. Mencarelli, and R. Plana, Solid-state Electron., Vol. 76, pp. 8-12, OCT 2012.

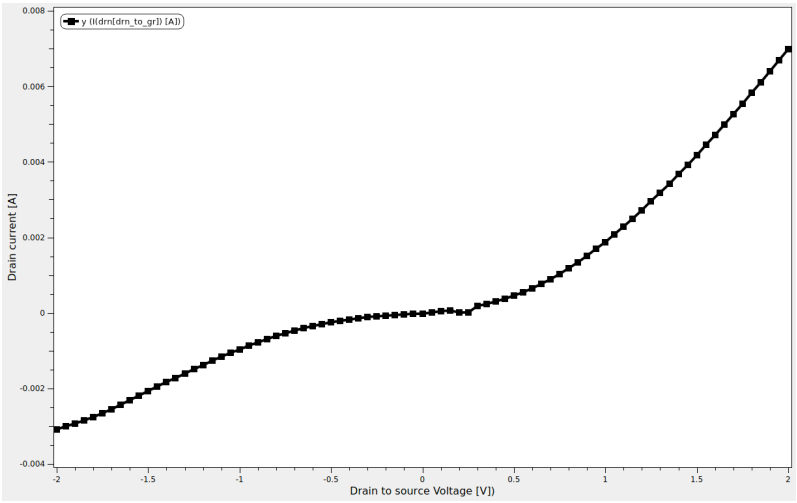

Figure 1: non-linear behavior of the graphene field effect transistors (GFET) shown with help of output characteristic curve at i.e. negative drain current vs negative drain to source Voltage at constant gate voltage of 1 V.

PAPER • **OPEN ACCESS**

Objective functions of distribution network expansion planning - a comprehensive and exhaustive review

To cite this article: Mandhir Kumar Verma *et al* 2019 *IOP Conf. Ser.: Mater. Sci. Eng.* **594** 012016

View the article online for updates and enhancements.

IOP ebooks™

Bringing you innovative digital publishing with leading voices to create your essential collection of books in STEM research.

Start exploring the collection - download the first chapter of every title for free.

This content was downloaded from IP address 14.139.251.100 on 23/09/2019 at 04:58

IOP Conf. Series: Materials Science and Engineering **594** (2019) 012016 doi:10.1088/1757-899X/594/1/012016

Objective functions of distribution network expansion planning - a comprehensive and exhaustive review

Mandhir Kumar Verma[1,*], Vinod Kumar Yadav[2] and V. Mukherjee[1]
[1]Dept. of Electrical Engineering, Indian Institute of Technology, Dhanbad, Jharkhand, India-826004
[2]Dept. of Electrical Engineering, Delhi Technological University, Delhi, India-110042
E-mail: *mandhirverma@gmail.com

Abstract. Utmost of elucidation about the research accomplished in an article is cleared from the objective function of the planning problem. An objective function is a mathematical expression which describe the existing condition of a system with numerous variables, in which alteration of these variables result in optimized value largest or smallest, depending on problem or desired value. That value may be obtained by minimizing or maximizing the objective function. In this paper, a review has been carried out on objective functions of distribution network expansion planning (DNEP). These objective functions have been classified into five main categories: financial, income related, technical, optimal size & location and social & economic. The selection of objective function clearly shows increasing penetration of distributed generation (DG), distributed energy storing systems (DESS) and fuel cells with renewable technologies. Most of the reviewed articles highlight these objectives in details, however; not all fields have been covered in any single work on DNEP. This review article aims to address this gap so that widespread DNEP can be achieved with flawlessness. Substantial information has been offered of research work done in the field of DNEP through this review article which will mitigate the impending researchers from the difficulties of getting apposite supervision.

1. Introduction

The classic objective of the distribution network expansion planning (DNEP) was to fulfil technical necessities (improvement of voltage profile, reliability, reduction of losses etc.). Later on, to ensure an economic and consistent energy supply, foremost aim of DNEP turn into determining an effective and least investment schedule [1]. Decision making progression becomes more complex task when one deals simultaneously to cover maximum aspects of the problem. Another characteristic features of distribution network operation and scheduling is that the judgement making problem is to be encountered with substantial level of ambiguous information. With more penetration of DG, the normal distribution networks becomes active distribution network. Depending upon the objectives functions considered for the expansion planning of distribution network, DNEP problem can be categorize into mono-objective problem and multi-objective problem [2]. The review of various articles reflects the shifting of DNEP from few objectives to multi-objective fulfillment. This paper provides a review on various objective functions utilized by various eminent researchers in the field of DNEP. These objective functions have been classified into five main categories: financial, income related, technical, optimal size & location and social & economic objectives. For original articles on various DNEP [1-80], literature survey has been summarized in tables 1-5.

Financial objectives are the most utilized objective function [1, 2, 4-19, 20-23, 25-33, 35-50, 52-61, 63-76, 78-80] which are categorize into two types: minimization of total expansion cost and maximization of distribution companies (DISCO's) net profit. Income related objectives functions have been separated out from the financial one [14, 49, 75] as these are essentially earnings of DISCO's that can be obtained by selling energy, getting subsidies in lieu of green technologies or by salvage cost.

Content from this work may be used under the terms of the Creative Commons Attribution 3.0 licence. Any further distribution of this work must maintain attribution to the author(s) and the title of the work, journal citation and DOI.
Published under licence by IOP Publishing Ltd

Concrete DNEP starts with technical objectives, which are the most affected part while doing expansion. These are classified into five types: energy losses minimization [3, 8, 15, 20, 33, 35, 45, 51, 53, 62, 67, 69, 70, 80], voltage stability & profile improvement [3, 13, 34, 45, 47, 51, 62, 67, 70, 80], reliability improvement [2, 6, 7, 21, 36, 69], line loading minimization [24, 77] and optimal power flow (OPF) solution [51]. While doing DNEP, it is obvious that new devices, equipment, switches [76], substations [2, 14] as well as DG and DESS [76] are needed to be installed. Among these, optimal sitting and sizing of DG is second most prominent objective function among all type of classifications. Few researchers have also given concerns of customer's profit and reducing planers workload while doing DNEP. These two concerns have been taken as maximization of social welfare function objective [77] and load forecasting [14].

The rest of the survey is organized into seven sections. These sections are divided mainly on basis of objective function classification. Section two is dedicated to classification of objective functions. A brief review on objective functions related to financial matter is mentioned in section three. Income related objectives are introduced and discussed in section four. Objective functions related to technical matter are outlines and classifies in section five. Optimal size and location objectives functions for DG, DESS, substation etc. are summarized in section six. A few researchers have also given attention to social and economic objectives which is presented in section seven. Finally section eight concludes the article along with short comings and future prospects.

2. Classification of objective functions

Depending upon aim of DNEP, objective functions are decided. The DNEP can be framed as a single-objective or a multi-objective expansion planning problem. Various objective functions considered by numerous renowned researchers have been taken in analogical order which depicts changing trends in selection of objective function. From the analysis of various objective functions, their classification and hierarchical distribution is performed and is summarized in Table 1.

According to review performed on various articles, it has been deducted that most prominent objective is to minimize total expansion cost. Rests are in total equivalent to this single objective alone. If a researcher has considered the problem as mono-objective, a single most optimal solution can be obtained but in case of multi objective problem, the objective become conflicting in it selves which have normally set of solutions rather than a unique and single solution [76]. Customarily multi-objective DNEP optimization technical hitches require minimizing or maximizing objective function ($f(x)$) as

$$f_{min}(x) = \left(f_1(x), f_2(x), \cdots f_n(x)\right) \quad (1)$$

$$f'_{max}(x) = \left(f_1'(x), f_2'(x), \cdots f_m'(x)\right) \quad (2)$$

s.t. various technical, economic, geographical etc. constraints. Discussion on constraints is not included in this review article.

Table 1. Objective functions classification of DNEP

S. No.	Objective functions	Reviewed articles	No. of research work reviewed*	%age of research work reviewed
	Financial objectives			
1	Minimization of total expansion cost	[1,2,4-19,21-23,25-33,35-50,52-61, 63-76,78-80]	73	91.25%
2	Maximization of net profit of DISCO's	[20,75]	2	02.50%
	Income related objectives			
3	Selling energy	[14,49,75]	3	03.75%
4	Award subsidies	[49]	1	01.25%
5	Salvage cost	[49,52]	2	02.50%
	Technical objectives			
6	Minimization of energy losses	[3,8,15,20,33,35,45,51,53,62, 67,69,70,80]	14	17.50%
7	Voltage stability & profile improvement	[3,13,34,45,47,51,62,67,70,80]	10	12.50%
8	Reliability improvement	[2,6,7,21,36,69]	6	07.50%
9	Optimal power flow (OPF) solution	[24,77]	2	02.50%
10	Minimize line loading	[51]	1	01.25%
	Optimal size and location (OSL) objectives			
11	OSL of DG	[10,11,16,22-24,26,27,32,33,36,37, 39,40,42,45,46,53,62,65-68,71,74, 75, 77,78,80]	29	36.25%
12	OSL of substation	[2,14,21]	3	03.75%
13	OSL of DESS	[76]	1	01.25%
14	OSL of switching devices	[76]	1	01.25%
	Social and economic objectives			
15	Maximization of social welfare function	[77]	1	01.25%
16	Load forecasting	[14]	1	01.25%

* The numeric values of number of papers and the percentage calculated on the basis of total papers reviewed in the references
**is done by cost reduction method also.

3. Financial objective functions

Objective functions related to finance are mainly of two types: primarily related to expenditure for expansion and secondly concerning profit for distribution companies (DISCO's).

3.1 Total expansion cost

DNEP models aims for finding the most cost-effective solution through minimizing investment cost in various equipment's, in their operation and maintenance and can be mentioned as exhaustive objective. Total expansion cost is highest taken objective function (with 91.3% reviewed work) (from Table 1). Besides equipment's concern, there are expenditure in energy losses, poor reliability, power imported, punishment for pollution and many more miscellaneous objective functions related to investment such as reinforcement costs, interest rate, cost of violating bus voltage limits and line loading limits, load curtailment cost, start-up costs (from either a cold stop or a hot stop), DSM incentive cost etc (Table 2).

Table 2. Various objective functions of DNEP related to expansion cost

S. No.	Objective function related to expansion cost	Reviewed articles	No. of research work reviewed	%age of research work reviewed
1	Installation	[1,2,4-19,21-23,25-33,35-49,52-61,63-76,78-80]	72	90.00%
2	Operation	[4,5,9-11,14-16,18,21,22,25,27,33,36-41,43-45,47-49,52,54, 56,58,60,61,63,66-68,71,74,75,78-80]	42	52.50%
3	Energy losses	[8,9,12,15,17,18,21,23,26-33,35,37-41,43,44,46, 48,49,52-58,61,64-66,68,69,73]	41	51.30%
4	Maintenance	[8-11,16,18,21,27,31-33,37-40,49,52,54,60,61,64,66,68,69, 71,72,75,80]	28	35.00%
5	Reliability index	[6,7,10,11,17,22,23,26-28,30-32,38-40,43,45,49,52,54,56,61, 63,64,68,72,73]	28	35.00%
6	Power imported	[16,23,25-27,33,43,49,50,56,59-61,66-68,71,72, 74,75,78, 79]	22	27.50%
7	Carbon punishment	[25,27,33,35,56,71]	06	07.50%
8	Miscellaneous	[6-11,17,23,26,28,30-32,35,38-40,43,48,52,58,61, 64,66,69, 72,73]	27	33.80%

Table 3. Various objective functions of DNEP related to installation cost

S. No.	Objective function related to inst. cost	Reviewed articles	No. of research work reviewed	%age of research work reviewed
1.	DG	[13,16,22,23,25-27,32,33,36,39,40,42,45,47,49,53,54,56, 58-61, 65-68,70,71,73-75,78,80]	34	42.50%
2.	Substations	[2,6,7,13-15,17,18,21,22,30,31,36-38,41,42,44-46,48,52,54-56, 58,59,61,65,66,67,69,70,74]	34	42.50%
3.	Distribution cable	[1,2,4-9,12,14,16-19,23,29,35,37,38,41,44,45,48,55,58,65,66,69, 72,78]	30	37.50%
4.	Feeders	[2,6,7,13,15,21,22,28,30,37,38,42,46,54,56, 59,61,64,67,68,70,74]	22	27.50%
5.	Transformers	[1,6,7,12,17,29,54,61,64,67]	10	12.50%
6.	Sectionalizing switches	[21,23,28,30,37,64,76]	07	08.75%
7.	DESS	[63,66,72,75,76,78,79]	07	08.75%
8.	Capacitors bank	[48,57,65,73]	04	05.00%
9.	New load points	[43,52]	02	02.50%
10.	Voltage regulators	[57,65]	02	02.50%
11.	Circuit breakers	[28]	01	01.25%
12.	Fuel cells	[73]	01	01.25%

3.1.1 *Installation cost.* This objective function is supreme prominent one among all expansion cost objective functions. The survey results are shown in Table 3 from which it can be concluded that 90% literature reviewed uses installation cost as one of the objective functions. Installation mainly includes those equipments which are back bone of distribution system and comprises of feeders, substations, transformers, reactive power sources (capacitor banks, inductors etc.), sectionalizing switches, protective devices (voltage regulators, circuit breakers etc.), fuel cells, distribution cable/line/conductors/branch, DG, DESS, new load points.

3.1.2 *Operation cost.* After installation of various devices, most of them also required financial assistance for their smooth operation and long life. The operation cost of electrical equipment's and devices have been considered in various articles which are summarize in Table 4. From Table 2 it can be concluded that 52.5% literature reviewed uses operation cost as objective function. These equipment and devices are: DG, substations, feeders, new branches, DESS, transformers and fuel cells.

3.1.3 *Maintenance cost.* All new and old equipment require maintenance whose cost is to be included in main objective function of DNEP and 35% literature reviewed uses maintenance cost as objective function.

3.1.4 *Energy losses cost.* In most of the cases, the losses cost is considered as energy losses and 51.3% literature reviewed uses energy loss cost as objective function.

3.1.5 *Reliability index.* 35% literature reviewed uses poor reliability cost as objective function. This function has also been termed as: costs of interruptions [17], reliability cost [22], non-distributed energy costs [23], cost for system reliability [27], customer interruption cost [28], energy not delivered cost [31], interruption cost [38], energy not served penalty cost [39,40], cost of energy not distributed (END) [45], energy not supplied cost [49], unserved energy cost [54], penalties cost for undelivered services [64], cost of load not served [72], expected customer outage cost (ECOST) [73] in various articles.

3.1.6 *Cost of power imported.* Power has been imported from big producers in case: the distribution network is operated by private players or there is increase in power demand and DISCOs are not interested in setting up DG or DESS options. 27.5% literature reviewed uses cost of power purchased as objective function. Depending upon the requirement, DISCOs can purchase active and reactive powers separately.

3.1.7 *Carbon punishment.* Pollution or carbon punishment is also termed as carbon emission cost or environmental compensation costs [33] or CO2 emission tax [71]. 7.5% literature reviewed (which has considered non-renewable resources-based DG) uses carbon punishment cost as objective function.

3.1.8 *Miscellaneous.* A few eminent researchers have considered some investment cost other than described above. Its summarized literature is given in Table 2 from which it can be concluded that 33.8% literature reviewed uses miscellaneous costs as objective function. Summarize in Table 5, these costs are reinforcement costs [10-12, 23, 25, 42, 43, 48, 49, 52, 57, 60, 64, 68, 71, 72] or re-conductoring or reinstallation cost, which is mainly done to strengthen the existing structure and is utilized in 20% of surveyed literature. The cost incurred in paying interest rate against the loan amount taken for expansion have been considered by [8, 9, 28, 48, 69] and is utilized in 6.25% of surveyed literature. Cost of violating limits (violating the bus voltage and line loading limits) [39, 40, 43] and is utilized in 3.75 % of surveyed literature, load (or DG) curtailment cost [35, 58] and is utilized in 2.5% of surveyed literature, start-up costs (from either a cold stop or a hot stop) [43] and is utilized in 1.25% of surveyed literature and demand side management (DSM) incentive cost [66] and is utilized in 1.25% of surveyed literature.

Table 4. Various objective functions of DNEP related to operation cost

S. No.	Objective function related to operation cost	Reviewed articles	No. of research work reviewed*	%age of research work reviewed
1.	DG	[16,22,25,27,33,36,39,40,43,45,47, 49,54,56,58, 60,61, 66-68,71,74,75, 78,80]	25	31.25%
2.	Substations	[17,18,21,22,36-38,41,44,45,48,52, 61,64,65]	15	18.75%
3.	Feeders	[15,21,22,37,38, 54,61,64]	8	10.00%
4.	New branches	[9,17,37,38,41,45,69]	7	08.75%
5.	DESS	[63,66,72,75]	4	05.00%
6.	Transformers	[15,17,61]	3	03.75%
7.	Fuel Cells	[73]	1	01.25%

Table 5. Various objective functions of DNEP related to miscellaneous cost

S. No.	Miscellaneous objective function	Reviewed articles	No. of research work reviewed*	%age of research work reviewed
1.	Reinforcement costs	[10-12,23,25,42,43, 48,49,52,57, 60,64,68,71,72]	16	20.00%
2.	Interest rate	[8,9,28,48,69]	5	06.25%
3.	Cost of violating limits	[39,40,43]	3	03.75%
4.	Load/DG curtailment cost	[35,58]	2	02.50%
5.	Start-up costs	[43]	1	01.25%
6.	DSM incentive cost	[66]	1	01.25%

3.2 DISCO's net profit maximization

It has been observed at some occasions that DISCOs are considered as sole owner of DG units whereas sometimes DG units are the investment made by external investors. For both these cases the objective function for maximizing net profit of DISCO's are different. In case DISCO does not expand the distribution system and purchase power from private investors, the objective function will be described as DISCO's profit index function ($DNP_{max,1}$) in which all terms are considered per year. In second case, DISCOs are considered as sole owner of DG units [75]. Both active and reactive powers are included in DNEP and DGs & DESSs are optimally scheduled to escalate profit of DISCO.

4. Income related objectives

The earnings and savings of DISCO's are considered in income related objectives. They are mainly of three types: selling energy, award of subsidies, salvage cost.

4.1 Selling energy

This objective is related to income from electricity sales, which in turn depends upon the tariffs according to type of customers. [14] has managed this objective with the help of geographic information system (GIS) based production management system (PMS) software. [49, 75] more precisely explain this objective by separating out active (P_r) and reactive (Q_r) power sale.

4.2 Award subsidies

DISCO's can be encouraged to use cleaner technologies, and to reduce carbon emission. In lieu of green technologies utilization for power production, DISCO's can be awarded subsidies [49] which will add to their income.

4.3 Salvage cost
[49] has also introduce salvage cost of DG units obtained at the end of planning period. This cost function can also be considered for other equipment.

5. Technical objectives
While doing DNEP, the study reveals that investment part has become more prominent then technical issues. Still without fulfilling technical objectives, DNEP can't be achieved. These are mainly energy losses minimization, voltage stability & profile improvement, reliability improvement, minimization of line loading and optimal power flow (OPF) solution.

5.1 Energy losses minimization
Energy losses minimization is the most utilized technical function (17.5%). Minimization of energy losses is also done by cost reduction method in some reviewed articles.

5.2 *Voltage stability & profile improvement*
Most of the researchers have maintained voltage stability by taking this objective as constraint. A few have taken it as objective function. The second most considered technical objective (12.5%), voltage stability & profile improvement is evaluated mainly by determining voltage stability index (VSI_{WN}) of whole distribution network [80].

5.3 Reliability improvement
Just like energy losses minimization objective, reliability improvement is also done by considering it as financial objective by many researchers. Reliability improvement (7.5%) is measured with the help of reliability index factor which is acknowledged by many names in available text [2, 6, 7, 21, 36, 69]. Most of the researchers have considered reliability as one of the main objective term but, in few reviewed articles, reliability has been considered as a constraint instead of objective function. Lowest $\mathcal{RI}$ factor shows better system reliability.

5.4 Minimize line loading
While doing DNEP with placement of reactive power sources and DG, overloading of few lines in network system occurs due to their incongruous engagement [51]. To determine intensity of line loading, indexing of line loading (LLI_{min}) is formulated w.r.t. its maximum power carrying capacity.

5.5 Optimal power flow (OPF) solution
Many articles encountered which are dedicated to advance and hybrid OPF methods for distribution networks. They are omitted because they are not dedicated to DNEP. Only few (2.5%) are found to be engaged in DNEP with also providing OPF solution [24, 77].

6. Optimal size and location (OSL) objectives
While doing DNEP, it is obvious that new devices, equipment, substations as well as DG and DESS are needed to be installed. Their optimal size and location determination is also important objectives which are taken by many researchers and are described below.

6.1 OSL of DG
After total expansion cost minimization objective function, OSL of DG objective is found to be second most employed objective function (37.5%) which is decided with the help of penetration capacity of DG.

6.2 OSL of substation
This objective function has been detected in few reviewed articles [2, 14, 21] and has been fulfilled with the help of software, product management system (PMS) which operates and provides results on the basis of practical geographical information system (GIS). The size has been decided by present demand and future uncertainty whereas location can be determined mathematically. To distinguish physical

distance and electrical distance between load center and substation locations, a correction factor with statistical sampling of prevailing low voltage feeders is obtained. This correction factor is termed as K.

6.3 OSL of DESS
[76] has decided OSL of DESS on the basis of reliability improvement factor. The reliability indexes are associated with momentary interruptions in case of determining OSL of battery banks. Momentary interruptions have been defined and evaluated with the help of MAIFI (Momentary Average Interruption Frequency Index).

6.4 OSL of switching devices
Similar to determination of OSL of DESS, [76] has determine the OSL of switching devices on the basis of long interruptions of power supply. Long interruptions have been defined and evaluated with the help of SAIDI (System Average Interruption Duration Index).

7. Social and economic objectives
While undertaking DNEP, a few researchers have also consider concerns of customer's profit and reducing planers workload. These two concerns have been taken as maximization of social welfare function objective and load forecasting.

7.1 Maximization of social welfare function
The social welfare function is a real-valued and differentiable term belongs to welfare economics. When applied to power systems, it can be defined as difference of end consumer's benefit and total cost of power produced [77] (both active and reactive power production) of DISCOs.

7.2 Load forecasting
[14] has utilize a decision-making support system software named as geographic information system (GIS) based production management system (PMS) which has been implemented on a practical system. Along with other objective fulfillment, this software also reduces the planner workload by doing load forecasting.

8. Conclusion
The sequence of this review study has considered a wide-ranging review of objective functions to be fulfilled while doing DNEP and found the changing trend of DNEP initially with reinforcement, then with new substations, conductoring, and then with penetration of DG in distribution network converting them into micro grids, then came utilization of DESS and last but not least utilization of fuel cells. Each article has utilized various and limited objectives to solve DNEP problems. The reviewed work shows that for achieving similar intentions of DNEP, different objective functions have been considered by various eminent researchers. A few objectives are there such as reliability improvement, energy losses etc. which have been considered by a few researchers as financial objective functions whereas by few as non-financial objective functions. This confusion should be removed and there inclusion must be done in single type of objective function. With increased penetration of green and proficient supply sources, the objectives of DNEP have moved from low cost solutions to somewhat expansive solutions. This review article aims to address this gap so that complete DNEP can be achieved with perfection. The suggested objective functions need to be enriched and articulated for application to a DNEP with multiple types of objective functions. It is also found that due to different regulations of each country, a few objectives have been taken by very less researchers such as carbon penalty, DCM incentive cost etc. these objective functions are prominent one and must be included by various DISCOs in general practice. It is anticipated that this review will be beneficial to the operators, engineers, manufacturers, scholars involved with DNEP for developing new strategies.

References

[1]. Carvalho P M S, Ferreira L A F M, Lobo F G and Barruncho L M F 2000 Distribution network expansion planning under uncertainty: a hedging algorithm in an evolutionary approach Power Delivery 15(1) 412-16.

[2]. Rosado I J R and Agustín J L B 2001 Reliability and costs optimization for distribution networks expansion using an evolutionary algorithm Power Systems 16(1) 111-18.
[3]. Asakura T, Genji T, Yura T, Hayashi N, and Fukuyama Y 2003 Long-term distribution network expansion planning by network reconfiguration and generation of construction plans Power Systems 18(3) 1196-204.
[4]. Vaziri M, Tomsovic K and Bose A 2004 A directed graph formulation of the multistage distribution expansion problem Power Delivery 19(3) 1335-41.
[5]. Vaziri M, Tomsovic K and Bose A 2004 Numerical analyses of a directed graph formulation of the multistage distribution expansion problem Power Delivery 19(3) 1348-54.
[6]. Fletcher R H and Strunz K 2007 Optimal distribution system horizon planning-part I: formulation Power Systems 22(2) 791-99.
[7]. Fletcher R H and Strunz K 2007 Optimal distribution system horizon planning-part II: application Power Systems 22(2) 862-70.
[8]. Carrano E G, Guimaraes F G, Takahashi R H C, Neto O M and Campelo F 2007 Electric distribution network expansion under load-evolution uncertainty using an immune system inspired algorithm Power Systems 22(2) 851-61.
[9]. Carrano E G, Cardoso R T N, Takahashi R H C, Fonseca C M and Neto O M 2008 Power distribution network expansion scheduling using dynamic programming genetic algorithm IET Gen., Trans. & Dist. 2(3) 444-55.
[10]. Haffner S, Pereira L F A, Pereira L A and Barreto L S 2008 Multistage model for distribution expansion planning with distributed generation-part I: problem formulation Power Delivery 23(2) 915-23.
[11]. Haffner S, Pereira L F A, Pereira L A and Barreto L S 2008 Multistage model for distribution expansion planning with distributed generation-part II: numerical results Power Delivery 23(2) 924-29.
[12]. Cossi A M, Romero R and Mantovani J R S 2009 Planning and projects of secondary electric power distribution systems Power Systems 24(3) 1599-608.
[13]. Mori H and Yoshida T 2009 An efficient multi-objective memetic algorithm for uncertainties in distribution network expansion planning IEEE Power & Energy Society General Meeting, Calgary, AB pp 1-6.
[14]. Luo F et al. 2009 A practical GIS-based decision-making support system for urban distribution network expansion planning International Conference on Sustainable Power Generation and Supply, Nanjing 1-6.
[15]. Najafi S, Hosseinian S H, Abedi M, Vahidnia A and Abachezadeh S 2009 A Framework for optimal planning in large distribution networks Power Systems 24(2) 1019-28.
[16]. Ouyang W, Cheng H, Zhang X, Yao L and Bazargan M 2010 Distribution network planning considering distributed generation by genetic algorithm combined with graph theory Electric Power Comp. and Systems 38(3) 325-39.
[17]. Popovic Z N and Popovic D S 2010 Graph theory based formulation of multi-period distribution expansion problems Elec. Power Sys. Research 80 1256-66.
[18]. Lavorato M, Rider M J, Garcia A V and Romero R 2010 Constructive heuristic algorithm for distribution system planning Power Systems 25(3) 1734-42.
[19]. Wang D T C, Ochoa L F and Harrison G P 2011 Modified GA and data envelopment analysis for multistage distribution network expansion planning under uncertainty Power Systems 26(2) 897-904.
[20]. Hsieh S C 2011 Bi-objective planning for distributed generations in distribution systems using Particle Swarm Optimization and Compromise Programming 4th Int. Conf. on Electric Utility Deregulation and Restruct. and Power Technologies (DRPT), Weihai, Shandong pp 168-173.
[21]. Sahoo N C, Ganguly S and Das D 2011 Simple heuristics-based selection of guides for multi-objective PSO with an application to electrical distribution system planning Engineering Applications of Artificial Intelligence 24 567-85.
[22]. Falaghi H, Singh C, Haghifam M R, Ramezani M 2011 DG integrated multistage distribution system expansion planning Elect. Power and Energy Sys. 33 1489-97.
[23]. Martins V F and Borges C L T 2011 Active distribution network integrated planning incorporating distributed generation and load response uncertainties Power Systems 26(4) 2164-72.
[24]. Sun H, Nikovski D, Ohno T, Takano T and Kojima Y 2011 A fast and robust load flow method for distribution systems with distributed generations Energy Procedia 12 236-44.
[25]. Soroudi A, Ehsan M and Zareipour H 2011 A practical eco-environmental distribution network planning model including fuel cells and non-renewable distributed energy resources Renewable Energy 36 179-88.
[26]. Borges C L T and Martins V F 2012 Multistage expansion planning for active distribution networks under demand and Distributed Generation uncertainties Elect. Power and Energy Sys. 36 107-16.
[27]. Zou K, Agalgaonkar A P, Muttaqi K M and Perera S 2012 Distribution system planning with incorporating DG reactive capability and system uncertainties Sust. Energy 3(1) 112-23.

[28]. Salehi J and Haghifam M R 2012 Long term distribution network planning considering urbanity uncertainties Elect. Power and Energy Sys. 42 321-33.
[29]. Mendoza J E, López M E, Pena H E and Labra D A 2012 Low voltage distribution optimization: Site, quantity and size of distribution transformers Elec. Power Sys. Research 91 52– 60.
[30]. Cossi A M, Silva L G W D, Lazaro R A R and Mantovani J R S 2012 Primary power distribution systems planning taking into account reliability, operation and expansion costs IET Gen., Tran. & Dist. 6(3) 274-84.
[31]. Tarôco C G, Carrano E G, Takahashi R H C and Neto O M 2012 A faster genetic algorithm for substation location and network design of power distribution systems IEEE Congress on Evolutionary Computation Brisbane QLD pp 1-6.
[32]. Millar R J, Kazemi S, Lehtonen M and Saarijarvi E 2012 Impact of MV connected microgrids on MV distribution planning Smart Grid 3(4) 2100-08.
[33]. Junjie M, Yulong W and Yang L 2012 Size and location of distributed generation in distribution system based on immune algorithm Systems Engineering Procedia 4 124-32.
[34]. Hu Z and Li F 2012 Cost-benefit analyses of active distribution network management, part I: annual benefit analysis Smart Grid 3(3) 1067-74.
[35]. Hu Z and Li F 2012 Cost-benefit analyses of active distribution network management, part II: investment reduction analysis Smart Grid 3(3) 1075-81.
[36]. Gitizadeh M, Vahed A A and Aghaei J 2013 Multistage distribution system expansion planning considering distributed generation using hybrid evolutionary algorithms App. Energy 10 655-66.
[37]. Ganguly S, Sahoo N C and Das D 2013 Multi-objective particle swarm optimization based on fuzzy-Pareto-dominance for possibilistic planning of electrical distribution systems incorporating distributed generation Fuzzy Sets and Systems 213 47-73.
[38]. Ganguly S, Sahoo N C and Das D 2013 Multi-objective planning of electrical distribution systems using dynamic programming Elect. Power and Energy Sys. 46 65-78.
[39]. Samper M E and Vargas A 2013 Investment decisions in distribution networks under uncertainty with distributed generation-part I: model formulation Power Systems 28(3) 2331-40.
[40]. Samper M E and Vargas A 2013 Investment decisions in distribution networks under uncertainty with distributed generation-part II: implementation and results Power Systems 28(3) 2341-51.
[41]. Camargo V, Lavorato M and Romero R 2013 Specialized genetic algorithm to solve the electrical distribution system expansion planning IEEE Power & Energy Society General Meeting, Vancouver BC pp. 1-5.
[42]. Saldarriaga C A, Hincapié R A and Salazar H 2013 A holistic approach for planning natural gas and electricity distribution networks Power Systems 28(4) 4052-63.
[43]. Zonkoly A M E 2013 Multistage expansion planning for distribution networks including unit commitment IET Gen., Tran. & Dist. 7(7) 766-78.
[44]. Jabr R A 2013 Polyhedral formulations and loop elimination constraints for distribution network expansion planning Power Systems 28(2) 1888-97.
[45]. Aghaei J, Muttaqi K M, Azizivahed A and Gitizadeh M 2014 Distribution expansion planning considering reliability and security of energy using modified PSO (Particle Swarm Optimization) algorithm Energy 65 398-411.
[46]. Ravadanegh S N and Roshanagh R G 2014 On optimal multistage electric power distribution networks expansion planning Elect. Power and Energy Sys. 54 487-97.
[47]. Muttaqi K M, Le A D T, Negnevitsky M and Ledwich G 2014 An algebraic approach for determination of DG parameters to support voltage profiles in radial distribution networks IEEE Smart Grid 5(3) 1351-60.
[48]. Franco J F, Rider M J and Romero R 2014 A mixed-integer quadratically-constrained programming model for the distribution system expansion planning Elect. Power and Energy Sys. 62 265-72.
[49]. Sadeghi M and Kalantar M 2014 Multi types DG expansion dynamic planning in distribution system under stochastic conditions using covariance matrix adaptation evolutionary strategy and monte-carlo simulation Energy Conversion and Mgt 87 455-71.
[50]. Gill S, Kockar I and Ault G W 2014 Dynamic optimal power flow for active distribution networks IEEE Trans. on Power Systems 29(1) 121-31.
[51]. Gallano R J C and Nerves A C 2014 Multi-objective optimization of distribution network reconfiguration with capacitor and distributed generator placement TENCON IEEE Region 10 Conference, Bangkok, pp 1-6.
[52]. Heidari S, Firuzabad M F and Kazemi S 2015 Power distribution network expansion planning considering distribution automation Power Systems 30(3) 1261-69.
[53]. Murty V V S N and Kumar A 2015 Optimal placement of DG in radial distribution systems based on new voltage stability index under load growth Elect. Power and Energy Sys. 69 246-56.

[54]. Delgado G M, Contreras J and Arroyo J M 2015 Joint expansion planning of distributed generation and distribution networks Power Systems 30(5) 2579-90.
[55]. Miloca S A, Volpi N M P, Yuan J, Pinto C L S 2015 Expansion planning problem in distribution systems with reliability evaluation: An application in real network using georeferenced database Elect. Power and Energy Sys. 70 9-16.
[56]. Bagheri A, Monsef H and Lesani H 2015 Integrated distribution network expansion planning incorporating distributed generation considering uncertainties, reliability, and operational conditions Elect. Power and Energy Sys. 73 56–70.
[57]. Gonçalves R R, Franco J F and Rider M J 2015 Short-term expansion planning of radial electrical distribution systems using mixed-integer linear programming IET Gen., Tran. & Dist. 9(3) 256-66.
[58]. Xing H, Cheng H, Zhang L, Zhang S and Zhang Y 2015 Second-order cone model for active distribution network expansion planning IEEE Power & Energy Society General Meeting, Denver CO pp 1-5.
[59]. Hemmati R, Hooshmand R A and Taheri N 2015 Distribution network expansion planning and DG placement in the presence of uncertainties Elect. Power and Energy Sys. 73 665-73.
[60]. Ahmadigorji M and Amjady N 2015 Optimal dynamic expansion planning of distribution systems considering non-renewable distributed generation using a new heuristic double-stage optimization solution approach App. Energy 156 655-65.
[61]. Shivaiea M, Ameli M T, Sepasian M S, Weinsier P D and Vahidinasab V 2015 A multistage framework for reliability-based distribution expansion planning considering distributed generations by a self-adaptive global-based harmony search algorithm Trans. Reliability Engg. and System Safety 139 68-81.
[62]. Mohan N, Ananthapadmanabha T and Kulkarni A D 2015 A weighted multiobjective index based optimal distributed generation planning in distribution system Procedia Technol. 21 279-86.
[63]. Saboori H, Hemmati R and Jirdehi M A 2015 Reliability improvement in radial electrical distribution network by optimal planning of energy storage systems Energy 93(2) 2299-312.
[64]. Mazhari S M, Monsef H and Romero R 2016 A Multi-Objective Distribution System Expansion Planning Incorporating Customer Choices on Reliability Power Systems 31(2) 1330-40.
[65]. Tabares A, Franco J F, Lavorato M and Rider M J 2016 Multistage long-term expansion planning of electrical distribution systems considering multiple alternatives Power Systems 31(3) 1900-14.
[66]. Xing H, Cheng H, Zhang Y and Zeng P 2016 Active distribution network expansion planning integrating dispersed energy storage systems IET Gen., Tran. & Dist. 10(3) 638-44.
[67]. Sayed M A E and Alsaffar M A 2016 Two stage methodology for optimal siting and sizing of distributed generation in medium voltage network IEEE Green Tech. Conf. (GreenTech) Kansas City MO pp 118-23.
[68]. Ahmadigorji M and Amjady N 2016 A multiyear DG-incorporated framework for expansion planning of distribution networks using binary chaotic shark smell optimization algorithm Energy 102 199-215.
[69]. Tarôco C G, Takahashi R H C and Carrano E G 2016 Multiobjective planning of power distribution networks with facility location for distributed generation Elec. Power Sys. Research 141 562-71.
[70]. Verma M K, Mukherjee V and Yadav V K 2016 Greenfield distribution network expansion strategy with hierarchical GA and MCDEA under uncertainty Elect. Power and Energy Sys. 79 245-52.
[71]. Ahmadigorji M, Amjady N and Dehghan S 2017 A novel two-stage evolutionary optimization method for multiyear expansion planning of distribution systems in presence of distributed generation Applied Soft Computing 52 1098-115.
[72]. Shen X, Shahidehpour M, Han Y, Zhu S and Zheng J 2017 Expansion planning of active distribution networks with centralized and distributed energy storage systems Sust. Energy 8(1) 126-34.
[73]. Hasanvand S, Nayeripour M, Waffenschmidt E and Abarghouei H F 2017 A new approach to transform an existing distribution network into a set of micro-grids for enhancing reliability and sustainability Applied Soft Computing 52 120-34.
[74]. Humayd A S B and Bhattacharya K 2017 Distribution system planning to accommodate distributed energy resources and PEVs Elec. Power Sys. Research 145 1-11.
[75]. Saboori H and Hemmati R 2017 Maximizing DISCO profit in active distribution networks by optimal planning of energy storage systems and distributed generators Ren. and Sust. Energy Reviews 71 365-72.
[76]. Pombo A V, Pinab J M and Pires V F 2017 Multiobjective formulation of the integration of storage systems within distribution networks for improving reliability Elec. Power Sys. Research 148 87-96.
[77]. Mokryani G, Hu Y F, Papadopoulos P, Niknam T and Aghaei J 2017 Deterministic approach for active distribution networks planning with high penetration of wind and solar power Ren. Energy 113 942-51.
[78]. Hemmati R, Saboori H and Siano P 2017 Coordinated short-term scheduling and long-term expansion planning in microgrids incorporating renewable energy resources and energy storage systems Energy 134 699-708.

[79]. Bai L, Jiang T, Li F, Chen H, Li X 2018 Distributed energy storage planning in soft open point based active distribution networks incorporating network reconfiguration and DG reactive power capability App. Energy 210 1082-91.
[80]. Li Y, Feng B, Li G, Qi J, Zhao D, MuY 2018 Optimal distributed generation planning in active distribution networks considering integration of energy storage App. Energy 210 1073-81.

This article has been accepted for publication in a future issue of this journal, but has not been fully edited. Content may change prior to final publication. Citation information: DOI 10.1109/TIA.2019.2933783, IEEE Transactions on Industry Applications

Optimized Resonant Converter by Implementing Shunt Branch Element as Magnetizing Inductance of Transformer in Electric Vehicle Chargers

Vijaya Vardhan Reddy. P, H. M. Suryawanshi, *Senior Member, IEEE,* Girish G. Talapur, and Makarand Sudhakar Ballal, *Senior Member, IEEE*

***Abstract*—An optimized resonant converter with zero voltage switching (ZVS) over extensive range of loading is proposed to integrate renewable energy sources to onboard charger. In conventional resonant circuit high frequency transformer (HF) parasitic components used as tank circuit, due to non-optimal magnetic components degrades the performance. Here, HF transformer is fabricated with optimized resonant tank circuit shunt branch inductance (L_p) as magnetizing inductance hence, eliminates the need for shunt branch inductance. The proposed resonant converter circuit design is optimized for minimum kVA rating, and better voltage regulation with both duty cycle and frequency control (mixed control method). Furthermore, the performance of the converter at very light is improved using proposed control method. Incorporating low $R_{DS}(ON)$ SiC-MOSFET and soft turn off the switches for wide load variation minimizes conduction, switching losses and improves efficiency. Opting powder core for the design of tank circuit reduces magnetic losses. A 3-kW prototype of the converter is built to verify the performance from no load to full load. The higher efficiency of the converter attained is 98.6% at 50% of the full load.**

***Index Terms*—Keywords: High frequency (HF), magnetizing inductance, resonant network, zero-voltage-switching (ZVS).**

I. Introduction

Population explosion and rapid industrialization demands excessive exploitation of fossil fuels to meet the human life power requirements. These non-renewable fossil fuels contribute to global warming, acidic environment and are not eco-friendly. Moreover, these fuels are at the verge of depletion. Aforementioned issues necessitate to more focus on expansion of clean renewable energy sources such as wind energy, photovoltaic arrays and fuels cells [1]-[3]. To maximize energy utilization from these intermittent sources, higher efficiency and wider load variation for such as onboard charger in Electric vehicles, DC-DC converters are widely adopted for these requirements [4]-[6]. In constant charge mode, variation in switching frequency is more than 500kHz for light load range and further losses are higher. Therefore, efficiency should be improved for effective energy utilization. Soft switched resonant converters are widely used to achieve high efficiency, reduced EMI, wide load regulation and high power density. Also, resonant converters are effective candidates for high power and high voltage applications. Therefore, for these application, a step up transformer is required to boost the lower voltage from input energy sources.

Two basic types of resonant converters are reported in the literature, namely, series resonant converter (SRC) and parallel resonant converter (PRC) [7]-[11]. Due to poor load regulation, lower efficiency at light load condition and inability to include the non idealities of the HF transformer these converters are not appropriate for high voltage. The parallel-series LCC resonant circuit have the combined desirable features of SRC and PRC. The LCC converter can operate with good efficiency over a wide range of load variation. HF transformer non idealities can be easily incorporated into the the tank circuit. However, magnetic inductance of the HF transformer is ignored in the analysis, which affects the converter performance drastically [12]-[14]. The dual active bridge (DAB) controlled by phase shift modulation, component stress are lower but this converters have a narrow ZVS range for wide load variation, ripple currents are high [15].

Resonant converter without shunt branch element has poor voltage regulation at light load, the switching frequency need to increase to very high to keep the output voltage regulated. This means more and more energy is circulating in the resonant tank instead of transferred to output, owing to which switching losses increases drastically, ZVS fails and resolution of DSP is limited hence leading to deteriorated performance of the converter.

To overcome the aforementioned issues, shunt branch is introduced for effective regulation at light load condition, but efficiency is low under very light load condition. The benefit of resonant converter with shunt branch is narrow switching frequency range with light load, ZVS capability with even no load and to regulate the output voltage at light load, with proposed mixed control method. Main advantage of the converter [16]-[18], is that the output terminals can even be short-circuited. Under short circuit condition, the entire current is limited by the resonant inductor. The circulating energy is reduced compared to series and parallel resonant circuits. In addition, by using higher-order resonant tanks, the designer has the choice of utilizing the parasitic inductance and capacitance, which always exist in the converter circuit, when

Manuscript received Januaury 30, 2019; revised April 14, 2019 and accepted July 15, 2019. This work was supported by the Department of Science and Technology and Science and Energy Research Board (DST-SERB) under Core Research Grant (CRG) project No. EMR/2017/003243 (*Corresponding author: Vijaya Vardhan Reddy.*)

Vijaya V. Reddy, H. M. Suryawanshi, Girish G. Talapur and Makarand S. Ballal are with the Department of Electrical Engineering, Visvesvaraya National Institute of Technology, Nagpur 440010, India (email id: vardhan258@gmail.com; hms_1963@rediffmail.com; girish223@gmail.com and drmsballal@rediffmail.com)

0093-9994 (c) 2019 IEEE. Personal use is permitted, but republication/redistribution requires IEEE permission. See http://www.ieee.org/publications_standards/publications/rights/index.html for more information.

This article has been accepted for publication in a future issue of this journal, but has not been fully edited. Content may change prior to final publication. Citation information: DOI 10.1109/TIA.2019.2933783, IEEE Transactions on Industry Applications

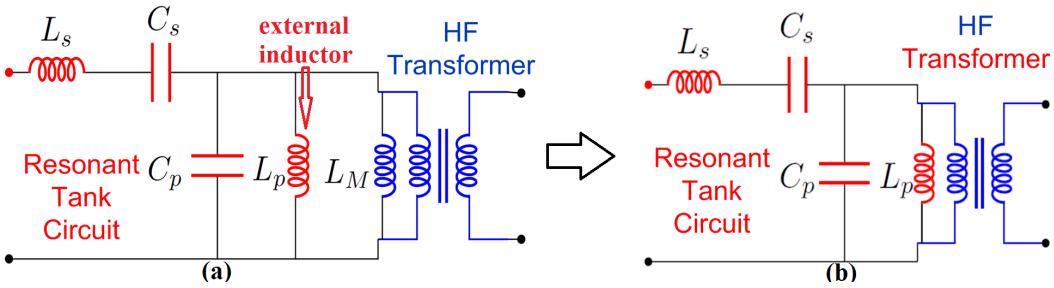

Fig. 1. High-voltage and high power resonant converter. (a) Optimal LC-LC resonant converter with HF transformer. (b) Fabricating with shunt element value (L_p) of Fig. (a) as the magnetizing inductance HF transformer.

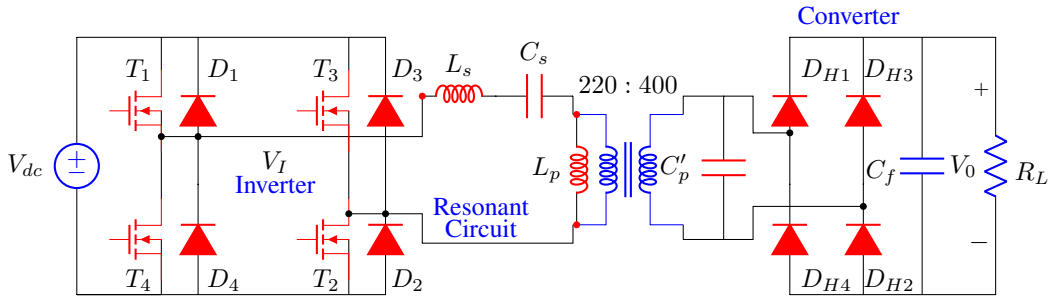

Fig. 2. Modified LC-LC Resonant Converter with shunt element as magnetizing inductance of HF transformer

operated at very high switching frequency. In previous works, first transformer is designed then their parasitic components L_m, C_w, and L_{lk} are employed to realize the resonant tank circuit (L_m, L_{lk}, and C_w are used as parallel inductor, series inductor, and parallel capacitor, respectively) [19]-[20]. However, as large number of turns in the transformer are used for the converter circuit, the non-optimal magnetic components degrade the performance of the converter. Therefore, in this paper based on optimized resonant tank circuit, shunt element of the converter is considered to be fabricated as the magnetising inductance of the HF transformer. Hence, shunt branch in the resonant tank is eliminated and volume of the converter is reduces considerably which improves the power density.

In the last two decades, development of efficient control techniques have been growing interests for dc-dc soft switched resonant converters [21]-[24]. Conventional method of frequency control from 100% load to light load leads to sharp increase in the switching frequency thus increases switching loss, resulting into performance deterioration [25]-[27]. To overcome the issue, hybrid control is introduced to regulate required output voltage. Using this method when switching frequency crosses certain limit then fixed duty cycle is adjusted to maintain constant output at light loading. However, other loading advantages of duty cycle control are ineffective and also the saturation of HF transformer core due to asymmetrical current leads to poor performance of the converter [28]-[29]. In contrast, the proposed converter is implemented with mixed control method where switching frequency and duty cycle are adjusted at the same time from full load to even very light load condition to maintain required output voltage. Moreover, it attains the advantage of wider ZVS operation with narrow range of frequency variation.

This paper presents an optimized resonant converter by manifesting shunt branch as magnetizing inductance of the HF transformer. The proposed resonant converter is optimized for minimum kVA rating and reduced harmonic distortion with mixed control method. Fabricating HF transformer with optimum value of shunt branch inductance (L_p) of the resonant tank circuit as magnetizing inductance eliminates one of the branch of the proposed resonant tank without effecting the performance of the converter. Therefore, volume of the converter is reduced considerably. The proposed mixed control method allows soft switching condition and constructive voltage regulation over wider range of load variation with narrow range of frequency variations. The critical point of proposed converter is the regulation of output voltage even under no load condition. The proposed converter tank circuit magnetic cores are developed using powder core, which have higher permeability, hence reduces the magnetic losses. Proposed converter provides step up voltage without grater turns ratio. Moreover, to reduce conduction losses low on state resistance SiC MOSFETs are used. The proposed converter with mixed control improves the performance of the onboard charger in Electric Vehicle even under very light load condition. Finally, 3-kW prototype of the proposed converter verifies improved performance with experimentation.

II. Circuit Description of Proposed Converter

The proposed optimal resonant converter comprises series and shunt branch elements of L_s, C_s, L_p, and C_p with HF transformer as shown in Fig. 1(a). Designing HF transformer with optimum shunt branch inductance of the resonant circuit as the magnetizing inductance as shown in Fig. 1(b). HF transformer provides step up voltage without higher turns ratio

0093-9994 (c) 2019 IEEE. Personal use is permitted, but republication/redistribution requires IEEE permission. See http://www.ieee.org/publications_standards/publications/rights/index.html for more information.

This article has been accepted for publication in a future issue of this journal, but has not been fully edited. Content may change prior to final publication. Citation information: DOI 10.1109/TIA.2019.2933783, IEEE Transactions on Industry Applications

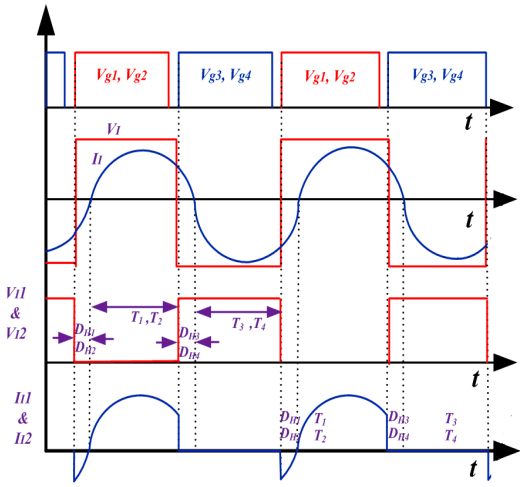

Fig. 3. Key waveforms of the proposed resonant converter

and utmost to least duty cycle operation. Here, T_1, T_2, T_3, and T_4 are wideband gap SiC MOSFET switches of inverter and the bridge rectifier consists of hyper fast diodes operated at optimum point. The diodes D_{H1} to D_{H4} carry load current before SiC switch is turned on to achieve ZVS. Fig. 2. shows the schematics of the proposed resonant converter. Renewable energy source voltage V_{dc} is applied to full bridge inverter. By implementation of mixed control method curtailment in frequency and duty cycle reduces switching and conduction loss. Thus, to study the behaviour of the converter it is expressed in terms of switching frequency and duty cycle. Key waveforms of converter operation using proposed control method are shown in Fig. 3. Fundamental resonant ac equivalent circuit is expressed in per unit for r^{th} harmonic is shown in Fig. 4. The input voltage $V_I(t)$ applied to the resonant tank circuit is symmetrical and expressed as

$$V_I(t) = \sum_{r=1,3}^{\infty} \frac{2\sqrt{2}V_{dc}}{r\pi}\sqrt{1-cos2\pi rD}\sin\left(r\omega_s t + \psi_r\right) \quad (1)$$

where D is duty cycle of the converter. The square waveform output V_I of full bridge inverter is fed to the resonant converter circuit, which results sinusoidal current waveform, this can be shifted lag by proposed control method. The resultant current of $i_s(t)$ is given by

$$i_s(t) = \sum_{r=1,3}^{\infty} \frac{2\sqrt{2}V_{dc}}{r\pi Z_{eq}\angle\phi_{eq}}\sqrt{1-cos2\pi rD}\sin\left(r\omega t + \psi_r\right) \quad (2)$$

where Z_{eq} represents input impedance of the converter, i.e.,

$$Z_{eq} = Z_s + Z_p \quad (3)$$

$$Z_s = j(X_{Ls} - X_{Cs}) = j(Q_s F_s - \frac{Q_s}{F_s}) \quad (4)$$

$$Z_p = \frac{jX_{p0}R_{ac}}{R_{ac} + jX_{p0}} \quad (5)$$

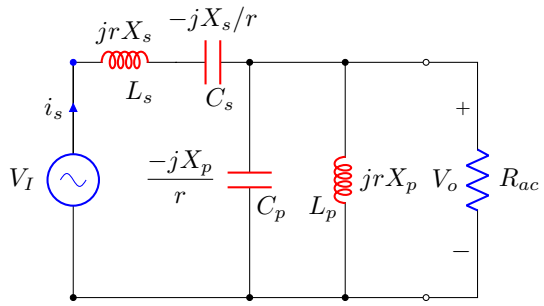

Fig. 4. Per unit r^{th} harmonic equivalent circuit

$$X_{p0} = \frac{X_{Lp}X_{Cp}}{X_{Cp} - X_{Lp}} = \frac{\frac{L_p}{L_s}\frac{C_s}{C_p}Q_s^2}{\frac{Q_s}{F_s}\frac{C_s}{C_p} - Q_s F_s \frac{L_p}{L_s}} \quad (6)$$

$$X_{Ls} = \omega_s L_s \text{ and } X_{Cs} = \frac{1}{\omega_s C_s} \quad (7)$$

$$X_{Lp} = \omega_s L_p \text{ and } X_{Cp} = \frac{1}{\omega_s C_p} \quad (8)$$

$$Q_s = \frac{\omega_0 L_s}{R'_L}, R_{ac} = \frac{8}{\pi^2}R'_L, \text{ and } R'_L = n^2 R_L \quad (9)$$

where X reactances, n turns ratio, R_L load resistance, R'_L as referred load resistance to primary side and Q_s is the quality factor. Low pass action of resonant tank filters out higher order harmonics but the dominant harmonics should be in acceptable level. Therefore, resultant output voltage is expressed by Kirchoff's current law, i.e,

$$V_o(t) = \sum_{r=1,3}^{\infty} \frac{2\sqrt{2}V_{dc}}{r\pi B_r\angle\varphi_r}\sqrt{1-cos2\pi rD}\sin\left(r\omega_s t + \psi_r\right) \quad (10)$$

Current through the parallel capacitor is expressed as

$$i_{C_p} = \sum_{r=1,3}^{\infty} \frac{2\sqrt{2}V_{dc}\sqrt{1-cos2\pi rD}}{r\pi X_p B_r\angle\varphi_r}\cos\left(r\omega_s t + \psi_r\right) \quad (11)$$

The current through the parallel inductor is given by

$$i_{L_p} = \sum_{r=1,3}^{\infty} \frac{2\sqrt{2}V_{dc}\sqrt{1-cos2\pi rD}}{r^2\pi X_p B_r\angle\varphi_r}\cos\left(r\omega_s t + \psi_r\right) \quad (12)$$

Voltage across the series capacitor is expressed as below

$$V_s = \sum_{r=1,3}^{\infty} \frac{2\sqrt{2}V_{dc}X_s}{r^2\pi Z_{eq}\angle\phi_{eq}}\sqrt{1-cos2\pi rD}\sin\left(r\omega_s t + \psi_r\right) \quad (13)$$

where ω_s switching frequency of the converter and $B_r = 1 - X_s/X_p(r-1/r)^2 + jXs/R_{ac}(r-1/r)$

$$\varphi_r = tan^{-1}\left(\frac{\frac{X_s}{R_{ac}}(r-\frac{1}{r})}{1-\frac{X_s}{X_p}(r-\frac{1}{r})^2}\right) \quad (14)$$

0093-9994 (c) 2019 IEEE. Personal use is permitted, but republication/redistribution requires IEEE permission. See http://www.ieee.org/publications_standards/publications/rights/index.html for more information.

This article has been accepted for publication in a future issue of this journal, but has not been fully edited. Content may change prior to final publication. Citation information: DOI 10.1109/TIA.2019.2933783, IEEE Transactions on Industry Applications

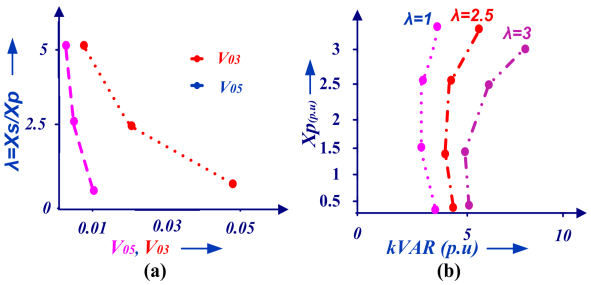

Fig. 5. (a) λ Vs third and fifth harmonics content of output voltage (V_{03}) and (V_{05}) (b) X_p Vs total kVAR rating

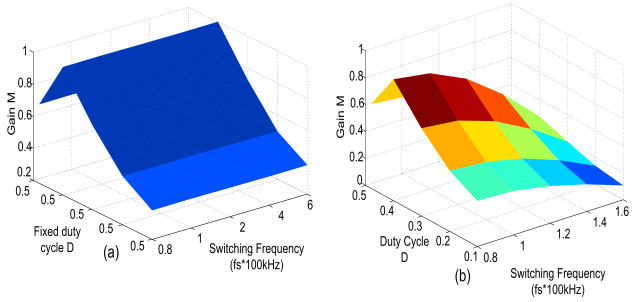

Fig. 6. Optimal design curves, (a) Conventional gain Vs switching Frequency variation (b) Proposed converter gain Vs dual control

III. Proposed Converter Analysis and Design

In order to get the resonant converter optimal parameters following design consideration are significant.

i. Acceptable level of ripple voltage.

ii. Output voltage of the converter under all load conditions should be constant.

A. Optimal resonant tank parameters

According to (10), the harmonic output voltage of the converter is given by

$$V_{or} = \frac{2\sqrt{1-cos2\pi rD}}{\pi r(1-\frac{X_s}{X_p}(r-\frac{1}{r})^2)}. \tag{15}$$

To reduce the ripple voltage, which is function of the harmonic content, optimal values of series and shunt reactances are chosen. Based on harmonic content $\lambda = X_s/X_p$ ratio of can be obtained from Fig. 5. Minimum kVA rating is the another parameter to get the optimal resonant converter elements. Therefore, kVA rating (p.u.) of the resonant converter w.r.t proposed mixed control as given below

$$\begin{aligned} TkVA &= \frac{4}{\pi}.\frac{4}{\pi}X_s(1-cos2\pi D) + \frac{4}{\pi}.\frac{4}{\pi X_p}(1-cos2\pi D) \\ &= \frac{16(1-cos2\pi D)}{\pi^2}(X_s+\frac{1}{X_p}). \end{aligned} \tag{16}$$

Fig. 5(a) shows the harmonic voltage of the converter with different values of λ. It can be seen that as λ increases, effect of higher order harmonics is reduced, but kVA rating increases from the Fig. 5(b). For optimal design of the converter minimum kVA rating and reduced dominant harmonics is to be considered. In this paper $\lambda = 2.5$, $X_p = 1.5$ and $D = 0.48$ chosen for optimal converter parameters.

B. Voltage gain (M) of the converter

The voltage gain of converter as a function of the conventional switching frequency F_s, requires wider range of normalized switching frequency for regulating output voltage from no-load to full load as shown in Fig. 6(a), and hence, the performance of the converter degrades due to increased switching losses. To overcome this here, the proposed converter gain is varied by both frequency and duty cycle (mixed control). Observation of the converter voltage gain variation with the proposed control method from no-load to full load is shown in Fig. 6(b). Converter overall voltage gain can be controlled by adjusting both the duty cycle and switching frequency is expressed as follow.

$$M = \frac{V_0}{V_{dc}} = \frac{V_I Z_p}{V_{dc} Z_{eq}} = \frac{2}{\pi}\frac{Z_p\sqrt{1-cos2\pi D}}{Z_{eq}}. \tag{17}$$

In order to regulated required output voltage from 100% load to no load using proposed control method, regression in duty cycle $D^{i+1} = D^i - bM^i$ and progression in switching frequency $F_s^{i+1} = F_s^i + aM^i$ are adjusted concurrently. Where i is the iteration, M is converter gain, a and b are constants.

C. Design of series Inductor

Design of series inductor for higher frequency can be done using powder core like sendust core, which have $B_m = 1T$ chosen. Sendust core offer minimal change in permeability or inductance (under 3% for $\mu_i = 125$) under AC excitation. Inductance change is less than 3% from ambient to 125^oC, overall losses are relatively low. Based on maximum current per unit cross section (J A/m^2) of the wire size without exceeding the limit, without overheat and the magnetic material can withstand maximum flux density (B_m) without saturation, Inductor is designed as area product without exceeding the limitations [30].

$$A_c * A_w = \frac{LI_{peak}I_{rms}}{K_w B_m J} \tag{18}$$

where A_w is the core window area, A_c is the core cross-sectional area, L is the series inductance, I_{peak} is the peak magnetizing current, J is the current density = $3A/mm^2$, K_w is the window utilization factor = 0.3, and $B_m = 1T$ for sendust core.

$$A = \frac{96.28\mu \times 20 \times 20/\sqrt{2}}{0.3 \times 1 \times 3 \times 10^6} = 3.02cm^4 \tag{19}$$

of cross sectional area $A_c = 1.75cm^2$ is chosen for Inductor design. Number of turns required for winding

$$N = \frac{LI_p}{B_m A_c} \approx 13. \tag{20}$$

but practically to utilizes core area 18 number of turns are considered. Litz wires, Kapton polyamide masking tape are used to reduce the skin effect and to have good thermal resistance.

0093-9994 (c) 2019 IEEE. Personal use is permitted, but republication/redistribution requires IEEE permission. See http://www.ieee.org/publications_standards/publications/rights/index.html for more information.

This article has been accepted for publication in a future issue of this journal, but has not been fully edited. Content may change prior to final publication. Citation information: DOI 10.1109/TIA.2019.2933783, IEEE Transactions on Industry Applications

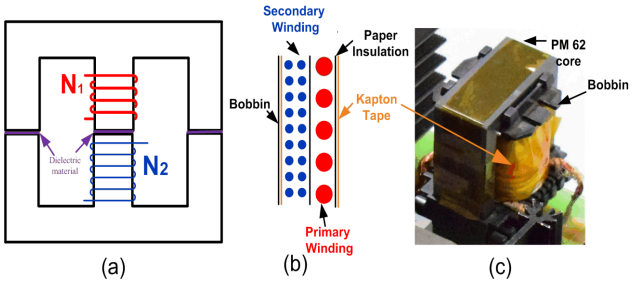

Fig. 7. Structure of HF transformer (a) Schematic representation (b)Winding structure (c) Actual photography of HF transformer.

D. Fabrication of HF Transformer

HF transformer is used to step up the voltage without large number of turns. Due to lesser number of turns in the transformer, leakage inductance is small. Optimal shunt branch inductance manifested as HF transformer magnetizing inductance. Therefore, the volume of the converter is considerably reduced by eliminating the shunt branch element. The prototype of HF transformer is shown in Fig. 7. The primary and secondary windings of the transformer are wound on Teflon bobbin which is placed on middle limb and Kapton tape is used as insulation wrapper across these primary and secondary windings as shown in Fig. 7(b). HF transformer is designed using ferrite core EE 46, because of comparatively low losses at high frequencies. A dielectric material used in HF transformer to get the required magnetizing inductance as shunt element inductance. For square wave of operation, the area product required to handle a given VA rating by the HF transformer is

$$A_T = \frac{VA}{2fB_{mT}K_{wT}J_T} = \frac{3000}{2 \times 100k \times 0.2 \times 3M \times 0.3}. \quad (21)$$

where, J_T is the current density = $3A/mm^2$, K_{wT} is the window utilization factor = 0.3, and $B_{mT} = 0.2T$ for ferrite core. Analytically number of primary turns $N_1 = 7$, and secondary turns $N_2 = 14$.

In general, HF transformer parasitic elements are used to realize all the branches of resonant converter tank circuit in low power applications. However, realization of HF transformer nonidealities as two or more branches of resonant tank circuit in high power application is cumbersome, due to the non-optimal magnetic components which degrade the performance of the converter. Therefore, external inductor and capacitor is used for network branch elements along with HF transformer as shown in Fig. 1(a). However, due to external inductor (L_p) size of the converter increases [16]. In contrast, in this paper based on optimized resonant tank circuit, shunt element of the converter is considered to be fabricated as the magnetising inductance of the HF transformer. Hence, the need of shunt branch (external L_p) in the tank circuit is eliminated is shown in Fig. 1(b). The total space consumed by the external L_p is 4 cm / 3.5 cm / 3.5 cm, which is less than 4% of the total volume measuring as 25 cm /13 cm / 4 cm. Utilization of external L_p leads to additional increase in size, which is reduced by fabricating HF transformer with L_p as L_m. Table I shows the comparison of converter size.

TABLE I
COMPARISON BETWEEN PROPOSED CONVERTER AND CONVERTER PRESENTED IN [16]

Parameter	Converter in [1]	Proposed converter
Size of L_p (cm)	$3.2 \times 3 \times 5$	$4 \times 3.5 \times 3.5$
Size of Converter (cm)	$10 \times 10 \times 5$	$25 \times 13 \times 4$
Space consumed by L_p	<10%	<5%
Effect	10% size increase	4% size reduces
Remarks	L_p is External	L_p is used for L_m
Power	500 W	3-kW
frequency	135kHz - 250kHz	104kHz - 150.6kHz

E. Different loss analysis of the proposed resonant converter

In proposed resonant converter with mixed control, experimental output power and input power are measured to estimate the efficiency and theoretical calculations are used to classify the different types of loss. Though excursion of frequency and duty cycle reduced along with soft-switching, the power loss still includes the switching loss of main switches ($P_{switching}$), the conduction loss of the rectifier, inverter switches and the magnetic loss of HF transformer and series inductor.

a) Switching power loss of inverter SiC switches are

$$P_{switching} = E_{off} \times f_s = V_{dc} I_{op} t_f \times f_s \quad (22)$$

where V_{dc} is dc supply, I_{op} working current, t_f fall time and f_s switching frequency. During the transition interval both the voltage across the device and the current through are substantially more than zero which leads to large instantaneous power loss.

b) Conduction loss include losses in inverter switches, freewheeling diodes and bridge rectifier. Losses occur due to the SiC MOSFET or freewheeling diode conduction, the total power dissipation during conduction is computed by multiplying square of the on-state current and on-state resistance.

$$P_{cond.switch} = 2I_s^2 \times R_{DS}(ON) \quad (23)$$

where $R_{DS}(ON)$ is the on-resistance of the main SiC switch. The input rms current of $i_s(t)$ as given below

$$i_s(t) = \frac{2V_{dc}}{\pi |Z_{eq}|} \sqrt{1 - cos2\pi D} \quad (24)$$

Combing (23) and (24), the conduction loss can be calculated by

$$P_{cond.switch} = \frac{8V_{dc}^2}{\pi^2 Z_{eq}^2}(1 - cos2\pi D) \times R_{DS}(ON) \quad (25)$$

c) Conduction loss of diode bridge rectifier will be calculated as

$$P_{cond.diode} = 2I_o V_f = 2V_f V_o / R_L \quad (26)$$

V_f is the forward voltage of the bridge rectifier diode.

d) Magnetic loss of the transformer can be calculated based

0093-9994 (c) 2019 IEEE. Personal use is permitted, but republication/redistribution requires IEEE permission. See http://www.ieee.org/publications_standards/publications/rights/index.html for more information.

This article has been accepted for publication in a future issue of this journal, but has not been fully edited. Content may change prior to final publication. Citation information: DOI 10.1109/TIA.2019.2933783, IEEE Transactions on Industry Applications

TABLE II
SPECIFICATIONS OF RESONANT CONVERTER HARDWARE

Components	Specifications
Power P	3-kW
Input Voltage V_{dc}	220 V
Output Voltage V_o	400 V
Sw.frequency f_s	104kHz- 150.6kHz
SiC MOSFET	C3M0065090D
Diode	RHRG75120
HF Transformer	Ferrite core PM 42
Output Capacitors	$100\mu F$, electrolytic
Turns Ratio n	0.55
Load Resistance R_L	53.33Ω
Series branch Inductance L_s	$96.28\mu H$
Series branch Capacitance C_s	$0.02631\mu F$
Parallel branch Inductance L_p	$38.5\mu H$
Parallel branch Capacitance C_p	$0.0657\mu F$

on Steinmetz equation, which is

$$P_{m.trans} = k_e f_s B_m^{\alpha} V_c \tag{27}$$

where k_e, α are the constants of the magnetic material, V_c is the magnetic core volume.

d) Magnetic loss of powder core inductor can be calculated by

$$P_{m.ind} = aB_{pk}^{b} f^{c} l_e A_e \tag{28}$$

$$\begin{aligned} B_{pk} =& 0.5(\mu)(\%\mu_i)(\mu_i)(100)(\Delta H) \\ \text{where } (\Delta H) =& \frac{N\Delta I_s}{l_e} \end{aligned} \tag{29}$$

where a, b, c are constants determined from curve fitting, number of turns (N), current (I_s), (l_e) and A_e are magnetic path length and area of cross section.

e) Dielectric loss of the tank circuit shunt capacitor (P_{die}): In high-power applications, high electric energy is stored in the insulator. The dielectric loss occurs due to the charging and discharging process of the electric energy. In the proposed resonant converter, the shunt branch capacitance is C_p. The Equivalent Series Resistor (R_s) of C_p can be calculated from the power loss dissipation factor $(tan\delta)$:

$$tan\delta = 2\pi f_s C_p R_s \tag{30}$$

therefore, R_s can be calculated as

$$R_s = tan\delta / 2\pi C_p f_s \tag{31}$$

The dielectric loss can be estimated by

$$P_{die} = i_{C_p}^2 R_s \tag{32}$$

Therefore, the dielectric loss is

$$P_{die} = \frac{4V_{dc}^2 tan\delta(1 - cos2\pi D)}{\pi^2 X_p^2 B^2 C_p f_s} \cos\left(\omega_s t + \psi - \varphi\right) \tag{33}$$

where the value δ is dielectric material power loss angle. The other losses are calculated based on the difference between the measured efficiency of the converter and measured losses of main components. The other loss includes ESR loss of switched capacitor, output capacitors and freewheeling diode.

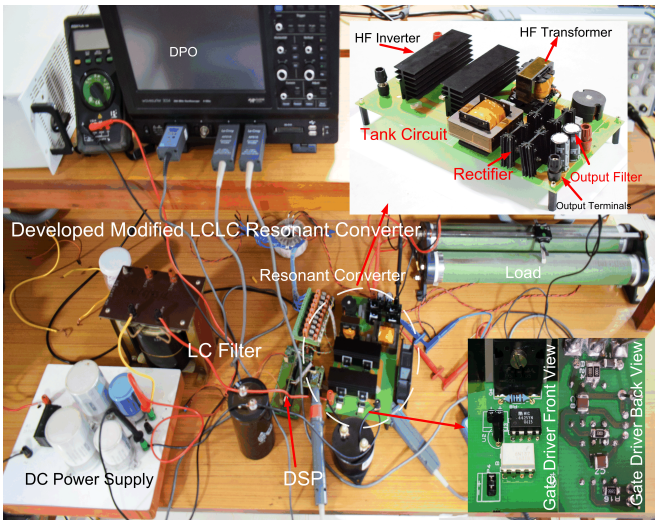

Fig. 8. Experimental Setup of Modified LC-LC Resonant converter

Based on the above analysis, combing (22), (25), (26), (27), (28) and (33), the total power loss of the converter can be calculated by

$$\begin{aligned} P_{total} =& 2E_{off} \times f_s + \frac{8V_{dc}^2}{\pi^2 Z_{eq}^2}(1 - cos2\pi D) + 2V_f V_o / R_L \\ &+ k_e f_s (B_m)^{\alpha} V_c + \frac{4V_{dc}^2 tan\delta(1 - cos2\pi D)}{\pi^2 X_p^2 B^2 C_p f_s} \\ &+ aB_{pk}^{b} f^{c} l_e A_e. \end{aligned} \tag{34}$$

IV. EXPERIMENTAL RESULTS OF THE PROPOSED CONVERTER

The proposed 3-kW, experimental prototype of resonant converter with shunt inductance as magnetizing inductance of HF transformer is fabricated in laboratory. The proposed resonant tank circuit design is based on optimal operating point. The converter is optimized for minimum kVA rating and reduced harmonic distortion. Fig. 8. shows the experimental setup of the proposed modified resonant converter. Specifications of hardware prototypes are shown in Table II. Fig. 9 shows the experimental results of the resonant full bridge inverter output voltage, resonant current, output voltage and current. Fig. 10 shows hardware waveforms at 25% full load and 10% full load, respectively. At 25% load, the switching frequency in excess of 192kHz at $D = 0.5$ was required, but with $D = 0.37$, switching frequency reduced to 112kHz. To regulate output voltage of basic series resonant converter with conventional frequency method at 10% full load, the switching frequency increased to more than 450kHz, owing to which switching losses increases drastically and ZVS fails. In contrast, with proposed mixed control, output voltage of this modified higher order resonant converter is well regulated with symmetrical current, which reduces core saturation, and the reduced operating switching frequency was 117.1kHz. In addition, even under very light load condition output voltage was controlled with ZVS condition.

0093-9994 (c) 2019 IEEE. Personal use is permitted, but republication/redistribution requires IEEE permission. See http://www.ieee.org/publications_standards/publications/rights/index.html for more information.

This article has been accepted for publication in a future issue of this journal, but has not been fully edited. Content may change prior to final publication. Citation information: DOI 10.1109/TIA.2019.2933783, IEEE Transactions on Industry Applications

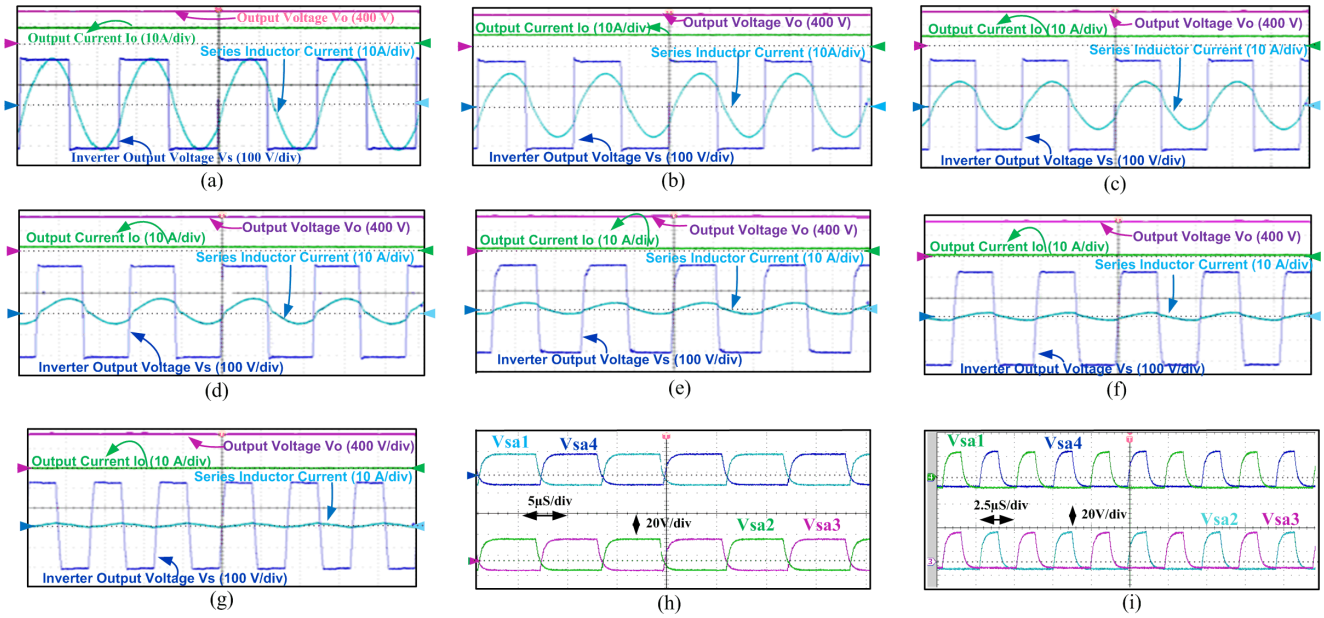

Fig. 9. Experimental results of the proposed converter, full bridge inverter Output voltage (100 V/div), series inductance current (10 A/div), Output voltage of the converter (400 V) and Output Current of the converter (10 A/div) for (a) full load, (b) 75% load, (c) 50% load, and (d) 25% load.(e) 10% load (f) 5%load (g) no load (h) Gate signals for the SiC MOSFET switches at D=0.48 (i) Gate signals at D=0.25

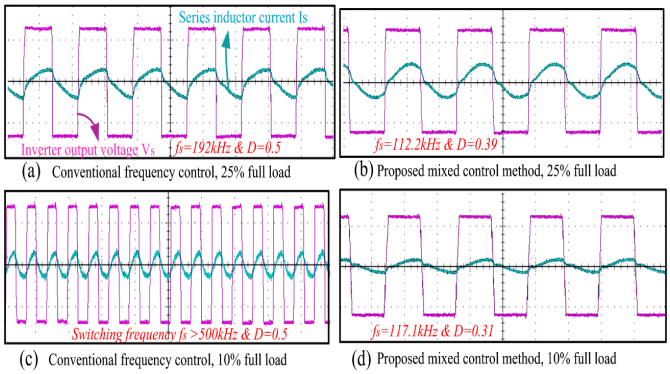

Fig. 10. Comparison of control methods (a) at 25% full load, $f = 192kHz$ & $D = 0.5$. (b) at 25% full load, proposed control method $f = 112.2kHz$ & $D = 0.39$ (c) at 10% full load, $f > 500kHz$ & $D = 0.5$. (d) at 10% full load, $f = 117.1$ & $D = 0.31$

The PI controller is used to compensate for the steady state error of the output voltage. The step change of load and reference input response is observed with the mixed control method, to verify the stability of the power converter. The PI controller is tuned accordingly to regulate the fine output voltage. Step load change response from 25% load to full load is shown in Fig. 11. In Fig. 11(a), conventional frequency control shows relatively higher settling time (time required to reach reference output voltage t_s) (35millisec). In Fig. 11(b), the proposed mixed control method shows decreased t_s (17millisec) because of additional duty cycle control reduces higher frequency changes to regulate the output voltage. Fig. 11(c) shows the reference input response from 390 V to 400 V, where output voltage tracks the reference voltage precisely with mixed control.

TABLE III
VALUES OF α MEASURED AT DIFFERENT LOAD CONDITION

Load	f_s,D	ϕ	φ	α
10% full load	117kHz, 0.31	89.9846	30.6	59.3846
5% full load	120kHz, 0.25	89.9847	36	53.9847
2% full load	139kHz, 0.2	89.98472	54	35.9871

ZVS under all load conditions is key requirement in higher voltage application to improve the efficiency of the converter. Hence, to ensure ZVS condition over wide load range, the resonant current $i_s(t)$ through resonant tank lags the voltage applied to the tank circuit as shown in Fig 12(a-b). Therefore, α should be greater than zero, which ensures ZVS condition.

$$\alpha = \phi - \psi > 0; \phi > \psi \Rightarrow \alpha > 0. \tag{35}$$

where ϕ and ψ are phase angles of the resonant current and voltage V_I. Therefore, α value estimated using (35) for different frequency and duty cycle is shown in Table III. To improve the performance of the converter, different types of losses are addressed and care has been taken to reduce them. In order to further reduce conduction losses of the proposed converter, SiC switch with lower on state resistance is selected, similarly diodes of bridge rectifier are also of higher voltage rating with low forward voltage to minimize the conduction losses as shown in Fig. 13. 3-kW prototype dc-dc resonant converter experimental results are summarized in Table IV. Loss analysis performed at full load, the distribution of different losses are shown in Fig. 14.

However, proposed control technique minimizes switching and conduction losses due to curtailment of duty cycle and switching frequency. In addition to this, Litz wires with small turns ratio for HF Transformer and inductor design aids in

0093-9994 (c) 2019 IEEE. Personal use is permitted, but republication/redistribution requires IEEE permission. See http://www.ieee.org/publications_standards/publications/rights/index.html for more information.

This article has been accepted for publication in a future issue of this journal, but has not been fully edited. Content may change prior to final publication. Citation information: DOI 10.1109/TIA.2019.2933783, IEEE Transactions on Industry Applications

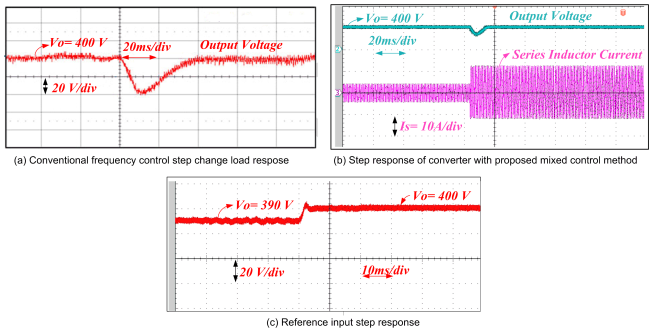

Fig. 11. Experimental results of step change performance of the converter with different control methods. (a) Output voltage regulation according to load change from 25% to full load with normal frequency control, (b) Output voltage adjustment according to load change from 25% to 100% with mixed control, (c) Output voltage tracking with reference input step change from 390 V to 400 V with mixed control method

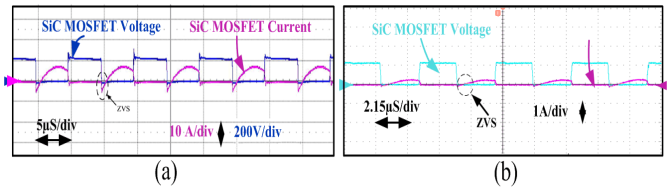

Fig. 12. Experimental result, (a) ZVS condition of SiC switch at 100% load. (b) ZVS condition of switch at 5% full load.

reduction of these losses. To overcome the magnetic losses in the proposed converter, powder core like sendust core and ferrite core are selected. While designing tank circuit magnetic material selection is very crucial which influences compactness of the converter. Sendust core is well known for the moderate cost and has significantly lower losses and substantially good thermal properties when compared to iron powdered core. For transformer design ferrite cores are best solution because eddy current losses are very less which will support higher efficiency, high flux density and distributed air gap helps to tolerate high DC current before the core saturates. Controller for the proposed resonant converter is developed by using TMS320F28335 launchpad. Fig. 15 shows efficiency analysis of the proposed modified converter for different loads. The performance of the converter demonstrates good efficiency across wider load range with the proposed control method. The maximum efficiency noticed for the developed converter is 98.6% at 50% of the load. It is observed from the efficiency curve, that the performance of the converter is significantly improved at very light load condition.

V. Conclusion

An optimal resonant converter with soft switching and HF transformer is designed with shunt branch inductance of the tank circuit as magnetizing inductance, eliminate the need of shunt branch of the tank circuit. The proposed converter is optimized for minimum kVA rating and reduced harmonic distortion. Effective voltage regulation and improvement of soft switching over wider loading range with narrow frequency excursions using proposed control method is achieved. Opting

TABLE IV
Experimental results of Proposed 3kW resonant converter

Parameter	Full load	75% load	50% load	5% load	no load
Switching frequency	104 kHz	108.1 kHz	110.5 kHz	120 kHz	150.7 kHz
Duty cycle	0.48	0.46	0.41	0.25	0.2
R_L	53.33 Ω	71.11 Ω	106.66 Ω	1066.6 Ω	30k Ω
Load	7.5 A	5.625 A	3.75 A	0.375 A	0.01 A
Efficiency	97.6%	98.01%	98.6%	92%	-

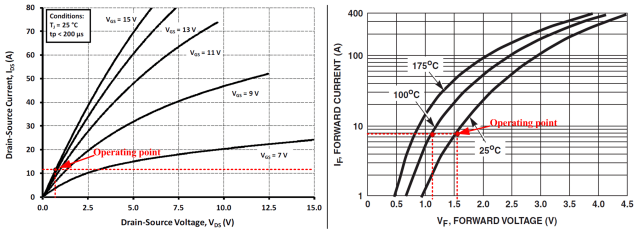

Fig. 13. Optimum operating point selection of SiC switch and diode

powder core with high permeability and low reluctance for the design of tank circuit reduces magnetic losses. By using SiC MOSFETs and diodes with low on state resistance minimizes conduction losses. A 3-kW proposed prototype of the proposed converter designed, developed and tested in the laboratory. Proposed converter maximum efficiency is 98.6% and attained at 50% load.

References

[1] J. M. Carrasco et al., "Power- electronic systems for the grid integration of renewable energy sources: A survey." *IEEE Trans. Ind. electron.,* vol. 53, no. 4, pp. 1002-1016, Jun 2006.

[2] S. Jain and V. Agarwal, "An integrated hybrid power supply for distributed generation applications fed by nonconventional energy sources,"*IEEE Trans. Energy Convers.,* vol. 23, no. 2, pp. 622-631, Jun. 2008.

[3] A. K. Rathore, A. K. S. Bhat, and R. Oruganti, "A comparison of soft-switched dc-dc converters for fuel cell to utility interface application", *IEEE Trans. Ind. Appl.,* vol. 128, no. 4, pp. 450-458, 2008.

[4] L. Solero, A. Lidozzi and J. A. Pomilio, "Design of multiple-input power converter for hybrid vehicles,"*in IEEE Trans. Power Electron,* vol. 20, no. 5, pp. 1007-1016, Sept. 2005.

[5] M. Liserre, T. Sauter, and J. Y. Hung, "Future energy systems: Integrating renewable energy sources into the smart power grid through industrial electronics,"*IEEE Ind. Electron. Mag.,* vol. 4, no. 1, pp. 18–37, Mar. 2010.

[6] L. Solero, "Nonconventional on-board charger for electric vehicle propulsion batteries," *in IEEE Trans. Vehi. Techn.,* vol. 50, no. 1, pp. 144-149, Jan. 2001.

[7] N. Azura, S. Iqbal, and S. Taib, "LLC resonant DC-DC converter for high voltage application," in Proc.*IEEE Appl. Energy Convers. (CENCON)*, pp. 90-95, Oct. 2014.

[8] W. Martinez, M. Yamamoto, Petar. Grbovic and C. A. Cortes, "Efficiency optimization of a single-phase boost DC-DC converter for electric vehicle applications," *IEEE Indus. Electron Soc. Dallas, TX, Conf.*, pp. 4279-4285, 2014.

[9] H. M. Suryawanshi, K. L. Thakre, S. G. Tarnekar, D. P. Kothary, and A. G. Kothari, "Power factor improvement and closed loop control of an AC-to-DC resonant converter," *IEE Proc. Electric Power Appl.,* vol. 149, no. 2, pp. 101-110, Mar. 2002.

[10] R. W. Erickson and D. Maksimovic "Fundamentals of Power Electronics," 2nd ed. New York, NY, USA: Springer-Verlag, 2001.

[11] A. K. Rathore, Devendra R. Patil and Dipti Srinivasan, "Non-isolated Bidirectional Soft-Switching Current-Fed LCL Resonant DC/DC Converter to Interface Energy Storage in DC Microgrid,"*IEEE Trans. Ind. Appl.* vol. 52, no. 2, Mar. 2016.

0093-9994 (c) 2019 IEEE. Personal use is permitted, but republication/redistribution requires IEEE permission. See http://www.ieee.org/publications_standards/publications/rights/index.html for more information.

This article has been accepted for publication in a future issue of this journal, but has not been fully edited. Content may change prior to final publication. Citation information: DOI 10.1109/TIA.2019.2933783, IEEE Transactions on Industry Applications

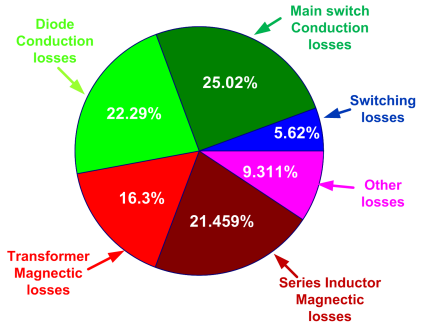

Fig. 14. %Loss distribution of proposed converter at full load.

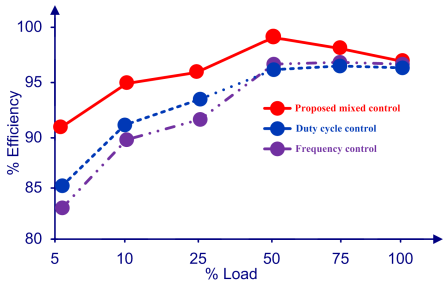

Fig. 15. Efficiency curves with respect to the load variations.

[12] J. A. Martin-Ramos, J. Diaz, A. M. Pernia, J. M. Lopera, and F. Nuno, "Dynamic and steady-state models for the PRC- LCC resonant topology with a capacitor as output filter," *IEEE Trans. Ind. Electron.,* vol. 54, no. 4, pp. 2262-2275, Aug. 2007.

[13] Yang. R, Ding. H, Xu. Y, and Xiang. Y, "An analytical steady-state model of LCC type series-parallel resonant converter with capacitive output filter," *IEEE Trans. on Power Electron.,* Vol. 29, no. 1, pp. 328-338, Jan. 2014.

[14] J. A. Martin-Ramos, A. M. Pernia, J. Diaz, F. Nuno, and J. A. Martinez, "Power supply for a high-voltage application," *IEEE Trans. Power Electron.,* vol. 23, no. 4, pp. 1608-1619, Jul. 2008.

[15] D. Fu, F. C. Lee, Y. Liu, and M. Xu, "Novel multi-element resonant converters for front-end dc/dc converters," in Proc. 39th *IEEE Annu. Power Electron. Spec. Conf.,* pp. 250-256, Jun. 15–19, 2008.

[16] Yang Chen, Hongliang Wang, Zhiyuan Hu, Yan-Fei Liu, Xiaodong Liu, Jahangir Afsharian, and Zhihua Yang "LCLC Converter With Optimal Capacitor Utilization for Hold-Up Mode Operation," *IEEE Trans. Power Electron.,* vol. 34, no. 3, pp. 2385-2396, Mar. 2019.

[17] Navid Shafiei, Majid Pahlevaninezhad, Hosein Farzanehfard, and Seyed Reza Motahari, " Analysis and Implementation of a Fixed-Frequency LCLC Resonant Converter With Capacitive Output Filter," *IEEE Trans. Ind. Electron.,* vol. 58, no. 10, pp. 4773- 4782, Oct. 2011.

[18] Bin Zhao ; Xin Zhang ; Zhe Zhang " Sequential Offline-Online-Offline (SO3) Measurement Approach for High Frequency LCLC Resonant Converters in the TWTA Applications,"*IEEE Trans. Ind. Electron.,* doi: 10.1109/TIE.2019.2898601

[19] Bin Zhao, Gang Wang, and William Gerard Hurley "Analysis and Performance of LCLC Resonant Converters for High-Voltage High-Frequency Applications," *IEEE Jour. Emerg. Sele. in Power Electron.,* vol. 5, no. 3, Sept. 2017.

[20] J. Biela and J. W. Kolar, "Using transformer parasitics for resonant converters - A review of the calculation of the stray capacitance of transformers," *IEEE Trans. Ind. Appl.*, vol. 44, no. 1, pp. 223–233, Jan./Feb. 2008.

[21] S. Y. Chen, Z. R. Li, and C.-L. Chen, "Analysis and design of single-stage ac/dc LLC resonant converter,"*IEEE Trans. Ind. Electron.,* vol. 59, no. 3, pp. 1538-1544, Mar. 2012.

[22] X. Fang, H. Hu, Z. J. Shen, and I. Batarseh," Operation mode analysis and peak gain approximation of the LLC resonant converter," *IEEE Trans. Power Electron.,* vol. 27, no. 4, pp. 1985-1995, Apr. 2012.

[23] J. Zhang, J. Liao, J. Wang, and Z. Qian, "A current-driving synchronous rectifier for an LLC resonant converter with voltage-doubler rectifier structure,"*IEEE Trans. Power Electron.,* vol. 27, no. 4, pp. 1894-1904, Apr. 2012.

[24] M. Jose Burdio, L. A. Barragan, D. Npvarro, and J. Acero, "Asymmetrical voltage-cancellation control for full-bridge series resonant inverters," *IEEE Trans. Power Electron.,* vol. 19, no. 2, pp. 461-469, 2004.

[25] S. Kislovski, "Linear variable inductor (LVI) in single-phase off-line telecomrectifiers,"*in Proc. IEEE Int. Telecom. Energy Conf.,* 1995, pp. 93-98.

[26] H. Xiao and S. Xie, "A ZVS bidirectional DC-DC converter with phase shift plus PWM control scheme,"*IEEE Trans. Power Electron.,* vol. 23, no. 2, pp. 813-823, Mar. 2008.

[27] Jie Lu, Ashish Kumar, and Khurram K. Afridi "Step-Down Impedance Control Network Resonant DC-DC Converter Utilizing an Enhanced Phase-Shift Control for Wide-Input-Range Operation," *IEEE Trans. Ind. Appl.*, vol. 54, no.5, pp. 4523-4536, Sept. 2018.

[28] Erdem Asa, Kerim Colak, and Dariusz Czarkowski "Analysis of a CLL Resonant Converter with Semi- Bridgeless Active Rectifier and Hybrid Control," *IEEE Trans. Ind. Electron.*, vol. 62, no. 11, pp. 6877- 6886, Nov. 2015.

[29] Hwa-Pyeong Park, Jee-Hoon Jung "PWM and PFM Hybrid Control Method for LLC Resonant Converters in High Switching Frequency Operation," *IEEE Trans. Ind. Electron.,*vol. 64, no. 1, pp. 253-263, Jan. 2017.

[30] M. K. Kazimierczuk, *"High-Frequency Magnetic Components",* 2nd ed. Chichester, U.K.: Wiley, 2014.

Vijaya Vardhan Reddy. P received the B.Tech degree in electrical and electronics engineering from PBR Visvodaya institute of Technology and Science, Kavali, India, and the M.Tech. degree in control systems engineering from IIT Kharagpur, India, in 2013. He is currently working towards the Ph.D. degree in electrical engineering with the Visvesvaraya National Institute of Technology, Nagpur, India.

During 2014, he worked with General Electric Global Research as IP Professional, Bangalore, India. His research interests include dc-dc converter, soft-switched resonant converter, and control system

H. M. Suryawanshi (M'06-SM'12) received the B.E. degree in Electrical Engineering from Walchand College of Engineering, Sangli, India, in 1988 and M.E. degree in Electrical Engineering from Indian Institute of Science, Bangalore, in 1994. He has been awarded Ph.D. degree by Nagpur University, Nagpur (India) in 1999.

He is currently working as Professor in the Department of Electrical Engineering, Visvesvaraya National Institute of Technology, Nagpur, (India).

He is the Chair Professor of Indian National Academy of Engineering (INAE), India. He is an Associate Editor of IEEE Transaction on Industrial Electronics, USA. He has received Fellow of INAE in 2012 for his outstanding research. He has received Institution of Electronics and Telecommunication Engineers (IETE)-Bimal Bose Award in 2009, IETE-Biman Behari Sen Memorial Award in 2017 for his leadership in Power Electronics in India. He has been a Guest Editor of the IEEE Transaction on Industrial Electronics Special Section: Z-Source Converters Topologies, Modulation Techniques, and Applications, 2017. His research interests include the field of Power Electronics, emphasising developmental of resonant converters, power factor correction, active power filters, FACTs devices, multilevel converters and electric drives.

0093-9994 (c) 2019 IEEE. Personal use is permitted, but republication/redistribution requires IEEE permission. See http://www.ieee.org/publications_standards/publications/rights/index.html for more information.

This article has been accepted for publication in a future issue of this journal, but has not been fully edited. Content may change prior to final publication. Citation information: DOI 10.1109/TIA.2019.2933783, IEEE Transactions on Industry Applications

Girish G. Talapur (S'15) received the B.Tech. degree in electrical and electronics engineering from the RGM College of Engineering and Technology, Nandyal, India, in 2009, and the M.Tech. degree in power systems from Delhi Technological University, New Delhi, India, in 2012. He is currently working toward the Ph.D. degree in electrical engineering with the Visvesvaraya National Institute of Technology, Nagpur, India. He is currently working in CG Power and Industrial Solutions Limted, Bhopal, India.

His research interests include high density power converters, distributed generation, ac microgrid, power quality, and dc microgrid

Makarand Sudhakar Ballal (M'15–SM'16) received the B.E. degree in electrical engineering from the Government College of Engineering, Aurangabad, India, in 1993, the M.Tech. degree in integrated power system from the Visvesvaraya National Institute of Technology, Nagpur, India, in 1997, and the Ph.D. degree from Rashtrasant Tukadoji Maharaj Nagpur University, Nagpur, in 2007.

He is currently a Professor with the Department of Electrical Engineering, Visvesvaraya National Institute of Technology. He has 15 years of experience in the power sector. He was with Maharashtra State Electricity Transmission Company Limited, Mumbai, India, from 1997 to 2012, where he was involved in the commissioning, installation, testing and maintenance of various HV and EHV electrical equipments and accessories. His current research interests include condition monitoring of electrical machines, power quality measurements, and power electronics and drives.

0093-9994 (c) 2019 IEEE. Personal use is permitted, but republication/redistribution requires IEEE permission. See http://www.ieee.org/publications_standards/publications/rights/index.html for more information.

Volume 7 Issue 2 (2019) 125-128 ISSN 2347 - 3258
International Journal of Advance Research and Innovation

Renewable Energy Fed DC Microgrid: An Overview

Apoorva Mishra, JN Rai
Department of Electrical Engineering, Delhi Technological University, Delhi-42, India.

Article Info
Article history:
Received 10 January 2019
Received in revised form
20 March 2019
Accepted 28 April 2019
Available online 15 June 2019

Keywords: Solar P-V, Wind turbine, DC microgrid, Flyback converter, Buck-Boost converter, MPPT

Abstract
This paper lays emphasis on need of renewable energy sources for power due to increase in the demand for energy and depletion of conventional sources of energy. We propose to integrate the renewable energy with our DC Micro grid. In this paper we study the interfacing of the Solar P-V , Wind Turbine with the DC Micro grid through the rectifier, Buck Boost and Fly back converter respectively. We present a model of a wind turbine using a Fly back converter as it can provide isolation due to the use of high frequency transformer in its design. This isolation provides the advantage of protection of the DC link from any fault on the wind turbine or synchronous generator side. The emphasis is to investigate performance of P-V with Buck Boost converter. We also apply the Perturb and Observe MPPT tracking technique on the respective converters at varying operating points to extract the maximum power and keep the DC-link voltage constant. Further the model of wind generator and solar energy performance on the MATLAB/SIMULINK environment is investigated..

1. Introduction

Due to increased exhaustion of the conventional energy resources we are trying to switch to non-conventional sources of energy which are renewable immaculate and ecological. They have several other advantages which includes (a) reduced transmission losses, (b) power quality improvement (c) improved reliability (d) reduction in emissions (e) provisions for heterogeneous power quality [1]. Systems should be installed according to the geographical parameters. Places where wind speed is high will benefit from the installations of wind turbines like the coastal regions of Tamil Nadu, Karnataka, Andhra Pradesh and Gujrat of the Indian subcontinent. Likewise Rajasthan, Punjab, Uttar Pradesh and Haryana and few amongst the many places benefitting from the solar power installations. The However accounting globally, Hydropower has the largest installations with total installation capacity being more than 1000GW which alone is 16% of the total energy used for electrification [2]. Also we see the performance of Solar P-V with Buck-Boost.

2. Wind Energy Conversion System Description

The system consists of a wind turbine connected to a synchronous machine which supplies AC power to a diode bridge rectifier which converts it to DC which is fed to a fly back converter which performs MPPT operation and maintains the constant grid voltage as shown in Fig.1

2.1 Wind Conversion system model

In the wind energy conversion system we obtain electrical energy from rotational energy obtained by the wind speed. The output power or torque of a wind turbine will depend on several factors like wind velocity, size and shape of the turbine, etc. [3]. A dynamic model of the wind turbine, governed by these parameters, is necessary to understand the behaviour of a wind turbine over its region of operation .Therefore by analysing its modelling, it is possible to control a wind turbine's performance to meet the desired operational characteristics [3]. Further the different performance characteristics and variables that play an important role in wind power generation, by deriving the speed and power relations are investigated [3].

$$E = \frac{1}{2}mv^2 \quad (1)$$

Here, m= mass of air; v= velocity of wind;
mass is obtained by:

$$m=\rho Ad \quad (2)$$

Here, ρ = air density, A= rotor blade swept area, d= covered distance by wind
mechanical power as-

$$P=\frac{E}{t}=\frac{\frac{1}{2}\rho Adv^2}{t}=\frac{1}{2}\rho Adv^3 \quad (3)$$

The wind turbine is used to deliver the maximum mechanical output power for corresponding wind velocity to track maximum power present in wind [4]. Fig 1 depicts that for tracking the maximum attainable power present in wind, the wind generator system rotor speed is varied widely[4]. This is performed using MPPT technique.

2.2 Maximum power point tracking technique

In the MPPT technique duty cycle of the converter is varied to keep the operating point , in this case the voltage of the generator so as to extricate maximum power . The grid voltage is kept constant and the current is varied. The MPPT controller senses the increment or decrement and a comparison is made with the previous values. The duty cycle of the converter is adjusted accordingly to keep the operating point so that maximum current is maintained and maximum power can be exploited as shown in the flowchart. The rotor velocity of the wind turbine system is also changed according to the duty ratio in accordance with the voltage of generator, current and power as in figure 2.

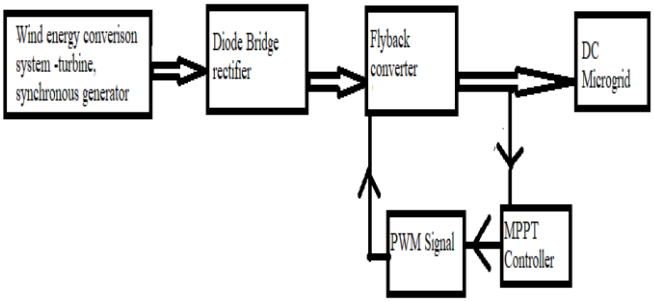

Fig.1: Block Diagram of wind connected DC Microgrid

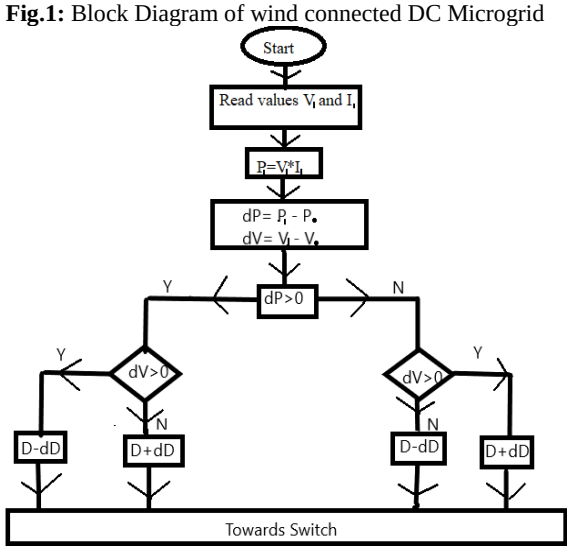

Fig 2: P&O flowchart MPPT

3. Verification of Applicability of Buck Boost Converter for MPPT

A model of Solar P-V was formed in MATLAB/SIMULINK as

Corresponding Author,
E-mail address: apoorvaald@gmail.com
All rights reserved: http://www.ijari.org

shown in Fig 4 . Voltage, Current and Power at various duty cycle was noted and found that the Power Vs duty cycle characteristics matched to the Solar P-V and Wind characteristics.

4. Simulink Models

A model is designed in MATLAB/SIMULINK for Flyback converter shown in Fig 3. Input voltage is considered 25V. Output voltage at various duty cycles is simulated and the result is obtained.

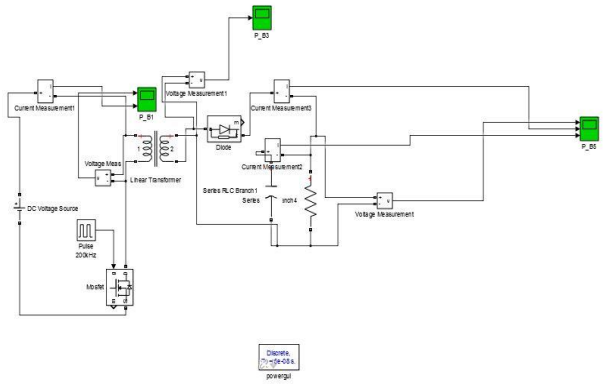

Fig 3: Flyback model simulation

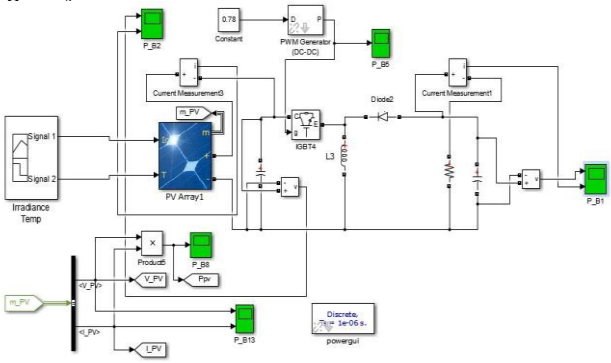

Fig 4: Simulation of Solar with Buck Boost

Duty Ratio	Vin	Iin	Pin	Vout	Iout	Pout
0.05	114.7	0.02	2.294	-7.5	-0.15	1.125
0.1	114.65	0.03	3.44	-14	-0.28	3.92
0.15	114.6	0.054	6.1884	-22	-0.45	9.9
0.2	114.55	0.165	18.9	-30.6	-0.62	18.97
0.25	114.23	0.4	45.692	-40	-0.8	32
0.3	114.2	0.55	62.81	-49	-1.1	53.9
0.35	114.17	0.8	91.2	-62.5	-1.3	81.25
0.4	114.05	0.98	111.72	-79.5	-1.57	124.815
0.45	114	1.75	199.5	-96.5	-1.92	185.28
0.5	113	2.5	282.5	-117	-2.5	292.5
0.55	112.5	4	450	-143	-3	429
0.6	111	6	666	-173.5	-3.47	602
0.65	110	8	880	-210	-4	840
0.7	106	12.5	1325	-260	-5.5	1430
0.75	100	20.5	2005	-312	-6.5	2028
0.77	92	22	2024	-330	-6.7	2211
0.78	88	24.9	2195	-331	-6.63	2194.53
0.79	80	25.7	2056	-322	-6.45	2076.9
0.8	70	26	1820	-305	-6	1830
0.85	35.5	26.1	926.55	-212.5	-4.3	913.75
0.9	12.5	26.16	327	-129.5	-2.6	336.7

Fig 5: Various measurements

The curves obtained were as follows

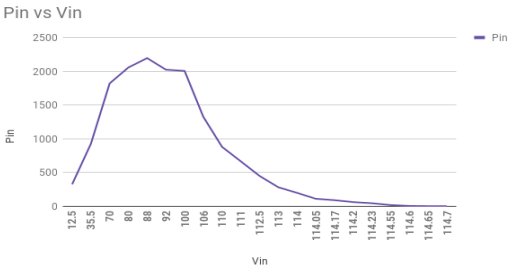

Fig 6: Power input Vs Voltage input

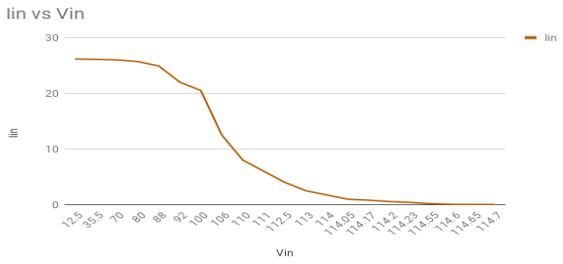

Fig 7: Current input Vs Voltage input

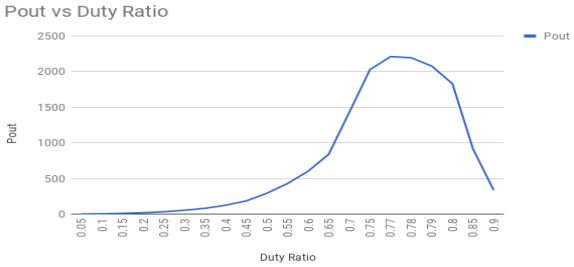

Fig 8: Power output Vs Duty Ratio

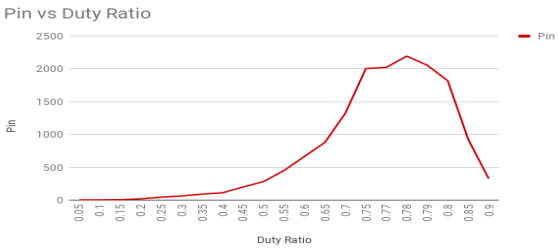

Fig 9: Power input Vs Duty Ratio

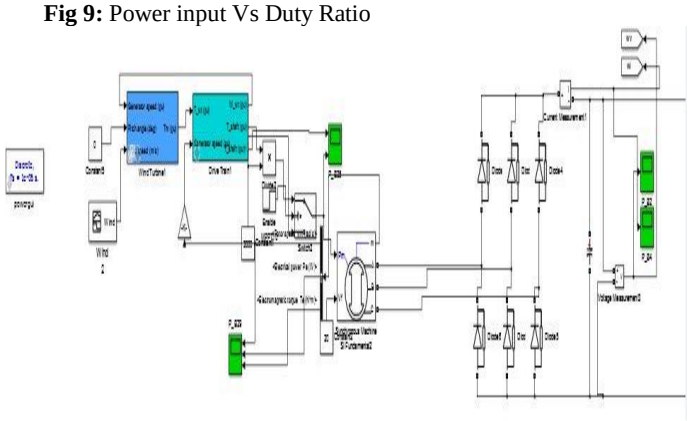

Fig. 10: Complete simulation of the wind system with flyback conveter and MPPT

Specifications of the wind turbine system are Synchronous Generator: 3 kVA, 415V, 50Hz.Figure 5 is the various measurements taken at various duty cycles and Figures 6,7,8,9 are the various characteristics plotted from the measurements. Further it is verified in the results section with output waveforms.

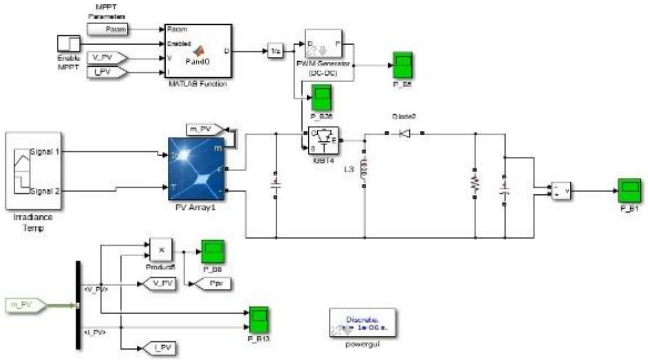

Fig. 11: Solar MPPT simulation

The parameters for this simulation were Solar Irradiation: 1000 W/meter square Temperature:25 degree Celsius ,Solar PV: Wp = 245 W, Voc = 38.23V, Isc = 8.67A, Vmp = 29.9V, Imp = 8.2A.

5.Results

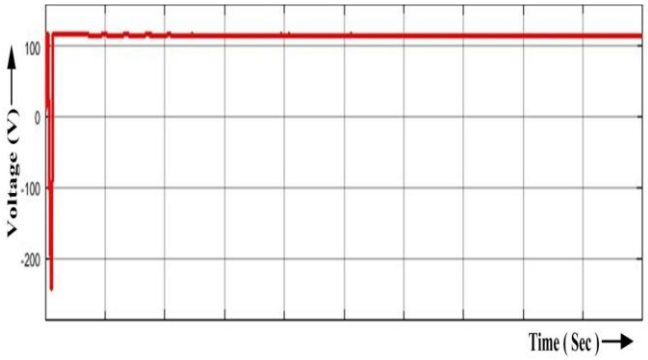

Fig 12: D-45% Input Voltage waveform for Fig 4.

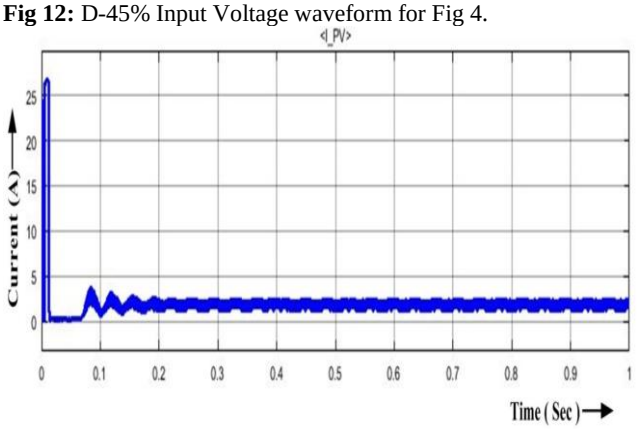

Fig 13: D-45% Input Current Waveform for Fig 4.

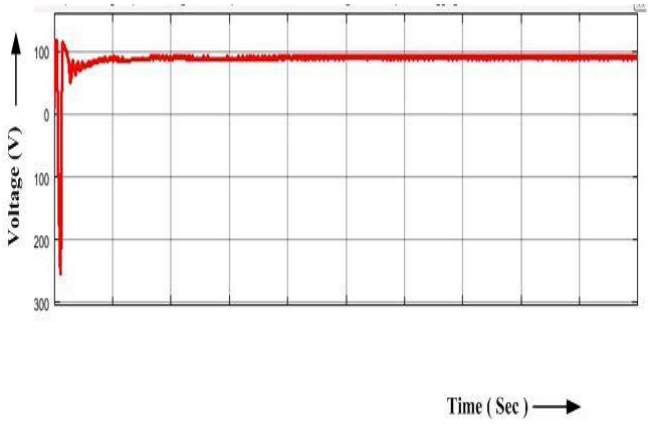

Fig 14: D-78% Input Voltage Waveform for Fig 4.

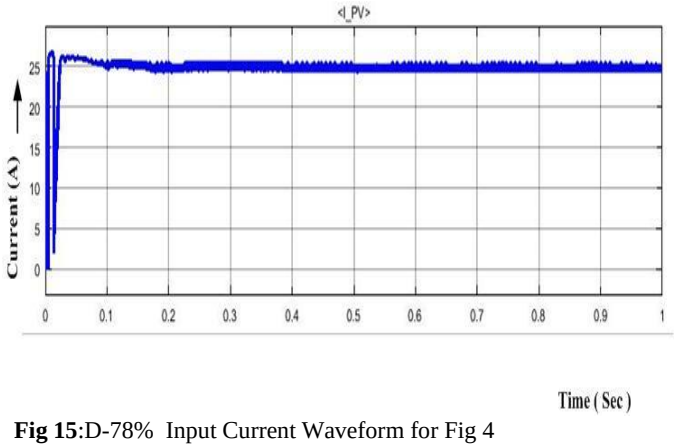

Fig 15:D-78% Input Current Waveform for Fig 4

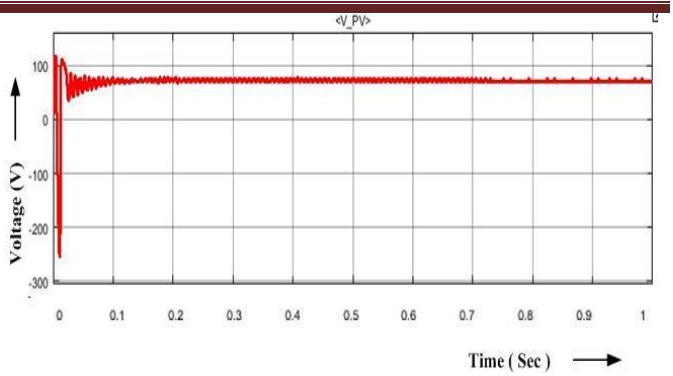

Fig 16: D-80% Input Voltage Waveform for Fig 4

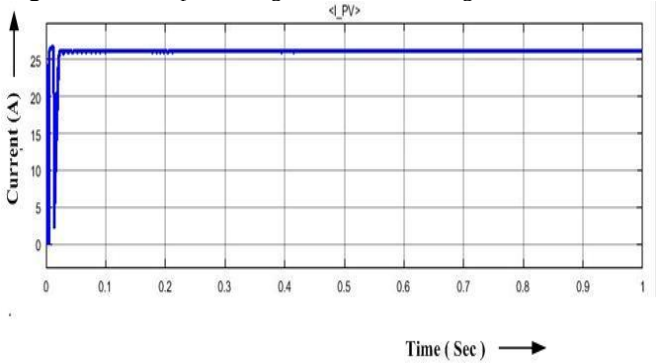

Fig 17: D-80% Input Current Waveform for Fig 4.

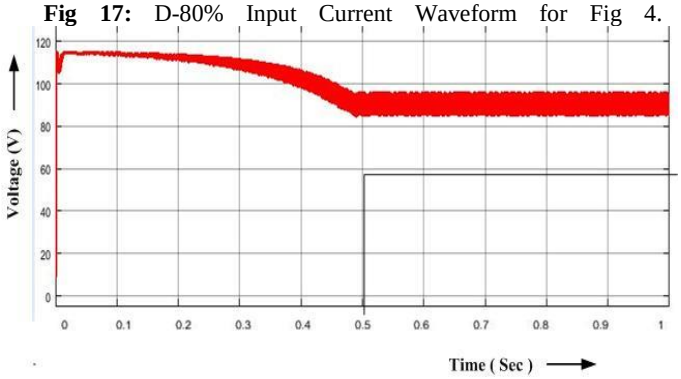

Fig 18: Input Voltage Waveform for Fig .11 with complete Solar MPPT.

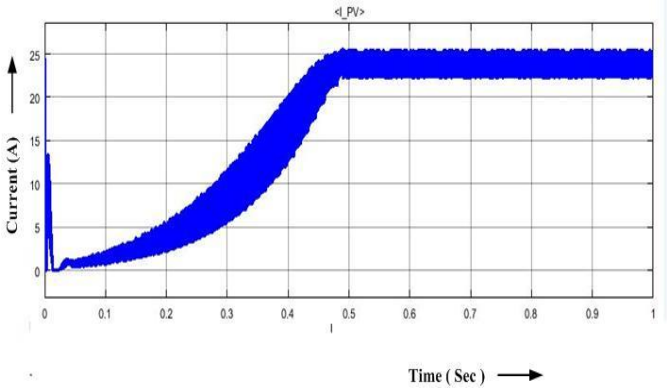

Fig 19: Input Current Waveform for for Fig .11 with complete Solar MPPT.

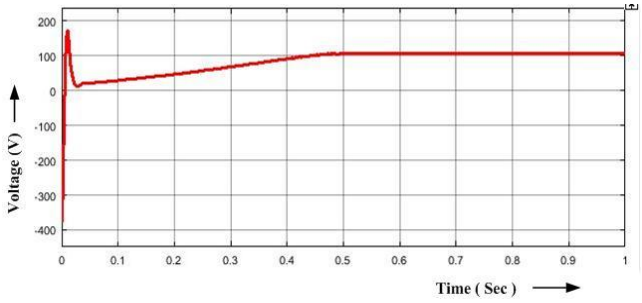

Fig 20: Output Voltage Waveform for Fig .11 with complete Solar MPPT.

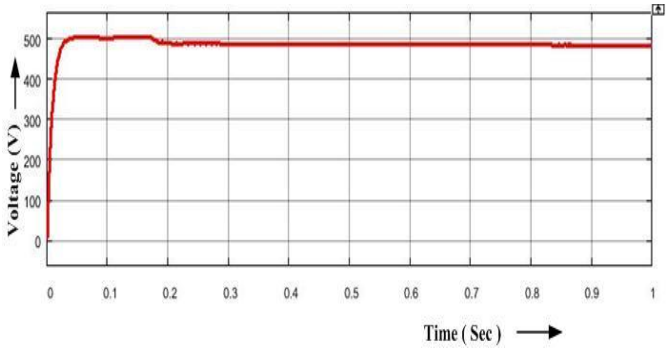

Fig 21: Output Voltage Waveform of Fig 10. Wind turbine with flyback converter.

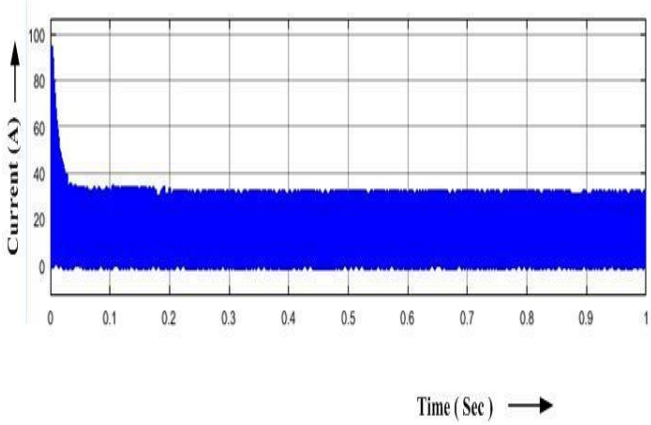

Fig 22: Output Current Waveform of Fig 10. Wind turbine with flyback converter.

6. Conclusions

In this study after analysing a lot, we found that the buck boost converter is applicable for MPPT as its Power Vs Duty Ratio graph and Power input Vs Voltage input graph is identical to the P-V characteristics of the solar panel and Power-speed characteristics of the wind system. It is also suggested to use Flyback Converters for MPPT as they are buck boost converters with isolation. This isolation provides the advantage of protection of the DC link from any fault. Fly back converters with higher turns ratio has application in higher power generation.

References

[1] SN Bhaskara, BH Chowdhury. Microgrids — A review of modeling, control, protection, simulation and future potential, 2012 IEEE Power & Energy Society General Meeting, 1, 2012.

[2] C Phurailatpam, R Sangral, BS Rajpurohit, SN Singh, FG Longatt. Design and Analysis of a DC Microgrid with Centralized Battery Energy Storage System, IEEE Indicon 2015, 1570171737.

[3] G Ofualagba, EU Ubeku. Wind Energy Conversion System-Wind Turbine Modeling, IEEE Power and Energy Society General Meeting - Conversion and Delivery of Electrical Energy in the 21st Century, 2008

[4] SS Gite, SH Pawar. Modeling of Wind Energy System with MPPT Control for DC Microgrid, IEEE 2017, Second International Conference on Electrical, Computer and Communication Technologies (ICECCT).

[5] K Strunz, E Abbasi, DN Huu. DC Microgrid for Wind and Solar Power Integration, IEEE journal of emerging and selected topics in power electronics, 2(1), 2014

Sentiment Analysis on Twitter Data: A Survey

Abhilash Mittal
Computer Science and Engineering Department
Delhi Technological University
New Delhi, India.
abhilashmittal23@gmail.com

Sanjay Patidar
Computer Science and Engineering Department
Delhi Technological University
New Delhi, India.
sanjaypatidar@dtu.ac.in

ABSTRACT
Twitter is the popular micro blogging site where thousands of people exchange their thoughts daily in the form of tweets. The characteristics of tweet is to be short and simple way of expressions. Though this paper will focus on sentiment analysis of twitter data. The research area of sentiment analysis are text data mining and NLP. In different form we can perform the sentiment analysis on twitter data. This research paper will focus on techniques of sentiment analysis where we will perform how to extract tweets from twitter. Eventually we will compare different sentiment analysis techniques and also the approaches containing twitter dataset.

CCS Concepts
• **Information systems→Database management system engines**.

Keywords
Social media; sentiment analysis; twitter data; text mining.

1. INTRODUCTION
Now a days twitter, facebook, whatsapp are getting so much attention from people and also they are getting very much popular among people. Sentiment analysis provides many opportunities to develop a new application. in the industrial field, sentiment analysis has big effect, like government organization and big companies, their desire is to know about what people think about their product, their market value. the aim of sentiment analysis is to find out the mood, behaviour and opinion of person from texts. for the sentiment analysis purpose, social networking used the various sentiment analysis techniques to take the public data. Sentiment analysis widely used in various domain such as finance, economics ,defence , politics. The data available on the social networking sites can be unstructured and structured. almost 80% data on the internet is unstructured. Sentiment analysis techniques are used to find out the people opinion on social media. Twitter is also a huge platform in that different idea, thought, opinion are presented and exchanged. It does not matter where people came from, what religious opinions they hold, rich or poor, educated or uneducated, they comment, compliment, discuss, argue,insist.

2. SENTIMENT ANALYSIS

Permission to make digital or hard copies of all or part of this work for personal or classroom use is granted without fee provided that copies are not made or distributed for profit or commercial advantage and that copies bear this notice and the full citation on the first page. Copyrights for components of this work owned by others than ACM must be honored. Abstracting with credit is permitted. To copy otherwise, or republish, to post on servers or to redistribute to lists, requires prior specific permission and/or a fee. Request permissions from Permissions@acm.org.
ICCCM 2019, July 27–29, 2019, Bangkok, Thailand
© 2019 Association for Computing Machinery.
ACM ISBN 978-1-4503-7195-7/19/07…$15.00
https://doi.org/10.1145/3348445.3348466

Sentiment analysis is the area of study where we deliberate the people's behavior related to any topic, about any chronicle. It is highly produces the big problem zone. It is having different tasks and multifarious names e.g. sentiment mining, subjectivity analysis, affect analysis, review mining etc.

2.1 Level of analysis
There are three different levels of sentiment analysis which are as follows:

2.1.1 Document Level Analysis
At this document level the task is to determine the the overall opinion of the document. It assumes that sentiment analysis at document level expresses opinions at a single entity[12].

2.1.2 Sentence Level Analysis
At this level the task is to determine the whether each and every sentences expressed a positive or negative or neutral opinion.

2.1.3 Entity/Aspect Level Analysis
It is also called feature level analysis. At this level we can find what people likes or dislikes but on the sentence level and document level we can't find what people likes or dislikes. This level perform finer-grained analysis.[11]

3. TWITTER
it is our aim to classify the tweets in various sentiment classes to perform sentiment analysis on twitter data. In this research field, to train a model several approaches have developed which is also used for testing to check its efficiency. It is challenging to perform sentiment analysis on twitter data. There are some reasons defined for this.

Bound tweet Sizesize of the tweets is bounded i.e. it is having only 280 characters which generate intensive statement.

By Using slang wordsthese slang words are bit different from English words. If we used slang words in our sentence then that slang words make an approach outmoded.

Twitter features twitter is permissive to use of URL's, hashtag(#) and user reference. In the twitter feature different processes are used to compare with other different words.

User diversity there are various ways to convey their opinion, people's used different language between the tweets while others used encore words or symbols to convey their emotions. [9]

4. SENTIMENTANALYSIS ON TWITTER DATA

This system basically consist of four stage named as: tweet retrieval, tweet pre-processing, classification algorithm and evaluation.

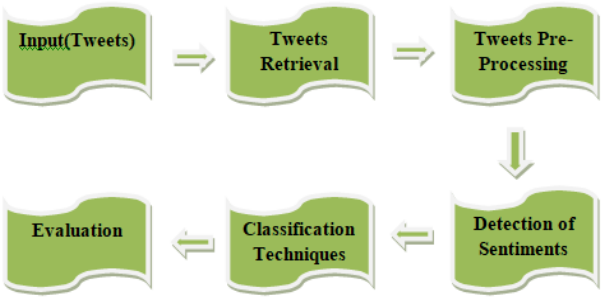

Figure 1. Working of Sentiment analysis in Twitter

Input (Keyword) in the beginning we will choose the subject, with related to that subject we will gather the tweet then after on those tweets we will perform the sentiment analysis.

Tweets Retrieval In this step, tweets will be retrieved, it can be in any form such as, unstructured, structured and semi structured . In sentiment analysis research can be done by the use of different programming language like python or R we can collect the tweets.

Pre-processing in the tweet pre-processing, data is filtered by removing the irrelevant data, inconsistent data and noisy data. Following tasks have to be performed while pre-processing:

- Removal of re-tweets(twitter data sets)
- Removing special characters, URLs, numbers and punctuations etc.
- Removing stopwords
- Stemming
- Tokenization

Sentiment Detection There are various application of sentiment analysis where it is mandatory to find out the sentiment like tweet classification and tweet mining.

In sentiment analysis our task is to find the polarity of the given word. It may be positive, negative or it may be neutral. By the use of different lexicons we can identify the polarity e.g. Bing Lui sentiment lexicons, sentiWord Net etc. which will estimate sentiment score and its strength etc. [11].

- Sentiment classification algorithm

Sentiment analysis can be classified into two approach i.e supervised learning and unsupervised learning. In supervised learning, naïvebayes, SVM and maximum entropy are used to perform the sentiment analysis whereas in unsupervised learning lexicon based, corpus based and dictionary based are used to perform the sentiment analysis. Furthermore Accuracy of classifier is depends on which training and testing dataset is used for which classification method

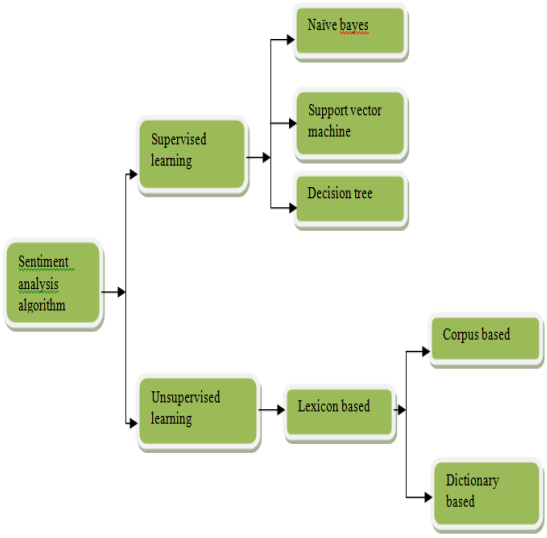

Figure2. Sentiment Analysis Techniques

Evaluation in sentiment analysis final output is analyzed to take decision whether we should opt it or not and then the result are displayed in term of bar graph, pie chart and line graph.

5. LITERATURE SURVEY

For mining the data, there are different text mining approaches are used.

Dhirajgurkhe, Niraj pal and RishitBhatia proposed how twitter data is processed firstly they collected data from various sources and eliminate those feature which does not contribute to find any polarity and then this data send into the sentiment classification engine i.e. naïve bayes classification algorithm which will calculate the probabilities i.e. how much data is corrected and predict the sentiment for the given query.[1]

M.bouazizi, T. ohtsuki have proposed the tweets which contain more than one sentiment called as multi class sentiment analysis. Where they have identify the exact sentiment conveyed by the user rather than the whole sentiment of the tweet. To identify this thing they have also used SENTA tool. They proposed an approach, with the help of this approach they have calculated the sentiment score whoever sentiment is having highest score that will be considered this process is called as "Quantification". [2]

Geetikagautam, DivakarYadav have discussed about customer review classification for which they have used twitter dataset which is already labeled. In this task they have used machine learning based algorithm i.e. naïve bayes, SVM, maximum entropy. They have worked on Python and NLTK for training the SVM, naïve bayes, maximum entropy. Naïve bayes is better techniques in term of accuracy and gives the better result compare to Maximum entropy. We can get the better result with compare to SVM by using the SVM with unigram model. And then further accuracy can be improved by semantic analytic followed by wordNet.[3].

AkshayAmolik, Niketanjivane, MahavirBhandari, Dr. m.venkatesan, a highly suitable model have discussed int his paper which will take the twitter data of upcoming Hollywood and bollywood movies. They are able to this task with the help of classifier and features like SVM and naïve bayes. Both of them

are used for high accuracy but in terms of precision naïve bayes is better than SVM and if we talk about recall then SVM is better than naïve bayes. By increasing the dataset we can increase the classification accuracy.[4]

Subhabrata Mukherjee et al. have discussed a hybrid system named as TwiSent which will resolve problem like spam tweet ,pragmatics, noisy text. Twisent consist of spell checker and pragmatics handler. spell checker finds the noisy text whereas pragmatics handler handles the pragmatics in tweets. Twisent gives better result compare to C-feel-IT system. The accuracy of finding the negative sentiment of Twisentsytem is high the C-Feel-IT.[5].

Dmitry Davidov, Oren Tsur, AriRappoport in this paper they have proposed a supervised sentiment classification structure which works well on twitter data. They have used K nearest neighbor and feature vector. the basic purpose of this framework is to identify and distinguish between sentiment types defined by smiley and tags.[6]

Neethu M S, Rajasree R, the author have used the machine learning techniques in this survey paper to explore the twitter data related to electronic product. They have used feature vector for the tweets classification . they have used three types of classifier i.e. SVM, naïve bayes, maximum entropy, and these classifier were tested using Matlab simulator. SVM and naïve bayes classifier are implemented using built in function. Whereas MaxEnt classifier is used by MaxEntsoftware. So basically the all classifier have nearly the same performance.[7].

Pulkit et al. built and proposed a model which extract tweet from twitter based on the post terror activities. they made their study on terrorist attack which was occurred in URI on 18 September 2016. They considered 59,988 tweet which had taken after the attack. They consider only those tweets which has #UriAttack, #uriattack. #uriattacks. They have used the naïve bayes and SVM to extract the last Re-tweet time and number of Re-tweet[13]

SudarshanSirsat et al. proposed a technique in sentiment analysis on twitter data where they have collected reviews of the product. They have used naïve bayesalgorithm which perform better in term of accuracy and efficiency. They have extracted 200 tweets where the average length of tweet was 70.105. the aim of this research is to identify the characteristic of tweet like how many times the tweet was liked and how many times they have Re-tweet the tweet.[18]

Hetuetal.built and proposed a model in sentiment analysis on twitter data based on anaconda python. They extract the dataset from kaggle in which they classify the people emotions based on positive and negative reviews. This model gives high accuracy on large dataset.[17]

Ali hasan et al. proposed a model using the hybrid approach that comprise sentiment analyzer machine learning. They took only those tweet that is followed by the hashtag(#) and contain the current political trends. Basically this model converts the urdu tweet into English tweet. They took 1690 tweet for training data and 400 for testing the data. They have used the naïve bayes and SVM classifier for training the dataset in weka and building a model. They have used three different libraries to calculate the subjectivity and polarity.[16]

FeddahAlhumaidiAlOtaibi et al. proposed a model by using the supervised and unsupervised algorithm. They wanted to know that which restaurant has more popularity between mcDonald and KFC by using the sentiment analysis. Moreover , they extracted 7000 tweets of both the restaurant by twitter API. The tweet was in English and they used R programming language. Because R programming language can perform big computational task. They have used several machine learning techniques but they found MaxEnt has performed better result compare to other technique. Moreover they have also found KFC have many neutral tweet and McDonald have more positive and negative tweet.[14]

Table 1. Summary of studies selected for review

Author	Datasets description	Techniques	Accuracy
Geetika gautam et.al [3]	Twitter dataset on customer review	SVM Max Entropy, Naïve Bayes Semantic Analysis (WordNet)	85.5% 83.8% 88.2% 89.9%
Seyed-Ali Bahrainian et al. [12]	Twitter data On Smartphones	Unigram feature,Naïve Bayes, MaxEnt,SVM Hybrid Approach	89.78%
Neethu M. S. et al. [7]	Twitter data on Electronic products	Naïve Bayes SVM Max Entropy Essemble	89.5% 90% 90% 90%
Apoorv Agarwal et al.[19]	10,000 manually Annotated Tweets	Unigram Kernel Senti-features Unigram + Senti features Kernel + Senti features	56.58% 60.60% 56.31% 60.50% 60.83%
Dhiraj Gurkhe et al. [1]	Twitter Data	Unigram Bigram Unigram+Bigram	81.2% 15% 67.5%

6. SENTIMENT ANALYSIS ALGORITHM

To classify the text classification problem in sentiment analysis, machine learning is used. In sentiment analysis, mainly there are two categories of learning algorithm.

6.1 Supervised learning

In the field of machine learning, different classification technique are used to classify the unlabeled data. These techniques used different classifier for training the dataset. Example of machine learning classifier naïve bayes, support vector machine, Decision Tree.These can be classified as supervised machine learning classifier which require training data set as prior. In supervised machine learning we do have several data point that describes features variable and target variable. The aim in supervised learning is to predict the final outcome variable given the predictor variable. The goal of supervised learning is to automate time consuming or expensive manual task.

6.1.1 Naïve bayes

Naïve bayes theorem is a classification method with the independent assumption between the predictors. In other words the approach of particular predictor of one class is not connected to closeness of some other class. Let's take an instance ,an apple may be considered a fruit if it is red in color, and if it is round in shape and if its diameter is consider to be three inches approximately. Despite of these feature are dependent on one another or in the presence of another feature. All these independent properties contribute to find the probability of naïve classifier that this is an apple. Naïve bayes is beneficial for big data sets and can be build easily.

6.1.2 Support vector machine

It is a supervised machine learning technique. SVM is well known used to perform in sentiment analysis. In SVM important information is represented in two vector where every vector is of size k. there is a classifier that separate the data in such a manner that margin should be maximum. SVM is used in sentiment classification and it perform better than naïve bayes in term of classification problem.[15]

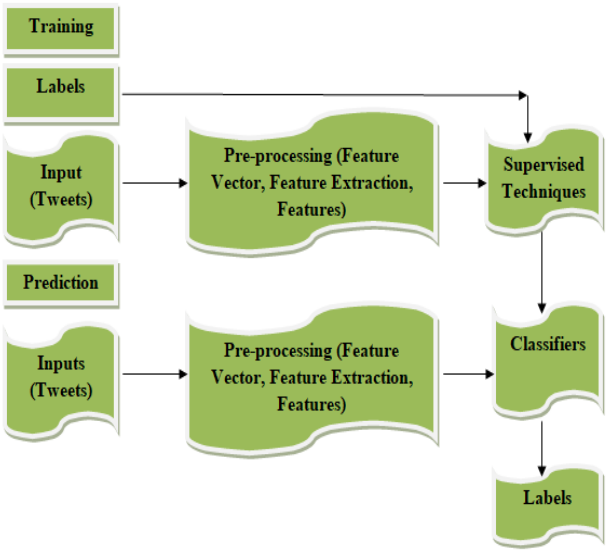

Figure 3. Supervised Learning Techniques used for Training and prediction of data

6.1.3 Decision Tree

Decision tree is a classification algorithm which comes under the supervised machine learning techniques. It is a graphical representation of all the possible solutions to a decision based on certain condition. Such as for every node there is two path "should we go through it is not" and it will come until we will get our aim. In the field of prediction and classification, decision tree play major role. There are various applications of decision tree. Decision tree is used in product design when there are series of decision and the next outcome depends on the previous outcomes. Another application of decision tree is when the user has some objective he wants to get max. profit or he may want to optimize the cost.

6.2 Unsupervised learning

It is an approach of machine learning. It does not use the information that is neither classified nor labeled. it allows the algorithm to perform on that information without human guidance. The task in the unsupervised learning to grouping of unsorted data according to patterns, differences, similarities without any previous information of data. In unsupervised learning there is no human guidance provided that means there is no training of data given to the machine. Therefore in unlabeled data, machine is unable to find the hidden structure by ourselves.

6.2.1 Lexicon Based

Lexicon based approach comes under the unsupervised learning approach. But it uses a dictionary for antonyms and synonyms of sentiments phrases and words with their corresponding opinionated guidelines. Furthermore lexicon based approach is further classified into two approaches i.e. dictionary and corpus based approach which is generally used by lexicon based to find sentiment.

6.2.1.1 Corpus based

It is mainly used to find the new opinionated words from a corpus by using a list of known sentiment words. And the other main use of corpus based approach is to build a sentiment dictionary with the help of other words. Generally this approach is not dominant compare to dictionary based because it needs dictionary of all English words.

6.2.1.2 Dictionary Based

It is used to compile the opinionated words. Generally dictionaries contains list of positive and negative sentiments. The procedure for the dictionary based approach is very easy. In the first stage we manually collect the list of known positive and negative words. Then the algorithm search for the synonyms and antonyms in the wordNet or online dictionaries for growing this dataset. Later they updated the wordlist if found Followed by next iterations. Then this process continues till we got no words to update the dictionaries. Finally when this process is finished then we clean the list manually.

7. CONCLUSION

The twitter data analysis has been made on various datasets to mine the sentiments or opinions. The area of opinion mining or sentiment analysis are defined in this paper where different authors have compared various techniques on a particular dataset to achieve better accuracy and they have also found that naïve bayes works faster than other techniques. The biggest drawback of supervised learning techniques is that it does not produces the best result when the datasest is not sufficient. However in lexicon

based approach, it is necessary to have all words in dictionary related to opinion, if so not then the performance will be degraded.

8. REFERENCES

[1] Gurkhe D., Pal N. and Rishit B. "Effective Sentiment Analysis of Social Media Datasets using Naïve Bayesian Classification." (2014).

[2] Bouazizi, M., Ohtsuki, T.: Multi-Class Sentiment Analysis in Twitter: What if Classification is Not the Answer. IEEE Access. 6, 64486-64502 (2018).

[3] Gautam, G., Yadav, D.: Sentiment analysis of twitter data using machine learning approaches and semantic analysis. 2014 Seventh International Conference on Contemporary Computing (IC3). (2014).

[4] Amolik, Akshay, et al. "Twitter sentiment analysis of movie reviews using machine learning techniques." International Journal of Engineering and Technology 7.6 (2016): 1-7.

[5] Mukherjee S., Malu A., Balamurali A.R, Bhattacharyya P."TwiSent: A Multistage System for Analyzing Sentiment in Twitter".

[6] Davidov D., Tsur O., Rappoport A." Enhanced Sentiment Learning Using Twitter Hashtags and Smileys".

[7] Neethu, M., Rajasree, R.: Sentiment analysis in twitter using machine learning techniques. 2013 Fourth International Conference on Computing, Communications and Networking Technologies (ICCCNT). (2013).

[8] Gupta B., et al. "Study of Twitter Sentiment Analysis using Machine Learning Algorithms on Python." (2017).

[9] Jagdale R., Shirsat V., and Deshmukh S. "Sentiment Analysis of Events from Twitter Using Open Source Tool." (2016).

[10] BongirwarV. :" A Survey on Sentence Level Sentiment Analysis" International Journal of Computer Science Trends and Technology (IJCST) – Volume 3 Issue 3, May-June 2015.

[11] Behdenna S., Barigou F. and Belalem G." Document Level Sentiment Analysis: A survey"(2018).

[12] Bahrainian, S., Dengel, A.: Sentiment Analysis and Summarization of Twitter Data. 2013 IEEE 16th International Conference on Computational Science and Engineering. (2013).

[13] PulkitGarg, HimanshuGarg, VirenderRanga "*Sentiment Analysis of the Uri Terror Attack UsingTwitter*" International Conference on Computing, Communication and Automation (ICCCA2017).

[14] Sahar A. El_Rahman, FeddahAlhumaidiAlOtaibi ,Wejdan Abdullah AlShehri " Sentiment Analysis of Twitter Data".

[15] AbdullahAlsaeedi, Mohammad ZubairKhan"A Study on Sentiment Analysis Techniques of Twitter Data" *(IJACSA) International Journal of Advanced Computer Science and Applications, Vol. 10, No. 2, 2019.*

[16] Ali Hasan, Sana Moin, Ahmad Karim and ShahaboddinShamshirband" Machine Learning-Based Sentiment Analysis forTwitter Accounts" 2018 by the authors. Licensee MDPI, Basel, Switzerland.

[17] HetuBhavsar, RichaManglani" Sentiment Analysis of Twitter Data using Python"International Research Journal of Engineering and Technology (IRJET) Mar 2019e-ISSN: 2395-0056 p-ISSN: 2395-0072.

[18] Prof. SudarshanSirsat, Dr.SujataRao, Dr.BhartiWukkadada"Sentiment Analysis on Twitter Data forproduct evaluation" IOSR Journal of Engineering (IOSRJEN) ISSN (e): 2250-3021, ISSN (p): 2278-8719PP 22-25.(2019)

[19] Apoorv Agarwal et al."Sentiment Analysis on Twitter Data" Proceedings of the Workshop on Language in Social Media (LSM 2011), pages 30–38, Portland, Oregon, 23 June 2011. c 2011 Association for Computational Linguistics.

This article has been accepted for publication in a future issue of this journal, but has not been fully edited. Content may change prior to final publication. Citation information: DOI 10.1109/TCDS.2019.2937796, IEEE Transactions on Cognitive and Developmental Systems

Sentiment Cognition from Words Shortlisted by Fuzzy Entropy

Srishti Vashishtha, and Seba Susan, *Member, IEEE*

***Abstract*—Sentiment analysis (SA) is the process of evaluating human emotions, opinions and reviews expressed in text to detect the writer's mental outlook towards a particular event, topic, product, service, etc. and assign a relevant sentiment. In SA, to highlight the correct words which contribute towards sentiment cognition is very difficult. Simulating this task of shortlisting of words by human observers is challenging due to complexity of human mind's processing. The use of fuzzy entropy is proposed in our work as an innovative step to tap sentiment quotients of online movie reviews. We have proposed a novel approach of shortlisting of words that help in sentiment cognition using a combination of fuzzy entropy, k-means clustering and sentiment lexicon SentiWordNet. We have addressed this challenging task of simulating the human cognition of words by developing a model that recognizes sentiment based on fuzzy scores derived from SentiWordNet in an automatic manner. Experiments on two benchmark movie review datasets-IMDB and polarity dataset by Pang and Lee, with training by LSTM neural networks, yields high accuracy for our approach as compared to other state-of-the-art-methods of SA.**

***Index Terms*—Sentiment Analysis, Human Cognition, Fuzzy Entropy, LSTM.**

I. Introduction

EMOTIONS enact a significant role in successful and effective human to human communication. It is an affective state expressed by human cognition process. Imitating human brain is one of the major challenges and constitute many key problems of artificial intelligence, including understanding natural language, reasoning and emotions. Comprehending the human mental state and deducing the way humans reason and convey information in their language is key to build up the human-machine interaction. Recent studies reveal that there exists a relationship between cognition and emotion; they are interdependent. Sentiment analysis is the process of evaluating human emotions, opinions, reviews expressed in text to detect the writer's mental outlook towards a particular event, topic, product, service, etc. and assign a relevant sentiment [1]. Hence, we require to build a novel cognition-inspired sentiment analysis framework to describe this relationship and help machines mimic human inference of sentiment from natural language. The sentiment is generally classified into binary polarity: positive or negative. This process uses natural language processing (NLP), combined with machine learning classification techniques. NLP is a range of computational techniques for the automatic analysis and representation of human language. Word level approaches to NLP are the first step towards understanding the natural language. NLP techniques can be applied at different levels- document, sentence, fine-grained, cross-domain, cross-lingual with supervised, unsupervised and probabilistic generative model-based approaches [2].

Rapid growth of internet has led to the creation of huge amount of text data, which is freely available on web. Sentiment analysis with NLP can be applied to this data. But in this enormous amount of text data, not all words are significant. Some words are more important than others for computing the sentiment and these get more visual attention. Attention models are integrated with sentiment analysis to highlight the key words in text [3]. Reading time of individual words is also an indicator of the semantic context in text [4],[5]. Many attention models are built using information embedded in text in local context [7-10]. Deep learning- based algorithms have further raised the performance of sentiment analysis [11], [12].

This work attempts to create a bridge between the human mind's processing of words during reading and NLP based sentiment analysis system. We propose a sentiment analysis system based on LSTM (Long Short-Term Memory) with the application of fuzzy logic for shortlisting the words. The fuzzy measure- fuzzy entropy is used to extract cognitive words which is fed into LSTM for training. These cognitive words build up a visual attention model that emulates the way human mind perceives text.

The rest of the paper is organized as follows. Section II present a summary of related work including visual attention model and fuzzy logic. Section III describes the fuzzy entropy measure implemented in our paper. The proposed methodology and experimental setup of our model is discussed in section IV and V respectively. In section VI, we discuss the results. Section VII summarizes the findings of the paper.

S. Vashishtha and S. Susan are with the Information Technology Department, Delhi Technological University, Delhi 110042 (email: srishtidtu@gmail.com and seba_406@yahoo.in)

2379-8920 (c) 2019 IEEE. Personal use is permitted, but republication/redistribution requires IEEE permission. See http://www.ieee.org/publications_standards/publications/rights/index.html for more information.

This article has been accepted for publication in a future issue of this journal, but has not been fully edited. Content may change prior to final publication. Citation information: DOI 10.1109/TCDS.2019.2937796, IEEE Transactions on Cognitive and Developmental Systems

II. RELATED WORK

This paper revolves around human inspired models of text perception, so we review several works from that perspective. Humans use natural language to communicate with each other. The first task of every text-based model is to decipher the natural language used by humans. Natural Language Processing (NLP) is a type of artificial intelligence involved with the interactions between computer and natural language used by human for everyday communication.

A. Natural Language Processing Tools for text pre-processing

NLP along with text mining is used to study relations between human emotions, feeling and opinions. Technologies based on NLP are becoming increasingly widespread. For example, in sentiment analysis, a piece of text written by a human can be broken down using NLP functions, followed by sentiment classification. Language processing delivers more natural human-machine interfaces, and more sophisticated access to stored information, hence it has come to play a central role in the multilingual information society [13]. Opinion mining requires several pre-processing steps in order to transform the natural language text into a form that a machine can interpret. One of the most useful steps is Part of Speech (POS) tagging. A word's POS tagging tell us the morphological affixes it can take. POS also assist in sentiment analysis application by helping select out nouns or other important words from a document [14]. Researchers use different POS Taggers: Stanford POS tagger used by [15], [16], [17] and NLTK POS tagger used by [13], [18]. There are many available toolkits for NLP: NLTK based on python [13], CoreNLP based on Java [19], LTP based on C++/python [20]. NLP techniques can be applied at various levels-document, sentence, fine-grained, cross-domain and cross-lingual with supervised, unsupervised, semi-supervised and probabilistic generative model-based approaches [2]. Our algorithm is a supervised lexicon-based approach at sentence level, it uses sentiment dictionary with opinion words and NLTK POS tagger to generate sentiment scores. The advantage of this approach is to attain stability as well as readability from a carefully designed lexicon to achieve high accuracy from a powerful supervised learning algorithm.

B. Sentiment Recognition by Machine Learning

Sentiment analysis is a language processing task which is applied to extract out the opinion expressed by humans in online reviews, social media, blogs, mobile applications, etc., and classify this opinion into different polarities like positive or negative. Singh *et al.* [24] has minutely analyzed demonetization policy that had occurred in India in 2017, from the common man's viewpoint, by applying the process of sentiment analysis. Pang *et al.* was one of the first research papers in sentiment analysis [21]. They classified the reviews into two classes- positive and negative using machine learning methods (Naive Bayes, maximum entropy and Support Vector Machine (SVM)). This paper doesn't incorporate human cognition. Poria *et al.* [22] proposed a sentiment analysis model that incorporates linguistics and common-sense computing to help machines imitate human inference of sentiment from natural language. SenticNet lexicon was used by them to calculate overall polarity of sentence, this calculation process is analogous to electronic circuits. Some researchers have performed sentiment analysis of textual data posed by humans on popular topics. Reference [23] developed an interactive visualization system SentiView, which interprets public sentiments posted by users in textual form on online forums and predicts short term trend of sentiments as well.

Performance of textual sentiment classification can be enhanced by using neural networks. Deep neural networks use convolution neural network (CNN) to extract out high level features from input sequence. In recent years, CNN has performed extraordinarily well on NLP tasks [25-28]. These research works fail to learn long-term dependencies. Recurrent neural networks are remarkable in text classification and are particularly favorable when data is sequential or have contextual view [29]. However, standard RNN suffers from the gradient vanishing problem where gradients may grow or decay exponentially over long sequences. To address this problem, Long-Short Term Memory model (LSTM) is introduced. LSTM is a type of RNN where newer information is more critical than older information (more recent words contain more weight on current neuron state). Recently, many papers have implemented LSTM for sentiment analysis [11-12], [29-31]. In order to extract deep features out of textual data and performing sentiment classification, the choice of LSTM classifier is the best. This is because LSTM is proficient in learning sequence characteristics, due to its ability to acquire syntax features of linguistics. In this paper, we have applied sentiment analysis on movie reviews and classified them as positive or negative using LSTM neural network. Cognitive features are extracted by incorporating visual attention model and fuzzy logic. These features emulate human mind, and are fed as input to LSTM network.

C. Visual Attention of Words

Attention is defined as the active direction of mind to an object, something that is interesting or important. Some inputs are indeed more important than others, with aspect to a particular goal. In this paper, the object is the word, so attention of words means the capability of human mind to concentrate on the subset of total words available to them. Algorithms can also assign attention, and they can learn how to do it better, by adjusting the weights they assign to different inputs. A recent trend in deep learning is to incorporate attention mechanisms. These attention mechanisms in neural networks are based on visual attention mechanism and related to human cognition. Long *et al.* [3] developed an attention model which is trained by cognitive features of eye-movement pattern data. They emphasized that not all words in text are equal, important words can be read in less time by human eye. A cognition based attention layer (CBA) for neural network-based sentiment analysis model is developed by using the

2379-8920 (c) 2019 IEEE. Personal use is permitted, but republication/redistribution requires IEEE permission. See http://www.ieee.org/publications_standards/publications/rights/index.html for more information.

This article has been accepted for publication in a future issue of this journal, but has not been fully edited. Content may change prior to final publication. Citation information: DOI 10.1109/TCDS.2019.2937796, IEEE Transactions on Cognitive and Developmental Systems

predicted reading time, which is dependent on eye-tracking data. This model performs better than [9], [32] because CBA gives higher weight to sentiment linked words. Readers' capability of understanding text depends upon two factors: text information and text energy [4]. Experiments reveal that the capability of understanding text is directly proportional to text information and inversely to text energy. Text energy is directly proportional to the sum of keywords in a text. This implies that if there are less keywords, the reader will consume less text energy and understand the text easily in less time. This motivated us to build our model that selects few important words, which is similar to a human mind that glances at only few keywords with less energy and understands the sentiment of text quickly. Experiments on finding significant keywords are fond amply in literature. Susan *et al.* used a maximum entropy partitioning method to find out unique elite keywords for document databases [6]. Demberg *et al.* [5] mentioned that readers' eyes fixate longer on words that have higher semantic roles, infrequent words, morphological complex words and ambiguous words. Tang *et al.* [7] works on only document level sentiment classification. It incorporates user and product level information into neural network, both of which greatly affect the interpretation of textual sentiment. Yang *et al*. developed a hierarchical attention network for document classification that has two levels of attention mechanism at word and sentence level [8]. These layers pick out qualitative informative words and sentences. This model outperformed Bag of Word method, Supervised Vector Machines, CNN, etc. and obtained better visualization. Tang *et al.* [7] only focused on local text information of user and product to address global data. Gui *et al.* [10] proposed a neural sentiment classification model by taking global user and product information. The attention mechanism is in both word and semantic levels. Compared to [5], this model contains less parameters and is more efficient in training. Eye-tracking technology has been used recently for sentiment analysis [18], [33-34]. Mishra *et al.* [18] built a model that uses traditional and cognitive features derived from eye-tracking patterns of human readers for sentiment analysis. When readers read sentiment bearing text, their eye-movement patterns can be interpreted to handle linguistic nuances better. These cognitive features grant sentiment analyzers the means to tackle complex constructs like irony, thwarting and sarcasm. This model computes subjective scores with the help of SentiWordNet lexicon [35]. Reference [36] discusses about critical spacing between words in a sentence. If the words are placed too close to each other (crowded) it will form a jumbled percept leading to combined features of those words that might mislead. An adequate amount of critical spacing is required between words, those who exceed this spacing comes into uncrowded window. Readers can perceive wrong results due to visual crowding. This concept deduces that visual layout of words is important for grasping correct words. In our work, the text is in printed format in an uncrowded window. Mostly papers have generated the cognitive features with eye-movement patterns but our algorithm generates the cognitive feature by selecting the important key words from text using fuzzy logic in automatic manner without human intervention. Our approach is the first of its kind to the best of our knowledge.

D. Fuzzy Solutions for Sentiment Analysis

Many researchers have applied fuzzy logic in sentiment analysis. References [37,38] have used trapezoidal fuzzy membership in sentiment analysis. Reference [37] performed multi-domain sentiment analysis by computing polarity of text using resources: SenticNet and General Inquirer and [38] applied fuzzy rules on the membership degree values to give output reflecting different intensities of sentiment. Some researchers have built their own lexicon to evaluate sentiment of user reviews from online websites [39,40]. Fuzzy rules can be applied on words [41,42] or phrases [43] of text to determine the sentiment of text. A fuzzy logic based approach developed by the authors in [44] computes the sentiment of cricket fans using SentiWordNet lexicon by analyzing their tweets. Sentiments are aggregated over a time period to plot their dynamic mood versus time. Bhoir *et al.* [41] used SentiWordNet lexicon but achieved low accuracy compared to learning by Naïve Bayes and SVM. Our work also uses SentiWordNet lexicon with higher accuracy results. Indhuja *et al.* [45] proposed a model that emulates the effect of linguistic hedges integrated in sentiment classification task. Feature Orientation dictionary with Linguistic Hedges and SentiWordNet lexicon are used in this model to store the features and identify the score of these features respectively. These papers have achieved limited accuracy due to the lack of training data. Moreover, none of these papers have incorporated selective human cognition of words with fuzzy logic. Our paper has evaluated the sentiment quotient of words using fuzzy entropy for extracting important words that aid in sentiment cognition. The next section discusses about the fuzzy measure-fuzzy entropy that has been used for the evaluation.

III. FUZZY ENTROPY

A fuzzy set A can be represented as $A=\{(x,\mu_A(x)\},x\in U$ where x is the element from the universal set U and $\mu_A(x)$ is the membership of element x and there are total n elements. Different fuzzy measures can be applied on a fuzzy set: cardinality, energy, entropy, specificity, etc. [46]. In our paper, we have applied entropy measure of fuzziness. Luca *et al.* [47] defined the fuzzy entropy of a fuzzy set as follows:

$$d(f)=H(f)+H(\overline{f}) \tag{1}$$

where $(\overline{f})$ is defined as 1-(f), the complement of the fuzzy set. This entropy is based on Shannon Entropy given by:

$$H(p)=-\sum_{i=1}^{n} p_i \log p_i \tag{2}$$

where p_i is the probability of the ith element and i =1,2…n. The equation for Shannon Fuzzy entropy, H_A, is obtained by

2379-8920 (c) 2019 IEEE. Personal use is permitted, but republication/redistribution requires IEEE permission. See http://www.ieee.org/publications_standards/publications/rights/index.html for more information.

This article has been accepted for publication in a future issue of this journal, but has not been fully edited. Content may change prior to final publication. Citation information: DOI 10.1109/TCDS.2019.2937796, IEEE Transactions on Cognitive and Developmental Systems

substituting p_i with membership $\mu_A(x_i)$ in (2) and using (1).

$$H_A = -\sum_{i=1}^{n}[\mu_A(x_i)\log\mu_A(x_i) + (1-\mu_A(x_i))\log(1-\mu_A(x_i))] \quad (3)$$

Different forms of fuzzy entropy have been proposed in literature; these measures satisfy the basic properties of fuzzy entropy [48-50]. The properties of fuzzy entropy are [47]:

1. H_A =0 if A is crisp set ($\mu_A(x_i)$ = 0 or 1 if $\forall x_i \in A$).
2. H_A is maximum if $\mu_A(x_i)$ =0.5 $\forall x_i \in A$.
3. $H_A \geq H_A^*$, where H_A^* is the entropy of A^*, a sharpened version of A.
4. $H_A = \overline{H_A}$, where $\overline{H_A}$ is the entropy of the complement set $\overline{A}$
5. H_A increases monotonically in the interval [0,0.5] and decreases monotonically in the interval [0.5,1].
6. H_A is a non-linear curve.
7. H_A is a concave function of $\mu_A(x_i)$.

These properties can be observed graphically in Fig. 1. For this purpose, we have evaluated the values of H_A corresponding to different values of $\mu_A(x_i)$, as shown in Table I:

TABLE I

ENTROPY VALUES H_A VERSUS μ_A VALUES

$\mu_A(x_i)$	$H_A(\mu_A(x_i))$
0	0
0.1	0.3251
0.2	0.5004
0.3	0.6109
0.4	0.6730
0.5	**0.6931**
0.6	0.6730
0.7	0.6109
0.8	0.5004
0.9	0.3251
1	0

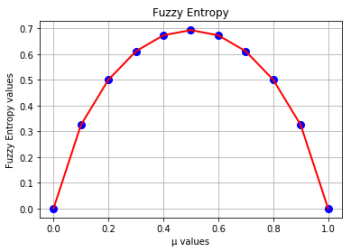

Fig. 1. Graph of Fuzzy Entropy.

In Fig. 1, it is clearly visible that fuzzy entropy value is 0 when $\mu_A(x_i)$ = 0 or 1, it attains maximum value at $\mu_A(x_i)$ =0.5. It is symmetric because it attains same value for complement set, for example H_A(0.3)=0.6109 and H_A (1-0.3)= H_A(0.7)=0.6109. The sixth property of fuzzy entropy is its non-linearity. It is clearly visible in Fig. 1 that the slope of the graph is not constant. The third property states that $H_A \geq H_A^*$ for the sharpened version of A. Sharpened means crisper, the entropy value is high when there is more fuzziness and its low when there is less fuzziness (crisp). We have applied this property in our work, to select the significant words in text. In sentiment analysis, the words that carry more emotion have got either very positive or very negative sentiment scores. So, we deal with extreme boundaries of $\mu_A(x_i)$ that correspond to low fuzzy entropy values. We remove the words which carry high fuzzy entropy values as they are insignificant and they don't contribute in evaluation of sentiment of text. In doing so, we take the advantage of properties 1-7 listed above since the non-linearity of the fuzzy entropy curve ensures that very few words are shortlisted. The symmetricity of the curve ensures that the minimum strength of positive and negative shortlisted scores remains the same.

IV. PROPOSED APPROACH

In this paper, we propose a supervised model that grades words for sentiment quotients using fuzzy entropy. k-means clustering is used to segregate the important words versus non-significant words and the significant words are finally trained using LSTM classifier. The shortlisted words in text are extracted in an automatic manner without any human intervention. Our model emulates the way the human brain thinks, by giving attention to significant words only. This section discusses the methodology adopted in this paper, starting with fuzzy logic, in the context of sentiment analysis.

A fuzzy set A can be represented as $A = \{(x, \mu_A(x)\}, x \in U$ where x is the element from the universal set U and $\mu_A(x)$ is the membership of element x. In our approach, Universe of Discourse is the set of all the words in each review. First of all, tokenization of review into sentences and sentences into words takes place. Words are tagged using NLTK POS Tagger [13] and lemmatized. Only those words that are nouns, adjectives, verbs or adverbs are used further. If the lemmatized word exists in SentiWordNet, its scores are obtained. Each word has positive and negative score ((6) and (7)) and can be interpreted as a fuzzy membership pertaining to the fuzzy sets Pos and Neg ((4) and (5)).

$$Pos = \{(a, \mu_{Pos}(a)\}, a \in X_i \quad (4)$$

$$Neg = \{(a, \mu_{Neg}(a)\}, a \in X_i \quad (5)$$

where a is the word. The membership functions $\mu_{Pos}(a)$ and $\mu_{Neg}(a)$ associated with the lemmatized word a are defined below. These are average positive and negative scores.

$$\mu_{Pos}(a) = \frac{\sum_{synsets}[syn.pos_score()]}{length(synsets)} \quad (6)$$

$$\mu_{Neg}(a) = \frac{\sum_{synsets}[syn.neg_score()]}{length(synsets)} \quad (7)$$

2379-8920 (c) 2019 IEEE. Personal use is permitted, but republication/redistribution requires IEEE permission. See http://www.ieee.org/publications_standards/publications/rights/index.html for more information.

This article has been accepted for publication in a future issue of this journal, but has not been fully edited. Content may change prior to final publication. Citation information: DOI 10.1109/TCDS.2019.2937796, IEEE Transactions on Cognitive and Developmental Systems

where $syn.pos_score()$ and $syn.neg_score()$ are the scores obtained from SentiWordNet; synset is the set of synonyms of each word present in SentiWordNet. We are assuming that the strength of human cognition can be measured using scores from SentiWordNet since human annotators have compiled this lexicon. The difference of positive and negative score is delta score $\mu_d(a)$, that is represented as:

$$\mu_d(a) = [\mu_{Pos}(a) - \mu_{Neg}(a)] \tag{8}$$

The normalization of delta score is fuzzy score *m* shown in (9), where $\mu_{Min}(a)$ and $\mu_{Max}(a)$ are maximum and minimum value of delta score in each sentence of review. Substituting the fuzzy score value *m* in the fuzzy entropy formula in (3), H_i is formulated in (10) and calculated for each word in a sentence.

$$m = \frac{\mu_d(a) - \mu_{Min}(a)}{\mu_{Max}(a) - \mu_{Min}(a)} \tag{9}$$

$$H_i = -[m\log(m+eps) + (1-m))\log((1-m)+eps)] \tag{10}$$

The fuzzy entropy for each word is calculated for all sentences in a review. k-means clustering [51] is applied on these entropy values to segregate them in to two clusters: low entropy and high entropy. Centroids (*c1* and *c2*) of each cluster is calculated, their mean, *threshold*, is computed, as shown in (11).

$$threshold = \frac{c1+c2}{2} \tag{11}$$

We are interested in the entropy values less than this *threshold*, the words corresponding to these entropy values are selected. These are the significant words which contribute in evaluating the sentiment of review. This *threshold* cuts the fuzzy entropy graph into two halves, the lower entropy values are selected as shown in Fig. 2. Suppose the computed *threshold*=0.4, entropy values less than 0.4 are selected, these values are marked in bold. k-means clustering is applied on all fuzzy entropy values of a review, it divides these values into two clusters. The cluster with values less than threshold is selected as depicted in Fig. 3. Algorithm1 describes the steps to extract shortlisted words from a review. These shortlisted words are trained on LSTM network to evaluate the sentiment of all reviews.

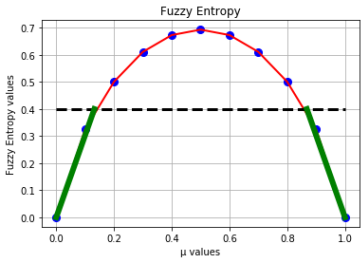

Fig. 2. Graph of Fuzzy Entropy with threshold=0.4.

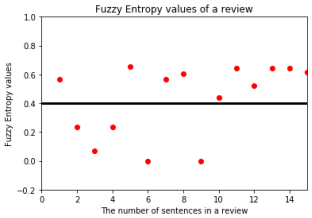

Fig. 3. k-means clustering applied on entropy values of a review.

Algorithm1 GetShortlistedWords

```
1:  function GetShortlistedWords(review)
2:  call GetFuzzyScore(review)

    1:  function GetFuzzyScore(review)
    2:  sentenceTokens = nltk. sent_tokenize(review)
    3:  for each sentenceToken in sentenceTokens do
    4:  processed_sentenceToken: Pre-Process sentenceToken
    5:  wordTokens = [nltk.word_tokenize(processed_sentenceToken)]
    6:  for each wordToken in wordTokens do
    7:  POS Tagging wordToken
    8:  lemmatizedWordToken = Lemmatize wordToken
    9:  if ((lemmatizedWordToken is Noun) OR
        (lemmatizedWordToken is Adjective)
        OR (lemmatizedWordToken is Verb) OR
        (lemmatizedWordToken is Adverb))
        AND (lemmatizedWordToken exists in SentiWordNet)
    10: Calculate average scores for wordToken using (6) and (7)
        avgPosScore = average Positive score;
        avgNegScore = average Negative scores;
    11: deltaScore = avgPosScore - avgNegScore (difference of above
        scores) using (8)
    12: fuzzyScore = Normalize deltaScore using (9)
    13: return listFuzzyScore = fuzzy Score for each word in each
        sentence of the review
    14: end function

3:  for each fuzzyScores in listFuzzyScore do
4:  call GetFuzzyEntropy(fuzzyScores)
    1:  function GetFuzzyEntropy(fuzzyScores)
    2:  For each fuzzyScore in fuzzyScores do
    3:  Calculate Fuzzy Entropy for fuzzyScore using (10)
    4:  Return fuzzyEntropy
    5:  End function
5:  fuzzyEntopies.Append = fuzzyEntropy
6:  return fuzzyEntropies

7:  call GetThresholdFromClustering(fuzzyEntropies)
    1:  Function GetThresholdFromClustering(fuzzyEntropies)
    2:  Create two clusters of low and high fuzzy Entropies
    3:  Calculate centroid of low and high clusters
    4:  Calculate threshold = Mean of Centroids using (11)
    5:  Return Threshold

8:  call GetFuzzyEntropy(fuzzyScores)
9:  FuzzyEntropyScores.Append = fuzzyEntropy
10: for each fuzzyEntropyScore in FuzzyEntropyScores
11: if fuzzyEntropyScore < threshold
12: ShortlistedWordTokens.Append = wordToken corresponding to that
    fuzzyEntropyScore
13: return ShortlistedWordTokens
14: end function
```

V. EXPERIMENTAL SETUP

In our approach, we have used two movie review datasets.

2379-8920 (c) 2019 IEEE. Personal use is permitted, but republication/redistribution requires IEEE permission. See http://www.ieee.org/publications_standards/publications/rights/index.html for more information.

This article has been accepted for publication in a future issue of this journal, but has not been fully edited. Content may change prior to final publication. Citation information: DOI 10.1109/TCDS.2019.2937796, IEEE Transactions on Cognitive and Developmental Systems

First one is the Movie Review Dataset IMDB[1]. Each movie review has several sentences. The IMDB dataset has a training set of 25,000 labeled instances and a testing set of 25,000 labeled instances; the dataset has positive and negative labels balanced in training and testing set. Many researchers have experimented on the IMDB dataset for sentiment analysis [11-12],[31], [52-53]. The second is polarity dataset v2.0 by Pang and Lee[2] [54]. This dataset contains 1000 positive and 1000 negative processed movie reviews. The train/test split of this dataset is 70-30 and we report 10-fold cross validation results. The code for our work is available online[3]. Our model is implemented on Keras, which is a popular python library, to create a LSTM network for classification task. Text-preprocessing is implemented using NLTK (natural language processing toolkit) python library [13]. Both datasets were preprocessed to a dictionary size of 5,000 words.

A LSTM sequential model with linear stack of layers is built up. The first layer is embedding layer with vocabulary size of 5,000 words with a zero-padded maximum sequence of 500 words per review and embedding size of 32. In second layer, 100 units of LSTM are added. The last layer is a fully-connected layer from the concatenated input to a single output. The layer is followed by a simple sigmoid activation function to limit the output between 0 and 1. The final yield is a single output.

The model is compiled using adam as optimizer and binary crossentropy as loss function. This loss calculates loss with two classes (0 and 1). In our experiments, 0 represents negative sentiment and 1 represents positive sentiment. The loss is calculated on the single and final output of the dense layer. The best network used a batch size of 64 and 3 epochs.

VI. RESULTS AND DISCUSSIONS

A. Comparison with other sentiment analysis techniques

In this section, we discuss the results of our proposed approach described in section IV. The comparison of our model and other models on the IMDB movie review dataset are shown in Table II. Beineke *et al.*, have used Naïve Bayes (NB) model for sentiment classification [56]. They have extracted a pair of derived features that are linearly combined to predict the sentiment. This method achieved the lowest accuracy of 65.9% as evident from Table II. Pang *et al.*, have considered the aspect of sentiment classification based on categorization study, with positive and negative sentiments [21]. They have undertaken the experiment with three different machine learning algorithms, such as NB, SVM, and Maximum Entropy. They have used bag-of word features framework to implement the machine learning algorithms. As per their analysis, NB algorithm shows poor result among the three algorithms and SVM algorithm yields the best result with accuracy 82.9%. Matsumoto *et al.*, have used the syntactic relationship among words as a basis of document level sentiment analysis [57].

The combined unigram+bigram as word feature gives an accuracy of 84.6%. Both the traditional and the proposed LSTM models in [31] plateaued at an accuracy just over 80%, with a maximum under 85%. Mullen and Collier have applied SVM algorithm for sentiment analysis where values are assigned to few selected words and then combined to form a model for classification and achieved 86% accuracy [58]. Authors in [53] proposed a hybrid supervised-unsupervised model when they created the IMDB review sentiment dataset. Their highest reported accuracy was 88.89% from their full model with additional unlabeled reviews and bag of words vectors. Authors in [55] experimented with multiple variation of machine learning models (NB, SVM, Maximum entropy, etc.) on the IMDB dataset. Their approach converted text reviews into numeric matrices using countvectorizer and TF-IDF, which were then given as input to machine learning algorithms for classification. The best accuracy achieved in [55] was 88.94% from their combined Unigram-Bigram-Trigram model using SVM. Our proposed model has achieved the highest accuracy of 89.80% in IMDB dataset.

We have compared our approach with different state-of-the-art methods of sentiment analysis on polarity dataset by Pang and Lee [54] in Table III. The SVM classifiers used in the comparison methods have gaussian (rbf) kernel with C=1.0 and auto-mode for gamma. Naïve Bayes classifier [56] achieves 71.17% and LSTM [31] gives an accuracy of 69.45%. Our proposed model has achieved the highest accuracy of 78.5% in this dataset.

We have performed t-test to determine if the results are statistically different. For t-tests we have compared the predicted output of our method with other comparison methods. In t-tests, the larger the t score, the more difference there is between groups. The smaller the t score, the more similarity there is between groups. A p-value is the probability that the results from the sample data occurred by chance. Low p-values are good; They indicate your data did not occur by chance. Since our t-scores are generally high and p-values are generally low, this implies the results of these comparison methods are statistically different as compared to our method's results. Our t-test results are shown for the IMDB dataset in Table II and for the polarity dataset by Pang and Lee in Table III.

Very few works have considered downsizing the sample set based on cognitive principles. We have implemented our model by generating cognitive words as features using fuzzy entropy measure, and these cognitive shortlisted words are fed as input to LSTM network. The application of fuzzy logic provides fuzzy reasoning and LSTM layers are able to use the information for a better interpretation of sentiments while classifying the reviews. LSTM is a more complicated function that learns to control the flow of information so as to prevent the vanishing gradient and allow the recurrent layer to more easily capture long-term dependencies. It is also proficient in learning sequence characteristics due to its ability to acquire syntax features of linguistics. The accuracy of our proposed model surpasses the previously published models.

[1] http://www.imdb.com/
[2] http://www.cs.cornell.edu/people/pabo/movie-review-data/
[3] https://github.com/SrishtiVashishtha/Sentiment-Cognition-from-Words-Shortlisted-by-Fuzzy-Entropy

2379-8920 (c) 2019 IEEE. Personal use is permitted, but republication/redistribution requires IEEE permission. See http://www.ieee.org/publications_standards/publications/rights/index.html for more information.

This article has been accepted for publication in a future issue of this journal, but has not been fully edited. Content may change prior to final publication. Citation information: DOI 10.1109/TCDS.2019.2937796, IEEE Transactions on Cognitive and Developmental Systems

TABLE II
COMPARISON OF OUR METHOD COMPARED TO OTHER SENTIMENT TECHNIQUES ON IMDB DATASET

Models	IMDB Accuracy (in %)	t-test Statistic Score	p-value
Naïve Bayes [56]	65.9	13.03	$9.31e^{-39}$
Unigram SVM [21]	82.9	-23.33	$8.389\ e^{-120}$
Unigram+Bigram [57]	84.6	-23.89	$1.821\ e^{-125}$
LSTM [31]	85	-18.04	$1.574\ e^{-22}$
SVM [58]	86	-227	0
Bag of Words [53]	88.89	-16.47	$8.10e^{-61}$
Unigram+Bigram+Trigram SVM [55]	88.94	-23.96	$3.388\ e^{-125}$
Our proposed model	89.80		

TABLE III
COMPARISON OF OUR METHOD COMPARED TO OTHER SENTIMENT TECHNIQUES ON PANG AND LEE DATASET

Models	Pang and Lee Accuracy (in %)	t-test Statistic Score	p-value
Naïve Bayes [56]	71.17	3.543	0.0004
Unigram SVM [21]	68	12.37	$3.31\ e^{-33}$
Unigram+Bigram [57]	61.5	17.51	$2.37\ e^{-61}$
LSTM [31]	69.5	-0.01	0.984
SVM [58]	49.7	43.66	$5.7e^{-250}$
Bag of Words [53]	68.5	14.08	$8.46\ e^{-42}$
Unigram+Bigram+Trigram SVM [55]	49.6	44.23	$3.5e^{-254}$
Our proposed model	78.5		

B. Sentiment Cognition from shortlisted words

1) Positive review example

We here demonstrate sentiment cognition from shortlisted words using our approach. The shortlisted words in a positive movie review are marked in bold as shown in Fig. 4. We can clearly observe the words like “great”, “hard”, “shines”, “best”, etc. are conveying positive emotion, thereby this review is classified as positive.

Bobbie Phillips, who in her own right has amassed a **great** list of credits as a **hard** working Hollywood actress, **shines** in this third installment of UPN and Village Roadshow is Chameleon series. Bobbie **delivers** this **role** to the viewers with **great** panache. The action and **stunts** were the **best** in the series.

Fig. 4. A positive movie review

2) Negative review example

Similarly, we next demonstrate the evaluation of negative sentiment cognition from shortlisted words. Fig. 5 depicts the shortlisted words marked in bold. The words “shame”, “bad”, “forget”, “not” convey negative emotion, hence this review is classified as negative.

It **is** a **shame**. There is an **interesting** idea here, but it gets **completely** lost in a confusion of Commodore 64 style computer effects and **bad** storytelling. It should be a fairly straightforward hunter/hunted kind of story, but the director and/or the writer **seem** like they **forgot** what the movie was **supposed** to be when they were about three days into shooting. **Not** much to **recommend** here, even the title **seems** to propel it into obscurity.

Fig. 5. A negative movie review

3) Challenging review example

There are some reviews where evaluating sentiment cognition from shortlisted words become difficult. Like in Fig. 6, the shortlisted words are “like”, “liked”, “not” and “artistic” are marked in bold. Here, some simple emotion words are left out due to presence of strong emotion words (“not”). The review is classified as negative.

I usually ignore whatever rating IMDb has when looking up a movie because I think I might **like** it anyway or whatever and I should at least give it a chance, but this time I wish I would paid attention. I know some people **liked** it, and I am **not** trying to say that they should **not**. The actors were either positively wooden or way over the top, and the film quality was awful, fuzzy and grainy and bland and **not** in an **artistic** way at all.

Fig. 6. A challenging movie review

C. Sensitivity Analysis for threshold selection

In this section, we discuss the sensitivity analysis of threshold selection. This threshold is based on k-means clustering of fuzzy entropy values. The following are different cases of shortlisted words under different thresholds, used to slice the fuzzy entropy graph for a movie review from IMDB dataset. All the values below threshold are selected. Fig. 7 depicts a sample review for the experiment.

the movie had extremely rich colour, in the way the house was decorated, in the clothes that the characters wore, in the open-skied daylight scenes that is in contrast to most horror movies, which, typically makes use of desaturated tones and gloomy environs (think Dark Water, which is another show i like) that gives this film a sense of aesthetics and joy when it was not in its, more, gripping moments.

Fig. 7. A sample movie review

2379-8920 (c) 2019 IEEE. Personal use is permitted, but republication/redistribution requires IEEE permission. See http://www.ieee.org/publications_standards/publications/rights/index.html for more information.

This article has been accepted for publication in a future issue of this journal, but has not been fully edited. Content may change prior to final publication. Citation information: DOI 10.1109/TCDS.2019.2937796, IEEE Transactions on Cognitive and Developmental Systems

1) Threshold is too low (0.1-0.2)

When the threshold is too low (0.1-0.2), very few words are shortlisted, hence polarity of review can't be determined. The shortlisted words are shown in bold in Fig. 8 and the corresponding fuzzy entropy graph with threshold 0.2 is shown in Fig. 9.

the movie had extremely rich colour, in the way the house was decorated, in the clothes that the characters wore, in the open-skied daylight scenes that is in contrast to most horror movies, which, typically makes use of desaturated tones and gloomy environs (think Dark Water, which is another show i like) that gives this film a sense of aesthetics and **joy** when it was **not** in its, more, gripping moments.

Fig. 8. Shortlisted words in movie review when threshold is 0.2

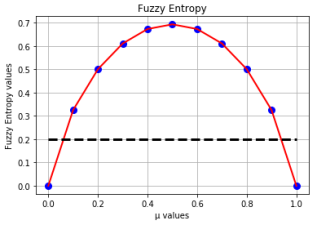

Fig. 9. Fuzzy entropy graph when threshold is 0.2

2) Threshold is too high (0.6)

When threshold is 0.6, more shortlisted words are obtained. Not all of these words are important, some extra words have been shortlisted which will predict the wrong polarity of the sentence. The shortlisted words are shown in bold in Fig. 10 and the corresponding fuzzy entropy graph with threshold 0.6 is shown in Fig. 11. We can clearly see when threshold is too high the graph is divided unequally, almost all fuzzy entropy values are selected.

the movie had **extremely rich** colour, in the way the house was **decorated**, in the clothes that the **characters** wore, in the open-skied daylight scenes that is in contrast to most horror movies, which, **typically makes use** of desaturated tones and **gloomy** environs (**think** Dark Water, which is another show i like) that gives this film a **sense** of **aesthetics** and **joy** when it was **not** in its, more, **gripping** moments.

Fig. 10. Shortlisted words in movie review when threshold is 0.6

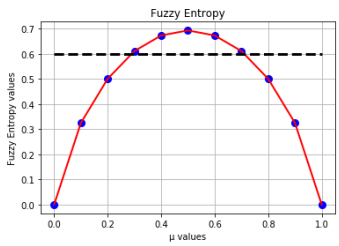

Fig. 11. Fuzzy entropy graph when threshold is 0.6

3) Threshold is medium (0.3-0.5)

When threshold is 0.4, some shortlisted words are obtained which are appropriate to determine the polarity of the sentence correctly. The shortlisted words are shown in bold in Fig. 12 and the corresponding fuzzy entropy graph with threshold 0.4 is shown in Fig. 13. We can observe this threshold divides the graph almost equally, the values lower than threshold are the significant words.

the movie had **extremely rich** colour, in the way the house was **decorated**, in the clothes that the **characters** wore, in the open-skied daylight scenes that is in contrast to most horror movies, which, typically makes use of desaturated tones and **gloomy** environs (think Dark Water, which is another show i like) that gives this film a sense of **aesthetics** and **joy** when it was **not** in its, more, **gripping** moments.

Fig. 12. Shortlisted words in movie review when threshold is 0.4

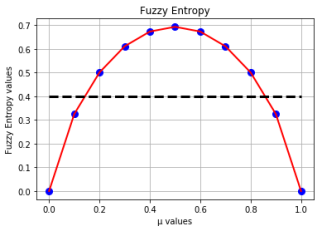

Fig. 13. Fuzzy entropy graph when threshold is 0.4

D. Sensitivity Analysis for threshold selection

The experiment was validated by word annotations by 15 human observers. Each observer's shortlisted words for the sample review were noted down. We followed the protocol for Manual Annotation Task. The annotator was asked to glance through the paragraph and write with memory the significant words they remember. An ethical clearance certificate was obtained from all the collaborators stating that their inputs could be utilized for research purpose without revealing of individual identity. Their motive of shortlisting words was not based on sentiment analysis. The compiled list of all shortlisted words for the positive review with their frequencies are shown in Fig. 14. We can infer that many people perceived negative words as well, like "horror" or "Dark" but out algorithm can correctly identify the positive sentiment words like "extremely", "rich", "joy", etc.

Fig. 14. Shortlisted words by human observations

We compared the shortlisted word list by machine (our fuzzy method) with each of the human annotators and computed the Precision, Recall and F-scores. These are presented in Table IV. We also predicted the sentiment for these shortlisted words using our fuzzy method (machine).

2379-8920 (c) 2019 IEEE. Personal use is permitted, but republication/redistribution requires IEEE permission. See http://www.ieee.org/publications_standards/publications/rights/index.html for more information.

This article has been accepted for publication in a future issue of this journal, but has not been fully edited. Content may change prior to final publication. Citation information: DOI 10.1109/TCDS.2019.2937796, IEEE Transactions on Cognitive and Developmental Systems

TABLE IV
COMPARISON OF OUR MACHINE METHOD COMPARED WITH HUMAN MIND

	Ma	HA1	HA2	HA3	HA4	HA5	HA6	HA7	HA8	HA9	HA10	HA11	HA12	HA13	HA14	HA15
Precision		0.56	0.22	0.44	0.44	0.44	0.33	0.33	0.33	0.22	0.22	0.33	0.56	0.44	0.56	0.44
Recall		0.56	0.2	0.44	0.4	0.4	0.38	0.38	0.33	0.22	0.29	0.3	0.5	0.36	0.44	0.4
F-Score		0.56	0.21	0.44	0.42	0.42	0.35	0.35	0.33	0.22	0.25	0.32	0.53	0.4	0.42	0.42
Sentiment	**Pos**	Pos	Neg	Pos	Pos	Pos	Neg	Pos	Pos	Neg	Neg	Neg	Neg	Neg	Neg	Neg

We can clearly observe the machine shortlisted words depicts positive sentiment and out of 15 only 6 predicted positive sentiment, rest predicted negative. Hence our fuzzy method (machine) predicts the correct sentiment at a higher rate than human annotators. In Table IV, Ma stands for Machine and HA stands for Human Annotators.

VII. CONCLUSION

Sentiment analysis is a language processing task which is applied to extract the opinion expressed by humans in online reviews, social media, blogs, mobile applications, etc., and classify this opinion into polarities like positive or negative. In this paper, we have proposed a model that extracts out the high sentiment cognition words from text in an automated way using fuzzy entropy measure for fuzzy reasoning. The fuzzy scores are extracted from SentiWordNet lexicon that has been compiled with the help of human annotations. Clustering technique is applied to these fuzzy entropy values to divide them into two clusters of significant and non-significant words. We are interested in the cluster with low fuzzy entropy values since they correspond to the important words which contribute in evaluation of the sentiment of text. Our approach emulates the way human mind works by glancing at only a few key important words in text, to determine the polarity of review. These shortlisted words are trained using a LSTM network. Our approach is implemented on two movie review datasets: IMDB and the polarity dataset by Pang and Lee. We have compared both datasets with other state-of-the-art methods of sentiment analysis. It is observed that our model has achieved the highest accuracies of 89.8% in IMDB and 78.5% in Pang and Lee datasets, as compared to other methods. We propose to incorporate eye movement data in our future work.

REFERENCES

[1] B. Pang, and L. Lee. "Opinion mining and sentiment analysis." *Foundations and Trends® in Information Retrieval* 2, no. 1–2 (2008): 1-135.

[2] S. Sun, C. Luo, and J. Chen. "A review of natural language processing techniques for opinion mining systems." *Information Fusion* 36 (2017): 10-25.

[3] Y. Long, Q. Lu, R. Xiang, M. Li, and C. Huang. "A cognition based attention model for sentiment analysis." In *Proceedings of the 2017 Conference on Empirical Methods in Natural Language Processing*, pp. 462-471. 2017.

[4] N. Fang, X. Luo, and W. Xu. "Evaluating the capability of text understanding based on cognitive principle." In *Audio, Language and Image Processing, 2008. ICALIP 2008. International Conference on*, pp. 1110-1114. IEEE, 2008.

[5] V. Demberg, and F. Keller. "Data from eye-tracking corpora as evidence for theories of syntactic processing complexity." *Cognition* 109, no. 2 (2008): 193-210.

[6] S. Susan, and J. Keshari. "Finding significant keywords for document databases by two-phase Maximum Entropy Partitioning." Pattern Recognition Letters 125 (2019): 195-205.

[7] D. Tang, B. Qin, and T. Liu. "Learning semantic representations of users and products for document level sentiment classification." In *Proceedings of the 53rd Annual Meeting of the Association for Computational Linguistics and the 7th International Joint Conference on Natural Language Processing (Volume 1: Long Papers)*, vol. 1, pp. 1014-1023. 2015.

[8] Z. Yang, D. Yang, C. Dyer, X. He, A. Smola, and E. Hovy. "Hierarchical attention networks for document classification." In *Proceedings of the 2016 Conference of the North American Chapter of the Association for Computational Linguistics: Human Language Technologies*, pp. 1480-1489. 2016.

[9] H. Chen, M. Sun, C. Tu, Y. Lin, and Z. Liu. "Neural sentiment classification with user and product attention." In *Proce edings of the 2016 Conference on Empirical Methods in Natural Language Processing*, pp. 1650-1659. 2016.

[10] L. Gui, R. Xu, Y. He, Q. Lu, and Z. Wei. "Intersubjectivity and Sentiment: From Language to Knowledge." In *IJCAI*, pp. 2789-2795. 2016.

[11] A. Yenter, and A. Verma. "Deep CNN-LSTM with combined kernels from multiple branches for IMDb review sentiment analysis." In *Ubiquitous Computing, Electronics and Mobile Communication Conference (UEMCON), 2017 IEEE 8th Annual*, pp. 540-546. IEEE, 2017.

[12] A. Hassan, and A. Mahmood. "Efficient Deep Learning Model for Text Classification Based on Recurrent and Convolutional Layers." In *Machine Learning and Applications (ICMLA), 2017 16th IEEE International Conference on*, pp. 1108-1113. IEEE, 2017.

[13] S. Bird, E. Klein, and E. Loper. *Natural language processing with Python: analyzing text with the natural language toolkit*. " O'Reilly Media, Inc.", 2009

[14] D. Jurafsky, and J. H. Martin. *Speech and language processing*. Vol. 3. London: Pearson, 2014.

[15] N. Gupta, and K. R. Abhinav. "Fuzzy sentiment analysis on microblogs for movie revenue prediction." In *Emerging Trends in Communication, Control, Signal Processing & Computing Applications (C2SPCA), 2013 International Conference on*, pp. 1-4. IEEE, 2013.

[16] Y. Arslan, A. Birturk, B. Djumabaev, and D. Küçük. "Real-time lexicon-based sentiment analysis experiments on Twitter with a mild (more information, less data) approach." In *Big Data (Big Data), 2017 IEEE International Conference on*, pp. 1892-1897. IEEE, 2017.

[17] D. C. Cavalcanti, R. BC Prudêncio, S. S. Pradhan, J. Y. Shah, and R. S. Pietrobon. "Good to be bad? Distinguishing between positive and negative citations in scientific impact." In *2011 23rd IEEE International Conference on Tools with Artificial Intelligence*, pp. 156-162. IEEE, 2011.

[18] A.Mishra, D. Kanojia, S. Nagar, K. Dey, and P.Bhattacharyya. "Leveraging cognitive features for sentiment analysis." *arXiv preprint arXiv:1701.05581*(2017).

[19] C.D. Manning, M. Surdeanu, J. Bauer, J. Finkel, S.J. Bethard, D. McClosky, The Stanford CoreNLP natural language processing toolkit, in: Proceedings of the 52nd Annual Meeting of the Association for Computational Linguistics: System Demonstrations, 2014, pp. 55–60.

[20] X. Qiu, Q. Zhang, X. Huang, Fudannlp: a toolkit for Chinese natural language processing, in: Proceedings of the 51st Annual Meeting of the Association for Computational Linguistics, 2013, pp. 49–54.

[21] B.Pang, L. Lee, and S. Vaithyanathan. "Thumbs up?: sentiment classification using machine learning techniques." In *Proceedings of the ACL-02 conference on Empirical methods in natural language processing-Volume 10*, pp. 79-86. Association for Computational Linguistics, 2002.

[22] S. Poria, E. Cambria, A. Gelbukh, F. Bisio, and A. Hussain. "Sentiment data flow analysis by means of dynamic linguistic patterns." *IEEE Computational Intelligence Magazine* 10, no. 4 (2015): 26-36.

2379-8920 (c) 2019 IEEE. Personal use is permitted, but republication/redistribution requires IEEE permission. See http://www.ieee.org/publications_standards/publications/rights/index.html for more information.

This article has been accepted for publication in a future issue of this journal, but has not been fully edited. Content may change prior to final publication. Citation information: DOI 10.1109/TCDS.2019.2937796, IEEE Transactions on Cognitive and Developmental Systems

[23] C. Wang, Z. Xiao, Y. Liu, Y. Xu, A. Zhou, and K. Zhang. "Sentiview: Sentiment analysis and visualization for internet popular topics." *IEEE transactions on human-machine systemss* 43, no. 6 (2013): 620-630.

[24] P. Singh, R. S. Sawhney, and K. S. Kahlon. "Sentiment analysis of demonetization of 500 &1000 rupee banknotes by Indian government." *ICT Express* 4, no. 3 (2018): 124-129.

[25] Y. Kim, Convolutional neural networks for sentence classification. In Proceedings of the 2014 Conference on Empirical Methods in Natural Language Processing (EMNLP). pages 1746-1751, Doha, Qatar, October 2014, Association for Computational linguistics

[26] R. Johnson, and T. Zhang, Effective use of word order for text categorization with convolutional neural networks. arXiv preprint arXiv:1412.1058, 2014.

[27] N. Kalchbrenner, E. Grefenstette, and P. Blunsom, A convolutional neural network for modelling sentences. arXiv preprint arXiv:1404.2188, 2014.

[28] X. Zhang, J. Zhao, and Y. LeCun. Character-level convolutional networks for text classification. in Advances in Neural Information Processing Systems. 2015.

[29] S. Lai, L. Xu, K. Liu, and J. Zhao, "Recurrent Convolutional Neural Networks for Text Classification," *In AAAI*, vol. 333, pp. 2267-2273, 2015.

[30] Q. Huang, R. Chen, X. Zheng, and Z. Dong. "Deep Sentiment Representation Based on CNN and LSTM." In *2017 International Conference on Green Informatics (ICGI)*, pp. 30-33. IEEE, 2017.

[31] L. Rahman, N. Mohammed, and A. Kalam Al Azad, "A new LSTM model by introducing biological cell state." In Electrical Engineering and Information Communication Technology (ICEEICT), 2016 3rd International Conference on, pp. 1-6, 2016.

[32] J. Xu, D. Chen, X. Qiu, and X. Huang. 2016. Cached long short-term memory neural networks for document-level sentiment classification. arXiv preprint arXiv:1610.04989.

[33]A. Joshi, A. Mishra, N. Senthamilselvan, and P. Bhattacharyya. 2014. Measuring sentiment annotation complexity of text. In *ACL (2)*, pages 36–41

[34] A. Mishra, A. Joshi, and P. Bhattacharyya. 2014. A cognitive study of subjectivity extraction in sentiment annotation. *ACL 2014*, page 142

[35] S. Baccianella, A. Esuli, and F. Sebastiani, 2010, May. Sentiwordnet 3.0: an enhanced lexical resource for sentiment analysis and opinion mining. In *Lrec* (Vol. 10, No. 2010, pp. 2200-2204).

[36] D. G. Pelli, and K. A. Tillman. "The uncrowded window of object recognition." *Nature neuroscience* 11, no. 10 (2008): 1129.

[37] M. Dragoni, and G. Petrucci. "A fuzzy-based strategy for multi-domain sentiment analysis." *International Journal of Approximate Reasoning* 93 (2018): 59-73.

[38] C. Jefferson, H. Liu, and M. Cocea. "Fuzzy approach for sentiment analysis." In *Fuzzy Systems (FUZZ-IEEE), 2017 IEEE International Conference on*, pp. 1-6. IEEE, 2017.

[39] S. Jusoh, and H.M. Alfawareh. "Applying fuzzy sets for opinion mining." In *Computer Applications Technology (ICCAT), 2013 International Conference on*, pp. 1-5. IEEE, 2013.

[40] M. Anagha, R.R. Kumar, K. Sreetha, and PC R. Raj. "Fuzzy logic based hybrid approach for sentiment analysis of Malayalam movie reviews." In *Signal Processing, Informatics, Communication and Energy Systems (SPICES), 2015 IEEE International Conference on*, pp. 1-4. IEEE, 2015.

[41] P. Bhoir, and S. Kolte. "Sentiment analysis of movie reviews using lexicon approach." In *Computational Intelligence and Computing Research (ICCIC), 2015 IEEE International Conference on*, pp. 1-6. IEEE, 2015

[42] S. Vashishtha, and S. Susan. "Fuzzy Rule based Unsupervised Sentiment Analysis from Social Media Posts." *Expert Systems with Applications* (2019): 112834.

[43] B. Agarwal, N. Mittal, and E. Cambria. "Enhancing sentiment classification performance using bi-tagged phrases." In *Data Mining Workshops (ICDMW), 2013 IEEE 13th International Conference on*, pp. 892-895. IEEE, 2013.

[44] S. Vashishtha, and S. Susan. "Fuzzy Logic Based Dynamic Plotting of Mood Swings from Tweets." In International Conference on Innovations in Bio-Inspired Computing and Applications, pp. 129-139. Springer, Cham, 2018.

[45] K. Indhuja, and PC R. Raj. "Fuzzy logic based sentiment analysis of product review documents." In *Computational Systems and Communications (ICCSC), 2014 First International Conference on*, pp. 18-22. IEEE, 2014

[46] W.Pedrycz, and F. Gomide. *Fuzzy systems engineering: toward human-centric computing*. John Wiley & Sons, 2007.

[47]A.D. Luca, and S. Termini. "A definition of a nonprobabilistic entropy in the setting of fuzzy sets theory." In *Readings in Fuzzy Sets for Intelligent Systems*, pp. 197-202. 1993.

[48] M. Qing, and T. Li. "Some properties and new formulae of fuzzy entropy." In *Networking, Sensing and Control, 2004 IEEE International Conference on*, vol. 1, pp. 401-406. IEEE, 2004.

[49] K.C. Deshmukh, K. C, and P. G. Khot. "Generalized Measures of Fuzzy Entropy and their Properties." In *World Academy of Science, Engineering and Technology International Journal of Mathematical and Computational Sciences on*, vol:5, no:8, 2011.

[50] S. Susan, and M. Hanmandlu. "A novel Fuzzy Entropy based on the non-extensive entropy and its application for feature selection." In *Fuzzy Systems (FUZZ), 2013 IEEE International Conference on*, pp. 1-8. IEEE, 2013.

[51] J. MacQueen. "Some methods for classification and analysis of multivariate observations." In *Proceedings of the fifth Berkeley symposium on mathematical statistics and probability*, vol. 1, no. 14, pp. 281-297. 1967.

[52] Y. Xiaohui, Y. Liu, J.X. Huang, and A. An. "Mining online reviews for predicting sales performance: A case study in the movie domain." *IEEE Transactions on Knowledge and Data engineering* 24, no. 4 (2012): 720-734.

[53] A.L. Maas, R. E. Daly, P. T. Pham, D. Huang, A.Y. Ng, and C. Potts. "Learning word vectors for sentiment analysis." In *Proceedings of the 49th annual meeting of the association for computational linguistics: Human language technologies-volume 1*, pp. 142-150. Association for Computational Linguistics, 2011.

[54] P. Bo and L. Lee. "A sentimental education: Sentiment analysis using subjectivity summarization based on minimum cuts." In Proceedings of the 42nd annual meeting on Association for Computational Linguistics, p. 271. Association for Computational Linguistics, 2004.

[55] A. Tripathy, A. Agrawal, and S. K. Rath. "Classification of sentiment reviews using n-gram machine learning approach." *Expert Systems with Applications* 57 (2016): 117-126.

[56] P. Beineke, T. Hastie, & S. Vaithyanathan (2004). The sentimental factor: improving review classification via human-provided information. In *Proceedings of the 42nd annual meeting on association for computational linguistics* (p. 263). Association for Computational Linguistics.

[57] S. Matsumoto, H. Takamura, & M. Okumura (2005). Sentiment classification using word sub-sequences and dependency sub-trees. In *Advances in knowledge discovery and data mining* (pp. 301–311). Berlin Heidelberg: Springer.

[58] T. Mullen, & N. Collier (2004). Sentiment analysis using support vector machines with diverse information sources. In *EMNLP: 4* (pp. 412–418)

Srishti Vashishtha has received B.Tech degree in Information Technology from Maharaja Surajmal Institute of Technology, GGSIPU, Delhi, M.Tech degree in Computer Science from University school of Information, Communication and Technology, GGSIPU, Delhi.

She is currently pursuing Ph.D. in Information Technology Department from Delhi Technological University, Delhi. Her area of interests includes Data Mining, Natural language Processing and Machine Learning.

Dr. Seba Susan has received Ph.D. from the Indian Institute of Technology, Delhi.

She is an Associate Professor in Information Technology Department, Delhi Technological University, Delhi. Her current research interests includes Computer Vision, Natural Language Processing, Machine Learning, Data Mining, Pattern Recognition, Image Processing, Fuzzy-Neural Networks, Soft Computing and area of specialization are Statistical inferencing and soft computing tools for Computer Vision, Data Mining and Machine Learning.

2379-8920 (c) 2019 IEEE. Personal use is permitted, but republication/redistribution requires IEEE permission. See http://www.ieee.org/publications_standards/publications/rights/index.html for more information.

Volume 7 Issue 2 (2019) 162-165 ISSN 2347 - 3258
International Journal of Advance Research and Innovation

Study and first law analysis of Gas Turbine-HRSG-ORC co-generation system with change in atmospheric temperature

Priyanshu Thakur, PV Ram Kumar
Department of Mechanical Engineering, Delhi Technological University, National Capital Region, New Delhi-110042, India

Article Info
Article history:
Received 23 January 2019
Received in revised form 20 March 2019
Accepted 10 April 2019
Available online 15 June 2019

Keywords
Gas Turbine, Heat Recovery Steam Geenrator, Organic Cycle, First law efficiecny.

Abstract
Gas turbine cogeneration system integrated with heat recovery steam generator and organic Rankine cycle provides an effective measure of waste heat recovery from exhaust gasses of gas turbine. The numerous study conducted to understand the variation in the performance of the integrated system has been done and the variation of performance with parameters such as turbine inlet temperature, compression ratio mass flow rate etc., has been carried out. The present paper investigates the variation in the performance of the system with change in the surrounding temperature. The paper provides the detailed first law analysis of the system and compares the first law efficiency obtained at different surrounding temperature to justify the location of use of the integrated system.

1. Introduction

With growing energy demand and issues of rise in environmental pollution at an unprecedented, the efficient utilization of available resources has become an issue of eminence importance. This bring into focus how effectively available resources can be managed without compromising the needs of the future generation thought sustainable development. Cogeneration system forms a part of such efficient utilisation of resources by ensuring the waste heat recovery from the available energy resource. The cogeneration system is defined in general terms as the process of producing more than one form of energy by utilising the same heating source such as thermal and electrical energy together from fossil fuels. Formally, World Alliance for Decentralisation Energy defines it as, "Process of producing both electrical and usable thermal energy (heating or cooling) at high efficiency and near the point use". And The Bureau of Energy Efficiency India defines cogeneration as "Sequential generation of two different form of energy from a single primary source, typically mechanical and thermal energy." [1]. Cogeneration system has been an integral form of energy generation dating backs to 1880 when electricity was not a primary source of energy and still continues to play an eminent role in the efficient energy management. The paper focus on one of such cogeneration system with gas turbine (GT) as prime mover and organic Ranking (ORC) present as bottoming cycle for waste heat recovery. ORC works in the same principle as common steam Rankine cycle. The only difference lies in the working fluid. ORC uses organic fluids or refrigerants as working fluid. The lower heat of vaporisation of these organic fluid make them suitable for working with a temperature source below 230℃ [2]. A lot of work has been conducted and good results are obtained in field of research for increasing the performance of the performance of ORC system. Researchers has examined different organic fluids for their performance. However over the recent years ORC as a bottom cycle for gas turbine cogeneration has been studied extensively. Khaljani M. et al, [3] has done one of the most detailed analysis of the system. In his work the energy, exergy and exergo-economic analysis has been carried out with R123 as the working fluid, parametric study has been done to understand the effect of various design variable on the change in efficiency, cost and its impact on environment. Ahmadi et al., [4] in his work has used integration ORC for tri-generation purpose, his work has shown combustion chamber and heat exchangers as two main source of irreversibility and has established through parametric study that compression ratio (r_p), turbine inlet temperature (TIT) and turbine isentropic efficiency are the parameters that affect the performance of the system significantly. Yari M. et al., [5] in has done a comparative study ORC system with regeneration, internal heat exchanger, and simple ORC to obtain higher efficiency. The work done in [5] has been taken as the base for validation of ORC system taken in [3].

This paper, however provide a different parametric study of the system for understanding the change in system behaviour with respect to surrounding temperature along with detailed first law analysis of the system through engineering equation solver software. The current system is validated by the results obtained in the [4] and this work open the area for the further work in mapping of different refrigerant at global level with respect to the surrounding temperature.

Corresponding Author,
E-mail address: priyanshu6995@gmail.com;pvrdce@gmail.com
All rights reserved: http://www.ijari.org

2. System Description

The Schematic Diagram of the GT-HSRG-ORC is given in Figure 1. It consists of the top cycle of GT and bottoming cycle of ORC. The ambient air at point 1, with pressure of 1 bar and temperature of 298.15 K, is compressed in air compressor. Then compressed air goes into air pre-heater and come out at a temperature of 850 K. In the combustion chamber, the fuel is injection pressure is at 12 bar to the incoming hot air from air pre-heater and combustion happens. After combustion the gases with a temperature of 1520 K then expand in the gas turbine and produce power of 30 MW [3]. To recover the energy of exhaust gases, hot gases after passing through the air pre-heater, are fed into a heat recovery steam generator. In the heat recovery steam generator, water with a pressure of 35 bar and temperature of 298.15 K enters the heat recovery steam generator and leaves it as saturated steam at the same pressure. Exhaust gases then enter to the evaporator where exchange heat with a bottoming cycle. ORC has five main components of the pump, the internal heat exchanger, evaporator, turbine and condenser. Organic working fluid in a saturated liquid phase is pumped to high pressure. After being heated in the internal heat exchanger enters the evaporator to receive the energy of exhaust gases and become saturated vapour. Afterwards, the working fluid with higher enthalpy enters turbine to produce power and expands to the condenser pressure. Superheated fluid after passing internal heat exchanger enters condenser and is condensed to saturated liquid phase.

3. Modelling

The thermodynamic modelling as well as energetic relations of the components of gas turbine cycle according to the relations given in [6], and HRSG according to the relations given in [7] and components of ORC according to the relations given in [5]. Table 1 gives the energy balance equation for various equipments of the cogeneration system.

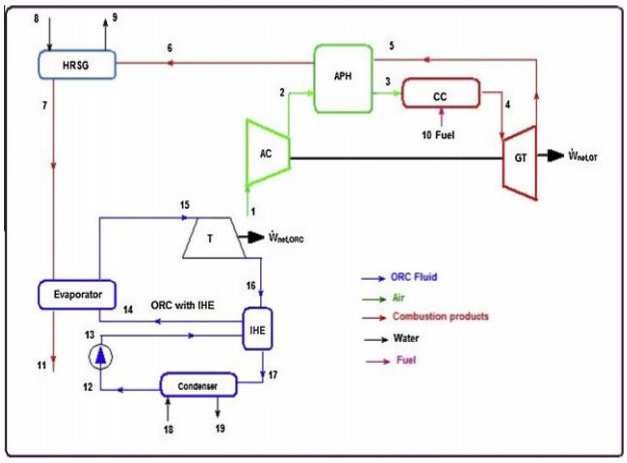

Fig.1: Schematic diagram of GT-HRSG/ORC system [4]

Table1: Energy balance equations GT-HRSG-ORC system [5-7]

Component	Energy Equation
Air compressor	$\eta_{ac} = \frac{(h_{2s} - h_1)}{h_2 - h_1} \quad \dot{W}_{AC} = m_{air}(h_2 - h_1)$
Air pre-heater	$h_3 - h_{2a} = (1+\tau)(h_{5a} - h_6)$
Combustion chamber	$-0.02\tau LHV_{CH_4} + h_a + \tau h_p - (1+\tau)h_p$
Gas turbine	$\eta_{GT} = (h_4 - h_5)/(h_4 - h_{5s}) \quad \dot{W}_{GT} = (\dot{m}_f + \dot{m}_{air})(h_4 - h_5)$
Pump	$\eta_p = \frac{v_{12}(p_{13} - p_{12})}{h_{13} - h_{12}} \quad \dot{W}_p = \dot{m}_{ORC}(h_{13} - h_{12})$
IHE	$(h_{14} - h_{13}) = (h_{16} - h_{17}), \in_{IHE} = (T_{11} - T_{14})/(T_{16} - T_{13})$
Evaporator	$(\dot{m}_{air} + \dot{m}_f)(h_7 - h_{11}) = \dot{m}_{ORC}(h_{15} - h_{14}), \dot{Q}_E = \dot{m}_{orc}(h_{15} - h_{14})$
Turbine	$\eta_T = (h_{15} - h_{16})/(h_{15s} - h_{15}), \dot{W}_T = \dot{m}_{ORC}(h_{15} - h_{16})$
Condenser	$\dot{m}_{ORC}(h_{17} - h_{12}) = \dot{m}_{water}(h_{19} - h_{18}), \dot{Q}_{COND} = \dot{m}_{ORC}(h_{17} - h_{12})$

The thermodynamic modelling and analysis was done on the basis of the following assumption:

1. All processes of the cycle are in steady state [6,7].
2. Air compressor and gas turbine are assumed adiabatic [7].
3. Lower heating value of the fuel (methane) is 50000 kJ/kg [7].
4. The principles of ideal gas mixtures are used for air and combustion products [7].
5. The pressure drops at air side and gas side are 5% and 3%, respectively [7].
6. Heat transfer from combustion chamber is 2% of lower heating value of the fuel. Other equipments work with no heat losses [7].
7. Heat recovery steam generator is designed in a single-pressure mode in which the water temperature and pressure at the inlet are 298.15 K and 35 bar, respectively. The HRSG outlet state is saturated vapour [4]
8. The organic working fluid enters the turbine as saturated vapour [4].

The basic input parameters of gas turbine and organic Rankine cycles are provided in Table 2, these includes the parameters which are being changed i.e., turbine inlet temperature as well as compression ratio, and range of variation has been provided according to the previously conducted research.

Table 2: Parameters used in the modelling (Source [4])

Parameters	Values
T1(K)	273.15-318.15
P1(bar)	1
$\dot{W}_{GT}$(MW)	30
T3(K)	850
T4(K)	1520
r_p	10
η_{AC}(%)	90
η_{GT}(%)	80
$\Delta T_{pp,HRSG}$(K)	25
Te(K)	375
Tc(K)	303.20
$\Delta T_{pp,E}$(K)	5
$\eta_{T(ORC)}$(%)	80%
$\eta_{p(ORC)}$(%)	85%
ε(%)	90

4. Results and Discussion

After the thermodynamic modelling of the system, validation of the model has been done by comparing the properties of working fluid at each point with the results obtained in [4]. R123 was used as a working fluid due to its lower global warming potential. This validation is provided in the appendix 1 of the paper. In this paper the performance of the system was studies on the basis of first law of thermodynamics only. The parametric study was done by varying the surrounding temperature and observing the change in behaviour of output by calculating the overall efficiency, total work output, total work output of ORC, mass flow rate of air and mass of heated water delivered. The alalyssi was done with the assumption that the electrical loadon the gas power plant is constant and power output of the gas turbine is kept constant at 30MW. The results obtained are shown in figure 2.

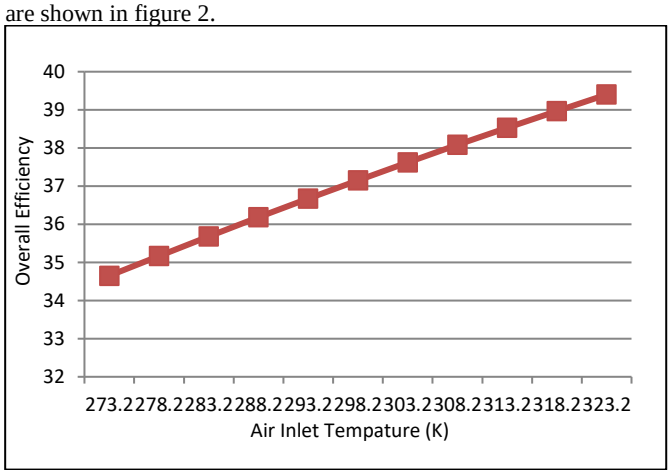

Fig.2 (a): Variation of overall efficiency with increase in surrounding temperature.

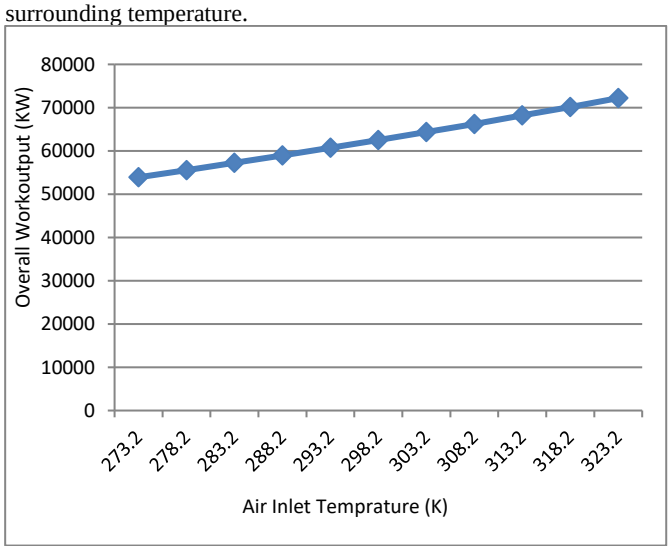

Fig.2 (b): Variation of work output with surrounding temperature.

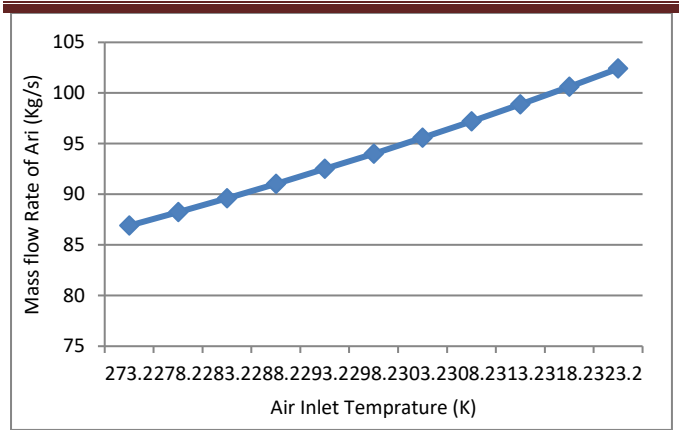

Fig.2 (c): Variation of mass flow rate of air with surrounding temperature

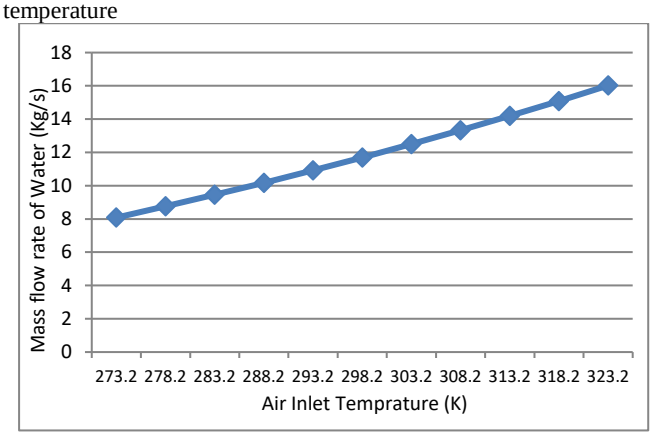

Fig.2 (d): Variation in steam output with change in surrounding temperature

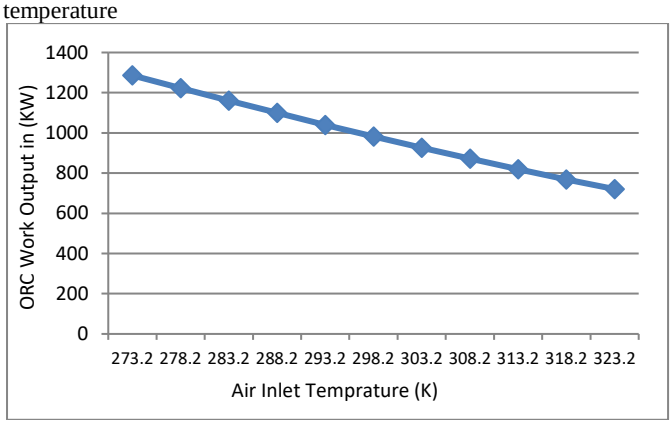

Fig.2 (e): Variation in work output of ORC with change in surrounding temperature.

Fig. 2: Variation on various output parameters with change in surrounding temperature

The result obtained shows that with increase in the temperature of inlet air, the overall efficiency of the system increases. This can be attributed to increase in the heated steam recovered at the HRSG which is higher than compared to decrease in the work output at ORC and increase work done at compressor. The overall work output of the system also have similar effect. The mass flow rate of the system increases, with increase in air inlet temperature, as a result of increased work input in compressor with net output and turbine inlet temperature remaining constant. Increased mass flow rate of air increases the mass of steam delivered in HRSG system which have a positive effect on overall efficiency and overall work output. However, with increase in the air inlet temperature the work output of the ORC decreases but since the delivered output is very small in compared to the overall turbine output its effect is significantly low for the current system. However in case of micro turbine power generation system this can be of eminent importance. The decrease in the output of ORC is attributed to the decreased temperature at outlet of the HRSG system as a result of increased mass flow rate of water with increase in the air inlet temperature. The air at outlet of HRSG act as the heat source for HRSG system. From the results obtained it can be observed that the temperature at the outlet of HRSG varies from 416K to 451K. Thurairaja K. et al., [9] in his work has provided the details of refrigerant that can be used in ORC at the given range of temperature of the heat source. In figure 3 a comparative analysis has been shown between various refrigerant which can be used for a heat source with temperature range of 416-451K in an ORC.

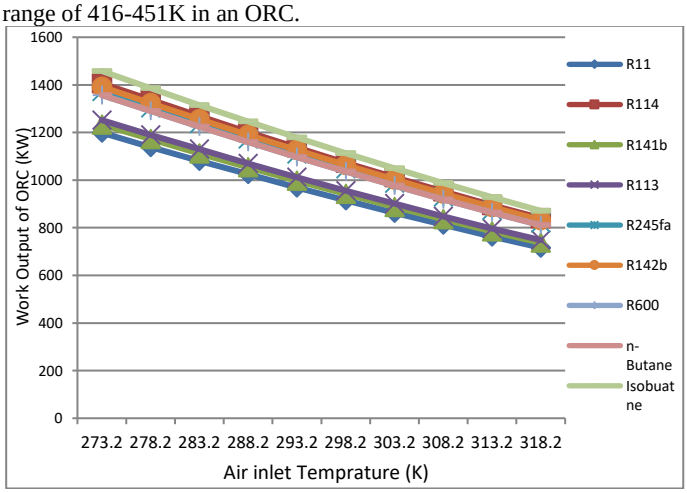

Fig. 3: Comparison of performance of various Organic fluid operating in bottoming cycle of cogeneration system.

It can be concluded from the above trend that increased surrounding temperature has a adverse effect on ORC work output for any organic working fluid. So it is recommended to increase the heat recovery through ORC in cogeneration system it should be operated in a cold region where air inlet temperature is lower. Among the various organic fluids used isobutene shows the most promising results. R-114, R-245fa, R-124b and R-600 give near about same performance. The work output obtained R-11, R-141b,R-113 and n-butane is comparative lower. However the difference is not very significant which makes their environmental impact study a significant part for choice of the organic fluid in the bottoming cycle.

Table 3 provides the point wise comparison of thermodynamic state of fluid under analysis of the given work with the values provided by reference [3] as the result.

Table 3: Comparison of thermodynamic properties of each stream of GT and ORC in present work and reference [3]

Stream	Working Fluid	T(K) in [3]	T(K)	P(bar) in [3]	P (bar)	ṁ (Kg/s) in [3]	ṁ (Kg/s)
1	Air	298.15	298.15	1.013	1.013	94.75	94.09
2	Air	603.5	603.1	10.13	10.13	94.75	94.09
3	Air	850	850	9.624	9.624	94.75	94.09
4	Combustion gases	1520	1520	9.142	9.142	96.454	95.782
5	Combustion gases	1016	1009	1.157	1.157	96.454	95.782
6	Combustion gases	789.6	743.3	1.122	1.122	96.454	95.782
7	Combustion gases	422.1	413	1.066	1.066	96.454	95.782
8	Water	298.15	298.15	35	35	15.21	13.41
9	Water	515.7	515.7	35	35	15.21	13.41
10	Fuel	298.15	298.15	12	12	1.704	1.692

11	Combustion gases	381.5	371.5	1.013	1.013	96.454	95.684
12	R123	303.2	303.2	1.097	1.099	21.61	24.12
13	R123	303.2	303.5	8.199	8.199	21.61	24.12
14	R123	316.5	316.2	8.199	8.199	21.61	24.12
15	R123	375	375	8.199	8.199	21.61	24.12
16	R123	323.8	323.8	1.097	1.099	21.61	24.12
17	R123	305.5	305.44	1.097	1.099	21.61	24.12

5. Conclusions

From the study of the system and its analysis based on the first law of thermodynamics following conclusion can be drawn.

- Increasing the surrounding temperature of the GT-HRSG-ORC integrated system increases mass flow rate of air as well as mass of steam generation.
- Increased mass of steam generation has a positive impact on the overall efficiency of the system which increases with increase in surrounding temperature.
- The work output through ORC decreases as a result of decreased temperature of air at inlet of evaporator.
- The decrease in ORC work output doesn't have a significant effect on the given system. However for micro gas turbine case it can make a significant difference.
- It is recommended to use the system in colder region if the waste heat recover through ORC is required to be enhanced.
- The comparative study between different organic fluid shows isobutene provides with the better result in compared to other organic fluid and is recommended to be used in cogeneration system.

In the present paper the work has been limited to first law analysis only however the second law analysis and cost variation with respect to surrounding condition can further be studied in detail in future and the comparative study between the organic fluid can be studied further with respect to their environmental impact.

Acknowledgment

The authors would like to acknowledge the efforts of the Department of Mechanical Engineering, Delhi Technological University for providing with the necessary resources to carry out the research work and would also like to acknowledge the effort of Institute of Engineers (India), Delhi Centre and IJARI for providing the platform of outlet for this work.

Nomenclature

HRSG	Heat Recovery Steam Generator
GT	Gas Turbine
IHE	Heat Exchanger
CC	Combustion Chamber
ORC	Organic Rankine Cycle
APH	Air Pre Heater
LHV	Lower Heating Value of Fuel
TIT	Turbine Inlet Temprature
η_{AC}	Compressor Efficiency
η_{comb}	Combustion Efficiency
η_{GT}	Turbine Efficiency
ε	Effectiveness
r_p	Compression Ratio
$\dot{W}$	Work Output
h	Enthaphy
s	Entropy
∇T_{pp}	Pitch Point Temperature Difference
Q	Heat
m	mass

Subscripts

p	Pump
T	Turbine
f	Fuel
ac/AC	Air Compressor
gt/GT	Gas Turbine
e	Evaporator
c	Comdensor

References

[1] Cogeneration, Chapter 7, Energy Efficiency in Thermal utilities, Guide Book 2 Bureau of Energy Efficiency, New Delhi, 155-https://beeindia.gov.in/sites/default/files/2Ch7.pdf

[2] BF Tchanche, G Lambrinos, A Frangoudakis, G Papadakis. Low grade heat conversion into power using ORC – A review of various application, Renewable and Sustainable Energy Review, 54(8), 2011, 3963-3979.

[3] M Khaljani, R Khoshbakti Saray, K Bahlouli. Comprehensive analysis of energy, exergy and exergo-economic of cogeneration of heat and power in combined gas turbine and Organic Rankine cycle, Energy conversion and Management, 97, 2015, 154-165.

[4] P Ahmadi, I Dincer, MA Rosen. Exergo-environmental analysis of an integrated organic Rankine cycle for trigeneration, Energy and Conversion Management , 64, 2012, 447-453.

[5] M Yari, S Mahmoudi. A thermodynamic study of waste heat recovery from GT-MHR using organic Rankine cycles, Heat and Mass Transfer, 47(2), 2011, 181-196.

[6]A Bejan. Thermoeconomic optimisation, Thermal design and optimization. G. Tsatsaronis, M Moran, New York USA, A Wiley Interscience publication , 1995, ch. 9, sec. 9.5 1996, 502-506.

[7] H Ghaebi, M Saidi, P Ahmadi. Exergoeconomic optimization of a trigeneration system for heating, cooling and power production purpose based on TRR method and using evolutionary algorithm. Appl Therm Engineerimg, 36, 2011, 113–25.

[8] K Thurairaja, A Wijewardane, S Jaysekara, C Ranasighe. Working fluid slection and performance evalutaion of ORC, 5th Tnt. Conf. Power and Energy System Engineering, CPESE, Nagoya, Germany, 9, 2018, 19-21.

Polymer 182 (2019) 121823

Contents lists available at ScienceDirect

Polymer

journal homepage: www.elsevier.com/locate/polymer

Synthesis and assessment of carboxymethyl tamarind kernel gum based novel superabsorbent hydrogels for agricultural applications

Khushbu, Sudhir G. Warkar*, Anil Kumar

Department of Applied Chemistry, Delhi Technological University, Delhi, India

HIGHLIGHTS

- Fabrication of novel, degradable CMTKG based superabsorbent hydrogels.
- Characterization of synthesized hydrogel with FTIR, TGA and swelling studies.
- Degradation studies of the synthesized hydrogels.
- Hydrogels effect on maximum water holding capacity, density, porosity and water retention capacity of soil.

ARTICLE INFO

Keywords:
Moisture retention
Superabsorbent hydrogels
Biopolymer
Agriculture
Soil conditioner

ABSTRACT

The novel superabsorbent hydrogels (SAH) were fabricated by interpenetrating carboxymethyl tamarind kernel gum with sodium-acrylate. The synthesis of SAH was verified by characterization using Fourier-transform infrared spectroscopy, thermo-gravimetric analysis, scanning electron microscopy and swelling studies under various solutions. The hydrogel formed was found out to be degradable (soil burial biodegradation test). Maximum water holding capacity, bulk density, porosity and water retention capacity of soil were evaluated to see the effects on soil by the hydrogel treatment. The hydrogel which absorbs up to 648 ml/g, post inclusion to soil, and showed significant enhancement in the moisture absorption (35%), porosity (7%) and water retension capacity compared to the untreated (control) soil. The effects of the hydrogel were also seen on the growth of chickpea plants. The synthesized SAH displayed promising potential as soil conditioner for agricultural applications.

1. Introduction

One of the most important inputs in agriculture is water. In rain fed agriculture, the sustainability of crop production majorly depends on availability of water. Even if a drought tolerant trait is introduced, water is not accessible to crops. Irrigation through dams, wells and other ground water sources is still not possible in many areas due to scarcity of groundwater and cost effectiveness. Rain is a free and first source of water but rainfall itself is becoming more and more unpredictable. This variability greatly affects soil which imposes crop production risks, especially on rain fed subsistence cultivation systems on marginal land. Since we know that world faces water and food crises. A growing population means more food to feed. Climate change is causing massive droughts and is expected to get much worse. Top soil erosion makes it harder to grow food and food scarcity leads to high prices which leads to social unrest [1]. To enhance the water utility competency in agriculture, a lot of methods are being implemented. Hydrogels are being explored for soil conditioning and water retention in agriculture because of its special properties [2,3]. All this led to hydrogels as they enhance the growth of the plant, harmless to flora and fauna and have good water intake and retain capacity.

Technically, hydrogels are tridimensional cross-linked hydrophilic polymers which possess the ability to assimilate a substantial volume of waters or other fluids and can swell without being dissolved off. While more practically, they are superabsorbent material that can hold hundreds of times its weight in water [4]. Reason being for their special properties are the hydrophilic functional groups that are connected to the polymeric backbone whereas their insolubility springs up from cross-links between network trails. The hydrogels which can absorb water up to 95% of their initial completely dry weight are usually known to be superabsorbent hydrogels (SAH) [5,6]. It helps to retain water in the soil by dispersing the absorbed water slowly, thus soil gets hydrated which capacitates the plant to sustain longer under water stress which consequently enhances the crop production. Henceforth,

* Corresponding author.
E-mail address: sudhirwarkar@gmail.com (S.G. Warkar).

https://doi.org/10.1016/j.polymer.2019.121823
Received 25 July 2019; Received in revised form 16 September 2019; Accepted 18 September 2019
Available online 19 September 2019
0032-3861/ © 2019 Published by Elsevier Ltd.

Table 1
Concentration of reactants used in synthesis and resultant swelling index.

Formulation	CMTKG(g)/distilled- water (mL)	Monomer (AA) (mL)	NaOH (g)	Distilled-water (mL)	Cross-linker (MBA) (mg)	Initiator (KPS) (g)	Swelling Index in distiled water (g/g)
H-1	0.1/10	7.1	4.2	13	17	0.1	359.20
H-2	0.2/10	7.1	4.2	13	17	0.1	414.33
H-3	0.3/10	7.1	4.2	13	17	0.1	648.19
H-4	0.1/10	7.1	4.2	13	26	0.1	320.27
H-5	0.2/10	7.1	4.2	13	26	0.1	396.22
H-6	0.3/10	7.1	4.2	13	26	0.1	531.39
H-7	0.1/10	7.1	4.2	13	35	0.05	153.10
H-8	0.1/10	7.1	4.2	13	35	0.1	227.32
H-9	0.1/10	7.1	4.2	13	35	0.4	200.07
H-10	0.1/10	7.1	4.2	13	35	0.8	158.41
H-11	0.2/10	7.1	4.2	13	35	0.1	318.45
H-12	0.3/10	7.1	4.2	13	35	0.1	429.74
H-13	0.3/10	7.1	4.2	13	44	0.1	341.11
H-14	0.3/10	7.1	4.2	13	53	0.1	223.31
H-15	0.15/10	7.1	4.2	13	17	0.1	387.29
H-16	0.25/10	7.1	4.2	13	17	0.1	503.34

SAH can act as a personal underground reservoir which encapsulates all the water that evaporates and helps in crop production in cases of drought [7]. In short, it can supplement rainfall to supply crop water needs [8]. These substances can be called as artificial humus because of the presence of carboxylic groups and their hydrophilicity. In comparison to humus, SAH have a higher density of hydrophilic cation binding groups and contains non aromatic moieties. Therefore, SAH are more pronounced per weight with respect to humus which consequently lowers down the chances of becoming hydrophobic, as humus does become the same in drought conditions [9].

The goal is to help farmers to grow more food with less water. Hence, for this to happen there are certain desirable properties for agriculture based hydrogels like they should be nontoxic, must not affect the nutrients of soil, must be stable in the soil and most importantly, they should be inexpensive [10]. Nowadays, most of the commercial hydrogels are made up of synthetic polymers, thus non-biodegradable and considered as pollutant for the soil. Due to alarming attention towards the environmental protection, development of natural polymers and hence biopolymer based SAH has become deal of great interest because of their environmental and commercial advantages. Presently, a lot of natural polymers based SAH have been synthesized using biopolymers and their derivatives such as chitosan [11], starch, alginate, cellulose and guar gum etc. [8,12–15].

Tamarind kernel gum (TKG) is a natural polymer and one the cheapest gums available as it is extracted from the seeds of tamarindus indica L. It is composed of xylose, galactose and glucose in the molar ratio of 1:2:3 [16]. TKG and its derivative have been used as a good alternative biopolymer to the synthetic polymers because of its biodegradability, varying solubility, non-toxicity and vulnerability to microbial degradation [17]. Number of TKG based modified products have been studied in various applications, such as textile, explosives, food industries, plywood and medical industries [12]. One such derivative of TKG is carboxymethyl tamarind kernel gum (CMTKG). It has better properties in comparison to TKG [18]. But very spare literature is handy on their utilization in the field of agriculture.

As per the research gap and capacity of carboxymethyl tamarind kernel gum (CMTKG), to the best of our knowledge, it is being used for the first time with sodium acrylate.

The present work elucidates synthesis, swelling studies, characterization and agricultural applications of carboxymethyl tamarind kernel gum (CMTKG) based novel SAH.

2. Experimental

2.1. Materials

CMTKG having 0.20° of substitution, was generously gifted by Hindustan Gum and chemicals ltd., Bhiwani, Haryana. Acrylic acid (AA, CDH, New Delhi), Potassium per sulphate (KPS, Fischer Scientific, Mumbai), N,N′-methylenebis(acrylamide) (MBA, Merck, Germany), Sodium hydroxide (Fischer Scientific, Mumbai) were used as received. Distilled water was used for the preparations of solutions.

2.2. Synthesis of SAH

The novel superabsorbent cross-linked hydrogels of CMTKG and sodium acrylate (SA) were fabricated by free radical copolymerization using KPS as an initiator and MBA as a cross-linker. In a typical procedure, this reaction was performed by dispersing desirable amount of CMTKG in 10 mL of distilled water. To this, a prefixed quantity of SA, MBA and KPS were mixed according to the desired ratios in a beaker and were stirred with the help of a magnetic stirrer. After 2 h, the resulting mixture was transferred into test tubes and kept in the hot water bath maintained at 60 °C for 2 h. The hydrogels then obtained were taken out by breaking the test tubes and cut into equal thin slices. Then, the hydrogels in the shape of small discs were immersed in distilled water for overnight so as to get rid of unreacted chemicals. Finally, the soaked hydrogel discs were first air dried and then in the oven at 50 °C till the arrival of constant weight [19].

The exact ratios of the reactants of reaction are summarized in Table 1. The combination which was found out to be the best is shown in bold.

2.3. Swelling studies

Swelling studies of the fabricated hydrogels were studied by gravimetric analysis. Fully dried hydrogel samples were accurately weighed and immersed in distilled water, solutions of pH 4, 9 and 12 (prepared by adding NaOH or HCl in their dilute version) and 0.9% NaCl.

After regular time interval, the swollen hydrogels were taken out and weighed after removing the surface water with filter paper (Fig. 2(a) & (b)). The swelling indexes were calculated using the given equation [20].

$$SI = (W_e - W_d) / W_d$$

where, SI is the swelling index of SAH, W_e is the weight of equilibrium swollen SAH while W_d is the initial weight of the dried SAH. All experiments were done in triplicate.

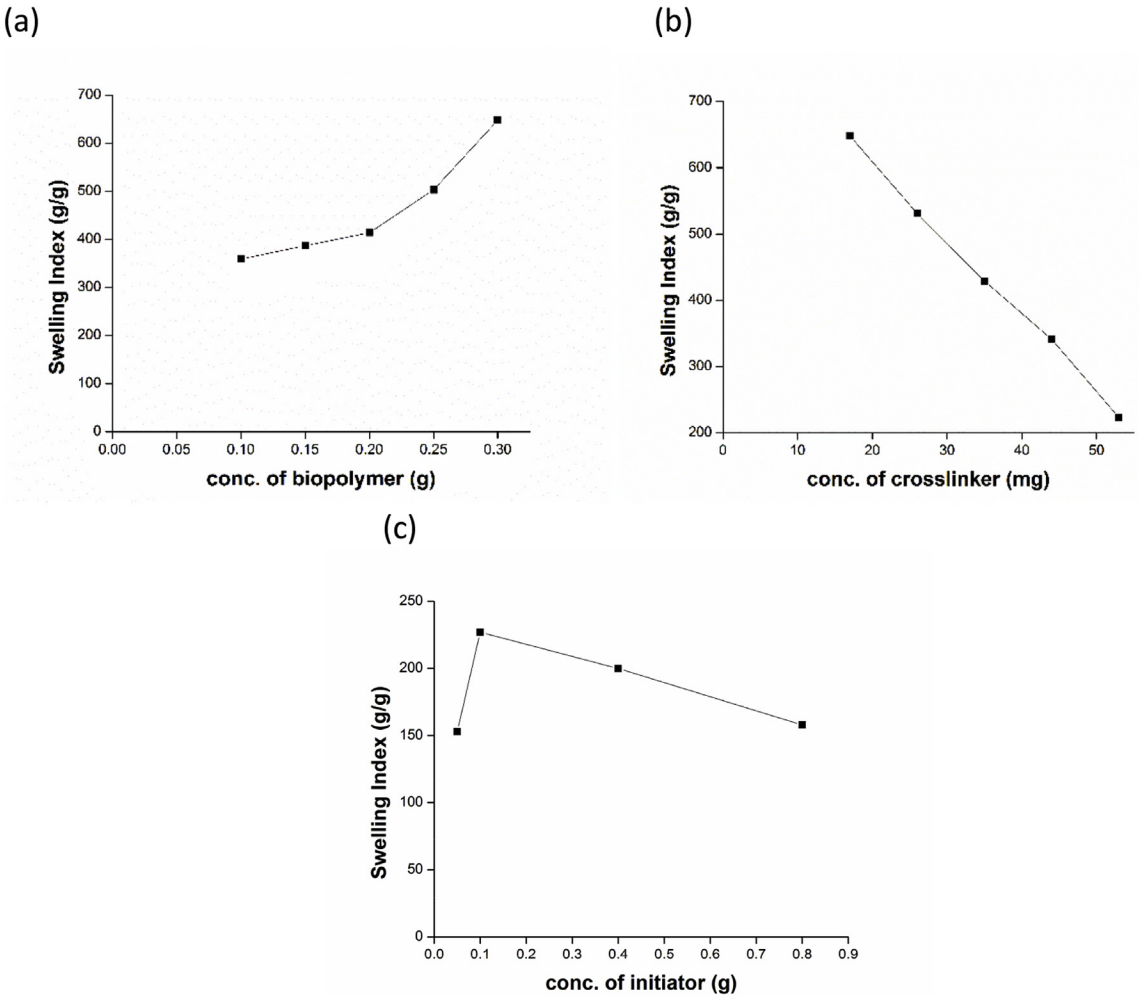

Fig. 1. Effects of reagent concentration on swelling index of the hydrogel. (a) Effect of biopolymer (b) Effect of cross-linker (c) Effect of initiator.

2.4. Characterization

2.4.1. Fourier-transform infrared (FTIR) spectroscopy

The FTIR spectra of CMTKG based SAH were recorded using a FTIR spectrophotometer in a solid state by KBr pellet method (Model: PerkinElmer spectrum version 10.5.3).

2.4.2. Thermal analysis

The thermo-gravimetric analysis (TGA) of CMTKG and its SAH were carried out using a PerkinElmer TGA by using N_2 atmosphere from 25 °C to 900 °C with 10 °C/min of uniform heating rate.

2.4.3. Scanning electron microscopy (SEM)

Surface morphology of CMTKG and its SAH were analyzed by SEM (Model: JEOL JSM-6610LV).

2.5. Degradation studies

Degradation of the fabricated SAH was done through soil burial method [3,21–23] for a period of 38 days. The predetermined quantities of SAH were kept into 50 mesh sieve bag and buried 5–6 cm deep inside the soil while maintaining the moisture in the soil. The samples were taken out at a particular interval of time and washed thoroughly in order to detach soil. The sample was then further dried and weighed. The degradation percentage was found out on the basis of dry weight of the SAH persisting in the soil after definite time period. The degradation studies were also done by analyzing the changes in the morphology of the SAH's surface (Fig. 4(a)(b)).

The percentage determination of left over dry content (DC) of SAH after each sampling period was found out by using the below mentioned formula [24]:

$$\%\ \text{DC remaining} = \frac{\text{weight of dry content at particular period}}{\text{weight of initial dry content}} \times 100$$

2.6. Applications of (CMTKG-PSA) SAH as a soil conditioner

The SAH formed was analyzed for the application in the field of agriculture as a soil conditioner by observing and calculating its effect on physical properties of soil including maximum water holding capacity, porosity, bulk density, particle density and water retention characteristics by planting chickpea seeds and also by using pressure-plate apparatus [24]. The composition of soil is as follows, Sand 89%, slit & clay 0.7% [25] having particle density 2.625 g/cm^3; bulk density 1.32 g/cm^3, was collected from Delhi Technological University.

For the determination of maximum water holding capacity (MWHC) of soil, definite quantity of fully air dried soil, filtered through 3 mm sieve, was made to treat with 0.1%, 0.2% & 0.3% of crushed SAH of particle size: 120–160 mesh, and for comparison, a sample of untreated soil was kept aside as control. To estimate the MWHC of soil, measured amount of the same was taken in a pot with tiny holes at the bottom followed by keeping filter paper in it. These soil samples were kept in the water bath in order to let the soil absorb water to its maximum capacity. After 6 h, the samples were removed from the water bath and

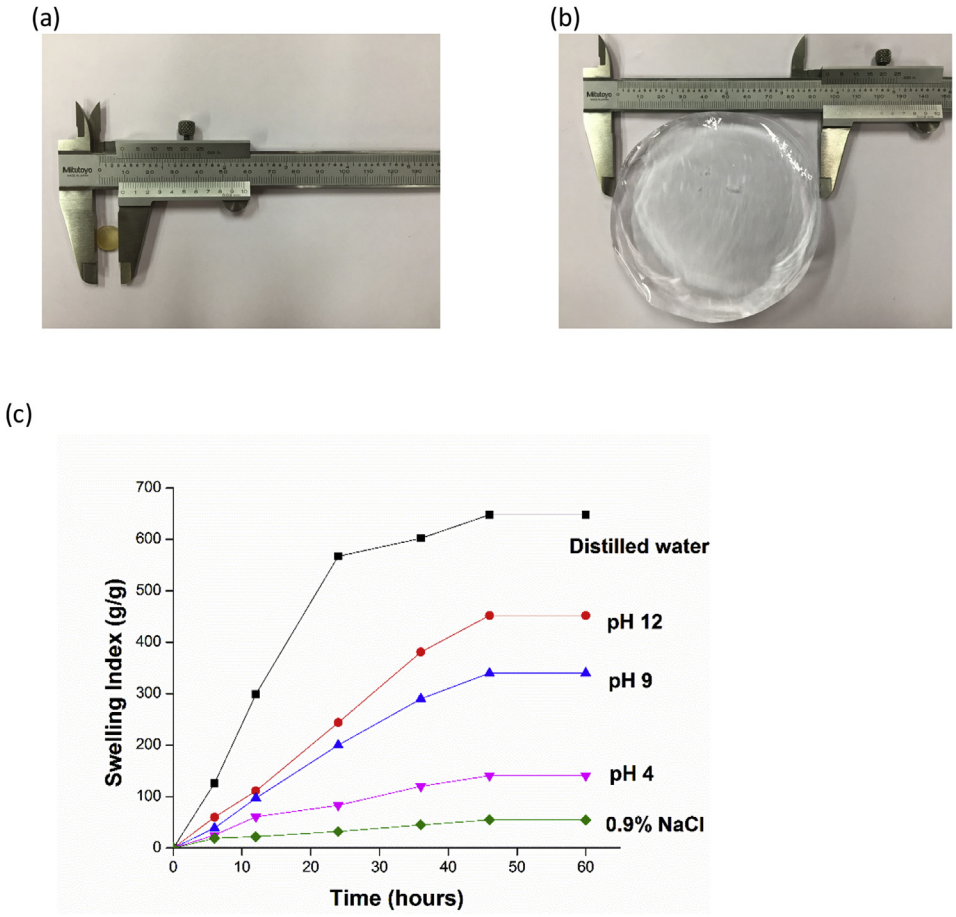

Fig. 2. Water absorption studies of CMTKG-PSA hydrogels. (a) Appearance of dry hydrogel (b) Appearance of swollen hydrgel (c) Absorption dynamics in different solvents.

surplus water was drained out. The net amount of water absorbed (MWHC) by the soil was determined as per the given equation.

MWHC of soil = weight of [whole pot – (wet filter paper + empty pot)]

Soil density was determined by taking the representative oven dried soil sample and was filtered through 2 mm sieve. Particle density of the control soil was calculated using pycnometer [26].

The determination of bulk density of powdered SAH having particle size between 120 and 160 mesh at different doses of 0.1%, 0.2%, and 0.3% w/w were mixed in the soil and taken in beakers which were having holes at the bottom, as explained in MWHC experiment setup. For comparison, control soil was also taken. The samples were then kept under room temperature conditions for a few days to enable drying. These dried samples were finally filtered through 2 mm sieve. Standard laboratory method was used for treated soil in determining the bulk density of all control and treated samples [27]. Porosity percentage was calculated with the help of the obtained values for particle and bulk density by using the formula:

P (%) = [1 – (BD/PD)] x 100

where, P = porosity, PD = particle density and BD = bulk density.

2.6.1. Water retention capacity by plantation method

In an effort to be beneficial to agriculture, especially effective in dry regions, testing of synthesized SAH for water retention was carried out in triplicates by growing chickpea seeds (cicer arietinum) into plants with and without using SAH.

2.6.2. Water retention capacity using pressure-plate apparatus

Pressure plate apparatus (Model: 1600 pressure extractor, Santabarbara, CA, USA) was used to study effect of SAH on water retention capacity of soil at different matric tensions of 0.33 bar (corresponding to field capacity), 1 bar, 5 bar and 15 bar (corresponding to permanent wilting point). The control (untreated soil) and soil treated with 100–160 mesh size SAH at different doses of 0.1, 0.2 and 0.3% was settled in rings made up of rubber which were arranged on ceramic plates. The samples were then allowed to saturate overnight with water. The plates were then set in pressure chamber applying various tensions until the flow of water ceased completely from the soil. This soil was then transferred into moisture boxes and weighed. These samples were dried in an oven at 100 °C for overnight, air cooled and reweighed. The following equation was used to calculate the total amount of water held by soil sample at particular pressure:

WC (% w/w) = $[(S_{wet} - S_{dry}) / S_{dry}]$ x 100

where, WC is the content of soil on weight basis, Swet is the weight of wet soil at a specific pressure, Sdry is the weight of dried soil.

3. Results and discussions

3.1. Mechanism of the formation of (CMTKG-PSA) SAH

In order to obtain SAH with maximum swelling index, different combinations of CMTKG, cross-linker (MBA), initiator (KPS) were tried during synthesis (Table 1).

The (CMTKG-PSA) SAH preparation scheme is depicted in Scheme 1. The initiator KPS was first decomposed at 60 °C to generate sulphate

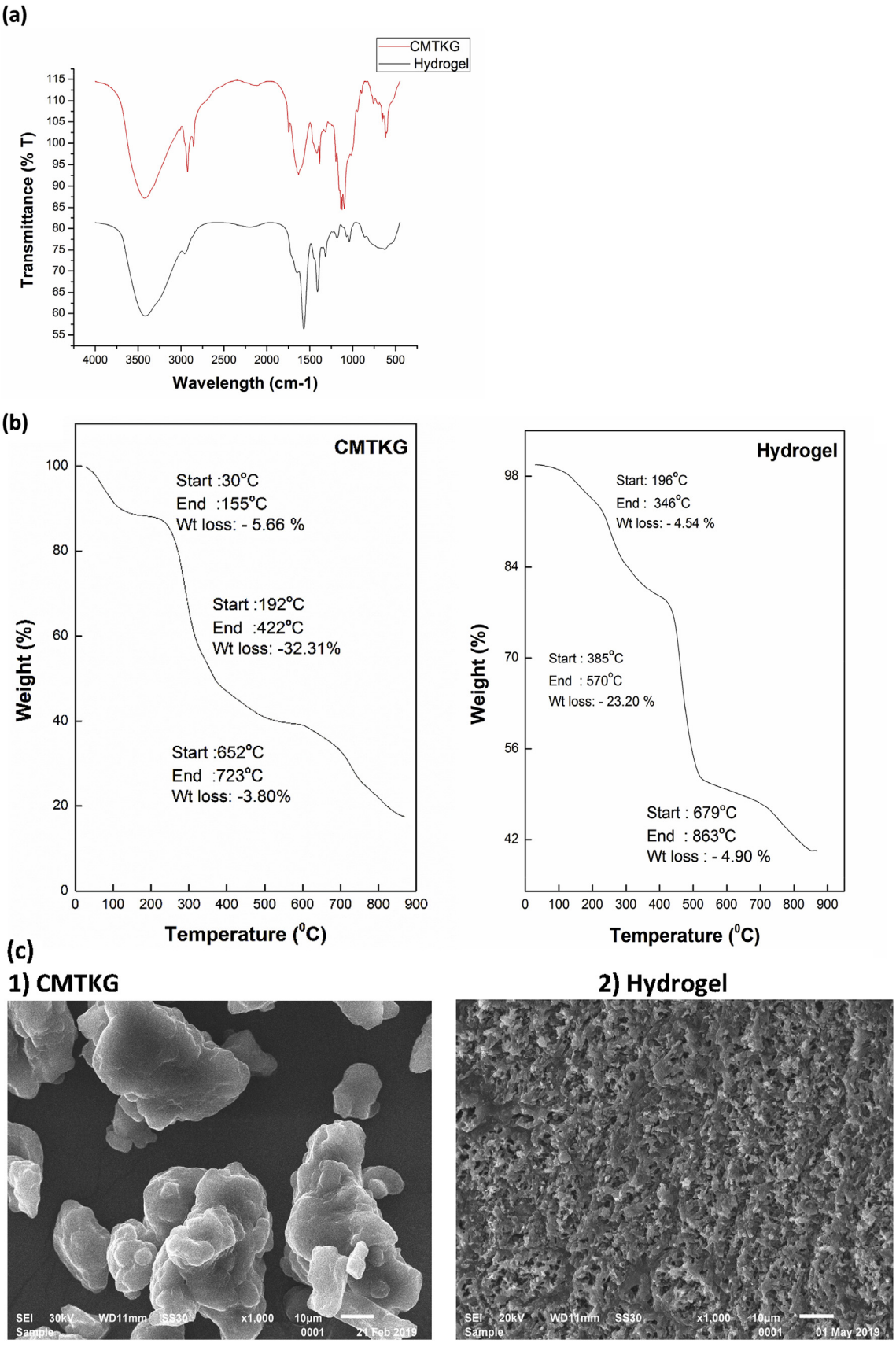

Fig. 3. Characterization of synthesized CMTKG-PSA hydrogel (a) FTIR analysis (b) TGA analysis (c) SEM study.

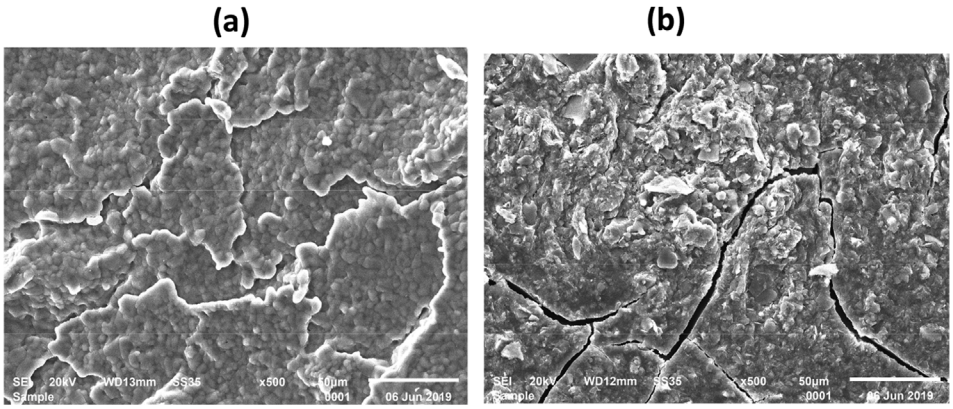

Fig. 4. Degradation studies of CMTKG-PSA hydrogel by soil burial method (a) Sem morphology after 20 days (b) Sem morphology after 38 days.

anion radicals. These radicals further formed macromolecular radicals on the substrates by extracting hydrogen atom(s) of the hydroxyl groups from the backbone of CMTKG. These active radicals were reacted with vinyl groups of SA to formulate covalent bonds and simultaneous generation of new radicals which can process propagation of chain to form poly sodium acrylate (PSA). Due to polyfunctionality of cross-linker, MBA (CH_2═CHCONHCH_2NHCOCH═CH_2), a macro radical with reactive sites was formed which can be utilized for cross-linking both the PSA and CMTKG through its –OH groups. This resulted into the formation of tri-dimensional network of CMTKG-PSA hydrogel.

It is relevant to mention that the SAH preparation was attempted solely with CMTKG (keeping all the reaction conditions identical), but it came out to be a jelly like mass and hence no hydrogel formation was observed.

3.2. Effect of biopolymer

The water absorption behavior of SAH was affected by the different concentration of the biopolymer, CMTKG. Different concentration of CMTKG showed significant effect on the capacity of water absorption

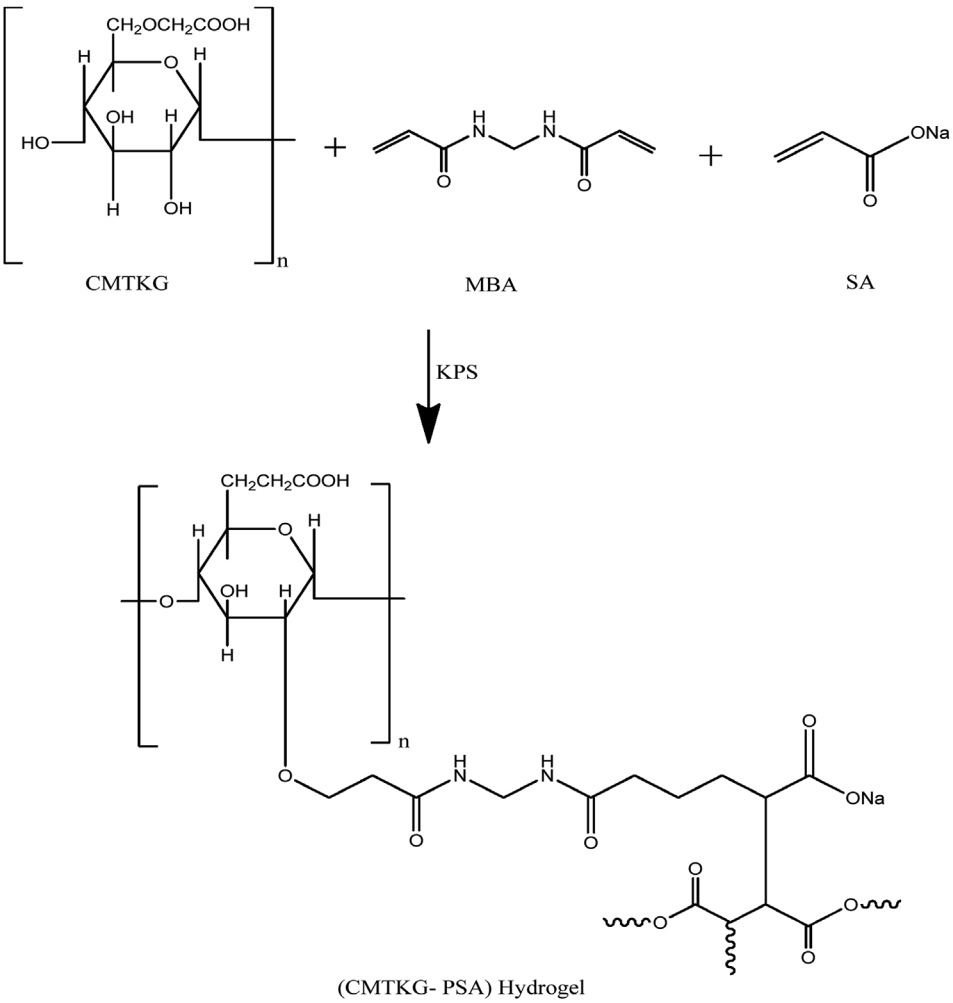

Scheme 1. Synthesis mechanism of CMTKG-PSA Hydrogel.

(swelling index) of SAH is evident in Fig. 1(a). This behavior may be due to the fact that as the concentration of CMTKG increased from 0.15 g to 0.3 g, the COO^- groups and the number of counter ions (Na^+) along the polymeric chains also got increased within the gel phase, resulting an amplification in the chain relaxation because of the repulsion among like charged COO^- groups. Furthermore, osmotic swelling pressure too got increased because of the increase in Na^+ (free counter ions) in the gel phase. Hence, these two factors play a significant part towards the increased swelling index of SAH with respect to the concentration of CMTKG [19]. Further, it can be noted that the synthesis of hydrogel with even higher concentration of biopolymer was also tried out but in that case the solution used to get very viscous and hence was very difficult to stir.

3.3. Effect of cross-linker

Cross-linking density is one of the important factors which affects swelling of SAH as explained by Flory's network theory [28]. SAH in terms of swelling undergo major changes even with a relatively small change in the concentration of cross-linker. In view of the swelling index of SAH, the relationship between the swelling index and the concentration of cross-linker, MBA was studied (Fig. 1(b)).

As the concentration of MBA increased from 17 mg to 53 mg, the swelling index decreased significantly. It is known that the dosage of cross-linker determines the cross-linking density. Hence, higher the concentration of MBA levels, more will be the cross-linking, which resulted in additional network formation. Consequently, the pore spaces among the frameworks of the tri-dimensional network would decrease which further reduced the free volume available inside the polymeric network of hydrogel, and restricting the water absorption rate. Hydrogels become harder and compact with excess cross-linking. It was observed that the hydrogel with even lesser concentration than 17 mg, resulted into the formation of jelly like product. This can be attributed to the insignificant network formation between the chains of polymers.

3.4. Effect of initiator

Reaction initiator plays a notable role in preparation of SAH by creating lot of active sites on the chains of polymer. Keeping the amount of cross-linker fixed at 35 mg, concentration of initiator, KPS, was varied and its outcome was studied in distilled water as shown in Fig. 1(c).

Initially, the water absorption increased and then reduced with the increase in the dosage of initiator. At 0.1 g of initiator concentration, maximum water absorbency was observed which was about 227 g/g. For the concentration below 0.1 g, sharp decline in water absorbency was observed. This can be attributed to slow disintegration of the KPS at lower concentration. This results in sedate reaction of polymerization leading into more concentration of soluble monomer. This results in the formation of loose hydrogel network leading to give less swelling. Again, decrease in water absorbency was observed beyond 0.1 g amount of the initiator because of the elevated collisions amid free-radicals and monomer due to fast velocity of reaction. This resulted in the increment of oligomer content in the network of hydrogel. It did not led to swelling because of the solubility of oligomeric part in water and hence swelling index of the SAH got decreased when concentration of initiator increased beyond 0.1 g [29].

3.5. Swelling studies

Swelling study of (CMTKG-PSA) SAH showed its huge potential to swell by holding water into its sponge-like framework. The swollen and dry SAH are shown in Fig. 2(a) (b). The swelling index of (CTKP-PSA) SAH for various solvents viz., pH 4, 9 and 12, 0.9% NaCl and distilled water have shown in Fig. 2(c). Swelling equilibrium was observed in about 46 h (h). Amongst the different solvents used, the highest swelling index was shown by the distilled water, it absorbed 648 g/g of distilled water.

For solutions at various pHs, the water absorption capacity increased from pH 4–12. At pH 4, 141 g/g swelling index was shown by the hydogel which at pH 9 increased to 340 g/g and at pH 12 increased further to 452 g/g. Improper ionization of the cross-linked network may be attributed for the lower swelling in acidic medium. Hence, a collapsed state was obtained at low pH. Whereas, at alkaline conditions, increase in electrostatic repulsions produced by the carboxylate anions (COO^-) in hydrogel might had widened the space present in the networks of SAH [30]. Water absorbency of the SAH was observed to be dropped drastically in case of 0.9% NaCl solution, where it absorbed 55 g/g of solvent. Significant reduction in the swelling capacity of hydrogel in the case of 0.9% NaCl solution is due to presence of high ionic concentration in surrounding which decreases the difference in the osmotic pressure between outer and inner phases. Consequently, restricts free entry of any solvent inside the 3-D network of SAH [31].

3.6. Characterization

3.6.1. FTIR spectroscopy

FTIR spectra of CMTKG and (CMTKG-PSA) SAH are as shown in Fig. 3(a). CMTKG showed characteristic broad absorption peak at 3428 cm^{-1} for –OH stretching vibrations. The symmetric and asymmetric vibration of $–COO^-$ moiety are assigned to 1415 cm^{-1} and 1631 cm^{-1}, respectively [32]. For the spectrum of SAH, a broad absorption band at 3418 cm^{-1} corresponded to the –OH stretching vibration and $–COO^-$ symmetric and asymmetric vibrations at 1410 cm^{-1} and 1568 cm^{-1}, respectively. This strong transmittance peak at 1568 cm^{-1} was linked with stretching vibration of C═O of the polysodium acrylate, whereas the occurrence of bands at 1039 cm^{-1} and 627 cm^{-1} were characteristic of the CTKP polysaccharide skeleton. The broad band at 627 cm^{-1} and a peak at 1317 cm^{-1} corresponded to the O═C–N and C–N groups of MBA [33]. This confirmed the presence of cross-linking. These together attributed to the successful cross-linking network between CMTKG chains and PSA.

3.6.2. Thermal analysis

Thermal stability of the SAH is expected to be more than its starting material, CMTKG. Hence, to confirm the same, comparative thermal studies were done. TGA thermograms of CMTKG and its cross-linked SAH are shown in Fig. 3(b). Weight loss was observed in three distinct zones in the case of CMTKG. The weight loss of 5.66%, at initial stage (30–155 °C) is attributed to the removal of moisture from the polymer. The second zone of weight loss (192–422 °C) could be because of the polymeric backbone degradation, i.e. decomposition of carboxymethyl and hydroxyl group of CMTKG [17,34] with 32.31% weight loss. This was followed by third zone of degradation (652–723 °C) with 3.80% weight loss. The weight loss was recorded in three zones in the case of (CMTKG-PSA) SAH also. First region (196–346 °C) was due to loss of unreacted cross-linker or monomers. The weight loss of 23.20% for Second region (385–570 °C) attributes to degradation of polymer backbone. The third region (679–863 °C) was found out with 4.90% of weight loss. However, the SAH had a higher mass percentage of about 79% until 400 °C was observed as compared to about 43% of the raw CMTKG at the same temperature. Similarly, at 850 °C, the SAH recorded more than 40% of residual mass in comparison to CMTKG with only 18% of residual mass. Hence, thermal stability of SAH was found to be much improved than the biopolymer.

3.6.3. Scanning electron microscopy (SEM)

SEM micrographs of CMTKG and (CMTKG-PSA) SAH, at various magnifications are shown in Fig. 3(c). This analysis showed the morphology of (CMTKG-PSA) SAH having lots of interspatial voids and spongy surface. It showed distinct and clear boundaries in a conventional network fashion whereas CMTKG exhibited a compact and non-

porous surface. At higher magnification, the gel network was observed that comprised both micro and macro pores. These pores are attributed for more swelling index as it permits direct penetration of the liquid in to the network of polymer by means of fluid diffusion.

3.7. Degradation studies

In agriculture, synthetic polymeric hydrogels are not preferred because of their non-biodegradable nature which leads to contamination of soil [35]. Here, (CMTKG-PSA) SAH were synthesized by mixing natural polymer with the synthetic polymer so as to upgrade its degradability in comparison to the synthetic hydrogels.

Rate of decomposition in the initial days was rapid followed by slower phase and relatively fast degradation rate. The rate of loss of weight were highest in the first 20 days where about 41% of the SAH was degraded in the soil whereas about 9% weight loss was observed from 20 to 38 days. The decomposition of polymers depends on various factors, e.g., oxygen content, pH, temperature, humidity, availability of mineral nutrients, which affects the growth of micro-organisms [36,37]. Rampant decay rate at initial phase can be due to decomposition of organic component of the SAH, CMTKG, which is uniformly blended with the other synthetic components. This decomposition was supported by soaking up of more soil micro-organisms in the network of swollen SAH while water absorption [3] which promoted the decay rate. This was supported by SEM studies, as depicted in Fig. 4(a), (b), where rapid phase degradation sample showed eroded and hollow surface morphology.

In the case of post 20 days, rate of decay got heavily reduced due to high water content in the network of SAH which might hinders oxygen from going into the hydrogel network and creating an anaerobic environment [38] that inhibit microbial growth and hence affecting the degradation rate.

3.8. Agricultural applications of (CMTKG-PSA) SAH

3.8.1. Maximum water holding capacity

It was established through the experiment that maximum water holding capacity or MWHC of soil significantly enhanced after treatment with (CMTKG-PSA) SAH. It can be seen in Fig. 5(a), (CMTKG-PSA) SAH at dosage of 0.1%, 0.2% and 0.3% was found to be effective in enhancing soil's MWHC.

MWHC of the control (untreated soil) was found to be 43.31% i.e. 43.31 g of water can be hold by 100 g of dried soil to reach saturation point. Addition of 0.1% of powdered SAH could enhance MWHC of soil by 10.8% to push it to 48.01%. Similarly, treatment with 0.2% and 0.3% further enhanced MWHC to 53.11% and 58.12% respectively which was 23.6% and 34.5% higher than that of the control. Intriguingly, for increase in SAH quantity by every 0.1%, approximately 11% inflation in MWHC was observed. To sum up, this experiment shows that the quantity of SAH mixed with soil is directly proportional to MWHC.

3.8.2. Soil density and porosity

Particle density (PD) is a peculiar characteristic of any soil, which was found as per standard procedure and was found out to be 2.625 g/cm^3. Using the value of PD, bulk density (BD) of control and distinctively treated soil was found out by following standard protocol (Singh et al., 2005). Fig. 5(b) and (c) depict the trends in BD and porosity of soil prior and post treatment with SAH.

Notable difference was observed in BD of SAH treated soil in contrast to control. In comparison to 1.32 g/cm^3 value of control, BD decreased by 3.0, 5.3 and 6.8% for 0.1, 0.2 and 0.3% SAH treated soil, respectively. BD and porosity have inverse relationship with each other. Porosity aids good health of soil by amplifying microbial count and soil aeration. In this experiment, about 50% of porosity observed for the control soil whereas for treated soils, it improved to 53%. The improvement in porosity may be due to the voids left in soil by the particles of SAH. There was not much difference between treated and control soil as the amount of SAH added was in the powdered form and hence the difference is notably visible in swollen stage only.

3.8.3. Water retention capacity by plantation

The determination of water retention capacity by planting chickpea seeds was conducted in triplicates by mixing SAH (0.5% (w/w)) with the soil (2 Kg) in one set of pots and while the other set, containing only soil, were kept as control. With 400 mL of water, ten healthy seeds were planted in all the pots. Germination was observed after 7 days in both type of sets. The pattern in growth of the plants was observed and special care was taken so that no pests affected the plants. There was not much difference observed in the growth of the plants in both type of sets for up to 18 days. However, after 18 days the plants in the pots containing untreated soil started wilting, while the plants in the pots containing soil with SAH were fresh. After 41 days, the plants in the pots having soil with SAH started wilting. The plants in soil with SAH were sustained fresh and green up to 41 days without any further addition of water (Fig. 6). Thus by mixing tiny amount of SAH, the moisture can easily be retained in the soil for as many as 41 days in comparison to just 18 days for untreated soil. Thus these SAH have competent water retention capacity in soil. It is notable to mention that the plants showed similar growth pattern in individual set of each category.

3.8.4. Water retention capacity using pressure-plate apparatus

Water retention under distinct matric potential of soil is a vital criterion which informs about the reachability of water to any plant. This plays crucial role under draught and stress condition and even little enhancement in water retention capacity of soil during pressure condition can boost the health of crops and the possibility of crop survival in case of severe draught.

The synthesized SAH has proven to be a successful utility, aiming increment in water retention property of soil at various pressure conditions as examined by pressure plate apparatus (Fig. 7). The difference was maximum at zero bar matric tension, where as compared to control (43.31% WHC i.e. water holding capacity), treated soil exhibited geometric elevation in the water retention, 48.01, 53.11 and 58.12% WHC for 0.1%, 0.2% and 0.3% of (CMTKG-PSA) SAH treatment respectively. A similar trend was observed at 0.33 bar tension, where as compared to controls 18.05%, treated soil showed 25.21, 26.62 and 27.62% WHC for 0.1, 0.2 and 0.3% CMTKG-PSA SAH treatment respectively. At high matric tension of 1 bar, 5 bar and 15 bar, similar trend was observed which clearly indicated that SAH treated soil could retain more water. At 15 bar pressure, this difference got reduced and control soil could retain 4.99% moisture as compared to 5.86% for 0.1% SAH, 7.06% for 0.2% SAH and 8.68% for 0.3% SAH. This reduced moisture retention at very high tension can be ascribed to the pressure exerted by neighboring soil particles which limit swelling and compress out initially absorbed water [39].

Out of the treatments, best result was given by 0.3% SAH, i.e. 3 g SAH per Kg of soil and significantly enhanced availability of water to plants in soil.

4. Conclusion

Novel degradable SAH with excellent water retaining property were synthesized from CMTKG. The moisture absorption and retention could improve significantly by adding slight amount of 0.1–0.3% (CMTKG-PSA) SAH into the soil. The maximum water holding capacity of soil was enhanced up to 35% and its porosity up to 7% of its original. The incorporation of the synthesized SAH in small dose in the soil showed notably higher moisture percentage retention even at the matric tension of 15 bar. Thus, the synthesized (CMTKG-PSA) SAH has the potential to be used in agriculture sector as water conserving agent and soil

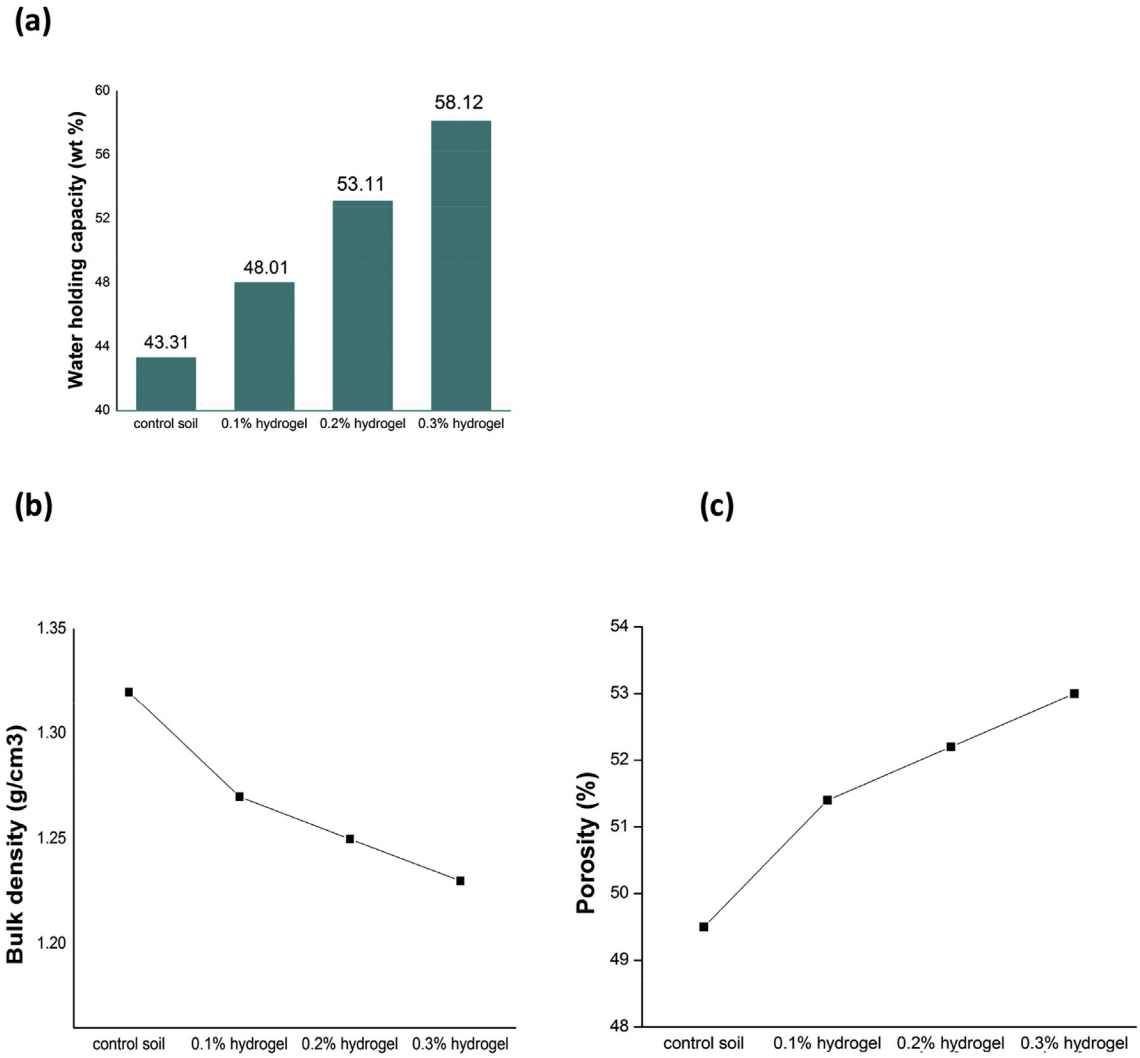

Fig. 5. Effect of hydrogel treatment on physical properties of soil (a) MWHC (b) Bulk density (c) Porosity.

Fig. 6. Effect of hydrogel treatment on chickpea plants after 41 days.

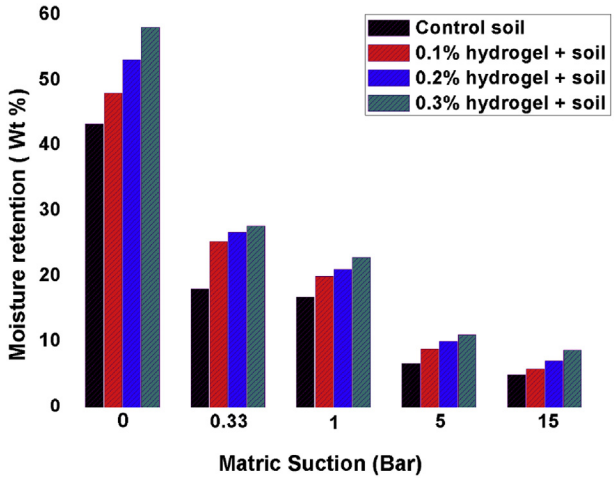

Fig. 7. Effect of hydrogel treatment on soil's moisture retention at distinct matric potential.

conditioner. These SAH can further be used as a nutrient carrier vehicle in the field of agriculture.

Conflicts of interest

There are no conflicts to declare.

Data availability

The raw/processed data required to reproduce these findings cannot be shared at this time as the data also forms part of an ongoing study.

References

[1] K. B, K.L. S, S.P. wani, Piara Singh, Climate Change and Sustainable Rain-Fed Agriculture : Challengea and Opportunities, (2009), pp. 221–239.

[2] L. Xie, M. Liu, B. Ni, X. Zhang, Y. Wang, Slow-release nitrogen and boron fertilizer from a functional superabsorbent formulation based on wheat straw and attapulgite, Chem. Eng. J. 167 (2011) 342–348, https://doi.org/10.1016/j.cej.2010.12.082.

[3] B. Ni, M. Liu, S. Lü, L. Xie, Y. Wang, Multifunctional slow-release Organic – Inorganic compound fertilizer, J. Agric. Food Chem. 58 (2010) 12373–12378, https://doi.org/10.1021/jf1029306.

[4] M.R. Guilherme, F.A. Aouada, A.R. Fajardo, A.F. Martins, A.T. Paulino, M.F.T. Davi, A.F. Rubira, E.C. Muniz, Superabsorbent hydrogels based on polysaccharides for application in agriculture as soil conditioner and nutrient carrier: a review, Eur. Polym. J. (2015), https://doi.org/10.1016/j.eurpolymj.2015.04.017.

[5] J. Kuang, K.Y. Yuk, K.M. Huh, Polysaccharide-based superporous hydrogels with fast swelling and superabsorbent properties, Carbohydr. Polym. 83 (2011) 284–290, https://doi.org/10.1016/j.carbpol.2010.07.052.

[6] R.A. Batista, P.J.P. Espitia, J. de S.S. Quintans, M.M. Freitas, M.Â. Cerqueira, J.A. Teixeira, J.C. Cardoso, Hydrogel as an alternative structure for food packaging systems, Carbohydr. Polym. 205 (2019) 106–116, https://doi.org/10.1016/j.carbpol.2018.10.006.

[7] K. Zhong, X.-L. Zheng, X.-Y. Mao, Z.-T. Lin, G.-B. Jiang, Sugarcane bagasse derivative-based superabsorbent containing phosphate rock with water–fertilizer integration, Carbohydr. Polym. 90 (2012) 820–826, https://doi.org/10.1016/j.carbpol.2012.06.006.

[8] K. Hemvichian, A. Chanthawong, P. Suwanmala, Synthesis and characterization of superabsorbent polymer prepared by radiation-induced graft copolymerization of acrylamide onto carboxymethyl cellulose for controlled release of agrochemicals, Radiat. Phys. Chem. 103 (2014) 167–171, https://doi.org/10.1016/j.radphyschem.2014.05.064.

[9] A. Hüttermann, L.J.B. Orikiriza, H. Agaba, Application of superabsorbent polymers for improving the ecological chemistry of degraded or polluted lands, Clean. - Soil, Air, Water 37 (2009) 517–526, https://doi.org/10.1002/clen.200900048.

[10] C.K.S. Pillai, Challenges for natural monomers and polymers: novel design strategies and engineering to develop advanced polymers, Des. Monomers Polym. 13 (2010) 87–121, https://doi.org/10.1163/138577210X12634696333190.

[11] S. Nangia, S. Warkar, D. Katyal, Pure and Applied Chemistry A Review on Environmental Applications of Chitosan Biopolymeric Hydrogel Based Composites, (2019), p. 1325, https://doi.org/10.1080/10601325.2018.1526041.

[12] R. Bhattacharyya, S.K. Ray, B. Mandal, A systematic method of synthesizing composite superabsorbent hydrogels from crosslink copolymer for removal of textile dyes from water, J. Ind. Eng. Chem. 19 (2013) 1191–1203, https://doi.org/10.1016/j.jiec.2012.12.017.

[13] Y. Zhou, S. Fu, L. Zhang, H. Zhan, Superabsorbent nanocomposite hydrogels made of carboxylated cellulose nanofibrils and CMC-g-p(AA-co-AM), Carbohydr. Polym. 97 (2013) 429–435, https://doi.org/10.1016/j.carbpol.2013.04.088.

[14] N. Thombare, U. Jha, S. Mishra, M.Z. Siddiqui, Guar gum as a promising starting material for diverse applications: a review, Int. J. Biol. Macromol. 88 (2016) 361–372, https://doi.org/10.1016/j.ijbiomac.2016.04.001.

[15] W.B. Wang, A.Q. Wang, Preparation, swelling and water-retention properties of crosslinked superabsorbent hydrogels based on guar gum, Adv. Mater. Res. 96 (2010) 177–182 https://doi.org/10.4028/www.scientific.net/AMR.96.177.

[16] S. Kshirsagar, A.P. Pandit, Curcumin pellets of carboxymethylated tamarind seed polysaccharide for the treatment of inflammatory bowel disease, Drug Deliv. Lett. 8 (2018) 29–40, https://doi.org/10.2174/2210303107666171106143357.

[17] S. Pal, G. Sen, S. Mishra, R.K. Dey, U. Jha, Carboxymethyl tamarind: synthesis, characterization and its application as novel drug-delivery agent, J. Appl. Polym. Sci. (2008), https://doi.org/10.1002/app.28455.

[18] J.H. T, Synthesis, characterization, and swelling behavior of superabsorbent hydrogel from sodium salt of partially carboxymethylated tamarind kernel powder-g-PAN, J. Appl. Polym. Sci. (2013), https://doi.org/10.1002/app.38910.

[19] A.P. Gupta, S.G. Warkar, Synthesis, characterization and swelling properties of poly (Acrylamide-cl-carboxymethylguargum) hydrogels, Int. J. Pharma Bio Sci. 6 (2015) 516–529 https://www.researchgate.net/publication/281927604_Synthesis_characterization_and_swelling_properties_of_poly_Acrylamide-cl-carboxymethylguargum_hydrogels , Accessed date: 20 February 2019.

[20] Y. Wang, J. Wang, Z. Yuan, H. Han, T. Li, L. Li, X. Guo, Chitosan cross-linked poly (acrylic acid) hydrogels: drug release control and mechanism, Colloids Surfaces B Biointerfaces 152 (2017) 252–259, https://doi.org/10.1016/j.colsurfb.2017.01.008.

[21] K. Sharma, V. Kumar, B.S. Kaith, V. Kumar, S. Som, S. Kalia, H.C. Swart, A study of the biodegradation behaviour of poly(methacrylic acid/aniline)-grafted gum ghatti by a soil burial method, RSC Adv. 4 (2014) 25637, https://doi.org/10.1039/c4ra03765k.

[22] B. Ni, M. Liu, S. Lü, Multifunctional slow-release urea fertilizer from ethylcellulose and superabsorbent coated formulations, Chem. Eng. J. 155 (2009) 892–898, https://doi.org/10.1016/j.cej.2009.08.025.

[23] K. Sharma, B.S. Kaith, V. Kumar, S. Kalia, V. Kumar, H.C. Swart, Synthesis and biodegradation studies of gamma irradiated electrically conductive hydrogels, Polym. Degrad. Stab. 107 (2014) 166–177, https://doi.org/10.1016/j.polymdegradstab.2014.05.014.

[24] N. Thombare, S. Mishra, M.Z. Siddiqui, U. Jha, D. Singh, G.R. Mahajan, Design and development of guar gum based novel, superabsorbent and moisture retaining hydrogels for agricultural applications, Carbohydr. Polym. 185 (2018) 169–178, https://doi.org/10.1016/j.carbpol.2018.01.018.

[25] G.W. G, J.W. Bauder, Particle-size analysis, Methods Soil Anal. Part 1—Physical Mineral. Methods, 1986, pp. 383–411, , https://doi.org/10.1007/978-1-4020-3995-9_406.

[26] A. Klute, G.R. Blake, K.H. Hartge, Bulk density, Methods Soil Anal. Part 1—Physical Mineral. Methods, Soil Science Society of America, American Society of Agronomy, 1986, pp. 363–375, , https://doi.org/10.2136/sssabookser5.1.2ed.c13.

[27] D. Singh, P.K. Chhonkar, B.S. Dwivedi, Manual on Soil, Plant and Water Analysis, Westville Publishing House, 2005, https://www.cabdirect.org/cabdirect/abstract/20073118818 , Accessed date: 20 February 2019.

[28] P.J. Flory, In Principles of Polymer Chemistry, (1953), https://doi.org/10.1126/science.119.3095.555-a.

[29] L. Wu, M. Liu, Rui Liang, Preparation and properties of a double-coated slow-release NPK compound fertilizer with superabsorbent and water-retention, Bioresour. Technol. 99 (2008) 547–554, https://doi.org/10.1016/j.biortech.2006.12.027.

[30] C. Chang, B. Duan, J. Cai, L. Zhang, Superabsorbent hydrogels based on cellulose for smart swelling and controllable delivery, Eur. Polym. J. 46 (2010) 92–100, https://doi.org/10.1016/j.eurpolymj.2009.04.033.

[31] Y. Zhao, J. Kang, T. Tan, Salt-, pH- and temperature-responsive semi-interpenetrating polymer network hydrogel based on poly(aspartic acid) and poly(acrylic acid), Polymer (2006), https://doi.org/10.1016/j.polymer.2006.08.056.

[32] J.H. Trivedi, Synthesis, characterization, and swelling behavior of superabsorbent hydrogel from sodium salt of partially carboxymethylated tamarind kernel powder-g-PAN, J. Appl. Polym. Sci. (2013), https://doi.org/10.1002/app.38910.

[33] B.V. Reddy, G.R. Rao, Vibrational spectra and modified valence force field for N,N'-methylenebisacrylamide, Indian J. Pure Appl. Phys. 46 (2008) 611–616.

[34] R.J. Dias, V.D. Havaldar, K.K. Mali, S.C. Dhawale, P.R. Kavitake, Sustained Delivery of Aceclofenac Interpenetrating Networks of Carboxymethyl Tamarind Gum and Chitosan for Sustained Delivery of Aceclofenac, (2017), https://doi.org/10.12991/mpj.2017.20.

[35] J.D. Stahl, M.D. Cameron, J. Haselbach, S.D. Aust, Biodegradation of superabsorbent polymers in soil - Springer, Bio Degrad 7 (2000) 83–88.

[36] H. Mittal, R. Jindal, B.S. Kaith, A. Maity, S.S. Ray, Flocculation and adsorption properties of biodegradable gum-ghatti-grafted poly(acrylamide-co-methacrylic acid) hydrogels, Carbohydr. Polym. (2015), https://doi.org/10.1016/j.carbpol.2014.09.026.

[37] M. Maiti, B.S. Kaith, R. Jindal, A.K. Jana, Synthesis and characterization of corn starch based green composites reinforced with Saccharum spontaneum L graft copolymers prepared under micro-wave and their effect on thermal, physio-chemical and mechanical properties, Polym. Degrad. Stab. (2010), https://doi.org/10.1016/j.polymdegradstab.2010.05.024.

[38] P. Cen, L. Xia, Production of cellulase by solid-state fermentation, Adv. Biochem. Eng./Biotechnol. (1999) 69–92, https://doi.org/10.1007/3-540-49194-5_4.

[39] M. Yangyuoru, E. Boateng, S. Adiku, D. Acquah, T. Adjadeh, F. Mawunya, Effects of natural and synthetic soil conditioners on soil moisture retention and maize yield, West African J. Appl. Ecol. 9 (2009) 1–8, https://doi.org/10.4314/wajae.v9i1.45676.

MADRID
inter.noise 2019
June 16 - 19
NOISE CONTROL FOR A BETTER ENVIRONMENT

TRAFFIC NOISE ANALYSIS USING RLS-90 MODEL IN URBAN CITY

Rajeev Kumar Mishra[1], Ankita R. Mishra[2] and Amit Singh[3]

[1,2,3]Department of Environmental Engineering, Delhi Technological University, Delhi, INDIA
Corresponding author: rajeevkumarmishra@dtu.ac.in

ABSTRACT

Traffic noise is considered as one of the important source of noise pollution and its contribution is approximately 75% of the total noise pollution in urban areas. Delhi is considered as second noisiest city in the world. Ten locations have been selected in Delhi on the basis of their land use pattern, to monitor the ambient noise level. The monitoring has been conducted during morning peak hours, off peak hours and evening peak hours. Sound level meter has been used to monitor the ambient noise level at the selected locations. During this study, RLS-90 Model has been used to predict the noise level at all the selected location. After data analysis, it was observed that the measured ambient noise level at all the locations were violating the permissible limits prescribed by CPCB. During monitoring, highest traffic noise level was observed at Ashram Chowk. This may be due to higher traffic volume as well as high traffic congestion at the particular location. The percentage error between monitored traffic noise level and predicted traffic noise level was found within the range of 0.5 % to 5.75%, which indicates the suitability and applicability of the model in a city like Delhi.

1. INTRODUCTION

Today all the developing as well as developed country are facing threat due to noise pollution after air and water pollution. Developing countries like India, migration of people from rural to urban areas expansion of cities, infrastructure development, population growth and urbanization are important factors resulting in motorization and consequent increase in levels of various urban pollution (Banerjee, et al 2008). The population of Delhi is approximately 11 million, which is the second highest population

in India and this number will be expected to expand by 40% in year 2021 (Census of India 2011). The vehicular population in the Delhi, jumped by 135.59 % from 1999-2000 to 2011-12 and vehicle population became 7.4 million in year 2011, amid a similar period the quantity of vehicles per thousand population expanded from 253 to 436. Likewise, it is noticed that the road network system of the capital has expanded from 28,508 km (year 2001) to 32,663 km (year 2011) (Economic survey of Delhi report 2012-2013), which is not even sufficient to accommodate the entire vehicle fleet. As a result of increasing traffic volume, congestion and poor traffic management in urban area, the traffic noise level has become so high that it exceeded the prescribed limit of CPCB. Traffic is one of the primary source of noise pollution in city like Delhi. A study conducted in Central London to observe that different types of vehicles contribute different level of noise pollution and also revealed that buses and trucks are more responsible in contributing to high traffic noise levels (Stephenson and Vulkan,1968). The noise level was found higher along all the busiest roads in all over Delhi (Akhter et al., 2012). Noise pollution can affect both health and behavior of all living beings. It can also damage physiological and psychological health. It can cause annoyance and aggression, high stress levels, hypertension, hearing loss, sleep disturbances and other harmful effects (Mishra et al 2010). The high noise level can also affect physiological and psychological health. It can contribute to cardiovascular effects and exposure to moderately high levels during a single eight-hour period causes a statistical rise in blood pressure of five to ten points and an increase in stress (NANMN report conducted by CPCB-2015-16). A social survey indicated that 73.8% of respondent residents were highly or moderately irritated by road traffic noise (Ali and Tamura, 2002)

To study the effect and to control the noise, different type of models like Federal highway administration (FHWA) model in USA, Calculation of road traffic noise (CORTN) model in UK, Stop and Go model in Bangkok and Richtlinien für den Lärmschutz an Straben (RLS-90) model in Germany, are used in different countries. These models are used to predict the noise level and help in the designing of noise barrier. In the present study, traffic noise level has been monitored at selected locations in Delhi. The road traffic noise prediction model i.e. RLS-90 has also been used to predict the noise level at all the selected locations. RLS90 model is based on the point source method with spreading ground attenuation, screening and reflection (Akhter et al., 2012). The forecasting of the traffic noise level at different year assumes that the only traffic volume is variable and another factor like road width, gradient, road surface, speed and traffic flow are constant.

2. METHODOLOGY

The noise monitoring procedure includes identification and selection of sampling locations, time duration for monitoring as well as the type of instrument used. The future traffic is predicted on the basis on observed traffic and expected annual growth rate of vehicles.

2.1 Site Selection

Total ten locations are selected in Delhi on the basis of their land use pattern. During site selection some of the locations are found under residential or commercial and silence zone. Land use pattern like locations having high rise building on one side or both sides and locations under the flyover bridge is the most affecting factor for variation in the noise level at different locations. Selected sites with their characteristics are presented in Table 1.

Table 1: List of selected noise monitoring sites in Delhi

Serial No.	Location	Area	One side	Other side
1.	Ashram Chowk	Mixed	Building	Building
2.	Lodhi road near Sai temple	Silence zone	Building	Open
3.	K.G& Tolstoy Marg	Silence zone	Building	Open
4.	Nirman Vihar	Commercial	Building	Building
5.	Pahrganj near police station	Commercial	Building	Building
6.	Peeragarhi Chowk	Commercial	Building	Open
7.	Patel Nagar Chowk	Mixed	Building	Open
8.	Shakti Nagar Chowk	Residential	Building	Building
9.	Kingsway Camp	Residential	Building	Building
10.	Badli mod near passport office	Mixed	Building	Open

2.2 Monitoring of Traffic Noise

The traffic noise level was monitored with the help of CESVA SC 260 sound level meter at the distance of 1m away from the edge of the road and the height of the sound level meter was taken as 1.5 m from the ground. This sound level meter is based on integrating averaging sound level meter and 1:1 and 1:3 octave band spectrum analyzers. It's monitored all frequencies (A- weight, C –weight and Z-weight) sound. Sound level meter calibrated before starting measuring of the traffic noise level.

2.3 RLS-90 model

RLS -90 model is used in the German for the prediction of the noise pollution level in highway and parking place. RLS- 90 is two parts:

(I). Sources level emission model (II). Propagation model

(I). **Sources level emission model**

In this model characteristic of the traffic flow, speed of the vehicles, type of the vehicles, according to its weight and texture of the road surface all these responsible factors of the L m E. Sources level emission calculated by the following formula:

$$L_M E = (Lm\ 25\ basic) + C_{speed} + C_{gradient} + C_{road\ surface} + C_{reflection}$$

Where,

$Lm = 37.3 + 10*\log\{m*(1+.082p)\}$

M=Mean hourly traffic volume

P =% truck exceeding 2.8 tones

- **Speed correction**

$$C_{speed} = L_{car} - 37.3 + 10*\log[100 + \{(10^{.1*c})*p / (100 + 8.23*P)\}]$$

$$L_{car} = 27.8 + 10*\log\{1 + (.002*V_{car})^3\}$$

$$L_{truck} = 23.1 + 12.5\log * (V_{car})$$

$$c = L_{truck} - L_{car}$$

Where,

V_{car} = Speed of the car

V_{truck} = Speed of the truck

(II). Propagation model

In this model noise level measured at the observation point noise is propagated energetic addition to the all contribution of the producing sources. Lengthy road and other meteorological factor affecting the noise level. Inverse relation between distance and sound, so that of the width of the road play important role.

$$Lm = Lm\ E + C_{section} + C_{spreading} + C_{ground\ absorbent} + C_{screening} + C_{met}$$

Where,

$C_{spreading}$ =spreading correction factor

$C_{ground\ absorbent}$ = Absorbent correction factor

$C_{screening}$ = Screening correction factor

C_{met} = Meteorological correction factor

3. RESULTS AND DISCUSSION

On the basis of collected data related to traffic noise study like traffic volume, average speed of vehicles, traffic noise data, the predicted value of noise level has been calculated at all the selected locations during peak and off-peak hours. The following sections discuss about the variation of monitored as well as predicted value of noise level during peak and off-peak hours.

3.1 Comparison between measured and predicted noise level during peak & off peak hours at Ashram Chowk

At Ashram Chowk, average noise level varied from 76.6 dB (A) to 80.1 dB (A) and 78.3 to 84.4 dB (A) during morning and evening peak hours respectively, whereas during off peak hours it was found as 77.3 dB(A). The variation of the noise level with respect to traffic volume is shown in Fig.1. In residential area average traffic noise level is quite higher than the standard noise level (55 dB (A)) because of the heavy traffic flow condition and due to the high rising building on both sides of the road. At the evening peak hour traffic noise level is maximum due to high traffic density or jam condition and honking effects. The percentage difference between observed average traffic noise level and predicted traffic noise level during morning peak hours, off peak hour and evening peak hours was found as 2.1%, 2.1% and 4.3% respectively, which indicates the applicability of the model.

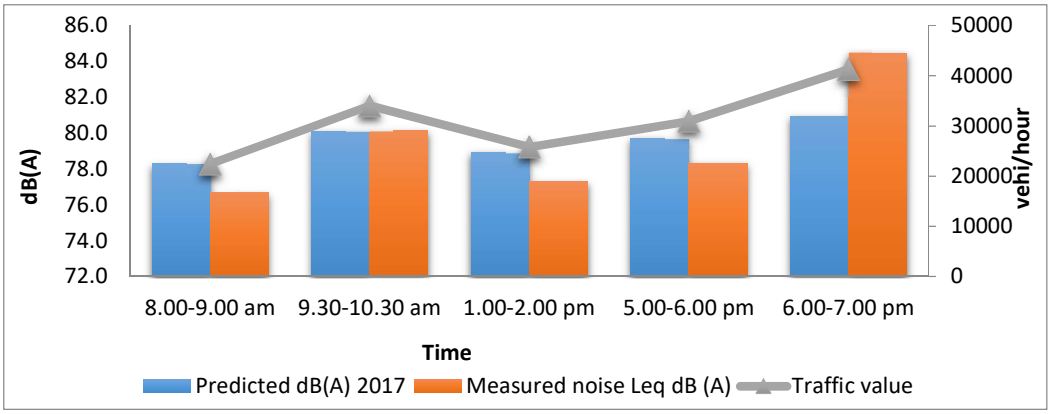

Fig 1. Variation of noise level during peak & off-peak hours at Ashram Chowk

3.2 Comparison between measured and predicted noise level during peak & off peak hours at Lodhi road

At this location, during peak hours the traffic volume was found between 6300 to 7340 vehicles per hour, whereas noise level varied from 70.2 to 74.8 dB (A). The Average

noise level at Lodhi road varied from 74.3 to 74.8 dB (A) in morning peak hour. On the other hand, the evening peak hours showed a variation in noise level i.e. 73.7 to 74.7 dB (A) (Fig.2). The average traffic noise level was found quite higher than the standard noise because of the heavy traffic flow condition and probably due to the irregular movement of vehicles. At this location, the percentage error was also calculated and found as 3.30, 1.38 and 3.12 respectively.

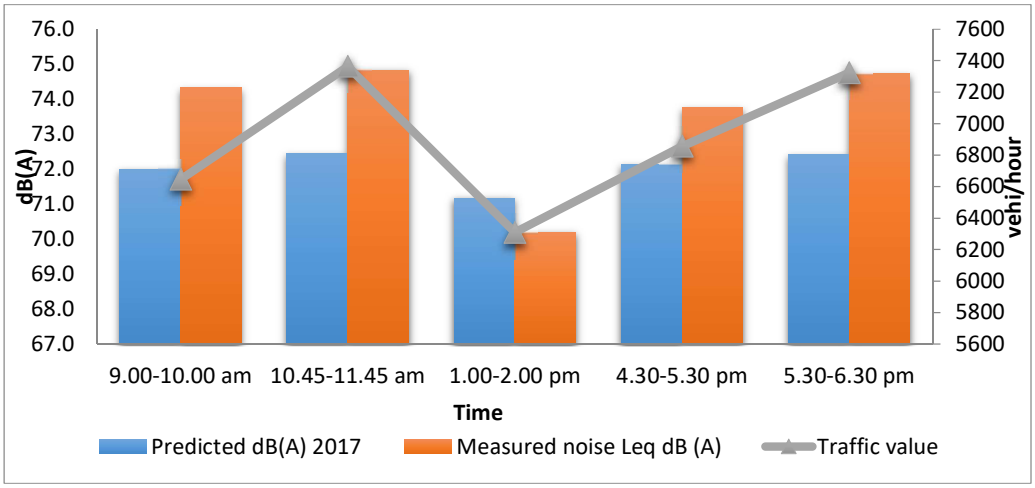

Fig 2. Temporal variation of traffic noise level at Lodhi road

3.3 Comparison between measured and predicted noise level during peak & off peak hours at K.G &Tolstoy Marg

It is depicted from figure 3 that the noise level at this location was found quite high as compared the Indian ambient standards. The morning peak hours showed a variation in noise level i.e. 72.8 to 74.7 dB (A), whereas 71.9 to 73.7 dB (A) during evening peak hours. The lowest noise level was found as 70.56 dB (A) during off-peak hours. The average traffic noise level at K.G & Tolstoy Marg was found high than the standard noise level i.e. 50 dB (A).

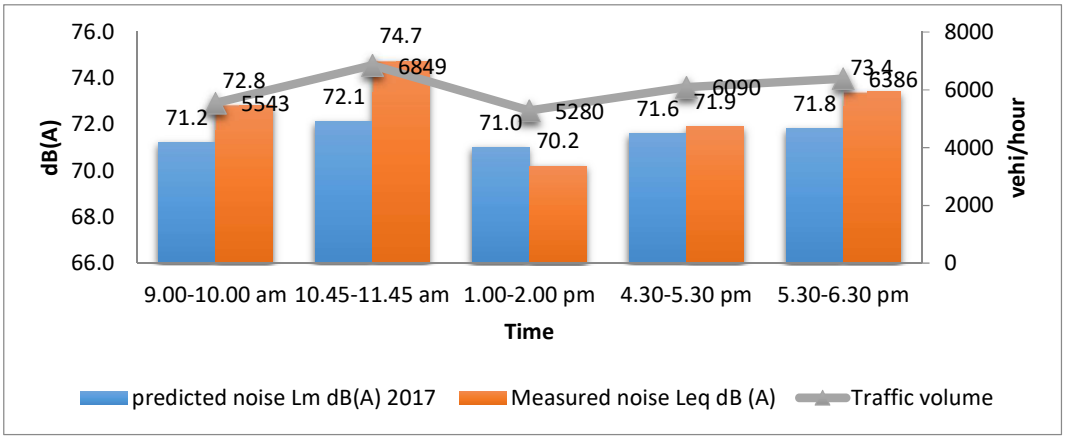

Fig 3. Temporal variation of traffic noise level at K.G & Tolstoy Marg

3.4 Comparison between measured and predicted noise level during peak & off peak hours at Nirman Vihar

The highest traffic noise was monitored during evening peak hour i.e. 6:00 to 7:00 pm, whereas minimum was also seen during morning peak hour i.e. 8:30 to 9:30 am (Fig. 4). From the analysis, it was concluded that the noise level found even during off-peak hour was higher than the ambient standards. The average traffic noise level at Nirman Vihar (commercial area) was also found higher than the prescribed standard i.e. 65 dB (A). It may be due to unavailability of parking facility at this location which may lead to higher traffic congestion and noise. The percentage error between predicted and measured traffic noise level was calculated during morning, off and evening peak hours and found as 3, 2.5 and 0.5 % respectively.

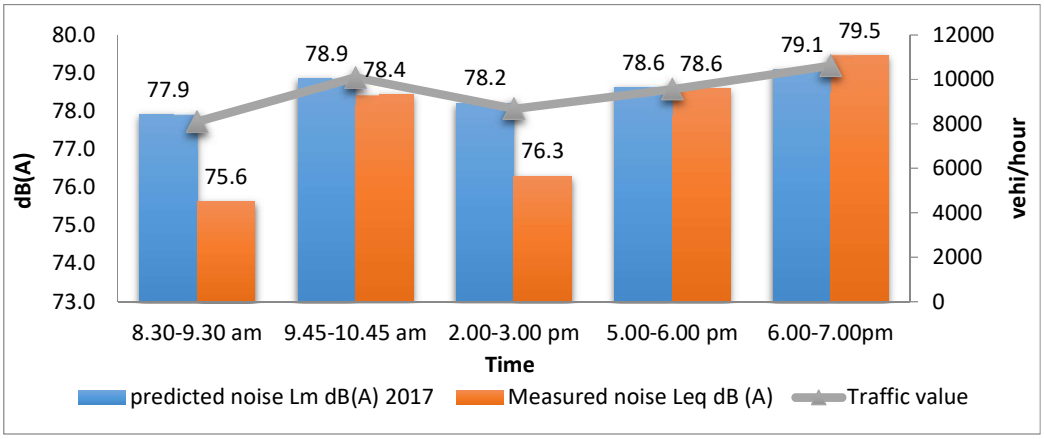

Fig 4. Traffic noise level variation during peak & off peak hours at Nirman Vihar

3.5 Comparison between measured and predicted noise level during peak & off peak hours at Paharganj

This location was categorized under commercial zone (Fig. 5). At this location, the average noise level was observed varying from 75.6 to 77.2 dB(A) in the morning peak hours and from 78.4 to 80.5 dB(A) during evening peak hours. The average traffic noise level at Paharganj (commercial area) was found quite higher than the standard noise level (65 dB(A)) because of the heavy traffic flow condition and high rising building on both sides of the road.

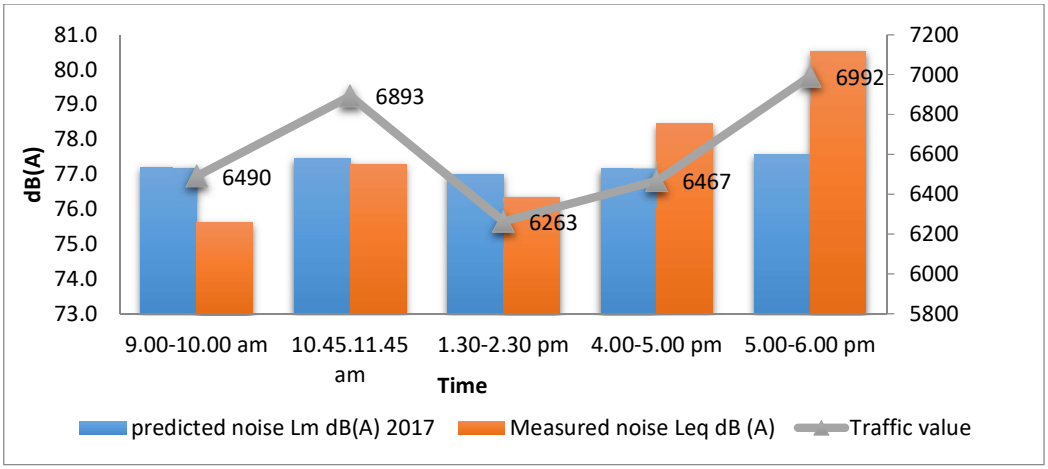

Fig 5. Temporal variation of traffic noise level at Paharganj Chowk

3.6 Comparison between measured and predicted noise level during peak & off peak hours at Peeragarhi Chowk

This location showed its highest noise level during 11:00 to 12:00 am. Average noise level at Peeragarhi vary from 75.1 to 80.7 dB (A) in the morning peak hours, in the evening peak hours vary from 77.6 to 79.1 dB (A), and during off peak hours noise level is 75.6 dB (A). The average traffic noise level at Peeragarhi Chowk (commercial area) is higher than the standard noise level (65 dB (A)) because of the area under the flyover bridge and heavy traffic flow condition. The percentage difference between modeled and observed noise level in the morning peak, off peak and even peak hours was obtained as 5.52, 3.87 and 1.84% respectively as shown in Fig. 6.

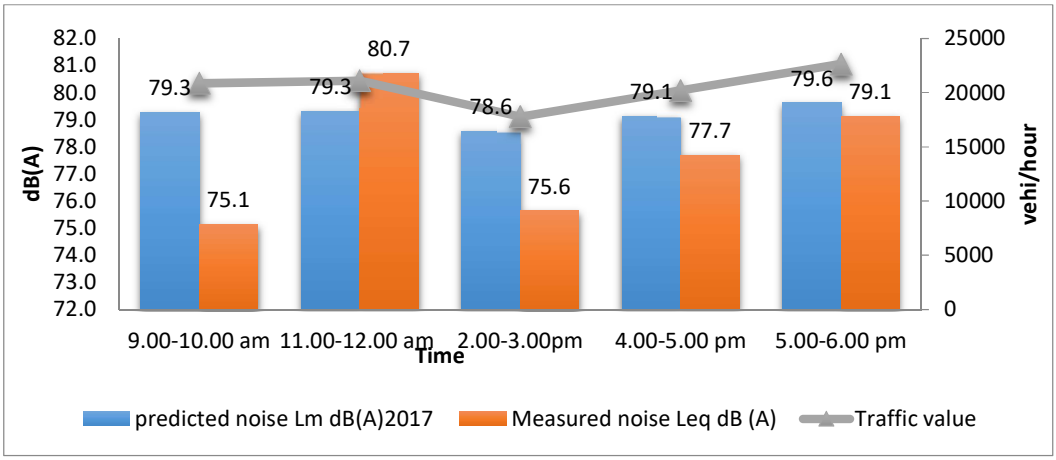

Fig 6. Variation of the traffic noise level during peak & off peak hours at Peeragarhi

3.7 Comparison between measured and predicted noise level during peak & off peak hours at Patel Nagar Chowk

At Patel Nagar Chowk, the highest traffic volume was observed during evening peak hours i.e. 6:00 to 7:00 pm, while the highest average noise level was also found during the same hour i.e. 76 dB (A). On the other hand, the predicted value during the same hours was 75.1 dB (A). At this site, the lowest noise level was found even high as compared to permissible limit. The average traffic noise level at Patel Nagar Chowk (residential area) was also found quite high than the standard noise level (55 dB (A)) due to heavy traffic flow and interrupted traffic conditions during evening time (Fig.7).

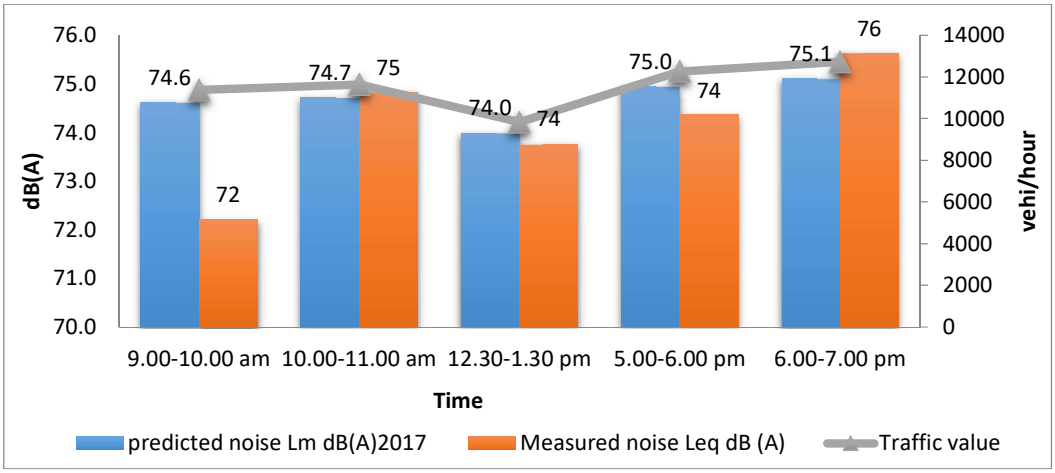

Fig 7. Variation of the traffic noise level during peak & off peak hours at Patel Nagar

3.8 Comparison between observed and predicted noise level at Shakti Nagar Chowk

This location was found under the category of residential land use pattern. At this location, very small difference of predicted noise level was found between peak and off-peak hours. Approximately similar kind of noisy condition was found during all time measurement of noise level at this location. With reference to traffic volume at this location, the hour 6:00 to 7:00 pm showed highest traffic i.e. 7749 vehicles/hour, whereas the observed traffic noise level was 79.5 dB(a), the highest one during all time scheduled measurement (Fig. 8). To check the suitability of the model, the percentage error of the predicted and monitored noise level was calculated and found as 5.3, 5.57 and 1% respectively during morning, off and evening peak hours.

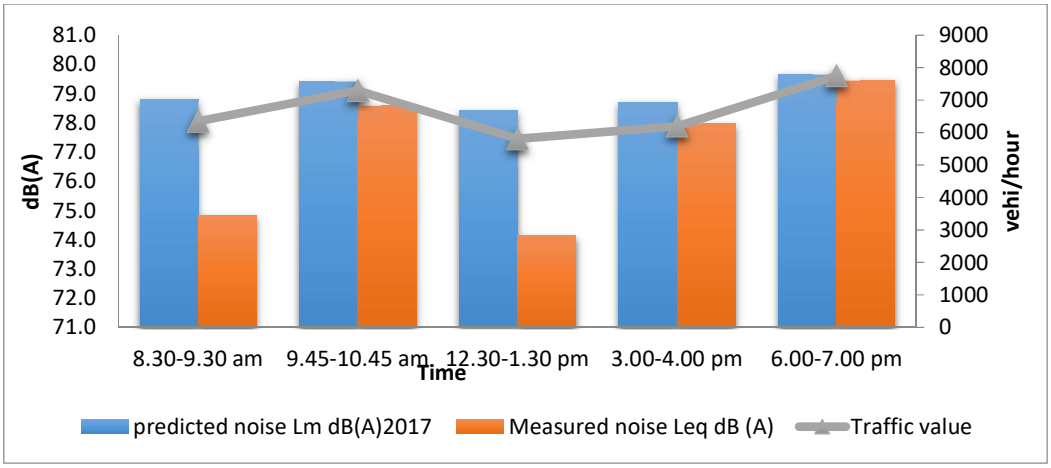

Fig 8. Traffic noise level during peak & off peak hours at Shakti Nagar Chowk

3.9 Comparison between measured and predicted noise level at Kingsway Camp

During traffic noise monitoring at this location, the maximum noise level was found as 75.1 dB (A) followed by 73.7 dB (A) during 11:00 to 12:00 pm and 6:30 to 7:30 pm respectively, whereas this hour also represented the highest traffic volume (Fig.9). The difference of noise level during morning peak hours, off peak hours and even peak hours was found as 1.26, 0.83 and 0.20 dB(A) respectively, and the percentage error was obtained as 1.75, 1.14 and 0.54 % respectively, which indicates the applicability and suitability of the model in city like Delhi.

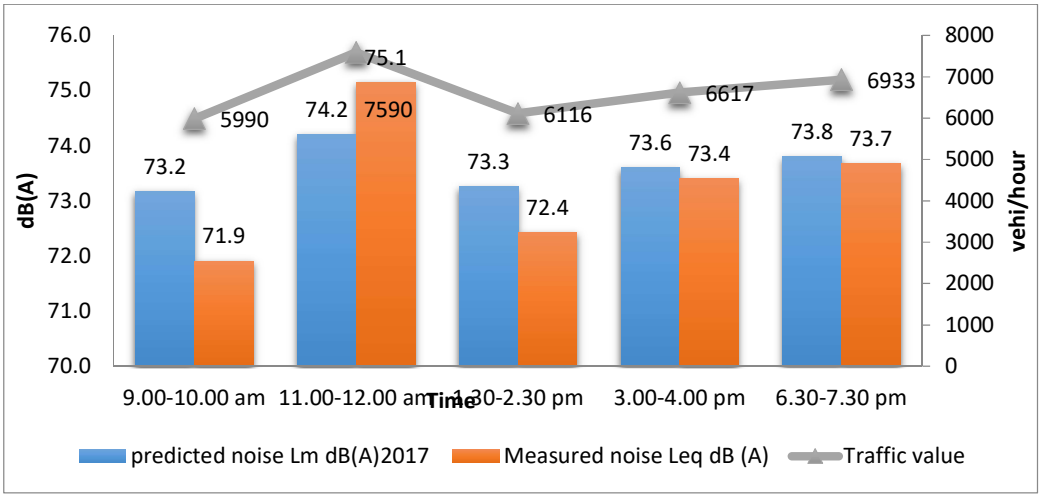

Fig 9. Variation of noise level at Kingsway Camp

3.10 Comparison between monitored and estimated noise level at Badli Mor

This location represents mix kind of land use pattern. The traffic volume was also found quite high during evening peak hour. The evening peak hour i.e. 6:30 to 7:30 pm showed a very high traffic noise i.e. 78.5 dB 78.5 dB (A), while the lowest was as 74.3 dB (a)

during off-peak hour. A direct association was observed between noise and traffic volume at this location (Fig. 10). The monitored data of this location was also used to calculate percentage error during morning peak hour, off-peak hour and evening peak hour and attained as 1.47, 1.38 and 2.35% respectively. This small percentage error indicates the applicability of RLS-90 model for this study.

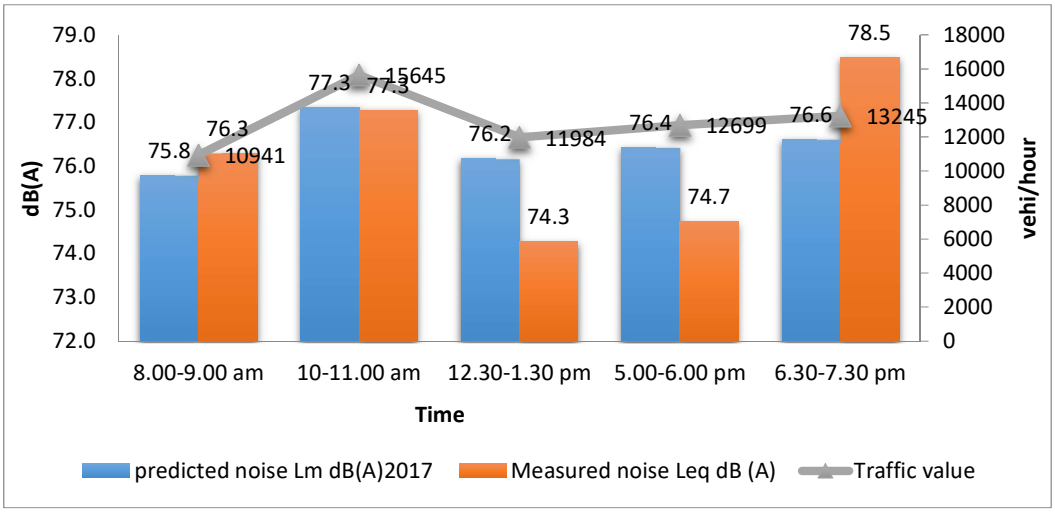

Fig 10. Temporal variation of traffic noise level at Badli Mor

On the basis of the comparative analysis between monitored and modeled traffic noise, at some locations, the measured noise level was found a little bit higher than the predicted one, whereas at some locations the predicted noise level was found a little bit more than the monitored noise level. At each location the percentage error has also been calculated and overall range of the percentage difference was found between the range of 0.5 to 5.75 %, which indicates the best suitability and applicability of this model in city like Delhi.

4. Forecasting of traffic noise level

Prediction of road traffic noise level by using RLS -90 model is found best suitable model in Indian heterogeneous traffic conditions. The same model has been used to forecast the traffic noise level for the year 2022, 2027 and 2032 (Table 2).

Table 2: Forecasting of traffic noise level for different years

Year / locations	Predicted noise level in 2017 dB(A)	Predicted noise level in 2022 dB(A)	Predicted noise level in 2027 dB(A)	Predicted noise level in 2032 dB(A)
Ashram Chowk	81.0	81.6	82.0	82.5
Lodhi Road near Sai temple	72.4	73.0	73.6	74.0

K.G & Tolstoy Marg	71.8	72.4	73.0	73.4
Nirman Vihar	79.1	79.7	80.2	80.7
Paharganj	77.6	78.1	78.7	79.1
Peeragarhi Chowk	79.6	80.2	80.8	81.2
Patel Nagar Chowk	75.11	75.71	76.25	76.72
Shakti Nagar Chowk	79.7	80.3	80.8	81.3
Kingsway Camp	73.8	74.4	75.0	75.4
Badli Mor	76.6	77.2	77.8	78.2

During this forecasting average annual vehicle growth rate is taken as 3% and other input parameters of the model assuming constant. Taking 2017 as a base year, road traffic noise has been predicted for different years i.e. 2022, 2027 and 2032. The forecasting of the traffic noise level at Ashram Chowk varied from 81 dB (A) to 82.5 dB(A) in 2017 to 2032 year, predicted traffic noise level much above the prescribed level due to heavy traffic flow and covered by high rise building on both sides of roads. Prediction of the traffic noise level at Lodhi road and K.G & Tolstoy Marg are varying from 72.4 to 74 and 71.8 to 73.4 dB (A) respectively, both locations consider as silence zone by CPCB. At Nirman Vihar traffic noise level predicted 79.1 to 80.7 dB(A) in 2017 to 2032 year. Paharganj Chowk which is near the New Delhi railway station, the traffic noise level has been predicted 77.6 to 79.1 dB (A).

5. CONCLUSION

After the analysis of the collected data, it is revealed that at each monitoring location, the traffic noise level was found more than the standard noise level as prescribed by CPCB. At Ashram Chowk, Nirman Vihar, Shakti Nagar and Peeragarhi Chowk the traffic noise level was observed much more during the evening time as compared to morning time. The reason behind this may be high traffic congestion and traffic volume during the evening period. It was observed that the locations covered by both sides high rising buildings and under the flyover bridge, having higher traffic noise level than the open or plain area. At silence zone area (Lodhi road and K.G. Marg), it was observed that the traffic noise level is more than prescribed standard noise level and sometime its was found equivalent to residential and commercial noise level. The developed model, i.e. RLS-90 gave very close results to the measured values. Percentage difference between predicted noise level and monitored noise level was found between 0.5 to 5.75%, which indicates the best suitability and applicability of this model in city like Delhi, whereas heterogeneous kind of traffic

is found. The forecasted noise level at all the locations were found much more than the permissible noise level, which indicates the mitigatory measure like noise barriers would be required at all the locations to curb the noise pollution and its associated adverse health problems.

6. REFERENCES

1. Akhtar, N., Kafeel, A., Gangopadhyay, S., "*Assessment of Road Noise Prediction Model (CoRTN) for Indian Conditions*", Indian journal of air pollution control, 12, 57 – 71, (2012).
2. Akhtar, N., Kafeel A., Gangopadhyay, S., "*Road Traffic Noise Mapping and a case study for Delhi Region*", International Journal of Applied Engineering and Technology, 2 (04), 39 – 45, (2012).
3. Ali, S. A. and Tamura, A., "*Road traffic noise mitigation strategies in Greater Cairo, Egypt*", Applied Acoustics, 63, 1257–1265, (2002).
4. Banerjee, D., Chakraborty, S.K., Bhattacharyya, S., Gangopadhyay, A., "*Modeling of road traffic noise in the industrial town of Asansol, India*", Transportation Research Part D, 13 (8), 539-541, (2008).
5. Census of India (2011). Available online at http://www.censusindia.gov.in/2011-provresults/PPT_2.html
6. Economic Survey of Delhi, (2012-2013). Available from Internet: <http://delhi.gov.in/wps/wcm/connect/DoIT_Planning/planning/misc./economic+survey+ of+delhi+2012-13>.
7. Mishra, R.K., Parida M., Rangnekar, S., "*Evaluation and analysis of traffic noise along bus rapid transit system corridor in Delhi*", International Journal of Environmental Science and Technology, 7 (4), 737-750, (2010).
8. Stephenson, R.J., Vulkan, G.H., "*Traffic noise*", Journal of Sound and Vibration, 7(2), 247-262, (1968).

Materials Today: Proceedings xxx (xxxx) xxx

Contents lists available at ScienceDirect

Materials Today: Proceedings

journal homepage: www.elsevier.com/locate/matpr

Tribological behavior of carbon coating for piston ring applications using Taguchi approach

Ankit Tyagi [a], SM Pandey [a], Qasim Murtaza [a], R.S. Walia [a], Mohit Tyagi [b,*]

[a] Department of Mechanical Engineering, Delhi Technological University, Delhi 110042, India
[b] Department of Industrial and Production Engineering, National Institute of Technology, Jalanadhar 144011, India

ARTICLE INFO

Article history:
Received 27 March 2019
Received in revised form 22 August 2019
Accepted 3 September 2019
Available online xxxx

Keywords:
Carbon coating
SEM-EDS
Taguchi optimization

ABSTRACT

The present work aims to develop carbon coating using HVOF technique and to enhance wear properties of carbon coating for piston ring applications utilizing Taguchi approach. SEM-EDS was utilized to characterize the worn out surfaces of composite coating. The optimal parameters were determined and anticipated utilizing S/N ratio. Significant factors for wear was sliding speed (59.89%) followed by temperature (28.71%) and load (9.18%).
© 2019 Elsevier Ltd. All rights reserved.
Peer-review under responsibility of the scientific committee of the 2nd International Conference on Computational and Experimental Methods in Mechanical Engineering.

1. Main text

The power generating parts in engine is required to be proficient to improve the performance of automobile vehicles and to make most extreme utilization of the IC engine working fluid (lubricants). Due to reasons over a ton of research is going on to enhance the efficiency and performance of IC engine [1]. Researchers examined that wear, COF and temperature are prominent factor that effects engine performance [2]. The wear behaviour of cylinders has been analysed the essential effect performance of IC engines with respect to control power loss, fuel utilization, and oil utilization. Consequently, the cylinder ring is one of the biggest source of COF and wear in automobiles [3–7]. Various kinds of coatings are used to improve the characteristic of the piston rings. Plasma Spray Coatings can be used to enhance engine performance and reduces friction and wear in piston rings [8]. The coating can build the hardness alongside phenomenal surface finish, accordingly diminishing the COF and wear rate on comparing with other techniques used for long terms [9]. Nanocomposite establishes two primary carbide materials utilized in thermal spray procedures to improve wear resistance and coefficient of friction sliding parts of automotive. CrC–NiCr HVOF coatings are better in execution than chrome plating than coat diverse sort of basic mechanical components (valves, piston rings).

The present work aims to develop carbon coating using HVOF technique and to enhance wear properties of carbon coating for piston ring applications utilizing Taguchi approach. The present work focussed upon finding the optimal process conditions for wear of carbon based composite coating. The optimal parameters was calculated and predicted using S/N ratio of ANOVA.

2. Experimental procedure

Initially cast iron substrate having dimension 10 mm diameter, was ground using 120–2000 grit emery paper and then polished with alumina paste. The composite powders such as NiCr, CrC, carbon powder and Mo were blend together in a mixer. HVOF thermal spray torch was used for carbon coating deposition. The carbon based composite powder was deposited with controlled rate at 40 g/min. The carbon composite coating thickness was about 300–400 μm. SEM-EDS was utilized to characterize the worn out surfaces of composite coating. High temperature tribometer was used to calculate the wear of composite coating. The maximum temperature, sliding speed and load range of tribometer is 800 °C, 3000 rpm and 200 N respectively. Fig. 1 shows (a) High temperature rotary tribometer (b) Pin and disc images before and after wear test. The experimental work and testing work (lab) was carried out in precision manufacturing lab, Delhi Technological University. The regressions values of experimental work of all factors are mentioned in Fig. 1 (c) and Table 1 as R_1, R_2, and R_3 respectively.

* Corresponding author.
E-mail address: mohitmied@gmail.com (M. Tyagi).

https://doi.org/10.1016/j.matpr.2019.09.004
2214-7853/© 2019 Elsevier Ltd. All rights reserved.
Peer-review under responsibility of the scientific committee of the 2nd International Conference on Computational and Experimental Methods in Mechanical Engineering.

Please cite this article as: A. Tyagi, S. Pandey, Q. Murtaza et al., Tribological behavior of carbon coating for piston ring applications using Taguchi approach, Materials Today: Proceedings, https://doi.org/10.1016/j.matpr.2019.09.004

Nomenclature

SEM	Scanning Electron Microscopy	Temp. (^{O}C)	Temperature
EDS	Energy-dispersive X-ray spectroscopy	N	Load
HVOF	High Velocity Oxy-Flame	S/N ratio	Signal to Noise ratio
IC engine	Internal Combustion engine	CrC	Chromium carbide
ANOVA	Analysis of Variance	μm	Micro-meters
%	Percentage	Mo	Molybdenum
COF	Coefficient of friction	OA	Orthogonal Array
SV (m/s)	Sliding Velocity		

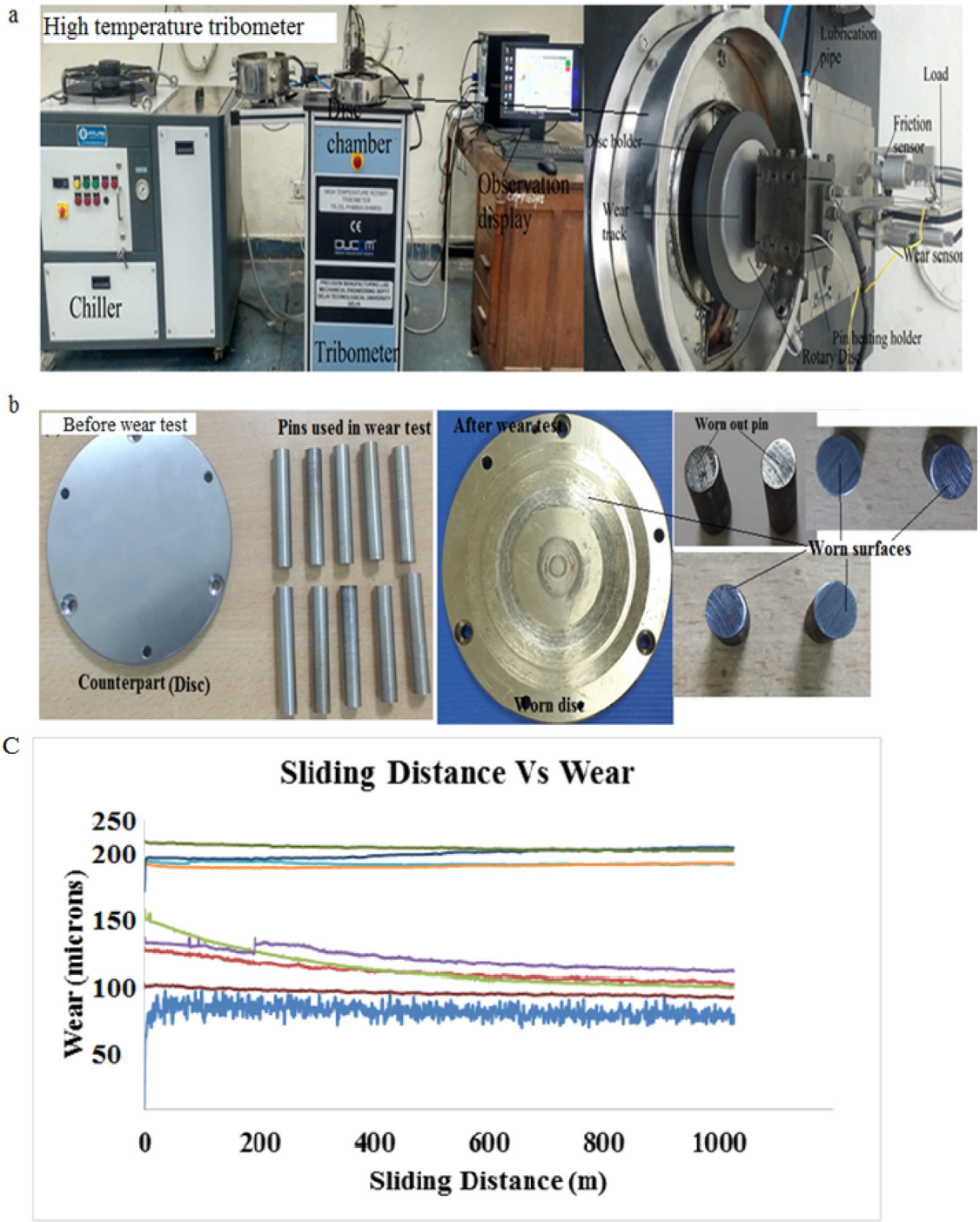

Fig. 1. (a) High temperature rotary tribometer; (b) Pin and disc images before and after wear test (c) Regression values of all factors.

Please cite this article as: A. Tyagi, S. Pandey, Q. Murtaza et al., Tribological behavior of carbon coating for piston ring applications using Taguchi approach, Materials Today: Proceedings, https://doi.org/10.1016/j.matpr.2019.09.004

Table 1
Experimental design and results of Taguchi L_9 OA for wear.

Trial no.	Temp. (°C)	SV (m/s)	Load (N)	Wear(micron)			S/N ratio (db)
				R_1	R_2	R_3	
1	100	1	10	230	230	230	−50.21
2	200	2	20	180	180	180	−45.10
3	300	3	30	100	100	100	−40.00
4	100	1	20	190	190	185	−45.49
5	200	2	30	140	140	140	−42.92
6	300	3	10	100	100	100	−40.00
7	100	1	30	120	120	120	−41.58
8	200	2	10	130	130	130	−42.27
9	300	3	20	80	70	70	−37.32

Mean(Overall) = 140.18.

Table 1 shows the experimental design and results of Taguchi L_9 as follows:

$$(S/N)LB = -10\log\left[\frac{1}{R}\sum_{j=1}^{R}\left(X_j^2\right)\right] \quad (1)$$

3. Results and discussions

3.1. Effects of parameters on wear (microns)

Table 2 and Fig. 2 shows the average values and main effects of wear.

Fig. 2 (a) shows as the temperature increases wear decreases. The wear result obtained at 300 °C temperature was highest on followed with 100 °C and 200 °C temp. for the carbon coating. S/N ratio of coating was lower most at 300 °C temperature followed with 100 °C and 200 °C temp. for the carbon coating.

From the Fig. 2(b), shows wear decreases as the SV increases, while S/N increases as SV increases. Wear result obtained at 3 m/s SV was highest on followed with 1 and 2 m/s sliding velocity for the carbon based composite coating.

The deviation of wear with load was shown in Fig. 2 (c). The wear obtained was minimum at maximum applied load of 30 N, while S/N ratio was maximum.

It was analysed and concluded from the results that as the temp., load and SV increases wear decreases due to formation of graphite like layer that is solid lubricant layer [10–17] or tribo-oxidative layer. The decrease in wear, and COF values of composite coating may be attributed due to formation of sulphides, oxides (MoS_2, and MoO_2), graphite layer (increase in carbon content), tribo- films, and micron size composite powders during test conditions. The friction coefficient value is increased in running in process, then become stable due to adhesive contact in dry conditions. Abrasion delamination and spalling may cause failure

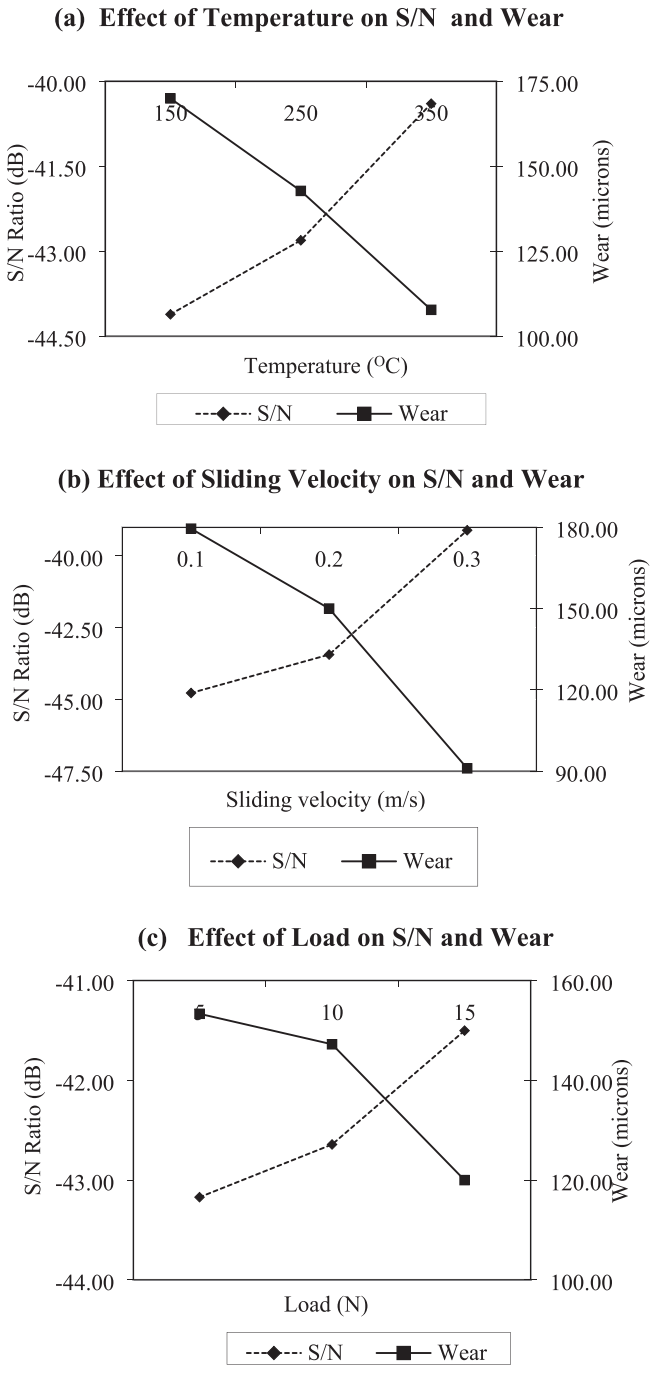

Fig. 2. Show wear deviation with (a) Temp. (°C); (b) SV (m/s); (c) Load (N).

Table 2
Average values and main effects of wear.

Parameter	Trial	Temperature (°C)		SV (m/s)		Load (N)	
Data		Raw Data	S/N Ratio	Raw Data	S/N Ratio	Raw Data	S/N Ratio
Average values (weight loss)	T1	170.00	−44.11	179.44	−44.77	153.33	−43.17
	T2	142.77	−42.80	150.00	−43.43	147.22	−42.64
	T3	107.77	−40.39	91.11	−39.10	120.00	−41.50
Main effect of weight loss	T2-T1	−27.22	1.30	−29.44	1.33	−6.11	0.52
	T3-T2	−35.00	2.42	−58.88	4.32	−27.22	1.14
Difference (T3-T2)-(T2-T1)		−7.77	1.10	−29.44	2.99	−21.11	0.61

Please cite this article as: A. Tyagi, S. Pandey, Q. Murtaza et al., Tribological behavior of carbon coating for piston ring applications using Taguchi approach, Materials Today: Proceedings, https://doi.org/10.1016/j.matpr.2019.09.004

of coating that may be due to one of the above-discussed reasons or the combinations. Also reported that delimitation causes due to the high value of contact stress which also causes to coating failure. The decrease in coefficient was more significant with an increase in sliding speed, load and temperature due to spalling or chipping off the composite coating.

Fig. 2 shows wear deviation and results obtained from deviation shows minimum values are at A_3, B_3 and C3 for average raw data and S/N ratio values. Wear mechanism of worn surfaces are shown in Fig. 3(a-d) and surface morphology reveals formation of oxide formation, cracks, micron size carbon particles, formation and delamination layer formation confirms erosion, indicates abrasive wear as dominant wear mechanism on developed coating. EDS results as shown in Fig. 3 (e) confirms the formation of tribo films and oxides, due to the increase in Carbon (C) and oxygen (O) contents. At variable temperature, sliding velocity and load wear occur

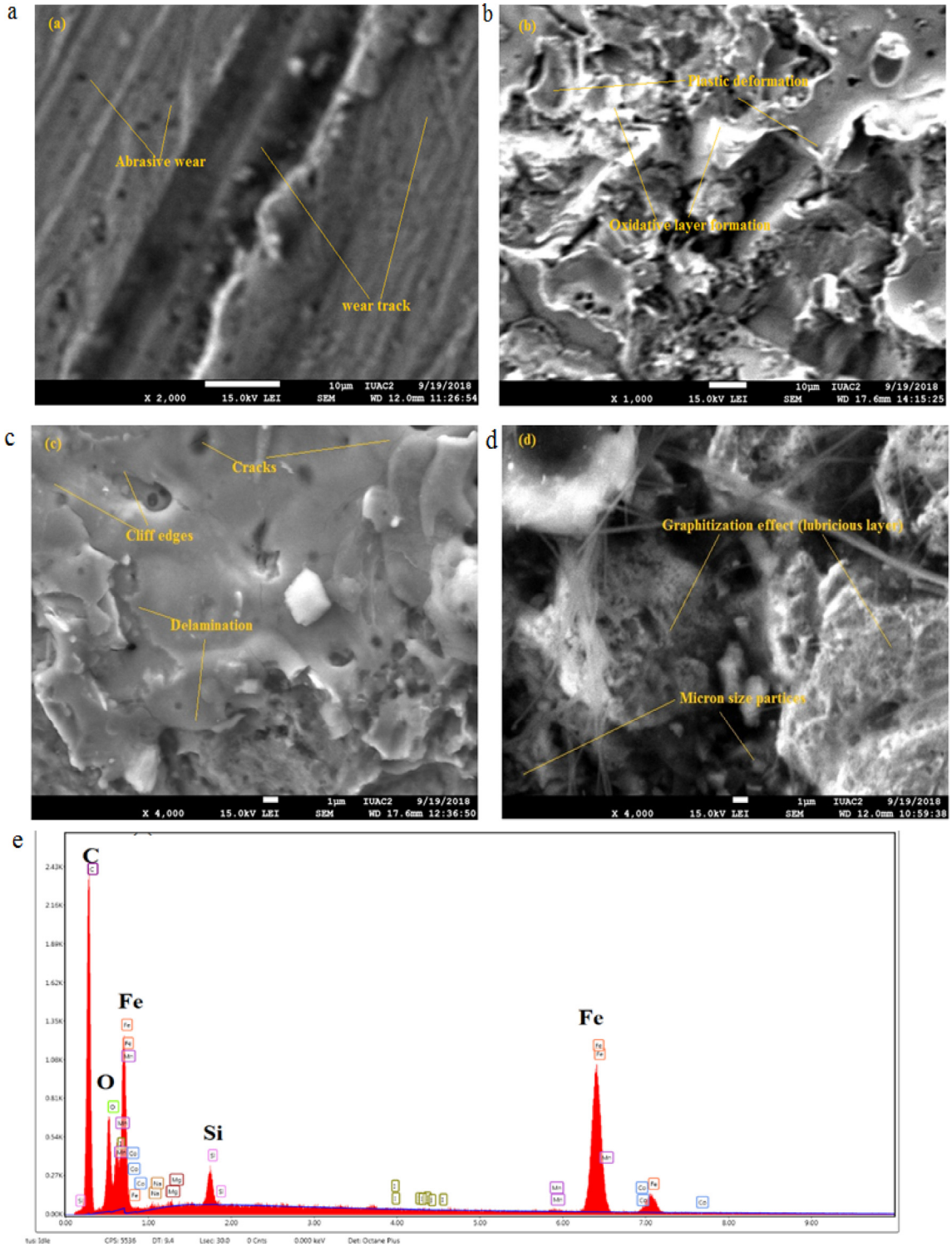

Fig. 3. (a-d) SEM result; (e) EDS image of worn out surfaces.

Please cite this article as: A. Tyagi, S. Pandey, Q. Murtaza et al., Tribological behavior of carbon coating for piston ring applications using Taguchi approach, Materials Today: Proceedings, https://doi.org/10.1016/j.matpr.2019.09.004

Table 3
Pooled ANOVA for wear.

Parameters	SS		SS'		V		F-Ratio		DOF		P (%)	
	Raw data	S/N data	Raw data	S/N data	Raw data	S/N data	Raw data	S/N data	Raw data	S/N data	Raw data	S/N data
Temperature (°C)	17512.96	21.34	17,410	21.13	8756.48	10.67	170.09	101.03	2	2	28.71	26.91
SV (m/s)	36412.96	52.60	36,310	52.39	18206.48	26.30	353.65	248.98	2	2	59.89	66.71
Load (N)	5668.51	4.36	5565.55	4.15	2834.25	2.18	55.05	20.66	2	2	9.18	5.29
E (Pooled)	1029.62	0.21	1338.51	0.84	51.48	0.10	–	–	20	2	2.20	1.07
Total	60624.07	78.52	60624.07	78.52	–	–	–	–	26	8	100	100

Table 4
Optimal values of wear.

Trails	Wear
A_3	107.77
B_3	91.11
C_3	120
T	140.18

mainly by ploughing (plastic deformation). The micron size of carbon particles work as an obstacle to plastic deformation [9] and results in abrasive wear resistance. However, the surface morphology of carbon coating revealed less plastic deformation, and formation of solid lubricant layer [10–17] between developed coating and counterbody occur during friction and wear test. Abrasion delamination and spalling may cause failure of coating that may be due to one of the above-discussed reasons or the combinations. Also reported that delimitation causes due to the high value of contact stress which also causes to coating failure.

Table 3 shows the pooled ANOVA values of wear. The optimal parameters was determined and anticipated utilizing S/N ratio. The significant factors for wear was sliding speed (59.89%) followed by temperature (28.71%) and load (9.18%).

3.1.1. Optimal performance estimation

3.1.1.1. Responses for optimal values for wear. Optimum level of average wear values are shows in Table 4. The estimated mean (μ) for optimum value for wear can be estimated by using Eq. (2) [18–23].

$$\mu_{COF} = A_3 + B_3 + C_3 - 2T$$
$$\mu_{wear} = 38.52 \quad (2)$$

The CI_{CE} value and CI_{POP} for 95% confidence interval was evaluated using Eqs. (3) and (4) [18–23]:

$$CI_{CE} = \sqrt{F_a(1,f_e)V_e\left[\frac{1}{n_{eff}} + \frac{1}{R}\right]} \quad (3)$$

$$CI_{POP} = \sqrt{\frac{F_a(1,f_e)V_e}{n_{eff}}} \quad (4)$$

The calculated values of ANOVA is:
$CI_{CE} = \pm 10.31$
$CI_{POP} = \pm 6.82$
The predicted values is:
CI_{CE}: $28.21 < \mu < 48.83$
CI_{POP}: $31.7 < \mu < 45.34$

3.1.1.2. Experiments of confirmation. Confirmation tests were performed for wear process parameters and optimal values of carbon coating for wear was restrained as 0.03 μm at trail 3 for load, temperature and sliding velocity.

4. Conclusions

In the present work, carbon based composite coating was successfully developed using HVOF techniques. The following results are obtained:

- The CI_{POP} range for wear: is: $31.7 < \mu < 45.34$.
- The CI_{CE} range for wear: is: $28.21 < \mu < 48.83$.
- The significant parameters for wear was sliding speed (59.89%) followed by temperature (28.71%) and load (9.18%).

References

[1] A. Skopp, N. Kelling, M. Woydt, L.M. Berger, Thermally sprayed titanium suboxide coatings for piston ring/cylinder liners under mixed lubrication and dry-running conditions, Wear 262 (2007) 1061–1070.
[2] Q. Liu, Y. Song, G. Xu, Z. Zhao, On the laser quenching of the groove of the piston head in large diesel engines, J. Mater. Eng. Perform. 7 (1998) 402–406.
[3] Tyagi, A., Murtaza, Q., Walia, RS., Effect of Reciprocating Frequency and Load on Wear Behaviour of Mo blend Composite Coating, International conference of advance research and innovation, 2019, 978-93-5346-3243.
[4] S.M. Pandey, Q. Murtaza, R.S. Walia, Study of dry wear behavior and morphological characteristic of 60% Mo-20% NiCr-10% CrC-10% Mo+ Fe based alloy coating by atmospheric plasma spray technique, Adv. Mater. Process. Technol. 3 (2018) 393–406.
[5] A. Tyagi, Q. Murtaza, R.S. Walia, S.M. Pandey, P. Tyagi, B. Bajaj, A critical review of diamond like carbon coating for wear resistance applications, Int. J. Refract Metal Hard Mater. 78 (2019) 107–122.
[6] R.J. Wood, Tribo-corrosion of coatings: a review, J. Phys. D Appl. Phys. 40 (2007) 5502.
[7] J. Chen, Y. Wang, H. Li, L. Ji, Y. Wu, Y. Lv, H. Zhou, Microstructure, morphology and properties of titanium containing graphite-like carbon films deposited by unbalanced magnetron sputtering, Tribol. Lett. 49 (2013) 47–59.
[8] Jian Wang, Feng-Lin Zhang, Teng Zhang, Wen-Guang Liu, Wei-Xiong Li, Yu-Mei Zhou, Preparation of Ni-P-diamond coatings with dry friction characteristics and abrasive wear resistance, Int. J. Refract Metal Hard Mater. 70 (2018) 32–38.
[9] M. Shabani, C.S. Abreu, J.R. Gomes, R.F. Silva, F.J. Oliveira, Effect of relative humidity and temperature on the tribology of multilayer micro/nanocrystalline CVD diamond coatings, Diam. Relat. Mater. 7 (2017) 190–198.
[10] N. Kumar, R. Ramadoss, A.T. Kozakov, K.J. Sankaran, S. Dash, A.K. Tyagi, N.H. Tai, I.-N. Lin, Humidity–dependent friction mechanism in an ultrananocrystalline diamond film, J. Phys. D: Appl. Phys. 46 (2013), 275501 (1)–275501(8).
[11] A.R. Konicek, C. Jaye, M.A. Hamilton, W.G. Sawyer, D.A. Fischer, R.W. Carpick, Near– Edge X–ray absorption fine structure imaging of spherical and flat counterfaces of ultra nanocrystalline diamond tribological contacts: a correlation of surface chemistry and friction, Tribol. Lett. 44 (2011) 99–106.
[12] Shenq Y. Luo, Jui-Kang Kuo, Brian Yeh, James C. Sung, Chuang-Wen Dai, Tsung J. Tsai, The tribology of nano-crystalline diamond, Mater. Chem. Phys. 72 (2001) 133–135.
[13] M. Kalin, E. Roman, J. Vižintin, The effect of temperature on the tribological mechanisms and reactivity of hydrogenated, amorphous diamond-like carbon coatings under oil-lubricated conditions, Thin Solid Films 515 (2007) 3644–3652.
[14] K.A.H Al Mahmud, M. Varman, M.A. Kalam, H.H. Masjuki, H.M. Mobarak, N.W. M. Zulkifli, Tribological characteristics of amorphous hydrogenated (a-C:H) and tetrahedral (ta-C) diamond-like carbon coating at different test temperatures in the presence of commercial lubricating oil, Surface Coat. Technol. 245 (2014) 133–147.
[15] N. Sharma, N. Kumar, A.K. Tyagi, Velocity dependence of coefficient of friction of diamond like carbon coatings, Solid State Phys. AIP Conf. Proc. 1447 (2012) 651–652.

Please cite this article as: A. Tyagi, S. Pandey, Q. Murtaza et al., Tribological behavior of carbon coating for piston ring applications using Taguchi approach, Materials Today: Proceedings, https://doi.org/10.1016/j.matpr.2019.09.004

[16] Dong-Wook Kim, Kyung-Woong Kim, Effects of sliding velocity and normal load on friction and wear characteristics of multi-layered diamond-like carbon (DLC) coating prepared by reactive sputtering, Wear 297 (2013) 722–730.
[17] Longchen Cui, Lu Zhibin, Liping Wang, Probing the low-friction mechanism of diamond-like carbon by varying of sliding velocity and vacuum pressure, Carbon 6 (6) (2014) 259–266.
[18] T. Goyal, R.S. Walia, T.S. Sidhu, Study of coating thickness of cold spray process using Taguchi method, Mater. Manuf. Process. 27 (2012) 185–192.
[19] R.S. Walia, H.S. Shan, P. Kumar, Parametric optimization of centrifugal force-assisted abrasive flow machining (CFAAFM) by the Taguchi method, Mater. Manuf. Process. 21 (2006) 375–382.
[20] B.S. Brar, R.S. Walia, V.P. Singh, Electrochemical-aided abrasive flow machining (ECA^2FM) process: a hybrid machining process, Int. J. Adv. Manuf. Technol. 79 (2015) 329–342.
[21] T. Goyal, R.S. Walia, T.S. Sidhu, Effect of parameters on coating density for cold spray process, Mater. Manuf. Process. 27 (2012) 193–200.
[22] A. Tyagi, Q. Murtaza, R.S. Walia, S.M. Pandey, Characterization and parametric optimization of tribological properties of Mo blend composite coating, Material Research Express, 2019, Accepted.
[23] A. Tyagi, R.S. Walia, Q. Murtaza, Tribological behavior of temperature dependent environment friendly thermal CVD diamond coating, Diamonds Related Mater. 96 (2019) 148–159.

Please cite this article as: A. Tyagi, S. Pandey, Q. Murtaza et al., Tribological behavior of carbon coating for piston ring applications using Taguchi approach, Materials Today: Proceedings, https://doi.org/10.1016/j.matpr.2019.09.004

I.J. Image, Graphics and Signal Processing, **2019, 8, 40-49**
Published Online August 2019 in MECS (http://www.mecs-press.org/)
DOI: 10.5815/ijigsp.2019.08.04

Visual Object Tracking by Fusion of Audio Imaging in Template Matching Framework

Satbir Singh
Dr.B R Ambedkar National Institute of Technology, Jalandhar, India
Email: satbir2008@ymail.com

Arun Khosla
Dr.B R Ambedkar National Institute of Technology, Jalandhar, India
Email: khoslaak@nitj.ac.in

Rajiv Kapoor
Dr.B R Ambedkar National Institute of Technology, Jalandhar, India
Email: rajivkapoor.dtu@gmail.com

Received: 04 April 2019; Accepted: 24 June 2019; Published: 08 August 2019

***Abstract*—**Audio imaging can play a fundamental role in computer vision, in particular in automated surveillance, boosting the accuracy of current systems based on standard optical cameras. We present here a method for object tracking application that fuses visual image with an audio image in the template-matching framework. Firstly, an improved template matching based tracking is presented that takes care of the chaotic movements in the template-matching algorithm. Then a fusion scheme is presented that makes use of deviations in the correlation scores pattern obtained across the individual frame in each imaging domain. The method is compared with various state of art trackers that perform track estimation using only visible imagery. Results highlight a significant improvement in the object tracking by the assistance of audio imaging using the proposed method under severe challenging vision conditions such as occlusions, object shape deformations, the presence of clutters and camouflage, etc.

***Index Terms*—**Audio Imaging, Template Matching, Object tracking, Information fusion.

I. Introduction

The video-alone tracking has many constraints especially under challenging visible conditions, such as illumination variation, occlusion, object appearance change, etc. To overcome these limitations, the research trends are moving towards the amalgamation of different sensing domain to aid the visible imagery tracking. New developments for fusion based tracking encourage the use of information through multiple cameras, thermal cameras, audio devices, radio waves, and light waves, etc. The detailed overview can be found in [1, 2, and 3].

We Humans observe a tremendous number of combined visual-audio examples and learn the correlation between them throughout their whole life [4] unconsciously. Because of the correlation between the sound and the visual events, humans are able to understand the object/event that is a sound generator and hence can localize the sound source even without any distinctive education. The motivation for the combined role of audio-visual information by the human in everyday life and its use is provided by the findings in psychology and cognitive science [4, 5, 6, 7, 8, and 9] on sound source localization capability of humans. The findings reveal that visual information correlated to sound improves the efficiency of search [8] and the accuracy of localization [7].

Some major advantages of audio information include Assistance in case of the limited field of view of a camera, providing additional hints in case of occlusion or similar structure clutter presence, Invariant to lighting variations in the scene, robustness, and reliability toward adverse weather circumstances like fog, dust, and snow. Acoustic information is also robust to camouflage for the reason that a sound source can be localized even if it is hidden behind other objects e.g. gunfire in a crowded scene.

The organization of the rest of the paper is presented in this paragraph. The implemented work procedure is explained in detail in Section II. It describes the improved correlation score based template matching used for object tracking in the individual sensing domain followed by the final fusion strategy applied. Section III provides the detail on experimental settings along with the discussion on the results acquired. Section IV highlights the concluding remarks and the future possibilities of the performed research.

II. Literature Review

The purpose of this section is to contemplate upon the previous work done for providing solution to the taken

Copyright © 2019 MECS

research problem. The study of different state of art techniques helps to understand the problem and its solution in a much organized manner.

Further as the need and significance of the audio-visual is explained earlier in the paper, it becomes important to cover the various practices involved in performing the said bi-modal fusion for the application of object tracking.

Previously, the audio information was found and used in its simple one-dimensional form, in which, the audio information was captured using a number of microphones. Then, certain audio features were obtained from the received sound signal. Finally, the information was used together in conjunction to take the final decision. Several issues like multi-target tracking [10, 11], robustness to reverberation [12], ground noise and interfering sources [13] and time-varying and intermittent sources [14] have been researched, making audio tracking a developed research field.

However, most of the system used for audio tracking are based on a limited number of microphones (typically < 20) spread in the environment. Such kind of layout does not ensure an efficient accuracy of localization and limits the number of sources that can be jointly localized. Further, the relation between the true location of the target and measurements from the microphones is characterized in a non-linear way that forces to use ad hoc tracking algorithms with complex models of measurement noise [15]. In addition, in order to make this information useful for amalgamation with visible mode information, a tedious task of calibration is required to be performed.

More recently, new techniques have been developed to record and generate acoustic images. Microphone arrays are capable of providing spatial information for incoming acoustic waves, as they can capture key information that would be impossible to acquire with single microphones [23]. Acoustic imaging microphone arrays (sometimes referred to as "acoustic cameras" [24]) often contain a camera which is usually located at the center of the array. An acoustic map, spawned using the microphone data, is put over as a transparency over the camera image. The output from acoustic beamforming applied to the signals acquired by a set of microphones encode at each pixel the sound intensity coming from each spatial direction. The devices generating audio imaging in such manner has numerous returns for the video based surveillance, such as the bimodal information can be easily fused together thanks to the pixel-to-pixel correspondence, which in turn diminishes the need of tedious calibration processes. Tracking can be performed taking as a measurement the cues of an image instead of cues of the single microphone's raw signal. The relation between measurement and state in tracking is straightforward. The overlap between acoustic and optical image allows a fair comparison between audio and video trackers. Apart from this, this technology is a completely passive technology, differently from active radars, optical and infrared cameras that require light emitters [25].

The proposed method presents an object tracking method developed specially for an advanced system that eliminates the need for calibration such as presented in [25]. Here, the image-audio arrangement is automatically mapped to an image-image scenario. So, common features can be extracted from both domains. This, in turn, can reduce the complexity of the fusion-based model.

In the last list of various audio-visual fusion based tracking schemes is presented in table 1. This tabulated analysis presents the citation of work, number of sensors used in the process and the comparative relation with the proposed technique that highlights the similarities and the differences among these.

Table 1. Various Audio-Visual Fusion based Tracking Methods

Research	**Sensors used**	**Comparison with proposed research technique**
Volkan Kilic et al. [16]	2 Circular Microphone arrays and 3 cameras	Aid used for object tracking is in the form of direction of arrival of sound and histogram probability matching as compared to the template match score in the proposed method. In addition, projection based homographic calibrations used.
Checka, Wilson, Siracusa, & Darrell [17]	2 cameras and 4 microphone arrays	Their model utilized particle filter framework, in which the foreground and background information was taken as visible cue, but short time Fourier transform of the received audio signal, was taken as the audio cue. So, both the cues were different and then were combined by converting them to probability distribution form.
Gehrig, Nickel, Ekenel, Klee, & McDonough [18]	4 cameras and 16 Microphone in array	This method was intended for an indoor system of a lecture hall with very less disturbance. It used Particle filter for object tracking and 3D projections for obtaining equivalent inputs from both audio and video signals.
Lim & Choi [19]	1 stereo camera and 3 microphones	It used particle filter for forming association between two modes, whereas the proposed method uses correlation based weighted fusion for the combined track estimate.
Megherbi, Ambelloui s, Colôt, & Cabestaing [20]	1 camera and 1 microphone	The audio features used were acoustic vectors composed of linear predictive coding coefficients (LPCC) of their speech. In addition, the visible features were based on histogram probability based distributions. Hence, both modality features were diverse which are same in the proposed research. Further, for fusion, Dempster's rule of combination in belief theory was used.
D'Arca, Hughes, Robertson, & Hopgood [21]	1 camera and 16 microphones	Main emphasis was on the condition of occlusion only. It used Kalman filter for fusion, but that is good for linear motion only. It used Time Difference of Arrival feature for audio source localization and height was determined by the visible signal.
Shivappa et al. [22]	4 cameras and 24 microphones	This method used Time Difference of Arrival from different microphone signals and used multi iterative decoding for fusion with visible tracker signal. The major differences were the use of a tough calibration technique that limited this algorithm in terms of speed.

Copyright © 2019 MECS

III. Proposed Work Methodology

Initially, the object tracking procedure for an individual domain was performed using a modified robust template matching approach. The simple template-matching algorithm is a popular method for object tracking. However, refinement of the algorithm is required to eliminate the issue of chaotic movements occurring in the template-matching framework. After, the application of amended template matching, the results obtained from individual sensing domain are intelligently fused to obtain the final track estimate. Fig. 1 presents the overall view of the work methodology. The complete section is divided into the following subsections:

A. Tracking using Correlation based Template matching

For tracking in an individual domain, a fast template matching process was incorporated. In this process, the object's initial template was made to slide across the image at the equivalently sized patch interval to find the resultant correlation coefficient values among the different regions of the current frame image. The following mathematical equation provides the formulation for this calculation.

$$s(x,y) = \frac{\sum_i \sum_j (I(x+i,y+j)-\bar{I})(R(i,j)-\bar{R})}{\sqrt{\{\sum_i \sum_j (I(x+i,y+j)-\bar{I})^2\}\{\sum_i \sum_j (R(i,j)-\bar{R})^2\}}} \quad (1)$$

In the above equation, I stands for the current frame image and R for the template region. Here, (i,j) and (x,y) resembles the pixel position in the template region of the object and the image frame respectively. Values, $\bar{R}$ and $\bar{I}$ represent the mean value of pixels in the template region and the corresponding image region with the size equivalent to the template size. The output $s(x,y)$ represent the score or the correlation based template-matching result of a rectangular region in the image with (x,y) as the starting pixel location.

For visible domain tracking, separate measures of R, G, and B were calculated and the combined correlation measure was calculated as the mean of these.

$$s^{VI}(x,y) = (s_r^{VI}(x,y) + s_g^{VI}(x,y) + s_b^{VI}(x,y))/3 \quad (2)$$

In the above equation, $s_r^{VI}(x,y)$, $s_g^{VI}(x,y)$, $s_b^{VI}(x,y)$ represent the individual color channel based correlation similarity score and $s^{VI}(x,y)$ denotes the combined value for visible imagery based output.

The computation from the audio-based sensor is very simple and easier because the information is sufficient by monochrome color representation only. Moreover, only the speaking person's voice gets a corresponding correlation coefficients were found using equation (1) and were resembled as: $s^{AI}(x,y)$.

B. Chaotic Movement Regulation for Template Match Tracking

To avoid superfluous anticipation activity of template matching algorithm, an extra measure was introduced to recheck the obtained track estimate. The state transition in the next frame was certified after verification using a Chaotic Movement Regulation Factor (CMRF). The value of this factor was computed using equation (3). In addition, the check step introduced for eliminating in-consistent tracking is presented by equation (4):

$$CMRF_t = \sqrt{(X_t - X_{t-1})^2 + (Y_t - Y_{t-1})^2} \quad (3)$$

Here, (X_t, Y_t) stands for initial coordinates of rectangular track estimate from the individual tracker at image frame at time interval t. In addition, the corresponding control action was taken was:

$$(X_t, Y_t) = \begin{cases} (X_{t-1}, Y_{t-1}), & if\ CMRF_t > D \\ (X_t, Y_t), & otherwise \end{cases} \quad (4)$$

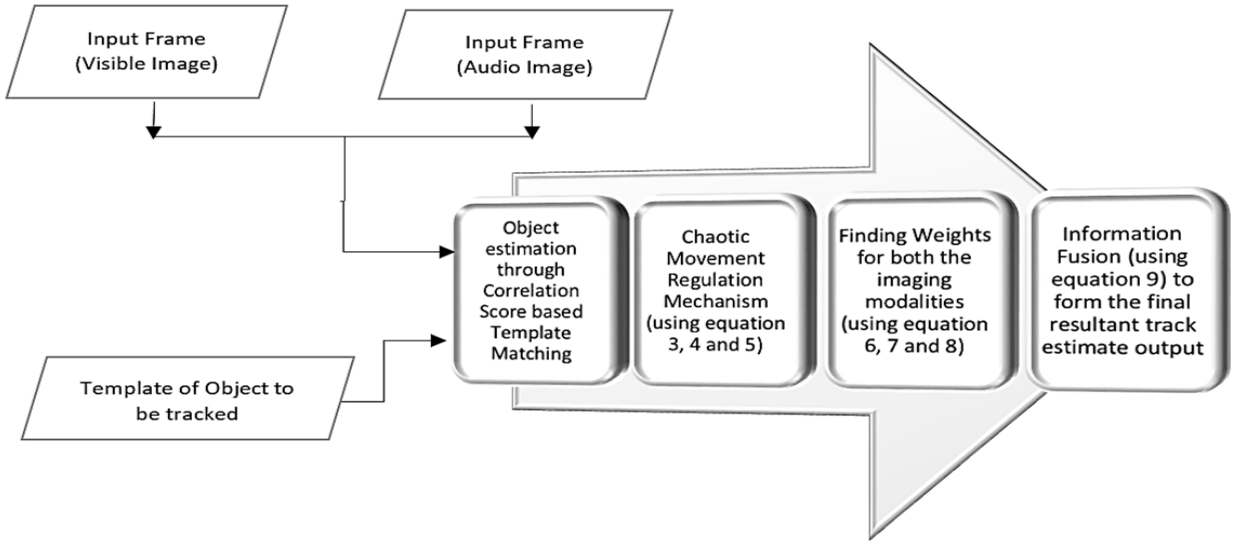

Fig.1. Block Diagram to illustrate the workflow of the proposed scheme

$$D = \sqrt[2]{(A^2 + B^2)} \quad (5)$$

The value of D was estimated using equation (5). It is interesting to note that the threshold parameter D was not chosen as an arbitrary value; rather it was made directly dependent on the dimensions of the object being tracked. Here, A and B represent the width and height of the target selected initially.

After regulating the correlation-based tracking, the final estimates for individual sensing domain were obtained. The maximum value of the correlation coefficient from the above process and the region corresponding to this was chosen as the track estimate from the individual modality. The maximum value of the correlation score for each domain were found among the different correlation values obtained. These were labeled as S_t^{VI}, S_t^{AI} and the region occupying this was saved as state estimates P_t^{VI}, P_t^{AI}respectively.

IV. Fusion Strategy

After the task of improved individual domain tracking estimate had been completed, the next task was to fuse the inputs from mutually exclusive track estimates. For achieving this, effective weights for each complimenting imagery were computed. The variation of the template matching based correlation score pattern throughout the current image frame was chosen as the basis of weighing these sources. The mode having more chances of a unique detection was provided the proportionally greater weight. The value of standard deviation was calculated among the different correlation scores obtained in a complete image frame of individual modality. It is interesting to note that more the pattern of correlation values is varying more are the chances of correct tracking estimate. The adaptation in weights from the individual imaging modality was performed using equations (6) to equation (8).

$$\sigma_t = \sigma_t^{VI}/(\sigma_t^{VI} + \sigma_t^{AI}) \quad (6)$$

$$W_t^{VI} = \frac{\sigma_t \; S_t^{VI}}{(\sigma_t \; S_t^{VI} + (1-\sigma_t) \; S_t^{AI})} \quad (7)$$

$$W_t^{AI} = \frac{(1-\sigma_t) \; S_t^{AI}}{(\sigma_t \; S_t^{VI} + (1-\sigma_t) \; S_t^{AI})} \quad (8)$$

In the above equations σ_t^{VI} and σ_t^{AI} represent the standard deviation value for the patterns of correlation scores obtained for individual imaging domain at the current time t. The tuning parameter for adjustments of weights was found using equation (6) and is denoted as σ_t. Next, the weights to these sources are provided accordingly using equation (7) and (8). Here, the parameters W_t^{VI} and W_t^{AI} denote the weighting factors for individual sensing imaging.

$$P_t^F = W_t^{VI} P_t^{VI} + W_t^{AI} P_t^{AI} \quad (9)$$

The final tracking estimate P_t^F is obtained using the earlier found tracking output of individual imaging modality values, P_t^{VI} and P_t^{AI}.

V. Experimental Results & Discussion

The testing of the proposed framework for audio imaging assisted video-based object tracking was done on three sequences available at [26]. The details of these sequences are presented in Table 2. The results along with discussion are presented according to the data sequence number. The performance of the Proposed Audio – Visual Fusion algorithm (PAVF) is compared with the alone visible trackers such as Visible alone Template Matching (VTM) and Visible Particle Filter [27] (VPF) algorithm. Along with this, the performance is also compared with a multi-cue vision based method that presents the fusion using intensity and gradient features (VCGF) [28]. All the experiments were performed using MATLAB software. The quantitative analysis is performed using some statistical parameters, whose detail is presented in the following paragraph.

The parameters opted for comparing the efficiency of the proposed algorithm are Root Square Positional Error Value (RSPEV), Precision Value (PV), Recall Measure Value (RMV) and finally the F1-Measure Value (FMV). The comparisons were obtained by taking the object's ground truth positions in the video sequence. The RSPEV resembles the closeness in the position of the track estimate with the actual position of the target, whereas PV and RV are the resultant of bounding box overlap efficiencies. PV is found as a ratio of intersection area of ground-truth bounding and estimated track bounding box to the area covered by the later. Whereas for RV, the numerator in the ratio remains as it is but the denominator is exchanged by the area of the ground truth bounding box. FMV is the combined measure that is equal to the Harmonic mean of PV and RV. F-score can be criticized in particular circumstances due to its bias as an evaluation metric. The mathematical calculations of these parameters are provided in the following four equations:

$$RSPEV_t = \sqrt{\left(G_t(x) - P_t^F(x)\right)^2 + \left(G_t(y) - P_t^F(y)\right)^2} \quad (10)$$

$$PV_t = G_t(area) \cap P_t(area)/P_t(area) \quad (11)$$

$$GV_t = G_t(area) \cap P_t(area)/G_t(area) \quad (12)$$

$$FMV_t = 2 \times P_t \times R_t/(P_t + R_t) \quad (13)$$

In above equations, $G_t(x)$ and $G_t(y)$ are the X and Y coordinate of starting point of the actual target state respectively, whereas, $P_t^F(x)$ and $P_t^F(y)$ represent the X and Y coordinate of starting point of the final track estimate found through applied fusion algorithm.

A. Sequence1:

The scenario for tracking the drone in the air can be observed in Fig. 2. The two frames illustrate that the drone appearance changes as it moves across the video sequence. In Fig. 2(a), some of the bottom view of the Drone is captured, whereas Fig. 2(b) mainly presents the side view of the Drone. Hence, it becomes difficult for any of the visual feature based object trackers to identify the drone with changing appearance. Moreover, throughout the whole sequence, the drone occurs many rotations, translations as well as its appearance changes in the visible domain.

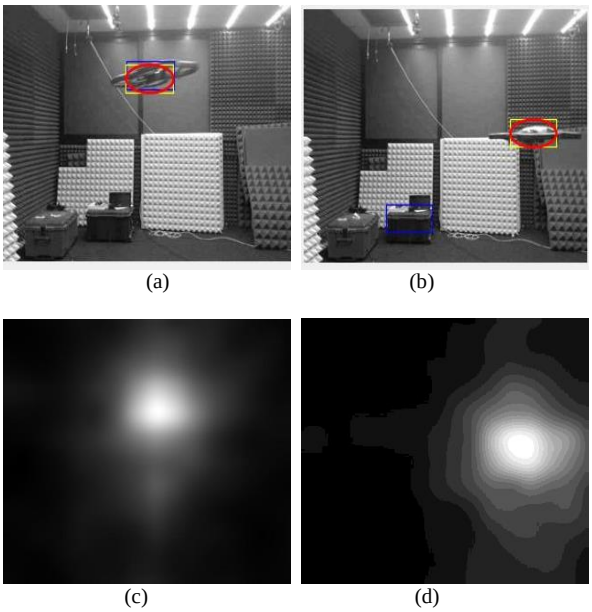

(a) (b)

(c) (d)

Fig.2. Illustration of Sequence 1: (a), (b) Frame 6 and Frame 100 of Visible Image of the sequence, (c), (d) Audio Imaging counterpart of (a) and (b) respectively.

But, the Audio Imaging produced is unaffected by these changes as shown in Fig. 2 (c) and Fig. 2(d). Therefore, in this case, the audio imaging becomes a more reliable source for tracking as compared to its visible counterpart. Hence, the proposed algorithm adjusts the weight favoring under these challenging conditions. The weight provided to the incorrect estimation of visible template matching tracker (shown in Blue rectangle in Fig. 2(c)) for frame number 100 is 0.095, whereas the weight provided for the same case to the audio image has a value of 0.905. In Fig. 2, the area covered under the yellow rectangle represent the track output from the audio imaging, whereas the red circle encloses the final output track estimate.

The same fact can be also be verified by going through the quantitative parameter analysis. Where the rest of the algorithm fails continuously from starting frame number 6 until the last frame number 150. Here, the analysis was started from frame number 6, because an appropriate template for matching was found in frame number 5 of the video. Hence, the tracking process was started thereafter. The plot of RSPEV for Drone sequence in Fig. 3 indicates that the audio imaging assisted tracking outperforms various visible tracking methods.

B. Sequence 2

This sequence is more difficult than the drone sequence because apart from the rotations and changing appearance of the object, the speaking person to be tracked comes across various partial and full occlusions in the visible domain. Further, there are similar visible appearance objects present in the scene.

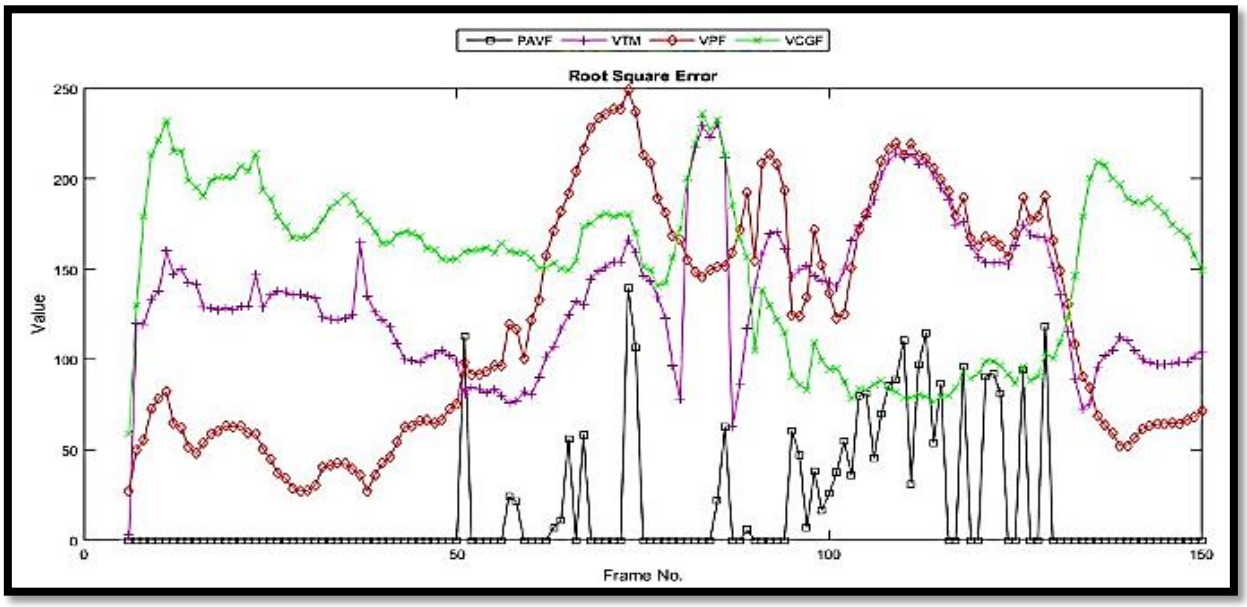

Fig.3. Plots for RSPEV comparisons for Sequence1

Table 2. Type Details of Dataset Sequence taken for experimentation

Dataset	Remarks	Challenges
Sequence 1 [26]	A 2 minutes long sequence, taken in a moderately reverberant environment. The goal is the tracking of a drone flying in the room, whose propellers are the only active audio sources.	The drone itself goes certain deformations in its size and shape during motion.
Sequence 2 [26]	A 2 minutes long sequence, taken in a moderately reverberant environment. The goal is the tracking of the face of a speaker moving in the room.	Presence of disturbing video and audio sources, generated by other people moving in the room
Sequence 3 [26]	Taken outdoor from a terrace, looking at a road about 50 m far from the device. The goal is the tracking of a motorbike.	Many disturbing sources are present, including wind flurries causing trees movements, a highway at about 500 m from the camera in the upper zone of the image

The video sequence is illustrated with the help of Fig. 4. The frame 10 of this visible-acoustic imaging dataset (presented in Fig. 4(a) and Fig. 4(c)) depicts that the partial occlusion condition does not seem to be a hurdle for the audio imaging. The object in the left image can be easily and robustly predicted from the right side acoustic image. Therefore, the fusion algorithm here can make the choice of heavily relying on the clearer differentiable image.

The case of Fig. 4 (b) and Fig. 4(d) present frame number 48 of sequence 2. In this, it is interesting to note that visible template matching is close to the location of the object but not pointing truly to the actual position (blue rectangle). Also, the audio imaging obtained is corrupted by random noise disturbances present. But, due to the mechanism provided in the proposed scheme for regulating the chaotic movements for template match using equation (3-6), the audio imaging tracker overcomes the effect of noises present and still provides a more reliable track estimate shown by an area under yellow rectangle. The weight values provided for this case are 0.36 for the visible tracker and 0.64 for the audio tracker. Finally, the final state estimate is enclosed by the red circle.

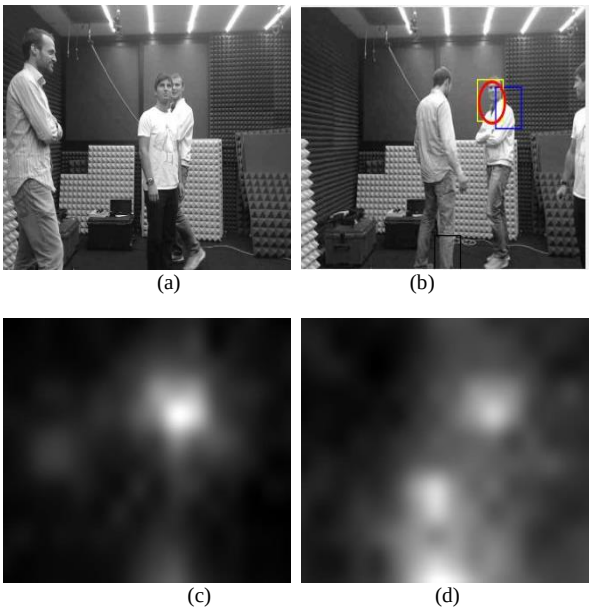

(a) (b) (c) (d)

Fig.4. Illustration of Sequence 2: (a), (b) Frame 10 and Frame 48 of Visible Image of the sequence, (c), (d) Audio Imaging counterpart of (a) and (b) respectively.

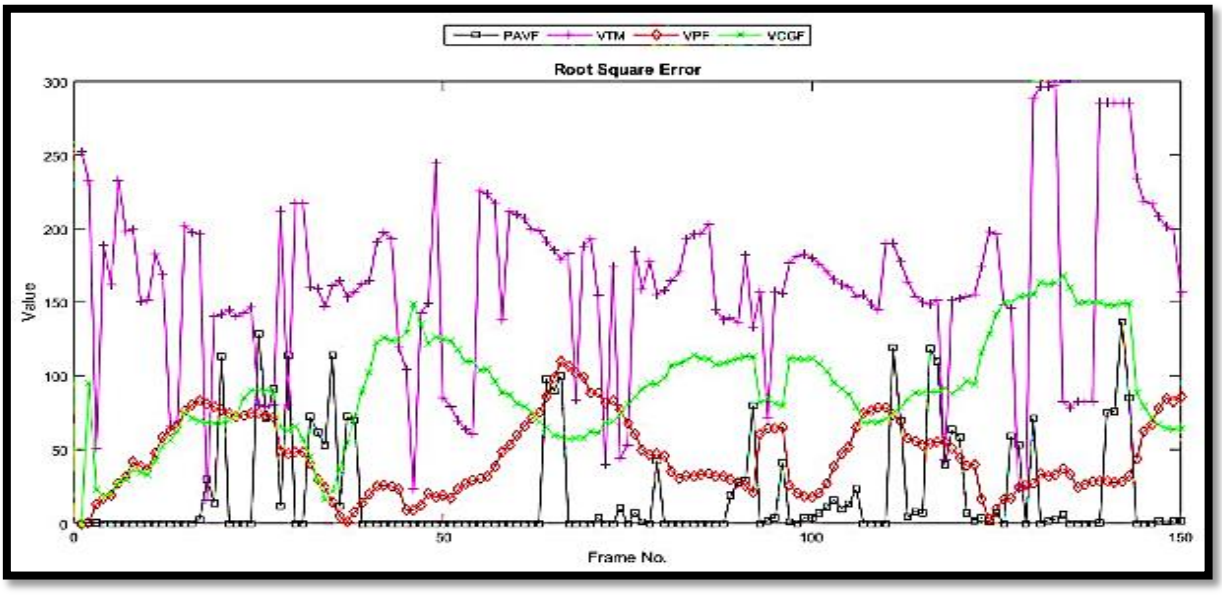

(a)

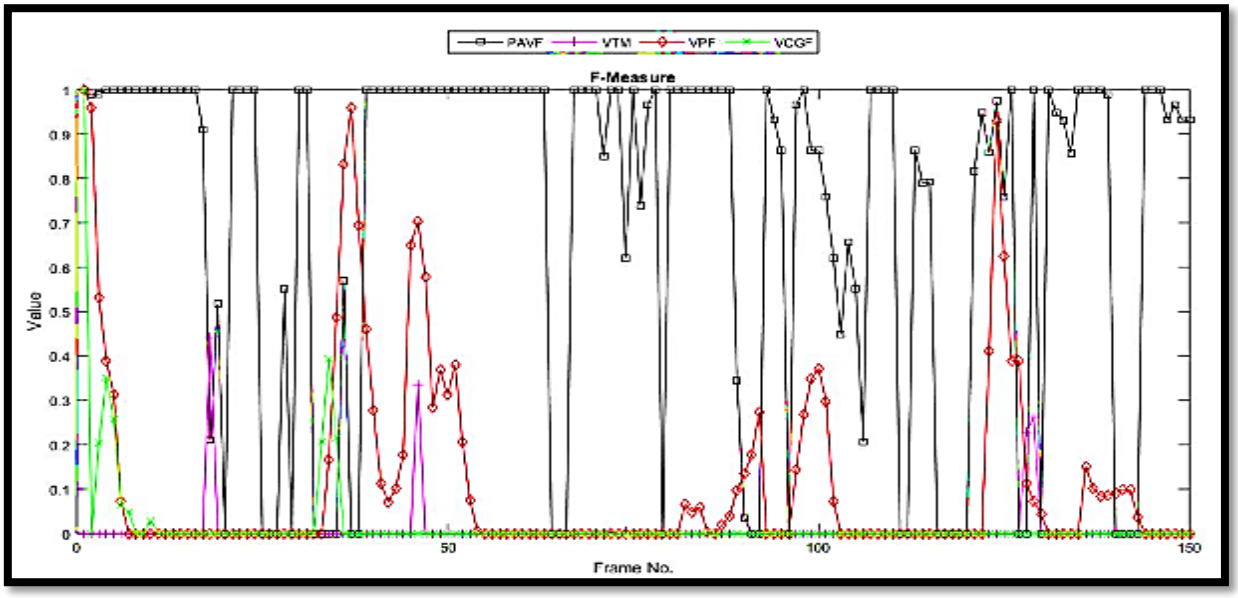

(b)

Fig.5. Plots for quantitative comparisons for Sequence2: (a) RSPEV and (b) FMV

The performance of the proposed algorithm was compared quantitatively and the resulting plots are presented in Fig. 5. Figure 5(a) illustrates the PRSE values. It is easy to deduce from this plot with the proposed method outperforms the other trackers. The assistance of Audio Imaging played an important role in improving the performance as explained in the above paragraphs. The proposed method also occur little errors in certain time intervals, where both the audio image as well as the video image is not providing cleaner hints in the sequence. Although the chaotic movement is controlled which results in small PRSE values during these difficult conditions, where the rest of algorithms fail miserably. The bounding box overlap ratio was formulated using F1-Measure calculations and Fig. 5(b) presents the obtained plot pattern.

C. Sequence 3

This sequence provides very tough challenges to the tracker. Fist, the size of the object to be tracked is very small as compared to the scene dimensions. Here, the scene is captured from a very far distance. The motorbike to be tracked is circled in green color in Fig. 6(a).

But for this frame, the audio image is comparatively better. It is shown in Fig. 6(c). The scenario in visible imagery also inhibits tough challenges such as a small-sized object, partial and full occlusions, Object rotation, the presence of clutters and similar appearance objects.

Also in Fig. 6(b), it is observed from the naked eye that the object has disappeared from the scene. But, actually, the biker gets occluded by the tree in its path. But, for acoustic imaging based signal, the presence of the object is relatively clear and is shown by Fig. 6(d). So, the single domain tracking would have been surely a failure for this type of sequence.

Apart from these, the audio signal here also encounters vague noises in bulk due to open highway recording, with sounds from vehicles and people present on the road. Since the recording was done on a terrace (an open noisy environment), it further worsened the situation for proper audio imaging. Hence, for this imagery, the results are not that promising as compared two earlier sequences.

But, one thing was surely determined that the assistance of audio imaging through the proposed fusion based tracking helps to resolve some of the major challenges for the vision-alone based object tracking. Table 3 and Table 4 provide the values of Average value of the statistical parameters per data sequence for providing the comparative analysis among different algorithms.

(a)

(b)

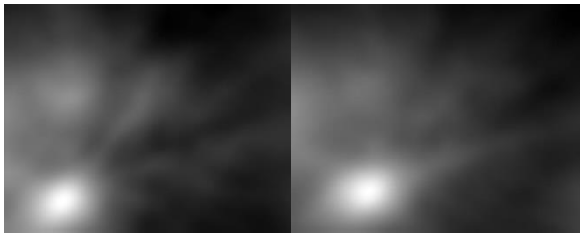

(c) (d)

Fig.6. Illustration of Sequence 3: (a), (b) frame 15 and frame 44 of Visible Image of the sequence, (c), (d) Audio Imaging counterpart of (a) and (b) respectively

Table 3. PRSE values for different algorithms

Algorithm	Sequence1	Sequence2	Sequence3	Average
PAVF	**13.24**	**18.12**	**35.14**	**22.17**
VTM	52.92	115.77	135.97	101.53
VPF	45.90	62.40	82.40	63.57
CGF	61.84	83.53	93.61	79.66

Table 4. F-Measure Score for various Algorithms

Algorithm	Sequence1	Sequence2	Sequence3	Average
PAVF	**0.81**	**0.78**	**0.66**	**0.75**
VTM	0.20	0.13	0.10	0.14
VPF	0.32	0.23	0.19	0.25
CGF	0.22	0.19	0.13	0.18

Here, the top performing algorithm is marked in bold letters. For PRSE, minimum value and for F-measure, maximum value is considered as the most efficient outcome respectively.

VI. Conclusion

We presented here a new development for object tracking using the audio imaging – visual imaging fusion in the template matching framework. Audio imaging can play an important role in computer vision, particularly for automated surveillance by boosting the accuracy of present systems. It has a great advantage in comparison to the primitive audio signal mode of information because it eliminates the need for tedious calibration process. In this paper, an improved template matching based tracking was presented that took care for the chaotic movement of the ordinary template-matching algorithm. Along with it, a fusion scheme was proposed that utilized the standard deviation values obtained from the correlation score pattern obtained throughout the individual frame in each imaging modality. Upon comparison with the state of art visible trackers, it was evident from the results that the proposed method brought considerable improvement in the object tracking process. The accuracy was judged in terms of positional errors and overlap efficiency. The lowest positional error with average value of 22.17 (compared to 101.53, 63.57, and 79.66) and highest overlap measure of 0.75 (compared to 0.14, 0.25, and 0.18) justified the contributions made by our method. Moreover, the performance of the algorithm in different visible conditions such as deformations in its size and shape (sequence 1), presence of disturbing video and audio sources, generated by other people moving in the room (sequence 2), and a difficult visible scene along with many disturbances (sequence 3) was comparatively appreciable. Although, the proposed method outperformed state of art methods in all the sequences, but there is still a scope for improvement, especially for the cases of presence of hefty noises (as was in the case of the third sequence of the outdoor motorbike). However, one can definitely say that conversion of sound to the imaging domain automatically is a plus point and for further work, various image enhancements techniques like image equalization algorithms and image filtering techniques (spatial domain, frequency domain, wavelet domain etc.) can be applied in the future for bringing further robustness to the process of Object Tracking.

References

[1] G. S. Walia and R. Kapoor, "Recent advances on multicue object tracking: a survey," *Artificial Intelligence Review*, vol. 46, no. 1, pp. 821–847, 2016.

[2] S. Singh, R. Kapoor, and A. Khosla, *Cross-Domain Usage in Real Time Video-Based Tracking*. U.S.A: IGI Global, 2017, pp. 105–129.

[3] J. Ma, Y. Ma, and C. Li, "Infrared and visible image fusion methods and applications: A survey," *Information Fusion*, vol. 45, pp. 153–178, 2018.

[4] W. W. Gaver, "What in the world do we hear: An ecological approach to auditory event perception," *Ecological psychology*, vol. 5, no. 1, pp. 1-29, 1993.

[5] B. Jones and B. Kabanoff, "Eye movements in auditory space perception," *Perception, & Psychophysics*, vol. 17, no. 3, pp. 241-245, 1975.

[6] P. Majdak, M. J. Goupell, and B. Laback, "3-d localization of virtual sound sources: Effects of visual environment, pointing method, and training," *Attention, Perception, & Psychophysics*, vol. 72, no. 2, pp. 454-469, 2010.

[7] B. R. Shelton and C. L. Searle, "The influence of vision on the absolute identification of sound-source position," *Perception & Psychophysics*, vol. 28, no. 6, pp. 589-596 1980.

[8] R. S. Bolia, W. R. D'Angelo, and R. L. McKinley, "Aurally aided visual search in three-dimensional space," *Human Factors*, vol. 41, no.4, pp. 664-669, 1999.

[9] D. R. Perrott, J. Cisneros, R. L. McKinley, and W. R. D'Angelo, "Aurally aided visual search under virtual and free-field listening conditions." *Human Factors*, vol. 38, no.4, pp. 702-715, 1996.

[10] M. F. Fallon and S. Godsill, "Acoustic source localization and tracking using track before detect," *IEEE*

Transactions on Audio, Speech, and Language Processing, vol. 18, no. 6 pp. 1228–1242, 2010.
[11] A. Plinge and G. Fink, "Multi-speaker tracking using multiple distributed microphone arrays," in *IEEE Int. Conf. on Acoust., Speech and Sig. Proc.* , May 2014, pp. 614–618.
[12] D. B. Ward, E. Lehmann, and R. Williamson, "Particle filtering algorithms for tracking an acoustic source in a reverberant environment," *IEEE Trans. On Speech and Audio Proc.*, vol. 11, no.6, pp. 826–836, 2003.
[13] K. Wu, S. T. Goh, and A. W. Khong, "Speaker localization and tracking in the presence of sound interference by exploiting speech harmonicity," *in IEEE International Conference on Acoustics, Speech and Signal Processing*, 2013, pp. 365–369.
[14] E. A. Lehmann and A. M. Johansson, "Particle filter with integrated voice activity detection for acoustic source tracking," *EURASIP Journal on Applied Signal Processing*, vol. 2007, no. 1, pp. 28–28, 2007.
[15] V. Cevher, R. Velmurugan, and J. H. McClellan, " Acoustic multi-target tracking using direction-of-arrival batches," *IEEE Transactions on Signal Processing*, vol. 55, no. 6, pp. 2810–2825, 2007.
[16] V. Kilic, M. Barnard, W. Wang, and J. Kittler, "Audio Assisted Robust Visual Tracking With Adaptive Particle Filtering," *IEEE Transactions on Multimedia*, vol. 17, no. 2, pp. 186–200, 2015.
[17] N. Checka, K. W. Wilson, M. R. Siracusa, and T.Darrell, "Multiple person and speaker activity tracking with a particle filter," *IEEE International Conference on Acoustics Speech and Signal Processing*, (1), V-881-4. 2004.
[18] K. Nickel, T. Gehrig, R. Stiefelhagen, and J. McDonough, "A joint particle filter for audio-visual speaker tracking," in proceedings of the 7th International Conference on Multimodal Interfaces, 2005.
[19] Y. Lim and J. Choi, "Speaker selection and tracking in a cluttered environment with audio and visual information," *IEEE Transactions on Consumer Electronics*, vol. 55, no. 3, pp. 1581–1589, 2009.
[20] N. Megherbi, S. Ambellouis, O. Colôt, and F. Cabestaing, "Joint audio-video people tracking using belief theory," in *IEEE International Conference on Advanced Video and Signal Based Surveillance*, p. 135–140, 2005
[21] E. D'Arca, A. Hughes, N. M. Robertson, and J. Hopgood, "Video tracking through occlusions by fast audio source localization," in *IEEE International Conference on Image Processing*, pp. 2660–2664, 2013.
[22] S. T. Shivappa, B. D. Rao, and M. M. Trivedi, "Audio-visual fusion and tracking with multilevel iterative decoding: Framework and experimental evaluation," *IEEE Journal on Selected Topics in Signal Processing*, vol. 4, no. 5, pp. 882–894, 2010.
[23] F. Su, "Acoustic Imaging Using a 64- Node Microphone Array and Beamformer System," thesis submitted to Carleton University Ottawa, Ontario, 2015.
[24] M. Legg, and S.Bradley, "A combined microphone and camera calibration technique with application to acoustic imaging," *IEEE Transactions on Image Processing*, vol. 22, no. 10, pp. 4028-4039, 2013.
[25] A. Zunino et al., "Seeing the Sound: a New Multimodal Imaging Device for Computer Vision," in *IEEE conference on Computer Vision Workshop*, pp. 693-701, 2015.
[26] http://www.iit.it/en/pavis/datasets/DualCam.html
[27] K. Nummiaro, E. K. Meier, and L. V. Gool, "An adaptive color-based particle filter," *Image Vis. Comput.*, vol. 21, no. 1, pp. 99–110, 2003.
[28] J. Xiao, R. Stolkin, M. Oussalah, and A. Leonardis, "Continuously Adaptive Data Fusion and Model Relearning for Particle Filter Tracking With Multiple Features," *IEEE Sens. J.*, vol. 16, no. 8, pp. 2639–2649, 2016.

Authors' Profiles

Satbir Singh Satbir Singh received M.E in Electronics and Communication Engineering from Thapar University, Patiala, India. He is presently working with Central scientific Instruments Organization, Chandigarh, India. Previously, he has a working experience as Senior Scientific Officer with Electronics and Communication Engineering Department of Delhi Technological University, Delhi and as a Project Engineer with Centre of Advanced Computing, Mohali, India. His research interests include signal processing, computer vision and IoT. Currently, he is pursuing Ph.D. from National Institute of Technology, Jalandhar, India.

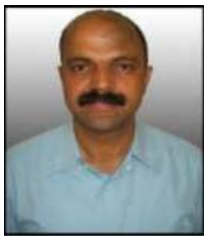

Arun Khosla Arun Khosla received his Ph.D. degree from Indraprastha University, Delhi in the field of Information Technology. He is presently working as Professor in the Department of Electronics and Communication Engineering, National Institute of Technology, Jalandhar, India. Dr. Khosla has been reviewer for various IEEE and other National and International conferences and also serves on the editorial board of International Journal of Swarm Intelligence Research. He is a life member of Indian Society of Technical Education.

Rajiv Kapoor Rajiv Kapoor received M.E. and Ph.D. degree in Electronics & Communication Engineering from Delhi College of Engineering, Delhi University. Dr. Kapoor presently working as Professor in Electronics & Communication Engineering Department, AIACT&R (Govt. of NCT of Delhi). He has authored over 90 research papers in various renowned international journal and conferences. His primary research interests are machine learning, computer vision, signal and image processing.

How to cite this paper: Satbir Singh, Arun Khosla, Rajiv Kapoor, " Visual Object Tracking by Fusion of Audio Imaging in Template Matching Framework", International Journal of Image, Graphics and Signal Processing(IJIGSP), Vol.11, No.8, pp. 40-49, 2019.DOI: 10.5815/ijigsp.2019.08.04

Copyright © 2019 MECS

Natural Language Engineering (2019), 1–20
doi:10.1017/S1351324919000421

CAMBRIDGE
UNIVERSITY PRESS

ARTICLE

Word sense disambiguation using implicit information

Goonjan Jain[1*] and D.K. Lobiyal[2]

[1]Department of Applied Mathematics, Delhi Technological University, New Delhi 110042, India and [2]School of Computer and Systems Sciences, Jawaharlal Nehru University, New Delhi 110067, India
*Corresponding author. Email: goonjan_jain@hotmail.com

(Received 17 October 2017; revised 21 June 2019; accepted 23 June 2019)

Abstract

Humans proficiently interpret the true sense of an ambiguous word by establishing association among words in a sentence. The complete sense of text is also based on implicit information, which is not explicitly mentioned. The absence of this implicit information is a significant problem for a computer program that attempts to determine the correct sense of ambiguous words. In this paper, we propose a novel method to uncover the implicit information that links the words of a sentence. We reveal this implicit information using a graph, which is then used to disambiguate the ambiguous word. The experiments show that the proposed algorithm interprets the correct sense for both homonyms and polysemous words. Our proposed algorithm has performed better than the approaches presented in the SemEval-2013 task for word sense disambiguation and has shown an accuracy of 79.6 percent, which is 2.5 percent better than the best unsupervised approach in SemEval-2007.

Keywords: Word sense disambiguation; Common sense; ConceptNet; Implicit information; Lexical priming

1. Introduction

The primary objective of word sense disambiguation (WSD) is to identify the correct sense of an ambiguous word based on the context it is used in Navigli (2009). WSD is critical for the accuracy and reliability of Natural Language Processing (NLP) tasks, such as Machine Translation (Vickrey *et al.* 2005); Carpuat and Wu (2005; 2007); (Chan, Ng, and Chiang 2007), Text Understanding (Kilgarriff 1997), Sentiment Analysis (Rentoumi *et. al.* 2009; Sumanth and Inkpen 2015; Hung and Chen 2016), Information Retrieval (Zhong and Ng 2012; Schadd and Roos 2015). Since the 1950s, many approaches have been proposed to assign senses to words (Weaver 1955).

Two of the main methodological approaches for assigning senses to words are the supervised and unsupervised methods. Supervised methods use semantically annotated corpora to train the system that is used to assign a correct sense to a word in context (Tratz *et al.* 2007; Zhong and Ng 2010; Wang, Rao, and Hu 2014). In contrast, unsupervised methods abstain from training and instead work directly on raw unannotated corpora (Mihalcea 2005; McCarthy *et al.* 2007; Tripodi and Pelillo 2017). In this paper, we propose an unsupervised approach.

Ambiguous words can be categorized as homonyms or polysemous words (Panman 1982). For example, consider the following usage of *bass* in different contexts.

1. I play $bass_1$ in a jazz band.
2. He was hungry and cooked $bass_2$.
3. The track has a wonderful $bass_3$ line.

The contexts of $bass_1$ and $bass_2$ are entirely different, and thus they are homonyms. However, $bass_1$ and $bass_3$ are semantically related and therefore are polysemous. While it is quite challenging

© Cambridge University Press 2019

Downloaded from https://www.cambridge.org/core. Columbia University - Law Library, on 17 Sep 2019 at 12:51:07, subject to the Cambridge Core terms of use, available at https://www.cambridge.org/core/terms. https://doi.org/10.1017/S1351324919000421

to disambiguate polysemous words, the proposed method disambiguates both homonyms and polysemous words.

Often the meaning of written and verbal communication is based on explicit and implicit information. Explicit information is something that is said or written, whereas implicit information is something that is meant but not said or written. Our brains process implicit information with precision to determine the correct meaning of the communication. For the examples given above, we can use common sense to understand that one cannot eat a musical instrument to satisfy hunger and similarly we cannot make music with a fish in hand. However, existing WSD techniques are unable to process this implicit information. There are many hurdles in doing this, one being a lack of contextual knowledge. The context of a word constitutes not only the words that surround the ambiguous word but also words that are not mentioned explicitly (Dunmore 1989; Fengning 1994). Taking both the word meaning and contextual information into account can efficiently solve the WSD problem.

To understand the meaning of a sentence, we use both words of the sentence and common sense. With common sense, we establish a relationship between the words, for example, "John booked a *table* for dinner." When we read this sentence, we infer several pieces of information, such as John had dinner in some restaurant, he made a prior booking, John is a person, he feels hungry and eats food. With this information, it becomes easier to perform WSD of an ambiguous word.

The approach proposed in this paper is based on a theory called lexical priming (Hoey 2005). This theory connects the lexical aspect of Corpus Linguistics and the priming aspect of Psycholinguistics. Priming takes place if exposure to one stimulus significantly increases the response to another stimulus. For example, *theatre* is recognized more quickly following *movie* than following *umbrella* (Wettler, Rapp, and Sedlmeier 2005). Lexical priming is based on the concept of lexical co-occurrence, which states that words are used along with other words and not in isolation. Every usage of a word is loaded with the context and co-texts in which it is encountered. Thus, our knowledge of a word includes the fact that it co-occurs with certain other words and in certain kinds of contexts (Hoey 2005). The validity and utility of this theory have been discussed in the literature (Pace-Sigge 2013; Rapp and Zock 2014). This theory guides the proposed algorithm, where we understand the meaning of the text by following links between the words of a sentence. Words may be linked directly or indirectly via previously attained knowledge. In this paper, we propose a novel algorithm to identify this attained knowledge that genuinely connects the words of a sentence.

We need an association network that contains knowledge about associations among words to implement the proposed algorithm. There are two methods to obtain such knowledge. One method is to ask people what a given term (*cat*) evokes in their mind (*dog, mouse,* etc.). Another method is to look at word co-occurrences in corpora and derive the associations from them (which, strictly speaking, pre-supposes that the human brain is also doing this). The proposed algorithm uses ConceptNet (Havasi, Speer, and Alonso 2007), which has gathered implicit pieces of knowledge using both of the methods mentioned above. ConceptNet was developed as a network of common sense knowledge, and is a semantic network containing information about the real world that computers should know for understanding written text.

1.1 ConceptNet

ConceptNet is a multilingual knowledge base in which words and phrases are related to one another via common sense. The knowledge contained in ConceptNet has been collected from a variety of resources, including crowdsourced resources, such as Wiktionary[a] and Open Mind Common Sense (OMCS) (Singh *et al.* 2002); purpose-driven games, such as Verbosity (von Ahn,

[a] https://en.wiktionary.org/wiki/Wiktionary:Main_Page.

Downloaded from https://www.cambridge.org/core. Columbia University - Law Library, on 17 Sep 2019 at 12:51:07, subject to the Cambridge Core terms of use, available at https://www.cambridge.org/core/terms. https://doi.org/10.1017/S1351324919000421

Figure 1. Single edge of ConceptNet.

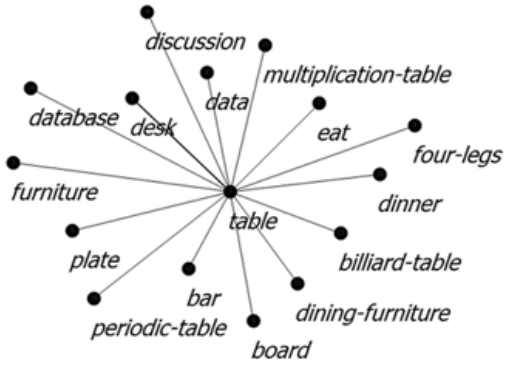

Figure 2. Example subgraph of ConceptNet with "Table" as an ambiguous word.

Keida, and Blum 2006); and expert-created resources, such as WordNet (Miller 1995; Fellbaum 1998). ConceptNet is a network of labeled nodes and edges. The nodes, or concepts, are words, word senses, and short phrases in a variety of different languages. These concepts are connected with a particular relation, which is represented as an edge. The proposition expressed by a relation between two concepts is called an assertion. Every object in ConceptNet has a uniform resource identifier (URI), which is structured similar to a path. URIs are meaningful and we can tell what the object is by looking at its URI. Different kind of objects are distinguished by the first element of the path, for example,

/c/: concept. For example, concept "car" in English has the URI "/c/en/car". Each concept has at least three components. The initial "/c" tells that the object is a concept. The next part tells the concept's language. Last part is the concept text.
/r/: language independent relations. For example, /r/IsA, /r/RelatedTo etc.
/a/: assertion, also known as edges. For example, the sentence "a car is used for driving" expresses an assertion, where the relation /r/UsedFor connects the concept /c/en/car to the concept /c/en/drive. The assertion has the URI: /a/[/r/UsedFor/, /c/en/car/, /c/en/drive/]

Figure 1 shows a single edge connecting two nodes where strings /c/en/car, /c/en/drive, and /r/UsedFor are URIs from ConceptNet. Figure 2 illustrates a subgraph of ConceptNet with *Table* as an ambiguous word. The *table* is connected to words belonging to different senses of its usage. The *table* is connected to *furniture, periodic table, eat* and *discussion*, which belong to different senses of the word.

"ConceptNet has no provision of representing ambiguous words or different senses of a word. It is simply a huge collection of words and phrases that are related to each other. Word senses are only distinguished by their part of speech."[b] For example, for a word *book*, there are 11 different senses of the word as a noun and 4 different senses of it as a verb in the WordNet. However, in ConceptNet we have only two different concepts pertaining to different senses of *book*, one as a verb and the other as a noun. Their URIs are "/c/en/book/v" and "/c/en/book/n", respectively. Each of these concepts is related to different concepts in ConceptNet.

In this paper, we have developed an algorithm for WSD, where a correct sense of an ambiguous word is suggested based on the similarity between the context of the ambiguous word, deduced using ConceptNet, and every one of its possible word senses.

The remainder of the paper is structured as follows: Section 2 gives a glimpse of some of the approaches proposed for unsupervised WSD in recent years. The detailed design and implementation methodology of our proposed work are explained in Section 3. The results of the evaluation

[b] https://github.com/commonsense/conceptnet5/wiki/FAQ

Downloaded from https://www.cambridge.org/core. Columbia University - Law Library, on 17 Sep 2019 at 12:51:07, subject to the Cambridge Core terms of use, available at https://www.cambridge.org/core/terms. https://doi.org/10.1017/S1351324919000421

of the proposed algorithm by undertaking various experiments and its comparison with other available algorithms are reported in Section 4. Finally, in Section 5, we conclude the work along with stating the possible future extensions of the work.

2. Related works

In this section, we give a brief survey of WSD approaches proposed in the literature. First, Lesk-based approaches are discussed. Then, we discuss a few of the graph-based approaches proposed in the literature. Later, we discuss ConceptNet-based approaches. We conclude this section by describing the identified research gap and the approach proposed to fill this gap.

Various dictionary-based and unsupervised approaches have been proposed in the literature, which try to identify the actual sense of a word. Actual sense is identified by exploiting the information derived from the word's context. The algorithms proposed by Lesk (1986), Banerjee and Pederson (2002), Patwardhan, Banerjee, and Pedersen (2003), Basile, Caputo, and Semeraro (2014) exploited pairwise semantic similarity among an ambiguous word and the words in its context. We discuss these approaches below.

In the Lesk algorithm (Lesk 1986), the definition, also known as gloss, of each sense of a word in a sentence is compared to the glosses of every other word in the sentence. The definition of a word is fetched from a dictionary. A word is assigned the sense for whose gloss shares the largest number of words in common with the glosses of the other words. An adapted version of the Lesk Algorithm was proposed by Banerjee and Pedersen (2002), who used WordNet instead of a dictionary for their algorithm. For comparison, the algorithm includes neighboring glosses and those of words related to the word to be disambiguated. Patwardhan *et al.* (2003) generalized this approach as a method of WSD. Basile *et al.* (2014) have proposed an enhanced form of the Lesk algorithm that is based on the distributional semantic model. The algorithm uses a word similarity function defined on a distributional semantic space to compute the gloss-context overlap. Authors of the enhanced Lesk algorithm adapted BabelNet (Navigli and Ponzetto 2012) as sense inventory.

Our work is in the continuation of the approach, where we identify a correct sense of a word by finding an overlap between words in context and glosses prepared using a knowledge base. All of the previously proposed approaches defined context as a collection of words of a sentence. However, in the proposed algorithm, the context includes both the words of a sentence and implicit words that are meant but not written.

Graph-based approaches have gained researchers' attention in the last few years. This is due to the native ability of graphs to organize contextual information as well as compute relations between word senses. This ability enables researchers to extract structural and semantic properties of the text. A few of the examples in the literature include Navigli and Lapata (2007; 2010), Sinha and Mihalcea (2007), Manion and Sainudiin (2014), Agirre, Lacalle, and Soroa (2014), Moro, Raganato, and Navigli (2014), Chaplot, Bhattacharyya, and Paranjape (2015), and Pina and Johansson (2016). We give a brief description of these approaches below.

Navigli and Lapata (2007; 2010) proposed an unsupervised WSD approach based on various measures of graph connectivity to deduce the relative importance of a node in the graph. The approach uses WordNet as a sense inventory as well as a knowledge base. This approach creates a graph, starting with WordNet senses as nodes, and then includes all the nodes and edges that exist on the paths between each pair of senses. It incorporates various local centrality measures and global connectivity measures to check the node's connectivity to all other nodes of the graph. The approach considered local centrality measures viz. degree, closeness, betweenness centrality, and their variants. Global connectivity measures used in the approach are compactness, graph entropy, etc. This approach showed that the local connectivity measures performed better than the global connectivity measures, particularly the degree centrality and PageRank.

Sinha and Mihalcea (2007) created a labeled graph such that there is a vertex for every possible sense for every word of the sentence. A weighted graph of label dependencies is built by adding

Downloaded from https://www.cambridge.org/core. Columbia University - Law Library, on 17 Sep 2019 at 12:51:07, subject to the Cambridge Core terms of use, available at https://www.cambridge.org/core/terms. https://doi.org/10.1017/S1351324919000421

a vertex for each admissible label and an edge for each pair of labels for which a dependency is identified. A maximum allowable distance can be set (MaxDist), indicating a constraint over the distance between words for which a label dependency is sought. Label dependencies are determined through the dependency function which encodes the relation between word senses. Scores are then assigned to vertices using a graph-based centrality algorithm. Sinha and Mihalcea (2007) experimented with various centrality measures viz. indegree, Closeness, Betweenness, and PageRank. The most likely set of labels is determined by identifying, for each word, the label that has the highest score.

Manion and Sainudiin (2014) introduced an approach named SUDOKU that tries to improve centrality. It is an iterative approach that simultaneously constructs a graph and disambiguates the words using a centrality function.

Agirre *et al.* (2014) proposed a new approach based on random walks, which uses WordNet and extended WordNet to create a graph. The modified PageRank random walk algorithm is used to include the context of the sentence for disambiguation. Acknowledging the intertwining of entity linking and WSD, Moro *et al.* (2014) proposed a unified graph-based approach for entity linking and WSD, calling it Bablefy.

Chaplot *et al.* (2015) proposed a new approach for unsupervised WSD. This approach was based on theories of sense dependency and selective dependency. *Sense dependency* states that the sense of a word does not depend on other words of the sentence but rather depends on the senses of the other words in the sentence. *Selective dependency* states that the sense of an ambiguous word is guided by only a few words of the sentence and their respective senses, and not by all words of the sentence. The goal of this approach is to maximize the joint probability of senses of all the words in a sentence, given a dependency structure of the sentence, frequency of senses, and similarity among them.

Pina and Johansson (2016) proposed another graph-based approach for WSD where sense and context embedding are constructed by applying the Skip-gram method to random walks over the sense graph. Their approach assigns a score to all the senses of an ambiguous word based on the dot product of the sense vector with the sum of the context vectors. It does not use any a priori sense probabilities and instead generates all information from the used knowledge base in the form of co-occurrence of concepts. The word is disambiguated by maximizing the sense score and selecting the sense with the highest score. It is successful in generating faster results compared to other methods.

We see much less work in the literature that uses ConceptNet for WSD. Two of the approaches based on ConceptNet are Blending (Havasi, Speer, and Pustejovsky (2010)) and ExtGM (Chen and Liu 2011). Blending (Havasi *et al.* 2010) uses a common sense reasoning technique, called blending, which combines knowledge from SemCor, WordNet, ConceptNet, Extended WordNet, and their ambiguated versions. The approach also uses the Brown1 and Brown2 corpus of SemCor 3.0 to gain knowledge about words that occur together in a sentence. With blending, a single vector space is created to model semantic similarity and associations, and data sets are included in the matrix using appropriate weighing factors. For disambiguation, an ad hoc category vector is created for each sentence, which represents words and meanings that are likely to appear in the sentence. For each word that is to be disambiguated, the sense of the word with the highest dot product with the ad hoc category's vector is declared as the correct sense of the word.

ExtGM (Chen and Liu 2011) first disambiguates concepts in ConceptNet, then tags each concept in a given assertion with one of the senses. It then combines ConceptNet and WordNet to create an enriched knowledge base. Chen and Liu (2011) did not develop any methodology for WSD, but instead implemented a WSD approach proposed by Galley and McKeown (2003) on their extended knowledge base.

We have identified a research gap while performing the literature survey. We identified that all of the approaches define the context of a sentence as consisting of words of the sentence. None of the approaches consider that the context of a sentence also includes implicit words, which truly

Downloaded from https://www.cambridge.org/core. Columbia University - Law Library, on 17 Sep 2019 at 12:51:07, subject to the Cambridge Core terms of use, available at https://www.cambridge.org/core/terms. https://doi.org/10.1017/S1351324919000421

guide the meaning of ambiguous words in a sentence. We also identified a high potential in ConceptNet to be used as a knowledge base. The common sense information that it has collected from volunteers makes it a rich and distinguished source of knowledge. In the proposed algorithm, we fetch the implicit words of a sentence using ConceptNet and then perform WSD of the ambiguous word using explicit and implicit information. As shown in the following section, the proposed algorithm successfully detects the implicit words that correctly describe the context of a sentence. The proposed algorithm ensures that a consistent solution of the WSD problem is found.

3. Proposed algorithm for disambiguation

The proposed algorithm proceeds incrementally and works sentence by sentence. Every sentence is processed using the Java-based Apache OpenNLP[c] toolkit. We performed stemming, part-of-speech (POS) tagging and chunking of each sentence using OpenNLP.

This algorithm has four phases:

1. Generate a graph representation of an input sentence.
2. Create an input sentence profile (ISP) of the input sentence.
3. Create a word sense profile (WSP) for every sense of the ambiguous word.
4. Interpret the ambiguous word.

3.1 Generate graph representation of an input sentence

We generate a graph representation of an input sentence to expose the connection between the words of a sentence. An input sentence contains an ambiguous word and other content words. We refer to content words, except for the ambiguous word, as well as phrases of the input sentence as *constituent terms*. The graph of a sentence is generated using constituent terms and ConceptNet. We add all the content words and phrases (NP, VP, ADJP, and ADVP) of the sentence in the initial sentence graph. However, preposition phrases (PPs) are avoided. PP generally has a preposition followed by a noun phrase. Since prepositions are noncontent words, they are not included in the initial graph; and the following noun phrase (NP) is already included. For example, consider the sentence "I play bass in a jazz band." The parse of the given sentence using OpenNLP is *"(TOP (S (NP (PRP I)) (VP (VBZ play) (NP (NN bass)) (PP (IN in) (NP (DT a) (NN jazz) (NN band)))))."* The content words in the sentence are—*play (VBZ), bass (NN), jazz (NN), band (NN)*. The phrases in the sentence are—noun phrase (NP)—*I, bass* and *a jazz band*; verb phrase (VP)—*play, play bass in a jazz band*; and preposition phrase (PP)—*in a jazz band*. Since we only consider content words, *I, a,* and *in* are omitted. Thus, for the given sentence, the constituent terms are *play, bass, jazz, band* and *jazz band*, which are also available in ConceptNet.

The graph is generated using ConceptNet as a knowledge base. We fetch a subgraph of ConceptNet with the ambiguous word as the centre of the graph. The constituent terms, which are spread across the graph, are connected to the ambiguous word via different paths of varying lengths. In ConceptNet, concepts are related to one another via different *Relations*, which provide vital information in understanding common sense knowledge. However, we are only interested in the concepts that are related to one another and not the type of relations that connect the concepts.

The following subsection gives more details on the method of graph creation.

3.1.1 Graph creation using spreading activation

'Spreading Activation is a method for searching associative networks, neural networks or semantic networks' (Collins and Loftus 1975). Experiments performed by various researchers have showcased its efficacy as a methodology for searching graphs (Meyer and Schvaneveldt 1971).

[c] https://opennlp.apache.org/. OpenNLP provides us with predefined models for stemming, POS tagging and chunking of a sentence. OpenNLP implements Porter Stemming algorithm for stemming and OpenNLP's parser is trained on Conll2000 shared task data.

Downloaded from https://www.cambridge.org/core. Columbia University - Law Library, on 17 Sep 2019 at 12:51:07, subject to the Cambridge Core terms of use, available at https://www.cambridge.org/core/terms. https://doi.org/10.1017/S1351324919000421

We implement spreading activation on ConceptNet to obtain a graph cocooned around an ambiguous word. We initiate the spreading process by assigning an initial weight T to an ambiguous word (w_a). The ambiguous word is the source node from where the activation begins. We used $T = 10$ in our experiments. Then, we spread this activation outward to other nodes linked to the source node. The weight decays with a decay factor (d) as activation propagates throughout the network. We used $d = 1$ in our experiments. The activation values range between 0 and 10. The weight starts at 10 and decays with every activation with a decay factor of $d = 1$. The spreading process stops if there is no node to traverse or if the weight has been reduced to 0. Different values of d affect the decaying value of spreading. If we increase the value of d, then the graph shrinks, resulting in a smaller graph.

Algorithm 1 Algorithm for Spreading Activation

Input: ConceptNet graph in the form of adjacency list, T is the weight, d is the decay factor, and w is the node to be spread outside. Initially, w=w_a, d=1, and T=10.
Output: Graph G, a subset of ConceptNet in the form of a list of edges

```
procedure SPREADING_ACTIVATION(w, d, t)
    processed[w] ← 1
    for vertex w_m adjacent to w do
        if (w, w_m) or (w_m, w) is not in G then
            Add Edge (w, w_m) to G
            if proceseed[w_m] = 0 or T-d ≥ 0 then
                return SPREADING_ACTIVATION(w_m, d, T − d)
            end if
        end if
    end for
end procedure
```

3.2 Create input sentence profile

The ISP of a sentence is a set of words or phrases that help a program understand the relationship between the constituent terms and the ambiguous word of a sentence based on common sense knowledge. We traverse the graph of the input sentence generated in the first step and find paths connecting every constituent term to the ambiguous word to create a profile of a sentence. We then use the depth first search to find the paths. The search starts from the ambiguous word (w_a), and we mark all the constituent terms (W_c) in the graph. Next, we find all paths from these constituent terms to w_a. Every node that lies along these paths becomes a member of the set of supporting terms (W_s) of the ISP. Since the operation is computationally expensive because of the high branching factor of the nodes, finding all the paths of different lengths is difficult and irrelevant. Therefore, we use a Threshold (L) to restrict the path lengths, that is $|pathLength| \leq L$. After performing multiple experiments (refer to Section 4), we fixed $L = 7$.

Let S be a set of constituent terms and ambiguous word of the input sentence. The ISP of a sentence is denoted by *ISP(S)*, such that, ISP(S) = $W_a \cup W_c \cup W_s$, where

W_a = {set of ambiguous words} = $\{w_a\}$
W_c = {set of constituent terms of a sentence} = S-$\{w_a\}$, includes all the content words and phrases (NP, VP, ADJP, and ADVP) of a sentence, except the ambiguous word.
W_s = {set of supporting terms}, are terms (both words and phrases) that enable a program to deduce the connection between an ambiguous word and constituent terms of the sentence under consideration. All the terms that lie along the paths from constituent terms to the ambiguous word are included in this set of supporting terms.

Downloaded from https://www.cambridge.org/core. Columbia University - Law Library, on 17 Sep 2019 at 12:51:07, subject to the Cambridge Core terms of use, available at https://www.cambridge.org/core/terms. https://doi.org/10.1017/S1351324919000421

3.3 Create Word Sense Profile (WSP)

We disambiguate ambiguous words by tagging them with a sense using WordNet as a word sense inventory. WordNet is an online lexical database that arranges words in terms of synonyms called synsets. Each synset represents a different sense, and each sense has a definition and a list of synonym words. Synsets are related to one another via lexical or semantic relations such as hypernymy, hyponymy, meronymy, antonymy. A gloss demonstrating sense usage also supports each sense.

This phase consists of the creation of a WSP (Chen and Liu 2011) for all the senses of the ambiguous word under consideration. A WSP is a set of words created using WordNet, and the WSP of a sense includes all synonyms in the synset, content words in their glosses, and words in semantically related synsets. For example, consider the second sense of the word *glass* (noun), which means a container used for drinking. It is represented as $\{glass_n^2\}$ where the subscript denotes the part-of-speech and the superscript denotes a sense number in WordNet. The WSP of a sense of *glass* is a union of all the words in the sets defined below.

WSP($glass_2^n$) = {drinking glass, container, made, glass, holding, liquids, drinking, beer glass, bumper, goblet, . . ., water glass, wine glass, glass, container}
Synonyms in synset: {drinking glass}
Content words in gloss: {container, made, glass, holding, liquids, drinking}
Semantically related synsets include:
Hyponyms: {beer glass, bumper, goblet, . . ., water glass, wine glass}
Meronym: {glass}
Hypernym: {container}

3.4 Interpret ambiguous word

To suggest a sense for the ambiguous word, we separately implement a set intersection operation between every WSP and ISP. In set theory, an intersection of two sets A and B is a set that contains all elements of A that also belongs to B. In the proposed algorithm, the ISP of the sentence, as well as all WSPs, are sets of words. On the application of set intersection, we obtain a set of words that belong to both the ISP and the corresponding WSP. The sense with an intersection set of highest cardinality is suggested as the correct sense. A conflict may arise when intersection sets of two or more senses have the highest and equal cardinality. Two such cases may occur. First, these senses are closely related. Second, the senses are different in context. The second case is considered as a failure case, as we cannot conclude a single sense for the ambiguous word. However, further processing is performed in the first case. The first case happens because WordNet is a fine-grained sense inventory where senses are very closely related. In this scenario, we further process these intersection sets, removing those concepts from intersection sets that are directly related to the ambiguous word but remotely to other constituent concepts.

For example, consider the usage of the word *bat* in the sentence "He batted the ball to the boundary." The ISP of the sentence is {ball, bat, boundary, hitting, smash, bang, beat, club, baseball, cricket, baseball stick, attack, hit six, run, four, score, batting, game, soft ball, stick, wooden stick, sport, racket, tennis, badminton, sports equipment}. There are five senses of the word *bat* in the WordNet. We thus applied intersection operation between the ISP and the WSPs. The highest cardinality intersection sets are $Intersect_4$ = {bat, club, cricket, hitting, sport} and $Intersect_5$ = {bat, club, hitting, ball, stick}. These sets are obtained by the intersection of WSP_4 with the ISP and WSP_5 with the ISP. The cardinalities of both intersection sets are equal. To resolve this, we find the words or phrases that are directly connected to *bat* and are not directly connected to the other constituent terms. We found that from $Intersect_4$, *club* is the only word that is directly connected to *bat* and remotely to others. However, in $Intersect_5$, *club, ball*, and *stick* are directly connected to *bat*. Therefore, we removed {club} from $Intersect_4$ and {club, ball, stick} from $Intersect_5$. After deleting these terms, the updated Intersect sets are given as $Intersect_4$ = {cricket, hitting, sport} and

Downloaded from https://www.cambridge.org/core. Columbia University - Law Library, on 17 Sep 2019 at 12:51:07, subject to the Cambridge Core terms of use, available at https://www.cambridge.org/core/terms. https://doi.org/10.1017/S1351324919000421

$Intersect_5$ = {hitting}. $Intersect_4$ has a higher cardinality; thus bat_n^4 is deduced as the right sense for the given ambiguous word. This kind of situation occurs in the case of very close senses which are even difficult for a human annotator to judge.

Algorithm 2 Algorithm for WSD using Implicit Information

Input: S - a set of constituent terms extracted from the given sentence, T - Threshold value for graph creation, d - decay factor, and L - Threshold for path length.

Let S= $\{w_1, w_2, \ldots, w_i, \ldots w_n\}$, where w_i represents the i^{th} $(1 \leq i \leq n)$ word or phrase in the input sentence.
Let w_a be an ambiguous word and constituent terms, W_c = S-$\{W_a\}$

Step 1: Create the ISP of the sentence using the following steps:
(i) Call Spreading_Activation(w_a, d, T)
(ii) Locate constituent terms, W_c, in the graph and find all paths connecting w_a to these concepts such that $|path_length| \leq$ L.
(iii) ISP = $\{c_i \mid$ concepts that lie along the paths from W_c to $w_a\}$

Step 2: Create WSPs of all the senses of the ambiguous word having the same part-of-speech. WSP($sense_j$) with $1 \leq j \leq m$, where m is the number of senses that a term has in WordNet.

Step 3: $Intersect_j$ = WSP($sense_j$) $\cap$ ISP

Step 4: If only one set, $Intersect_h$, has the highest cardinality, suggest $sense_h$ as the correct sense. Else go to Step 5.

Step 5: If more than one intersection set exists, let $Intersect_x$ and $Intersect_y$, such that their cardinalities are maximum and equal. Remove the words from intersection sets ($Intersect_x$ and $Intersect_y$) that are directly related to the ambiguous word w_a but remotely to other constituent terms, W_c. The updated Intersect set with the highest cardinality is given as the correct sense.

3.5 Illustrative examples

In this section, we discuss various examples to demonstrate how our proposed algorithm successfully interprets the correct sense of an ambiguous word. Even a graph generated for a simple sentence becomes a complex graph due to the size of ConceptNet. Therefore, for the sake of brevity and to make our examples understandable, we give excerpts of our original graphs, which include only a few of the most relevant concepts. We demonstrate the algorithm for the examples mentioned in Section 1. Since all the example sentences have the same ambiguous word, we define WSPs for all the senses of word $bass_n$ once.

WSP($bass_n^1$) = {bass, lowest part, treble, pitch, concert pitch, soprano, tenor, low frequency, alto, tone, tune, high pitch, key, low pitch, high frequency, musical range};
WSP($bass_n^2$) = {bass, thorough bass, basso continuo, bass part, figured bass, part, voice, secondo, continuo, primo, ground bass, voice part};
WSP ($bass_n^3$) = {bass, vocalizer, musician, player, lowest voice, singer, adult male singer, performer, performing artist, vocalist, entertainer, basso, instrumentalist};
WSP($bass_n^4$) = {bass, sea bass, striper, seafood, food, family Serranidae, solid food, lean flesh, striped bass, saltwater fish, edible fish, shellfish, roe, Atlantic Coast, United States, elongated body, long spiny dorsal fin};

Downloaded from https://www.cambridge.org/core. Columbia University - Law Library, on 17 Sep 2019 at 12:51:07, subject to the Cambridge Core terms of use, available at https://www.cambridge.org/core/terms. https://doi.org/10.1017/S1351324919000421

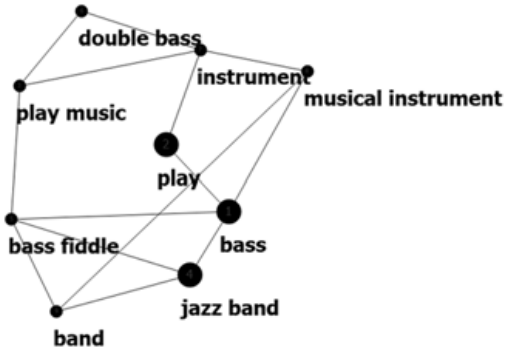

Figure 3. Excerpt of the graphical expansion for the sentence 'I play bass in a jazz band.'

WSP($bass_n^5$) = {bass, freshwater bass, North American, freshwater fish, lean flesh, flesh, large-mouth bass, smallmouth bass, North American food, game fish};
WSP($bass_n^6$) = {bass, basso, basso profundo, very deep bass voice, singing voice, lowest adult male singing voice, singing voice, lowest, voice, vocalization, vocalisation, vocalism, phonation, vox, bass voice, baritone, baritone voice};
WSP($bass_n^7$) = {bass, member, lowest range, musical instrument, bass violin, bull fiddle, double bass, contrabass, family of musical instruments, bass fiddle, string bass, bass guitar, instrument, bass horn, sousaphone, tuba, bombardon, bombard, produce musical tones, sounds};
WSP($bass_n^8$) = {bass, nontechnical name, percoid, edible marine, percoid fish, percoidean, freshwater spiny-finned fish, freshwater bass}.

(i) I play *bass* in a jazz band.

An excerpt of graphical expansion for this sentence is shown in Figure 3. We can see that the constituent terms, *jazz band* and *play*, are directly related to the ambiguous word (*bass*). Obtaining constituents terms early in the graph makes the task more comfortable, but this does not help provide any information about how these terms are related to one another via common sense knowledge. This also demonstrates that a small value of the Threshold (L) is not a very good choice to opt for.

For any given sentence, the ISP is represented as ISP(S) = $W_a \cup W_c \cup W_s$. For the given sentence, W_a = {bass}; W_c = {play, jazz band}; and W_s = {double bass, play music, bass fiddle, instrument, musical instrument, band}. Therefore, the ISP for the given sentence is ISP(S) = {bass, play, jazz band, double bass, play music, bass fiddle, instrument, musical instrument, band}. Next, we find the intersection of ISP(S) with all the WSPs defined above. $Intersect_1$ = {bass}; $Intersect_2$ = {bass}; $Intersect_3$ = {bass}; $Intersect_4$ = {bass}; $Intersect_5$ = {bass}; $Intersect_6$ = {bass}; $Intersect_7$ = {bass, musical instrument, instrument, bass fiddle, double bass}; $Intersect_8$ = {bass}. Looking at the Intersect sets, we can conclude that $Intersect_7$ has the highest cardinality and therefore $bass_n^7$ is the deduced right sense for the ambiguous word.

(ii) He was hungry and cooked *bass*.

Following a similar approach used for the creation of the ISP for the previous sentence, the ISP created for this sentence is {hungry, cook, bass, eat, food, hunger, fish, cook food, seafood, freshwater fish, freshwater bass, eat food} (refer Figure 4). The intersection sets generated as a result of intersection operation between the ISP and WSPs are $Intersect_1$ = {bass}; $Intersect_2$ = {bass}; $Intersect_3$ = {bass}; $Intersect_4$ = {bass, food, seafood}; $Intersect_5$ = {bass, freshwater fish, freshwater bass}; $Intersect_6$ = {bass}; $Intersect_7$ = {bass}; $Intersect_8$ = {bass, fish, freshwater bass}. The intersection sets with the highest cardinality are $Intersect_4$, $Intersect_5$, and $Intersect_8$. Now, by applying Step 5 of our algorithm, no removals occur from $Intersect_4$. Both *freshwater fish* and *freshwater bass* are removed from $Intersect_5$, as they are directly related to *bass* but remotely related to *cook* and *hungry*. From $Intersect_8$, only *freshwater bass* is deleted for the reason mentioned above. However, *fish* remains within $Intersect_8$, as this is directly related with *hungry*. Therefore, the

Downloaded from https://www.cambridge.org/core. Columbia University - Law Library, on 17 Sep 2019 at 12:51:07, subject to the Cambridge Core terms of use, available at https://www.cambridge.org/core/terms. https://doi.org/10.1017/S1351324919000421

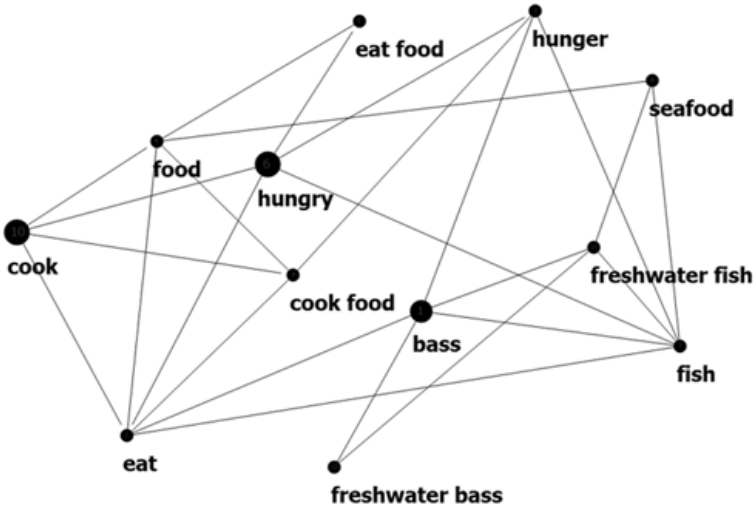

Figure 4. Excerpt of the graphical expansion for the sentence 'He was hungry and cooked bass.'

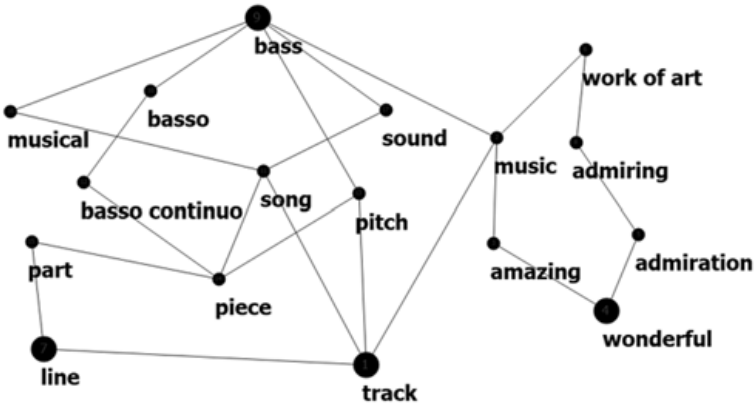

Figure 5. Excerpt of the graphical expansion for the sentence 'The track has wonderful bass line.'

updated intersection sets are $Intersect_4$ = {bass, food, seafood}; $Intersect_5$ = {bass}; $Intersect_8$ = {bass, fish}. $Intersect_4$ is of highest cardinality. Therefore, the deduced sense for *bass* in the given context is $bass_n^4$.

(iii) The track has a wonderful *bass* line.

The graph (Figure 5) shows the connectivity between *track* and *bass* via different paths. One path is *track-music-bass* and another path is *track-song-piece-basso continuo-basso-bass*. A music listener relates with the first path, whereas a music composer relates closely with the second path. Thus, the graph uncovers the relationship between terms based on the knowledge of different people. The ISP for the given sentence is ISP = {bass, wonderful, track, line, pitch, basso, basso continuo, amazing, admiration, admiring, work of art, music, part, piece, song, sound} (refer Figure 5). The intersection of the ISP with the WSPs generates the following intersect sets. $Intersect_1$ = {bass, pitch}; $Intersect_2$ = {bass, basso continuo, part}; $Intersect_3$ = {bass}; $Intersect_4$ = {bass}; $Intersect_5$ = {bass}; $Intersect_6$ = {bass, basso}; $Intersect_7$ = {bass}; $Intersect_8$ = {bass}. Among these obtained intersect sets, $Intersect_2$ has the highest cardinality. Therefore, $bass_n^2$ is the correct sense of the word *bass* in the sentence.

(iv) Please install the *patch*.

In the given input sentence, *patch* is the ambiguous word. The WSPs for all the senses of the word *patch* as a noun are listed below.

WSP($patch_n^1$) = {patch, spot, speckle, dapple, fleck, maculation, marking, design, pattern, figure, crisscross, cross, mark};

Downloaded from https://www.cambridge.org/core. Columbia University - Law Library, on 17 Sep 2019 at 12:51:07, subject to the Cambridge Core terms of use, available at https://www.cambridge.org/core/terms. https://doi.org/10.1017/S1351324919000421

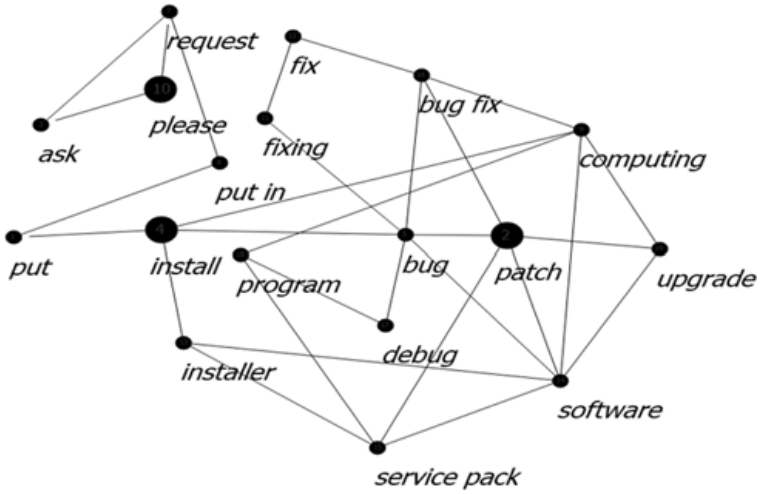

Figure 6. Excerpt of the graphical expansion for the sentence 'Please install the patch.'

WSP($patch_n^2$) = {patch, plot, plot of land, plot of ground, small area. Ground, vegetation, bean plot, cabbage patch, tract, piece of land, piece of ground, parcel of land, parcel};
WSP($patch_n^3$) = {patch, piece of cloth, piece of material, decoration, mend, cover, fabric, piece, part, portion};
WSP($patch_n^4$) = {patch, while, piece, spell, period, indeterminate length, bad weather};
WSP($patch_n^5$) = {patch, commands, correct, bug, computer program, programme, computer programme, instructions, computer, execute, interpret, software, package, code};
WSP($patch_n^6$) = {patch, temporary hookup, connection, limited time, connection, connecter, connector, connective, connexion, lash-up, contrivance};
WSP($patch_n^7$) = {patch, mend, darn, sewing, repair, worn, torn hole, stitchery, needlework, needle, thread, needlecraft, binding, stitch, applique, binding, patchwork};
WSP($patch_n^8$) = {patch, eyepatch, cloth, covering, eye, cloth covering, artifact, artefact, covers, protect, shelter, conceal};
WSP($patch_n^9$) = {patch, bandage, injured, part of body, covers, protects, adhesive bandage, capeline bandage, cast, plaster cast, compression bandage, amputation, medical, dressing, gauze, plastic, fabric tape, adhesive}.

A part of graphical expansion for the sentence is given in Figure 6. The ISP for the sentence is ISP ={patch, software, bug, computing, program, installer, service pack, upgrade, debug, please, request, put in, put, fix, bug fix}. The intersection of the ISP and WSPs generates the following intersection sets. $Intersect_1$ = {patch}; $Intersect_2$ = {patch}; $Intersect_3$ = {patch}; $Intersect_4$ = {patch}; $Intersect_5$ = {patch, software, bug}; $Intersect_6$ = {patch}; $Intersect_7$ = {patch}; $Intersect_8$ = {patch}; $Intersect_9$ = {patch}. As is evident, the intersection set $Intersect_5$ has the highest cardinality. Therefore, $patch_n^5$ is the correct sense for the word *patch* in the given sentence.

To demonstrate the effectiveness of the proposed algorithm on a verb, such as "be", let us take an example sentence of "He is a good singer." The word to be disambiguated is *is*. WordNet indicates "be" as the base form of the verb "is", and thus we use *be* as the word to be disambiguated. The ISP of the sentence is {be, good, singer, to be, being, am, music, is, human, human being, person, artist, music}. Then we create the WSPs for all 13 senses of the word *be* in WordNet. The WSPs are given below:

WSP(be_v^1) = {be, is, equality, being, John, rich, good, answer, look, suffer, hurt, be well, feel, stay, remain, rest, continue, sparkle, scintillate, coruscate, confuse, throw, fuddle, befuddle, confound, rank, point, want, need, require, compact, pack, rest, cut};
WSP(be_v^2) = {be, is, identical, someone, something, president, John Smith, house};

Downloaded from https://www.cambridge.org/core. Columbia University - Law Library, on 17 Sep 2019 at 12:51:07, subject to the Cambridge Core terms of use, available at https://www.cambridge.org/core/terms. https://doi.org/10.1017/S1351324919000421

WSP(be_v^3) = {be, occupy, certain position, area, somewhere, where, umbrella, toolshed, is, back, what, behind, behavior, this, stretch, stretch along, attend, go to, fill, populate, dwell, live, inhabit, reach, extend to, touch, run, go, pass, lead, extend};
WSP(be_v^4) = {be, exist, existence, extant, God, there, come, preexist, coexist, cohabit, indwell, prevail, hold, obtain, consist, lie in, lie, distribute, dwell};
WSP(be_v^5) = {be, happen, occur, take place, lost, wallet, this, during, visit, parent's house, there, two hundred people, funeral, lot, noise, kitchen};
WSP(be_v^6) = {be, equal, identical, equivalent, one dollar, equals, 1000 rubles, days, equate, correspond, match, fit, check, jibe, gibe, tally, agree, represent, stand for, correspond, translate};
WSP(be_v^7) = {be, constitute, represent, make up, comprise, form, compose, make, form, range, straddle, fall into, fall under, present, pose, supplement, money, income, stone wall, backdrop, performance, constitute, entire, belonging, children, made up, chorus, sum, represents, income, year, few, men, army};
WSP(be_v^8) = {be, follow, work, specific, place, specific place, specific subject, function, herpetologist, resident philosopher, vet, cox};
WSP(be_v^9) = {be, embody, personify, represent, character, stage, Derek Jacobi, Hamlet, body, exemplify, typify, symbolize, symbolize, stand for};
WSP(be_v^{10}) = {be, spend, use time, hour, take, occupy, use up, space};
WSP(be_v^{11}) = {be, live, have life, alive, great leader, no more, grandfather, lived, end of war, survive, last, live on, go, endure, hold up, hold out, living};
WSP(be_v^{12}) = {be, remain, unmolested, undisturbed, uninterrupted, infinitive form, let, stay, rest};
WSP(be_v^{13}) = {cost, be, priced at, set back, knock back, put back}.

Next, we perform an intersection of the ISP with the WSPs. We determine that $Intersection_1$ = {being, is, good} has the highest cardinality and thus be_n^1 is deduced as the correct sense of *be* in the above example.

4. Experimental results and discussion

In this section, we first describe how the Threshold value (L) for the proposed algorithm has been found. Next, we describe various performed experiments and obtained results and their interpretation. To evaluate the performance of our algorithm, we compute three measures, viz. precision, recall, and f1-measure. Since our algorithm provides an answer to all ambiguous words, the values for precision, recall, and f1-measure are the same.

- *Precision (P)*—the percentage of correct senses out of the total identified senses;
- *Recall (R)*—the percentage of the number of correctly identified senses to the total number of words in the data set; and
- *F1-measure*—combination of precision and recall, F1-measure = (2*P*R/ (P+R)).

4.1 Tuning of threshold (L) value

For the proposed algorithm, the value of Threshold (L) is tuned using two data sets viz. SemEval-2010 task 17 (Agirre *et al.* 2010) and SemEval-2015 task 13 (Moro and Navigli 2015). The text in the first data set is from the ecology domain, whereas the text in the second data set is composed of data from four different domains: medical, drug, math, and social issues. A total of 794 words out of 1,398 words were disambiguated in the first data set, and the highest F1-measure of 56.79 was obtained at $L = 7$. A total of 819 words were disambiguated out of 1,261 words from the second test set and the highest F1-measure of 64.96 was obtained at $L = 7$. The results are shown in Tables 1 and 2. With this observation, we set the Threshold (L) for our algorithm at $L = 7$.

Downloaded from https://www.cambridge.org/core. Columbia University - Law Library, on 17 Sep 2019 at 12:51:07, subject to the Cambridge Core terms of use, available at https://www.cambridge.org/core/terms. https://doi.org/10.1017/S1351324919000421

Table 1. Impact of Threshold (L) on the F1-measure of the proposed algorithm for the SemEval-2010 Task 7 data set

Threshold (L)	F1-measure
5	51·21
6	55·87
7	56·79
8	54·30
9	49·55

Table 2. Impact of Threshold (L) on the F1-measure of the proposed algorithm for the SemEval-2015 Task 13 data set

Threshold (L)	F1-measure
5	61·23
6	63·88
7	64·96
8	63·62
9	60·33

4.2 Experiments performed

To test our algorithm, we ran it with two distinct data sets. One was provided for *SemEval-2013 Task 12: Multilingual Word Sense Disambiguation* and other for *SemEval 2007 Task 7: Coarse-Grained English All-Words Task*. One of the significant differences in these two data sets is their sense granularities. While the SemEval-2007 task uses coarse-grained word senses, the SemEval-2013 task relies on fine-grained distinctions. Since only nouns are tagged in the SemEval-2013 task, we also tested our algorithm with the SemEval-2007 test data set, which is an all-word WSD task. A scorer was provided along with the data sets to ensure consistent scoring of the algorithms. We also obtained our results using the official scorer of these tasks.

4.2.1 Testing on SemEval-2013 Task 12: Multilingual word sense disambiguation

We ran our algorithm on a test set of Semeval-2013 task for multilingual word sense disambiguation (Navigli, Jurgens, and Vannelle 2013). The test set consisted of 13 articles covering different domains. For English, there were 1644 words of running text consisting of 1502 single-words and 85 multiword expressions. For the task, participating systems were given the flexibility to use either BabelNet or its two main subsets, viz. WordNet and Wikipedia, as a sense inventory. We used WordNet as a sense inventory for annotating ambiguous words in our experiments. To do so, we restricted ourselves to items annotated with BabelNet synsets that contain WordNet senses for the ambiguous word.

The proposed algorithm correctly tagged 1012 words out of 1502 single-words and all the multiword expressions when tested with the test set. It did so with an F1-measure of 69.13 at $L = 7$. However, the highest F1-measure of 69.30 was achieved with $L = 6$. Table 3 has a comparison of the results of the proposed algorithm with the results of the algorithms that were submitted in the SemEval-2013 task. We have also compared our algorithm with the most frequent sense

Downloaded from https://www.cambridge.org/core. Columbia University - Law Library, on 17 Sep 2019 at 12:51:07, subject to the Cambridge Core terms of use, available at https://www.cambridge.org/core/terms. https://doi.org/10.1017/S1351324919000421

Table 3. Comparison results with systems participating in SEMEVAL-2013 Task 12

Team	System	F1-measure
GETALP	WN-1	51·4
UMCC-DLSI	RUN2	64·7
Proposed algorithm		69·13
MFS		63·0

Table 4. F1 scores for 13 articles in the SemEval-2013 Task 12 (for WordNet)(T.=Translated)

Text	Description[a]	Length	F1-measure
1	General environment	194	70·2
2	T. Politics	76	52·7
3	T. Economics (Wall street)	69	62·1
4	News, General	109	66·9
5	T. Economics (Banks)	53	49·2
6	Web general	190	69·8
7	T. Sports	178	45·2
8	Science	135	65·1
9	Geopolitics economics	159	61·4
10	General law	138	64·9
11	T. Sport	76	59·7
12	T. Political	170	59·1
13	T. Economics (Deutsche bank)	97	63·2

[a] (Schwab *et al.* 2013)

Table 5. Impact of Threshold (L) on the F1-measure of the proposed algorithm for the SemEval-2013 test set

Threshold(L)	F1-measure	Threshold(L)	F1-measure
1	35·64	6	69·30
2	42·90	7	69·13
3	49·97	8	67·29
4	58·73	9	63·71
5	65·41	10	62·90

(MFS) baseline. MFS of an ambiguous word is the sense with maximum frequency in the training data. Table 4 depicts the document level F1 scores for the data set, and Table 5 depicts the influence of L on the results for the 2013 data set.

We also performed an investigation with Wikipedia and BabelNet sense inventories. Wikipedia sense synset consists of a page title with an optional label. The structured relations include redirect pages, disambiguation pages, internal links, interlanguage links, and categories. For example,

Downloaded from https://www.cambridge.org/core. Columbia University - Law Library, on 17 Sep 2019 at 12:51:07, subject to the Cambridge Core terms of use, available at https://www.cambridge.org/core/terms. https://doi.org/10.1017/S1351324919000421

Table 6. Impact of Threshold (L) on the F1-measure of the proposed algorithm for the SemEval-2007 Task 7 data set

Threshold(L)	F1-measure	Threshold(L)	F1-measure
1	38·91	6	69·94
2	44·25	7	79·63
3	54·30	8	78·47
4	59·22	9	77·36
5	68·73	10	72·68

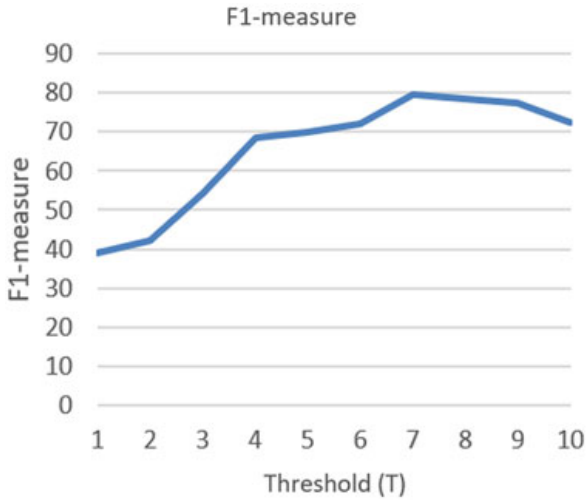

Figure 7. (Colour online) Graphical representation of Threshold (L) versus F1-measure.

consider the word "play". Its synset consists of {play, play(theatre)}. With this little information in a synset, the results were not very encouraging with our algorithm, but the results we obtained from BabelNet are quite inspiring. However, the purpose of our research was to investigate the applicability of WordNet because it is available for Indian languages too, whereas BabelNet does not incorporate most Indian languages.

4.2.2 Testing on SemEval-2007 Task 7: Coarse-grained english all-words task

The SemEval 2007 test set for coarse WSD (Navigli and Lapata 2007) contains five documents belonging to different domains, viz. journalism, book review, travel, computer science, and biography. Out of 2269 ambiguous words, 1807 words were tagged correctly using a Threshold (L) value of 7. This gives an F1-measure of 79.63 (1807/2269).

In Table 6, we summarize the impact of the Threshold (L) on the proposed algorithm. Performance of the algorithm improved with an initial increase in the value of L. However, after a certain limit, the performance began to deteriorate with an increase in the value of L. The relationship between L and F1-measure is shown in Figure 7. The reason for such behaviour is that as the graph size increased with an increasing L, more concepts came into consideration. These concepts were from diverse domains and were not related to our domain of discourse. This hampers the performance of the algorithm.

Out of 2269 word instances, 678 words were monosemous and 1591 were polysemous per the coarse sense inventory. The proposed algorithm correctly tagged all of the monosemous words and 1159 of the polysemous words. Table 7 below summarizes these statistics.

During our experiments, we noticed that a few senses were incorrectly identified because of the unavailability of information in ConceptNet. The reason for this is that common sense knowledge is vast, and ConceptNet is yet not an exhaustive resource that has captured all of the

Downloaded from https://www.cambridge.org/core. Columbia University - Law Library, on 17 Sep 2019 at 12:51:07, subject to the Cambridge Core terms of use, available at https://www.cambridge.org/core/terms. https://doi.org/10.1017/S1351324919000421

Table 7. Statistics of the performance of the proposed algorithm for monosomy and polysemy

	Monosemous		Polysemous	
	Instances	Correct	Instances	Correct
Noun	358	358	750	594
Verb	86	86	505	382
Adjective	141	141	221	136
Adverb	93	93	115	47

The first two numeric columns give the number of instances and the number of correct instances of monosemous words. The last two numeric columns represent the total number of instances and the number of correct instances for polysemous words.

Table 8. Performance of different unsupervised coarse WSD algorithms on the SemEval-2007 test set

Algorithm	F1-measure	Methodology
ExtGM	82·8	Unsupervised
Blending	80·8	Unsupervised
Proposed algorithm	79·63	Unsupervised
SUSSX-FR	77·04	Unsupervised
WFS baseline	63·44	
MFS baseline	78·9	
Random baseline	62·7	

available knowledge. Furthermore, many sentences that are available in ConceptNet are incorrect and meaningless. For example, sentences such as "It is a tree" with assertion It→ ISA → Tree fail to provide any relevant information. Dangling sentences such as "Tree is a often" are incomplete and ambiguous. Such sentences were added into the system because volunteers of the OMCS project created the sentences and there were no quality controls to prevent volunteers from entering meaningless data. The presence of such irrelevant information degrades the performance of the proposed algorithm.

There are only a few algorithms that make use of common sense knowledge for WSD. We compared the performance of the proposed algorithm with the ExtGM approach (Chen and Liu 2011), Blending Approach (Havasi *et al.* 2010), and SUSSX-FR (Koeling and McCarthy 2007). The ExtGM approach (Chen and Liu 2011) disambiguates assertions of ConceptNet and then performs WSD. The Blending Approach (Havasi *et al.* 2010) makes use of ConceptNet. SUSSX-FR (Koeling and McCarthy 2007) is the best-unsupervised WSD system that participated in the Semeval-2007 coarse-grained all-words WSD task. We have taken various baseline approaches to compare the performance of the proposed algorithm viz. WFS (WordNet First Sense) baseline, MFS (Most Frequent Sense) baseline, and RB (Random Baseline). The results of all these algorithms along with the proposed algorithm are shown in Table 8.

The approaches ExtGM (Chen and Liu 2011) and Blending (Havasi *et al.* 2010) gave better results than our proposed algorithm. The approach by Chen and Liu (2011) first disambiguates concepts of ConceptNet using WordNet as a sense inventory. It then merges disambiguated

Downloaded from https://www.cambridge.org/core. Columbia University - Law Library, on 17 Sep 2019 at 12:51:07, subject to the Cambridge Core terms of use, available at https://www.cambridge.org/core/terms. https://doi.org/10.1017/S1351324919000421

Table 9. Performance of the proposed algorithm on different data sets

S. No.	Dataset	F1-measure (By proposed algorithm)	Threshold(L)
1	SemEval 2013 fine-grained	69·3	6
2	SemEval 2007 coarse-grained	79·63	7
3	SemEval 2007 fine-grained	57·23	7
4	SemEval 3 fine-grained	63·01	7
5	SemEval 2 fine-grained	66·67	6

ConceptNet with WordNet and performs WSD of text using this enriched resource. The blending approach proposed by Havasi *et al.* (2010) blends various knowledge bases viz. ConceptNet, WordNet, Extended WordNet, and their ambiguated versions. They also use the Brown1 and Brown2 corpus of SemCor 3.0 to gain knowledge about words that occur together in a sentence. Thus, their approach is also corpus dependent. The blending approach was implemented solely for coarse WSD. In the proposed algorithm, we neither disambiguate ConceptNet, which itself is an enormous task, nor do we merge varied knowledge bases, which is computationally tedious. Instead, we traverse the ConceptNet graph and include all the concepts lying in the path from the constituent terms to the ambiguous word. This gives us implicit terms that connect the words/terms of the sentence together. We then use this information to disambiguate the words in the text. The proposed algorithm is simpler than both of the proposed approaches, and the results are close to current state-of-art algorithms.

We also tested the proposed algorithm on five more data sets. The results obtained from these tests reinforce our decision to use 7 as the value for the Threshold (L). The results are shown in Table 9. For three data sets, the proposed algorithm gave the best results when L was set to 7. For the other two data sets, the F1-measure was highest when L was set to 6. However, the F1-measure at $L = 6$ was only marginally higher than the F1-measure at $L = 7$. Therefore, taking the above observations into consideration, we proposed $L = 7$ to be used for the test sets.

5. Conclusion and future work

WSD is an essential task in NLP, and context plays an important role in disambiguating an ambiguous word. The context of a sentence is comprised of the words in the sentence as well as implicit information, which is not said aloud. The work presented here successfully demonstrated that the knowledge of implicit information could significantly improve a computer program's power to disambiguate an ambiguous word. The proposed algorithm has an accuracy of 69.3 percent, which is higher than all the unsupervised WordNet-based systems submitted in the SemEval-2013 competition. We were successful in disambiguating 79.63 percent of the lexical sample data set of Semeval-2007.

The proposed algorithm is a very humble attempt at disambiguation, and there is large scope for further improvement. Common sense knowledge is extremely significant, and an enormous amount of knowledge needs to be added in ConceptNet. Therefore, we will use OpenIE approaches in our future work to collect as many assertions as possible, which will increase the ConceptNet knowledge base. We will also attempt to include the relationships between the nodes of ConceptNet in the proposed algorithm. This will help create a better understanding of the context of the sentence, and thus a better WSD. We also plan to extend the proposed algorithm to work with Indian languages, and we will attempt to merge WordNet into ConceptNet for better evaluation.

Downloaded from https://www.cambridge.org/core. Columbia University - Law Library, on 17 Sep 2019 at 12:51:07, subject to the Cambridge Core terms of use, available at https://www.cambridge.org/core/terms. https://doi.org/10.1017/S1351324919000421

References

Agirre E., Lacalle O.L, Felbaum C., Hsieh S., Tesconi M., Monachini M., Vossen P. and Segers, R. (2010). SemEval-2010 task 17: All-words word Sense Disambiguation on a specific domain. In *Proceedings of the 5th International Workshop on Semantic Evaluations, ACL 2010*, pp. 75–80.

Agirre E., Lacalle O.L and Soroa, A. (2014). Random walks for knowledge based word sense disambiguation. *Computational Linguistics* **40,** 57–84.

Banerjee S. and Pedersen, T. (2002). An adapted lesk algorithm for word sense disambiguation using Wordnet. In: Gelbukh A. (eds) Computational Linguistics and Intelligent Text Processing. CICLing 2002. *Lecture notes in Computer Science*, vol 2276, pp. 136–145. Springer, Berlin, Heidelberg.

Basile P., Caputo A. and Semeraro G. (2014). An enhanced lesk word sense disambiguation algorithm through a distributional semantic model. In *Proceedings of COLING 2014, 25th International Conference on Computational Linguistics*, pp. 1591–1600.

Carpuat M. and Wu D. (2005). Word sense disambiguation vs. statistical machine translation. In *Proceedings of the 43rd Annual Meeting of the Association for Computational Linguistics (ACL-05)*, Association for Computational Linguistics, pp. 387–394. Stroudsburg, PA, USA.

Carpuat M. and Wu D. (2007). Improving statistical machine translation using word sense disambiguation. In *Proceedings of the Joint Conference on Empirical Methods in Natural Language Processing and Computational Natural Language Learning (EMNLP/CoNLL'07)*, pp. 61–72.

Chan Y.S., Ng H.T. and Chiang D. (2007). Word sense disambiguation improves statistical machine translation. In *Proceedings of Annual Meeting-Association for Computational Linguistics, ACL-2007*, pp. 33–40.

Chaplot D.S., Bhattacharyya P. and Paranjape A. (2015). Unsupervised word sense disambiguation using Markov random field and dependency parser. In *Proceedings of the Twenty-Ninth AAAI Conference on Artificial Intelligence*, Texas, Austin, pp. 2217–2223.

Chen J. and Liu J. (2011). Combining WordNet and ConceptNet for word sense disambiguation. In *Proceedings of the 5th International Joint Conference on Natural Language Processing*, pp. 686–694.

Collins A.M. and Loftus E.F. (1975). A spreading activation theory of semantic processing. *Psychological Review* **82**, 407–428.

Dunmore D. (1989). Using contextual clues to infer word meaning: an evaluation of current exercise types. *Reading in a Foreign Language* **6**, 337–347.

Fellbaum C. (1998). *WordNet: An Electronic Lexical Database*. Cambridge, MA: MIT Press.

Fengning Y. (1994). Context clues - a key to vocabulary development. *People's Republic of China-forum* **32**(3), 39.

Galley M. and McKeown K. (2003). Improving word sense disambiguation in lexical chaining. In *Proceedings of the 18th International Joint Conference on Artificial Intelligence*, pp. 1486–88.

Havasi C., Speer R. and Alonso, J. (2007). ConceptNet 3: a flexible, multilingual semantic network for common sense knowledge. In *Recent Advances in Natural Language Processing*, September, Borovets, Bulgaria, pp. 27–33.

Havasi C., Speer R. and Pustejovsky J. (2010). Coarse word sense disambiguation using common sense. In *Common Sense Knowledge: papers from AAAI Fall Symposium.*

Hoey M. (2005). *Lexical Priming. A New Theory of Words and Language*. London: Routledge.

Hung C. and Chen S.-J. (2016). Word sense disambiguation based sentiment lexicon for sentiment analysis. *Knowledge Based Systems* **110,** 224–232.

Kilgarriff A. (1997). I don't believe in word senses. *Computers and the Humanities* **31**, 91–113.

Koeling R. and McCarthy D. (2007). Sussx. WSD using automatically acquired predominant senses. In *Proceedings of the 4th International Workshop on Semantic Evaluations*, pp. 314–317.

Lesk M. (1986). Automatic sense disambiguation using machine readable dictionaries: how to tell a pine cone from an ice cream cone. In *SIGDOC'86: Proceedings of the 5th annual international conference on Systems documentation*, pp. 24–26.

Manion S.L. and Sainudiin R. (2014). An iterative sudoku style approach to subgraph-based word sense disambiguation. In *Proceedings of the Third Joint Conference on Lexical and Computational Semantics (* SEM 2014)*, pp. 40–50.

McCarthy D., Koeling R., Weeds J. and Carroll J. (2007). Unsupervised acquisition of predominant word senses. *Computational Linguistics* **33**, 553–590.

Meyer D.E. and Schvaneveldt R.W. (1971). Facilitation in recognizing pairs of words: evidence of a dependence between retrieval operations. *Journal of Experimental Psychology* **90**, 227–234.

Mihalcea R. (2005) Unsupervised large-vocabulary word sense disambiguation with graph-based algorithms for sequence data labeling. In *Proceedings of the Conference on Human Language Technology and Empirical Methods in Natural Language Processing*, pp. 411–418.

Miller G. (1995). WordNet: a lexical database for english. *Communications of the ACM* **38**, 39–41.

Moro, A. and Navigli, R. (2015). SemEval-2015 task 13: multilingual all-words sense disambiguation and entity linking. In *Proceedings of the 9th International Workshop on Semantic Evaluation (SemEval-2015)*, pp. 288–297.

Moro A., Raganato A. and Navigli R. (2014). Entity linking meets word sense disambiguation: a unified approach. *Transactions of the Association for Computational Linguistics* **2**, 231–244.

Navigli R. (2009). Word sense disambiguation: a survey. *ACM Computing Surveys* **41**, 10.1–10.69.

Downloaded from https://www.cambridge.org/core. Columbia University - Law Library, on 17 Sep 2019 at 12:51:07, subject to the Cambridge Core terms of use, available at https://www.cambridge.org/core/terms. https://doi.org/10.1017/S1351324919000421

Navigli R., Jurgens D. and Vannella D. (2013). SemEval-2013 task 12: multilingual word sense disambiguation. In *Seventh International Workshop on Semantic Evaluation (SemEval 2013)*, pp. 222–231.
Navigli R. and Lapata M. (2007). Graph connectivity measures for unsupervised word sense disambiguation. In *Proceedings of IJCAI'07*, pp. 1683–1688.
Navigli R. and Lapata M. (2010). An experimental study of graph connectivity for unsupervised word sense disambiguation. *IEEE Transactions on Pattern Analysis and Machine Intelligence* **32**, 678–692.
Navigli R. and Litkowski K.C. (2007). SemEval- 2007: task summary. SemEval Web site. http://nlp.cs.swarthmore.edu/semeval/tasks/task07/summary.shtml.
Navigli R. and Ponzetto S. (2012). BabelNet: the automatic construction, evaluation, and application of a wide-coverage multilingual semantic network. *Artificial Intelligence* **193**, 217–250.
Pace-Sigge M. (2013). The concept of lexical priming in the context of language use. *ICAME Journal* **37**, 149–173.
Panman O. (1982). Homonymy and polysemy. *Lingua* **58**, 105–136.
Patwardhan S., Banerjee S. and Pedersen T. (2003). Using measures of semantic relatedness for word sense disambiguation. In *Proceedings of CICLing'03*, pp. 241–257.
Pina L.N. and Johansson R. (2016). Embedding sense for efficient graph-based word sense disambiguation. In *Proceedings of 2016 Workshop on Graph Based Methods for Natural Language Processing, NAACL-HLT*, pp. 1–5.
Rapp R. and Zock M. (2014). The CogALex-IV shared task on the lexical access problem. In *Proceedings of the 4th Workshop on Cognitive Aspects of the Lexicon*, pp. 1–14.
Rentoumi V., Giannakopoulos G., Karkaletsis V. and Vouros G.A. (2009). Sentiment analysis of figurative language using a word sense disambiguation approach. In *Proceedings of RANLP*, pp. 370–54d.
Schadd F.C. and Roos N. (2015). Word-sense disambiguation for ontology mapping: concept disambiguation using virtual documents and information retrieval techniques. *Journal on Data Semantics* **4**, 167–186.
Schwab D., Tchechmedjiev A., Goulian J., Nasiruddin M., Sérasset G. and Blanchon H. (2013). GETALP: Propagation of a Lesk Measure through an ant colony algorithm. In *Seventh International Workshop on Semantic Evaluation (SemEval 2013)*, pp. 232–240.
Singh P., Lin T., Mueller E.T., Lim G., Perkins T. and Zhu W.L. (2002). Open mind common sense: knowledge acquisition from general public. In *Proceedings of On the Move to Meaningful Internet Systems*, pp. 1223–1237.
Sinha R. and Mihalcea R. (2007). Unsupervised graph-based word sense disambiguation using measures of word semantic similarity. In *Proceedings of ICSC*, pp. 363–369.
Sumanth, C. and Inkpen, D. (2015). How much does word sense disambiguation help in sentiment analysis of micropost data? In *Proceedings of the 6th (WASSA 2015)*, pp. 115–121.
Tratz S., Sanfilippo A., Gregory M., Chappell A., Posse C. and Whitney P. (2007). PNNL: a supervised maximum entropy approach to word sense disambiguation. In *Proceedings of the 4th International Workshop on Semantic Evaluations*, pp. 264–267.
Tripodi R. and Pelillo M. (2017). A Game theoretic approach to word sense disambiguation. *Computational Linguistics* **43**, 31–70.
Vickrey D., Biewald L., Teyssier M. and Koller D. (2005). Word-sense disambiguation for machine translation. In *Proceedings of the Conference on Human Language Technology and Empirical Methods in Natural Language Processing*, pp. 771–778.
von Ahn L., Keida M. and Blum M. (2006). Verbosity: A game for collecting common sense facts. In *Proceedings of SIGCHI Conference on Human Fctors in Computing Systems*, pp. 75–78.
Wang T., Rao J. and Hu, Q. (2014). Supervised word sense disambiguation using semantic diffusion kernel. *Engineering Applications of Artificial Intelligence* **27**, 167–174.
Weaver W. (1955). Translation. *Machine Translation of Languages* **14**, 15–23.
Wettler M., Rapp R. and Sedlmeier P. (2005). Free word associations correspond to contiguities between words in texts. *Journal of Quantitative Linguistics* **12**, 111–122.
Zhong Z. and Ng H.T. (2010) It makes sense: a wide-coverage word sense disambiguation system for free text. In *Proceedings of the ACL 2010 System Demonstrations*, pp. 78–83.
Zhong Z. and Ng H.T. (2012). Word Sense Disambiguation improves information retrieval. In *Proceedings of ACL 2012*, pp. 273–282.

Cite this article: Jain G and Lobiyal D.K. Word sense disambiguation using implicit information. *Natural Language Engineering* https://doi.org/10.1017/S1351324919000421

Downloaded from https://www.cambridge.org/core. Columbia University - Law Library, on 17 Sep 2019 at 12:51:07, subject to the Cambridge Core terms of use, available at https://www.cambridge.org/core/terms. https://doi.org/10.1017/S1351324919000421